

UNIVERSITY OF ŽILINA



TRANSCOM PROCEEDINGS 2015

**11-th EUROPEAN CONFERENCE
OF YOUNG RESEARCHERS AND SCIENTISTS**

under the auspices of

Tatiana Čorejová
Rector of the University of Žilina

**SECTION 6
MACHINES AND EQUIPMENT
TRANSPORT MEANS
APPLIED MECHANICS**

ŽILINA June 22 - 24, 2015
SLOVAK REPUBLIC

Edited by Mária Maňurová, Michal Mokryš

© University of Žilina, 2015

ISBN: 978-80-554-1048-7

ISSN of Transcom Proceedings CD-Rom version: 1339-9799

ISSN of Transcom Proceedings online version: 1339-9829

(<http://www.transcom-conference.com/transcom-archive>)

TRANSCOM 2015

11th European conference of young researchers and scientists

TRANSCOM 2015, the 11th international conference of young European scientists, postgraduate students and their tutors, aims to establish and expand international contacts and co-operation. The main purpose of the conference is to provide young scientists with an encouraging and stimulating environment in which they present results of their research to the scientific community. TRANSCOM has been organised regularly every other year since 1995. Between 160 and 400 young researchers and scientists participate regularly in the event. The conference is organised for postgraduate students and young scientists up to the age of 35 and their tutors. Young workers are expected to present the results they had achieved.

The conference is organised by the University of Žilina. It is the university with about 13 000 graduate and postgraduate students. The university offers Bachelor, Master and PhD programmes in the fields of transport, telecommunications, forensic engineering, management operations, information systems, in mechanical, civil, electrical, special engineering and in social sciences incl. natural sciences.

SECTIONS AND SCIENTIFIC COMMITTEE

1. TRANSPORT AND COMMUNICATIONS TECHNOLOGY.

Scientific committee: Adamko Norbert (SK), Bugaj Martin (SK), Buzna Ľuboš (SK), Drozdziel Paweł (PL), Jánošíková Eudmila (SK), Madleňák Radovan (SK), Rievaj Vladimír (SK), Teichmann Dušan (CZ)

2. ECONOMICS AND MANAGEMENT.

Scientific committee: Blašková Martina (SK), Hittmár Štefan (SK), Borkowski Stanisław (PL), Gregor Milan (SK), Kucharčíková Alžbeta (SK), Matuszek Józef (PL), Mičieta Branislav (SK), Rostášová Mária (SK), Sroka Włodzimierz (PL), Tomová Anna (SK), Zhivitskaya Helena (BLR)

3. INFORMATION AND COMMUNICATION TECHNOLOGIES.

Scientific committee: Dado Milan (SK), Hudec Róbert (SK), Kharchenko Vyacheslav (UKR), Klimo Martin (SK), Kršák Emil (SK), Matiaško Karol (SK), Pancierz Krzysztof (PL), Spalek Juraj (SK), Švadlenka Libor (CZ), Vaculík Juraj (SK), Vašínek Vladimír (CZ), Vrček Neven (HR)

4. ELECTRIC POWER SYSTEMS. ELECTRICAL AND ELECTRONIC ENGINEERING.

Scientific committee: Altus Juraj (SK), Brandštetter Pavel (CZ), Bury Peter (SK), Cacciato Mario (I), Čáповá Klára (SK), Dobrucký Branislav (SK), Chernoyarov Oleg Vyacheslavovich (RU), Janoušek Ladislav (SK), Luft Mirosław (PL), Szychta Elżbieta (PL), Špánik Pavol (SK), Vittek Ján (SK)

5. MATERIAL ENGINEERING. MECHANICAL ENGINEERING TECHNOLOGIES.

Scientific committee: Adamczak Stanisław (PL), Guagliano Mario (I), Konečná Radomila (SK), Kunz Ludvík (CZ), Kuric Ivan (SK), Meško Jozef (SK), Neslušán Miroslav (SK), Takács János (H), Ungureanu Nicolae Stelian (RO)

6. MACHINES AND EQUIPMENT. TRANSPORT MEANS. APPLIED MECHANICS.

Scientific committee: Gerlici Juraj (SK), Chudzikiewicz Andrzej (PL), Malcho Milan (SK), Medvecký Štefan (SK), Zapoměl Jaroslav (CZ), Žmindák Milan (SK)

7. CIVIL ENGINEERING.

Scientific committee: Bujňák Ján (SK), Ižvolt Libor (SK), Segalini Andrea (I)

8. NATURAL SCIENCES (APPLIED MATHEMATICS). SOCIAL SCIENCES.

Scientific committee: Dopita Miroslav (CZ), Dzhalladova Irrada (UKR), Grecmanová Helena (SK), Katuščák Dušan (SK), Marčoková Mariana (SK), Růžičková Miroslava (SK), Šindelářová Jaromíra (CZ)

9. SECURITY ENGINEERING. FORENSIC ENGINEERING.

Scientific committee: Kasanický Gustáv (SK), Kohút Pavol (SK), Navrátil Leoš (CZ), Řehák David (CZ), Sventeková Eva (SK), Šimák Ladislav (SK), Zagorecki Adam (UK), Zamiar Zenon (PL)

ORGANIZING COMMITTEE

CHAIRPERSONS

Čelko Ján, Bokúvka Otakar

EXECUTIVE SECRETARY

Vráblová Helena

MEMBERS

Baš'ovanský Ronald, Belan Juraj, Bendík Ján, Brída Peter, Brúna Marek, Bulej Vladimír, Cíba Jakub, Čičmancová Silvia, Dulina Luboslav, Ďurovec Martin, Florková Zuzana, Gašová Zuzana, Grajcaríková Petra, Grejták Marek, Herda Miloš, Hóger Marek, Hrbček Jozef, Hruboš Marián, Hudák Martin, Koman Gabriel, Kutaj Milan, Kuzmová Mária, Kvet Michal, Magdolen Marián, Malichová Eva, Maňurová Mária, Masárová Gabriela, Metruk Rastislav, Murgašová Veronika, Nosek Radovan, Odrobiňák Jaroslav, Olešnaníková Veronika, Oriěšková Veronika, Palkechová Marcela, Porubiaková Andrea, Pšenáková Zuzana, Račko Ján, Rusinková Jana, Rypáková Martina, Semanová Štefánia, Stankovičová Zuzana, Šarafín Peter, Šimková Ivana, Šušlik Luboš, Vaško Alan, Vincúrová Gabriela.



**SECTION 6 MACHINES AND EQUIPMENT
TRANSPORT MEANS
APPLIED MECHANICS**

REVIEWERS:

Bašťovanský Ronald
Blatnický Miroslav
Bokůvka Otakar
Brumerčík František
Čaja Alexander
Dižo Ján
Durčanský Peter
Dzimko Marián
Galliková Jana
Gerlici Juraj
Grenčík Juraj
Harušinec Jozef
Holubčík Michal
Hrček Slavomír
Juřena Tomáš
Kalinčák Daniel
Kohár Róbert
Koňár Radoslav

Kučera Ľuboš
Kukuča Pavol
Lack Tomáš
Łukasz Orman
Malcho Milan
Naď Milan
Nemec Martin
Nosek Radovan
Nový František
Pilát Peter
Poprocký Roman
Silvester Poljak
Stuchlý Vladimír
Suchánek Andrej
Šťastniak Pavol
Vaško Milan
Zvolenský Peter
Žmindák Milan

Note:

Author/s are responsible for language contents of their papers

CONTENTS

BARAN, PETER – BREZÁNI, MILOŠ – KUKUČA, PAVOL, Žilina, Slovak Republic: The measuring system and adjustment of compression ratio in prototype of Stirling engine with non conventional mechanism FIK	8
BAVLNA, LUKÁŠ – ZVOLENSKÝ, PETER, Žilina, Slovak Republic: Simulation of acoustics energy propagation through the floor structure of passenger coach	14
BEZÁK, PETER – BEZÁK, JURAJ, Žilina, Slovak Republic: Use of advanced technologies to design and produce headlights for electric vehicle EDISON	20
BREZÁNI, MILOŠ – BARAN, PETER, Žilina, Slovak Republic: Using of waste heat of internal combustion engines and types of heat exchangers.....	30
BRUMERČÍK, FRANTIŠEK – SOJCAK, DUSAN – NIEOCZYM, ALEKSANDER, Žilina, Slovak Republic: Construction of Primary Circuit VVER 440V/213 nuclear power plant	36
BUCALA, JÁN – ŽARNAY, MARTIN – POLJAK, SILVESTER – RADEK, NORBERT, Žilina, Slovak Republic: Application of Wear Resistant Coatings for Autonomous Drilling Devices Working in Extreme Conditions	42
DIŽO, JÁN – BLATNICKÝ, MIROSLAV, Žilina, Slovak Republic: Development of a Flexible Multibody System of a Rail Vehicle.....	48
GAJDOŠÍK, TOMÁŠ – BUCALA, JÁN – TOMÁŠIKOVÁ, MÁRIA, Žilina, Slovak Republic: The Vibrodiagnostics of Toothed Planetary Gearboxes	54
GALLIKOVÁ, JANA – POPROCKÝ, ROMAN, Žilina, Slovak Republic: Computer-aided analysis and the consequences of failures of the selected vehicle subsystem	58
HAUSER, VLADIMÍR, Žilina, Slovak Republic: Rail-wheel contact of tramways vehicles in arc track.....	64
HEJMA, PETR – KLIMENDA, FRANTIŠEK – KAMPO, JAN, Usti nad Labem, Czech Republic: Length of weld of welding machine	70
HRABOVSKÝ, PETER – PAPUČÍK, ŠTEFAN, Žilina, Slovak Republic: Comparing Heat Transfer of Heat Pipe and Copper Bar.....	76
HRABOVSKÝ, PETER – PAPUČÍK, ŠTEFAN – LENHARD, RICHARD, Žilina, Slovak Republic: Comparing Thermal Conductivity of Heat Pipe and Copper Bar.	82
CHABADOVÁ, JANA – PAPUČÍK, ŠTEFAN – JANDAČKA, JOZEF –PILÁT, PETER, Žilina, Slovak Republic: Emissions measurements during the combustion of wood pellets.....	88
CHUDZIKIEWICZ, ANDRZEJ – SOWINSKA, MAGDALENA, Warsaw, Poland: Modelling and Simulations of Dynamics of the Low-floor Tramcar with Independently Rotating Wheels	94
JOBB, MARIÁN – KOSA, ĽUBOŠ – NEMEC, PATRIK – MALCHO, MILAN, Žilina, Slovak Republic: Effect of high temperature on the performance parameters gravitational heat pipe, filled with different working medium	100
KALIČÁKOVÁ, ZDEŇKA – DRASTICHOVÁ, VENDULA – MIČKA, VLADIMÍR – KRPEC, KAMIL, Ostrava, Czech Republic: Simulation of Emissions of Nanoparticles from Braking Processes on a Dynamometer with Regard to Distribution of Pollutants.....	105

KASANICKÝ, MARTIN – LENHARD, RICHARD – MALCHO, MILAN, Žilina, Slovak Republic: Optimization of Atypical Heat Exchanger with Using CFD Simulation	111
KASANICKÝ, MARTIN – ČAJA, ALEXANDER – MALCHO, MILAN, Žilina, Slovak Republic: The Device for Measuring the Thickness of the Falling Condensate in the Gravity Assisted Heat Pipe.....	115
KOSA, ĽUBOŠ – ČAJA, ALEXANDER – KASANICKÝ, MARTIN, Žilina, Slovak Republic: Comparison of cooling electro static converters with classic ribbed cooler and heat pipes	119
KOSA, ĽUBOŠ – JOBB, MARIÁN – NEMEC, PATRIK – MALCHO, MILAN, Žilina, Slovak Republic: Dependent of Working Position and Working Diameter at Thermal Performance Gravitational Heat Pipe.....	125
KOVALÍČEK, MATÚŠ – BUCALA, JÁN – BRONČEK, JOZEF, Žilina, Slovak Republic: Influence of heat treatment on coefficient of friction between DLC (WCC) deposited layer and bearing steel 100Cr6	131
KULPA, JAKUB – WITKOWSKI, GRZEGORZ, Kielce, Poland: Multisensory measurements in modern production techniques	136
LENHARD, RICHARD – KASANICKÝ, MARTIN, Žilina, Slovak Republic: Indirect Heat Water Heaters	141
MAŇUROVÁ, MÁRIA – SUCHÁNEK, ANDREJ, Žilina, Slovak Republic: Creation of a tilting bogie model for simulation purpose.....	145
MAŇUROVÁ, MÁRIA – SUCHÁNEK, ANDREJ, Žilina, Slovak Republic: Suspension of tilting bogie specification for calculations of dynamical behavior evaluation.....	151
MARKOWSKI, JAROSŁAW – PIELECHA, JACEK – JASIŃSKI, REMIGIUSZ – ŚLUSARZ, GRZEGORZ – WIRKOWSKI, PAWEŁ, Poznan, Poland: Methodology of Assessment of Exhaust Gas Flow for a Small Jet Engine.....	157
MELNIK, RAFAŁ – SOWIŃSKI, BOGDAN, Warsaw, Poland: Validation of the Rail Vehicles' Suspension Damage Model.....	162
MIČIETA, JOZEF – HÁJEK, JIŘÍ – JANDAČKA, JOZEF, Žilina, Slovak Republic: Simplified Model of Combustion Process in Fuel Bed	166
MIKOLAJČÍK, MARTIN – KALINČÁK, DANIEL, Žilina, Slovak Republic: Hybridization way of better fuel utilization and decreasing emission	173
MŁODZIŃSKA, DIANA – JURECKI, RAFAŁ S. – SZUMSKA, EMILIA, Kielce, Poland: The rotational speed differences of the vehicle wheels equipped and non-equipped with ABS system	179
MOČILAN, MARTIN – ŽMINDÁK, MILAN, Žilina, Slovak Republic: Thermo-Mechanical Finite Element Analysis of Mold for Piston Casting	184
PALACKA, MATEJ – HOLUBČÍK, MICHAL – VICIAN, PETER, Žilina, Slovak Republic: Increasing the Accuracy of Thermal Power of the Large Heat Source by Using Sensor Calibration.....	190
PECHÁČ, PETER – SÁGA, MILAN, Žilina, Slovak Republic: Comparison Study of Fully Stress Design Algorithms for Discrete Optimization of Truss Structures.....	195
REZNIČÁK, ŠTEFAN – MALCHO, MILAN, Žilina, Slovak Republic: Energy Accumulation and Storage of Natural Gas in the Form of Compressed Natural Gas, Liquefied Natural Gas and Methane Hydrates	201

REZNIČÁK, ŠTEFAN – SMATANOVÁ, HELENA – KAPJOR, ANDREJ, Žilina, Slovak Republic: The Heat Transfer from the Complex Shaped Piping System	205
RUMAN, FRANTIŠEK – GREŇČÍK, JURAJ, Žilina, Slovak Republic: Methodology for calculating the LCC and LCP with the support of software	210
SADKOWSKI, WOJCIECH – PASTUSZKO, ROBERT – MARCINIEWSKI, MATEUSZ – LUDWINEK, KRZYSZTOF – KANIOWSKI, ROBERT, Kielce, Poland: Simulation comparison of the operating characteristics of conventional and a new type of Stirling engine	216
SAWCZUK, WOJCIECH – KOWALCZYK, JAKUB – ULBRICH, DARIUSZ, Poznan, Poland: Process evaluation of the braking disc brake of a rail vehicle using vibration friction pad	222
STANKOVIČOVÁ, ZUZANA – DEKÝŠ, VLADIMÍR – NOVÁK, PAVOL – UHRÍČÍK, MILAN – SAPIETA, MILAN – RADZISZEWSKI, LESZEK, Žilina, Slovak Republic: Thermal stress analysis of the plate with hole at fatigue testing machine.....	226
SUCHÁNEK, ANDREJ – HARUŠINEC, JOZEF, Žilina, Slovak Republic: Evaluation of structural properties of braked railway wheel.....	232
SULOVCOVÁ, KATARÍNA – JANDAČKA, JOZEF – PAPUČÍK, ŠTEFAN, Žilina, Slovak Republic: Visualization and measurement of flow in flue gas path by particle image velocimetry method.....	238
ŠŤASTNIAK, PAVOL, Žilina, Slovak Republic: Design of Non-Standard Long Railway Wagon with Variable Use of Loading Platform.....	242
ŠTEFAŇAKOVÁ, VERONIKA, Žilina, Slovak Republic: Modification of spring element in the system for the angle of attack setting.....	248
TOMASIKOVA, MARIA – KRZYWONOS, LESZEK – BRUMERCIK, FRANTISEK, Žilina, Slovak Republic: Vehicle suspension and damping	255
TOMASIKOVA, MARIA – MACHROWSKA, ANNA – BRUMERCIK FRANTISEK, Žilina, Slovak Republic: Vehicle steering geometry.....	260
TOMASIKOVA, MARIA – NIEOCZYM, ALEKSANDER – BRUMERCIK, FRANTISEK, Žilina, Slovak Republic: Vehicle drivetrain modelling.....	265
UHRÍČÍK, MILAN – KOPAS, PETER, Žilina, Slovak Republic: Determine the Fatigue Lifetime for Aluminium Alloy EN AW 2007.T3 During Cyclic Bending – Torsion Loading Under In-and-out of Phase Shift $\varphi = 0^\circ$ and $\varphi = 90^\circ$	269
VALČÁKOVÁ, LENKA, Žilina, Slovak Republic: RAILBCOT – SIMRAIL System Dynamics analysis.....	275
WEIS, PETER, Žilina, Slovak Republic: Examination of Modal Characteristics of currying frame and gearbox for extruder	283

The measuring system and adjustment of compression ratio in prototype of Stirling engine with non-conventional mechanism FIK

*Peter Baran, * Miloš Brezáni, * Pavol Kukuča

*University of Transport, Faculty of Mechanical Engineering, Department of Transport and Handling Machines, Univerzitna 2, 01026 Žilina, Slovakia, {peter.baran, milos.brezani, pavol.kukuca}@fstroj.uniza.sk

Abstract. This paper deals with the measurement system of the thermodynamic processes and adjusting of compression ratio in the prototype of Stirling engine with unconventional mechanism. The measuring system consists of sensors which are integrated in the cylinder head, interconnecting pipes and output shaft of the engine prototype. Compression ratio must be observed by the mathematical concept of thermal cycling. The volume of the interconnecting pipes was detected through a virtual model and the method of weighing the regenerator, where volume was detected by calculation according to the density of the material. Pipe dimensions were measured and compared with a virtual model.

Keywords: Measurement system, FIK mechanism, Compression ratio, Stirling engine.

1. Introduction

Stirling engines are currently used in the production of electricity. There are several types of mechanisms, which by design are suitable for use in a Stirling heat engine [2]. Engines with non-conventional mechanisms may have several advantages when used in practice. In the case of prototype devices of Stirling engines, which verify the functionality of the machine it is necessary to determine the progress of thermodynamic phenomena taking place at the premises of the rollers and therefore need to create and implement measuring system on a machine.

Compression ratio is an important factor in designing of internal combustion engine [3]. In the case of Stirling engine with a nonconventional mechanism FIK constitutes regenerator (consisting of rings of steel wire net) part of the volume in the interconnecting pipe. Since it is not possible to determine the volume through a virtual model, because of the relatively large number of the rings, volume was determined by measuring of weight and recalculation by equation of density.

1.1. Description of swing mechanism

FIK mechanism (Fig. 1, Fig. 2) is a swinging system, which is characterized, that the center of the swinging plate during the rotation of the shaft acting circular motion [1].

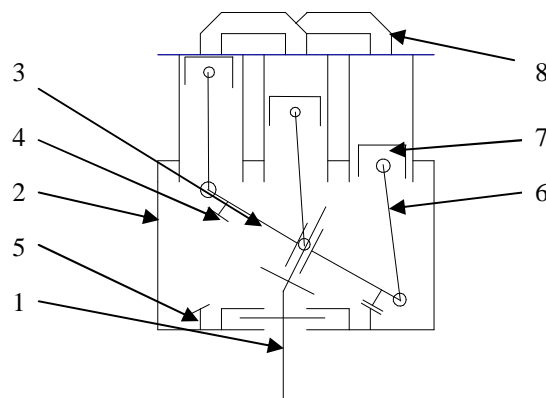


Fig. 1. Mechanism FIK: 1- Crankshaft, 2- crankcase, 3- swinging plate, 4- bevel wheel (part of swinging plate), 5- bevel wheel (part of crankcase), 6- ball joint segment, 7- piston, 8- head cylinder and regenerator pipe.

1.2. Measuring system

The measuring system (Fig. 2, Fig. 3) consists of pressure and temperature sensors, RPM sensor and the cooling cylinder is provided through non-return valve inlet pressure.

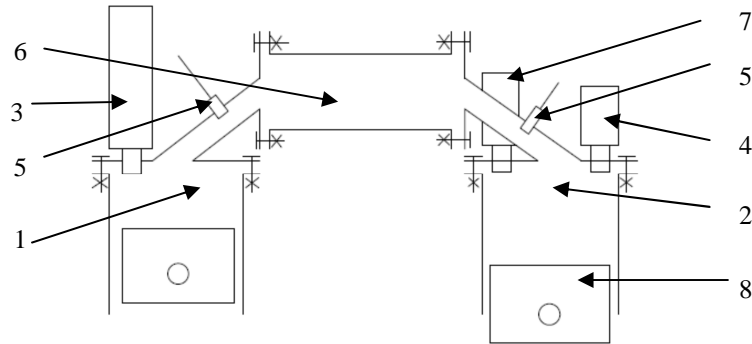


Fig. 2. Schematic representation of the measurement system in head cylinder: 1- Heat cylinder, 2- cooled cylinder, 3- Heat cylinder pressure sensor, 4- Cooled cylinder pressure sensor, 5- Temperature sensor, 6- regenerator, 7- Non- return valve, 8- Piston.

RPM sensor (Fig.3) is connected with a rubber coupling on the output shaft. This sensor is located at the bottom of the flywheel.

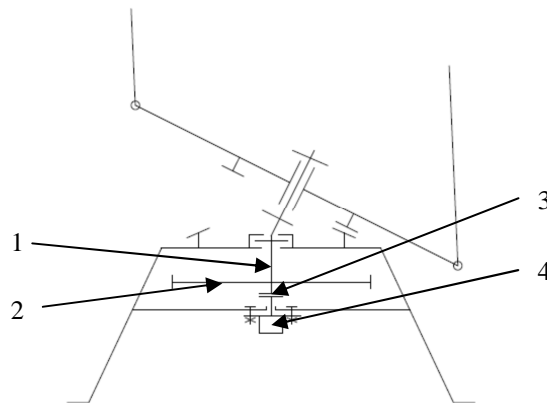


Fig. 3. RPM sensor: 1- Output shaft (crankshaft), 2- flywheel, 3- rubber coupling, 4- RPM sensor

Engineering design of assembling sensors: Proposal sensors (Fig.4) location in head valves and interconnection pipe.

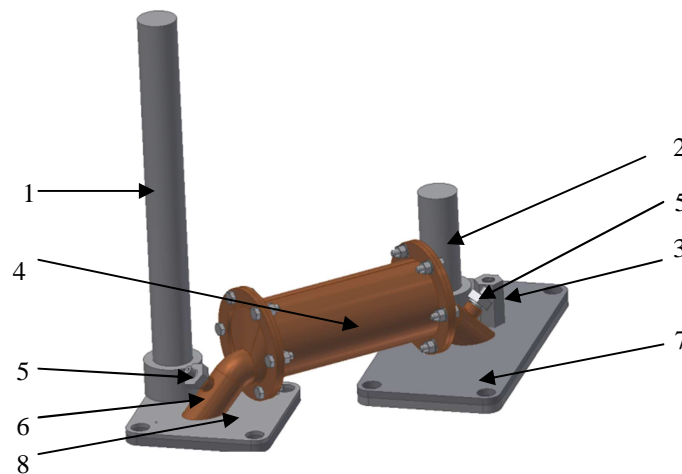


Fig. 4. Virtual model of head valves interconnection pipes and regenerator pipe with sensors: 1- Heat cylinder pressure sensor, 2- Cooled cylinder pressure sensor, 3- Non- return valve, 4- Regenerator pipe, 5- Temperature sensor connection 6- Interconnection pipe, 7- Cooled cylinder head valve, 8- Heat cylinder head valve.

The measurement system used for measuring the waveform of pressure, temperature changes in the individual pairs and is indispensable for the operation of the air supercharging system.

2. Adjustment of the compression ratio

2.1. Dead volumes

In this case, we add up all the dead volumes in a pair of prototype Stirling engine. Then subtract the volume of regenerator. The volume of the regenerator is determined by calculation through the density of the material.

Dead volume (Fig. 5) of the interconnecting pipes and cylinders consists of these individual parts:

- V_C - Volume between the cylinder head and the piston top dead center
- V_H - Volume in the cylinder head hole
- V_K - Volume in knuckle
- V_F - Volume in the flange
- V_T - Volume in regenerator tube
- V_R - Volume of regenerator

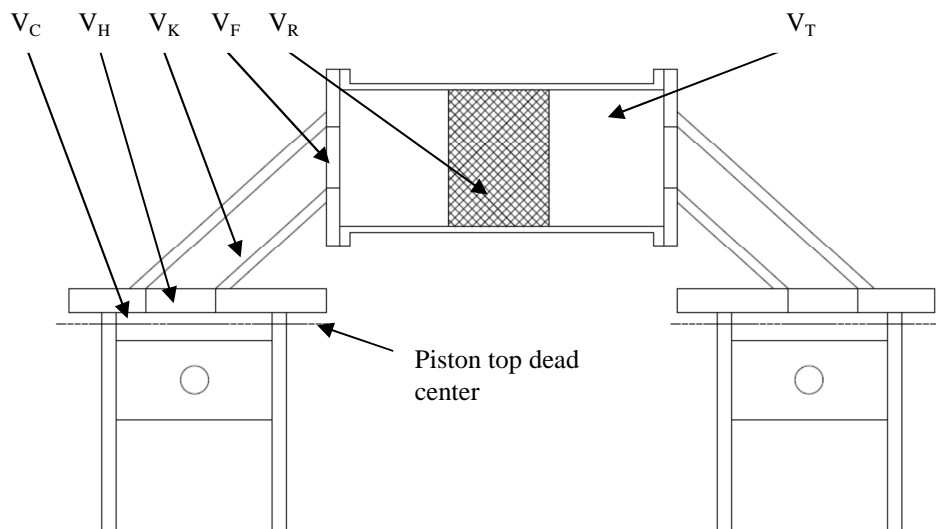


Fig. 5. Schematic model of dead volumes in interconnecting pipe.

The total dead volume (V_D) is generally given by (1):

$$V_D = [2 \cdot (V_C + V_H + V_K + V_F) + V_T] - V_R \quad (1)$$

To determine the volume of regenerator, we first measured the mass of all steel rings in both pairs, and then assigned them to half. The total mass of the rings was 104 grams, it follows 52 grams to one regenerator tube. Through the formula for the calculation of material density (2), we express the volume (density of steel is $\rho_R = 7800 \text{ kg} \cdot \text{m}^{-3}$).

$$\rho_R = m/V_R \quad (2)$$

$$\begin{aligned} \rho_R &= m/V_R \\ V_R &= m/\rho_R; \\ V_R &= 0.052\text{kg}/7800 \text{ kg} \cdot \text{m}^{-3} \\ V_R &= 6666.66\text{mm}^3 \end{aligned}$$



Fig. 6. Weight measurement of steel rings.

Volumes V_C , V_H , V_K , V_F and V_T were determined through a virtual model of the engine, which parts are identical with a real prototype model.

$$V_D = 302044.27 \text{ mm}^3$$

2.2. Compression ratio

The compression ratio ε (3) is determined by the equation [4]. The Fig. 7 shows the position of the pistons in maximal compression. In this position, none of the pistons is in the top dead center (TDC), and therefore to determine the volume V_2 it is necessary to add to the dead volume V_D volume V_{TDC} .

$$\varepsilon = V_1/V_2 \quad (3)$$

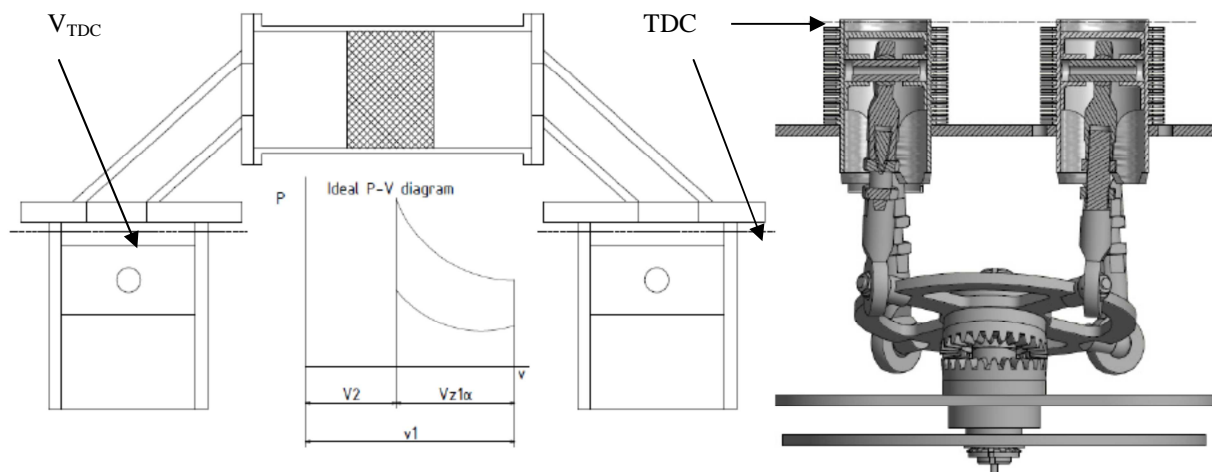


Fig. 7. Scheme (left) and the position of the pistons at the maximum compression. Position of piston, virtual model (right) .

Calculation of volume V_2 (4):

$$V_2 = (2 \cdot V_{TDC}) + V_D \quad (4)$$

$$V_2 = 391161.436 \text{ mm}^3$$

The Fig. 8 shows the position of the pistons V1 volume. In this position, none of the pistons is in the lower dead center (LDC).

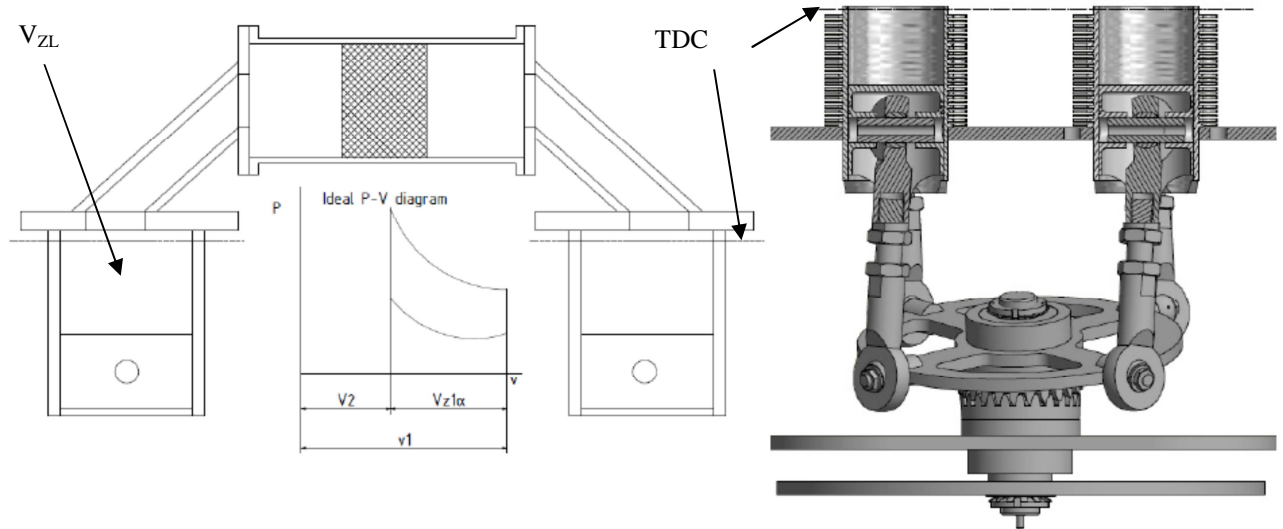


Fig. 8. Scheme (left) and the position of the pistons in V1 volume. Position of piston, virtual model (right).

Volume V_{ZL} (cylinder size) can be determined by measuring the height of the bottom edge of the piston to TDC by virtual model. Calculation of volume V1 (5):

$$V1 = (2 \cdot V_{ZL}) + V_D \quad (5)$$

$$V1 = 839689.564 \text{mm}^3$$

Calculation of compression ratio (3):

$$\varepsilon = V1/V2 \quad (3)$$

$$\varepsilon = 2.146$$

Comparison of compression ratio by virtual model (ε_M) and calculation (6) by Stirling engine type α (ε_α):

- D- piston diameter
- Z- Piston stroke

$$\varepsilon_M = 2.146$$

$$\varepsilon_\alpha = \frac{\sqrt{2} \cdot \frac{\pi \cdot D^2}{4} \cdot Z}{V2} + 1 \quad (6)$$

$$\varepsilon_\alpha = 2.15$$

3. Conclusion

By measuring the weight of steel rings regenerator and their integration into the regenerator pipe the compression ratio was set. The computational model set compression ratio of 2.1. Deviation from rated compression ratio is caused by deficiency of steel rings. Setting of the compression ratio will be one of the basic preconditions for correct measurements. These measured values serve as basic elements for the diagnosis of piping and regenerator system. Initial diagnosis is to verify the tightness of connecting pipes and leakages of the medium (air) through the pistons.

References

- [1] Isteník, R. *Distribution and unconventional mechanisms of internal combustion engines*. Žilina 2008. (In Slovak).
- [2] Holubčík M., Ďurčanský P., Jandačka J. *Analysis of open and closed cycle of hot air engine in cogeneration using dendromass* 2012.
- [3] Punov P., Evtimov T. *Numerical study the influence of the intake system on the volumetric efficiency and in cylinder parameters of a gasoline IC engine*. 2006.
- [4] Bigoš, P., Puškár, M. *The optimal amount of compression ratio*. Acta Mechanica Slovaca. Roč. 12, 2008. (In Slovak).

Acknowledgement

This contribution is the result of the project implementation: Modern methods of teaching of control and diagnostic systems of engine vehicles, ITMS code 26110230107, supported by the Operational Programme Educational.



The Agency
of the Ministry of Education, Science, Research and Sport
of the Slovak Republic
for the Structural Funds EU





Simulation of acoustics energy propagation through the floor structure of passenger coach

*Lukáš Bavlina, *Peter Zvolenský

University of Žilina, Faculty of Mechanical Engineering, Department of Transport and Handling Machines,
Univerzitná 2, 01026 Žilina, Slovakia, {lukas.bavlina, peter.zvolensky}@fstroj.uniza.sk

Abstract. Acoustic properties can be detected not just experimentally, but also by computing and choosing adequate tools for the simulation of selected physical process. Simulation can detect the acoustic properties of materials used in the design of vehicles. Acquired information on the behaviour of different acoustic materials can consequently be used in the design of sound resistant structures of railway vehicles. In the program COMSOL Multiphysics by function poroacoustics was simulated propagation of acoustic energy through the sandwich floor structure of the passenger coach. In the floor structure was used high-absorbent fibrous material STERED[®]. This paper deals with proposal of using material STERED[®] in the structure of the passenger coach floor during modernization and with identification acoustics effect of material STERED[®].

Keywords: Noise, STERED[®], Mineral wool, Passenger coach.

1. Introduction

Nowadays we concentrate attention to the design, but also to the modification, modernization and reconstruction of transport to a wide spectrum of operating parameters. One of the important parameters, which dominates in the selection of a suitable vehicle, is comfort. Word comfort very often introduces silence. Rate of noise level which is generated in the interior of a vehicle is also a rate of quality evaluation of a structure. Attention is paid to reducing noise in interior of vehicles, which is radiated through structure of the floor, in the railway traffic.

2. Analysis

In the modernization of rail vehicles there is not often any change of shape and dimensional parameters of construction, but particularly in the use of new materials. At the present, in the construction of the floor of passenger coach series Bdghmeer as thermal and sound insulation is used a “technical insulation mineral wool LFM 5 Alu R from company Knauf Insulation“. Mineral and rock wool have in comparison with more modern thermal and sound insulations many disadvantages. It is dangerous to health, material having a low elasticity which lost over time. It is coming to ageing and loss volume and drastically losing heat-insulating properties [1]. Modernization of the floor includes fully dismantling of individual layers except the trapezoidal steel sheet having a support function. From trapezoidal steel sheet old paint is removed and new glaze is applied. The structure of layer is maintained. Old materials are replaced with new materials.

In the modernization of the passenger coach floor no change will occur in the shape and dimensions of the structure and no change will occur in the use of new types of materials. There is only restoring the properties of the materials from which the floor is made. When we want maintain shape and dimensions of the structures and improve ride comfort, we must use new types of acoustical materials.

Possible solution can be material STERED[®], which is novelty on the market of thermal and sound insulation material. STERED[®] used in the construction of the floor is suitable solution, because has excellent acoustic properties.

The input material consists from textile parts waste of new cars, but also from separated textile parts of cars after end of life. Separation of textile material produces significant volumes of textile materials of specific qualities. This material is characterized by:

- Excellent properties that are not changed in time.
- Material was originally used in the cars and was determined to sound and thermal insulation while must meet the criteria of strict requirements especially for health and safety.

To define the behaviour of new sound-insulating material STERED[®] in the floor construction of the passenger carriage, it is important to perform a computer simulations, which proves the expected acoustic effect in operating conditions [2].

3. Simulation of sound pressure propagation through construction of floor

For simulation of the sound pressure transfer through floor construction of the passenger coach series Bdgmeer was chosen as an appropriate tool program COMSOL Multiphysics 4.4. The aim of the simulation is to implement frequency analysis and detect any differences between the attenuation spectrums of the used materials.

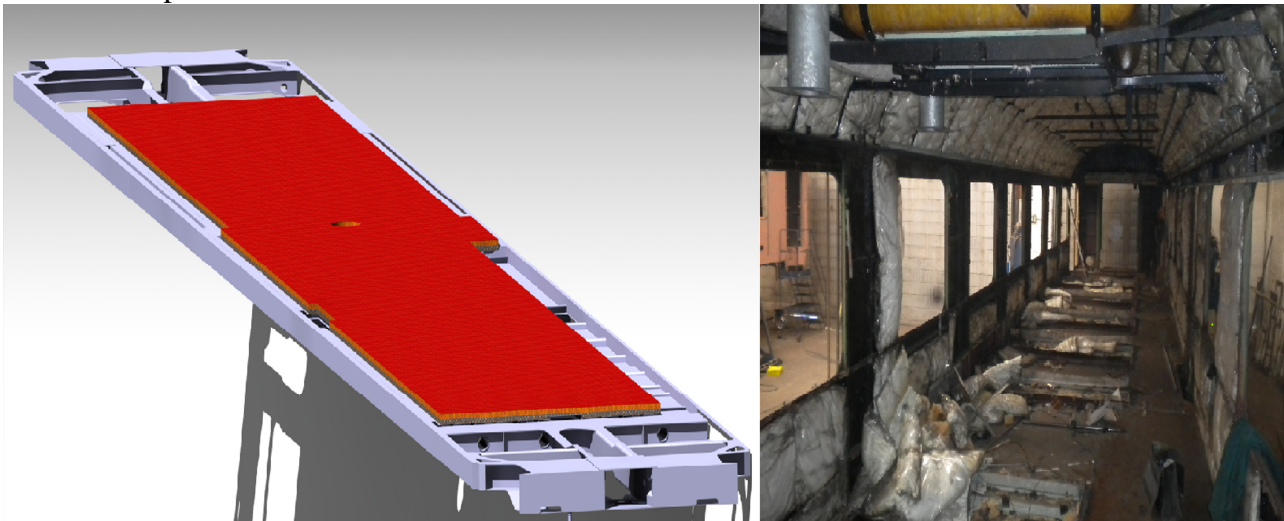


Fig. 1 The floor structure of the passenger coach series Bdgmeer created in CATIA V5R21 and picture of passenger coach during the modernization .

3.1. Poroacoustics

The program COMSOL Multiphysics offers an important function “poroacoustics”. By using this function we can add extended spectrum of parameters to a material and it can be considered as a porous media. The sound doesn’t spread only through the fibres of material, but as well as through the fluid medium which is in pores among the fibres. This medium is usually air [1]. This case, the Johnson-Champoux-Allard model was used. The Johnson-Champoux-Allard model is an equivalent fluid model that mimics two limiting behaviours of the full poroelastic material model defined by Biot’s theory. The first is the rigid porous matrix model (1) and the second is the limp porous matrix model (3). An equivalent fluid model is computationally less demanding than the full poroelastic model. However, they are only physical correct for certain choices of material parameters. Both models are based on describing the frequency dependent, effective density $\rho(\omega)$ and the effective bulk modulus $K(\omega)$ of the saturating fluid inside the porous matrix. The following parameters used in the (2) are given in (Tab. 1) have decisive effect on the acoustic properties of investigated materials. These parameters were used in the simulation, and are acquired from the

manufacturers of materials. The parameters were acquired in a laboratory of the manufacturer in accordance with the relevant standards.

Value	Symbol	Units	Mineral wool	STERED® ID
Flow resistance	R_f	[kPa.s/m ²]	5	5÷100
Thermal characteristic length	L_{th}	[m]	650.10 ⁻⁶	205.10 ⁻⁶
Viscous characteristics length	L_v	[m]	420.10 ⁻⁶	97.10 ⁻⁶
Fluid Density	ρ_f	[kg/m ³]	1.204	1.204
Dynamic viscosity for air	μ	[Pa.s]	1.818.10 ⁻⁵	1.818.10 ⁻⁵
Speed of sound in air	c	[m.s ⁻¹]	343	343
Thermal conductivity	k	[W/(m.K)]	0.04	0.054
Porosity	ε_p	1	0.95	0.99
Tortuosity	τ	1	1.03	1.38
Absolute pressure	P_o	[atm]	1	1
Prandtl number	P_r	1	1	1
Porous material density	ρ_d	[kg/m ³]	50	200

Tab. 1 Material parameters.

$$\rho_{rig} = \frac{\tau\rho_f}{\varepsilon_p} \left[1 + \frac{R_f\varepsilon_p}{i\omega\rho_f\tau} \sqrt{1 + \frac{4i\omega\tau^2\mu\rho_f}{R_f^2L_v^2\varepsilon_p^2}} \right] \quad (1)$$

$$K_{eq} = \frac{\gamma P_o}{\varepsilon_p} \left[\gamma - (\gamma - 1) \left(1 + \frac{8\mu}{i\omega L_{th}^2 P_r \rho_f} \sqrt{1 + \frac{i\omega L_{th}^2 P_r \rho_f}{16\mu}} \right)^{-1} \right]^{-1} \quad (2)$$

$$\rho_{limp} = \frac{\rho_{rig}\rho_{av} - \rho_f^2}{\rho_{av} + \rho_{rig} - 2\rho_f} \quad (3)$$

$$\rho_{av} = \rho_d + \varepsilon_p\rho_f \quad (4)$$

$$L_v = \frac{1}{s} \sqrt{\frac{8\mu\tau}{\varepsilon_p R_f}} \quad (5)$$

$$L_{th} = \frac{2V_p}{S_p} \approx 2L_v \quad (6)$$

The most significant effect on the acoustic properties of porous material has the thermal characteristic length and viscous characteristic length. These parameters can be obtained using equations (5, 6). The thermal and viscous characteristic lengths are, by definition, scalar quantities. For spherical pores, the value of L_{th} is close to the value of the radius of the pore. Value L_v is close to the value of the size of the inter-connection between two pores. Thus, from 2D or 3D acquisitions of the material microstructure, an estimation of the thermal and viscous characteristic length can be obtained. The main difficulty encountered with these methods is to define a macroscopic single value (or mean value) L_{th} , from a disperse microscopic information [3].

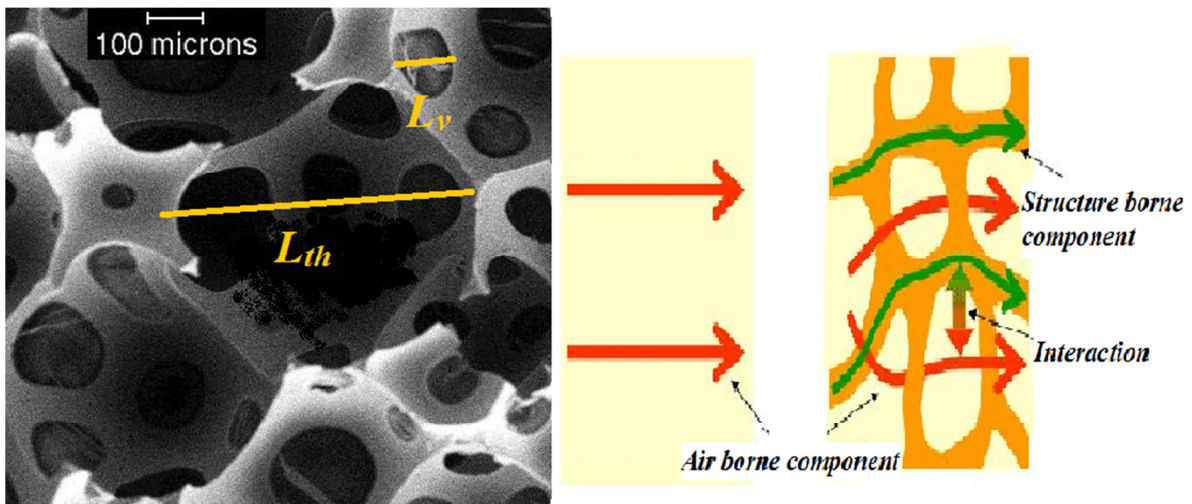


Fig. 2 Thermal and viscous characteristic length [4] and wave propagation in porous material [3].



Fig. 3 Mineral wool Knauf insulation LMF 5 Alu R [5] and STERED[®] [2].

The surface of trapezoidal steel sheet is exposed to acoustic pressure of 20 Pa (120 dB). The frequency range of this sound is from 5 Hz to 20 kHz, with step 5 Hz. During the simulation, it is possible to monitor propagation acoustic pressure through the construction into interior in this spectrum. The aim is to find a material with a better attenuation ability of low-frequency sounds than mineral wool. Attenuation can be determined by comparing the measured frequency analysis in individual layers of floor construction and in interior of the passenger coach, both in the current condition as well as when the material STERED[®] is used. This can be achieved by interesting “Point graph” function, where it is possible in the individual points (Fig. 5) to record the sound pressure depending on the excitation frequency. For simulation wasn't used 3D model, because it is very complicated, but a simplified cross-sectional of construction in 2D was used.

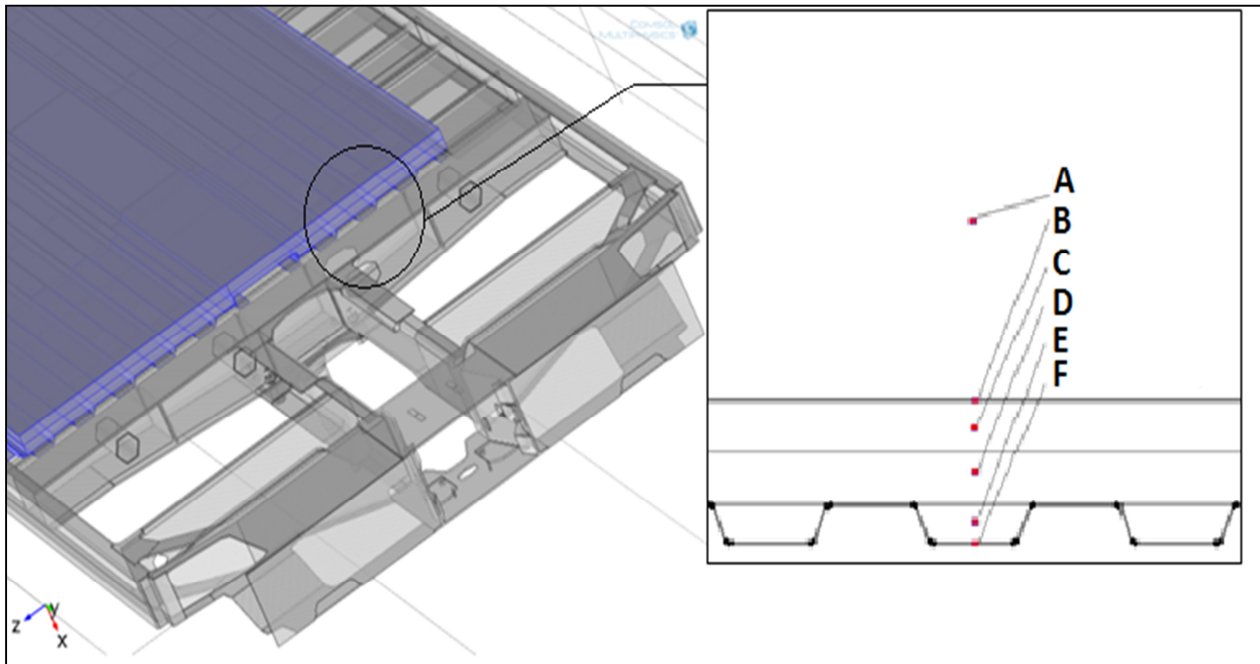
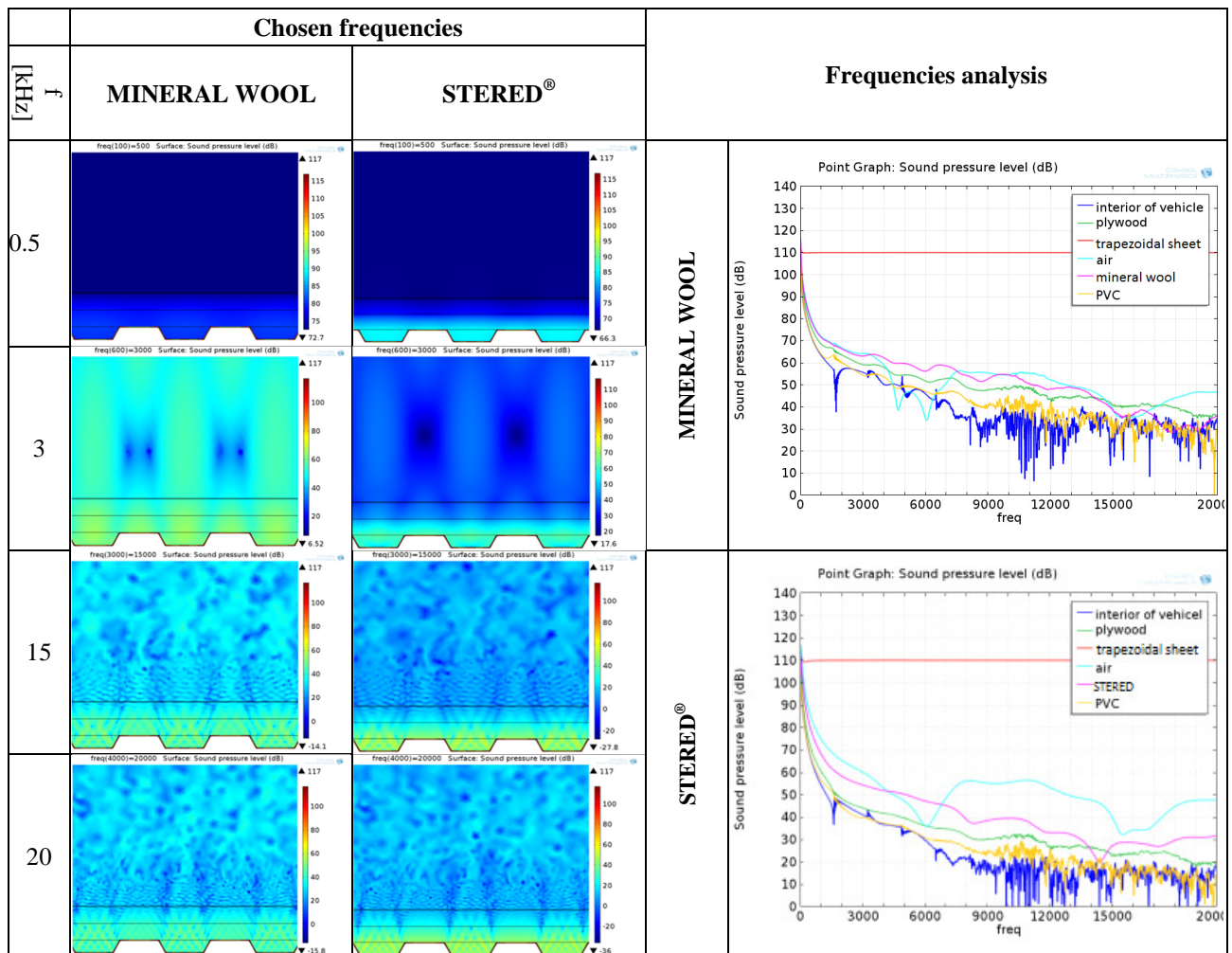


Fig. 4 Measured points, which is located in layers of floor. A- interior of passenger carriage, B – PVC, C – plywood, D – STERED[®]/Mineral wool, E – Air, F – Trapezoidal steel sheet .

4. Results of simulation



Tab. 2 Results of simulation.



5. Conclusion

By using “poroacoustic” function in COMSOL Multiphysics, the initial noise, which is generated by bogie of passenger carriage and propagations through the floor, was simulated.

Results of simulations are shown in the frequency spectrums of noise, which is transferred through the floor in different points of the floor structure.

It was detected that results of the simulation depend on the choice of input conditions, the acoustic properties of the passenger carriage floor and the material properties of the porous material in the floor. Other possibilities of verification of expected acoustic properties of the selected insulating material will continue.

The dependencies of sound reduction of used material for the selected frequencies of noise generated by bogie are shown. From these initial simulations the expected sound-insulating properties of selected materials can be observed.

We assume that in the consequent research the simulation conditions will be made more precise as well as the statistical analysis and complex evaluation of continuous results of simulation in order to perform the verification of experiments in real service on railways will be done.

References

- [1] Trevor J. Cox, Peter D'. *Acoustic Absorbers and Diffusers: Theory, Design and Application*. s.l. : CRC Press, 2009. p. 156. ISBN 0203893050, 9780203893050.
- [2] <http://www.stered.sk>. [Online] 2014. <http://www.stered.sk/technologia>. [in Slovak]
- [3] Jaouen, Luc. <http://apmr.matelys.com/>. [Online] 8. 1 2015. <http://apmr.matelys.com/Parameters/Characterization/Acoustics/ThermalCharacteristicLength.html>.
- [4] Technology, Wison. <http://wisonpower.com/>. http://wisonpower.com/sub/product_view.php?idx=94&cat_no=. [Online] 2015. [Date: 24. 2 2015.]
- [5] <http://www.knaufinsulation.sk>. [Online] 2014. <http://www.knaufinsulation.sk/lamelove-pasy/nobasil-lmf-5-alur>. [in Slovak]



Use of advanced technologies to design and produce headlights for electric vehicle EDISON

*Peter Bezák, *Juraj Bezák

*University of Žilina, Faculty of Mechanical engineering, Department of Design and Mechanical elements, Univerzitna 8215/1, 010 26 Žilina, Slovakia, peter.bezak@fstroj.uniza.sk

Abstract. This article describes the methodology of designing the headlight for electromobile from initial design concepts to construction documentation. Structural design was created using CAD software CATIA V5. In addition to alternative designs strength and thermal analysis of the top plastic cover of the headlamp was created. FEM analysis was created in software ANSYS Workbench for the purpose of understanding the behavior of the material used under normal operating conditions. Prototype parts of headlights were produced by Department of Design and Mechanical Elements and, after careful adjustment and testing installed in built electric vehicle EDISON. Plastic headlight cover made by 3D printer Vantage and retaining plate for lighting modules - HELLA was the main objective of production.

Keywords: Construction design, Software ANSYS, Headlight, 3D printer, Electric vehicle, FDM.

1. Introduction

In this article we talk about Electric vehicle EDISON, which was designed and built at the University of Žilina, Department of Design and Mechanical Elements . Edison was constructed by teachers and students of the University of Žilina.



Fig. 1. Electric vehicle EDISON .

Electric vehicle or EV is car that is using electricity for his power. As a source of energy is usually used battery that must be charged before driving from an external source. Range of the electric car depends on the capacity of the battery. Electric vehicles are currently the most environmentally friendly methods of transport. The advantage of electric car is zero emission production, reduction of operating costs and lower noise. Another advantage is that they do not produce exhaust gas. Technological breakthrough in the development of electric cars started by the development of electronics and control systems, by the development of new types of batteries (eg.

SCIB battery), but mostly by the rapid rise in energy fuels - especially oil and thus gasoline. The advantage of electric cars is a simpler design. A car - drive can be placed directly in the wheels, the control electronics and battery set in the bottom part of vehicle. The body can be constructed more variable based on the same chassis [2].

Car headlights are an inseparable part of each vehicle, ensure road safety in low light conditions and at night. The first headlights that were made, had clear circular cover glass and a parabolic reflector. With increasing speeds and increasing traffic density it was necessary to shine away to long distances, while not disturbing oncoming drivers. It was necessary to guide the flow of light rays. Guiding Light began with breaking light beams on structured cover glass of headlight. The constantly rising speed of cars required to see far ahead, so another feature of lighting was added - lighting into the distance. Technically, it was resolved by using two-filament bulb or with additional lighting equipment intended for this function. Later, the idea was to "see around corners", which at the Citroën DS 19 was in 1967 implemented by rotation of internal reflectors in the direction of rotation of the steering wheel. Today's modern cars, solve this problem by using fog lights or special lamp integrated on the sides of the bumper. Latest technical innovation is intelligent adaptive headlights that are computer controlled [3].

2. Experiment

The experimental part of this article describes the design methodology of electric headlights for electric vehicle EDISON. The main part of the engineering design of the headlights, consists of the design study, 3D body scanning and related calculations in ANSYS Workbench applications. Simulation of manufacturing the plastic cover of the headlamp using rapid prototyping methods is also included. Proposed headlamps must meet operational, legislative, safety and other requirements.

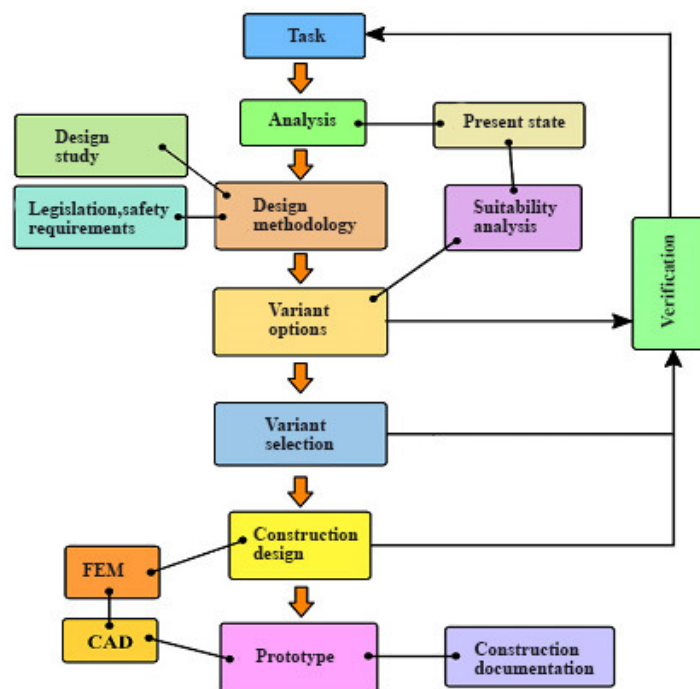


Fig. 2. Methodology scheme of car headlight design.

2.1. 3D digitalization of car body

In the first phase of design solutions of headlights for EDISON it was necessary to digitalize(3d scanning) the body of car, due to the creation of borders (spatial and dimensional). These were later used like reference for CAD modeling. Scanning was performed by using a 3D scanner ZScanner 700 from Z Corporation.



Fig. 3. ZScanner 700 od firmy Z CORPORATION.

Technical specification	
Weight	980 g
Dimensions	160x260x210 mm
Measurement	18 000 cycles/s
Laser class	II (safe for eye)
Resolution axis Z	0.1 mm
Accuracy:	do 0.05 mm
ISO	20 μm + 0,2L/1000
Output files	STL, RAW

Tab. 1. 3D scanner parameters

It was necessary to stick to the body with a series of small targets, which help the scanner focusing the laser beam (Fig. 3) before scanning.



Fig. 4. Car body with positional targets.



Fig. 5. 3D digitalization of car body.

Scan data were directly transmitted to a computer and recorded in program- ZScan from ZCorporation. The output file of this program is STL (Standard Tessellation Language) ,widely used in rapid prototyping and Computer Aided Manufacturing. Processed STL data were further used in CAD application (in our case, in CATIA V5) that supports this type of files. Car body with cover plates, tires and suspension can be seen on Fig. 5,6.

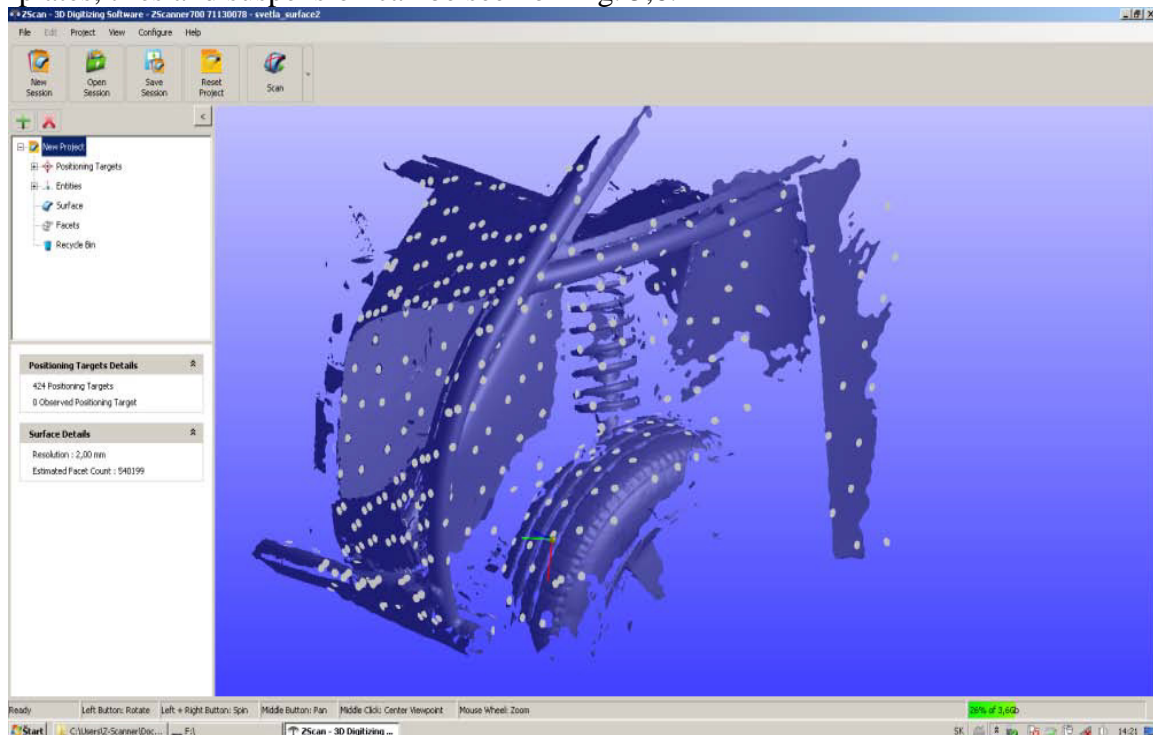


Fig. 6. 3D data in software ZScan.

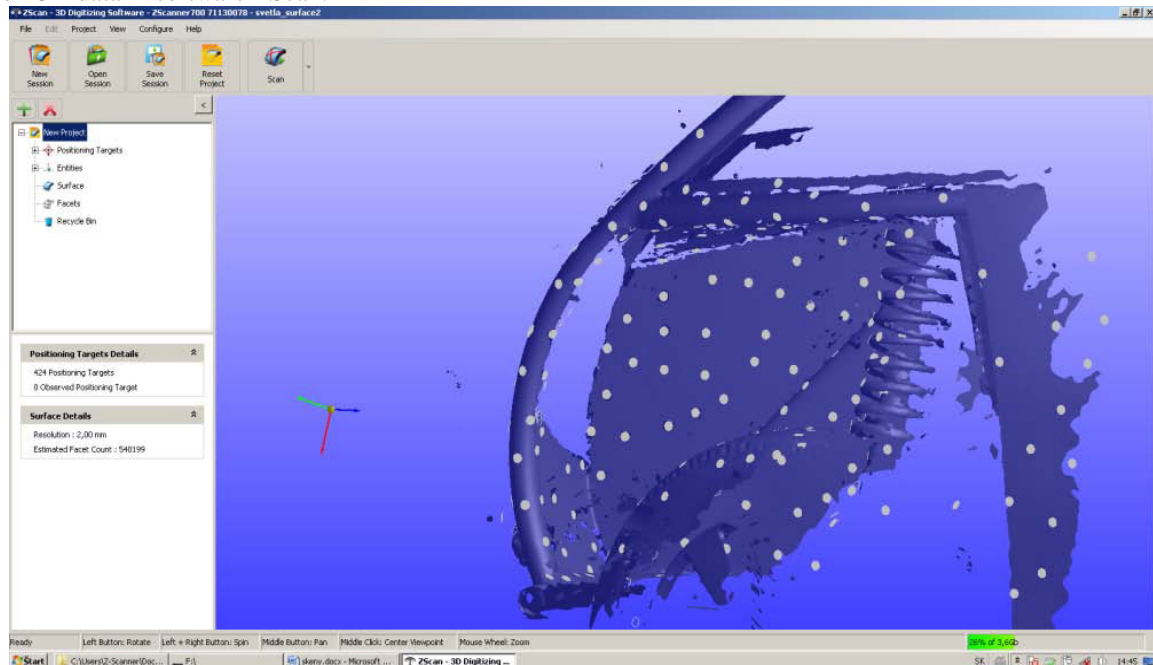


Fig. 7. 3D data in software ZScan (side).

2.2. Design sketch of car headlights

Design concepts of shape and location of the headlights were developed regarding the overall design of the car and vision of its creators, before concepting each alternative design.

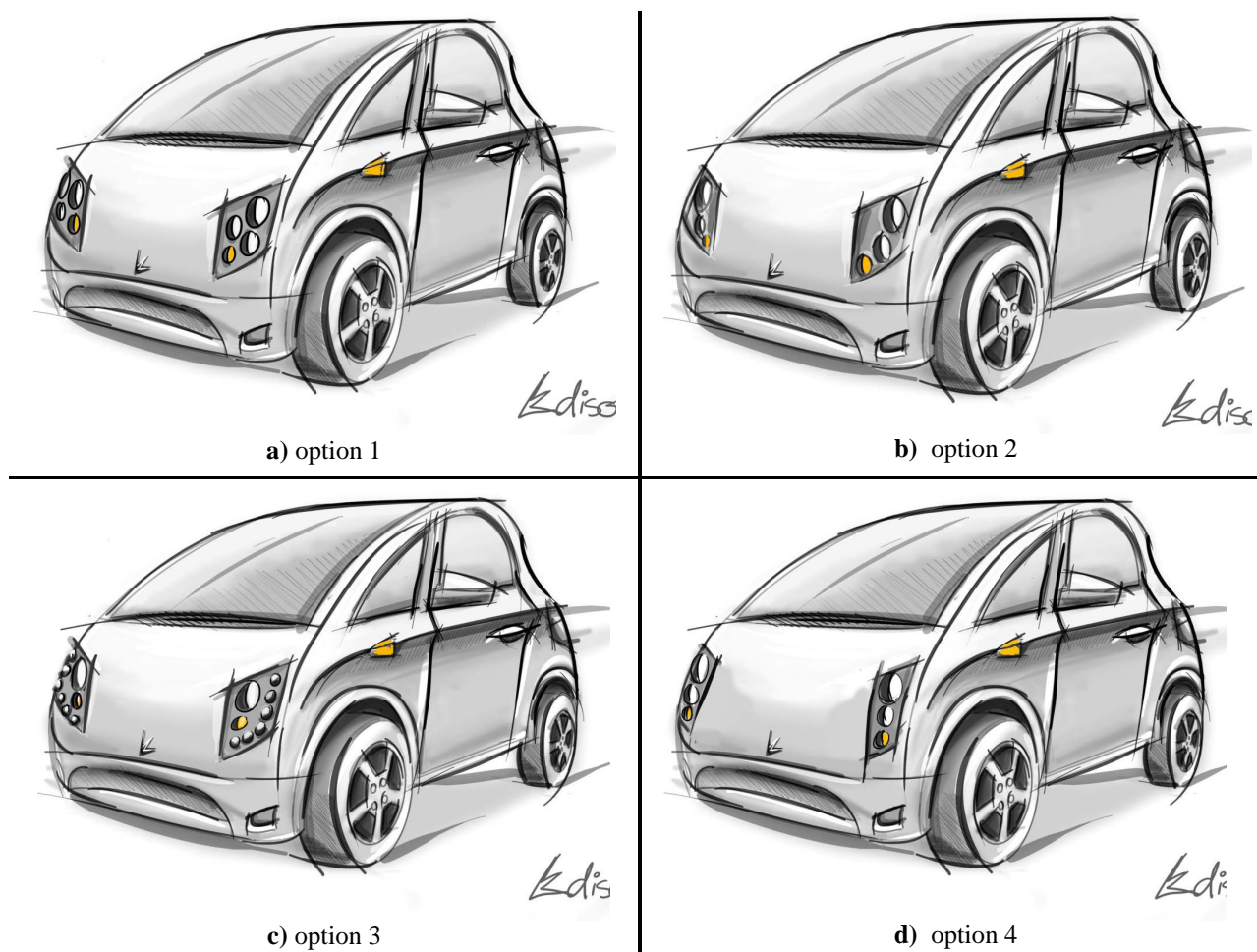


Fig. 8. Design sketches of different options for car headlights.

The concept and design of the headlights had to match the basic legislative requirements and government regulations, and also regarding UNECE and EC / EEC directives. In particular, it should be followed by Decree no. 166/1997 of the Ministry of Transport, Posts and Telecommunications of the Slovak Republic Collection of Laws, §40- Section 49, which deals with the conditions of vehicle traffic on the roads. Law no. 725/2004 Z.z. which deals with the exchange of halogen headlamps for xenon [4].

Regarding the Directive on the approximation of the laws of the Member States relating to motor vehicle headlamps which function is main-beam and / or dipped-beam headlamps and incandescent electric filament lamps for such headlamps No 76/761 / EEC of 27 July 1976 [5].

Tab. 2 summarizes the score for each variant of headlights.

Attributes		Significance coeff.	Options								Best solution	
			1		2		3		4		p _i	p _i ·v _i
			p	p.v	p	p.v	p	p.v	p	p.v		
a) critical												
1	lifetime	1	2	2	3	3	4	4	4	4	4	4
2	design		1	1	4	4	1	1	3	3	4	4
3	Legislation		1	1	4	4	4	4	1	1	4	4
4	price		2	2	4	4	1	1	1	1	4	4
5	Energy consumption		2	2	3	3	1	1	4	4	4	4
6	dimensions		2	2	4	4	2	2	4	4	4	4
7	features		4	4	4	4	4	4	4	4	4	4

b) very important												
8	connectivity with the electrical wiring	0,5	3	1,5	4	2	3	1,5	2	1	4	2
9	resistance to weather conditions		2	1	2	1	4	2	4	2	4	2
10	Easy of maintenance		2	1	4	2	3	1,5	2	1	4	2
11	Low noise and vibration		2	1	3	1,5	1	0,5	3	1,5	4	2
12	resistance to damage		3	1,5	4	2	2	1	1	0,5	4	2
13	chemical resistance		3	1,5	3	1,5	3	1,5	3	1,5	4	2
14	Corrosion resistance		2	1	2	1	3	1,5	3	1,5	4	2
c) imoportant												
15	enclosures	0,2	2	0,4	2	0,4	3	0,6	3	0,6	4	0,8
16	Easy of use		4	0,8	4	0,8	4	0,8	4	0,8	4	0,8
17	manufacturability at school		4	0,8	4	0,8	4	0,8	4	0,8	4	0,8
d) informative												
18	weights	0,1	3	0,3	4	0,4	2	0,2	3	0,3	4	0,4
19	Used materials		3	0,3	3	0,3	3	0,3	3	0,3	4	0,4
20	control		3	0,3	4	0,4	4	0,4	4	0,4	4	0,4
Summary				25,4		40,1		29,6		33,2		45,6
Technical value				0,557		0,879		0,649		0,728		1

Tab. 2. Rating variants.

Tab. 2. shows that the variant **No. 2** has the best score - the highest technical value and the best satisfies all selection criteria.

3. Final variant

Body lamp is made of sheet metal holder, where are placed lighting modules from HELLA. Specifically, the 50 mm Bi-halogen module, which provides the function of passing and driving lights in one housing. Module is 12V with 55W bulb H7. The cover glass of the module is free of optical elements. Daily function and position lamp provides 60 mm 12 V LED module. Directional lights are 60 mm including premium P21W bulb. Top headlight cover is made of PC-ABS thermoplastic. The plastic part is provided with threaded inserts for assembly on plate. Headlight range adjustment is depending on the load and is carried out manually by the electric motor. Motor is held in place by a plastic holder fixed to the plate. FIG. 9 shows light modules used for headlight.

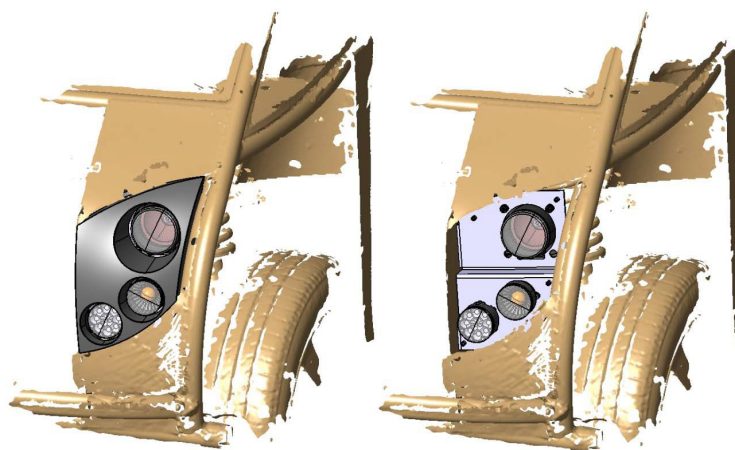


Fig. 9. Final variant with and without cover.

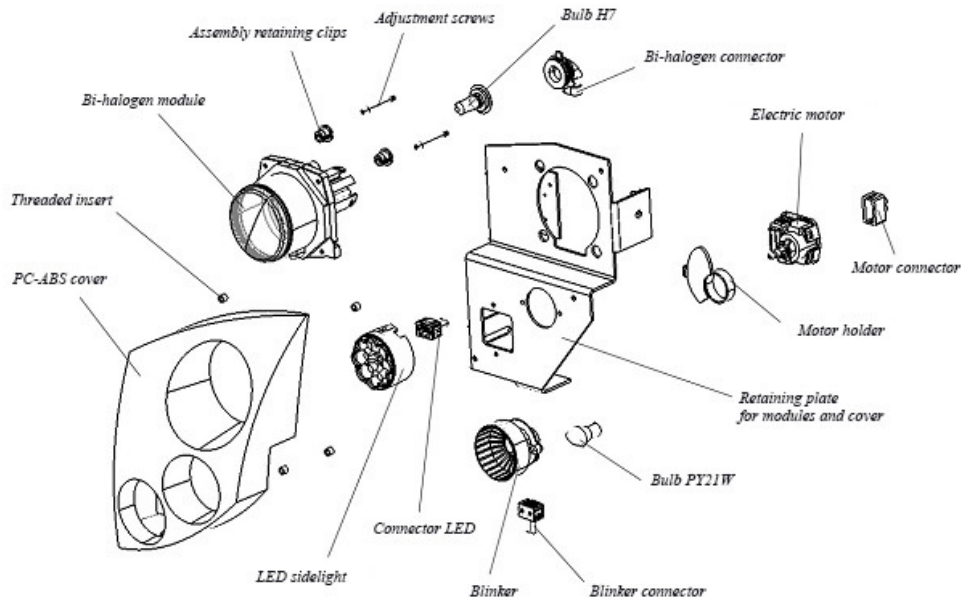


Fig. 10. Detailed scheme of final variant.

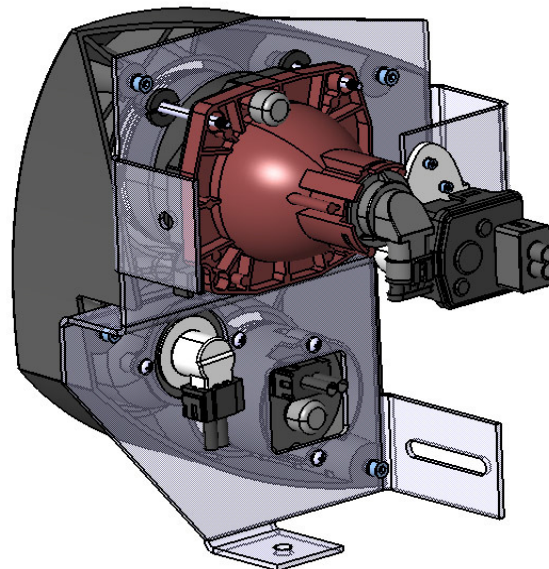


Fig. 11. Headlight (from back).

Top plastic cover (Fig. 12) of headlight was made of PC-ABS thermoplastic and was produced on the 3D printer. The cover is provided with ribs to increase stiffness and strength [6]. Cover is installed on retaining plate with screws (Fig. 11).

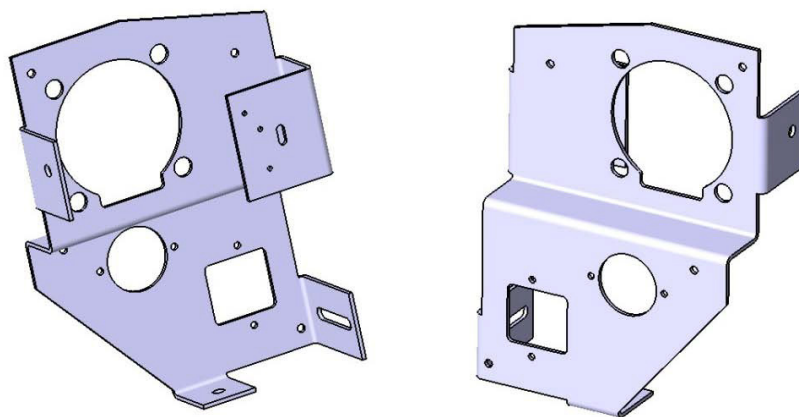


Fig. 12. Retaining plate for lighting modules.

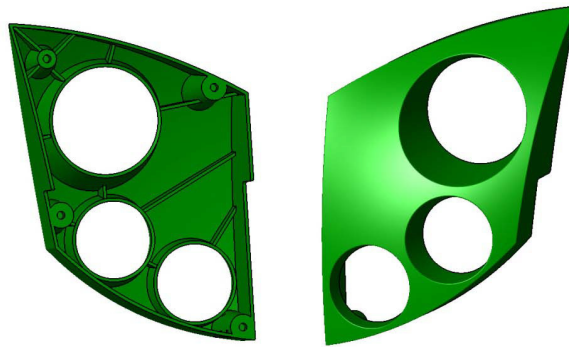


Fig. 13. PC - Cover of headlights.



Fig. 14. Electric vehicle EDISON.

3.1. Simulation of printing the plastic cover

Sequences of images that simulate the printing of the top plastic cover of the headlight can be seen on Fig.15 Cover was printed on a 3D printer Vantage SE (Fig. 13) from Stratasys, which uses FDM technology (Fused Deposition Modeling). The printer is suitable for the production of strong and accurate prototypes.



Fig. 14. 3D printer VANTAGE SE.

Printer specifications:

- materials: ABS, ABSi, PC, PC-ABS a PS-ISO,
- printing dimensions (X,Y,Z) max. 406 x 355 x, 406 mm,
- washable support system,
- layer thickness 0.125/0.17 mm,
- speed 1cm³/ 8 min,
- possibility of building functional sets of permanent,
- parts.

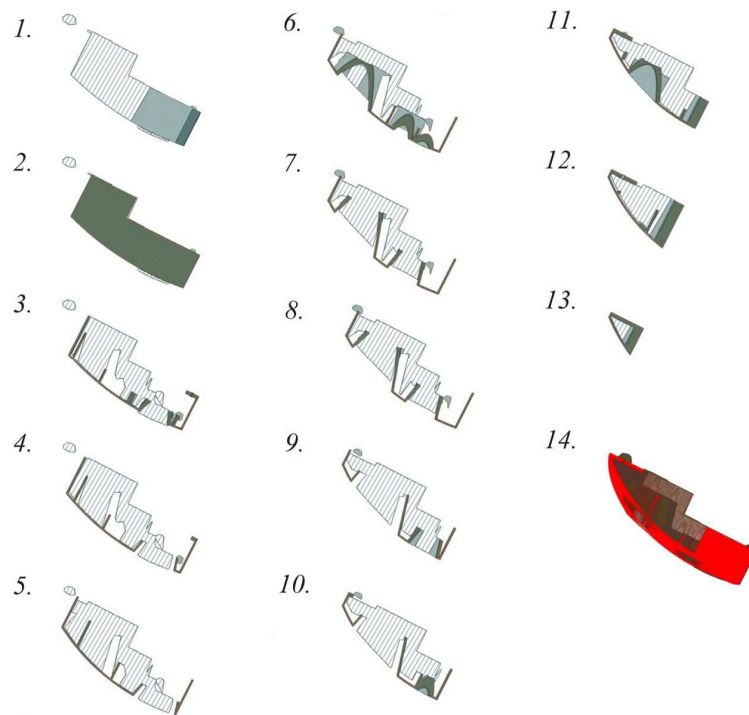


Fig. 15. Simulation of printing the cover in software Insight.

Prototypes produced by this method are rigid and even over time don't lose their mechanical properties.

3.2. Technical - economic assessment

Tab. 3 shows the costs of production, which consist of the cost of materials and cost of construction.

Components	Amount	Price in EUR/piece no TAX	Price in EUR/piece including TAX
Production of metal brackets for lighting modules	2	18	36
Production of plastic headlight covers	2	750	1500
Bi-halogen modules	2	166,4	332,8
Blinkers	2	47,4	94,8
LED side lights	2	133,2	266,4
Adjusting motors	2	71,7	143,4
Connector bi-halogen	2	0,3	0,6
Bulb H7	2	3,9	7,8
Bulb PY21W	2	0,8	1,6
Connector LED/blinker	4	0,5	1
Threaded inserts	8	0,3	2,4
Screws	30	0,1	3
Nuts	30	0,12	3,6
Washers	22	0,08	1,76
Summary			2395,16

Tab. 3. Cost of production of headlight for EDISON.

Tab. 4 shows the calculated approximate time-consuming of production left headlight for electric vehicle EDISON.



<i>Operation</i>	<i>Time frame in (h)</i>
Production of metal brackets for headlights	1,5
Production of plastic covers	40
Installation of threaded inserts in plastic. coverage	1
Assembling headlights	3
<i>Summary</i>	45,5

Tab. 4. Production time of headlights.

Some of the data in technical - economic assessment were determined only on the basis of theoretical assumptions.

4. Conclusion

This article describes the design methodology of the headlights from initial design concepts to construction documentation. Structural design was created by using CAD support CATIA V5. With the help of the Department of Design and Mechanical Elements production of prototypes took place. After careful adjustment and testing these components were installed in electric vehicle EDISON. Plastic headlight cover made on 3D printer Vantage and retaining plate for lighting modules from HELLA has been the main objective of manufacturing.

Acknowledgement

Thank you to prof. Ing. Ľuboš Kučera, PhD. for his valuable advice and comments.

References

- [1] GAJDÁČ, I., MIKITA, M., KUČERA, Ľ. *The modular design of electric vehicles*. Ai magazine : journal about the automotive industry, mechanical engineering and economics. - ISSN 1337-7612. Vol. 5, No. 2 (2012). (In Slovak)
- [2] [22.7.2014], <http://sk.wikipedia.org/wiki/Elektromobil>. (In Slovak)
- [3] FABIAN, M. et al. 2010. *Automobile headlights – history, development, shapes*. Industry and Design. Leaderpress, 2011, Vol. 4, No. 1, pp. 50 – 53. (In Slovak)
- [4] Ministry of Transport, Posts and Telecommunications of the Slovak Republic dated 17 March 1997 on special schools as amended by Decree of the Ministry of Education of the Slovak Republic No. 116/1997 Collection of Laws / National Council of the Slovak Republic. – Efficient from 17.3.1997.- Collection of Laws – Section 54 (1997). (In Slovak)
- [5] HLAVŇA, V. et al. 2006. *The means of transport - theory*. Žilina: EDIS, 2006. 295 p. ISBN 80-8070-498-8. (In Slovak)
- [6] BÉKÉS, J., ČELKO, M., ČERVENÝ, L. 1962. *Metalworking*. Bratislava: SNTL, 1962. 500 p. ISBN 63-021-62. (In Slovak)



Using of waste heat of internal combustion engines and types of heat exchangers

*Miloš Brezáni, *Peter Baran

* Department of Transport and Handling Machines, University of Zilina, Univerzitná 1, 010 26 ŽILINA, Slovakia, {milos.brezani, peter.baran}@fstroj.uniza.sk

Abstract. Article discusses about the use of heat exchangers for stationary combustion engines and cogeneration units. The paper is dedicated to the problem of unused thermal energy in stationary engines. It analyses possibilities of accumulation of heat energy and its possible application in various fields. The paper deals with the classification of heat exchangers and with the subsequent description of design solutions of heat exchangers types used in given field.

Keywords: Heat exchangers, Cogeneration units, Waste heat, Combustion engines, Unused energy.

1. Introduction

Nowadays if we omit alternating economic crisis. We can talk about ecological time. Political thinking towards just environmental but also economical, gives new insight into the lifestyle and comfort of man. A great impact just on these aspects has energetic. It is due to the increasing energy demands of human society, on which depends in no small measure the environmental burden and efficiency of energy use.

Possibility how to reduce energy consumption, is the way of savings. Reduction in fuel consumption can be utilized in a direction, which deals with the production of several types of energy, and possibly also of the products from the primary source at the same time. To this category can include cogeneration, trigeneration and polygeneration. Find a use for the heat is not as easy as in the case of electrical energy. But nevertheless is being offered several options, such as use of heat for hot water or direct water heating and its subsequent use for houses or large objects, depending on the performance of the cogeneration unit itself. Another option would be to use the absorption unit to transform heat to cold, making it possible to extend services to the production of cold water, for example for supply of air conditioners.

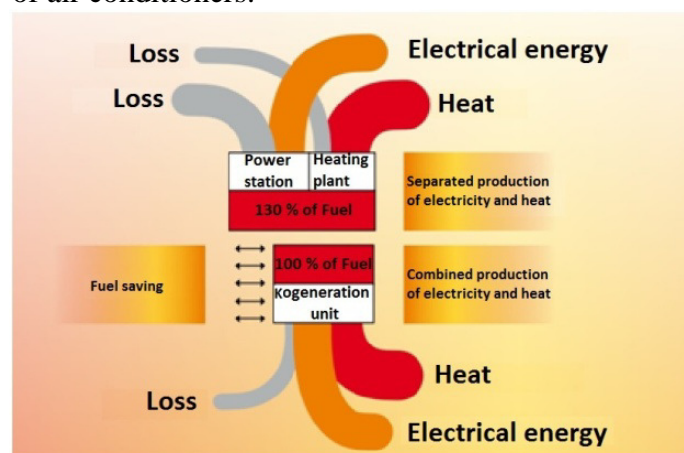


Fig. 1 Cogeneration principle.

For all these systems the energy transformation is decisive the method how to submit it. For this intention in case of heat is used inseparable part of most of the systems which is called the thermal coupling node. Thereby may be various types of heat exchangers, coolers, condensers etc. The most

common devices nowadays belong heat exchangers. In this case, for the generation of thermal energy from the exhaust gas and its subsequent use in other applications.

2. Use of heat exchangers in cogeneration units and stationary internal combustion engines.

For use of stationary internal combustion engine to generate electricity, or in other applications, arises a waste heat [1]. In most cases, this heat is not used in any way, but today's time more and more forcing producers and consumers to invest in technology that can leverage the potential of unused energy and contribute to cost saving. To this end has started to use exhaust gas heat exchangers. An exhaust heat exchanger is positioned on the exhaust pipe, removing heat flue gases, which could then be used for various applications.

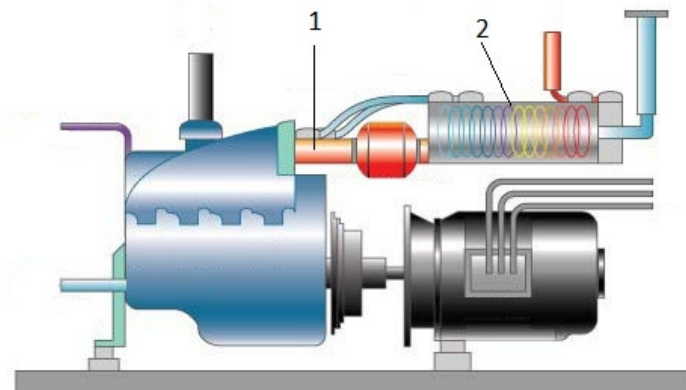


Fig. 2 Position of exhaust gas exchanger in stationary combustion engine (1. Exhaust gas pipe, 2. Exhaust gas heat exchanger).

Exhaust gas temperature at the start of the exhaust pipe is in the range 500-700 °C. This means that the exhaust gases offer a great potential for utilization of waste heat. The exhaust gases in the most of cases heat up liquid, which can subsequently be used in several ways.

3. Use of thermal energy from stationary engines

Possibilities of using waste heat are several. The most common include heating domestic hot water and heating. Smaller stationary engines can cover claims of houses alternatively smaller buildings. Using the largest units with up to 2 MW, or combining multiple units into a single source of energy can cover demands for heating and DHW for larger building or complex of several buildings.

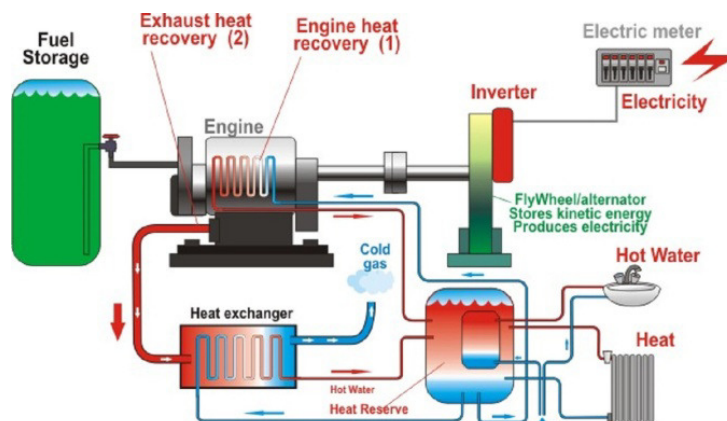


Fig. 3 Cogeneration unit with supply of heating water and hot domestic water.



A further possibility is the use of waste heat to accumulate in the storage tanks, and its subsequent use, if needs. In the Nordic countries, the use of waste heat necessary to ensure of the right engine function. Heat is used for heating of intake air and in a case of engine shutdown for maintaining the operating temperature for the purpose to avoid cold starts. With the similar principle is already dealing automakers like BMW with their technology Efficient Dynamics. Automakers already knows for a long time, that the heating of combustion engine in winter requires more fuel and the engine also produces larger amounts of emissions. Thus the engine is warmer, thus there is less friction and decreases consumption and CO₂ emissions [2]. BMW engineers have calculated that the warmed engine after start in the winter consumes about 10% less fuel than a cold engine.

The heat exchanger which heats the fluids and shortens warm-up phase of the engine is already commonly used in gasoline engines. The faster the heated oil in the gearbox and the engine is at operating temperature, the lower the energy losses by friction and fuel consumption. For diesel engines, BMW sees the potential saving in heating the interior. Modern units are already so efficient that the waste heat from them is unable to heat cabin. Therefore, in vehicles with diesel engines is started mounted auxiliary electric heater with 1000 W power, which in winter increases fuel consumption by an average of 1 l per 100 km. In this regard can help heated interior by heat exchanger. Attachments electric heaters will thus become superfluous. The heat exchanger, like in gasoline engines may also participate in faster heating of diesel engine to operating temperature.

4. Heat exchanger

Device used for targeted transfer heat energy from the one heat medium to another one, according to the second law of thermodynamics, is called a heat exchanger [3]. These facilities include a large group and can be found in many sorts of systems without us realizing it. According to the purpose and primarily according to the action, which takes place in the heat exchanger can be divided into the condensers, evaporators, coolers, regenerative heat exchangers etc. Another division is quite normal according to the method of heat transfer, ie whether there is contact between the media etc.

Heat exchangers are divided into:

- Recuperative - media are separated by a solid impermeable wall and not coming into contact
- Regenerative - occurs periodically substituted flow heating and cooling media in the defined area.
- Contact - media come together for some time in contact without chemical reaction, and then are separated.
- Mixing - media are in a certain place mixed and continuing as a mixture.

The most commonly used type of heat exchanger is recuperative. This group primarily include tubular and plate heat exchanger. From the point of view flow is the most common counter-flow design, which results in better heat distribution than in parallel flow design.

4.1. Tube heat exchanger

In this type of exchanger, heat exchange takes place between the tube and the tubular-space. Tubular space normally consists of pipes or tubes of circular cross section, but we can meet with cross-sections of other shapes such as oval, square etc. To reduce the dimensional parameters of tubular exchangers can use all sorts of ways to increase the area of the pipe from the side of the pipe as well as the tubular space. For this purpose are used, for example ribs.

Tube heat exchangers can be divided according to the construction on:

- With shaped tubes
- With straight pipes
 - Tube in tube

- Tube in the shell

Design with shaped tubes represent different tube axis arranged in the shape of a helix, spiral etc., located in the shell.

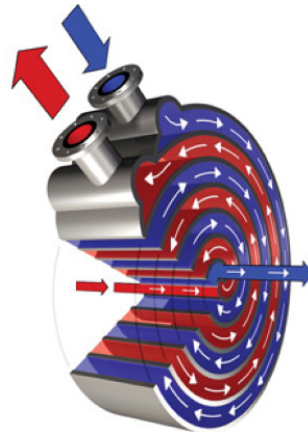


Fig. 4 Spiral tube heat exchanger.

Exchangers in design tube in tube are among the simplest device in the above category. It's occurred like dismountable and non-dismountable which are exclusively for pure thermal media.



Fig. 5 Shell & tube heat exchanger.

In general the tube exchanger with jacket is the most commonly used heat exchanger, where the main structure consists of a tube bundle placed in the shell of a cylindrical shape. These exchangers are manufactured at many different versions, depending on the configuration of inlet and outlet orifices, pipes, construction attachment of different thermal dilatation of tubes and plastics etc. This type of heat exchanger typically includes partitions that perform two basic functions. Arrestment of tubes resulting in a reduction of bending and vibration and also primarily direct the flow of media that is purposely altered to the cross-flow that increase the intensity of heat transfer. The system also has the disadvantage that, with the inclusion of partitions create higher pressure drop.

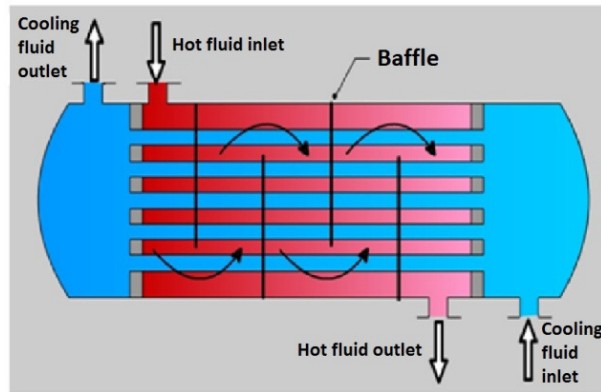


Fig. 6 Tube heat exchanger with baffles.

Tube heat exchangers are characterized by good heat resistance and affordable price. However, their disadvantages are small compactness and high weight. The case of the pipes with small diameter, in which is the aqueous medium dirty it's expected gradual decrease of the cross-section pipe up to its complete clogging.



Fig. 7 Real construction of tube heat exchanger with baffles.

4.2. Plate heat exchanger

Plate heat exchangers are based on a patent that has already been registered in 1878 by German inventor Albrecht Dracke. This principle, when one liquid cooling another liquid and liquids are flowing on both sides of group thin metal plates, became the basis for the construction of the heat exchanger - commercial plate pasteurizer Alfa Laval.

For more than 130 years was plate heat exchangers developed and structurally modified to devices that are used in thousands of different applications in all industries. Plate heat exchanger was previously designed for heating and cooling of the milk, but now is commonly used for heating and cooling in industrial processes and it is the basis of air-conditioning in buildings or it provides heating of hot water for hundreds of millions of people.

This type of heat exchanger is characterized with a row lying plates which bear shaped reinforcements create turbulence of heat transfer medium and enlarge the heat-conveying surface. The heat transfer medium, as shown in the figure flows between the slabs of small thickness, whereby the heat is transmitted between substances mainly convective. Plate heat exchangers can be sorted into dismountable and non-dismountable. Non-dismountable exchangers are usually occur in the brazing or welding design, which can also be used in case of the aggressive heat transfer medium. For plate heat exchangers is a clear advantage of their higher performance per unit area, therefore low weight and small size which is for the same performance about 5 times smaller than in tubular heat exchangers. However, the benefits are offset by higher prices and demanding production technology.

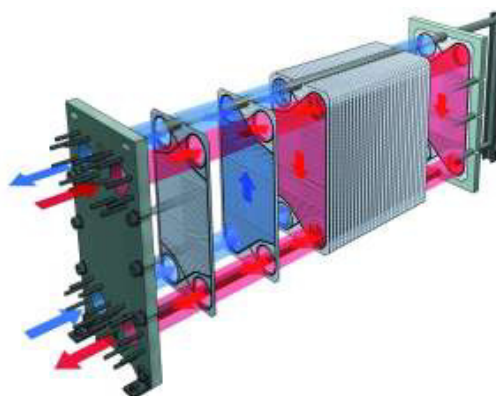


Fig. 8 Plate heat exchanger.

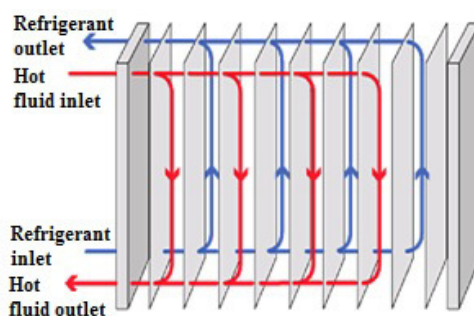


Fig. 9 Fluid flow in plate heat exchanger.

5. Conclusion

Nowadays, everyone looking for ways to save the largest amount of funds. Hence arise technology with which we can use energy from waste heat for other applications. Exhaust gas heat exchangers are increasingly appearing in conjunction with stationary combustion engines and automotive industries. Use of this technology to many manufacturers interesting solution as fuel economy and reduce emissions. The rate of fuel savings and overall efficiency of the plant will require yet another survey, which I will dedicate next steps in my work.

Acknowledgement

The acknowledgement heading is of the same style as the heading references "Reference" and it is not numbered. The text of acknowledgements is of the style "Text".

The authors are asked to pay special attention to the form of references. The NAMES OF AUTHORS should be typed in capitals, the Titles of Journals, Books or Proceedings in italics with the first capital letter in all significant words. The titles of articles are typed similarly as the basic text without the first capital letter in all words. When referenced in the text, enclose the citation number in square brackets, for example [1].

References

- [1] Holubčík, M., Hužvár, J. Jandačka, J. *Combined production of heat and electricity with use of micro cogeneration*, IN-TECH 2011 International Conference on Innovative Technologies. 2011. ISBN 978-80-904502-6-4
- [2] Kovalčík, A. Toporcer, E. Hlavňa, V. *Gaseous emissions of a combined cogeneration unit*. TRANSCOM 2009 : 8-th European conference of young research and scientific workers : Žilina June 22-24, 2009, Slovak Republic. Section 6: Machines and equipments. Applied mechanics. - Žilina: University of Žilina, 2009. - ISBN 978-80-554-0031-0.
- [3] Nemeč, P.: Hužvár, J. *Proposal of heat exchanger in micro-cogeneration unit, configuration with biomass combustion*. Development of materials science in research and education : the nineteenth joint seminar. [Bratislava: Slovak Society for Industrial Chemistry, 2009]. ISBN 978-80-89088-81-2. - S. 28-29.



Construction of Primary Circuit VVER 440V/213 nuclear power plant

*Frantisek Brumercik, **Dusan Sojcek, ***Aleksander Nieoczym

*University of Zilina, Faculty of mechanical engineering, Department of Design and Machine Elements,
Univerzitna 1, 01026 Žilina, Slovakia, brumercikf@fstroj.uniza.sk

**Enersense International Oy Gallen-Kallelankatu 7, 28100 Pori, Finland, dusan.sojcek@e-sense.eu

***University of Lublin, Department of Machine Elements and Mechatronics, 01026 Lublin, Poland,
a.nieoczym@pollub.pl

Abstract. The article describes construction of primary circuit, its features and technical layout. VVER reactors are special design of Pressurized Water Reactors with some particular design features. VVER reactors are the most frequently build reactor type in the world, proposed and build by Rosatom. Beside this, we can also notice reactors EPR (European pressured reactor) proposed and build by Areva. Basically primary circuit consists from Reactor, Main circulating piping (MCP), steam generator, main circulating pump, main closure valve and pressurized system. Besides primary circuit there are auxiliary system and safety system for safe operation. Nowadays build reactors are defined as III+ generation with advanced technology.

Keywords: VVER 440/ 213, Reactor, Main pump, Steam generator, Pressured system, Main valve, Parameters, Primary circuit.

1. Introduction

VVER-type reactor development was started by OKB “GIDROPRESS” in 1955. The first reactor of 210 MW (el.) power was commissioned at Unit I of Novovoronezh NPP (NV NPP) in 1964. A number of basic engineering solutions developed for the first VVER were of original character and most of them became traditional features for subsequent VVER generations. Such solutions included the following [1, 2]:

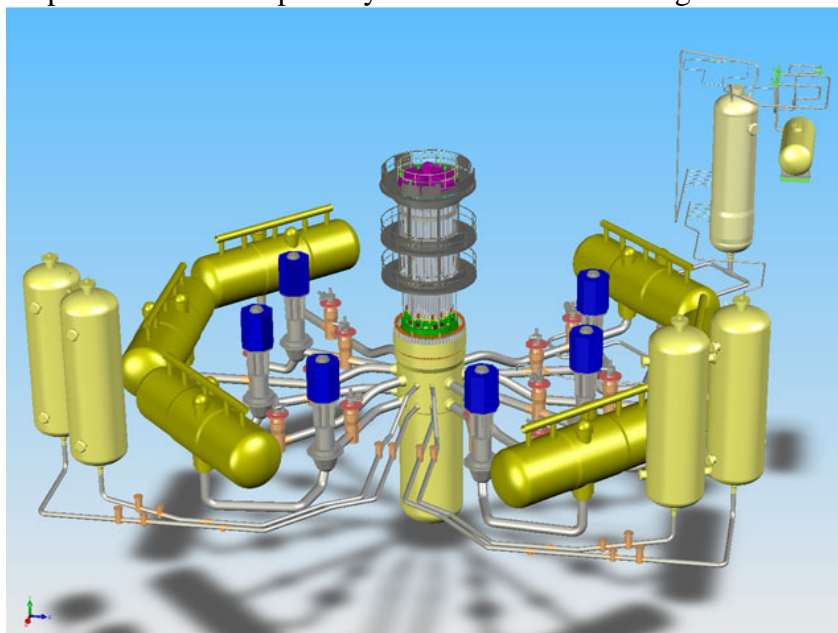
- A hexagonal grid for the arrangement of fuel assemblies (FAs) in the reactor core and accordingly the shape of fuel assemblies is hexahedral; the fuel rods in fuel assembly are arranged in triangular grid,
- Zirconium–niobium alloy is used as the material for fuel rod claddings,
- Possibility to transport all large-sized equipment by railway to enable a complete manufacturing process under factory conditions,
- High-strength alloyed carbon steel, which is serviceable in high neutron radiation fluxes, is used as the reactor vessel material,
- The bottom part of reactor vessel, which has no nozzles or any other holes, contains the core,
- The reactor vessel is manufactured of solid-forged shells without longitudinal welds,
- CPS (control and protection system) drives, outlets of temperature and power control systems are arranged on the removable upper head unit of the reactor,
- An original design of horizontal type steam generators with a tube sheet in the form of two cylindrical heads,
- Austenitic stainless steel is used as the material of steam generator HX tubes.

2. VVER 440 Primary circuit design description

The VVER 440 primary circuit consists of subsystems, which are described below. The main subsystems are:

- Reactor Vessel and Internals,
- Reactor coolant system,
- Main Gate Valve,
- Reactor Coolant Pump,
- Steam Generator PGV -4.

The model and parameters of the primary circuit are shown in Fig. 1.



Main design parameters of the VVER-440

Thermal power, nominal, MW	1,375
Primary pressure, MPa	12.26
Steam generator vessel pressure, MPa	4.6
Reactor coolant flow, m ³ /h	41,000
Reactor outlet temperature, °C	300
Number of fuel assemblies, pcs.	312
Number of CPS assemblies, pcs.	37
Uranium loading, t	41.5
Fuel enrichment in isotope U-235, %	3.6 ^a

^aFuel average enrichment is increased to 4.87% in the course of FA design improvement.

Fig. 1. VVER 440/213 primary circuit 3D model and parameters. Source: <http://www.tesnet.cz/en/sluzby-inzenyrske-modelovani.php>.

2.1 Reactor Vessel and Internals

The VVER reactor vessel design is based on meeting the following requirements:

- Proven materials and structures,
- Complete manufacture of the vessel with workshop testing included,
- Possibility of vessel transport by railway,
- Possibility of vessel in-service inspection.

The vessel is made of heat-resistant chromium–molybdenum steel of Grade 15Kh2MFA. The steel and the welding materials were chosen from the results of numerous analyses of mechanical properties, the absence of susceptibility to brittle fracture, the absence of thermal embrittlement, durability, and irradiation resistance. The steel was proven in manufacturing and it has been used in the fabrication of all VVER 440 reactor vessels (Fig. 2).

The upper cylindrical part of V-230 reactor vessel has 5 inlet and 5 outlet D_{nom} 500 nozzles for coolant to flow and one D_{nom} 100 nozzle for pressure-measurement pulse tubes and level gauge. The D_{nom} 500 nozzles are located in two rows away from the area of maximum neutron irradiation.

Four D_{nom} 250 nozzles were additionally included in the design for the V-213 reactor vessel for the application of the emergency core cooling system (ECCS). Two nozzles of this diameter are placed in each row of D_{nom} 500 nozzles.

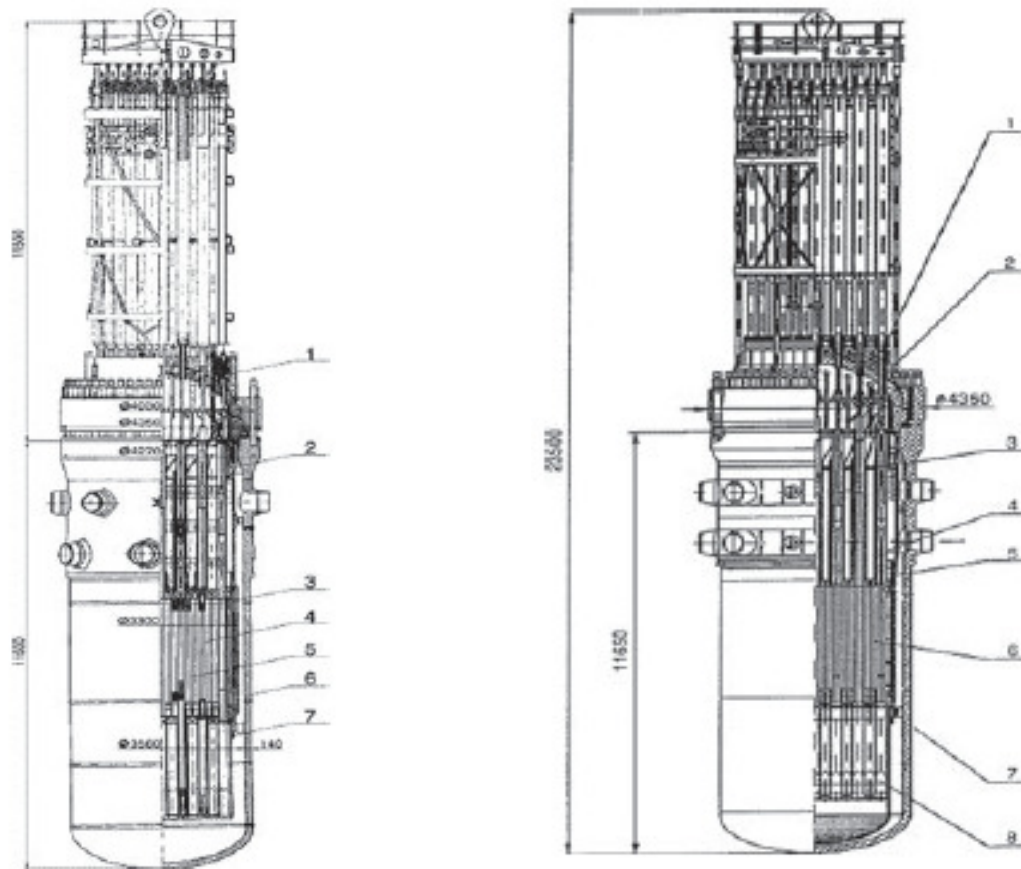


Fig. 2. Reactor V-230 (left), 1 - Top head, 2 – protective tube unit, 3 - Core barrel, 4-ERC assembly, 5 - working assembly, 6 - Vessel, 7 – Core barrel bottom. Reactor V-213 (right), 1 – ERC drive, 2 – Top head unit, 3 – Protective tube unit, 4 – intermediate rod, 5 – Core barrel, 6 – Reactor core, 7 – Reactor vessel, 8 – Core barrel bottom.

2.2 Reactor coolant system

Under normal operating conditions both V-230 and V-213 reactor types are cooled by six circulation loops of the main coolant pipeline (MCP). The pipelines are located in an airtight compartment around reactor concrete cavity (fig. 3). Each circulation loop is welded to the inlet and outlet nozzles of reactor vessel. The pipelines contain a reactor coolant pump (RCP) and a steam generator connected by D_{nom} 500 pipelines. The pipelines are made of stainless steel (05Kh18N19T).

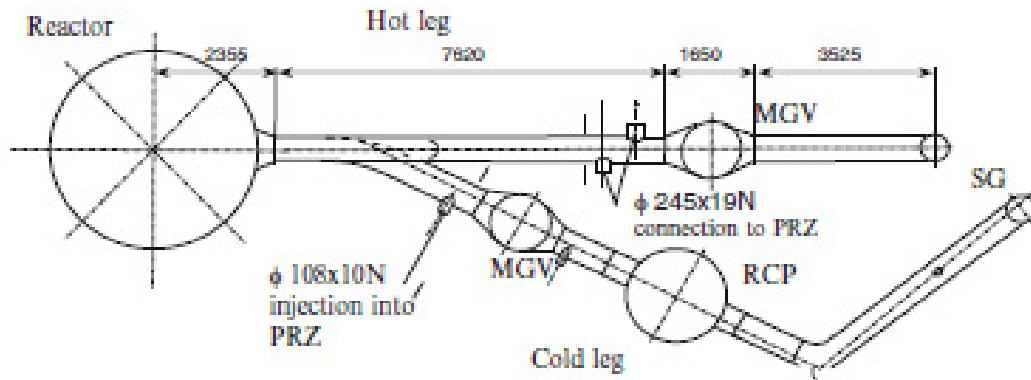


Fig. 3. Circulation loop 1 of reactor V – 213, MG V – Main Gate Valve, RCP – Reactor coolant pump.

2.3 Main Gate Valve

There is an annular shoulder on the internal surface of the vessel, which is located between the rows of nozzles that separate the inlet and outlet coolant flows (fig. 4). The shoulder allows the alignment of the core barrel with respect to the vessel. Corrosion-resistant cladding of internal surface was only applied to the area of vessel-to-top head joint in the first V-230 reactor vessels (6 vessels). All other vessels were covered with corrosion-resistant cladding all over the internal surface.

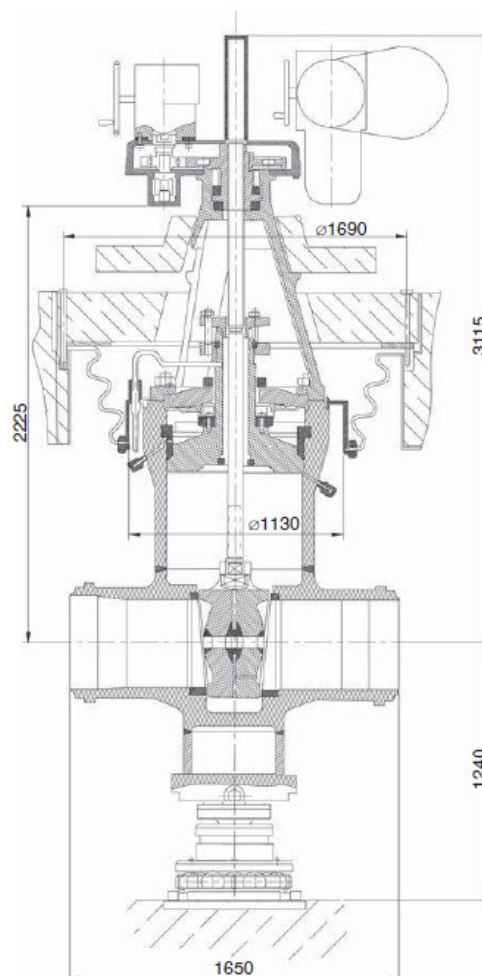


Fig. 4. Main gate valve.

2.4 Reactor Coolant Pump

Reactor plants of the V-230 type are featured with centrifugal one-stage vertical pumps of the packless type with an integrated electric drive of type GCN-310. The pumps (RCP) are used in the primary coolant circuit (fig. 5). Such leakproof pumps have been proved to be highly reliable with no leaks of radioactive primary water and they are simple in operation. Disadvantages of these pumps include low efficiency due to the high electromagnetic losses on sealing metal partition of electric motor and a small inertia coastdown in the case of the loss of power. Note that with reactor plants of the type V-230, the coastdown of four RCPs in case of loss of power together with coastdown of the turbine generators, power supply to these RCPs is provided by the terminals of the station service generator located on one shaft with the main generator. Reactor plant V-213 is featured with pumps of GCN-317 having mechanical sealing of the shaft, equipped with flywheels. The pump of GCN 317 is equipped with antireversing mechanism.

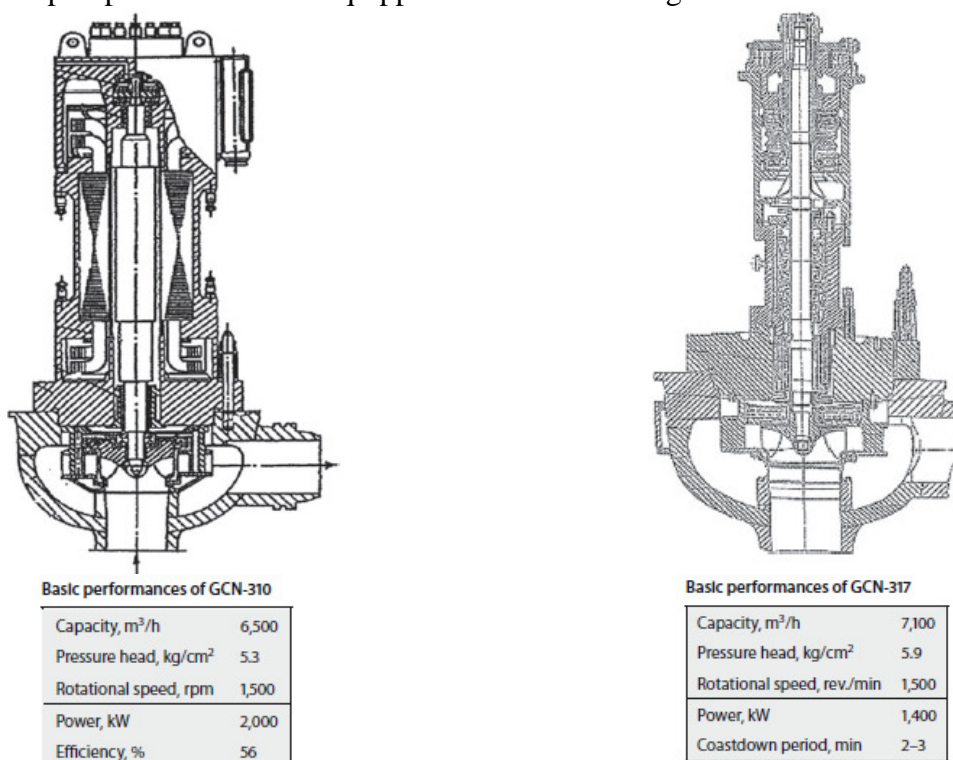
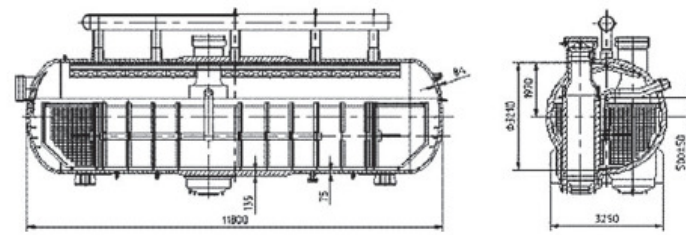


Fig. 5. Reactor Coolant Pumps and its parameters.

2.4 Steam Generator PGV -4

The basic structural feature of VVER steam generator is the horizontal arrangement of the cylindrical vessel, the submerged heating tube bundle, the cylindrical vertical collectors of the tubes, natural circulation of the boiler water, and an integrated steam separation system (fig. 6). Tube bundle consists of 5,146 stainless tubes with the outer diameter of 16 mm and wall thickness of 1,4 mm. The entire heat exchange surface is equal to 2,570 m².

The important advantage of horizontal steam generators is that there is a large water inventory in the secondary circuit. This large water volume provides favorable inertial characteristics for the whole of the reactor plant under transient and accident processes, thereby essentially enhancing its safety.



Steam generator performances

Steam capacity, t/h	452
Feedwater temperature, nominal, °C	223
Feedwater temperature with high pressure heater (HPH) switched off, °C	164
Steam pressure (abs.), MPa	4.71
Steam temperature, °C	260
Feedwater flowrate, t/h	453
Steam humidity at SG outlet (maximum), %	0.25

Fig. 6. Steam generator PGV -4 and its parameters.

3. Conclusion

Nowadays energetic field faces to chose main direction in matter to keep stable global energetic balance. Of course with considering environmental issues not just during operation of plant but also during construction and later on decommissioning. All of us very well know about CO₂ reduction and which source of energy is considered as main pollutant, but we still need stable sources of energy for our homes and industry. However renewable energy is now in main discussion in EU countries. But here it appears that we have problems to keep transmission line in balance and to direct flow of energy via countries [3].

This article just in short shows some basic features of nuclear power plant and its process criteria. It is one of possibility to produce big amount of energy. Yes, in this matter is necessary to talk about safety, big CAPEX and nuclear fuel storage what is really long term issue basically issue for our generation. In the face of all there are still plans to be finished (Mochovce, Olkiluoto, etc.) and build (Hanhikivi 1) new power plants. It is just to believe in new technology and implemented improved, independent, redundant safety system and we can discover the way of synergy between nuclear power and renewable energy source.

References

- [1] BRUMERČÍK, F. – SOJČÁK, D.: *Mechanical design aspects in HRSG waste heat recovery boilers*. TRANSCOM 2013 : 10-th European conference of young research and scientific workers : Žilina, June 24-26, 2013, Slovak Republic. - Žilina: University of Žilina, 2013. - ISBN 978-80-554-0695-4.
- [2] BRUMERČÍK, F. – SOJČÁK, D.: *Emission reduction and optimalization techniques in flue gas path of power plant equipment*. TRANSCOM 2013 : 10-th European conference of young research and scientific workers : Žilina, June 24-26, 2013, Slovak Republic. - Žilina: University of Žilina, 2013. - ISBN 978-80-554-0695-4.
- [3] RAYAPROLU, K.: *Boiler for Power and Process*. CRC Press, Taylor & Francis Group, 2009



Application of Wear Resistant Coatings for Autonomous Drilling Devices Working in Extreme Conditions

*Ján Bucala, *Martin Žarnay, *Silvester Poljak, **Norbert Radek

*University of Žilina, Faculty of Mechanical Engineering, Department of Design and Mechanical Elements, Univerzitná 1, 01026 Žilina, Slovakia, {jan.bucala, martin.zarnay, silvester.poljak}@fstroj.uniza.sk

**Kielce University of Technology, The Centre for Laser Technologies of Metals, 25-314, Kielce, Poland, norrad@tu.kielce.pl

Abstract. This article deals with the comparison of properties of two coating with same chemical composition (50% WC and 50% Cu), but different coating treatment, which can be used for contact surfaces of anchoring system of geothermal borehole autonomous device called Plasmabit. The main object of our investigations was the coefficient of friction between tribological pair consisting of coating – friction body and wear resistance of WC-Cu (tungsten carbide - copper) coatings. These data are very important for the next phase of development of the autonomous devices which are able to operate in deep geothermal borehole with high temperatures and pressures. The choice of suitable material and its surface treatment are key factors for force generation and expected lifetime of Plasmabit's anchoring system.

Keywords: Plasmabit, Anchoring system, Wear resistant coatings, Coefficient of friction.

1. Introduction

The price of geothermal boreholes grows exponentially with the depth when using current drilling methods. New technologies promising lower prices are currently being researched. One of the most promising technologies is high energy electric plasma, the technology which is compatible with liquid environments. This technology is directly integrated into Plasmabit – innovative device developed by company GA Drilling and promising linear price growth with the depth. It is autonomous system capable of its own movement in the borehole and the device itself consists of many subsystems such as system for movement and anchoring, system for rock disintegration (Plasmatron), control and management systems. Electric energy, cooling and technological water are supplied from the surface. Plasmabit should be able to work at pressures up to 100MPa and temperatures up to 360°C. Simplified 3D model of Plasmabit with basic principle of anchoring system can be seen on Fig. 1.

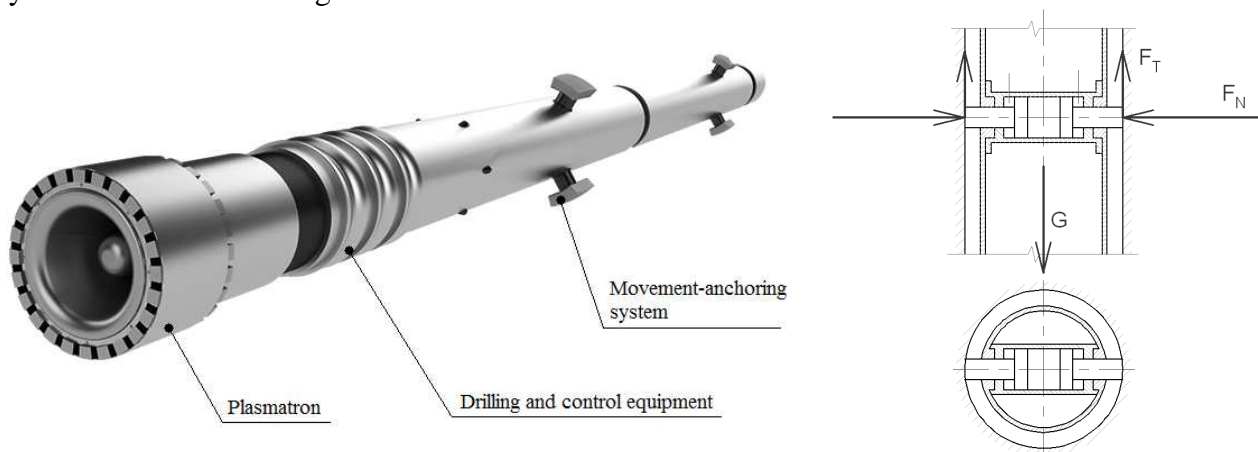


Fig. 1. Plasmabit – main parts and principle of anchoring system.

GA Drilling cooperates with Faculty of mechanical engineering of University of Žilina on the project “Autonomous robust mechatronic systems for ultra-deep geothermal boreholes” dealing with the design of Plasmabit’s movement-anchoring system. This system allows Plasmabit to move axially in the irregularly shaped borehole with deviation of borehole from vertical axis. In order to anchor Plasmabit to the surface of the borehole, anchoring elements are pushed against the surface of the borehole until the normal force of required magnitude is generated.

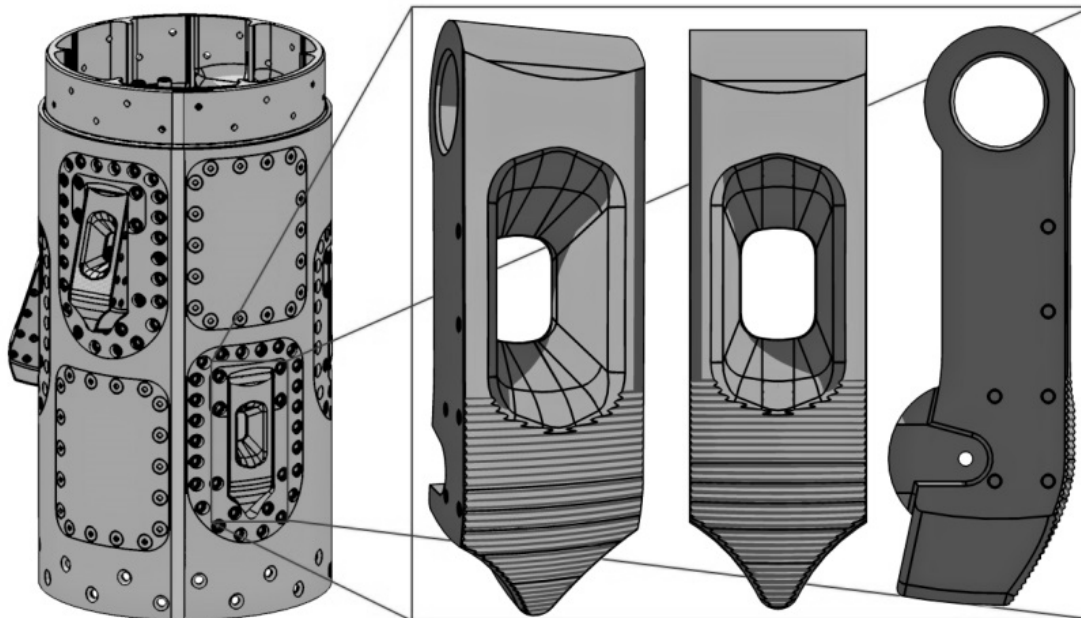


Fig. 2. Anchoring module of Plasmabit with enlarged anchoring element.

Anchoring elements will operate under high pressure and high temperature and will be exposed to high abrasive wear due to the contact with the surface of the borehole and also because of sharp small size particles which are produced during plasma rock disintegration process and later become part of drilling fluid. Therefore the choice of the material with suitable coating is decisive factor from the perspective of a lifetime and also for the value of the coefficient of friction between the anchoring element and the surface of the borehole.

The coatings with different mechanical properties than the substrate itself can be interesting option because of increased hardness, higher coefficient of friction and decreased price. Currently we are experimenting with WC-Cu coatings with different content of WC and Cu. These coatings can be used in the applications requiring high wear resistance and high coefficient of friction such as rock grinders. An electro-spark deposition (ESD) was used to deposit the coating to the surface. The deposition of the coating is achieved by an electrical circuit, which generates sparks between the electrode and the substrate. Electrical pulses of high frequency and high direct current between the electrode (anode) and substrate (cathode) release very hot micro-particles of electrode material, resulting in continuous micro-welding coating on the work-piece surface. The attributes of WC-Cu coating can be altered by subsequent laser treatment.

2. Samples, measurement devices and conditions

Linear tribometer which is available at Department of design and mechanical elements was used for the evaluation of surface properties of different coatings. This tribometer works on ball-on-flat principle and can reproduce loads similar to those expected in real life conditions. The tribological pair for every test consists of the samples made of carbon steel C45 with coating consisting of 50% WC and 50% Cu which is deposited onto its upper surface and grade 14 109 (according to STN) steel ball with 5 mm diameter and hardness of 58 HRC which corresponds to the hardness of granite. Steel is more suitable for the task because of its exact material properties and

the integrity of the material. Granite on the other hand is susceptible to cracks and disintegration during the process and has different material characteristic depending on exact material composition.

It was impossible for the samples to have exact size and shape as is shown on Fig. 2 because there are certain limitations within the design of the tribometer. Two 50% WC – 50% Cu samples with dimensions of 30 x 70 x 4 mm were used during experiment. Figure 3 shows surface structure of coating a) deposited by the ESD and of coating b) deposited by the ESD with laser treatment. The Nd:YAG laser (impulse mode), model BLS 720 was used. The sample was modified by using the following parameters: spot diameter $d = 0.7$ mm, power $P = 60$ W, laser beam velocity $v = 250$ mm/min, nozzle-workpiece distance $f = 6$ mm, pulse duration $t_i = 0.4$ ms, pulse repetition frequency $f = 50$ Hz, beam shift jump $S = 0.4$ mm, nitrogen gas shield $Q = 25$ l/min.

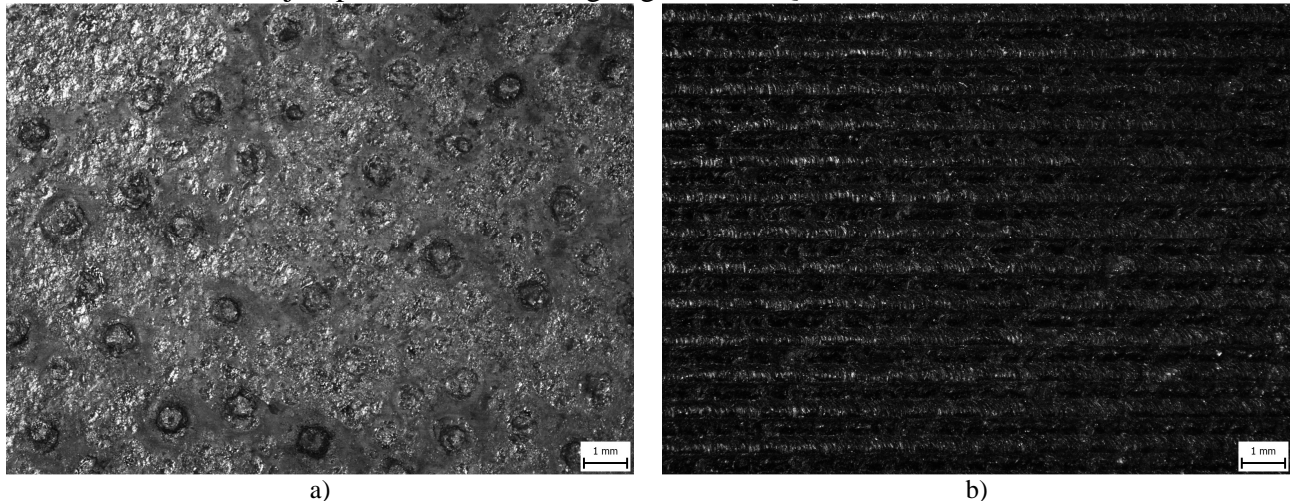


Fig. 3. Coatings used in experiment.

The surface structure of both coatings is very different. ESD deposited coating has very uneven surface structure. There are certain areas with higher copper content which are visible as rough circles. The laser treatment led to the homogenization of chemical composition of the coating, structure refinement, and crystallization of phases supersaturated due to the occurrence of temperature gradients and high cooling rate. Previous research conducted by Norbert Radek indicates that laser treatment refined the structure and some microcracks disappeared. However, 9% decrease in the Vickers microhardness occurred and average value of the coefficient of friction slightly decreased after laser treatment.

The most important part of our research is to measure the coefficient of friction for given tribological pairs in order to compare and evaluate coatings and determine whether these coatings are suitable for anchoring elements or not. Friction force F_N between the coating and steel ball is given by following equation:

$$F_T = F_N \cdot \mu \quad (1)$$

where F_N is normal force and μ represents coefficient of friction. Normal force is generated by the weight applied to the tip with steel ball and friction force is measured with tensometric sensor which is installed directly in the tribometer.

2.1. Experiment conditions

Experiment conditions such as laboratory temperature (20 °C), humidity and material of steel ball were the same for every experiment. The load for every test was determined according to given parameters and was constant during our experiments, values of 1N, 5N and 10N were used. Time for each test was chosen according to the overall length of tribological track with value of 100 meters (1000 cycles) or 500 meters (5000 cycles).

3. Results

The parameters used for tribological tests on 50% WC + 50% Cu coating are listed in table 1. There were 5 different tests performed on this sample, each corresponding to different track.

Track	Load [N]	Distance [m]	Cycles [1]	Mass [g]	
				Before	After
1	1	100	1000	56.5193	56.5192
2	5	100	1000	56.5192	56.5189
3	10	100	1000	56.5189	56.5179
4	5	500	5000	56.5179	56.5167
5	10	500	5000	56.5167	56.5159

Tab. 1. Tribological test parameters for ESD deposited coating 50% WC + 50% Cu.

The parameters used for tribological tests on 50% WC + 50% Cu coating with laser treatment are listed in table 2. The mass of the sample was evaluated after every test in order to measure its wear.

Track	Load [N]	Distance [m]	Cycles [1]	Mass [g]	
				Before	After
1	1	100	1000	56.1478	56.1474
2	5	100	1000	56.1474	56.1469
3	10	100	1000	56.1469	56.1453
4	5	500	5000	56.1453	56.1434
5	10	500	5000	56.1434	56.1412

Tab. 2. Tribological test parameters for ESD deposited coating 50% WC + 50% Cu with laser treatment.

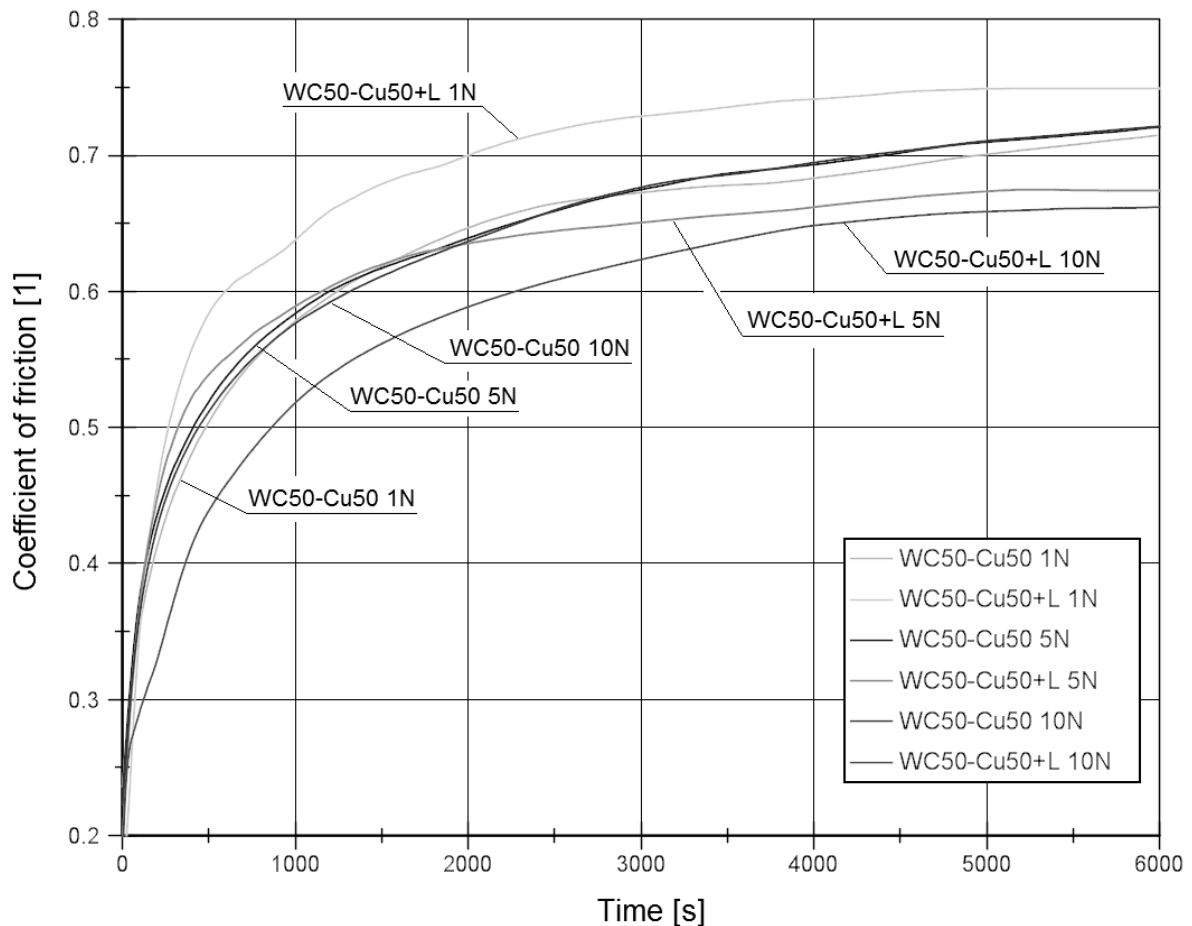


Fig. 4. Comparison of ESD deposited coatings used in 100 meter tests.

We decided to divide the results to two separate graphs because of different length of the tests. The coefficient of friction as a function of time for both samples with tribological track length of 100 m is shown on Fig. 4. The loads 1N, 5N and 10N used for the tests on both samples are listed here. The coefficient of friction has growing tendency for all tests, starting at 0.2 and rising to values over 0.75 after 6000 seconds. Many tests showed that value of the coefficient of friction started to be constant after reaching 5000 seconds. The highest value of 0.85 was reached by 1N load on 50% WC + 50% Cu sample with laser treatment. By comparing test results with corresponding loads it is clear that laser treated sample achieved lower values of the coefficient of friction. There is only one exception – 1N load. Situation was different here because the sample with laser treatment reached higher value of the coefficient of friction.

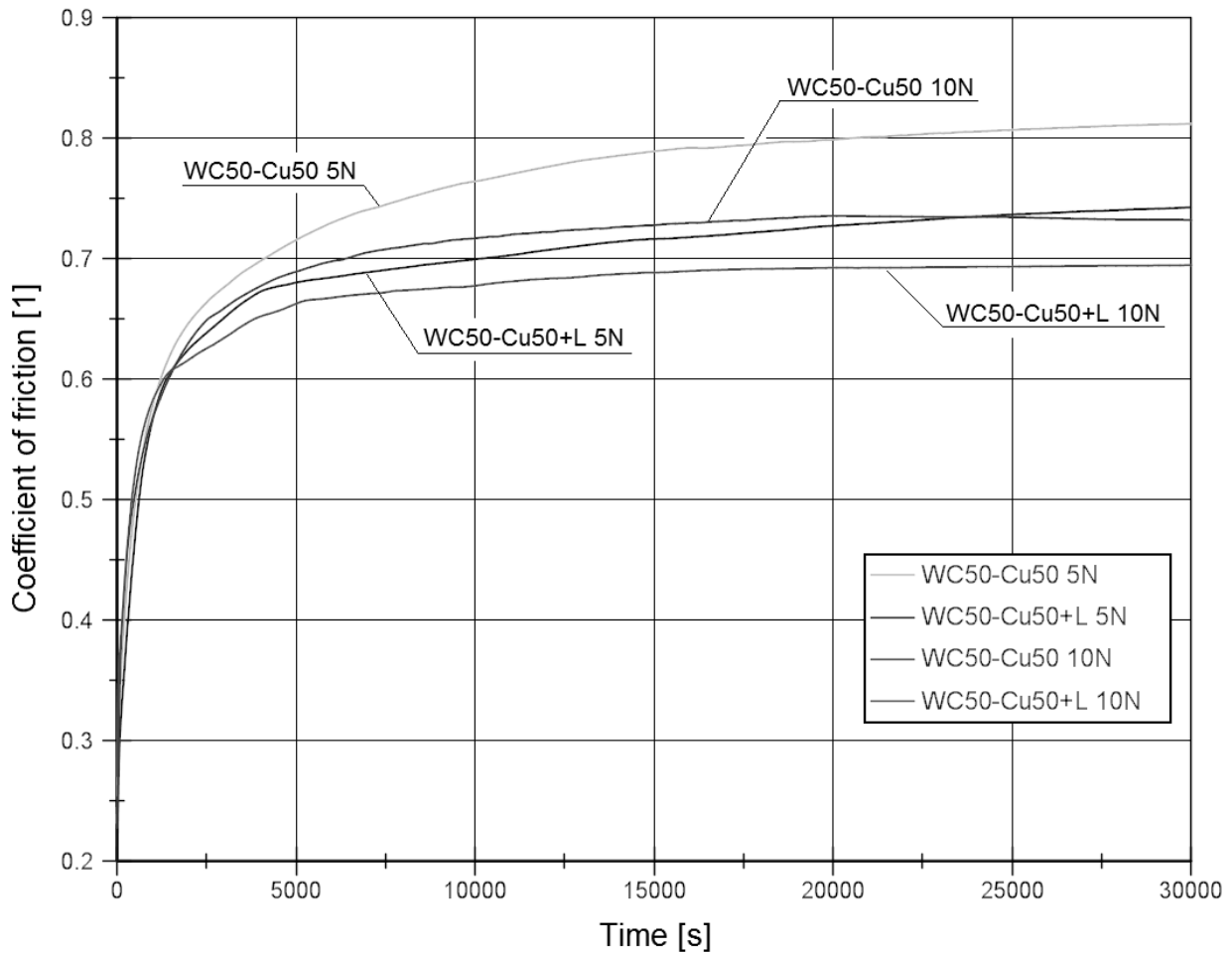


Fig. 5. Comparison of ESD deposited coatings used in 500 meter tests.

The coefficient of friction as a function of time for both samples with tribological track length of 500 m can be seen on Fig. 5. The growing tendency of the coefficient of friction was observed for all tests, starting at 0.2 and rising to values over 0.69 after 30000 seconds. The tests performed on the sample with laser treatment showed that value of the coefficient of friction become constant after reaching approximately 20000 seconds. The tests done on sample without laser treatment have slightly rising tendency even after reaching 30000 seconds. The highest value of 0.82 was reached by 5N load on 50% WC + 50% Cu sample without laser treatment. By comparing test results with corresponding loads it is clear that the sample without laser treatment achieved higher values of the coefficient of friction.

The samples were weighted after every test which means we can compare results and determine whether the coating is wear resistant or not. Wear process occurred on both samples and material loss due to wear reached values no higher than 2.2 milligrams for 500 m tests. The values lower

than 1.6 milligrams were obtained during short tests. Wear rate was always lower on the coating without laser treatment.

Wear of steel balls used in our tests was also evaluated. Wear rate of all steel balls was higher for the coating without laser treatment. Steel balls used for 10N and 100 meter test are on Fig. 6. The ball a) corresponds to the coating without laser treatment while b) was used on laser treated coating.

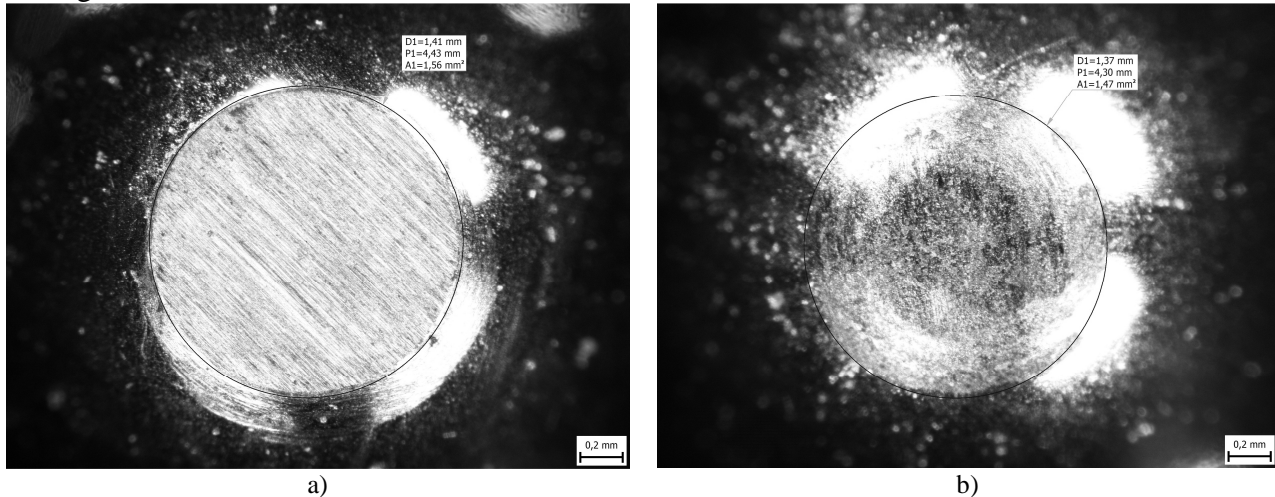


Fig. 6. Steel balls used in 10N and 100m test.

4. Conclusion

Both coatings (with and without laser treatment) achieved very high coefficient of friction which makes these coatings suitable for use as the coatings for anchoring elements. By comparing both coating it is clear that the coating without laser treatment reached higher coefficient of friction by 5 to 9%. As far as wear is concerned wear rate is much higher for the coating with laser treatment by 60 to 200% depending on length and load used during our tests. That means that 50% WC + 50% Cu coating without laser treatment is more wear resistant than laser treated coating. When wear resistance and coefficient of friction are taken into account, the coating without laser treatment is more suitable for our purposes.

More experiments will be performed in the near future. We are planning to evaluate the impact of different content of main components in WC-Cu coatings on wear resistance and on coefficient of friction as these coatings clearly show great promise for our application.

Acknowledgement

This publication is the result of the project implementation: „Autonomous Robust Mechatronic Systems for Ultra Deep Geothermal Boreholes“, ITMS code 26220220139, supported by the Research & Development Operational Programme funded by the ERDF.

References

- [1] BRONČEK, J. *Tribologické aspekty pohybového systému Plazmabitú*. University of Žilina, 2012 (Research report)
- [2] HOLMBERG, K. – MATTHEWS, A. *Coatings tribology*. 2nd ed. Amsterdam: Elsevier 2009, ISBN 978-0-444-52750-9
- [3] RADEK, N. – BRONČEK, J. – SHALAPKO, J. *Influence of laser treatment on microstructure and tribological properties of electro-spark deposited coatings* in *Technológ*, 02 (2014), pages 95-98, ISSN 1337-8996
- [4] <http://www.gadrilling.com/technology/>



Development of a Flexible Multibody System of a Rail Vehicle

*Ján Dižo, *Miroslav Blatnický

*University of Žilina, Faculty of Mechanical Engineering, Univerzitná 2, 010 26 Žilina, Slovakia,
jan.dizo@fstroj.uniza.sk, miroslav.blatnicky@fstroj.uniza.sk

Abstract. Computer modelling and simulation tools are nowadays widely used in the field of a rail vehicle design. These virtual reality tools allow to perform static analyses of rail vehicle parts and dynamic analyses of a rail vehicle multibody system. The finite element method is most commonly used for static analyses and the multibody system dynamics is used for dynamic analyses. Dynamic analyses performing is mainly necessary in the field of rail vehicle design. The goal of this paper is an implementation of flexible bodies into the rail vehicle multibody system. The implementation of flexible bodies into the rail vehicle multibody system allows extending the using of simulations, especially for an assessment of an influence of flexible bodies on running properties of the rail vehicle.

Keywords: Multibody system dynamics, Rail vehicle, Computer modelling, Flexible bodies.

1. Introduction

Rail vehicle production composes number of parts. First it is the design phase, then the development phase and the optimisation phase, further the production of a rail vehicle, the verification and validation of a rail vehicle and finally the commissioning of a rail vehicle. Computer software allows performing complex simulations. Thus, shorter development periods and rising requirements like durability, efficiency or mass reduction which intensifies the usage of lightweight structures demand precise simulations. In this way costly experiments and prototypes can be reduced using computer aided simulations.

2. Formulations of flexible multibody system dynamics

Dynamic behaviour and properties of rail vehicle are described by means of the multibody system dynamics. The standard multibody system of a rail vehicle is composed of rigid elements which are connected by ideal joints, coupling elements, contact elements and force elements. In the field of rail vehicle dynamics the phenomena of the contact between a wheel and a rail enters into account.

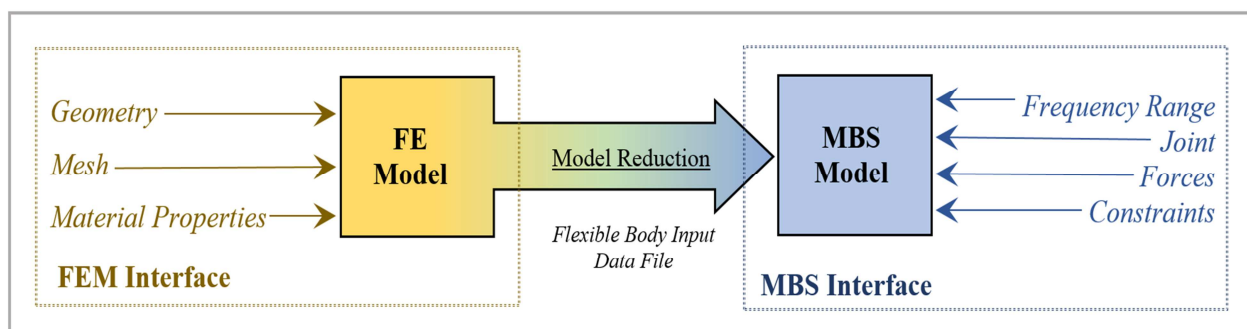


Fig. 1. The workflow of creating flexible bodies.

The MBS with flexible bodies has to be applied for applications of the rail vehicle dynamics where the deformations of the bodies have to be considered

Flexible bodies are introduced into the multibody system of rail vehicle by using of the finite element method. The reduction of the linear flexible degrees of freedom is the principal step for an efficient simulation of a flexible multibody system of a rail vehicle [9]. The Fig. 1 gives an overview of the workflow when working with flexible bodies in MBS software.

2.1. Figures and Tables

There are several methods for the kinematic description of the motion of the flexible bodies that are subjected to large displacements.

It is implemented in several commercial software as well as research general purpose multibody computer software.

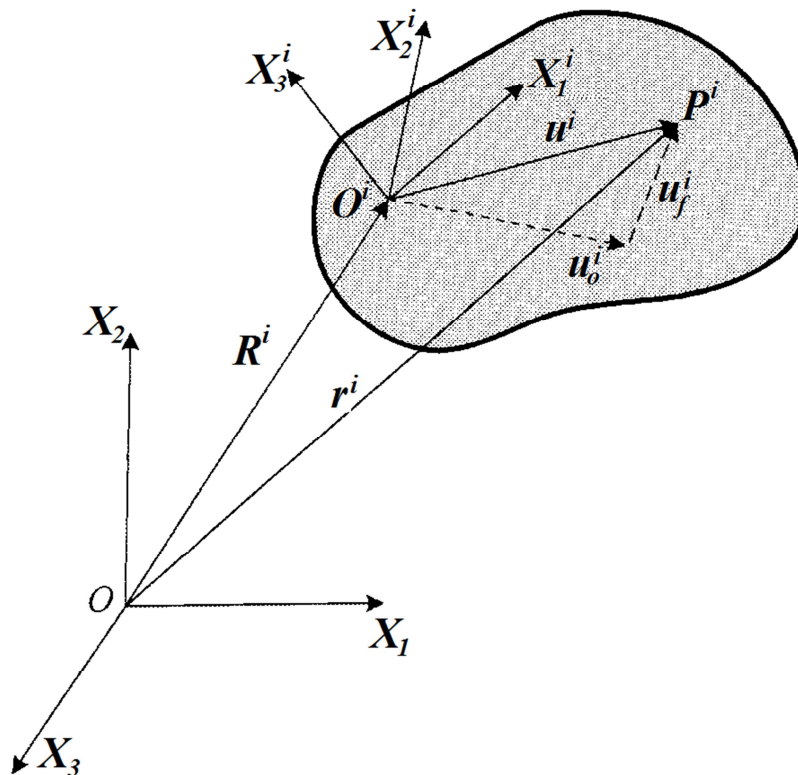


Fig. 2 Representation of the flexible body kinematic.

In this approach, two sets of coordinates are used to describe the configuration of the flexible bodies – one set describing the location and orientation of a selected body coordinate system and second is to separate the motion of the body into a large nonlinear motion of the reference frame and a small linear elastic deformation with respect to the reference frame.

In this description, the global position on the flexible body I can be written as:

$$\mathbf{r}^i = \mathbf{R}^i + \mathbf{A}^i (\bar{\mathbf{u}}_o^i + \bar{\mathbf{u}}_f^i); \quad (1)$$

where all the vectors that appear in this equation are shown in Fig. 2. and \mathbf{A}^i is the transformation matrix for defining the orientation of the body coordinate system with respect to the global coordinate system.

Using the dynamic description introduced above, the principle of virtual work in dynamics of Lagrange's equation can be used to systematically develop the dynamic equation of motion of the flexible bodies that undergo large reference displacements. In the floating frame of reference formulation, the equations of motion are formulated in terms of a coupled set of reference and flexible coordinates. In case of using the floating frame of reference formulation approach, the equations of motion of a flexible body in the multibody system of rail vehicle can be written in the general form:



$$\mathbf{M}^i \ddot{\mathbf{y}}^i + \mathbf{K}^i \mathbf{y}^i = \mathbf{q}_e^i + \mathbf{q}_v^i + \mathbf{q}_c^i; \quad (2)$$

where \mathbf{M} is the mass matrix, \mathbf{K} is the stiffness matrix, \mathbf{y} , $\ddot{\mathbf{y}}$ are vectors of the coordinates, accelerations, \mathbf{q}_e is vector of externally applied forces and \mathbf{q}_v is the vector of Coriolis forces and centrifugal forces and \mathbf{q}_c is the vector of the constraint forces. The equations of motion of the multibody system can be expressed as:

$$\mathbf{M}\ddot{\mathbf{y}} + \mathbf{K}\mathbf{y} = \mathbf{q}_e + \mathbf{q}_v + \mathbf{q}_c. \quad (3)$$

The vector of coordinates \mathbf{y} can be partitioned:

$$\mathbf{y} = [\mathbf{y}_r^T, \mathbf{y}_f^T]^T; \quad (4)$$

where subscripts r and f refer, respectively, to reference and flexible coordinates. Using the equation (4), the equation of motion of the flexible multibody system are:

$$\begin{bmatrix} \mathbf{M}_{rr} & \mathbf{M}_{rf} \\ \mathbf{M}_{fr} & \mathbf{M}_{ff} \end{bmatrix} \begin{bmatrix} \ddot{\mathbf{y}}_r \\ \ddot{\mathbf{y}}_f \end{bmatrix} + \begin{bmatrix} \mathbf{0} & \mathbf{0} \\ \mathbf{0} & \mathbf{K}_{ff} \end{bmatrix} = \begin{bmatrix} (\mathbf{q}_e)_r \\ (\mathbf{q}_e)_f \end{bmatrix} + \begin{bmatrix} (\mathbf{q}_v)_r \\ (\mathbf{q}_v)_f \end{bmatrix} + \begin{bmatrix} (\mathbf{q}_c)_r \\ (\mathbf{q}_c)_f \end{bmatrix}. \quad (5)$$

The floating frame of reference formulation leads to a highly nonlinear mass matrix as the result of the inertia coupling between the reference motion and the elastic deformation. On the other hand, the stiffness matrix is the same as the stiffness matrix used in the structural dynamics due the fact that the flexible coordinates are defined with respect to the coordinate system of the body.

3. Process of flexible body creation for multibody system dynamics

In the field of flexible multibody system of rail vehicle it is needed to perform reduction of a flexible body. Flexible body creation and flexible body reduction includes three main operations:

- 1) creating the finite element model of rail vehicle component,
- 2) import the finite element model into the software for a multibody system dynamics,
- 3) creating the flexible multibody system of the rail vehicle.

Before the import the finite element model of rail vehicle component into the multibody software it is necessary to perform reducing degrees of freedom of the finite element model of rail vehicle component. Reduction of the finite element model consists of several phases:

- setting up location of the interface nodes; the interface nodes allow connecting the flexible body to each other in the multibody system of a rail vehicle,
- connecting the interface nodes with the flexible body structure,
- defining the coupling nodes as retained nodes,
- and finally defining the retained degrees of freedom [18].

When the finite element model of the rail vehicle component is reduced, it is possible generating the input files, which is required for multibody software. This file contains all necessary information about flexibility and properties of selected rail vehicle component. Once the input data of flexible body are imported into the multibody software, it is possible apply to the flexible body joints, constraints, force elements etc. Deformations of the flexible body are caused by these boundary conditions and loads [15].

In this paper is introduced creation of the finite element model of the bogie frame. It is the bogie frame Y25, which is the most commonly used for the freight rail vehicle in the Central and Eastern Europe [19, 20, 21].

The procedure of the flexible rail vehicle component preparation consists of several parts. Firstly we have to be created the 3D model of a rail vehicle component. This model can be imported into finite element method software (Fig.4), where we can create a mesh, perform modal analyses, analyses of flexible component behaviour and also reduction of the rail vehicle component. Than the flexible body can be used for implementation of flexible body into multibody dynamic model of

rail vehicle [14, 22]. For the reduction of the flexible body the definition of interface nodes is required. Interfaces nodes are defined in those locations where the other components of the bogie and body of freight wagon are mounted to the bogie frame. There are locations on axle guides, on the centre pivot and on side bearers. Interface nodes on axle guides serve to the interconnection with axle boxes and interface nodes on the centre pivots and side bearers allow interconnection between the bogie and body of wagon

Example of the interface node is shown in Fig. 4. Interface node is coupled with nodes from the finite element mesh by using is shown the detail of interface node (INode) and relevant constraint equation created on the friction surface of the axle guide. In this interface node are defined friction forces between the bogie frame and the axlebox in the multibody system of the freight wagon.

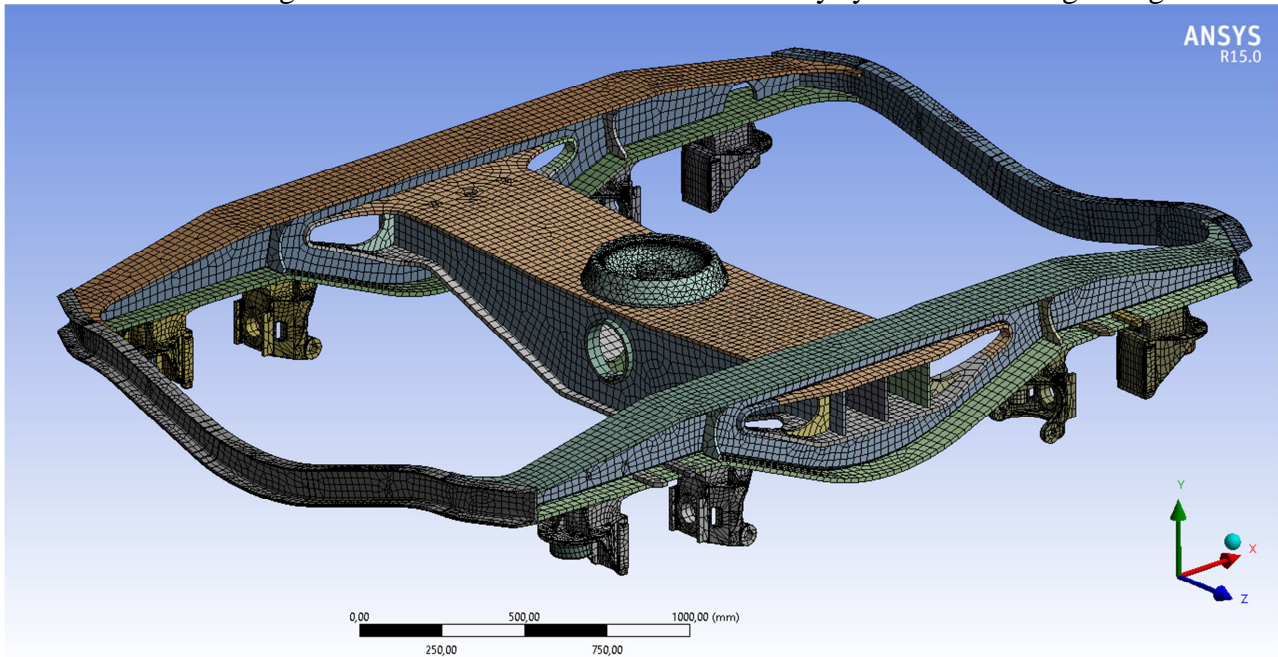


Fig. 3 Finite element model of bogie frame in Ansys.

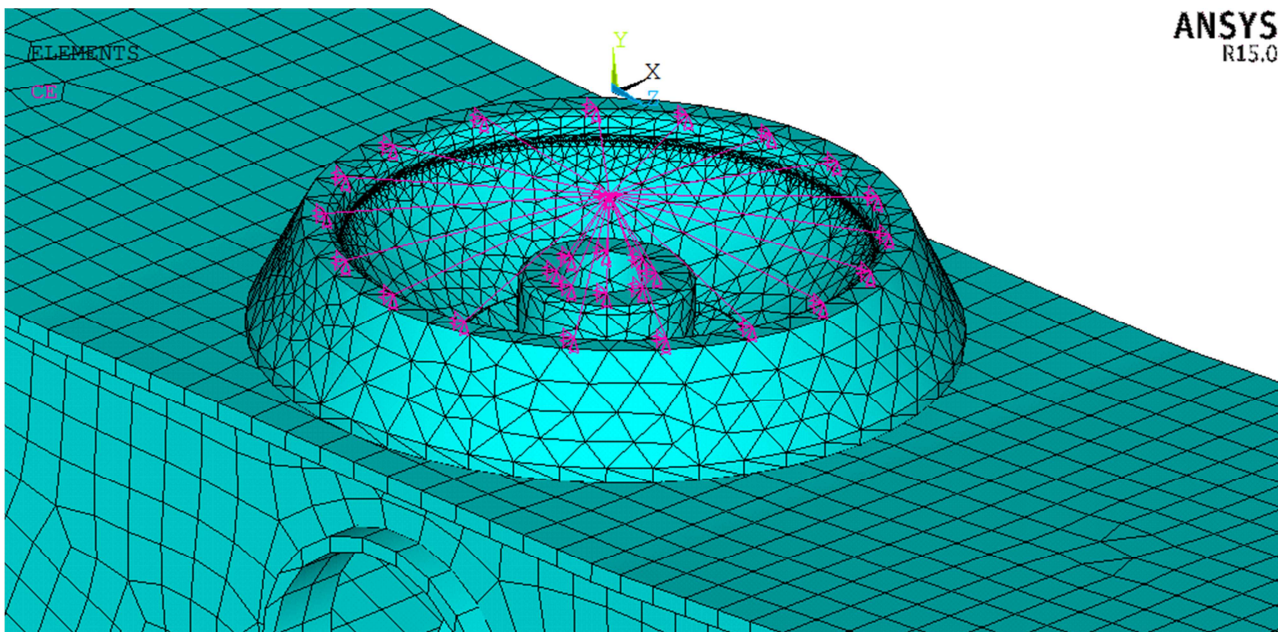


Fig. 4 Interface node on the centre pivot of the bogie frame.

When the flexible component of a freight wagon will be imported into the multibody software, will be created a flexible multibody system of a freight wagon. Such flexible multibody system will provide an advantage, that it will be perform simulation, which bring a better evaluation of the rail

vehicle properties. Multibody dynamics in which is considered a flexibility of body allow to perform such simulations which better confirm real vehicle behaviour under operational conditions.

4. Conclusion

The aim of this article was described options for using the multibody dynamics for simulation of a rail vehicle including a flexible component. There are described the most commonly used approach to the reduction of the flexible body. Including the flexible bodies into multibody system dynamics simulations of a rail vehicle running provide advanced opportunities for evaluation of rail vehicle properties, also stress in the structure of the rail vehicle components under real operational conditions.

Railway-Educational Centre of Rail Vehicles (VVCKV)

Acknowledgement

This paper was created during the processing of the project No. APVV-0842-11: “Equivalent railway operation load simulator on the roller rig”. The work is also supported by the Scientific Grant Agency of the Ministry of Education of the Slovak Republic and the Slovak Academy of Sciences in project No. 1/0347/12: “Railway wheel tread profile wear research under the rail vehicle in operation conditions simulation on the test bench.”, project No. 1/0383/12: “The rail vehicle running properties research with the help of a computer simulation.” and No. 1/1098/11: “Stress Distribution in a Braked Railway Wheel”.



The Agency
of the Ministry of Education, Science, Research and Sport
of the Slovak Republic
for the Structural Funds EU



This contribution is the result of the project implementation: „Development of two types of freight wagons with bogies for non-standard wheelbase or track wheelset, complying with the criteria for interoperability, Environmental Issues, safety and reliability,“ ITMS code 26220220070, supported by the Operational Programme Research and Development.

„We support research activities in Slovakia / Project is co-financed from EU sources”

References

- [1] HARUSINEC, J., DIZO, J., STASTNIAK, P. *The Computer Simulation of the Goods Wagon by Y25 Bogies* (in Slovak). Technolog, University of Zilina – EDIS Zilina, ISBN 1337-8996. 2013.
- [2] KLIMENDA, F., NANGOLO, F. *System identification for Underdamped Mechanical Systems*. In: 52nd International Conference on Experimental Stress Analysis, EAN 2014, Mariansle Lazne, Czech Republic, June 2-5 2014, 2014. ISBN 978-1-63266-822-6.
- [3] LACK, T., GERLICI, J. *Wheel/rail Tangential Contact Stress Evaluation by Means of the Modified Strip Method*. Communications – Scientific Letters of the University of Zilina, vol. 16. No. 3a, 2014, 33-39. ISSN 1335-4205.
- [4] LACK, T., GERLICI, J. *Wheel/rail Tangential Contact Stress Evaluation by Means of the Modified Strip Method*. Communications – Scientific Letters of the University of Zilina, vol. 16. No. 3a, 2014. ISSN 1335-4205.
- [5] SHABANA, A. A. *Flexible Multibody Dynamics: Review of Past Recent Developments*. Multibody System Dynamics 1. 1997.
- [6] SIMPACK documentation 2014, *user guide* (part of the program package).



- [7] SKOCILAS, J., SKOCILASOVA, B., SOUKUP, J. *Determination of the Rheological Properties of Thin Plate under Transient Vibration*. Latin American J. of Solids and Structures. Brazil Society for mechatronics and Engineering. 2014. ISSN 1679-7817 (print), 1679-7825 (online).
- [8] STASTNIAK, P. HARUSINEC, J., GERLICI, J., LACK, T. *Stress analysis of the modified bogie frame of type Y25*. In: Dynamics of rigid and deformable bodies, 2013Proceedings XI. International Scientific Conference, Ústí nad Labem, October 9-11 2013. - Ústí nad Labem: FVTM UJEP, 2013. - ISBN 978-80-7414-607-7.
- [9] STASTNIAK, P. HARUSINEC, J., GERLICI, J., LACK, T. *Railway vehicles design solutions for intermodal transport*. In: Computational and experimental methods in applied mechanics I. - Ústí nad Labem: FVTM UJEP, 2013. - ISBN 978-80-7414-609-1.
- [10] STASTNIAK, P., HARUSINEC, J., GERLICI, J., LACK, T. *Structural analysis of the construction freight bogie wagon (In Slovak)*. In: Strojirenske technologie – the journal for science, research and production. – ISSN 1211-4162. – Vol. 18. No. 2, 2013.
- [11] SVOBODA, M., SOUKUP, J., PETRENKO, A. *Use of FEM programs in solving general unbalance simple mechanical system rigid, flexible stored bodies*. In: 52nd International Conference on Experimental Stress Analysis, EAN 2014, Mariánské Lázně, Czech Republic, June 2-5 2014, 2014. ISBN 978-1-63266-822-6.
- [12] VASKO, M., LEITNER, B., SAGA, M.: *Computational Fatigue Damage Prediction of the Lorry Frames under Random Excitation*. Communications – Scientific Letters of the University of Žilina, vol. 12, No. 4, 2010.



The Vibrodiagnostics of Toothed Planetary Gearboxes

*Tomáš Gajdošík, *Ján Bucala, *Mária Tomášiková

*University of Žilina, Faculty of Mechanical Engineering, Department of Design and Mechanical Elements, Univerzitná 2, 01026 Žilina, Slovakia, {tomas.gajdosik, jan.bucala, maria.tomasikova}@fstroj.uniza.sk

Abstract. The article deals with the description of diagnostic device used on Department of Design and Mechanical Elements at University of Žilina in Žilina which has been developed in order to measure, diagnose and evaluate faults of gearboxes with toothed gears by vibrodiagnostics. Recent measurements of artificially created and damaged gearboxes are described in this article. The last chapter is dedicated to comparison of two different vibrodiagnostic methods – SKF method and SPM method. The comparison was made to verify all our previously measured data by SKF method and technique and also to directly compare the results of both diagnostic methods used for one gearbox.

Keywords: Vibrodiagnostics, Frequency, Operational damage.

1. Introduction and description of diagnostic device

Vibrodiagnostic is considered to be one of most progressive maintenance methods. It offers possibilities to diagnose status and conditions of devices while they are fully operational [1]. Diagnostic device has been constructed on Department of Design and Mechanical Elements in order to measure and evaluate faults of components by analyzing frequency spectra of gearboxes (Fig. 1). Laboratory research primarily aims at diagnostic of damaged gears of planetary gearboxes.

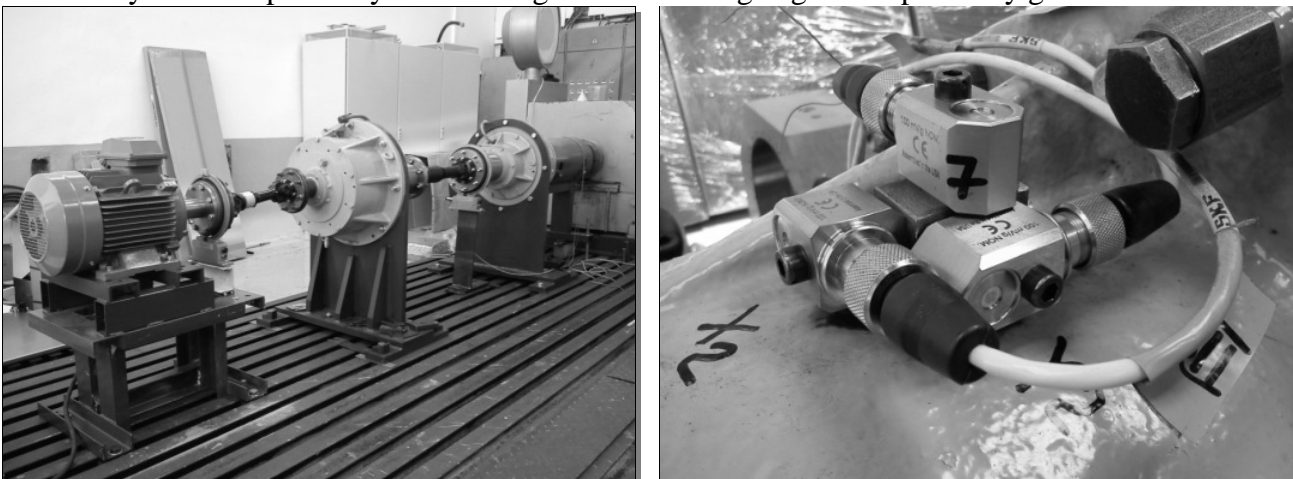


Fig. 1. Diagnostic device used on Department of Design and Mechanical Elements for diagnostic of planetary gearboxes faults (left) and placement of vibration sensors (right).

Diagnostic device consists of one 15 kW electromotor controlled by a phase shifter, two planetary gearboxes type A2000 mounted in series and also one dynamometer. Components are coupled together by cardan shafts. Diagnostic device is supplemented with noncontact sensors HBM T10F for RMP and torque measurement. Gearbox A 2000 is planetary gearbox with two planetary gearings with spur involute gears [2].

Diagnostic apparatus was purchased from SKF and it contains six acceleration sensors with resolution of 100 mV/g, on-line diagnostic unit IMx-S and PC equipped with @plitude analyst software. Both frequency analysis and envelope method for signal processing are used to determine gearbox faults.

Gearbox A2000 was tested for fault response at 1470 ± 10 RPM. Input shaft can rotate both clockwise and anticlockwise according to current needs.

2. Previous measurements

The first step for our research was to collect data from undamaged gearbox. After all data were analyzed and evaluated, we could create artificial damage on measured gearbox. Sun gear of the first planetary gearing was the first to be damaged.

The first damage to be measured was notch on face area of one tooth of sun gear. This type of damage was created in order to create significant vibration response in frequency spectrum of vibrations of whole gearbox and this type of damage was identified easily. After all necessary data were measured and fault response was identified in spectra of vibrations velocity (filter 3), small pitting damage was made on the opposite surface of already damaged tooth. The response of pitting in frequency spectrum was not as significant as it was in the case of notch damage, but it could be clearly seen and easily identified.

As the experiment continued, we extended small pitting to the half of teeth of sun gear and later to every tooth. Area affected by pitting of damaged teeth extended to 40 – 50 % of teeth surface with this operation and data were measured. The gearbox was disassembled and artificially damaged sun gear was replaced by sun gear damaged by real pitting on the half of its teeth. The gearbox was assembled once again and measurements were made in order to compare artificial and real pitting. Comparison of our data showed that responses for artificial and real pitting were very similar which also confirmed correctness of our measurement method.

The last of measured faults was damage of sun gear by removing one of its teeth. 50 % of tooth material was removed for the first phase and later whole tooth was removed. The damage in the form of another notch, this time on the surface of one tooth of planet gear, was added and measurements were made.

3. Comparative measurements between two different methods

Comparative measurements were made in cooperation with vibrodiagnostic specialists from SPM Instrument s.r.o. SPM HD and SPM Spectrum methods were used to examine currents status of the gearbox. Gearbox was damaged by missing tooth and pitting on sun gear and notch type damage was made on satellite gear.

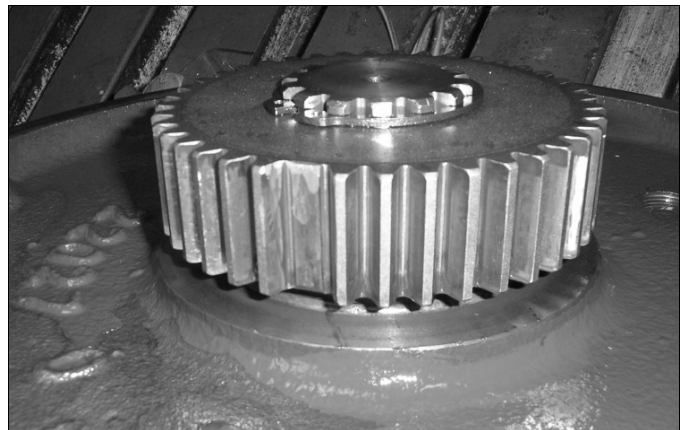


Fig. 2. Damaged sun gear with one missing tooth.

Frequency spectre measured by SPM HD method is shown on Fig. 3. Teeth frequency of damaged gear (54.976 Hz) and its harmonic frequencies within spectre are marked by numbers. Fig. 10 contains data measured by enveloped accelerations method filter 3 where teeth frequency and its harmonic frequencies of damaged gear (55 Hz) are also marked by numbers. Spectra on both

figures are very similar with small difference of amplitude magnitude for 6th, 7th and 8th harmonic frequency because these harmonic frequencies have much lower amplitudes with enveloped accelerations method.

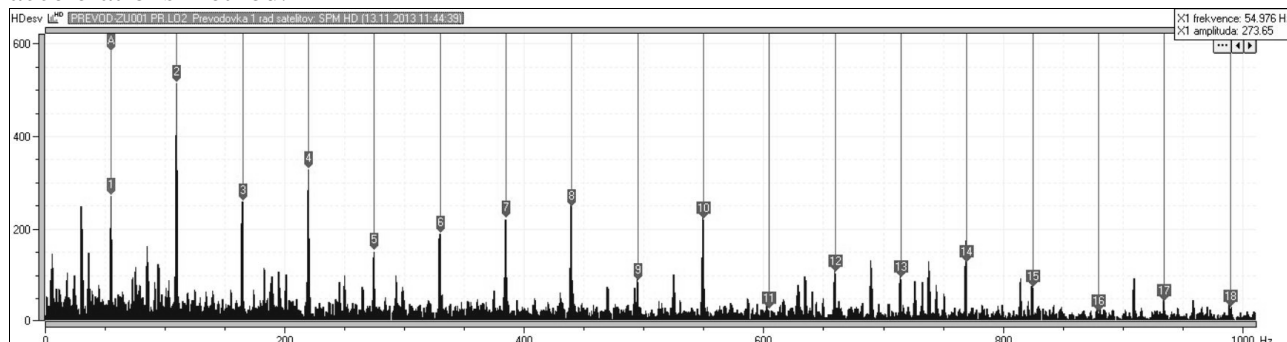


Fig. 3. Frequency spectrum measured by SPM HD method.

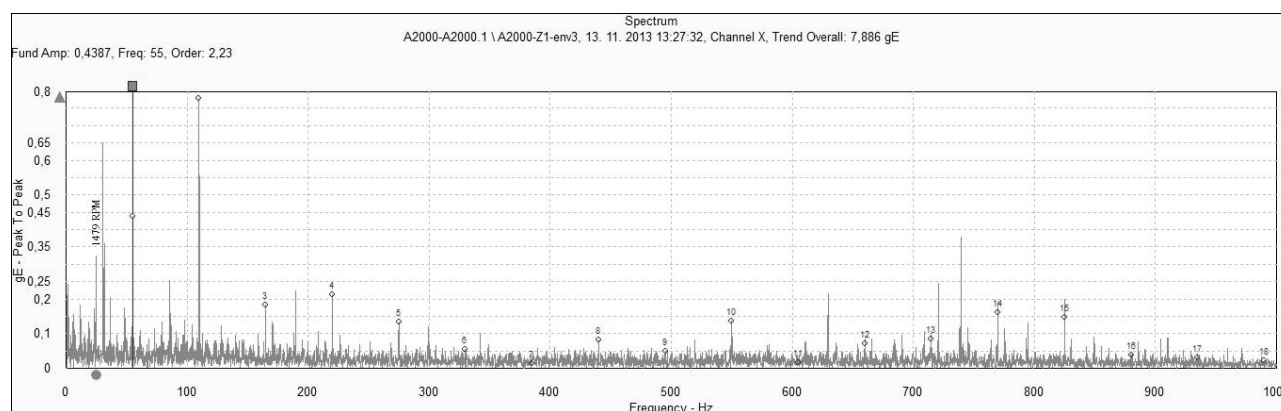


Fig. 4. Frequency spectrum measured by enveloped accelerations method (SKF).

Vibrations velocity frequency spectrum obtained by SPM Spectrum method can be seen on Fig. 5. Spectrum shape is very similar with SKF methods in direct comparison (Fig. 6), difference is in amplitude magnitudes. Spectra on both figures have highlighted amplitudes of lateral band with the delta of teeth frequency of damaged sun gear (55 Hz) and amplitude of lateral band of gear contact frequency of first planetary gearing which has high value of amplitude dominating whole spectrum.

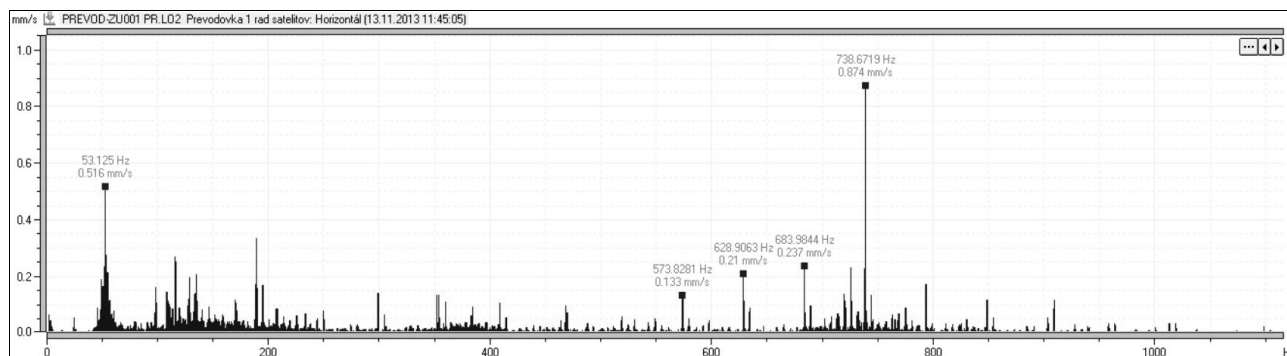


Fig. 5. Frequency spectrum of vibrations velocity measured by SPM Spectrum method.

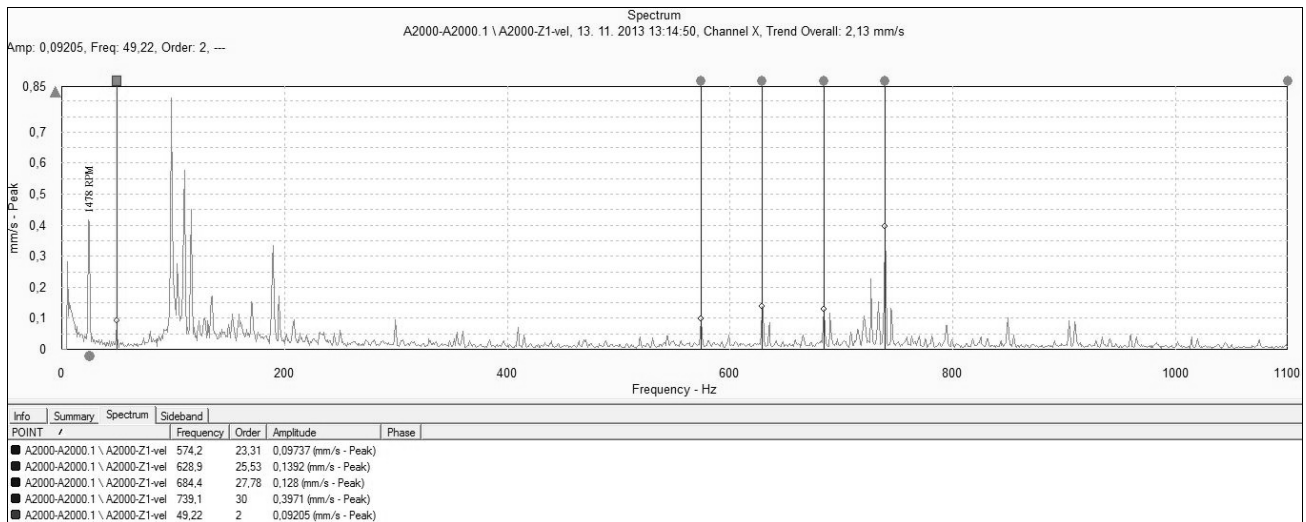


Fig. 6. Frequency spectrum of vibrations velocity measured by SKF diagnostic methods.

It is necessary to mention that influence of damaged planet gear has not been detected neither in vibrations velocity spectrum and neither in enveloped accelerations spectrum.

4. Conclusion

Comparative measurements between two different methods, one by SKF and another by SPM proved that these techniques are very similar and we were able to confirm correctness of previously measured data. Based on comparison of both methods, we can confirm that fault response in frequency spectrum is almost exactly the same even when different signal processing method is used. These results confirm that all measured data so far are correct and can be applied for industrial measurements.

Acknowledgments

This article was created with support of Slovak Research and Development Agency (SRDA) under project no. APVV 087-10: “Intelligent diagnostic systems of gearboxes and their components”.

We would like to thank to prof. Ľuboš Kučera, PhD. for every provided advice and technical help. This article would not be possible to be written without his help.

References

- [1] PRODAJ, J. *Application of a diagnosis of selected nodes of stationary and mobile transmission systems*. (In Slovak) [PhD thesis], Žilina 2012
- [2] GAJDOŠÍK, T., BUCALA, J., KOVALÍČEK, M. *Vibrodiagnostic of gearboxes* [Transcom 2013], Žilina 2013
- [3] KUČERA, Ľ., GAJDOŠÍK, T. *The Vibrodiagnostic of Gears* [ICMD 2013], Liberec 2013
- [4] KUČERA, Ľ., GAJDOŠÍK, T., BUCALA, J. *The Vibrodiagnostics of Damaged Gears of Planetary Gearboxes*, Komunikácie 2014



Computer-aided analysis and the consequences of failures of the selected vehicle subsystem

*Jana Galliková, *Roman Poprocký

*University of Žilina, Faculty of Mechanical Engineering, Department of Transport and Handling Machines, Univerzitná 1, 010 26 Žilina, Slovakia, {jana.gallikova, roman.poprocky}@fstroj.uniza.sk

Abstract. The paper deals with computer-aided analysis of failure modes and effects of the selected vehicle subsystem. It describes the construction of subsystem, its individual components and defines the various parameters. Limits values of wear and damage of the subsystem in operation, having a significant impact on the safety of rail operations are presented. The results obtained from FMEA is developed in the program 6.5 APIS for the causes and consequences of failures Besides the depiction of FMEA data in standardized form sheets, informative graphs and statistics can support your presentations. Critical parts are determined and measures to mitigate the effects of failures are prosed.

Keywords: Maintenance, Failure mode and effect analysis (FMEA), Critical parts.

1. Introduction

The FME(C)A is a design tool used to systematically analyze postulated component failures and identify the resultant effects on system operations. The analysis is sometimes characterized as consisting of two sub-analyses, the first being the failure modes and effects analysis (FMEA), and the second, the criticality analysis (CA). Successful development of an FMEA requires that the analyst include all significant failure modes for each contributing element or part in the system. FMEAs can be performed at the system, subsystem, assembly, subassembly or part level. The FMECA should be a living document during development of a hardware design. It should be scheduled and completed concurrently with the design. If completed in a timely manner, the FMECA can help guide design decisions. The usefulness of the FMECA as a design tool and in the decision-making process is dependent on the effectiveness and timeliness with which design problems are identified. Timeliness is probably the most important consideration. In the extreme case, the FMECA would be of little value to the design decision process if the analysis is performed after the hardware is built. While the FMECA identifies all part failure modes, its primary benefit is the early identification of all critical and catastrophic subsystem or system failure modes so they can be eliminated or minimized through design modification at the earliest point in the development effort; therefore, the FMECA should be performed at the system level as soon as preliminary design information is available and extended to the lower levels as the detail design progresses [6].

2. FMEA

When analyzing the possible failures and their causes all data are stored in the database, depending on whether the proposal or process is evaluated. Five successive steps are performed during the analysis:

1. Elements and Systems.
2. Functional structure and function of a system.
3. Analysis of possible failures, their causes and possible consequences. Assessment of their significance and likelihood of occurrence, as well as the possibility of detection the failure.

4. Risk Assessment (RPN), consideration of consequences types.
5. Optimization, setting priorities for corrective actions and evaluation of their effectiveness.

Following example is used or showing you a practical example of FMEA analysis. The bogie is Y25 bogie for two-axle freight wagons – it corresponds to UIC 510 regulation. The bogie can be designed for a maximum speed of 100 km/h (22.5 tons axle load) or 120 km/h (20.0 tons axle load).

The main parts of the running gear are:

1. wheelsets,
2. the axle bearings,
3. wheelsets guidance,
4. suspension,
5. bogie frame [6].

3. Network structures of freight bogie by FMEA

In the production structure is based on knowledge of equipment whose structure we want to create. The system consists of individual elements of the system which is to describe a structural context hierarchically grouped into the system.

The first step is the creation of the system structure. It is also necessary to establish the elements of the structure and their functions and failures. Then we can create function networks and failure networks. It is important that a list of all possible or potential modes of failure of the system was drawn up - this is the basis of FMEA [2, 5].

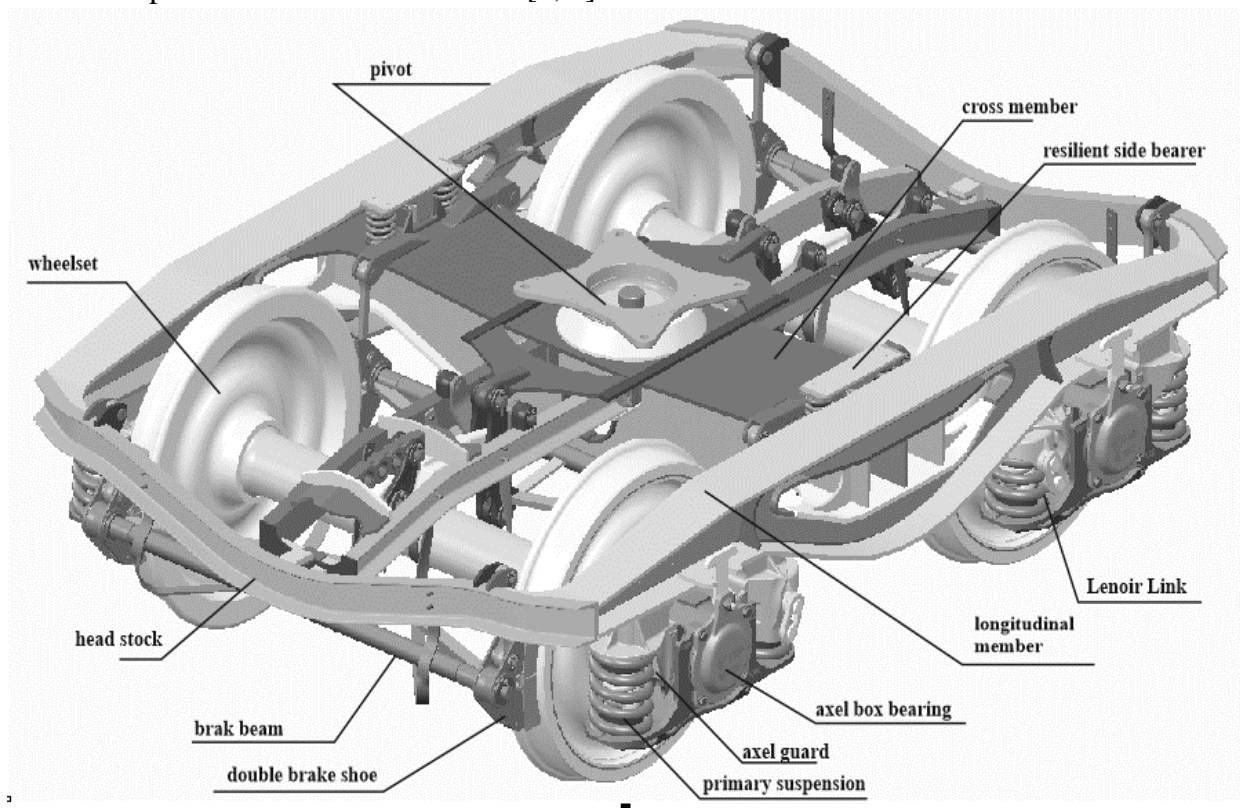





Fig. 1. Model of freight bogie Y25 [1].

Wheel profile wear are arisen on wheelsets, wheel flange wear and breaks. Grooves and clapped locations on the circumference of the shaft axle deeper than the 0.54 mm, inside distance between wheels with larger difference than ± 3 mm from the face value are disallowed. In Tab.1 some critical parts of wheelsets are shown.

Failures of wheelset	Causes	Measures
<p>Excessive radial wear of a wheel profile</p> 	<p>Dynamic and thermal stress of a wheel</p>	<p>The excessive radial wear of wheel profile is removed by means of the wheel profile lathe turning, if the monoblock have the sufficient thickness yet. The monoblock is rejected, when the ultrasonic flaw detection confirms the break which is expanding into the monoblock under the allowable value.</p>
<p>Stuck material on a wheel profile</p> 	<p>Sticked materials are produced because the material from rails or brake block is stucked to the tread</p>	<p>Sticked materials are produced because the material from rails or brake block is stucked to the tread.</p>
<p>Crumbled material on the tread</p> 	<p>Fatigue effect</p>	<p>The wheel profile of the monoblock is lathe turned. The wheel profile has to be up to the V99/1 standard. Limited dimensions of the wheel profile are checked.</p>

Tab. 1 Example of critical parts of wheelset [1].

Each element of the system is in the system, independently of the structural arrangements different functions, respectively tasks. For the performance of the functions of one system components are typically needed as the function of other elements of the system.

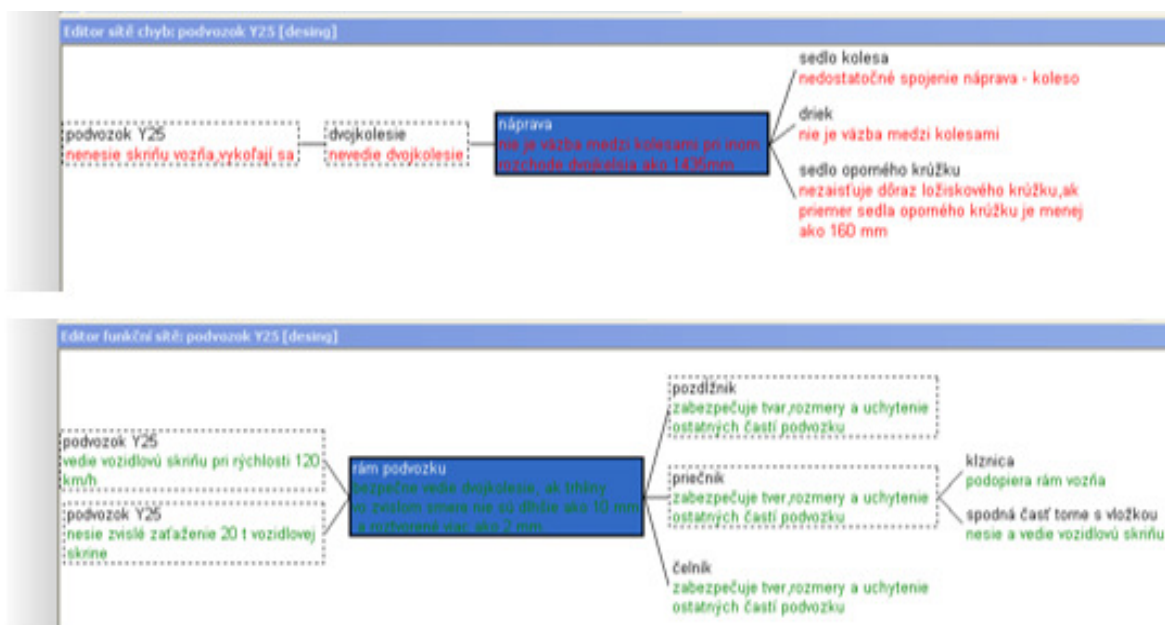


Fig. 2. Example of function network for bogie frame and failure network for axle [5].

For each element examined in the system, it is necessary to create function network and failure network. The next step is a risk assessment. Values of probability, severity and detectability are entered (Fig.2).

The example of FMEA analysis can be seen in Fig. 3.

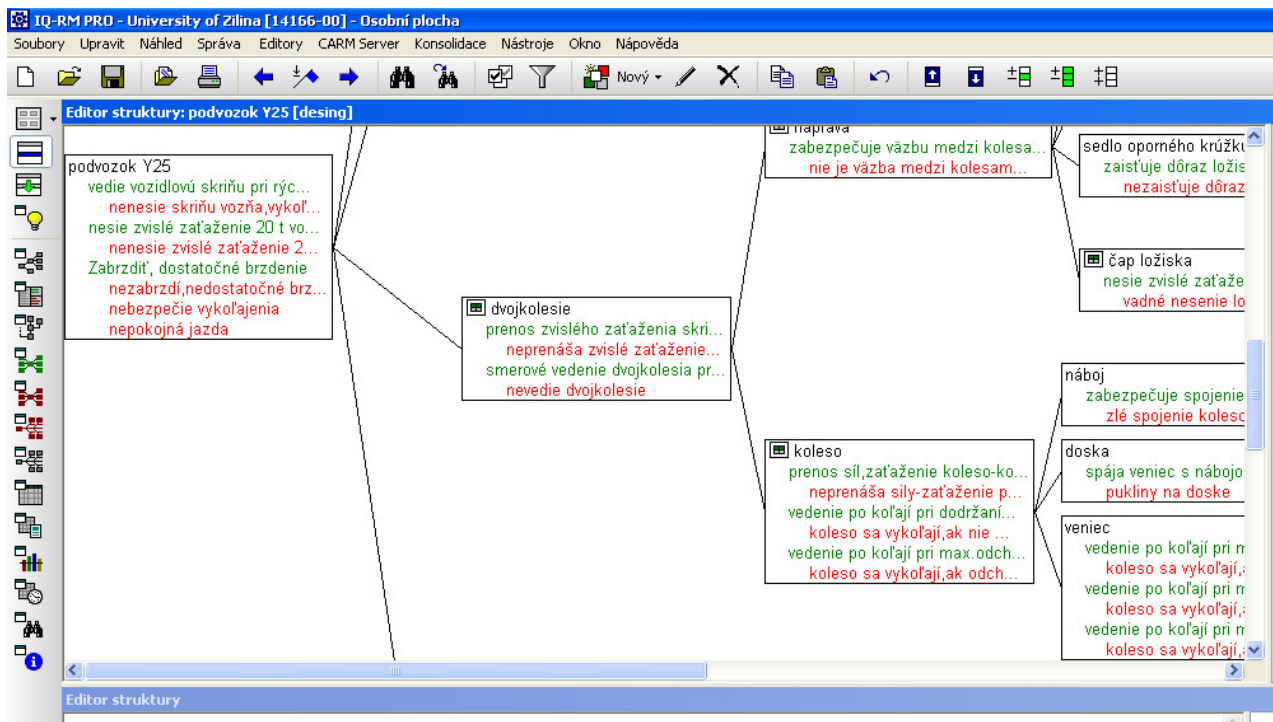


Fig. 3 View of the freight bogie structure with the structure of function and failures networks [1].

4. Risk assessment

The next step of FMEA is risk assessment. It is based on a compilation of forms, resulting in the knowledge of the risk of failure. This risk assessment is a measure of the consequences of failures.

The risk assessment of the system is assigned at the design and planning of the available measures to reduce their occurrence and detection. The measure of this evaluation is an indicator – RPN – level of risk/priority, which consists of three factors:

S – the importance of the seriousness of the occurrence of failure causes

O – the probability of occurrence of failure causes,

D – the probability of detection of failure causes, or it's result

These elements S, O a D can take any value from 1 to 10, where the level of risk is expressed by their mathematical product [2, 5].



EQ-RM PRD - University of Žilina [14166-00] - Osobní plocha

Soubory Upravit Náhled Správa Editory CARM Server Konsolidace Nástroje Okno Nápověda

Editor struktury: podvozok Y25 [desing]

Editor formuláře: YDA 96 /YDA 06: náprava (podvozok Y25 [desing])

Následky chyb	Z	K	Druh chyb	Příčiny chyb	Preventivní opatření	Opatření detekce	D	RPN	O/T
				F M E A desing		Číslo: Strana:			
Typ/Mo del/Vyhotovení/Várka: podvozok Y25				Věcný kód:		Zodpovědný:		Vytvořeno:	
				Stav opatření:		Firma:			
FMEA/Systémový element: náprava				Věcný kód:		Zodpovědný:		Vytvořeno:	
				Stav opatření:		Firma:		Změněno:	
Následky chyb	S	K	Druh chyb	Příčiny chyb	Preventivní opatření	Opatření detekce	D	RPN	O/T
Systémový element: náprava									
Funkce: zabezpečuje väzbu medzi kolesami 1435 mm									
nevedie dvojkolesie	10		nie je väzba medzi kolesami pri inom rozcho de dvojkolesia ako 1435mm	nedostatočné spojenie náprava - koleso	Počáteční stav: 16.3.2012				
				nie je väzba medzi kolesami	vizuálna prehliadka	4 meranie	1	40	
				nezaistíuje dôraz ložiskového krúžku, ak priemer sedla oporného krúžku je menej ako 160 mm	Počáteční stav: 16.3.2012				
					vizuálna prehliadka	4 meranie	1	40	
					Počáteční stav: 16.3.2012				
					žiadna	2 meranie	5	100	

Fig. 4 Form of risk assessment for axel.

Proposal of detection measures

In the proposed preventive maintenance, two methods to detect failures – visual inspection and defectoscopy are proposed. The role of the visual inspection is based on more frequent intervals by visual inspection to avoid unexpected failures that could have consequences in the loss of human life or in removal of the air brake system from operation. The role of the defectoscopy is based on a more frequent interval using the defectoscopy for preventing accidental failures that are not detectable by visual inspection.

Proposal of preventive measures

In FMEA analysis, it was found that it is appropriate to change all intervals of control components after running 200 000 km or 300 000 km, depending on the component, thus the current maintenance system will be more expensive but minimizes the risk of failures and the consequences associated with them.

Analysis of differences

In Fig.5 we can see that there was a significant reduction in RPN values on proposed detection methods, as well as preventive measures. RPN values for the first stage of the preventive maintenance are in the range from 400 to 180. RPN values range from 80 to 32 when we use preventive measures.

The green columns in the figure represent RPN values for individual components and well-defined cause failures when we use the first level of the preventive maintenance [3, 5].

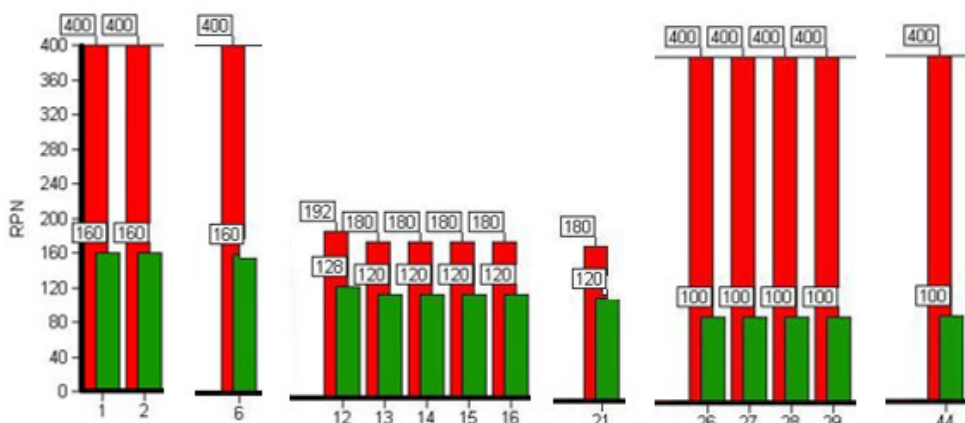


Fig. 5 The cause of failures [1].

4. Conclusion

From economical point of view, it is important to prevent a single failure by detecting the failure in time on the bogie. This is possible by using the diagnostic tool, whose task is to detect internal cracks and damage. Another way how to detect damage on the individual components is by carrying out planned preventative inspections. Their main role is to inspect parts that are most stressed when driving after passing the specific number of kilometers, or a specified time period.

The strategic task of the diagnostic system is to replace the current methodology according to schedule of vehicles maintenance with more convenient methodology according to the actual functional situation and the actual technical state, or to create an optimum combination of schedule and according to the actual situation.

The aim of introducing the diagnosis and the automatic diagnosis of vehicles is increasing the actual availability of vehicles, increase their reliability and operational safety, improve the quality and efficiency of maintenance and repair industry through control and decision-making activities. Objectification is increased with the level of automation of diagnostic activities. At the same time, demands on the quality of all activities related to the operation, maintenance and repair of vehicles are increasing.

Acknowledgement

This contribution is the result of the project implementation: Modern methods of teaching of control and diagnostic systems of engine vehicles, ITMS code 26110230107, supported by the Operational Programme Educational.



The Agency
of the Ministry of Education, Science, Research and Sport
of the Slovak Republic
for the Structural Funds EU



References

- [1] CHOBOT, L.: *Computer-aided analysis and the consequences of failures of the selected type of bogie (In Slovak)*. Diploma thesis. University of Žilina, 2012.
- [2] GREŇČÍK, J. a kol.: *Maintenance management: Synergies of theory and practice*, released Slovak Maintenance Society, BEKI design, s.r.o. Košice, ISBN 978-80-89522-03-3, Košice 2013 p. 373-390
- [3] GREŇČÍK, J. – RUMAN, F.: *Proposal of new maintenance system of air brake system on semi-trailer combination aimed at increase of operational safety*. In: *Bus – Technique, Eksploatacja, systemy Transportowe*, Nr 3/2013, ISSN 1509-5878
- [4] STUHLÝ, V. – POPROCKÝ R.: *Maintenance of machinery (In Slovak)*. EDIS- publishers, ISBN: 978-80-554-0845-3, Žilina, 2014 p. 152-243
- [5] STUHLÝ, V. – POPROCKÝ R.: *The concept of maintenance RCM: tutorial 9: tutorial – 2. edition – Žilina: University of Žilina, 2005, ISBN 80-8070-567-1*
- [6] STUHLÝ, V. - *The use of RCM to design the content of the maintenance of the chassis GP 200 passenger wagons (In Slovak): ICTKI 2012: International Conference of Technology Knowledge and Information 2012 : 4. international conference, Ústí nad Labem, 23.-24.1.2012, Czech Republic - JAN EVANGELYSTA PURKYŇĚ UNIVERSITY IN ÚSTÍ NAD LABEM, 2012. - ISBN 978-80-7414-433-2. - CD-ROM, p. 237-244.*



Rail-wheel contact of tramways vehicles in arc track

*Vladimír Hauser

*University of Žilina, Faculty of Mechanical Engineering, Department of Transport and Handling Machines,
Univerzitná 1, 01026 Žilina, Slovakia, vladimir.hauser@fstroj.uniza.sk

Abstract. In rail transport, it is necessary to solve the issue of passing the wheelset through arc track. With reduction of the radius of the track arc, the angles of attack and guiding forces acting on the vehicle grow. In the past, there was sometimes used one very special kind of rail to ease passing through arcs track with very small radius. This rail makes possible riding of the flange for wheel, which is situated on the outer side of arc track. This way was allowed on standard gauge track passing of some vehicles through arc track with radius up to 30 meters. This way of passing arc tracks was sometimes used in narrow ratios on sidings of producers. This paper considers the suitability of a similar solution for tramways urban transport, where is at the crossroads and at the turn-back places often used arc tracks of very small radius.

Keywords: Special rail, Wheelset, Track arc of very small radius, Wheel-rail contact geometry.

1. Introduction

When wheelset runs through arc track, it is necessary, that the wheel on the inner side of track arc underwent a little smaller distance than the wheel situated on the outer side of track. The wheelset is one solid part, so it is not possible to achieve different angular velocity of wheels situated on one axle. Wheelset is situated in the track with a transverse clearance. The wheel tread has cone, respectively curved shape. While transverse deflection of the wheelset from track axle, the instantaneous rolling radius of the wheel is changed. So is created a presumption of rolling the wheelset through a curved trajectory, as shows Fig. 1.

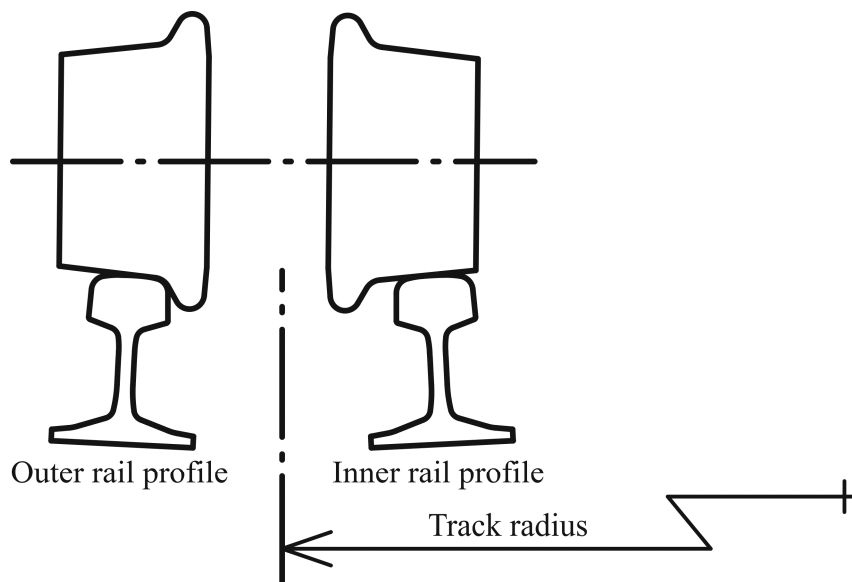


Fig. 1. Wheelset situated in arc track.

In arcs track of small radius, this mechanism of passing arcs cannot ensure passing by clean rolling – without slipping. Slip takes place mostly on the wheel situated on the inner side of arc track. It results in significant wear of wheels and rails in a typical way. Passage of the vehicle

through such wear rails causes considerable dynamic stress of traction vehicle and track, giving a sharp noise.

This problem can be partially solved by designing the wheel treads profile with a larger conicity. Such solution can be used only for low-speed vehicles. Larger conicity of the wheel treads profile causes instability of higher-speed ride. Therefore generally are build arc track with larger radius.

One specific case is the rail vehicles of urban public transport. Those vehicles often need to pass through arc track with radius up to 17 meters. In this case there are significant Wheel slips provided by sharp sounds and rolling contact depreciation.

Partial improvement of the situation can provide flange lubrication. Another possibility is the use of vehicles with independent wheels on one axle. But this complicates construction of the bogies, their traction and the maintenance.

2. Description of the current state

I analyzed the current state in environment of Transport Company of Bratislava on the basis of publicly available information. Rail vehicles for urban transport does not fall within the scope of the railways technical standards. All operating parameters, rail-wheel contact geometry including, fall within the competence of the transport company of corresponding city.

The behavior of the wheelset during passage the arc track is influenced by many parameters. One of these is rail-wheel contact geometry. The current state of rail-wheel contact is shown in Fig. 2. There is used wheel profile TRAM-DPB and rail profile NT1.

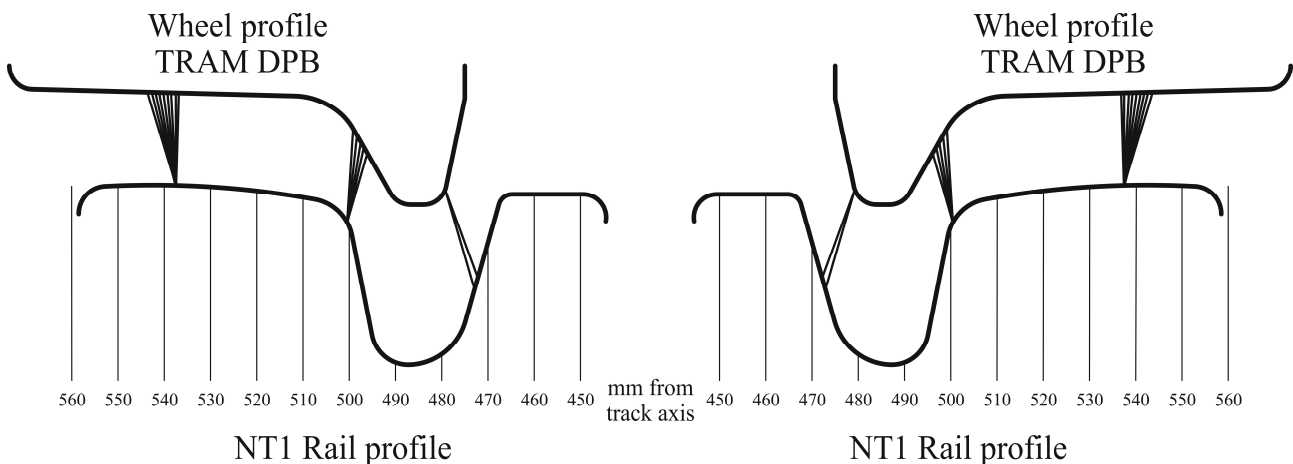


Fig. 2. Contact points function - the current state of rail-wheel contact.

On the basis of Fig. 2 is shown that this wheel profile TRAM-DPB is not suitable for running on a rail shape NT1. When running in a straight track, it is worn only one place on the top of the rail. When running in arc track, there is a two-point rail-wheel contact. It is again an unfavorable state. The contact points are unequally distributed on the surface of both parts. The small conicity of the wheel's running surface does not allow to change the wheel radius in arcs track in sufficient range – like is shown on Fig. 1.

The existing vehicles are operating on lines, where is necessary to overcome arcs track of very small radius. On the crossroads and at the turn-back places are usually used tracks with a radius up to 20 meters. Exceptionally are used tracks with a radius up to 17 meters. Passing of such arcs track leads to two point rail-wheel contact. There is a slip between wheel and rail, forming typical wear of rails. It can be assumed that a significant part of the wheel wear is caused just by transition through arcs of very small radius.

Notable is also the noise burden of the environment resulting from such operation. Those negative phenomena are nowadays suppressed only by flange lubrication in the second contact

point area. Therefore are in the track before tight arcs, installed special equipment – lubricating points, as is shown in Fig. 3. This is not a satisfactory solution in reducing noise, especially in wet weather.

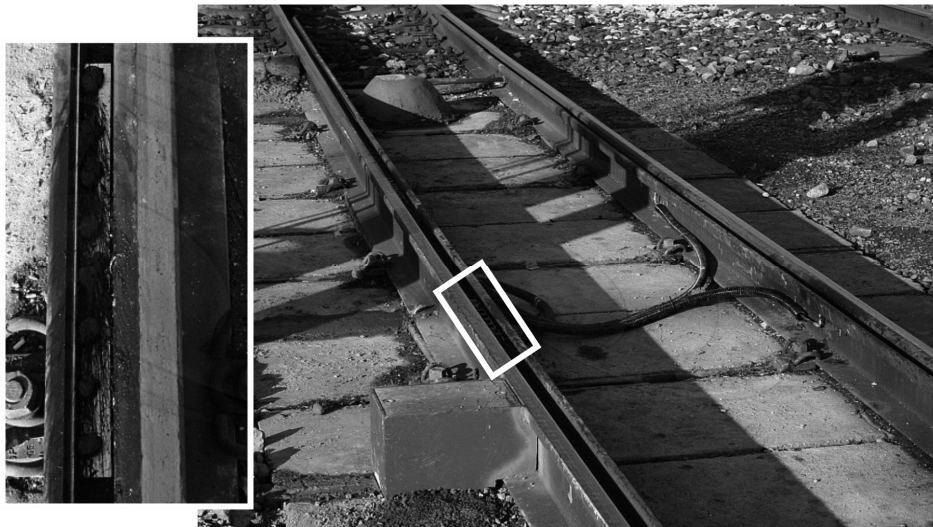


Fig. 3. Lubricating point installed in the track.

Usage of bogies with independent wheels on one axle cut probably provided only a partial solution. Nowadays are developed some new types of tram-bogies, which realize radial shooting of each wheel in track arcs using special mechanical coupling. The wheels are not connected by an axle, so are created the conditions for better behavior of the bogie when running trough curved track. An example of such bogie shows Fig 4.

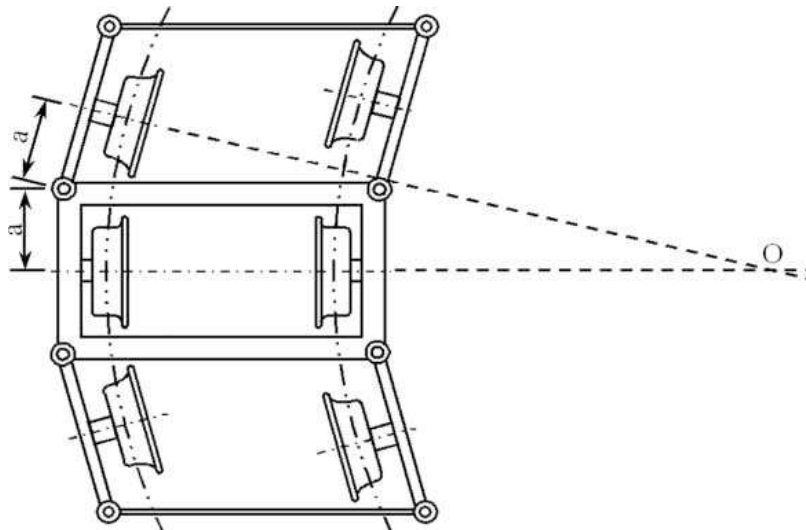


Fig. 4. An example of a new developed bogie.

Potential usage of such bogies would require costly exchange vehicle fleet. Complicated conception of those bogies, as well as construction of the traction, would probably require complicated and expansive maintenance.

3. The proposed solution

The proposed solution is based on knowledge of the properties of one very specific kind of rail, which was used in tight curves on siding of certain producers, at the beginning of the 20th century.

The track of nominal gauge 1435 mm was special designed to make possible riding of the flange for wheel, which is situated on the outer side of arc track. The principle of this track shows Fig. 5.

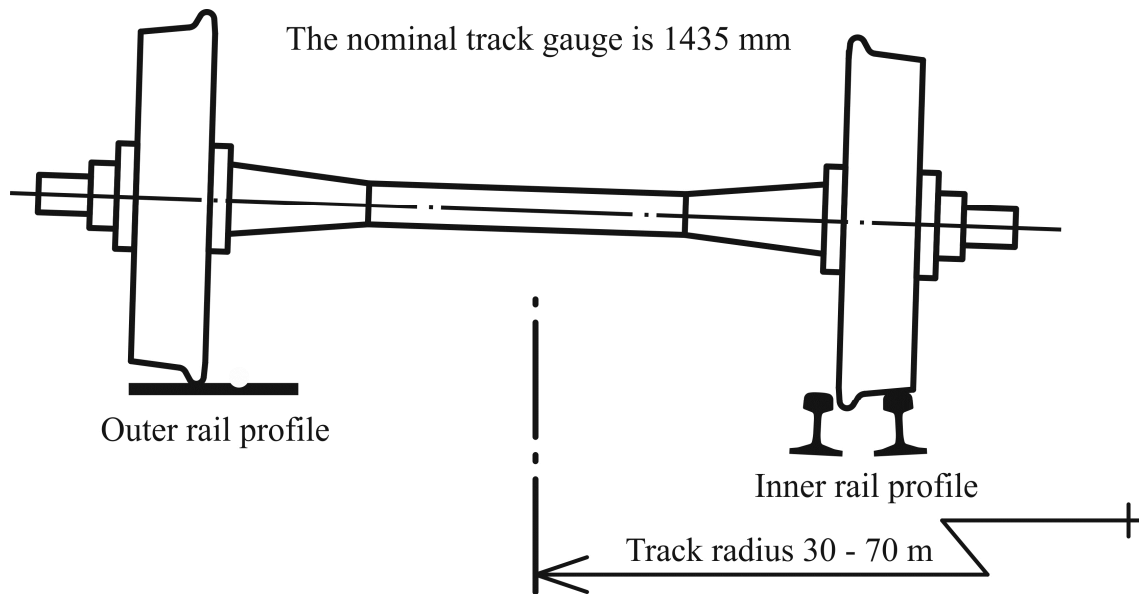


Fig. 5. The principle of very special kind of rail, used at the beginning of the 20th century.

Thus strongly enlarged difference of rolling radius of the wheels on the same axle allowed some vehicles to pass trough track arc radius up to 30 meters. Construction of such track was progressed through several innovations. The last version even allowed passing of 3-axle engines. The changeover place between casual track and special track is shown at Fig. 6.

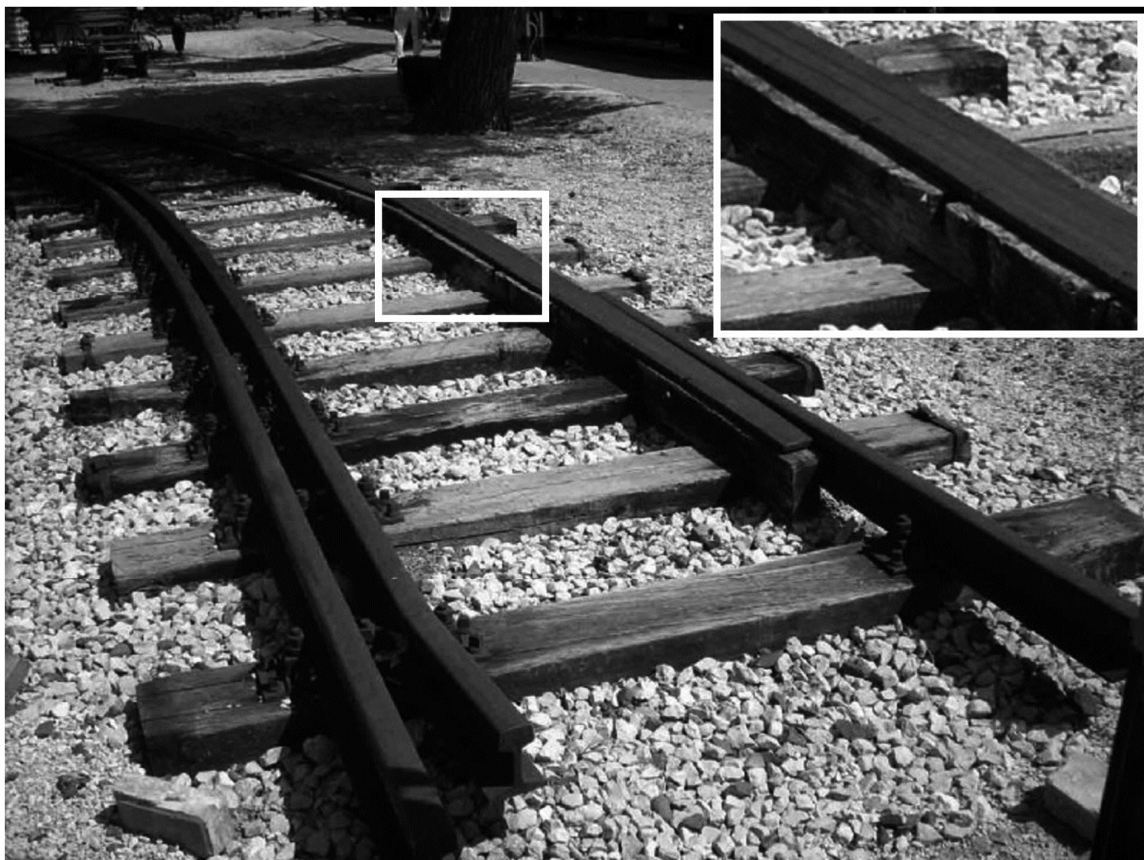


Fig. 6. The changeover place between casual track and special track.

Operation on this track had some special rules. For example, all couplers must be disconnected, so the train must be always pushed by the locomotive. Only 2-axle wagon with short axle-distance could be used. The speed limit on the track was 10 km/h.

Based on the information obtained by analyzing the special rails, I propose to solve the issue of passing trams through arc track of small radius using of special rails geometry. The special geometry should to make possible riding of the flange for wheel, which is situated on the outer side of arc track.

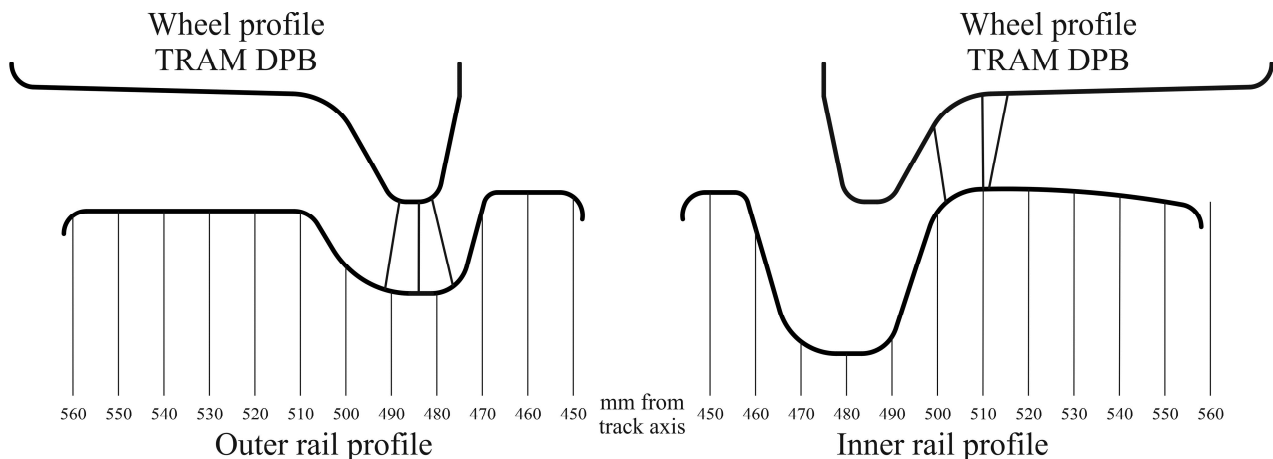


Fig. 7. Contact points function - proposed rail-wheel contact in arc, track radius 18 meters.

Fig. 7 shows the proposed rails geometry. The left part of the picture shows the rail-wheel situation on the outer side of arc track. The right part of the picture shows the rail-wheel situation on the inner side of arc track.

Riding flange of the wheel situated on the outer side of arc track causes enlargement of rolling radius difference by jump. The wheelset tends to accrue to the inner rail. Therefore, the geometry of the inner rail is designed to allow fine tuning of the wheel rolling radius to the value, which is needed for passing the track arc without slip between wheel and rail.

For the transition between straight track of current geometry and sharp curved track of proposed geometry will be used rails with the varying profile according to the arc track radius.

Geometry of the rails is proposed special to wheel profile TRAM-DPB. This solution offers of the kinematic point of view more advantageous way of passing arc track. It is expected, that the proposed rail profile will reduce the longitudinal forces in the wheelset guidance by two-third. Moreover, the proposed rail profile will reduce the longitudinal forces in rail-wheel contact by one half. Therefore the wear and noise reduction can be expected. The proposed solution will be able to use for the existing vehicle fleet. After wear of the current rail in sharp arcs, they can be easy replaced by newly designed rails.

4. Conclusion

I expect that the newly designed track geometry can have a significant positive impact on driving properties of trams in arc tracks with extremely small radius. The use of the proposed track can minimize noise emission and can reduce wear rate of the rail-wheel contact in the arcs with very small radius. Nowadays is checked the proposed rails geometry in the light of driving dynamics of the vehicle. It should also be aimed on solving the transition from straight track of the current geometry to arc track with newly designed geometry.

The new proposed rails geometry (Fig. 7) can be useful in arc with very small radius. It can't be useful in the arcs with casual radius (Radius over than 50m). But the currently used wheel profile TRAM-DPB is nowise suitable for running at currently used rail profile NT1. It would be appropriate first to design wheel profile optimized for running at rail profile NT1. So could be



solved the wear and noise problem in the arcs with casual radius. The special rail geometry should be designed in respect of the correct wheel geometry.

References

- [1] GERLICI, J., LACK, T. *The Rail – Wheel contact*. 1st ed. Edis: Žilina, 2004. (In Slovak)
- [2] KALINČÁK, D. *Rail vehicles I*. 1st ed. Edis: Žilina, 2008. (In Slovak)
- [3] WANG, W., SUDA, Y., MICHITSUJI, Y. *Running performance of steering truck with independently rotating wheel considering traction and braking*. Vehicle System Dynamics, 2008.
- [4] JURIKA, L., Šestina, V. *100 years of the Trams in Bratislava*. 1st ed. Alfa: Bratislava, 1995. (In Slovak)
- [5] HONS, J. *The Transport History in the ČSSR territory*. Alfa: Bratislava, 1975 (In Slovak)
- [6] PURGINA, J. *The development of the Railways in Slovakia since 1837 focused to Bratislava*. SAV: Bratislava, 1959. (In Slovak)
- [7] HANUŠ, E. *The Birth of the Railways in Slovakia*. Dopravní nakladatelství: Praha, 1959. (In Slovak)
- [8] TNŽ 73 63 61. *The geometric location and rail layout of railways using the 1000 mm gauge*, ŽSR: Bratislava, 2007. (In Slovak)



Length of weld of welding machine

*Petr Hejma, *František Klimenda, *Jan Kampo

Jan Evangelisty Purkyne University, Faculty of Production Technology and Management, Department of Machines and Mechanics, Usti nad Labem, 400 01 Usti nad Labem, Czech Republic, hejma@fvfm.ujep.cz

Abstract: Some welding robots don't have implemented the own calculation of the length of weld from welding program enrollment. This is complicates the techno-economic parameters of the welding process. These calculations have to be made analytically. For simple calculations straight line welds can be used a linear interpolation. . For complicated welds (e.g. welding of pipes) we must for calculations length of weld used a straight line, circle or curvilinear interpolation. This article deals by the calculation of length of welds from enrollment of welding program which is generated by welding robot. For this calculation is used the circular interpolation.

Keywords: Welding robot, Welding program, Straight line, Circle interpolations.

1. Introduction

The statistical data of the CNC programs are an important basis for process of optimization. The software for creations of CNC programs (e.g. EdgeCam) usually consists of a time record of active motion of tool. From these information, the cutting speed length can be found. The accuracy of this length of cut is sufficient for a many applications in industry. The different situation is for industrial robots, where these information is often lacking. Determining the length of path of movement of the industrial robot is sometimes important. In most case we are looking for only coordinate of endpoints (e.g. moving of components from point A to point B, i.e. coordinates of these points). In some cases this is an indication of the path of length of the end point of the robot substantial (e.g. a welding robots, where we need know the length of weld). In this case the time of the weld id recorded (e.g. time of the arc burning, i.e. from the time function of the electric current that is flowing through the welding wire), but to obtaining this information we need installation of other measurement and evaluation devices.

2. Methodic

The method that is used to obtain the statistical data from CNC program of welding is usually dependent on the type of programming. The programming can be performed by

- *absolute method* – description of welding program, in which the position of the robot is defined by the number of pulses of electric current to the stepper motors of the individual axes of the robot. The number of pulses is a direct proportional to the rotation of individual step of motors
- *relative method* – description of welding program, in which the position of the robot, i.e. position of TCP (Tool Centre Point - the end of the welding wire) is assigned to the chosen coordinate system and is thus defined in Cartesian coordinates. Performing the positional commands defined in enrollment program the robot control system continuously calculates by the inverse kinematic.

To obtain the information from welding program we must know the syntax of welding program. The methodology has been processed for welding program of firma Yaskawa. To explain this

All three parts of the welding program (Tab. 1) are interconnected alphanumeric designation $Cvwxyz$ (where v, w, x, y and z are whole numbers, e.g. C00011).

Format of the program was modified by algorithm which was implemented in PHP (hypertext preprocessor) for further calculations. The first and the third column were paired, shown in Tab. 1. To appropriate cells of the table editor were divided the individual numbers. The rows that do not contribute to the technological commands (instructions for crossing the robot) were removed.

The result of this modification is shown in Fig. 1

	A	B	C	D	E	F	G	H	I
1			B_{ix}	B_{iy}	B_{iz}	R_{ix}	R_{iy}	R_{iz}	
2	INST	MOVC	720,073	-746,649	-9,263	173,3554	7,9775	-8,9394	11
3	WELD	ARCON							
4	INST	MOVC	719,792	-748,441	-4,339	173,3549	7,9768	-8,9399	11
5	INST	MOVC	712,982	-756,642	6,695	173,8917	8,0508	-23,4548	11
6	INST	MOVC	700,625	-765,761	8,751	173,8909	8,051	-56,9822	11
7	INST	MOVC	687,257	-772,185	-0,699	173,8888	8,0545	-92,1418	11
8	WELD	ARCOF							
9	INST	MOVJ	1320,485	-0,256	640,569	-179,931	-76,1011	-0,0713	100

Fig. 1. Dates of welding program who are needed for analysis.

In Fig. 1 the column A defines the character of instruction, column B defines the specific command. The further specification is listed in columns C up to I, where columns C up to H define the position and the column I defines the speed. The command "MOVJ" defines the speed in % of maximum speed.

The input dates for calculation are the coordinates of the points $B_i = [B_{ix}; B_{iy}; B_{iz}]$. We assume that we process n points, i.e. B_1, \dots, B_n .

For each pair of consecutive points the length of the linear interpolation can be determine. For each set of three of consecutive points the length of the circular interpolation can be determine.

Let the lengths of the linear interpolations between the points B_i, B_{i+1} be denoted L_i , for $i = 1, \dots, n-1$, circular interpolations between points B_i, B_{i+1}, B_{i+2} , be denoted o_i , for $i = 1, \dots, n-3$ and let the circular interpolation of the three last points B_{n-2}, B_{n-1}, B_n be o_{n-2} . The calculation for last triad of points differs by determining the angle, which correspond to the circular arc. The total length of the composed of weld from commands of the circular interpolation is defined as the sum of o_i for $i = 1, \dots, n-2$. This circular interpolation is from the command "ARCON" to the command "ARCOF". This article describes the calculation for one weld. To calculate more welds the second index (e.g. j) for identification of individual welds can be used.

Linear interpolation – length between the points B_i and B_{i+1} is given by

$$L_i = \sqrt{(B_{(i+1)x} - B_{ix})^2 + (B_{(i+1)y} - B_{iy})^2 + (B_{(i+1)z} - B_{iz})^2} \text{ for } i = 1, 2, \dots, n-1 \quad (1)$$

Circular interpolation – weld which is composed from commands for circular interpolation can be defined by n points, while $n \geq 3$.

The example of weld which is defined by commands of circular interpolation. It is intended by 5 points – Fig. 2. The weld of points are identified by B_1 up to B_5 . We can use the circular interpolation for interspaces a circle by triplet of consecutive points, if this points do not lie on a straight line.

The default consideration: The points B_i, B_{i+1} and B_{i+2} defines a triangle in space. Finding the circular circumscribing this triangle and calculating the length of the arc is challenging. The circular arc is defined by a circle, specified by points B_i, B_{i+1} a B_{i+2} . From point B_1 to point B_{n-2} the length of a circular arc o_i between points B_i , and B_{i+1} (where $i = 1, \dots, n-3$) can be calculated. The length of circular arc o_{n-2} can be found from the point B_{n-2} to point B_n ($B_{n-2}; B_{n-1}; B_n$). To determine the length of the arc we must determine the center and radius of a circle that is passing through the actual three points, angle that is corresponding to the circular arc, and finally the length of arc. The coordinate

of the center of lines B_i, B_{i+1} and B_{i+1}, B_{i+2} can be determine for each set of three consecutive points. Thereafter we need to determine the direction vectors axis of triangle B_i, B_{i+1}, B_{i+2} . The lines which correspond to the axes of a triangle can't be parallel or skew lines (because the points of triangle do not lay on the circle). These lines are intersecting in a single point – center of the search circle.

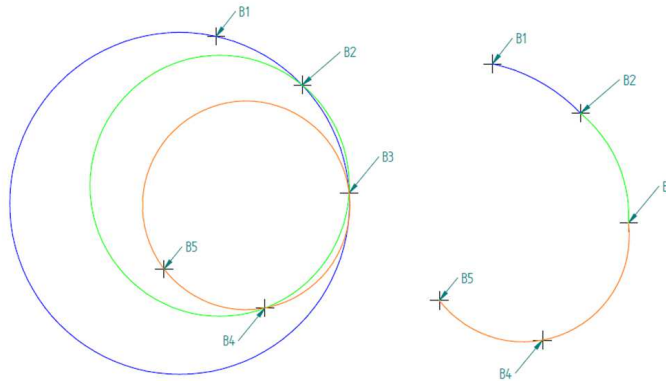


Fig. 2. Circular interpolation.

Subtracting the coordinates of two points in space the following are obtain

$$\vec{u} = B_{i+1} - B_i = (u_x; u_y; u_z) \quad (2)$$

$$\vec{v} = B_{i+2} - B_{i+1} = (v_x; v_y; v_z) \quad (3)$$

The plane τ is defined by the points B_i, B_{i+1} and B_{i+2} . In this plane lies the direction vectors \vec{u} and \vec{v} . The normal vector \vec{n} of plane τ is expressed by vector product of the direction vectors \vec{u} and \vec{v}

$$\vec{n} = \vec{u} \times \vec{v} = (u_y v_z - u_z v_y, u_z v_x - u_x v_z, u_x v_y - u_y v_x) = (n_x; n_y; n_z) \quad (4)$$

The vectors \vec{u} and \vec{v} form two side of a triangle (B_i, B_{i+1} a B_{i+2}). The coordinate of the center of these parties are calculated from these two sides. These sides are formed by vector \vec{u} (line B_i, B_{i+1} – (5)) and \vec{v} (line B_i, B_{i+2} – (6)).

$$S_{B_i, i+1} = \left[\frac{B_{(i)x} + B_{(i+1)x}}{2}; \frac{B_{(i)y} + B_{(i+1)y}}{2}; \frac{B_{(i)z} + B_{(i+1)z}}{2} \right] \quad (5)$$

$$S_{B_i, i+2} = \left[\frac{B_{(i)x} + B_{(i+2)x}}{2}; \frac{B_{(i)y} + B_{(i+2)y}}{2}; \frac{B_{(i)z} + B_{(i+2)z}}{2} \right] \quad (6)$$

In this article we are looking a circumscribed circle by points B_i, B_{i+1} a B_{i+2} , which is formed a triangle (the center of the circumscribed circle V_i is lies on the intersection of the axes pages).

The vectors \vec{w}_1 (7) a \vec{w}_2 (8) result from the vector product of the normal vector \vec{n} and vectors \vec{u} and \vec{v} . The vector \vec{w}_1 is perpendicular on the vector \vec{u} and vector \vec{w}_2 is perpendicular on the vector \vec{v} . The vector \vec{w}_1 is used as the direction vector of the line p_1 . This line lies in the plane τ and pass through the center of the line B_i, B_{i+1} and will be perpendicular to it. The vector \vec{w}_2 is used as the direction vector of the line p_2 . This line lies in the plane τ and passes through the center of the line B_i, B_{i+2} and is perpendicular to it.

$$\vec{w}_1 = (u_y n_z - u_z n_y, u_z n_x - u_x n_z, u_x n_y - u_y n_x) = (w_{(1)x}; w_{(1)y}; w_{(1)z}) \quad (7)$$

$$\vec{w}_2 = (n_y v_z - n_z v_y, n_z v_x - n_x v_z, n_x v_y - n_y v_x) = (w_{(2)x}; w_{(2)y}; w_{(2)z}) \quad (8)$$

Equation (9) is a parametric equation of a straight line p_1 and equation (10) is a parametrical equation of a straight line p_2 .



$$x = S_{(B_{i,i+1})_x} + t \cdot w_{(1)_x}; \quad y = S_{(B_{i,i+1})_y} + t \cdot w_{(1)_y}; \quad z = S_{(B_{i,i+1})_z} + t \cdot w_{(1)_z}, \quad t \in \mathfrak{R} \quad (9)$$

$$x = S_{(B_{i,i+2})_x} + s \cdot w_{(2)_x}; \quad y = S_{(B_{i,i+2})_y} + s \cdot w_{(2)_y}; \quad z = S_{(B_{i,i+2})_z} + s \cdot w_{(2)_z}, \quad s \in \mathfrak{R} \quad (10)$$

The coordinate of the lines p_1 and p_2 will be equal in the intersection. The coordinates of the center of the circle is obtain by solving these three equations (9, 10) with two unknowns t, s . These equations have a single solution. The coordinates of the center V_i circumscribed circle of the triangle (B_i, B_{i+1} a B_{i+2}) we are determine by substituting the parameter t into the parametrical equation of straight line (9).

$$V_i = [V_{ix}; V_{iy}; V_{iz}] \quad (11)$$

The size of the radius of the circumscribing circle is given by

$$R_i = \sqrt{(B_{ix} - V_{ix})^2 + (B_{iy} - V_{iy})^2 + (B_{iz} - V_{iz})^2} \quad (12)$$

Therefore expressing the vectors that are designed by center V_i and by individual points (h_1, h_2 for all triplets of except the last and h_1, h_3 for the last triad), the following is obtained

$$h_1 = (B_{ix} - V_{ix}; B_{iy} - V_{iy}; B_{iz} - V_{iz}) = (h_{1x}; h_{1y}; h_{1z}) \quad (13)$$

$$h_2 = (B_{(i+1)x} - V_{ix}; B_{(i+1)y} - V_{iy}; B_{(i+1)z} - V_{iz}) = (h_{2x}; h_{2y}; h_{2z}) \quad (14)$$

$$h_3 = (B_{(i+2)x} - V_{ix}; B_{(i+2)y} - V_{iy}; B_{(i+2)z} - V_{iz}) = (h_{3x}; h_{3y}; h_{3z}) \quad (15)$$

The angle φ_i between two adjacent vectors is given as following scalar product

$$\varphi_i = \arccos \frac{h_{1x}h_{2x} + h_{1y}h_{2y} + h_{1z}h_{2z}}{\sqrt{h_{1x}^2 + h_{1y}^2 + h_{1z}^2} \sqrt{h_{2x}^2 + h_{2y}^2 + h_{2z}^2}} \text{ e.i.} \quad (16)$$

$$\varphi_i = \arccos \frac{h_{1x}h_{3x} + h_{1y}h_{3y} + h_{1z}h_{3z}}{\sqrt{h_{1x}^2 + h_{1y}^2 + h_{1z}^2} \sqrt{h_{3x}^2 + h_{3y}^2 + h_{3z}^2}}$$

The length of arc between two adjacent points is then

$$o_i = \varphi_i \cdot R_i \quad (17)$$

The total length of the weld o is composed from commands of circular interpolation. That is composed from the command "ARCON" to the command "ARCOF"

$$o = \sum_{i=1}^{n-2} \varphi_i \cdot R_i \quad (18)$$

3. Solution and discussion

This article has shown the challenges faced when welding a weld flange to a tube of diameter 48 mm by means of a welding robot. The program for the welding robot was shown in Tab. 1. The coordinate of points which the weld passes were shown in Fig. 1. The length of the weld was determined by analytical method using the circular interpolation method that consists of five points. The fifth point determine the end of the welding wire. The coordinate of this points (B_1 up to B_5), the length of the individual weld arc from which the weld and total length o of the circular interpolation are shown in Tab. 2. The accuracy of this circular interpolation was subsequently verified by experimental measured data of the centerline of the weld. The midline was created by finger of the welding robot, where the welding wire has been replaced by a measuring device.



i	B_i [mm]	o_i [mm]	o [mm]
1	$B_1 = [720,073; -746,649; -9,263]$	$o_1 = 5,261$ $o_2 = 15,658$ $o_3 = 33,822$	$o = 54,741$
2	$B_2 = [719,792; -748,441; -4,339]$		
3	$B_3 = [712,982; -756,642; 6,695]$		
4	$B_4 = [700,625; -765,761; 8,751]$		
5	$B_5 = [687,257; -772,185; -0,699]$		

Tab. 2. Calculation of the weld length.

Using this device the circular interpolation length was measured at 54,9 mm. By analytical method the length was given as 54,74 mm. The relative error between the measured and calculate data was 0,16 mm, meanwhile the absolute error was found at 0,3%.

4. Conclusion

The article describes the proposed methodology for calculating the length of the weld, which is defined by the linear and the circular interpolation method. In the CNC program are description the coordinates of the points, that is defined the interpolation. From the data of the welding program using the linear and the circular interpolation, the individual length of welds are determined. The basic for the analytical solution of the length of weld are the coordination of the individual points. Therefore we must use the relative method of welding program was used. The above example of calculation and the experimental solution has a very good agreement between the calculated and experimental solutions. If can be concluded that the proposed method is suitable for determining the length of the weld from the welding program of the welding robot.

Acknowledgement

The research work is supported by the SGS – UJEP, Czech Republic.

References

- [1] BARTSCH, H. J. *Mathematical formulas*. (In Czech) Praha: Mladá fronta, 2002.
- [2] BURDA, P. *Algebra and analytic geometry*. (In Czech) Ostrava 1997.
- [3] Robots manual Yaskawa.
- [4] BLATNÝ, J. *Standardization of interface*. (In Czech) MON, Praha, 1990.
- [5] NIEBEL, B., FREIVALDS, A. *1999 Methods, standards, and work design*. (10th ed.) New York WCB/McGraw-Hill
- [6] STADLER, W. *Analytical Robotics and Mechatronics*. McGraw-Hill Inc., 1995., 7-ISBN 0-07-060608-0.



Comparing Heat Transfer of Heat Pipe and Copper Bar.

Peter Hrabovský, Štefan Papučík

University of Žilina, Faculty of Mechanical Engineering, Department of Power Engineering, Univerzitná 1,
01026 Žilina, Slovakia, {peter.hrabovsky, stefan.papucik}@fstroj.uniza.sk.

Abstract. This article discusses the comparison heat transfer between the copper bar and the heat pipe, which is made of copper and water is distilled working fluid. The significance of this experiment consists in comparing of the heat transfer in two individual samples. On the basis of measured and calculated data can be constructed the plot on which we can see the contrast of heat transfer between heat pipe and copper bar.

Keywords: Heat pipe, Full copper bar, Heat transfer.

1. Introduction

This paper deals with comparing the heat transfer of the heat pipe and copper bar of the same diameter and length. Based on measurements of the two samples we can draw conclusions creating imaginary material which will have similar properties as thermal heat transfer tube. This imaginary material we can use for simulation of heat transfer instead of heat pipe.

1.1. Heat transfer

The most efficient method of heat transfer is conduction. This mode of heat transfer occurs when there is a temperature gradient across a body. In this case, the energy is transferred from a high temperature region to low temperature region due to random molecular motion (diffusion). Conduction occurs similarly in liquids and gases. Regions with greater molecular kinetic energy will pass their thermal energy to regions with less molecular energy through direct molecular collisions. In metals, a significant portion of the transported thermal energy is also carried by conduction-band electrons. Different materials have varying abilities to conduct heat [1].

Heat pipes employ evaporative cooling to transfer thermal energy from one point to another by the evaporation and condensation of a working fluid or coolant. Heat pipes rely on a temperature difference between the ends of the pipe, and cannot lower temperatures at either end beyond the ambient temperature (hence they tend to equalize the temperature within the pipe) [2].

When one end of the heat pipe is heated the working fluid inside the pipe at that end evaporates and increases the vapor pressure inside the cavity of the heat pipe. The latent heat of evaporation is absorbed by the vaporization of the working fluid reduces the temperature at the hot end of the pipe [3].

The vapor pressure over the hot liquid working fluid at the hot end of the pipe is higher than the equilibrium vapor pressure over the condensing working fluid at the cooler end of the pipe, and this pressure difference drives a rapid mass transfer to the condensing end where the excess vapor condenses, releases its latent heat, and warms the cool end of the pipe. Non-condensing gases (caused by contamination for instance) in the vapor impede the gas flow and reduce the effectiveness of the heat pipe, particularly at low temperatures, where vapor pressures are low. The speed of molecules in a gas is approximately the speed of sound, and in the absence of noncondensing gases (i.e., if there is only a gas phase present) this is the upper limit to the velocity with which they could travel in the heat pipe. In practice, the speed of the vapor through the heat pipe is limited by the rate of condensation at the cold end and far lower than the molecular speed [4].

The condensed working fluid then flows back to the hot end of the pipe. In the case of vertically oriented heat pipes the fluid may be moved by the force of gravity. In the case of heat pipes containing wicks, the fluid is returned by capillary action [5].

2. Copper bar

Copper and copper alloys are widely used in a variety of products that enable and enhance our everyday lives. They have excellent electrical and thermal conductivities, exhibit good strength and formability, have outstanding resistance to corrosion and fatigue, and are generally non-magnetic. Pure copper is used extensively for electrical wire and cable, electrical contacts and various other parts that are required to pass electrical current. Coppers and certain brasses, bronzes and copper nickels are used extensively for automotive radiators, heat exchangers, home heating systems, solar collectors, and various other applications requiring rapid conduction of heat across or along a metal section. Because of their outstanding ability to withstand corrosion, coppers, brasses, bronzes and copper nickels are also used for pipes, valves and fittings in systems carrying potable water, process water or other aqueous fluids, and industrial gases. Measurement sample is in figure below (Fig. 1). The sample consist of copper bar in length 400 mm and diameter 18 mm.



Fig. 1. Copper bar.

3. Heat pipe

We used a heat pipe to transfer heat from the heat source to the point of consumption of heat with high efficiency and low temperature difference. It is a sealed device in which the net substance (water) exist in the liquid and the gas phase at a pressure below atmospheric pressure (vacuum). Cleanliness of the working fluid is an important parameter for the efficiency of the heat pipe, in terms of heat transfer. The actual heat pipe (**Chyba! Nenašiel sa žiaden zdroj odkazov.**) consists of evaporation, condensation, and the adiabatic section. In the evaporator the working fluid is evaporated at a temperature below normal conditions. In the adiabatic section is not exchanged heat transfer through the ambient area, due to the isolation of a few working fluid to the wall of the heat pipe condensation film of condensed working fluid. In the condenser the vapor of working fluid condenses on the walls of the heat pipe, which transmit latent (condensing) heat through the walls of the heat pipe to the heat consumption point [6].

Filling of the heat pipe in this experiment is the distilled water. The production process of the heat pipe consists of the preparation of the material, the soldering of components, filling the working fluid and its evaporation to required volume. The final volume of the working fluid is about 20% of the total volume of the heat pipe, which is about 16 ml of water. This volume has been established on the basis of previous experiments that compared the effectiveness of the heat pipe at various percentages volumes of the working fluid. The value 20% of the working fluid in the heat pipe reached the best results. The diameter of the heat pipe is 18 mm and length 400 mm.

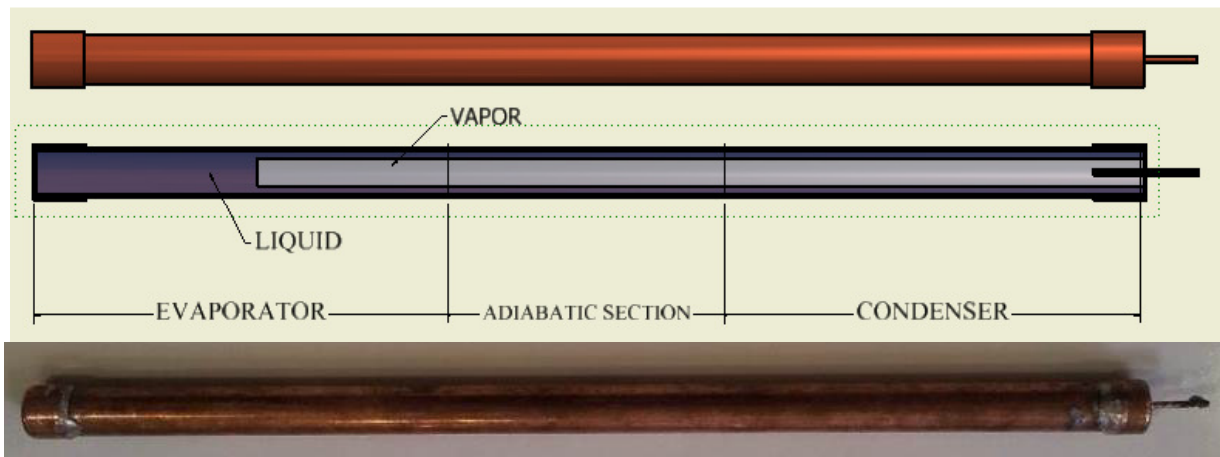


Fig. 2. Heat pipe.

4. Experimental device

Device of experiment consists of two parts (cases), on which the fixed the copper bar or the heat pipe. In Fig. 3 is shown the experimental device.

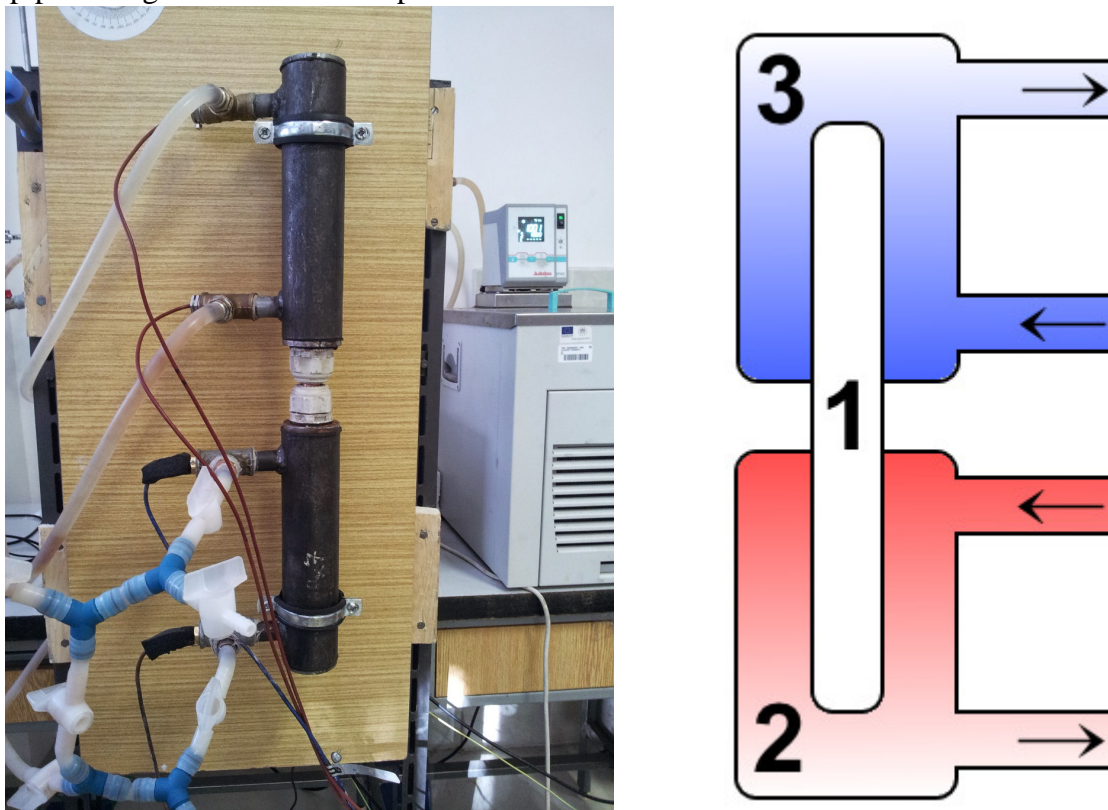


Fig. 3. Real view on the experimental device in left and scheme of experimental device in right.

A case situated in the upper part, (**Chyba! Nenašiel sa žiaden zdroj odkazov.** ref. 3) is the part of a cooling device. It is connect to the cooling device, the cooling medium is water. The water circulates in a closed circuit between the cooling device and the case. In the cooling circuit included the safe cases, in which there are devices for measuring the temperature at entry and exit of water. In the circuit is included flow meter too that shows speed of flow of the refrigerant in a closed circuit. A case situated at the bottom part (**Chyba! Nenašiel sa žiaden zdroj odkazov.** ref. 2) is the heating of the device. It is connected to the heating device, the working medium is water. In a closed heater circuit included thermocouples for temperature measurement inlet and outlet water from the case, flow meter for flow measurement.. The circuit contents a valves that get disconnect

the heater case when it is need for cooling with cold water, while avoiding the cooling of heating up the water in the heater circuit. Measured samples are mounted in the cases by caulked joints with seals, which are not being relaxed, possible leakage of cooling or heating of the working fluid.

4.1. Measurement of copper bar

In the figure (Fig. 4), and in the table (Tab. 1), below we can see full process and measurement values of copper bar. The heated water was about 70 °C, the cooler water was about 10 °C. In such a flow rate of cooling water, we measured power of copper bar about 60 W. We can see that the outlet temperature of cooling water is stable.

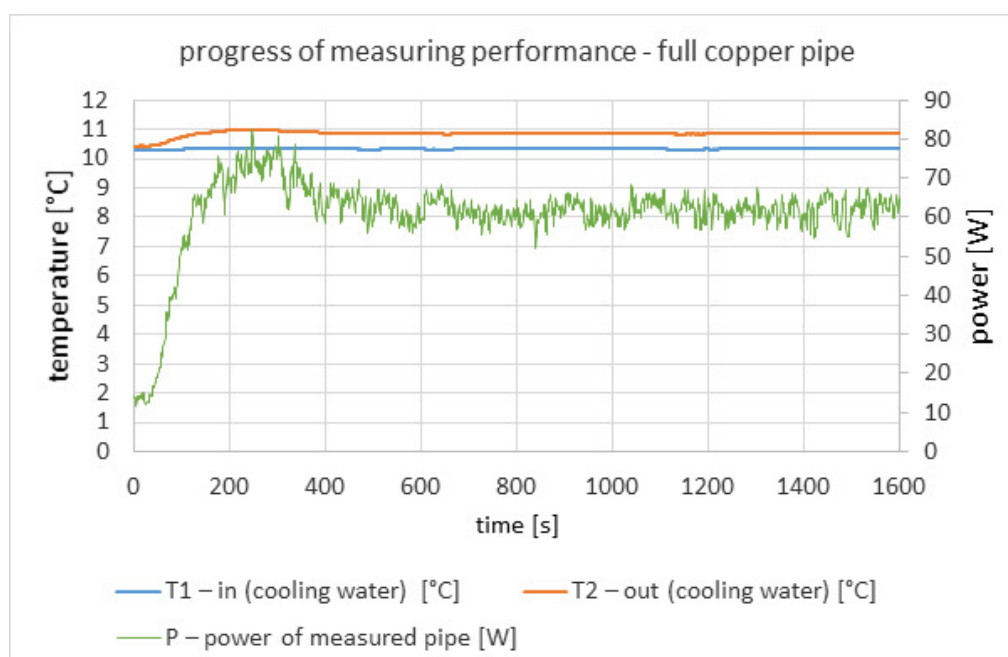


Fig. 4. Full process of measurement of copper bar.

Time step of measuring	Temperature of heating water		Mass flow of heating water	Temperature of cooling water		Mass flow of cooling water	P – power of measured pipe
	Inlet	Outlet		Inlet	Outlet		
[s]	[°C]	[°C]	[kg.s ⁻¹]	[°C]	[°C]	[kg.s ⁻¹]	[W]
400	71.83	71.65	0.078078	10.34	10.87	0.026247	58.38613
500	72.45	71.79	0.077724	10.32	10.85	0.026247	58.38678
600	72.58	71.85	0.078694	10.33	10.84	0.027418	58.68832
700	72.63	71.79	0.078854	10.34	10.85	0.028253	60.47726
800	72.69	71.62	0.078688	10.34	10.84	0.029591	62.09821
900	72.7	71.36	0.078688	10.34	10.85	0.02842	60.83512
1000	72.71	71.06	0.076899	10.35	10.85	0.029591	62.09786
1100	72.72	70.87	0.078362	10.33	10.85	0.028588	62.3931
1200	72.69	70.74	0.078363	10.33	10.84	0.03026	64.77187
1300	72.66	70.63	0.078365	10.34	10.85	0.028922	61.90868
1400	72.69	70.61	0.077713	10.36	10.87	0.027919	59.76089
1500	72.72	70.61	0.077712	10.37	10.88	0.028922	61.90764
1600	72.7	70.57	0.07755	10.34	10.86	0.029591	64.58197

Tab. 1. Table of measurement values of copper bar.

4.2. Measurement of copper bar

In the figure (Fig. 5) and in the table (**Chyba! Nenašiel sa žiaden zdroj odkazov.**) below we can see full process and measurement values of heat pipe. The heated water was about 70 °C, the cooler water was about 10 °C. In such a flow rate of cooling water, we measured power of heat pipe about 500 W. We can see that the outlet temperature is increasing compared to copper bar.

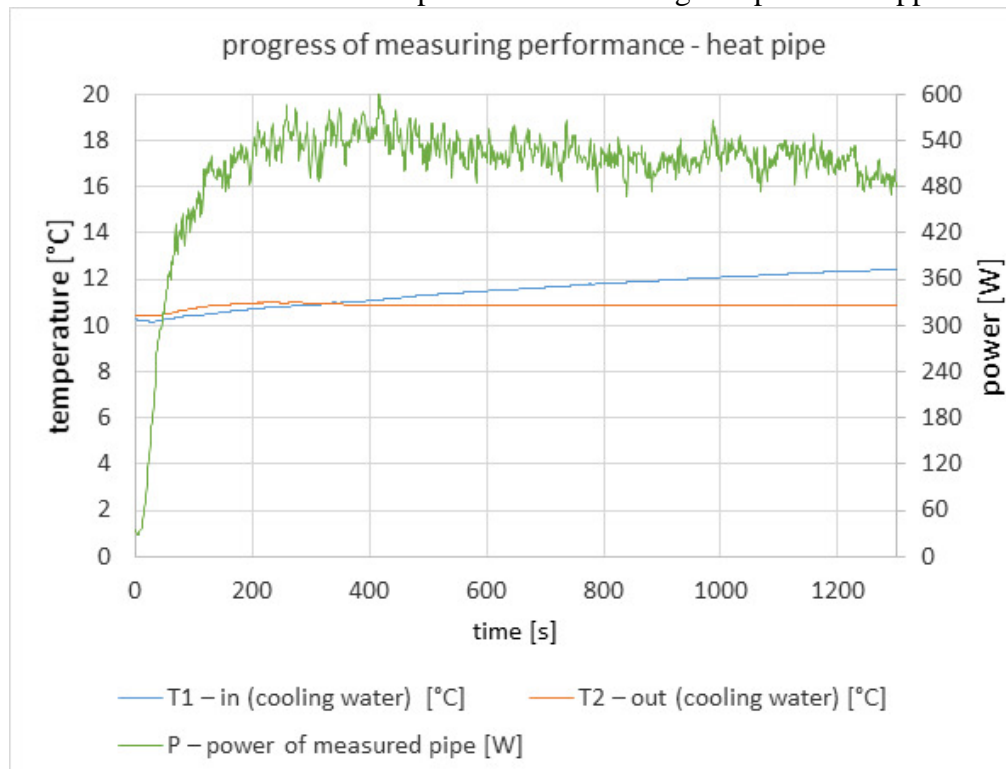


Fig. 5. Full process of measurement of heat pipe.

Time step of measuring	Temperature of heating		Mass flow of heating water	Temperature of cooling		Mass flow of cooling water	P – power of measured pipe
	Inlet	Outlet		Inlet	Outlet		
[s]	[°C]	[°C]	[kg.s ⁻¹]	[°C]	[°C]	[kg.s ⁻¹]	[W]
100	57.63	51.48	0.06984	10.43	14.11	0.02859	441.35
200	67.58	61.87	0.07012	10.72	14.96	0.02959	526.24
300	70.96	65.85	0.07405	10.87	15.32	0.02674	499.21
400	72.25	67.54	0.07578	11.06	15.60	0.02825	537.89
500	72.77	68.38	0.07462	11.31	15.70	0.02891	532.36
600	73.00	68.76	0.07575	11.48	15.69	0.02925	516.40
700	73.08	68.93	0.07591	11.64	15.82	0.03008	527.33
800	73.12	69.05	0.07591	11.81	15.96	0.03008	523.49
900	73.12	69.07	0.07623	11.94	16.04	0.03041	522.90
1000	73.09	69.02	0.07542	12.07	16.14	0.03008	513.34
1100	73.07	69.00	0.07575	12.21	16.35	0.03074	533.72
1200	73.03	68.99	0.07575	12.34	16.32	0.03091	515.86
1300	73.01	68.98	0.07591	12.44	16.18	0.03091	484.74

Tab. 2. Table of measurement values of the heat pipe.



5. Conclusion

Results of this experiment emerge from heat transfer of the copper bar and of the heat pipe. The heat pipe have got the better conductive properties as copper bar. Based on this experiment we can prepare simulation of heat pipe, when we use a substitute material instead of the heat pipe. The substitute material shows us the results of the thermal conduction of heat pipe.

Acknowledgement

This article was elaborated within the solution of project KEGA č.029ŽU-4/2015 „Heat recovery from the technological processes“.

References

- [1] KASANICKY, M., GAVLAS, S., VANTUCH, M., MALCHO, M. *Possibilities of using carbon dioxide as fillers for heat pipe to obtain low-potential geothermal energy*. Experimental fluid mechanics, 2012
- [2] PATSCH, M, LABAJ, J. *Influence of glycerin combustion in experimental burner on production of emissions*. Acta Metallurgica Slovaca conference. ISSN 1338-1660
- [3] NEMEC, P., CAJA, A. *Heat transfer intensification applying thermal tubes*. Acta Metallurgica Slovaca, 2009, vol. 15, No. 1, pp. 215-220.
- [4] NEMEC, P., CAJA, A. *Heat transport visualization of heat pipe by thermovision*. Experimental fluid mechanics, 2010, ISBN 978-80-7372-670-6, pp. 431-434.
- [5] NEMEC, P. *Influence heat transfer limitations of heat pipes on their cooling power*. Transcom, 2009, ISBN 978-80-554-0031-0, pp. 103-108.
- [6] NEMEC, P., MALCHO, M., SMITKA, M., MATUSOV, J. *Performance parameters of clodes loop thermosyphon*. Communications Scientific Letters of the University of Zilina, 2012



Comparing Thermal Conductivity of Heat Pipe and Copper Bar.

Peter Hrabovský, Štefan Papučík, Richard Lenhard

University of Žilina, Faculty of Mechanical Engineering, Department of Power Engineering, Univerzitná 1,
01026 Žilina, Slovakia, {peter.hrabovsky, stefan.papucik, richard.lenhard}@fstroj.uniza.sk.

Abstract. This article discusses the comparison the thermal conductivity between the copper bar and the heat pipe, which is made of copper and a working fluid is the distilled water. The significance of this experiment consists in comparing the thermal performance of heat transfer individual samples. On the basis of measured and calculated data can be constructed the plot on which we can design the replacement material, which will, for the most part with the thermal performance of the heat pipe. Material model that allows us to replace the heat pipe, simplify process of mathematical simulation in a computer software ANSYS.

Keywords: Heat pipe, Copper bar, Heat transfer, Thermal conductivity.

1. Introduction

This paper deals with comparing the thermal conductivity of the heat pipe and copper bar of the same diameter and length. Based on measurements of the two samples we can draw conclusions creating imaginary material which will have similar properties as thermal heat transfer tube. This imaginary material we can use for simulation of heat transfer instead of heat pipe at.

1.1. Thermal conductivity

Thermal conductivity is a material property that tells us and how effectively the material is able to conduct heat. It is the amount of heat per unit of time must pass through the body of per unit of length was a unit temperature gradient (temperature gradient, that is, the proportion of the temperature difference at the ends of the rod and the length of the rod) [1]. It is assumed that the heat is spreading in one direction. In other words: Thermal diffusivity is power (ie. Heat per unit of time) which passes every square meter 1 meter thick plate, which one party has a temperature of 1 Kelvin higher than the other. The characteristic unit of thermal conductivity is $[W \cdot m^{-1} \cdot K^{-1}]$ [2].

2. Copper bar

One sample is a copper bar (Fig. 1). The dimensions of sample is length 400 mm and diameter 18 mm. Material is copper because copper is most used by design of heat exchangers. We use the copper in heating technology, electronics and real life as material of coin.



Fig. 1. Copper bar.

3. Heat pipe

We used a heat pipe to transfer heat from the heat source to the point of consumption of heat with high efficiency and low temperature difference. It is a sealed device in which the net substance (water) exist in the liquid and the gas phase at a pressure below atmospheric pressure (vacuum). Cleanliness of the working fluid is an important parameter for the efficiency of the heat pipe, in terms of heat transfer [3]. The actual heat pipe (**Chyba! Nenašiel sa žiaden zdroj odkazov.**) consists of evaporation, condensation, and the adiabatic section. In the evaporator the working fluid is evaporated at a temperature below normal conditions. In the adiabatic section is not exchanged heat transfer through the ambient area, due to the isolation of a few working fluid to the wall of the heat pipe condensation film of condensed working fluid. In the condenser the vapor of working fluid condenses on the walls of the heat pipe, which transmit latent (condensing) heat through the walls of the heat pipe to the heat consumption point [4].

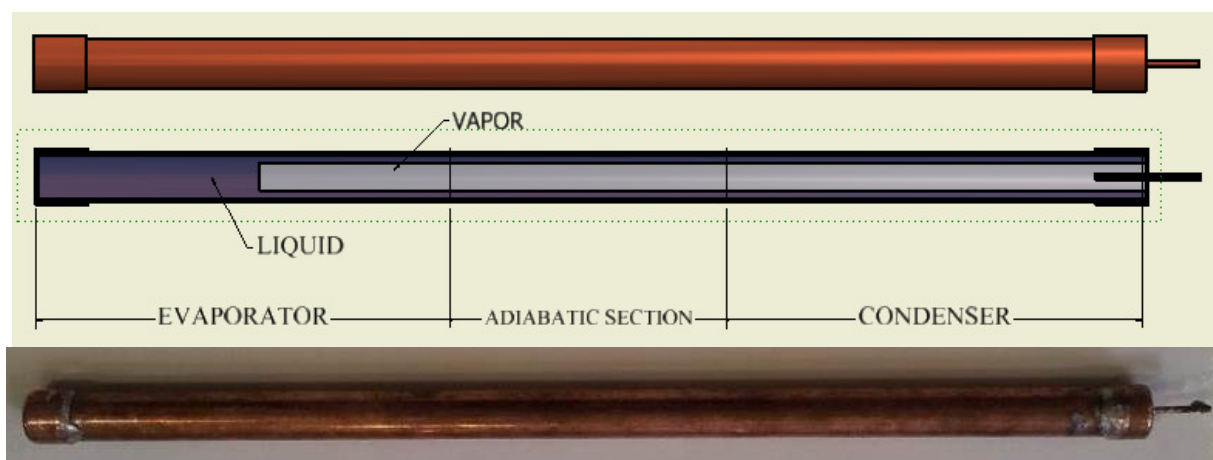


Fig. 2. Heat pipe.

Filling of the heat pipe in this experiment is the distilled water. The production process of the heat pipe consists of the preparation of the material, the soldering of components, filling the working fluid and its evaporation to required volume. The final volume of the working fluid is about 20% of the total volume of the heat pipe, which is about 16 ml of water. This volume has been established on the basis of previous experiments that compared the effectiveness of the heat pipe at various percentages volumes of the working fluid. The value 20% of the working fluid in the heat pipe reached the best results. The diameter of the heat pipe is 18 mm and length 400 mm.

4. Model of simulation

Model consists of three parts: two cases and one sample (copper bar, heat pipe). The one of two samples is fixed in two cases. In Fig. 3 is shown the position of cases and sample in a reality and in a scheme.

A case situated in the upper part, is the part of a cooling device. It is connect to the cooling device, the cooling medium is water. The water circulates in a closed circuit between the cooling device and the case. In the cooling circuit included the safe cases, in which there are devices for measuring the temperature at entry and exit of water. In the circuit is included flow meter too that shows speed of flow of the cooling fluid in a closed circuit. A case situated at the bottom part is the heating of the device. It is connected to the heating device, the working medium is water. In a closed heater circuit included thermocouples for temperature measurement inlet and outlet water from the case, flow meter for flow measurement.. The circuit contents a valves that get disconnect the heater case when it is need for cooling with cold water, while avoiding the cooling of heating up the water in the heater circuit. Measured samples are mounted in the cases by caulked joints with seals, which are not being relaxed, possible leakage of cooling or heating of the working fluid.

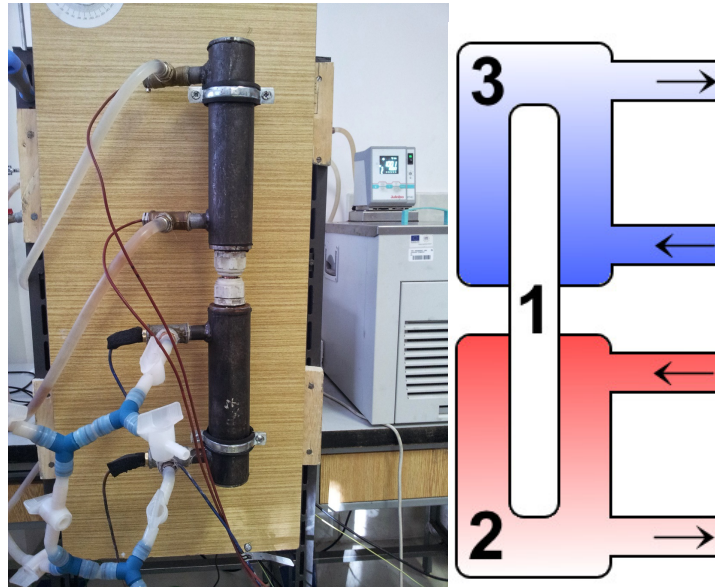


Fig. 3. Real view on the experimental device in left and scheme of experimental test device in right.

The mesh (Fig. 4) of this model consist of 239 302 cells, 1 552 487 faces and 1 306 224 nodes.

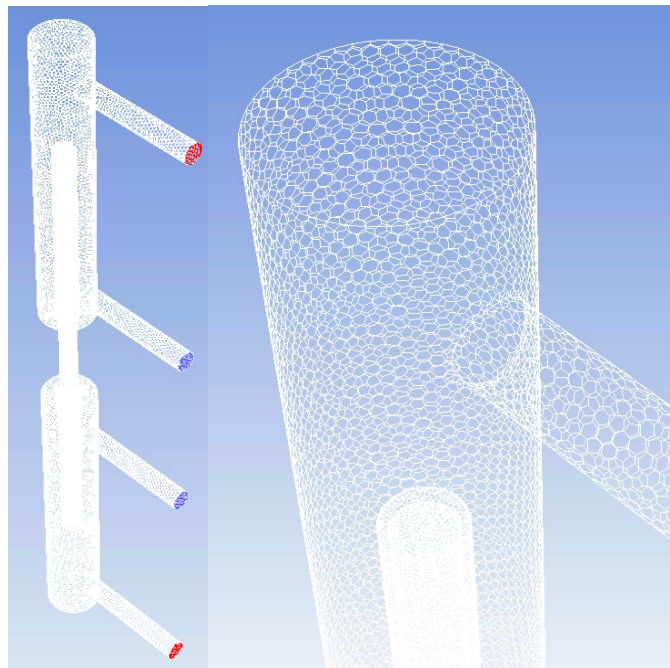


Fig. 4. Mesh of model.

Mains volumes (Fig. 3) are cool water (3) about 10 °C in cooling system, hot water (2) about 70 °C in heating system, samples (1) there are copper bar and heat pipe which is substitute of water vapour.

5. Results of simulation

Simulation of copper bar get us a result similar to averages measurements values. In Fig. 5 is shown heat transfer in copper bar. The heat transfer rate is low. The simulation of this sample was realized with tabular values.

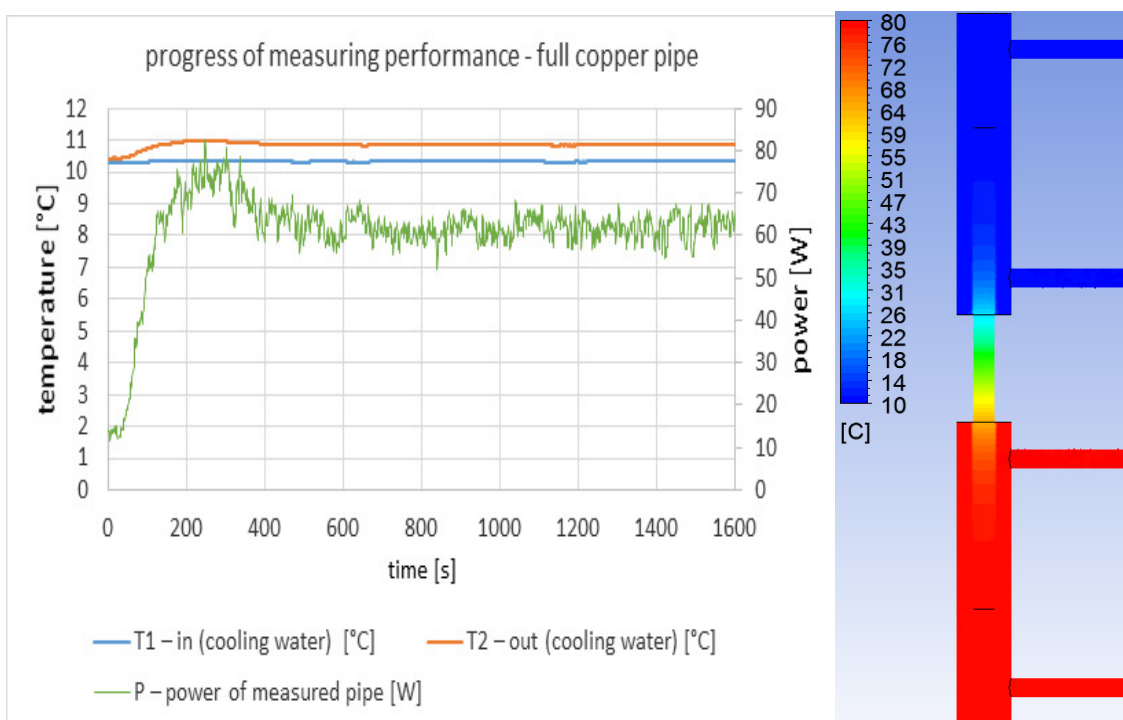


Fig. 5. Heat transfer in copper bar.

In the Fig. 5 we can see the progress of heat transfer in copper bar. The main parameter to influence on the power is called thermal conductivity. From the thermal conductivity emerge the thermal resistance.

The Tab. 1 below is shown us the general thermal properties of copper material.

Property	Value	Unit
Atomic number	29	
Atomic weight	63.54	
Density	8920	kg.m ⁻³
Specific heat	3860	J.kg ⁻¹
Thermal conductivity	394	W.m ⁻¹ .K ⁻¹

Tab. 1. Thermal properties of copper material.

The Tab. 2 is shown measurement values of copper bar in last experiment.

Time step of [s]	Temperature of [°C]		Mass flow of heating water [kg.s ⁻¹]	Temperature of [°C]		Mass flow of cooling [kg.s ⁻¹]	P – power of measured [W]
	Inlet	Outlet		Inlet	Outlet		
400	71.83	71.65	0.07808	10.34	10.87	0.02625	58.37
500	72.45	71.79	0.07772	10.32	10.85	0.02625	58.39
600	72.58	71.85	0.07869	10.33	10.84	0.02742	58.69
700	72.63	71.79	0.07885	10.34	10.85	0.02825	60.48
800	72.69	71.62	0.07869	10.34	10.84	0.02959	62.10
900	72.70	71.36	0.07869	10.34	10.85	0.02842	60.84
1000	72.71	71.06	0.07690	10.35	10.85	0.02959	62.10
1100	72.72	70.87	0.07836	10.33	10.85	0.02859	62.39
1200	72.69	70.74	0.07836	10.33	10.84	0.03026	64.77
1300	72.66	70.63	0.07837	10.34	10.85	0.02892	61.91
1400	72.69	70.61	0.07771	10.36	10.87	0.02792	59.76
1500	72.72	70.61	0.07771	10.37	10.88	0.02892	61.91
1600	72.7	70.57	0.07755	10.34	10.86	0.02959	64.58

Tab. 2. Measurement values of copper bar

Simulation of heat pipe was in progress of more than one steps. One parameter was changed in every step. The parameter is called thermal conductivity. It begin at value 500 [W.m⁻¹.K⁻¹] and continue in 2500, 5000, 10000, 15000, 20000, 25000, 30000, 40000, 45000, 50000 [W.m⁻¹.K⁻¹]. Based on this simulation is substitution (imaginary) material instead of heat pipe. The material is

water-vapour. The water-vapour exist in heat pipe at the action of heat transfer between the ends of sample.

In the Fig. 6 we can see the heat transfer of heat pipe with different thermal conductivity. Here is shown the intensity of heat transfer. With increased thermal conductivity rate of heat transfer grows.

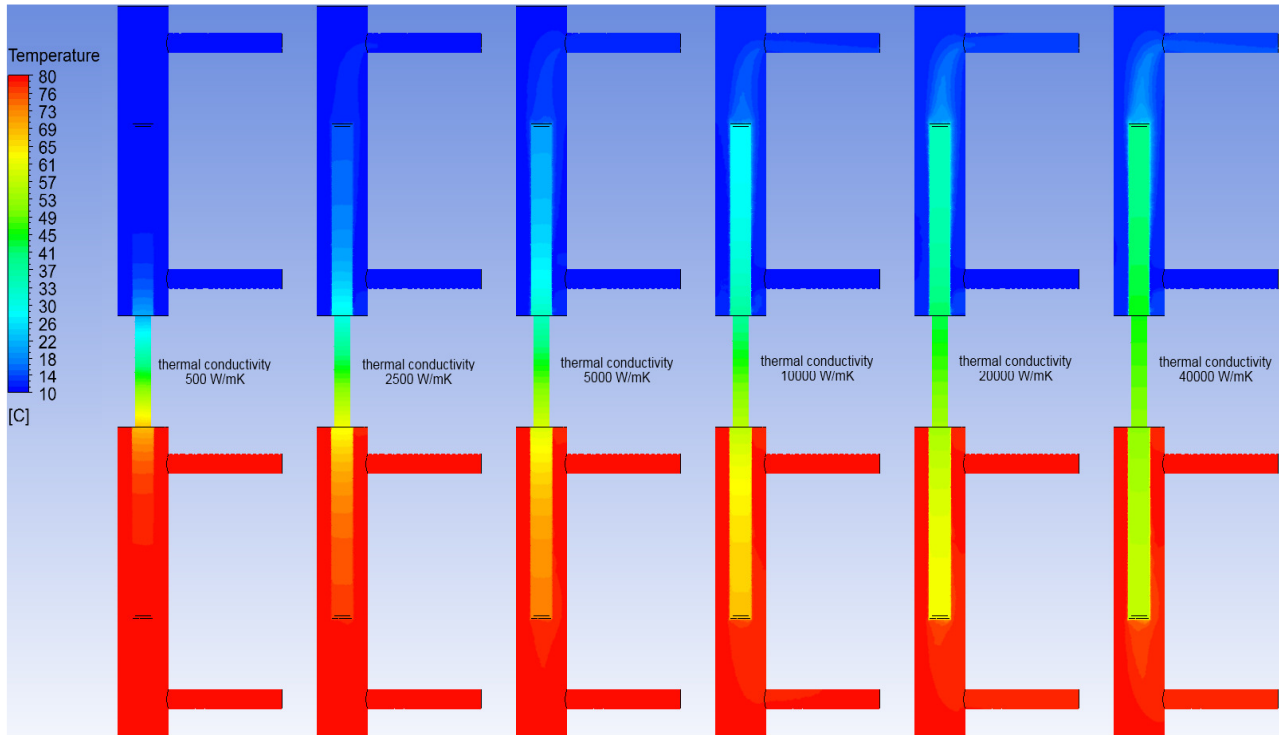


Fig. 6. Heat transfer at different thermal conductivity.

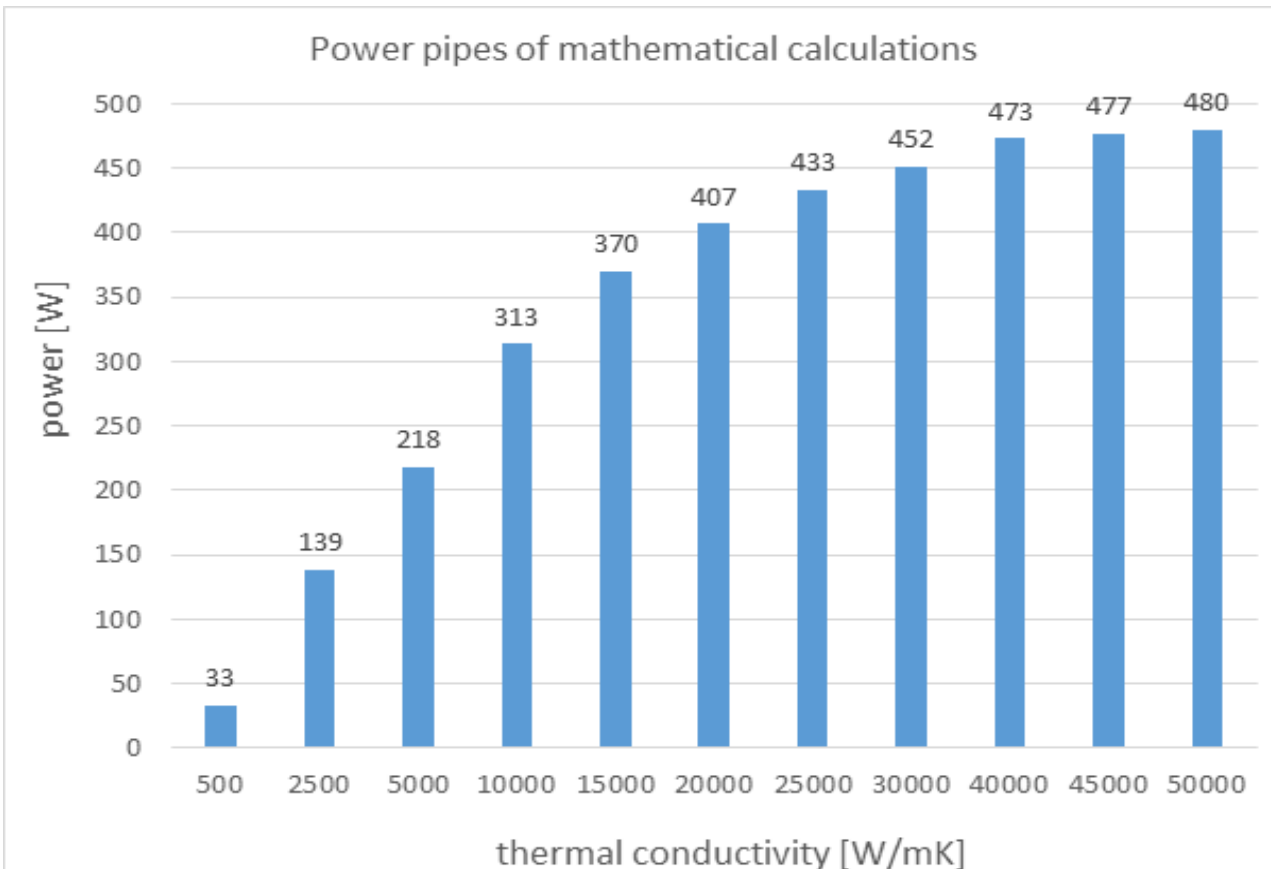


Fig. 7. Depend the thermal conductivity on power of heat pipes.



In Fig. 7 we can see depend of thermal conductivity on power of heat pipe. The values are compute with simulation software ANSYS. With increased thermal conductivity grows the heat transfer. As the substitute (imaginary) material instead of the heat pipe was water-vapor. We changed one parameter which is called thermal conductivity. At value of thermal conductivity 50 000 [W.m⁻¹.K⁻¹] is the power of heat pipe about 480 [W]. The value of power is similar as the measurement value in Tab. 3.

Time step of measuring	Temperature of heating		Mass flow of heating water	Temperature of cooling		Mass flow of cooling water	P – power of measured pipe
	Inlet	Outlet		Inlet	Outlet		
[s]	[°C]	[°C]	[kg.s-1]	[°C]	[°C]	[kg.s-1]	[W]
100	57.63	51.48	0.06984	10.43	14.11	0.02859	441.35
200	67.58	61.87	0.07012	10.72	14.96	0.02959	526.24
300	70.96	65.85	0.07405	10.87	15.32	0.02674	499.20
400	72.25	67.54	0.07578	11.06	15.60	0.02825	537.89
500	72.77	68.38	0.07462	11.31	15.70	0.02891	532.36
600	73.00	68.76	0.07575	11.48	15.69	0.02925	516.40
700	73.08	68.93	0.07591	11.64	15.82	0.03008	527.33
800	73.12	69.05	0.07591	11.81	15.96	0.03008	523.49
900	73.12	69.07	0.07623	11.94	16.04	0.03041	522.90
1000	73.09	69.02	0.07542	12.07	16.14	0.03008	513.34
1100	73.07	69.00	0.07575	12.21	16.35	0.03074	533.72
1200	73.03	68.99	0.07575	12.34	16.32	0.03091	515.86
1300	73.01	68.98	0.07591	12.44	16.18	0.03091	484.74

Tab. 3. Measurement values of heat pipe.

6. Conclusion

At this simulation, we determine a possibility of substitution of heat pipe with another material with changed of some parameter. We have approximated to real conditions of real heat pipe. This simulation is valid only for specific heat pipe, which is overwritten upper in section 3. This simulation is steady time. The new transient time simulation is in progress now.

Acknowledgement

This article was elaborated within the solution of project KEGA č.029ŽU-4/2015 „Heat recovery from the technological processes“.

References

- [1] PATSCH, M, LABAJ, J. *Influence of glycerin combustion in experimental burner on production of emissions*. Acta Metallurgica Slovaca conference. ISSN 1338-1660
- [2] NEMEC, P., CAJA, A. *Heat transfer intensification applying thermal tubes*. Acta Metallurgica Slovaca, 2009, vol. 15, No. 1, pp. 215-220.
- [3] NEMEC, P., CAJA, A. *Heat transport visualization of heat pipe by thermovision*. Experimental fluid mechanics, 2010, ISBN 978-80-7372-670-6, pp. 431-434.
- [4] NOSEK, R. - HOLUBČÍK, M. *Measurement of particulate matter during the combustion of phytomass in small heat sources*. Power control and optimization, proceeding of seventh global conference, Yangon, Myanmar, 2013.



Emissions measurements during the combustion of wood pellets

*Jana Chabadová, *Štefan Papučík, *Jozef Jandačka, *Peter Pilát

*University of Žilina, Faculty of Mechanical Engineering, Department of Power Engineering, Univerzitná 8215/1, 01026 Žilina, Slovakia, stefan.papucik, jozef.jandacka, jana.chabadova, peter.pilat@fstroj.uniza.sk

Abstract. Several aspects affecting the production of particulate. One of the greatest impacts is combustion air volume and its division into primary and secondary part. The article describes experimental device, where it was investigated effect of combustion air volume on particulate matters production, measuring method, measured and analysed achieved results.

Keywords: Particulate matter, Wood pellets, Combustion.

1. Introduction

Air quality significantly affects the status of the environment, human health, as well as individual ecosystems. The biggest problem in air quality at present represents pollution particulate matter (PM). Significantly to this contributes combustion biomass, although most particulate pollutants come from transport. One of the main conditions affecting the combustion process is an adequate supply. If we bring in a large number of furnace air temperature drops unburned gases escape and therefore of the energy escapes us. If the supply is insufficient, there is no burning of volatile matter and combustion is complete.

2. Measurement

Use The basic task of emission measurement is to determine the mass concentration pollutants. Measured weights laid pollutant concentrations are in the range from several [$\text{mg} \cdot \text{m}^{-3}$] to several [$\text{g} \cdot \text{m}^{-3}$]. Each measurement must always consists of a status conditions in cross-section measurements, determination of the main components in the exhaust gas, determine the total volumetric flow rate and determine the median concentration of fluid in the gas stream. As the measurement method was used gravimetric method, which is a manual single method of sampling probe of the gas flow. It is based on the Mean concentrations of the collection of one or more points of the cross section, followed by gravimetric measurement evaluation. Solid additives are shed in an external filter. Representative sample is transferred sample probe suitable shape and the correct speed according to isokinetic conditions:

$$w_{s,i} = w_i \rightarrow c_{s,i} = c_i \quad (1)$$

This equation sets out the requirement that the sampling rate was in the wellhead $w_{s,j}$ [$\text{m} \cdot \text{s}^{-1}$] the same as the speed w_i [$\text{m} \cdot \text{s}^{-1}$] gas flow, then the concentration of the wellhead $c_{s,i}$ [$\text{g} \cdot \text{m}^{-3}$] exhaust flow is equal to the concentration in the stream or [$\text{g} \cdot \text{m}^{-3}$]. Isokinetic conditions are achieved by controlling.

The aim was to analyse measurements of particulate matter from the combustion of wood pellets in various stoppage primary and secondary air. Measurement was implemented in the boiler with nominal output 25kW. This is an automatic boiler with automatic ignition hot. Screw conveyor transports fuel from the hopper to the burner, fuel evenly spread over the surface grid provides diffuser. The air required for combustion is supplied by fan, primary air is supplied to the fuel joints in the grate, and secondary air is fed to the burner holes in the rear wall of the burner. Flow of the

flue gas through the heat exchanger, where is transferred heat to the heating water. Cooled exhaust gases going up the chimney outlet port. The technical parameters of the furnace are shown in chart. The measurement was implemented at various stoppage primary and secondary air.

Samples were collected sample probe directly from the chimney. For separation of PM10 and PM2.5 was used a three-stage separator MSSSI impactor designed for filtration and separation particulate emissions directly in the chimney. The compact design allows the combined current separation of PM10 and PM2.5. The bottom of the holder is placed on a membrane filter diameter 47 mm. We used wood pellets as fuel with a diameter of 6 cm, a bulk density of 650 kg m⁻³ and calorific 17.5MJ.kg⁻¹.

Automatic boiler Verner A251LS (Fig. 1 and Tab. 1) allows you to change the fan speed in the range from 1 to 7 degree. Prior to measurement on an experimental boiler measured mass flows of air at various stoppage primary and secondary air fan and individual levels. Tab. 2 shows the mass flow of air at various fan stoppage extensions are the primary and secondary air from the manufacturer, which was the primary and secondary element to eject 6.8 cm to 3.1 cm.

Rated power	25 kW
Efficiency	92%
Water tank capacity	85 l
Hopper	240 l
Volume ashtray	18 l
Flue gases temperature at rated power	160 °C
Fuel consumption at rated power	5.8 kg.h ⁻¹
Emission class	3
Efficiency class	3

Tab. 1. Technical parameters of the boiler.



Fig. 1. Boiler Verner A251LS.

fan	primary air [kg.hod ⁻¹]	secondary air [kg.hod ⁻¹]	total air [kg.hod ⁻¹]
1	27.82	2.68	30.50
2	20.92	2.02	22.95
3	68.84	8.20	77.05
4	91.68	12.95	104.63
5	104.16	15.19	119.36
6	120.29	18.22	138.52
7	138.05	21.67	159.72

Tab. 2. Measured values of mass flow.

For quality evaluation of combustion process was content of flue gases measured by flue gases analyser ABB AO 2020 (Fig. 2). Advice is assigned on analysis of gaseous pollutants. Gas offtake is one point with inox probe. On inlet of the sample to the offtake pipe is in preserved box heated ceramic filter, captured mechanical dirtiness. Sample continues by offtake pipe to the measuring system. Pipe is heated for noncondensing of the sample. Measured gas is leded to the refrigerator. In the next step is gas leded through the valves and filters to the analyser. Analyser ABB AO 2020 is set according the requirements and the nature of measurement. In the case of emission measuring from wood combustion in the fireplace stoves were used measuring advices URAS 26 and MAGNOS 206. For a more accurate analysis of emission and power parameters of the individual settings of intake air into the pellet burner was always measured circa 120 min. During the combustion process of one fuel portion was recorded the following values: ambient temperature T_o [°C], chimney pressure p_k [Pa], flue gases temperature T_k [°C], outlet water temperature from the boiler [°C], inlet water temperature to the boiler t_r [°C], volume flow of heatchange Q_{vh} [m³.h⁻¹], speed of inlet air to the burner [m.s⁻¹], temperature of inlet air to the burner [°C], constitution of flue gases : oxygen O₂ [%], carbon dioxide CO₂ [%], carbon monoxide CO [ppm], nitrogen oxide NO_x [ppm], sulphur dioxide SO₂ [ppm].



Fig. 2. Emissions analyser (ABB).

Samples for analysis of particulate matters (PM) were sampled disposable by probe of TECCORA Company, directly from the chimney. For separation of the particles PM10 (particulate matters in range from 2.5 μm to 10 μm) and PM2.5 (particulate matters smaller than 2.5 μm) was used three- stage separation impactor MSSI intended for filtration and separation of particulate matter directly in the chimney. Combined compact design allows simultaneous separation of PM10

and PM2.5. At the bottom is placed holder for membrane filter diameter of 47 mm. Measurements were carried out at various fan stoppage.

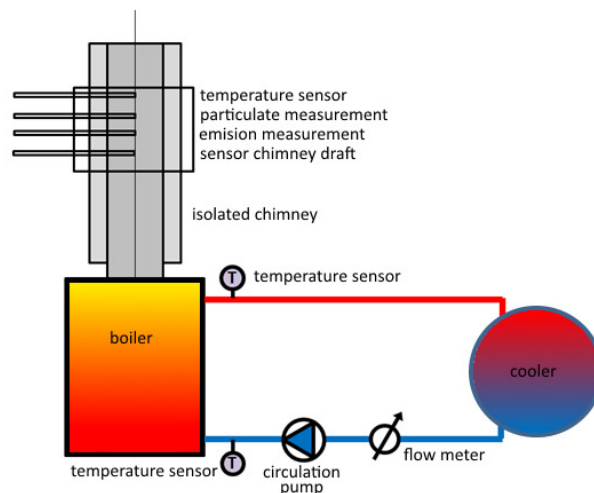


Fig. 3. Scheme experimental measurement.

In experimental measurements of the boiler output is set to half (Fig. 3). During measurements were recorded at 20 second intervals on the emissions, ambient temperature, exhaust temperature, fuel loss. Interval measurement itself was 30min. Based on measurements of the mass flow of primary and secondary air entering the combustion process in a small heat source is used to manually overfill fan heat source on values: 1,3,6,7. During the measurement of performance and emission parameters of the extensions are fan # 1 to the insufficient supply of air for the combustion process, and therefore used as 3,6,7 The settings. In the picture we can see tar No.2 established the impactor that created the extensions are worth the No.1 fan, respectively: the minimum speed (Fig. 4).

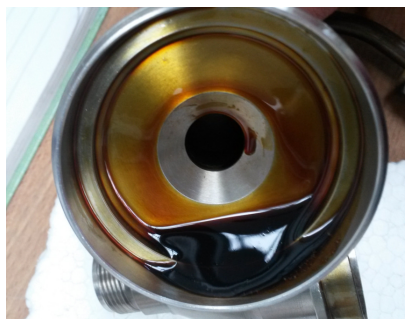


Fig. 4. Tar established the impactor.

3. The evaluation of measurement

Use The basic task of emission measurement is to determine the mass concentration pollutants. Measured weights laid pollutant concentrations are in the range

On the first graph (Fig. 5) is showed selected record from one measurement running during 30 min., and effect of combustion at fan setting on speed number 3 on production of individual pollutants and power of small heat source. From the running is possible to observe a significant increasing of all pollutants during fuel metering from the screw feeder to the combustion chamber, while at the same time decreased power. This phenomenon can be observed in all realized combination of primary and secondary mass flow incoming to the combustion process.

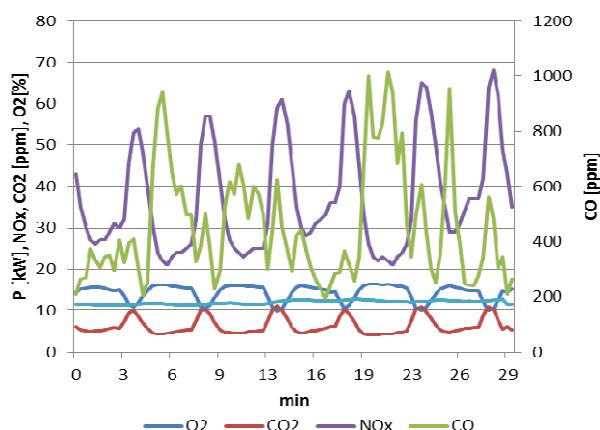


Fig. 5. One measurement running during 30 min.

From the perspective of the average values of each combination in primary and secondary mass flow changes can be observed a considerable effect of combustion air amount on combustion quality (Fig. 6, 7). From the perspective of power is the best setting of fan (primary and secondary air setting) on value No 6. Then the experimental small heat source achieves the best efficiency and performance (Fig. 6).

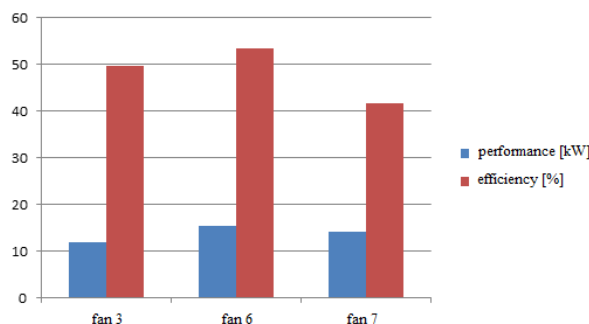


Fig. 6. Performance and efficiency.

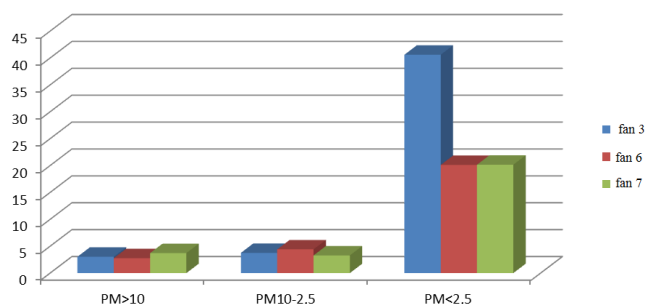


Fig. 7. Production of particulate matter.

If we look on the analysis of measured data from the aspect of particulate matter (Fig.8), is possible to observe similar process of particulate matters (PM) production with the same variant of combustion like in the previous analysis. From the aspect of PM production we accord least mass number of PM in range 10 μm and more. Similar results were recorded also for PM10 particles, which are in the range of 2.5 μm to 10 μm . Surprisingly was found, that at the combustion of ecological fuels from biomass are most produced smallest particles PM, which are most dangerous for the human body. PM 2.5 are smaller than 2.5 μm . In terms of redistribution and intensity on the formation of PM particles from burning biomass in the process, we observe an increase in the formation of PM at pinching inlet air, or fan settings on value 3. The biggest effect of combustion air pinching was on the creation of PM2.5. Formation of particles larger than PM10 and PM10 was in all variants redistribution and intensity of combustion air into the combustion process approximately the same.



4. Conclusion

From previously conducted preliminary analyses show that even a slight interference with the process combustion in a small heat source using superstructures intensity entering primary and secondary air can fundamentally affect the quality of combustion and emission performance terms. From these introductory analyses is observed significant fluctuation of pollutants production, dangerous for the human health, produced from the combustion process at incorrect setting of primary and secondary air. From this perspective is important to deal with redistribution and intensity of combustion air and its effect on combustion process, with which we will interest in the next experiments.

Acknowledgement

This article was created within the frame of project KEGA 070ZU-4/2013 “Modern sources for heating”

The research is supported by the European Regional Development Fund and the Slovak state budget for the project “Research Centre of University of Žilina” ITMS 26220220183 acknowledgement heading is of the same style as the heading references “Reference” and it is not numbered. The text of acknowledgements is of the style “Text”.

References

- [1] DZURENDA, L. *Spaľovanie dreva a kôry*. TU Zvolen, 2005.
- [2] RAJNIAK, I a kol. *Tepelno-energetické a emisné merania*, Bratislava 1997, ISBN 80-88683-20-3
- [3] CHABADOVA, J. *Emisie pri spaľovaní dendromasy*, Písomná časť dizertačnej skúšky, 2009
- [4] NAJSER, J., PEER, V., VANTÚCH, M. *Biomass gasification for liquid fuel production*. XIX. international scientific conference: 09.04.-11.04.2014 Liptovský Ján, Slovakia. - Žilina: University of Žilina, 2014. - ISBN 978-80-554-0855-2. - S. 73-76.
- [5] KLENOVČANOVÁ, A., BRESTOVIČ, T. *Štúdium tepelného obsahu vybraných druhov biomasy a odpadov / A. Klenovčanová, T. Brestovič, R. Čap - 2007*. In: Acta Metallurgica Slovaca. Roč. 13, mimoriadne č. 3 (2007), s. 160-165. - ISSN 1335-1532
- [6] JOHNSON, F., LECKNER, B., BOROVEC, K., OCHODEK, T., NOSKIEVIČ, P. *An Experimental Study of In-furnace Processes and Dynamic Behaviour of a 235 MW CFB Boiler*. „VGB PowerTech 3/2004“, str. 82-87, Volume 84/2004, ISSN 1435-3199
- [7] RAJZINGER, J., KNIZAT, B. *Citlivostná analýza vybraných fyzikálnych veličín zemného plynu*. Fluid Mechanics and Thermomechanics. Medzinárodná vedecká konferencia katedier mechaniky tekutín a termomechaniky. XXV. Bratislava : STU v Bratislave, 2006. ISBN 80-227-2434-3.
- [8] VITÁZEK, I., HAVELKA, J. *Termodynamické parametre zemného plynu 2009*. Zborník zo XVII. Medzinárodnej vedeckej konferencie „Aplikácia experimentálnych a numerických metód v mechanike tekutín a energetike“. Žilina: ŽU, 2010, s. 341-346. ISBN 978-80-554-0189-8.
- [9] PATSCH, M., LÁBAJ, J. *Experimental burner for glycerin combustion*. IN-TECH 2011 : proceedings of international conference on innovative technologies : 01.09.2011 to 03.09.2011, Bratislava, Slovakia. - [S.l.]: Jan Kudláček, 2011. - ISBN 978-80-904502-6-4. - S. 429-431.
- [10] NOSEK, R. - HOLUBČÍK, M.: *Measurement of particulate matter during the combustion of phytomass in small heat sources*. Power control and optimization, proceeding of seventh global conference, Yangon, Myanmar, 2013. ISBN 978-983-44483-63.
- [11] HOLUBČÍK, M. – JACHNIAK, E. – SMATANOVÁ, H. *Differences between pellets from biomass made in manufactory and in domestic conditions*. AIP Conference Proceedings, Volume 1608, 2014, Pages 48-53, ISSN: 0094-243X
- [12] VANTUCH, M., HUZVAR, J., KAPJOR, A. *Heat transfer from oriented heat exchange areas*. EPJ Web of Conference [elektronický zdroj]. - ISSN 2100-014X. - Vol. 67, art. no. 02122 (2014), online, [5] s.



Modelling and Simulations of Dynamics of the Low-floor Tramcar with Independently Rotating Wheels

*Andrzej Chudzikiewicz, *Magdalena Sowińska

*Warsaw University of Technology, Faculty of Transport, Koszykowa 75, 00-662 Warsaw, Poland,
ach@wt.pw.edu.pl

Abstract. The article is devoted to the analysis of numerical simulation results of the tramcar dynamics. It presents the mathematical model of the one section of the low-floor tram with the bogie with independently rotating wheels. The simulations were performed according to different scenarios, connected with the track geometry, which seem to be dangerous for the tram behaviour e.g.: curving, gauge narrowing, track buckling, etc. Special attention was paid on wheels lateral displacement and forces occurring in contact of wheels and rails. The simulation results reveal characteristic features of such an unconventional system of the tram, which can oftenly demonstrate dynamics considered worse than in the conventional case of the tramcar.

Keywords: Low-floor tramcar, Independently rotating wheels.

1. Introduction

Currently, the demand of the urban transport providers on the modern tramcars leads designers to the new point of view on the tramcar construction. However, the realization of the goal which is a constant improvement of the passengers comfort cannot be fulfilled further. The reason is a construction of the bogies, which makes the introduction of 100% low floor impossible. The researchers adjust to new design requirements and analyse the unconventional wheelsets with independently rotating wheels.

In this study there was made an attempt of development of the model of unconventional bogie in the tramcar section. As the characteristic features of the dynamics of such a wheelsets are still not well known, several simulations were performed in order to recognize the behaviour of the system. The results of simulations were analysed and general conclusions derived.

1.1. Literature Background

Studies on the concept of independently rotating wheels have concentrated generally on the steering strategies of running gear that could overcome the drawbacks of IRW bogie design. Positions [1, 2, 3] deal with the active control of the wheelsets, paper [4] surveys various possibilities of its control. Goodall in [5] presents experimental approach on torque control of IRW wheelsets. Paper [6] deals with the linear model of a bogie with independently rotating wheels and paper [7] with comparison of mathematical modelling of both conventional and unconventional bogies.

2. Model

The three dimensional model of tramcar dynamics was considered in all cases of simulations. The one section of the tramcar has 20 degrees of freedom and consists of four rigid bodies which are:

- car body, which has 6 degrees of freedom,
- bogie frame body, which has 6 degrees of freedom,

- two wheelsets with independently rotating wheels which has 4 degrees of freedom each.
 The section of the tramcar with marked degrees of freedom of car body is presented in Fig. 1.

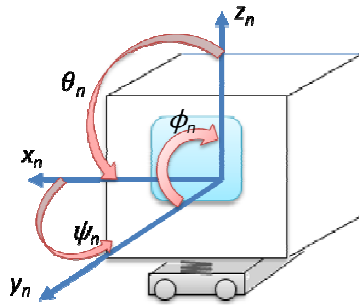


Fig. 1. Tramcar section scheme with degrees of freedom of the car body.

The unconventional wheelset with independently rotating wheels has a cranked axle which allows to lower the floor in the whole tramcar inner space. Such a wheelset has wheels mounted on the common axle with the use of bearing system which enables independent rotation of wheels. In this case, the wheelset has 4 degrees of freedom as it is visible in Fig. 2a. The analysis of dynamics of the wheelset is limited to the motion in a horizontal plane. Whole model of the bogie has 14 degrees of freedom and it is symmetric respect to x axis as it is captured in the Fig. 2b.

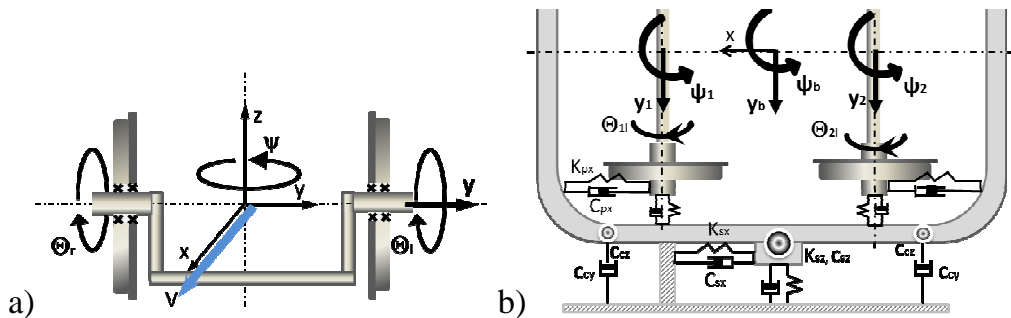


Fig. 2. a) the wheelset model b) the bogie model with elastic-damping elements marked.

Bodies are connected with the elastic and damping elements which have linear characteristics.

The vehicle's motion is investigated in the non-inertial frame connected with the centreline of a track. The Fastsim procedure was involved in the numerical calculations. However, the procedure had to be modified in terms of creepages form, because of the free rolling of the wheels. For that reason, the longitudinal creepage was assumed zero. The wheels used for the simulations were Ri60 type and rail profiles were typical grooved tramway track rails.

3. Simulation study

Fig. 3 presents three different track geometries assumed for the simulations.

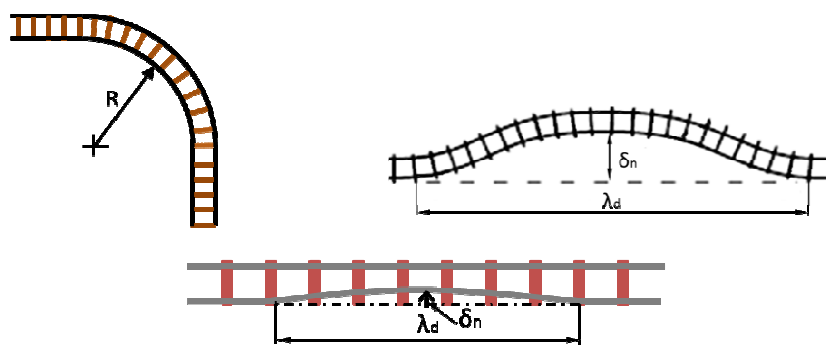


Fig. 3. Tracks taken for the simulations: a) steady curving b) buckled track c) track with lateral misalignment.

Fig. 3a presents track in the steady curving case and it is modelled as a quarter of the circle with straight entrance and exit, Fig. 3b pictures buckled track modelled as half of the sinusoid of 50 cm amplitude and long 10 m and Fig. 3c a track with lateral sinusoidal misalignment of 1 cm and 2 cm amplitude of right rail long 5 m. Simulations were performed according to different velocities and track parameters.

Fig. 4 presents lateral displacement of the wheelset's centre of mass during the ride on the curve (Fig. 3a) with velocity of 20 km/h. It compares two curves of different radius: 20 and 50 m.

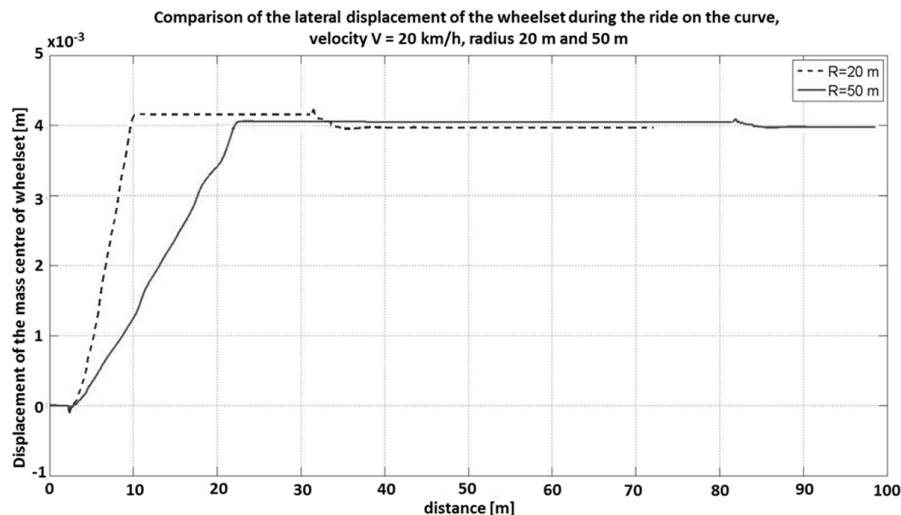


Fig. 4. Lateral displacement of the wheelset during the steady curving; 20 and 50 m radius, 20 km/h.

The wheelset displaces faster to the maximal position on the tighter curve than on the curve of 50 m radius. The maximal position means the position when the wheel flange is in contact with the rail. In both cases such situation occurs. After exiting the curve the wheelsets remain displaced. The centre of the wheelset mass does not return to the central position on the track. Fig. 5 shows the yaw angle of the wheelset in the same case of the track scenario.

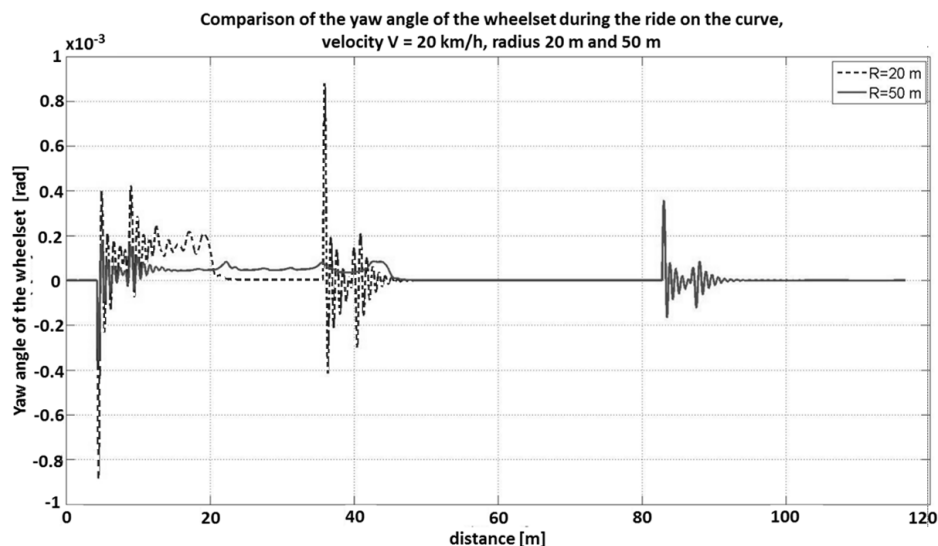


Fig. 5. Yaw angle of the wheelset during the steady curving; 20 and 50 m radius, 20 km/h.

It is shown, that independently rotating wheels wheelsets have the ability of radial positioning, because the yaw angle stabilizes on the zero value during the ride on the curve. The comparison of wheelset lateral displacement on the curve of 50 m radius in two cases of velocity is shown in Fig. 6. It reveals the same features which is slow climbing up to the flange, remaining of the flange in the constant contact with the rail and no self-centring ability.

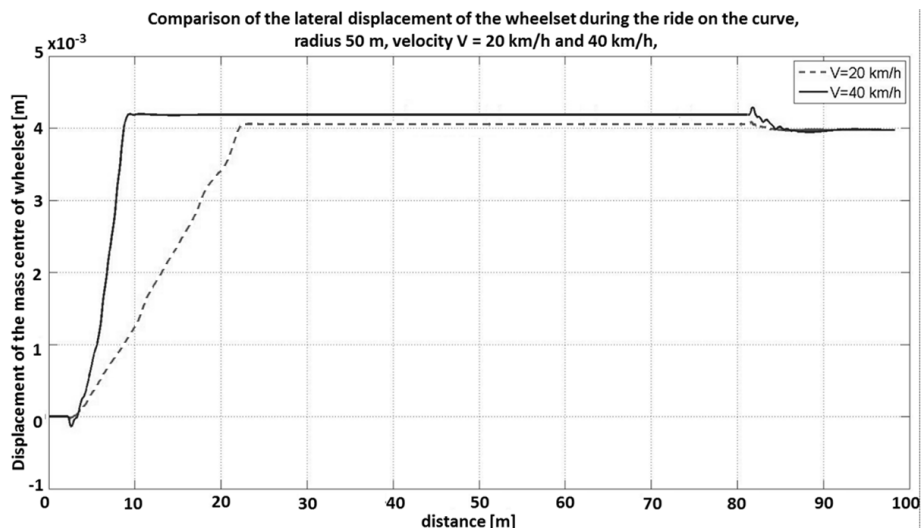


Fig. 6. Lateral displacement of the wheelset during the steady curving; 50 m radius, 20 and 40 km/h

Fig. 7 presents the lateral forces in the area of contact between the wheel and rail during the ride on the curve of 50 m radius with the velocity of 40 km/h. The graph compares forces on the left and right side of the wheelset.

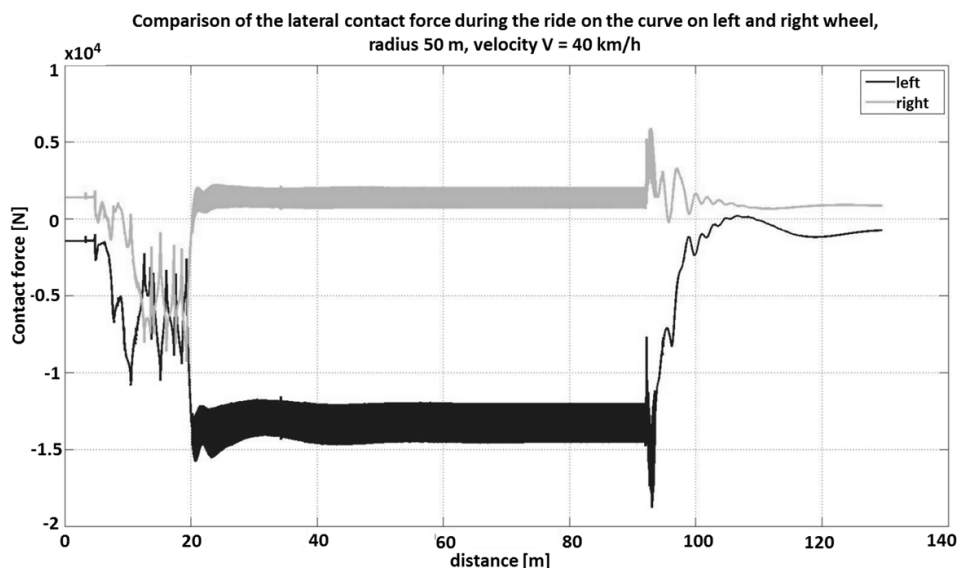


Fig. 7. Lateral contact forces on the left and right wheel during the steady curving; 50 m radius, 40 km/h.

When the tramcar turns right on the curve, the lateral forces in the outer wheel area of contact are about 1.4 kN and in the inner wheel area of contact are about 0.15 kN. Forces have the oscillating character around these values because of the flange-rail contact on the curve.

Next interesting features of such a wheelset appear in the simulation results of the ride on the buckled track. As it is visible in Fig. 8, the wheelsets perform distinctly different motion in the case of velocity of 40 km/h and 60 km/h. When the velocity is 40 km/h, the wheelset has smaller displacements on the buckled section of the track than 60 km/h case. After exiting to the straight track the wheelset which rides with the 40 km/h approaches shortly the centreline of the track and then returns to the previous position. When the ride velocity is 60 km/h, the wheelset after exiting the buckled section passes the centreline and takes the maximum position on the other side of the track and does not return to the centre.

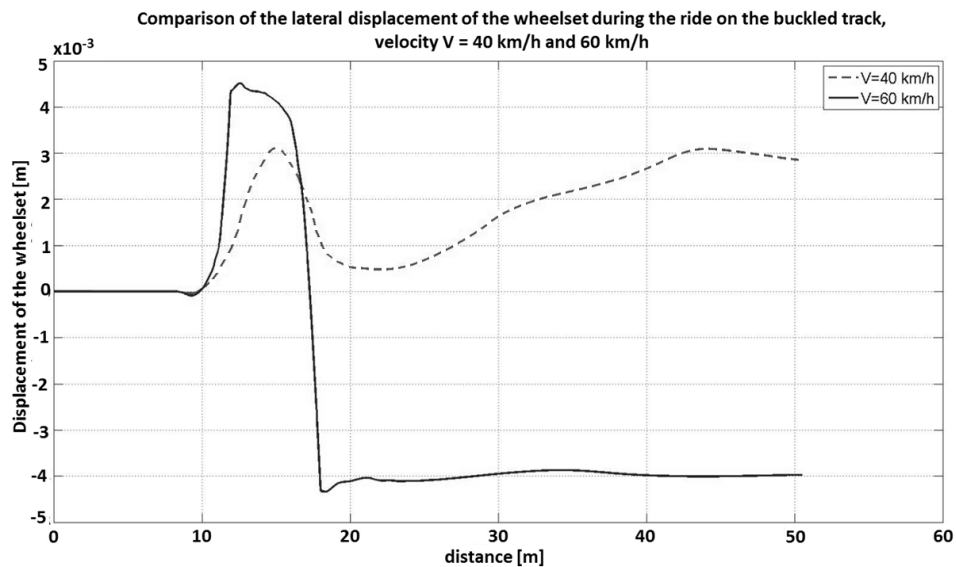


Fig. 8. Lateral displacement of the wheelset during the ride on the buckling; 40 and 60 km/h.

Fig. 9 presents the lateral forces in the area of left and right wheel contact with the rail during the ride on the buckled track. When the velocity is equal to 40 km/h, the forces are approximately equal to 1.2 kN on the entrance and exit from the buckled section.

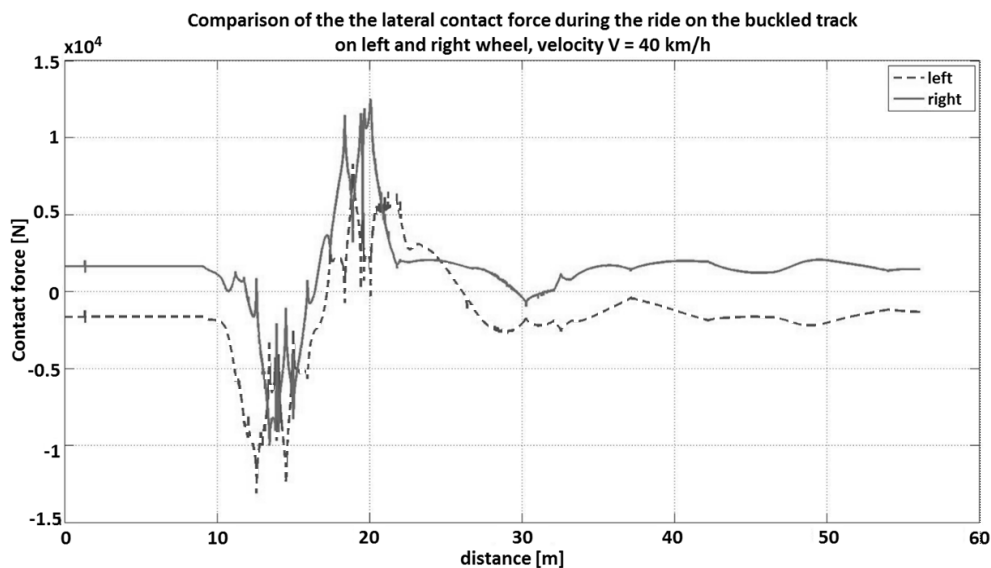


Fig. 9. Lateral contact forces on the left and right wheel during the ride on the buckling; 40 km/h.

The simulation results have also shown, that when the velocity increases to 60 km/h, the lateral forces values are 5 times bigger than in 40 km/h case. Fig. 10 presents lateral displacement of the wheelset on the last type of the track, which is a track with the lateral misalignment of one of the rails. This graph compares the answer of the IRW wheelsets on the misalignment of different amplitude – 1 cm and 2 cm. The ride velocity is constant and equal to 20 km/h. This scenario shows strong influence of misalignment on lateral motion of the wheelset. The system nearly does not notice the 1 cm amplitude misalignment, what cannot be observed in case of 2 cm amplitude. In this case, the lateral displacements of the wheelset are increasing till the flange-rail contact and then decrease towards the centreline of the track.

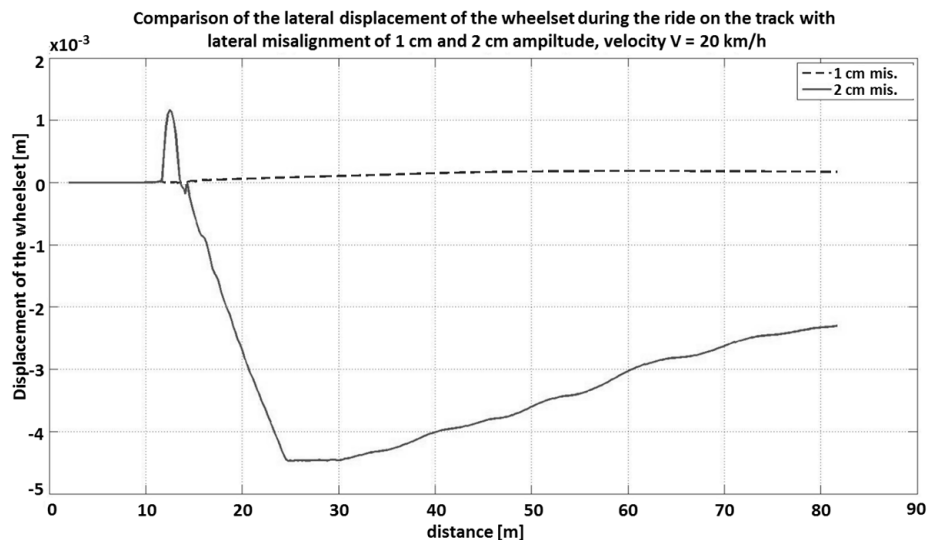


Fig. 10. Lateral displacement of the wheelset during the ride track with lateral misalignment; 1 and 2 cm amp., 20 km/h.

4. Conclusion

The paper presents examples of simulation results of the low floor tramcar motion performed according to different scenarios. Analysis of the results focuses on the lateral displacements of the wheelset's centre of mass, yaw angle of the wheelsets and lateral forces in the area of wheel and rail contact. The numerical model have shown that new wheelset type requires modified mathematical model of contact what mainly involves form of the creepages. Various simulations were performed for real wheel and rail profiles and different track geometries and revealed the characteristic features of independently rotating wheels bogie, which are: no self-centring ability, easy radial positioning, long contact of the flange with the rail. The scenarios of the ride on the buckled track and track with lateral misalignment give an insight on how strong influence on the bogie motion has the ride velocity and size of the irregularity. The responses of the system are hardly predictable.

Acknowledgement

The work was done as a part of the research project WND-DEM-1-493 / 000, „Support for scientific research and development on a demonstration scale DEMONSTRATOR+”.

References

- [1] GOODALL, R.M. – HONG, L. Solid axle and independently rotating wheelsets - A control engineering assessment of stability, *Vehicle System Dynamics*, vol. 33, 2000.
- [2] MIYAMOTO, M. – SATO, T. *Study on the stabilization of railway vehicles with independently rotating wheels by control of steering on wheelset (1 Axle trailer bogie)*, JSME, 10th Conf. Transportation 01-36, 2001.
- [3] OBATA, R. – TANIFUJI, K. – SOMA, H. – MASUDA, T. *Curving performance of a rail vehicle with independently rotating wheels by torque difference control*, *Transaction of the Japan Society of Mechanical Engineers Series C*, vol. 72, no. 716, 2006.
- [4] MEI, T.X. – GOODALL, R.M. *Practical strategies for controlling railway wheelsets independently rotating wheels*, ASME, vol. 125, 2003.
- [5] LIANG, B. – IWNICKI, S.D. *An experimental study of independently rotating wheels for railway vehicles*, IEEE Proc. Int. Conf. Mechatronics and Automation, 2007.
- [6] CHO, Y. - KWAK, J. *Development of a new analytical model for a railway vehicle equipped with independently rotating wheels*, *International Journal of Automotive Technology*, vol. 13, no. 7, 2012.
- [7] JAWAHAR, P.M. – GUPTA, K.N. *Mathematical modelling for lateral dynamic simulation of a railway vehicle with conventional and unconventional wheelset*, *Mathematical and Computer Modelling*, vol. 14, 1990.



Effect of high temperature on the performance parameters gravitational heat pipe, filled with different working medium

*Marián Jobb, *Ľuboš Kosa, *Patrik Nemec, *Milan Malcho

*University of Žilina, Faculty of Mechanical Engineering, Department of Power Engineering, Univerzitna 8215/1, 01026 Žilina, Slovakia, {marian.jobb, lubos.kosa, patrik.nemec, milan.malcho}@fstroj.uniza.sk

Abstract. The paper presents the results of performances gravity heat pipe filled with three different working substances: water, alcohol and oil. Power heat pipe was measured at high temperatures ranging from 160°C to 480°C. This paper describes the experimental measurement of performance parameters and wiring diagram.

Keywords: Gravitational heat pipe, Performance parameters, High temperature.

1. Introduction

In the area of research and development in the energy sector are now people focus not only on the development of alternative fuels, reducing emissions and attracting new sources of energy, but also for efficient heat transfer, whether for cooling various components in electrical engineering, computer science, engineering or in the recovery of waste heating and transport of heat in heating [1, 2].

Heat pipes are precisely such equipment heat transfer while maintaining low temperature differences. Therefore, the development and optimization of the key to greater efficiency and broader application of heat pipes [3]. The advantage of the heat pipe is that even in the smaller sizes can transmit high heat output, while its construction is simple with a long life, reliability and durability [4].

2. Theoretical analysis of gravitational heat pipes

Construction of gravity heat pipe is the simplest and also the principle is the basis for other types. A heat pipe consists of a closed outer shell and a working fluid provided within the tube. The tube operates in a vertical or slightly inclined position with the coupling portion located always above the evaporation portion. The evaporation of the working fluid evaporates and condenses the condensation part. The condensate then runs to the evaporation of the force of gravity along the smooth inner wall [5, 6]. The transferred heat flow depends on the thermal resistance of the liquid film on the wall of the condensation part. The correct operation of the tube is conditioned in such a dosage amount of working fluid, in the range of operating parameters to avoid insufficient wetting of the surface evaporation and thus decreased performance. Conversely, too much excess liquid in the vapor of boiling results in the release of large steam bubbles form when the shock phenomena. Heat transfer between the vapor phase of the working fluid and the inner wall of the tube is particularly influenced by the character of flow in the falling film of liquid.

GRAVITY HEAT PIPE STRUCTURE

FIG. 1

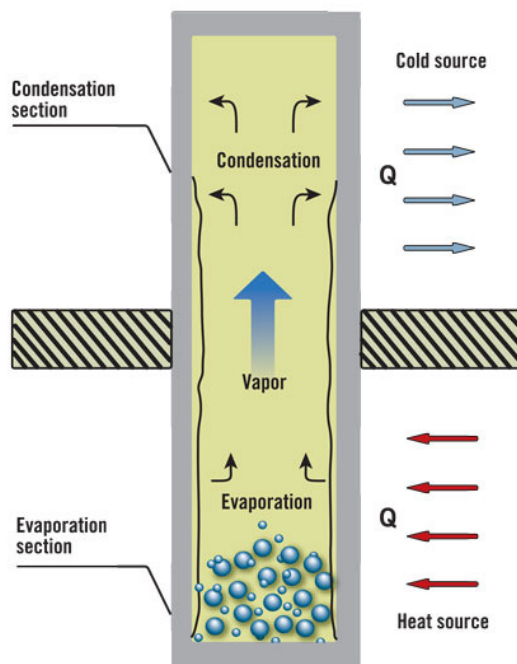


Fig. 1. Function of gravitation heat pipe (<http://www.ogj.com/content/dam/ogj/print-articles/Volume%20111/mar-4/z130304OGJdhu01.jpg>).

3. Proposal for measuring equipment

The equipment (Fig. 2) was designed and constructed so that the detection performance of heat pipe in the simplest and safest. The actual determination of the performance of the heat pipe is based on the difference the input and output temperatures of the cooling water passing through the cooling device located on the condensation part of the heat pipe.

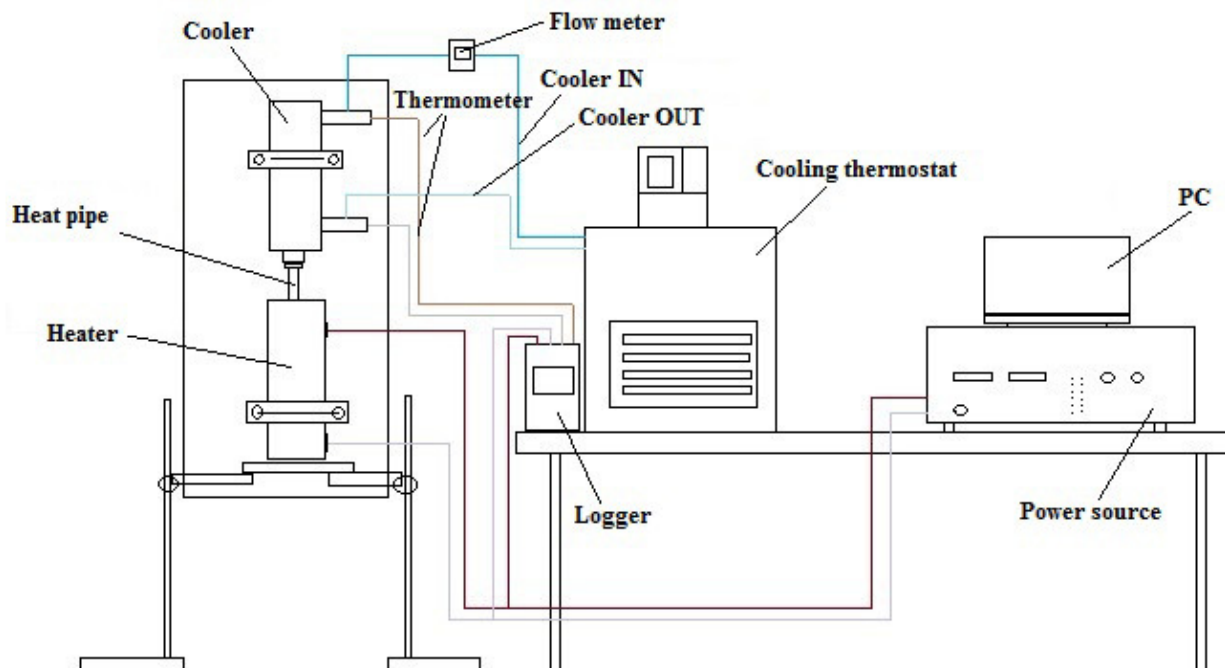


Fig. 2. Schematic diagram of the measuring device for the detection performance of the heat pipe.



Fig. 3. The measuring device for the detection performance of the heat pipe.

4. Measurement procedure

Heat pipes of internal diameter 10 mm and a length of 500 mm were filled with the working fluid into 20% of its capacity. Measurements were carried out on the heat pipe filled with three working substances: heat transfer oil Mol Thermol 68, distilled water and 98% alcohol. Heated part of the heat pipe was placed in the heating element and the condensing portion was placed in a cooling. The individual tubes were exposed to three different heat through at 160°C, 320°C and 480°C and at these temperatures were recorded measurements. The measurement was repeated three times on each tube, to check the results.

After placing the tube into the measuring device (Fig. 3), we set the source voltage 40V and 1.1A current. Thus, we set the parameters allowed 10 minutes to equilibrate and then we started by measuring exchanges and computer record measured values. The body after stabilization of the treated tube at 160°C. Computer us every 10 seconds a record of temperature at the inlet of the cooling and temperature in the extract. Cooling equipment we set the required 15°C. After 10 minutes, the measurement and recording of data, we voltage Power supply current increased and set to 80V and 2.3A. In this setting, the heating element after stabilization, treated the heater portion of the tube temperature of 320°C. Measurement and writing values for this setting also lasted 10 minutes. The third and final change in the settings, the increase in voltage 120V and current to 3.5A. Again, the 10-minute stabilization followed by a 10 minute measuring and logging values. This setting was able to develop a radiator temperature 480°C

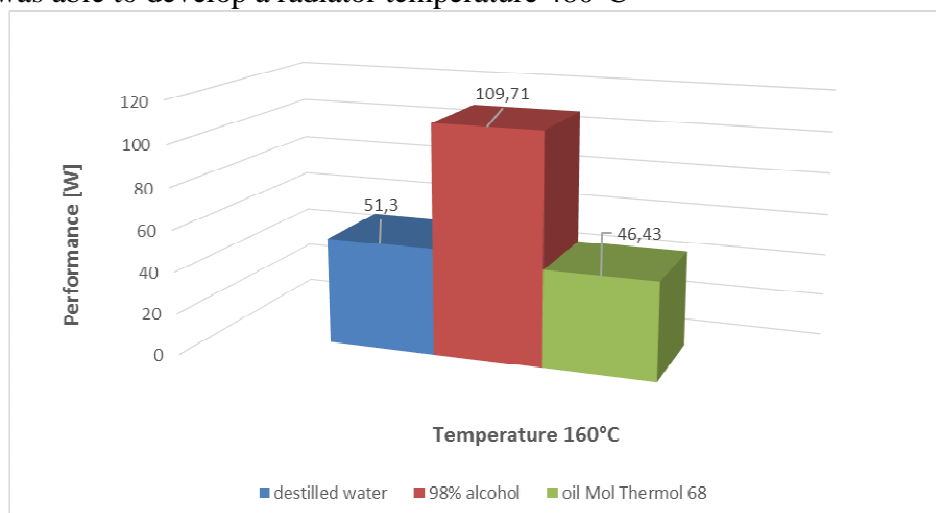


Fig. 4. Power heat pipes at 160°C.

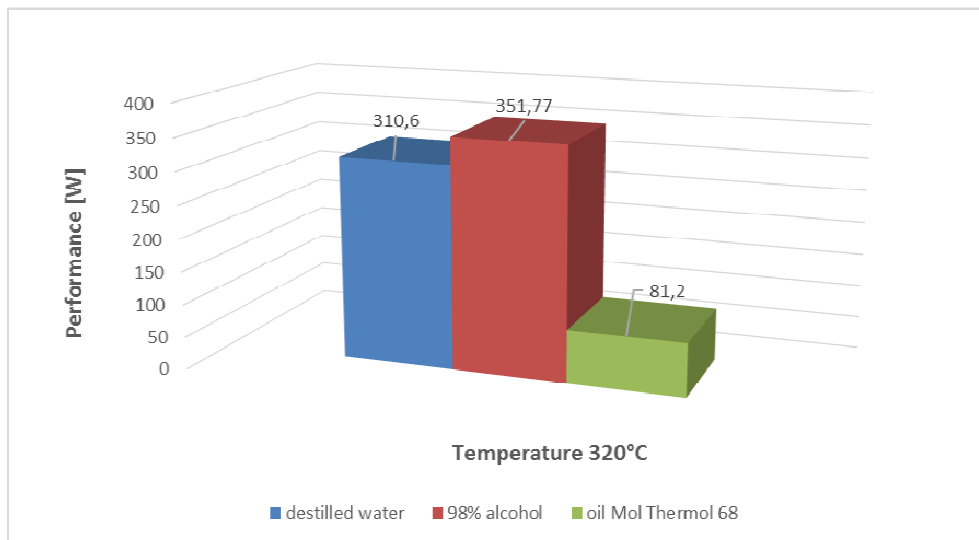


Fig. 5. Power heat pipes at 320°C.

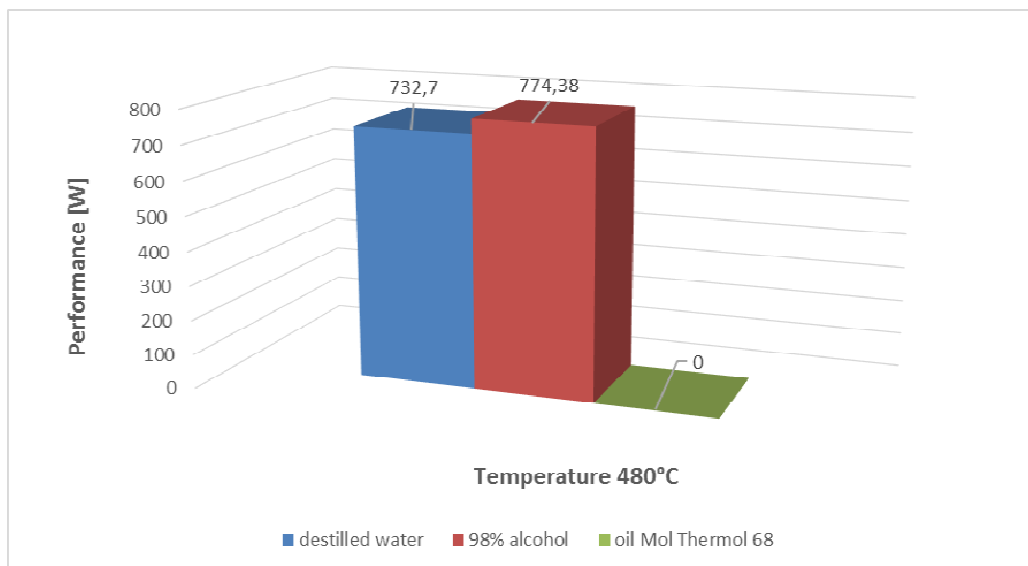


Fig. 6. Power heat pipes at 480°C.

5. Conclusion

When using heat pipe filled with oil and set at 120V and 3.5A occurred during the temperature rise in the destruction of the heat pipe at the end of the tin solder (Fig. 4). The measured heat at the time of destruction was 327°C. This phenomenon is repeated at the same temperature, in a further tube. The oil in the tube and evaporated under-tube so could not function properly and cooling off. Nonevaporated and heated oil thus causing destruction tin solder.

The calculated performance of the tubes are shown graphically in Fig. 5, 6, 7 and graphs shows that TT-filled spirit achieve the greatest results. The aim of the measurements was to test the life and performance of gravitational copper heat pipe at the high temperatures which are reached in the industry (e.g. industrial furnaces, zinc, foundries, etc.). To measure the performance has been verified that the heat transfer oil Mol Thermol 68 is not suitable as the operating medium used in the heat pipe at high temperatures.



Fig. 7. The destruction of the heat pipe using oil - working medium.

Acknowledgement

The research is supported by European regional development fund and Slovak state budget by the project Research centre of University of Žilina", ITMS 26220220183 (50%).

This work is supported by the financial assistance of the project APVV - 0577-10 " Cooling of power electronic systems by cooling cycles without mechanical drive" (50%).

References

- [1] REAY, D. A., KEW, P. A. *Heatpipes, Theory, Design and Applications*. Fifth Edition, USA, 2006.
- [2] HOLUBČÍK, M., ĎURČANSKÝ, P., JANDAČKA, J. and NOSEK, R. *Design of heat exchanger for ericsson-brayton piston engine*. The Scientific World Journal, Volume 2014, 2014, Article number 138254, ISSN: 23566140, DOI: 10.1155/2014/138254
- [3] LENHARD, R., KADUCHOVÁ, K. and PAPUČÍK, Š. *Analysis of the fill amount influence on the heat performance of heat pipe*. International Conference on Application of Experimental and Numerical Methods in Fluid Mechanics and Energetics 2014, XIX.AEaNMiFMaE 2014; Liptovský Jan; Slovakia; 9 April 2014 through 11 April 2014; Code 107300, ISBN: 978-073541244-6, DOI: 10.1063/1.4892724
- [4] NOSEK, R., GAVLAS, S., LENHARD, R., SEDLAK, V., ARVESEN, H.M. *Condenser optimization of heat pipe*. *Komunikácie*, Volume 16, Issue 3A, 2014, Pages 62-66, ISSN: 13354205
- [5] VANTÚCH, M., HUŽVÁR, J. and KAPJOR, A. *Heat transfer from oriented heat exchange areas* [Prenos tepla z orientovaných teplovýmenných plôch] EPJ Web of Conference [elektronický zdroj]. - ISSN 2100-014X. - Vol. 67, art. no. 02122 (2014)
- [6] FAGHRI, A. *Heat Pipe Science and Technology*. Washington DC. Taylor & Francis, 1995.



Simulation of Emissions of Nanoparticles from Braking Processes on a Dynamometer with Regard to Distribution of Pollutants

*Zdeňka Kaličáková, *Vendula Drastichová, *Vladimír Mička, **Kamil Krpec

*VSB – Technical University of Ostrava, Faculty of Safety Engineering, Lumírova 13, Ostrava - Výškovice,
700 30, Czech Republic, {zdenka.kalicakova, vendula.drastichova}@vsb.cz

**VSB – Technical University of Ostrava, Energy Research Centre, 17.listopadu 15/2172, Ostrava – Poruba,
708 33, Czech Republic, {kamil.krpec}@vsb.cz

Abstract. Motor traffic ranks among the main sources of air pollution in urban regions. It turns out that dust particles, especially particles smaller than 0.1 μm , may be the most significant in terms of health from the whole range of pollutants, e.g. exhaust gases, abrasions of brake pads, car paint abrasions or tyre abrasions, produced by vehicles. The performed experiments related to abrasion of brake pads, and indicated that particles smaller than 100 nm are released in the air. Nanoparticles settle very slowly and remain in the air for a long time, which significantly contributes to air pollution in areas with high density of traffic. The size of particles and its composition are related to potential effects of the particles on health and possible health hazards. The aim of the work is to determine numerical concentrations and perform chemical analyses of individual emission fractions from the testing dynamometer of frictional properties of automotive brake pads.

Keywords: Pollutants, Brake pads, Dynamometer.

1. Introduction

People have always been exposed to particles, and owing to the evolutionary process, we adapted to the environment we developed in. Nowadays, human organism is because of the quick technical development exposed to either purposefully or unintentionally produced nanoparticles (particles of 1 nm to 100 nm), with which human body is incapable of dealing with [1, 2].

Sources producing nanoparticles, i.e. Ultra Fine Particles (UFP), can be divided into natural and anthropogenic. Natural sources of nanoparticles are for example volcanic activity, sandstorms or soil erosion. Anthropogenic sources of UFP, primarily within urban areas, are local combustion chambers, industry and traffic [3].

Nanoparticles are typical for their very slow sedimentation of submicron fractions that remain in the air for a very long time. Nanoparticles also significantly contribute to air pollution in areas with high density of traffic, e.g. in Moravian Silesian Region, and may enter human organism via airways, and thus endanger general state of health. For that reason, the risk arising from inhalational exposition of human body to these materials, to which heavy metals can be bond, considerably increases. The size of particles and its composition also negatively influence state of human health and possible health hazards [4]. There are metallic elements that are released to the environment during braking, which are given off from brake pads. Brake pads are composed of iron, barium, copper, aluminium, zinc, tin, lead and other metals [5]. It is impossible to eliminate or degrade heavy metals from the environment. We can only influence the quantitative component of their occurrence in the environment, provided that the source is anthropogenic. Harmful effect of heavy metals cannot be unequivocally classified for each metal as they themselves are part of human organism. Metals in the form of nanoparticles may remain in the air for quite a long period of time and are able to transport themselves through components of the environment. Some of the heavy

metals and their compounds cause dysfunction of blood formation, damage to nervous system or damages of internal organs [6, 7, 8].

Interest in potential effect of heavy metals on human health and the environment had been increasing recently. Some studies suggest that metals from vehicles have negative effects on the environment, however, we must not ignore the impact of other sources too (e.g. exhaust gases and tire wear). Other studies described effects of brake pad metals on water quality [9].

Even though it is typical to study emissions of exhaust gases and their impact on the environment in the field of motor traffic, the importance attached to abrasion of brakes is much smaller. During braking, a thermal-oxidation degradation of organic compounds, present in the brake lining, comes about. This process leads to formation and release of volatile organic compounds (VOC). Polycyclic aromatic hydrocarbons (PAH) were also detected in the abrasion. These volatile products emerging during abrasion may negatively influence the environment, and should be paid close attention to. These substances show mutagenic character [7, 9, 10]. The particles released during abrasion of brakes may be qualified as air dust or small particles. Abrasion of brakes in motor traffic consists of particles in the size of 10 nm to 20 μm . The smallest particles in the size of nanometres may be easily inhaled into airway, which may lead to formation of oxidative stress and inflammation. It has been proven that nanoparticles, if inhaled and penetrated to human organism, are transmitted by blood and taken to target tissues such as the liver, kidney and brain. Owing to the minuscule size of nanoparticles, their sedimentation is very slow and if released in the air, they may be transferred thousands of kilometres from their source [10, 11].

2. Experiment

The measurement was performed on the testing dynamometer of frictional properties of vehicular brake pads (Link M2800, see Fig. 1). Two types of brake pads were tested - low metallic and non-asbestos composites. Frictional composites with reduced metal content that include 5 – 15 % of metallic content, are mostly comprised of ceramic fibres and other padding materials. They make less noise during braking than other types of frictional composites. Non-asbestos frictional composites (NAO - Non-Asbestos Organic) that include metallic content up to 5 %, are made of organic materials, such as fibres, rubber, glass, Kevlar and high-temperature resin [12].



Fig. 1. Testing dynamometer of frictional properties of vehicular brake pads (Link M2800).

To evaluate analysed emissions from braking on the dynamometer (Fig. 2), we used scanning mobility particle sizer (SMPS), which measures the amount of particles along with their dimensions from the size of 10 nm to 200 nm with the use of detection of electric mobility [13]. We presupposed an excess concentration of released particles, thus it was necessary to dilute the taken sample. The dilution factor was set at 100:1 and the dilution machine flow rate was 1 litre/min [14]. Furthermore, the sampling system NANO ID SELECT 005 was employed. The system collected particles of the size from 2 nm to 35 μm . The particles were assorted

in compliance with their size into 12 fractions. The sampling system of the device is divided into 2 collection parts - cascade impactor and diffusion cell [15, 16].

The samples taken were analysed using the method of Inductively Coupled Plasma Mass Spectrometry (ICP-MS). The ICP-MS represents an ultrametric analytic method serving to determine the volume of metric amounts of individual elements in the analysed sample. This method allows to analyse almost all elements starting from lithium up to uranium with the sensitivity from units of ppm up to hundreds of ppm. Another advantage of the method is the possibility to simultaneously set several elements [17].

To determine mass concentration of elements, we used the Respiratory Tract Deposition Model that serves to determine the mass of individual metals as an accumulative dose of the total and alveolar deposited fraction of aerosol in the affected part of the respiratory tract [18].

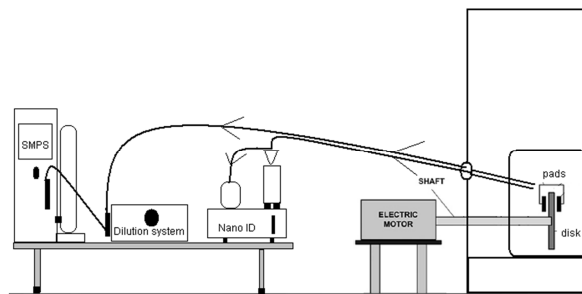


Fig. 2. Layout scheme of the experiment.

3. Results

The Fig. 3 to Fig. 8 depict size distribution of mass concentration of the metals selected by means of the ICRP model. You may see three types of markings on the graphs. The marking called "In the air" represents the mass of the metal that is released in the air, the "DF" marking represents the mass of the metal that is deposited in the alveolar area of lungs, and the "DFal" marking represents the mass of the metal that is deposited in the alveolar and tracheobronchial area of lungs.

For non-asbestos friction composites NAO of a brake pad:

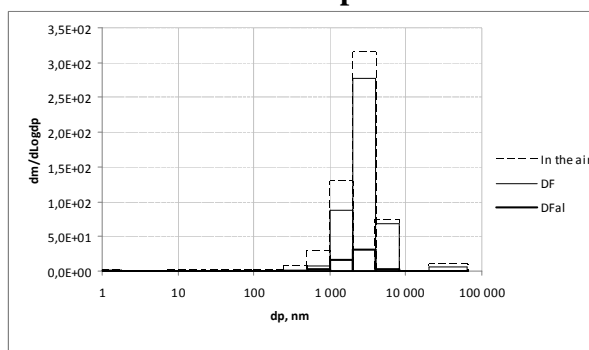


Fig. 3. Deposition of alveolar and total fraction of copper in accordance with the inhale model ICRP.

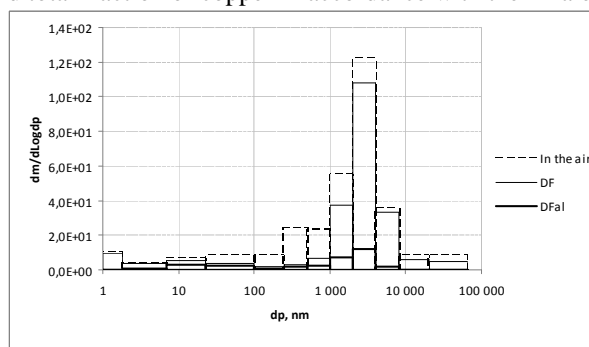


Fig. 4. Deposition of alveolar and total fraction of copper in accordance with the inhale model.

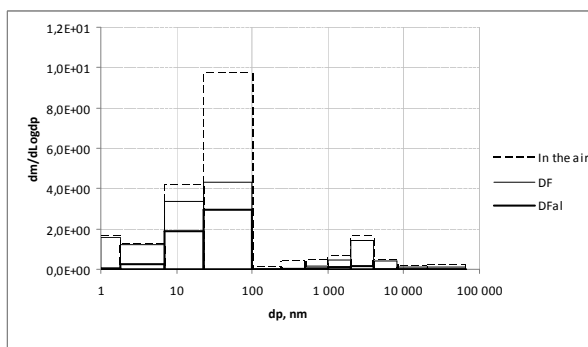


Fig. 5. Deposition of alveolar and total fraction of manganese in accordance with the inhale model ICRP.

For low metallic brake pads (LOW METAL brake pads):

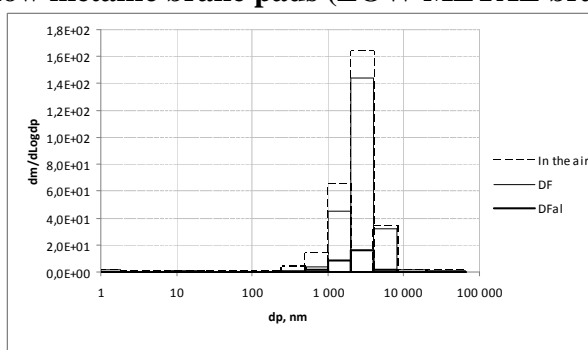


Fig. 6. Deposition of alveolar and total fraction of copper in accordance with the inhale model ICRP.

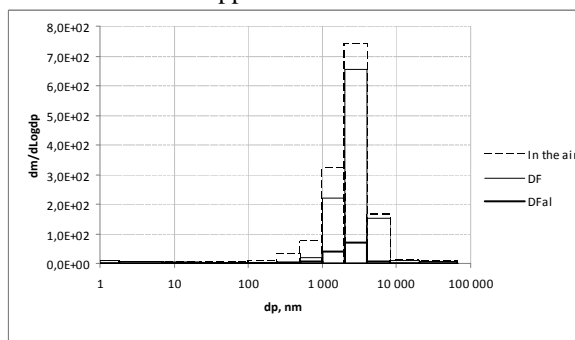


Fig. 7. Deposition of alveolar and total fraction of iron in accordance with the inhale model ICRP.

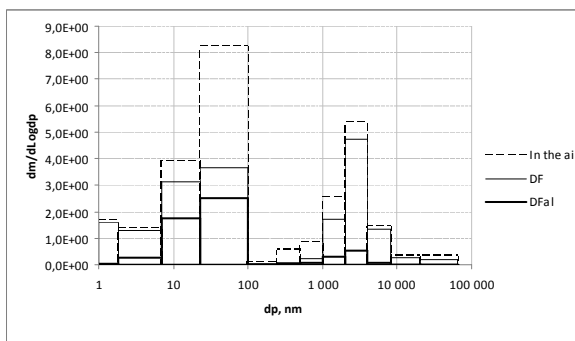


Fig. 8. Deposition of alveolar and total fraction of manganese in accordance with the inhale model ICRP.

For illustrative purposes, a few graphical depictions of these spectra were chosen from several measurements performed by the SMPS device. Testing conditions: 30-80 km/h, 30 bars - pressure of brake pads on a brake disc.

Fig. 9 depicts only particles of the size of 100 nm with temperatures from 50 - 300 °C. The measuring time was 3 minutes and 25 seconds, several brake cycles were performed during this period of time. The NAO (Non-asbestos organic) type of brake pads was used.

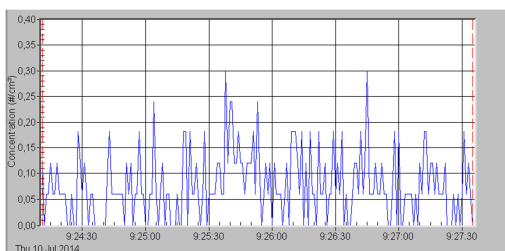


Fig. 9. Size distribution of 100nm particle (with the dilution machine).

Fig. 10 depicts only particles of the size of 100 nm with temperatures from 50 – 300 °C. The measuring time was a little less than 7 minutes, several brake cycles were performed during this period of time. The low metallic (low metal) type of brake pads was used. The concentration of particles of the size of 100nm ranged maximally to 30 particles/cm³.

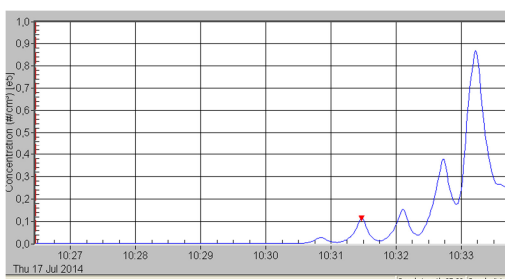


Fig. 10. Size distribution of 100nm particle (without the dilution machine).

4. Conclusion

We performed sampling and monitoring of fine particles, which were released in the course of abrasion of brake pads on a dynamometer. Thereafter, chemical composition of the samples was determined using the ICP-MS method. Presence of the following metals was proved: Al, Cr, Cu, Fe, Zn, Pb, Mo and Co. In case of non-asbestos friction composites (NAO), manganese predominated within ultrafine particles, copper and iron predominated within larger particles. In case of friction composites with low content of metals (low metal), manganese predominated within ultrafine particles, and iron predominated within larger particles.

Sampling was completed with monitoring of particles SMPS that uses the method based on electric mobility of particles. In case of non-asbestos friction composites (NAO), particles of the size of 200 nm predominated. In case of friction composites with low content of metals (low metal), particles of the size under 100 nm predominated.

The performed experiments on abrasion of brake pads showed that particles smaller than 100nm are released in the air. And so it turned out that braking processes represent a source of air contamination by nanoparticles, inclusive of particles that, thanks to their size and also their chemical composition, pose potential risk for human health.

Acknowledgement

This work originated as a part of solution of the project SP2015/169 Comparison of Estimate of Professional Exposition of Aerosol Particles with Substantial Toxic and Carcinogenic Effect by means of an Empiric, Physically-Chemical Model and Experiment with the Management of Health Hazards on Workplace and the project SP2015/132 Emission of Fine Particles of Anthropogenic Activities (household heating, braking processes of vehicles).



References

- [1] NOHAVICA, D. *Risks of Nanomaterials and Nanotechnologies for Human Health and the Environment*. 2011. Available in Czech at: https://moodle.fp.tul.cz/nano/pluginfile.php/1401/mod_resource/content/1/nohavica-clanek-o-nanotoxicite.pdf.
- [2] KALIČÁKOVÁ, Z., et al. *Urban Air Pollution by Nanoparticles in the Ostrava Region*. 2013. Available in English at: <http://iopscience.iop.org/1742-6596/429/1/012005?fromSearchPage=true>.
- [3] SKREHOT, P. RUPOVÁ, M. *Nano-safety*. 1. ed. Prague: Occupational Safety Research Institute, 2011. 230 s. ISBN 978-80-86973-89-0.
- [4] HINDS, W.C. *Aerosol Technology*, John Wiley & Sons, Inc., New York, 1999.
- [5] FARA, Milan. (2003) *Toxicologically Dangerous Substances in Emission PM10*. PRAGUE. Project. Chzech Hydrometeorological Institute. Available in Czech at: http://old.chmi.cz/uoco/prj/vav_740_3_02/dp1dod.pdf.
- [6] FILIPOVÁ, Z, KUKUTSCHOVÁ, J., MAŠLÁŇ, M. *Danger of Nanomaterials*. 1. ed. in Olomouc: Palacký University, 2012. ISBN 978-80-244-3201-4.
- [7] COX, R.L. *Engineered Tribological Composites*. 1st ed. Warrendale: SAE International, 2012. 505 p. ISBN 978-0-7680-3485-1
- [8] FILIP, P., WEISS, Z., RAFAJA, D. *On Friction Layer Formation in Polymer Matrix Composite Materials for Brake Applications*, *Wear* 252, 2002.
- [9] VAŠAK, R. *Problems of Asbestos and its Effect on the Environment*. 2007, Zlín. Bachelor Theses. Tomáš Baťa University. Available in Czech at: https://dspace.k.utb.cz/bitstream/handle/10563/3029/va%C5%A1k_2007_bp.pdf?sequence=1.
- [10] KUKUTSCHOVÁ, J.; MORAVEC, P.; TOMÁŠEK, V.; MATĚJKA, V.; SMOLÍK, J.; SCHWARZ, J.; SEIDLEROVÁ, J.; ŠAFÁŘOVÁ, K.; FILIP, P.: *On Airborne Nano/Micro-sized Wear Particles Released from Low-Metallic Automotive Brakes*, Original Research Article, *Environmental Pollution*, Volume 159, Issue 4, April 2011.
- [11] KUKUTSCHOVÁ, J., ROUBÍČEK, V., MAŠLÁŇ, M., JANČÍK, D., SLOVÁK, V., MALACHOVÁ, K.; PAVLÍČKOVÁ, Z., FILIP, P.: *Wear Performance and Wear Debris of Semimetallic Automotive Brake Materials*. *Wear*, Volume 268, Issues 1–2, 4 January 2010, pp. 86-93.
- [12] ANDREW, J. *Braking of Road Vehicles*. Butterworth-Heinemann, 2013. ISBN 978-012-3973-146.
- [13] TSI. *Scanning Mobility Particle Sizer™ SPMeter Model 3936*. 2013 Available in English at: http://www.tsi.com/uploadedFiles/_Site_Root/Products/Literature/Spec_Sheets/SMPS3936-3034.pdf.
- [14] DILUTION SYSTEM MODEL 3332. 2014. Available in English at: http://www.tsi.com/uploadedFiles/_Site_Root/Products/Literature/Application_Notes/3332_Dilution_System_Appnote_3332-001-web.pdf.
- [15] NANEUM. *SamplerNano-ID™ Select*. 2015. Available at: <http://www.naneum.com/products/particle-measurement/samplers/nano-id-select.html>.
- [16] WIDE RANDE AEROSOL SAMPLING SYSTEM. *Nano ID Select 005*. Canterbury, 2009.
- [17] MIHALJEVIČ, M., STRNAD, L., ŠEBEK, O. *Use of Mass Spectrometry with Inductively Bound Plasma in Geochemistry*. *Chemické listy*. 2004, NO. 98. Available in Czech at: http://www.chemicke-listy.cz/docs/full/2004_03_02.pdf.
- [18] ICRP. *Human Respiratory Tract Model for Radiological Protection*. Publication 66. Ann. ICRP 24 (1-3), 1994.



Optimization of Atypical Heat Exchanger with Using CFD Simulation

*Martin Kasanický, *Richard Lenhard, *Milan Malcho

*University of Žilina, Faculty of Mechanical Engineering, Department of Power Engineering, Univerzitna 1, 01026 Žilina, Slovakia, {martin.kasanicky, richard.lenhard, milan.malcho}@fstroj.uniza.sk

Abstract. This article deals with the optimization of atypical heat exchanger with using CFD simulations of 8 variants. In an effort to find a suitable heat exchanger geometry in terms of pressure and in terms of heat - transfer properties.

Keywords: Heat pipe, Heat exchanger, CFD simulation, Pressure drop.

1. Identification of Solved Issue

The heat exchanger will serve as a heater and as a cooler in the device for measuring the thickness of a falling condensate in gravity assisted heat pipe with using optical triangulation method (hereinafter DMTFC). This device is located in Fig. 1.

Heater and the cooler will be connected to circulation thermostat Julabo, heat transfer fluid is distilled water. The problem with these thermostats are relatively low available pressure. In particular, is the value of 0.7 bar at the volumetric flow rate of 26 l min^{-1} . Therefore, the task is to optimize the heat exchanger, which will have the best possible heat transfer coefficient at the lowest pressure drop. The material of the heat exchanger is stainless steel.

On Fig. 2. is shown only one part of the exchanger. Complete exchanger will also contain his counterpart and both parts will be welded.

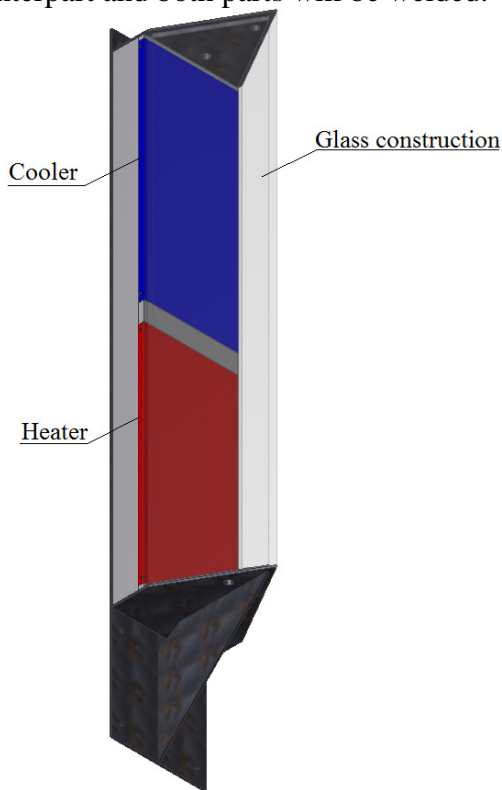


Fig. 1. The main concept of DMTFC.

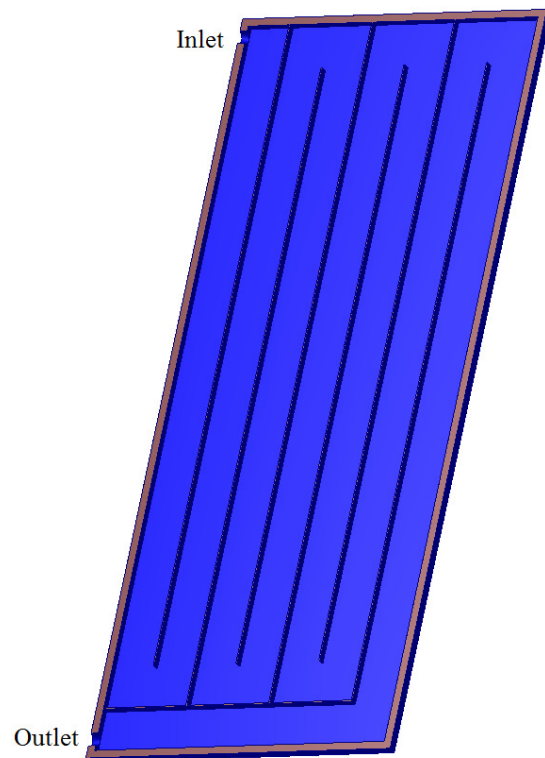


Fig. 2. The basic design of the heat exchanger.

The problem with this design is to estimate the right number of barriers in the exchanger, not to exceed the required pressure drop. For that reason was made a simulation in ANSYS CFX with 0, 2, 4, 6, 8, 10, 12 and 14 of the barriers. 14 barriers is the maximum capacity of the structure while maintaining the same uniform geometry for all simulations.

2. Simulation of Individual Variants

The calculated area of individual variants was implemented by hexahedral mesh created with ICEM CFD. The entire model features of three meshes. The first is the interior of the heat exchanger (this mesh is shown in Fig. 3.), the second mesh is the wall of heat exchanger through which the heat is transient to DMTCF and the third is a layer of a falling condensate in DMTCF (heat - transfer medium in the heat pipe is also distilled water). Turbulence model for both fluid domain is k-ε.

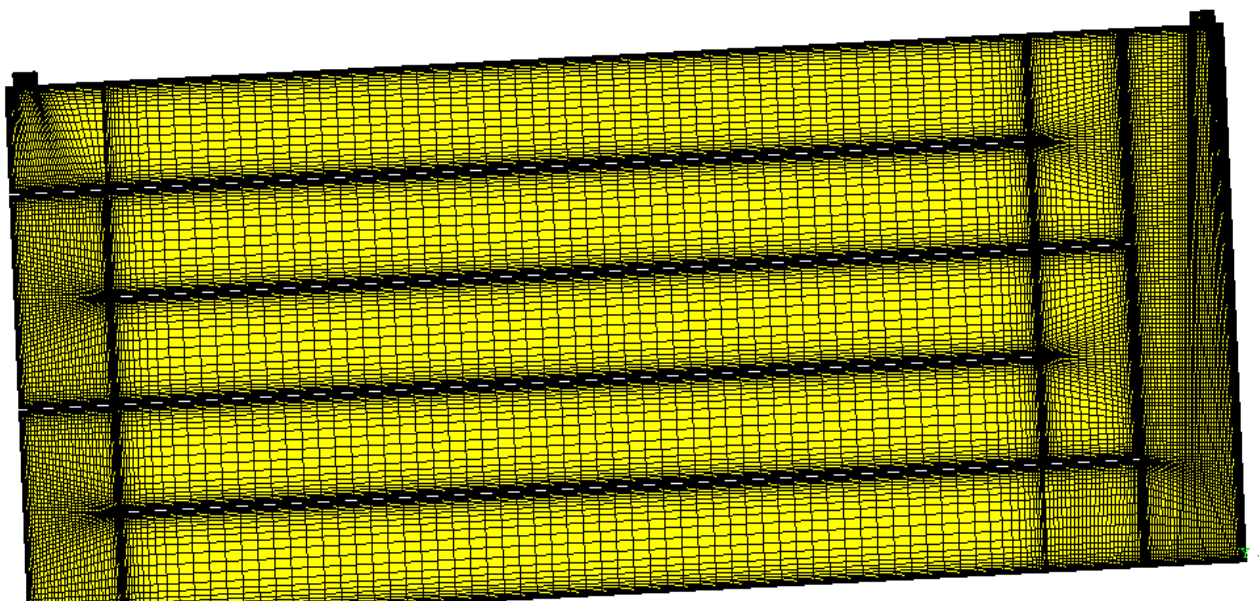


Fig. 3. The mesh of 4-barriered heat exchanger.

Boundary conditions are: input speed into the exchanger, which is derived from the maximum volumetric flow of water in circulating thermostat and the pressure at the outlet of the exchanger. Next, input speed of a falling condensate and its output pressure. These values were estimated by calculating the rate of falling of condensate, but its accuracy is questionable. It should be noted, however, that simulation is designed as an optimization nature, where the most important element is just the pressure drop through the heat exchanger and the second row is the heat transfer coefficient coefficient, whose value is calculated based on the estimated values given boundary conditions and, therefore, its value may be regarded as for comparison against other simulations. Boundary conditions are shown in Tab. 1.

The normal velocity in heat exchanger inlet	4.4	m.s ⁻¹
Temperature of water inlet	80	°C
Pressure behind the heat exchanger	1	bar
The normal velocity of falling condensate (estimated)	0.025	m.s ⁻¹
Temperature of falling condensate (estimated)	30	°C
Pressure of condnsate in an end of the computation area	3	bar

Tab. 1. Boundary conditions.

3. Evaluation of Simulations

The calculation results of the individual simulations are in Tab. 2. and Fig. 4.

Account of barriers	Pressure drop [kPa]	Heat transfer coefficient [$\text{W}\cdot\text{m}^{-2}\cdot\text{K}^{-1}$]
0	14,9	4091
2	17,9	5709
4	27,3	7593
6	40,7	8949
8	67,3	10678
10	109,9	12765
12	171,8	14598
14	257,1	16365

Tab. 2. Pressure drop and heat transfer coefficients of individual variants.

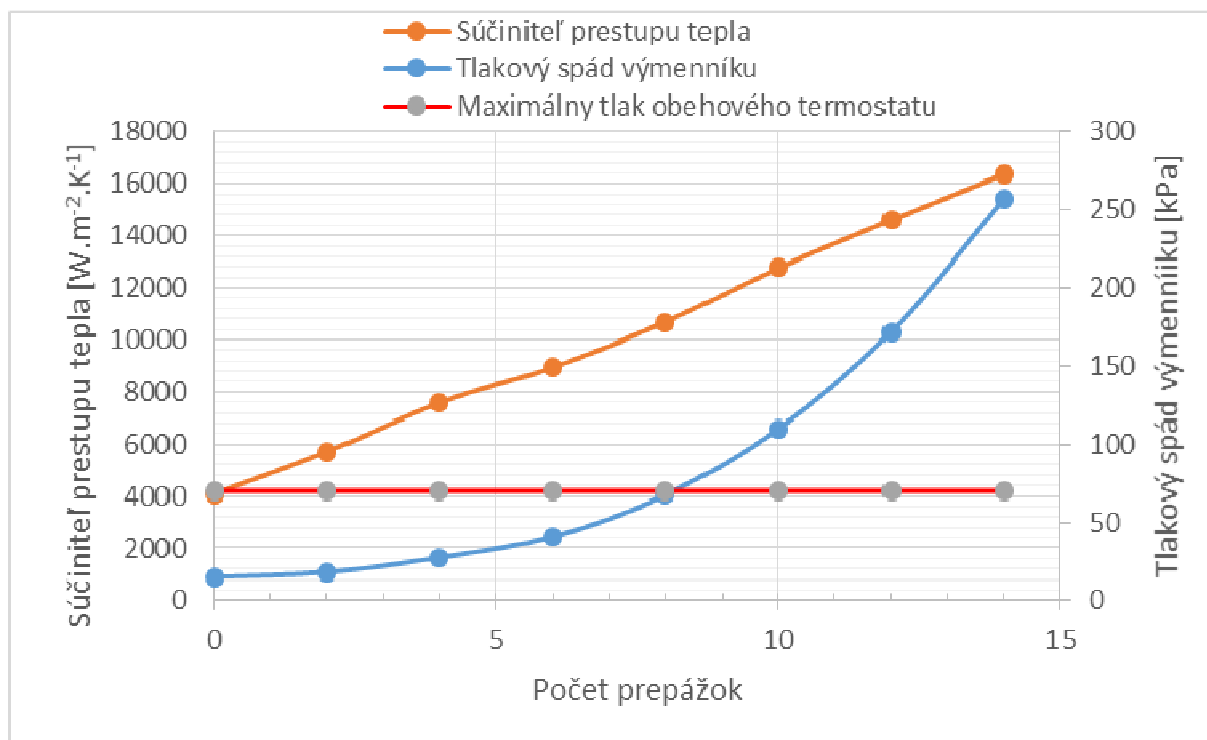


Fig. 4. The dependence of the coefficient of heat transfer and pressure drop of the number of partitions exchanger.

Based on the calculated results can be determined that the optimum heat exchanger should have eight barriers since reaching 67.3 kPa. However, the maximum pressure of the circulation thermostat of 70 kPa and it should also in mind the fact, that the exchanger is connected with piping, which also causes a certain pressure drop. For this reason can be considered as optimal exchanger with six barriers.

The graph in Fig. 4. also shows that, while the heat-transfer coefficient varies almost linearly in substance, the pressure drop increases convex. This is logical, because the only changing parameter is the internal flow speed in the heat exchanger, which increases with increasing amount of barriers. Fig. 5 is a comparison of velocity vector fields in heat exchangers with the number of barricades 0, 6 and 14.

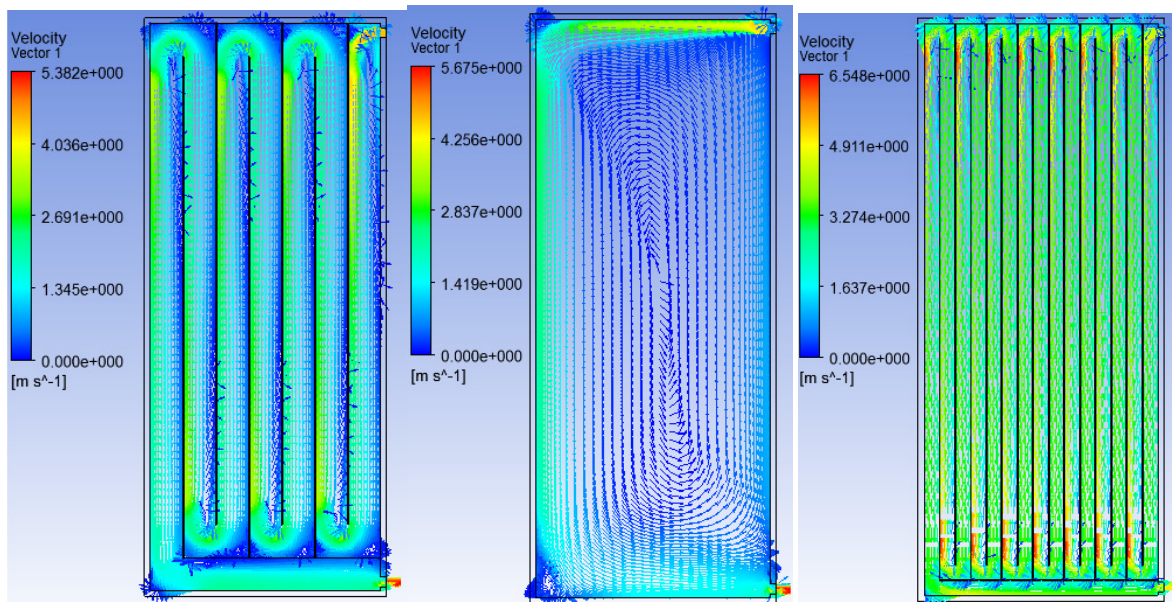


Fig. 5. Comparison of velocity vector fields with the number of partitions 0, 6 and 14.

From the figure it can be observed that while in the first two cases, the maximum flow rate achieved at the outlet of the heat exchanger, because there is the narrowest cross section, in the third case is the highest velocity after barrier.

4. Conclusion

From the simulation results may generally be concluded that if the only change in calculation is the number of barricades and therefore a different internal flow velocity, heat transfer coefficient varies linearly, but the pressure drop varies parabolically. Therefore, in terms of energy preferred to select a smaller number of partitions.

Acknowledgement

This work was financially supported by the project APVV 0577-10 "cooling of power electronic systems without mechanical drives"

References

- [1] FAGHRI, A., ZHANG, Y. *Transport phenomena in multiphase systems*. Academic Press, 2006
- [2] M. KASANICKÝ M., LENHARD, R., MALCHO, M., *Mathematical Model of Heat Transport through Gravity* AENMATE proceeding, 2014.
- [3] SULOVCOVA, K., JANDAČKA J. *Option of solid pollutants abatement in flue gas path*. In *Komunikacie*, Volume 15, Issue 4, 2013, Pages 44-47
- [4] NEMEC P., ČAJA, A., LENHARD. R. *Visualization of heat transport in heat pipes using thermocamera* In *Archives of Thermodynamics*, Volume 31, Issue 4, 2010, Pages 125-132



The Device for Measuring the Thickness of the Falling Condensate in the Gravity Assisted Heat Pipe

*Martin Kasanický, *Alexander Čaja, *Milan Malcho

*University of Žilina, Faculty of Mechanical Engineering, Department of Power Engineering, Univerzitna 1, 01026 Žilina, Slovakia, {martin.kasanicky, alexander.čaja, milan.malcho}@fstroj.uniza.sk

Abstract. The main problem of designing systems which uses heat pipes is a large number of variables, whether it is a traditional - gravity, or advanced - capillary, pulsating, heat pipes. This article is a basic methodology for measuring the thickness of the falling condensate in gravitational heat pipes, with using the optical triangulation method, and the evaluation of risks associated with this method.

Keywords: Heat pipe, Optical triangulation, Falling condensate.

1. Introduction

CFD simulations of gravity assisted heat pipes (GAHP) are nowadays common practice. However, the current CFD models are not robust and flexible enough to capture a wide range of conditions occurring within the heat pipe. For this reason it is necessary to pay more attention to adapting these models in order to capture larger number of functional states within GAHP.

2. Theoretical Background of the Draft

Nowadays there are many approaches to calculate the heat pipes properties. One of these approaches is the calculation of GAHP heat performance parameters is based on knowledge of the falling condensate thickness. According to [1], the average value of Nusselt Reynolds number in the laminar flow region can be stated as

$$Nu = \frac{\alpha_L}{\lambda_L} = \left[\frac{\eta_L^2}{\rho_L \cdot (\rho_L - \rho_V) \cdot g} \right]^{\frac{1}{3}} = \frac{4}{3} \cdot \frac{(\delta^*)^3}{x^*} + \frac{2 \cdot (\delta^*)^2 \cdot \tau_\delta^*}{x^*}, \quad (1)$$

$$Re_\delta = \frac{4}{3} \cdot (\delta^*)^3 + 2 \cdot (\delta^*)^2 \cdot \tau_\delta^* \quad (2)$$

where α_L is the heat transfer coefficient of the liquid phase, λ_L is thermal conductivity of the liquid phase, η_L dynamic viscosity of the liquid phase, ρ_L and ρ_V density of liquid and vapour phase respectively and g is the gravity acceleration. Another – dimensionless variables are expressed as follows

$$\delta^* = \frac{\delta}{L_F}, \quad (3)$$

$$x^* = \left(\frac{x}{L_F} \right) \cdot \frac{4 \cdot c_{pL} \cdot \Delta T}{Pr_L \cdot l_V}, \quad (4)$$

$$\tau_{\delta}^* = \frac{\tau_{\delta}}{(\rho_L - \rho_V) \cdot g}, \quad (5)$$

where δ is the falling condensate thickness, x is the coordinate in direction of the flow (by common configuration it is vertical downwards direction), c_{pL} is the constant pressure specific heat of the liquid phase, ΔT is the temperature difference between wall and liquid, Pr_L is the Prandtl number of liquid phase, l_V is heat of evaporation, τ_{δ} is the interfacial shear stress between liquid and vapor phase and

$$L_F = \left[\frac{\eta_L^2}{\rho_L \cdot (\rho_L - \rho_V) \cdot g} \right]^{\frac{1}{3}} \quad (6)$$

With combination of equations 3,4 and 5 we can get equation criteria equation

$$x^* = (\delta^*)^4 \frac{4}{3} \cdot (\delta^*)^3 \cdot \tau_{\delta}^* \quad (7)$$

The last formula is an expression of one variable through the second and, therefore, it is necessary to solve the system of equations iteratively. It should be noted, however, that the knowledge of the thickness of the condensate, the system of equation can be solved with a single variable (is also relative, since all material constants are a function of its temperature, which varies with the thickness of the condensate in the y direction, but for the purpose of further assume, it can be considered as a constant.). The above equations are valid for laminar flow regime of falling condensate. For turbulent flow it can be also used a wide range of correlations that can be found in the referenced literature.

3. Optical Triangulation Method

The method is based on of this method is to light the walls of the tube and at the same time the layer of condensate running down the laser beam and the reflection from the two capture facility using a CCD camera, as shown the layout in Fig. 1.

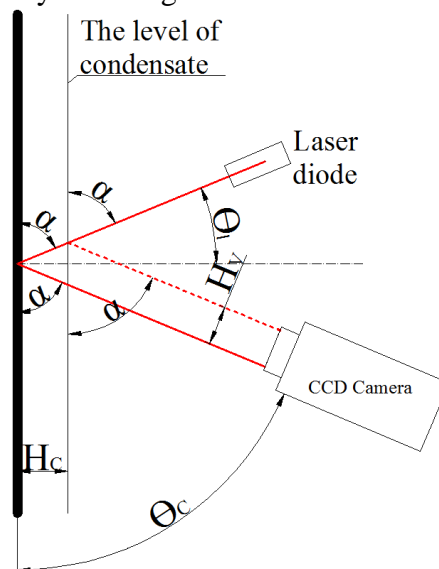


Fig. 1. The principle of optical triangulation.

Based on the layout, the condensate thickness equation can be determined as

$$H_c = \frac{H_V \cdot G_x}{\cos(\Theta_c)} \cdot \left[\frac{1}{1 + \text{tg}(\Theta_c) \cdot \text{tg}(\Theta_c)} \right] \quad (8)$$

Where H_C is condensate thickness, H_V is the distance shown at CCD camera, G_X is the optic magnification, θ_C is angle which make camera with the drenched wall and θ_L the angle which make laser beam with the wall. Optical principle of the method was tested on glass-plate, in which water has sprayed.



Fig. 2. Experimental device to test the applicability of the method.

On the basis of this experiment it was evaluated the optimal color of the laser beam recorded by CCD camera is in the green part of the light spectrum. The experiment also showed that the distilled water at ambient temperature (20 °C) is not an appropriate medium for the thickness measurement by using this method, because the glass surface does not form a continuous film. This deficiency may be removed by heating the water to a higher temperature because the increased temperature decreases surface tension value. When using ethanol system worked properly.

4. Design of the Device for Condensate Thickness Measurement

The suggested device will be constructed according to the scheme in Fig. 3. and Fig. 4. The basis of the device is a glass construction with a hollow triangular prism, which will work as GAHP. The glass structure is inserted in a steel frame, which is attached by screws to the wall. Anticipated working liquids in heat pipe will be distilled water and ethanol. Triangular cross-section construction is designed by means of the elimination of refraction passing through a glass wall, or on the side of the laser beam emitted from the diode, or reflections on the side of the CCD camera. Principle of operation of GAHP will be driven by using two heat exchangers. One will work as a heater (evaporator) and the other as a cooler (condenser). The two heat exchangers are coequal.

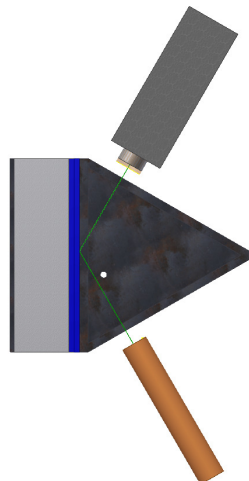


Fig. 4. Detail of the device.

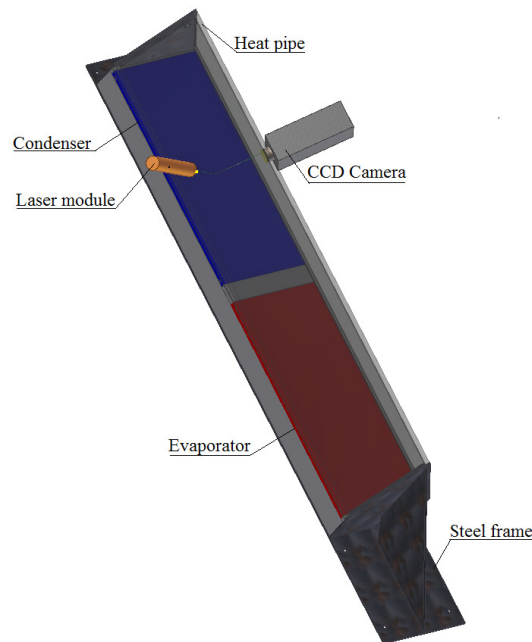


Fig. 3. Schematic of measuring the thickness of the condensate in GAHP.

Each exchanger is individually connected to the circulation thermostat Julabo and heat transfer fluid is distilled water. In each independent circuit will be used PT100 temperature sensors at the inlet and the outlet of the heat exchanger and also has a flow meter, in order to use a calorimetric method to express performance at separate heat exchangers, as well as the actual power delivered by the heat pipe.

The pressure and the amount of charge in the heat pipe will be accomplished by gradual evaporation of the working fluid of the heat pipe. The entire device will be thoroughly insulated using extruded polystyrene. The polystyrene plates for the other two glass surfaces are still in addition, supported by two permanent magnets in order to be able to move them vertically and with them move the laser module and a CCD camera in the vertical direction (the horizontal direction as well as, to obtain the biggest possible picture on heat pipe main wall). On these polystyrene plates will be, from the outside, in addition placed heating infra-foil to prevent condensation on these glass surfaces. Such condensation would be impossible to measure the thickness of the condensing optical triangulation method.

Acknowledgement

This work was financially supported by the project APVV 0577-10 "Cooling of power electronic systems without mechanical drives".

References

- [1] FAGHRI, A., ZHANG, Y. *Transport phenomena in multiphase systems*. Academic Press, 2006.
- [2] LENHARD, R., MALCHO, M. *Numerical simulation device for the transport of geothermal heat with forced circulation of media*. In *Mathematical and computer modelling*, Volume 57, Issue 1-2, January 2013.
- [3] NEMEC, P., MALCHO, M., SMITKA, M., MATUSOV, J. *Performance parameters of a closed loop thermosyphon*. In *Komunikacie*, Volume 14, Issue 4 A, 2012.
- [4] NEMEC P., ČAJA, A., LENHARD. R. *Visualization of heat transport in heat pipes using thermocamera* In *Archives of Thermodynamics*, Volume 31, Issue 4, 2010.
- [5] MALCHO, M., JANDAČKA, J., VANTÚCH, M., KAPJOR, A., GAVLAS, S. *Transfer of low-potential heat from a deep borehole by means of a heat pipe and heat pump* In *Komunikacie*, Volume 14, Issue 4 A, 2012,



Comparison of cooling electro static converters with classic ribbed cooler and heat pipes

*Luboš Kosa, *Alexander Čaja, *Martin Kasanický

*University of Žilina, Faculty of Mechanical Engineering, Department of Power Engineering, Univerzitna 2, 01026 Žilina, Slovakia, {alexander.caja, lubos.kosa, martin.kasanicky}@fstroj.uniza.sk

Abstract. In recent years saw a great increase miniaturization of some heat-stressed equipment mainly in electronics and mechatronics. Design and produce a more complex and energy-consuming equipment. When the device is efficient, then the majority even higher heat loss-making power, which is necessary in order to maintain safe operating temperatures due. The paper deals with the problem of heat dissipation of electrostatic converters using a ribbed radiator or heat pipes. Normally for cooling electrostatic devices use different types of cooling using finned heat sinks that use the principle of free or forced convection often. To achieve the forced convection is used by various fans, resulting in increased risk of failure, because these devices have moving parts. Therefore it is developing such types cooling that these fans not need. As a prospective cooling appears use of heat pipes.

Keywords: Heat pipe, Cooling, Heat transport, Heat loss.

1. Introduction

The electrostatic converter is a device used to change the parameters of current and voltage used for railway wagons. For this converter was studied suitable cooling system. Commonly used static converters are mainly cooled by air flow around the surface, and there is only the convective heat transfer. To ensure air flow fans are mainly used with suitably shaped plates. However, this increases the failure rate and the difficulty of maintaining, because the fans contain moving parts which are wear out by the own operations. Therefore, consideration is given to change cooling methods of electrostatic converters. The best way seems to use heat pipes. Heat pipes are working on the principle of phase change of the working fluid, so that no moving parts are maintenance free and their thermal conductivity is much higher than that of metallic materials of the same diameter solid section. Their main duty is to lead the heat generated by electrostatic converter into place with lower ambient temperature, and there it through ribbed cooler transmit into the surroundings by natural convection.

To get an idea of the quantity of heat produced by a particular method of heat transfer in the actual inverter, and a subsequent proposal from the best cooling method had to be electrostatic converter scanning a first in terms of output and losses. To measure these heat outputs and losses, as well as the cooling systems themselves can use either the original electrostatic converter, which is used in practice, or geometrically similar model. Due to the temperature measurements inside the body energy converter was to compare different methods of cooling produced geometrically identical model. In the case of the original electrostatic converter would need to drill holes for mounting thermocouples near the winding transformers. Would risk damaging the insulation or could follow to its destruction and thus destroy the transformer itself. In addition, the actual converter would have to be supplied and also burdened with too high currents and voltages. From the following operational and safety reasons was used a model of the electrostatic converter.

The base model consists of an aluminum container that is used for the mass production of transformers electrostatic converters. To pack is inserted two electrical insulating toroids, which were equipped with ohmic resistances, which are shaped winding transformer



Fig. 1 Location of the transformer in the machine housing.

The resistors are connected in series and the total resistance is $\sim 10 \Omega$, corresponding winding resistance in real static converters. The Joule heat generating resistor is DC powered from a regulated voltage source. Based on this assumption and the known values of voltage and current was determined the theoretical heat output model. This performance was later verified to measurement of heat loss in a thermostatic chamber. This performance was later verified to measurement of heat loss in a thermostatic chamber.

In addition to resistance toroids were entered into the model and temperature sensors - thermocouple. Their location was selected to be the minimum of the thermocouples recorded a temperature as accurately as possible on the surface and inside the ring, also in the vicinity of the aluminum hub. The distribution of thermocouples is shown in Fig. 2. The space between the toroid and the container was filled mass model, which thermal and electrical insulating properties were similar thermal and electrical properties of the resin used in mass production.

Completely primary intention was to use an aluminum mandrel positioned in the middle of converter and fixed to the bottom of the outer packaging. The mandrel serves to faster heat dissipation from inside the converter. However, this method does not seem sufficient. While the mandrel diverting heat more quickly to the surface, the insufficient cooling due to the small surface of transmission and a low coefficient of heat transmission of the outer coating to the environment.

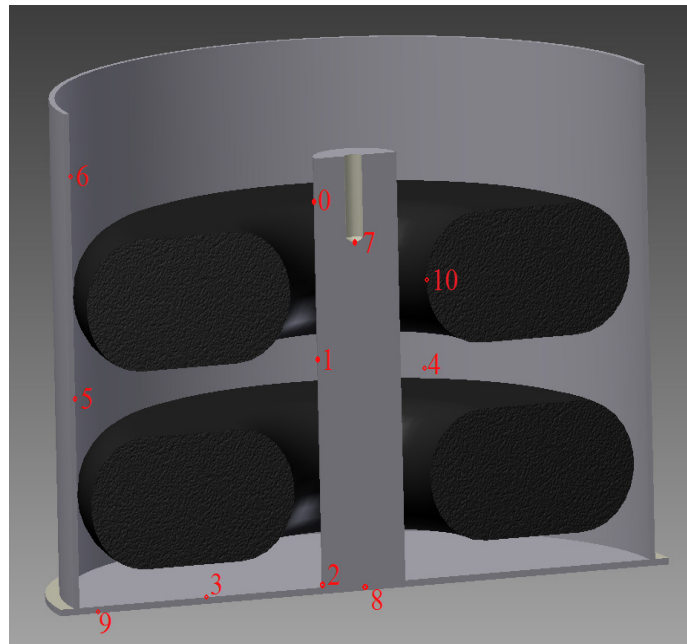


Fig. 2 Location of thermocouples in the model of the electrostatic converter.

2. Measurement temperatures on the inverter in a thermostatic chamber

In order to assess the properties of each cooling systems static an energy converter, it was necessary to provide several temperature levels at which it would be simulated release of heat loss and constant power to determine the temperature distribution of the measured points in stationary mode. For this reason, was conducted a range of experiments at three different ambient temperatures and two heat output generated by Joule heating simulating power dissipation 30 and 50 W. All temperatures and heat output, respectively voltage and electric current regulated power supply were measurement by logger and they are recorded on a computer screen so as to reaching steady state level of the different temperatures, and that the system got to thermodynamic equilibrium.



Fig. 3 Model of electrostatic converter without cooler.



Fig. 4 Model of electrostatic converter with cooler.



Fig. 5 Model of electrostatic converter with heat pipe.

The individual measures were carried out to compare the three types of heat transfer - convection from the surface of the transformer, convection of the heat sink located on the surface and by heat pipe placed in an aluminum mandrel transformer.

All measurements were made in a thermostatic chamber, where they were simulated three different temperatures at two different heat output of the heat loss model. The heat output of the model was controlled by source of electrical energy on the values of 30 W and 50 W, the temperature were set in a chamber by thermostatic control to 30°C, 50°C and 70°C. Measurements were conducted at two different heat output. The reason was that the static power converters are used transformers of different power. Size frame, which are stored, remains the same. Temperature range was chosen based on experience with the use of energy converters. In normal operation is usually ambient temperature of about 40°C, but if the converter is not sufficiently cooled and is fully charged, it reaches the ambient temperature in the frame to 70°C.

In the transformer were generally measured temperatures in ten different points. For comparison, however, selected only two of them. The first section characterizes the place with the highest measured temperature. This is because, in order to detect the intensity of heat transfer from the center of the transformer. The second point is characterized by a point at the surface. Watched the intensity of cooling, depending on ambient temperature.

3. Evaluation of measured variables

From figure No .6 follows that in performance of heat 30 W and about 70 ° C, the differences between the various methods of heat removal is stationary significant, particularly with regard to free-cooling heat sink and the other two types of cooling, the best way of cooling the heat removal using heat pipe.

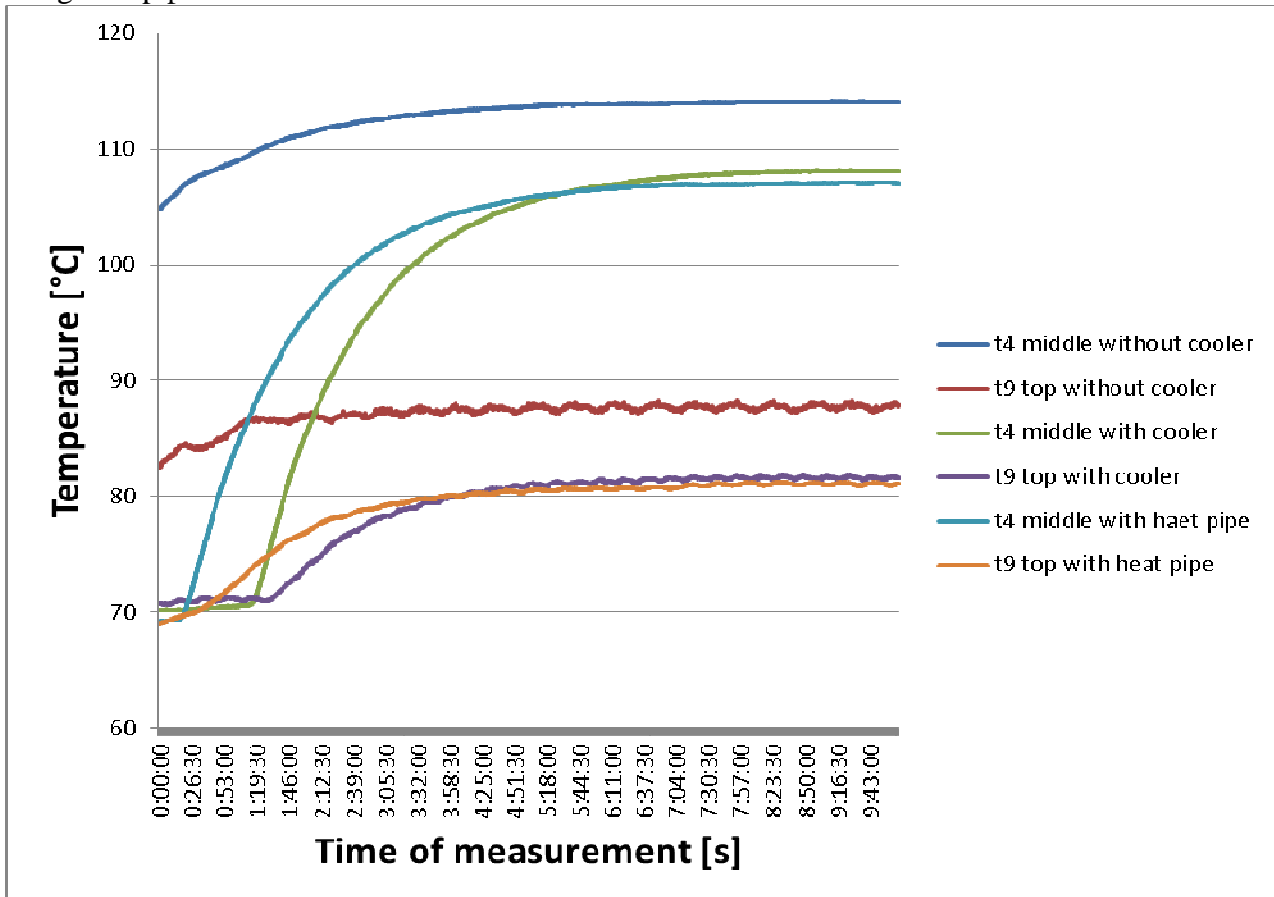


Fig. 6 Comparison of the temperature curve at selected locations inverter for each method of cooling in heat output of 30 W and an ambient temperature of 70°C.

Behind the cooling by the heat pipe followed heat transport by a ribbed cooler with vertical ribs and highest temperatures drop to remove the same cooling performance at the same ambient temperature needs to plain sheath inverter without ribs. The temperature difference on the surface and inside the body of the inverter in this case the cooling without heat and the remaining types of cooling is about 6-7 ° C

4. Conclusion

In the experiment, we investigated the course of temperatures in heat-exposed areas of the body of the converter. The results show that there is still the possibility of optimizing the construction of such facilities. The new structure of static converter will enable transport the heat produced as power loss and thus ensure a reduction in temperature, especially in winding isolation transformer of the converter and contribute to increasing the reliability of the device.

Acknowledgement

This work was part of the project APVV – 0557 – 10.



References

- [1] NEMEC, P., MALCHO, M., HOLUBČÍK, M. *Heat removal from bipolar transistor by loop heat pipe with nickel and copper porous structures*. The scientific world journal, 2014, ISSN 1537-744X.
- [2] NEMEC, P., MALCHO, M., HOLUBČÍK, M. *Experimental investigation thermal performance and visualization heat transfer dynamics of mesh screen wick heat pipes*. IN-TECH 2014, ISSN 1849-0662
- [3] NEMEC, P., ČAJA, A., MALCHO, M. *Testing thermal properties of cooling device with heat pipes to improve his heat transfer ability*. Journal of energy and power engineering, 2014, ISSN 1934-8975.
- [4] NEMEC, P., SMITKA, M., MALCHO, M., JANDAČKA, J. *Porovnanie konvenčného a nekonvenčného spôsobu chladenia tranzistorov*, ElectroScope, 2013, ISSN 1802-4564
- [5] KASANICKÝ, M., LENHARD, R., MALCHO, M. *Mathematical model of heat transport through gravity assisted heat pipe in order to set length of the pipe*, AIP Conference Proceedings, Vol. 1608. 2014, ISSN 0094-243X



Dependent of Working Position and Working Diameter at Thermal Performance Gravitational Heat Pipe

*Luboš Kosa, *Marián Jobb, *Patrik Nemec, *Milan Malcho

*University of Žilina, Faculty of Mechanical Engineering, Department of Power Engineering, Univerzitná 8215/1, 01026 Žilina, Slovakia, {lubos.kosa, marian.jobb, patrik.nemec, milan.malcho}@fstroj.uniza.sk

Abstract. One of more alternatives of heat transfer without the using of mechanical equipment is the use of the heat pipe. Heat pipes are easy to manufacture and maintenance of low input investment cost. The advantage of using the heat pipe is its use in hermetic closed electronic device which is separated exchange of air between the device and the environment. This experiment deals with the influence of changes in the working tube diameter and changing the working position on performance parameters. Changing the working position and the tube diameter changes the thermal performance of the heat pipe. The result of this paper is finding the optimal diameter with ideal working substance for the greatest heat transfer for 1cm^2 sectional area tube.

Keywords: Gravitation heat pipe, Thermal performance, Diameter, Angle, Water.

1. Introduction

The general principle of heat pipes using gravity, commonly classified as two phase thermosyphon, dates back to the steam age and Angier March Perkins and his son Loftus Perkins and the "Perkins Tube", which saw widespread use in locomotive boilers and working ovens. Capillary-based heat pipes were first suggested by R.S. Gaugler of General Motors in 1942, who patented the idea, but did not develop it further. A heat pipe is a heat-transfer device that combines the principles of both thermal conductivity and phase transition to efficiently manage the transfer of heat between two solid interfaces [5].

At the hot interface of a heat pipe a liquid in contact with a thermally conductive solid surface turns into a vapor by absorbing heat from that surface. The vapor then travels along the heat pipe to the cold interface and condenses back into a liquid - releasing the latent heat. The liquid then returns to the hot interface through either capillary action, centrifugal force, or gravity, and the cycle repeats. (Fig.1) Due to the very high heat transfer coefficients for boiling and condensation, heat pipes are highly effective thermal conductors [6].

Heat pipe consists of a sealed pipe or tube made of a material that is compatible with the working fluid such as copper for water heat pipes, or aluminium for ammonia heat pipes. A vacuum pump is used to remove the air from the empty heat pipe. The heat pipe is partially filled with a working fluid and then sealed. The working fluid mass is chosen so that the heat pipe contains both vapor and liquid over the operating temperature range. Water heat pipes are sometimes filled by partially filling with water, heating until the water boils and displaces the air, and then sealed while hot. Working fluids are chosen according to the temperatures at which the heat pipe must operate [7].

The advantage of heat pipes over many other heat-dissipation mechanisms is their great efficiency in transferring heat. Heat pipes contain no mechanical moving parts and typically require no maintenance. The advantage of the heat pipe is a fast start action of the heat transfer, their geometric shape, weight. Heat pipes are used for cooling electronic devices and increasingly begin to apply computer technology. Another possibility of using heat pipes in solar collectors, where in the condensation part is arranged a heat exchanger which is heated.

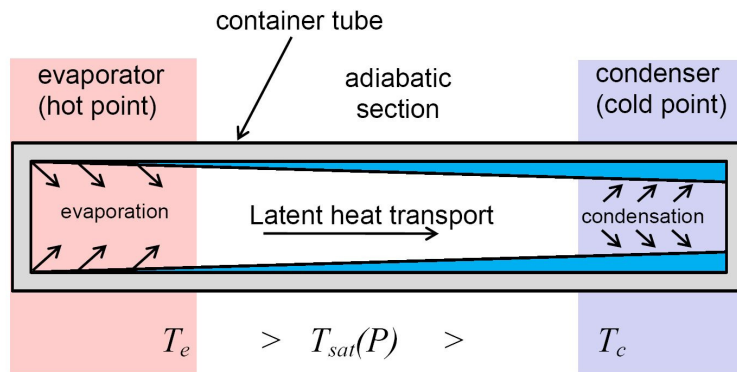


Fig. 1. Function of gravitation heat pipe [3].

2. Method of experiment

For experimentally measurement the performance of the heat pipes were chosen method of measuring with water. To measure were used gravity heat pipe of copper material of the same length of 50 cm. Heat pipes are different diameter pipes (DN12, DN15, DN18, DN22, and DN28). The working medium of the experimental measurements were used distilled water and we change a measurement angle of heat pipe. For better working conditions was achieved starting internal pressure of the heat pipe 800 Pa. For recording the measured values, we used the program AMR WinControl from AHLBORN. Measuring consisted of heating the evaporator section by a circulating medium at 80 °C, wherein the evaporation taking place within the working medium of the heat pipe. Cooling the condensation section by a circulating medium at 20°C, wherein working medium was evaporation. For experimental measurements were recorded temperature inflow and outflow on water the condenser and the flow medium.

2.1. Used materials

For experimentally measurement we used copper pipe of the length 50cm, copper fittings and copper capillary tubing's (Fig.2). Working medium of the experimental measurements were used distilled water. Ideal of amount of working medium is 25% full volume tube.

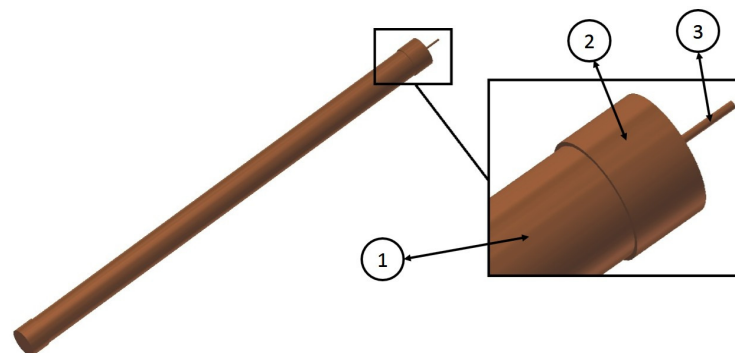


Fig. 2. Experimental heat pipe was consist for 1- copper pipe, 2- copper fitting, 3- copper capillary tubing.

2.2. Measurement of thermal performance of gravitation heat pipe

We chose the calorimetric equation (1) for obtaining to the results of thermal performance heat pipe, which describes the heat transfer bodies, forming isolated system, covered by the law of conservation of energy. The law of conservation of energy is that all the heat that the exchange of a single body transfer, the second body receives. We can suppose that there is no change in the type

of energy, heat energy can't be changed, for example into mechanical energy, and the substances are chemically inert, doesn't generates heat from chemical reactions:

$$\dot{Q} = \dot{m} \cdot c \cdot \Delta t \quad (1)$$

where \dot{Q} is a heat flux in W, \dot{m} represents the mass flow in $\text{kg}\cdot\text{s}^{-1}$, c represents the specific heat capacity water where $20^\circ\text{C} = 4183 \text{ J}\cdot\text{Kg}^{-1}\cdot\text{K}^{-1}$ and Δt represents the temperature gradient in K

For experimental measurement we build a measuring equipment (Fig.3) consist with 1-protractor, 2-flow meter, 3-outlet temperature, 4-inlet temperature, 5-condenser, 6-evaporator, 7-water heating for evaporator, 8-cooling water for condenser.

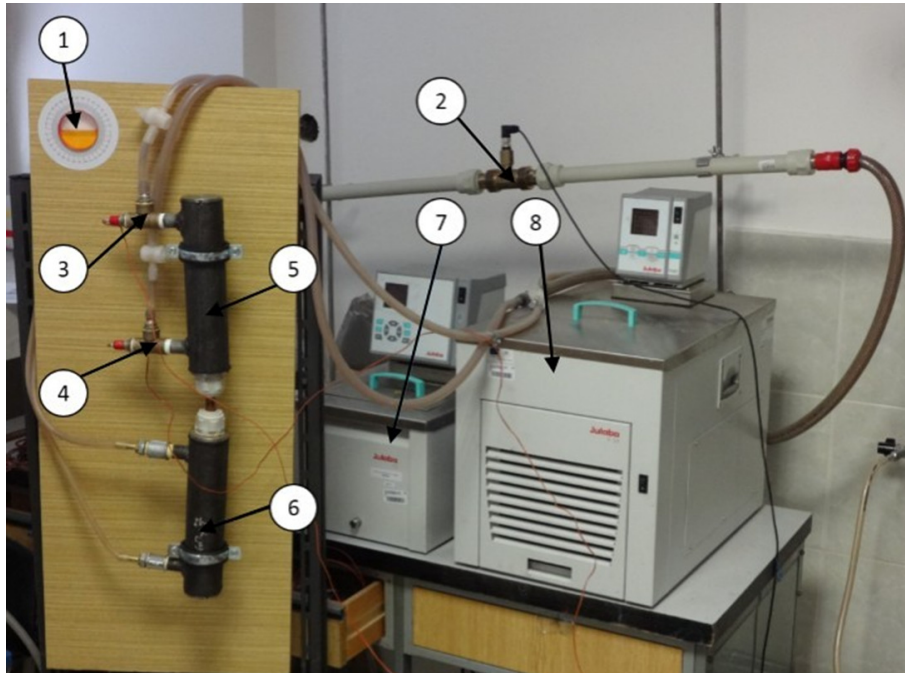


Fig. 3: Experimental measuring equipment.

3. Evaluation measuring of thermal performance gravitation heat pipe

During the experiments are confirmed the assumptions that the biggest diameter and different working position change thermal performance a heat pipe. The main object of experimental was find ideal working position and ideal diameter for tube. We find the biggest thermal performance for heat pipe in 1cm^2 of section tube. All heat pipes were stuffed 25% their full volume with working medium. We recorded mass flow and temperature difference outlet and inlet of cooling water.

Temperature difference (K)	DN 12	DN 15	DN 18	DN 22	DN 28
0	0.45	1.2	1.76	2	2.27
15	0.45	1.41	1.75	2.15	2.06
30	0.47	1.53	1.80	2.12	2.17
45	0.51	1.62	1.80	2.09	2.16
60	0.52	2.10	1.98	2.16	2.27
75	0.51	0.88	1.86	2.23	2.18

Tab. 1. Temperature difference per different diameter and working position.

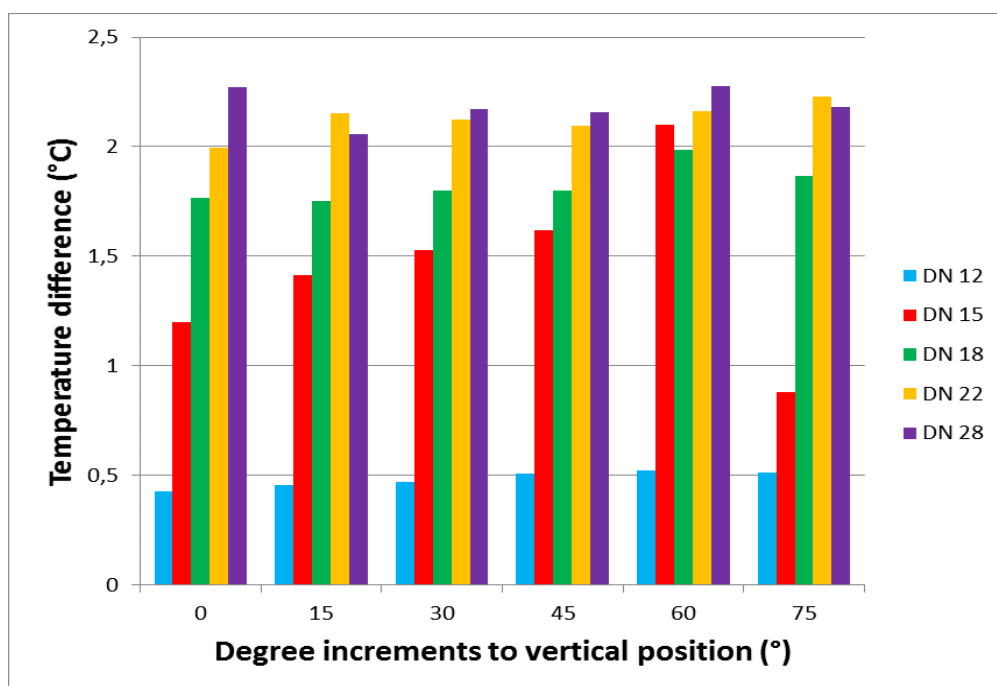


Fig. 4. Dependence temperature difference per different diameter and working position .

Fig. 4 is average value different temperature where the biggest diameter DN28 have the biggest different of temperature at vertical angle and 60 degree.

Mass flow (Kg.s ⁻¹)	DN 12	DN 15	DN 18	DN 22	DN 28
0	0.0635	0.058	0.06	0.062	0.064
15	0.0635	0.054	0.06	0.062	0.064
30	0.0635	0.05	0.06	0.062	0.064
45	0.0635	0.05	0.06	0.062	0.064
60	0.0635	0.034	0.06	0.062	0.064
75	0.0635	0.063	0.06	0.062	0.064

Tab. 2. Mass flow in measurement of heat pipe per different diameter and working position.

Tab. 2 shows the average value of mass flow where mass flow will be similar on full measurement.

For the evaluation we used equation number 1 where specific heat capacity water was $20^{\circ}\text{C} = 4183 \text{ J.Kg}^{-1}.\text{K}^{-1}$.

Thermal performance (W)	DN 12	DN 15	DN 18	DN 22	DN 28
0	112.8	291.92	445.12	516.3	604.7
15	120.8	318.27	442.44	556.12	548.08
30	125.1	318.58	454.41	548.74	577.58
45	135.1	333.57	454.37	541.32	575.21
60	138	296.03	500.55	559.53	604.32
75	136.3	230.64	470.27	575.93	578.19

Tab. 3. Thermal performance of gravitation heat pipe per different diameter and working position

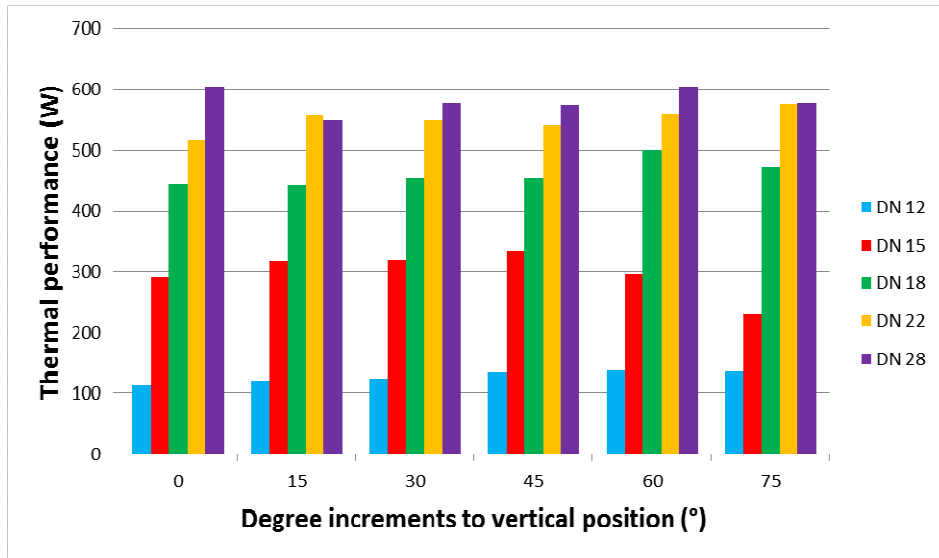


Fig. 5: Difference of thermal performance for gravitation heat pipe per different diameter and working position

Fig.5 shows the average value of thermal performance heat pipe when we used different diameter and different working position. We expect when the biggest diameter have the biggest thermal performance so we want find the biggest thermal performance for 1cm² sectional tube. We used the equation number 2 where we division thermal performance with sectional area of tube.

$$\dot{Q}_s = \frac{\dot{Q}}{S} \quad (2)$$

Where \dot{Q} a heat flux in W, S is represents the sectional area of tube cm².

Thermal performance for 1cm ² sectional tube W	DN 12	DN 15	DN 18	DN 22	DN 28
0	99.74	165.20	174.90	135.83	98.2
15	106.8	180.12	173.85	146.31	89.00
30	110.64	180.29	178.55	144.37	93.79
45	119.41	188.78	178.54	142.41	93.41
60	122.03	167.53	196.68	147.20	98.14
75	120.5	130.52	184.78	151.52	93.89

Tab. 4. Thermal performance for 1cm² sectional area tube per different diameter and working position .

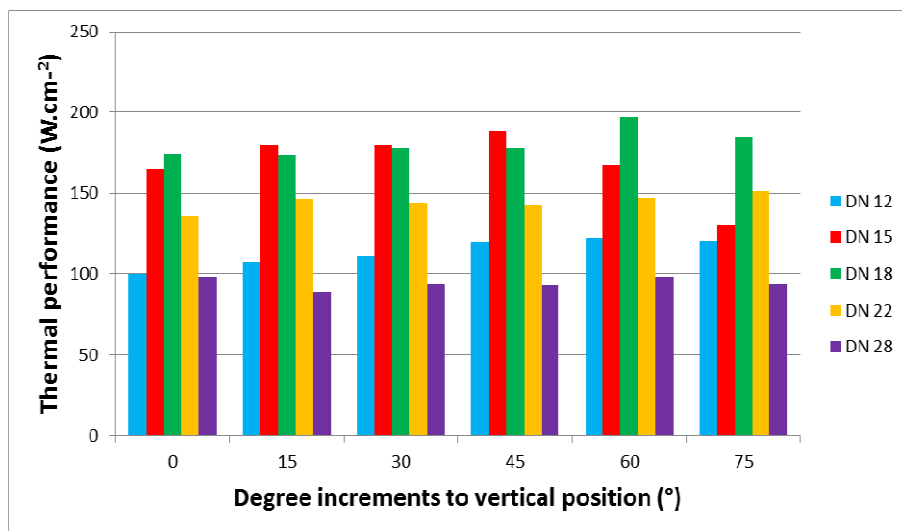


Fig. 6. Difference of thermal performance for gravitation heat pipe per different diameter and working position .



Fig. 6 shows different between working position and different diameter of tube. The best working position is around 60 degree and the best diameter is a DN 18 where thermal performance is a 196.68 W.cm^2 .

The worst diameter is a DN 28 where thermal performance is a biggest but thermal performance for 1cm^2 sectional area tube is a least.

4. Conclusion

We measured the effect of the diameter and type of working position gravity heat pipe for thermal performance characteristics of the device. Measurements we found that the extension of the diameter also increases the heat output of the heat pipes by gravity. The greatest progress transferred power 604.7W reached gravity heat pipe DN 28 with a vertical working position, but due to the cross-sectional area of 1 cm^2 reached the highest transmitted power 196.68 W gravity heat pipe DN18 with a 60 degree working position.

Acknowledgement

The research is supported by European regional development fund and Slovak state budget by the project Research centre of University of Žilina", ITMS 26220220183 (50%).

This work is supported by the financial assistance of the project APVV - 0577-10 " Cooling of power electronic systems by cooling cycles without mechanical drive" (50%).

References

- [1] HOLUBČÍK, M., ĎURČANSKÝ, P., JANDAČKA, J. and NOSEK, R. *Design of heat exchanger for ericsson-brayton piston engine*. The Scientific World Journal, Volume 2014, ISSN: 23566140,
- [2] LENHARD, R., KADUCHOVÁ, K. and PAPUČÍK, Š. *Analysis of the fill amount influence on the heat performance of heat pipe*. International Conference on Application of Experimental and Numerical Methods in Fluid Mechanics and Energetics 2014, XIX.AEaNMiFMaE 2014; Liptovsky Jan; Slovakia; ISBN: 978-073541244-6,
- [3] NIKOLAYEV, V. S. *Modeling of pulsating heat pipe (PHP)* <http://www.pmmh.espci.fr/~vnikol/PHP.html>
- [4] NOSEK, R., GAVLAS, S., LENHARD, R., SEDLAK, V., ARVESEN, H.M. *Condenser optimization of heat pipe*, Komunikacie, Volume 16, Issue 3A, 2014, Pages 62-66, ISSN: 13354205
- [5] PETERSON, G.,P. *An introduction to heat pipes modeling, testing, and application*. 2010, ISBM 0-471-30512-X
- [6] REAY, D., KEW, P. and MCGLEN, R. *Heat pipes – Theory, design and applications*, sixth edition, 2014, ISBN: 978-0-08-098266-3
- [7] SILVERSTEIN, C., C. *Design and technology of heat pipes for cooling and heat exchange*. 2011, ISBN 0-89116-859-1
- [8] VANTÚCH, M., HUŽVÁR, J. and KAPJOR, A. *Heat transfer from oriented heat exchange areas* [Prenos tepla z orientovaných teplovýmenných plôch] EPJ Web of Conference [elektronický zdroj]. - ISSN 2100-014X. - Vol. 67.



Influence of heat treatment on coefficient of friction between DLC (WCC) deposited layer and bearing steel 100Cr6

*Matúš Kovalíček, *Ján Bucala, *Jozef Bronček

*University of Žilina, Faculty of Mechanical Engineering, Department of Design and Mechanical Elements, Univerzitna 2, 01026 Žilina, Slovakia, {matus.kovalicek, jan.bucala, jozef.broncek}@fstroj.uniza.sk

Abstract. DLC coatings are wear resistant, have low coefficient of friction and are widely used in industry, in medicine and for decorative purposes. This article focuses on tribological properties of DLC coatings based on WCC deposited on substrate made from grade 100Cr6 bearing steel.

Keywords: Tribology, Coefficient of friction, Bearing steel 100Cr6, WC/C based DLC coating

1. Introduction

Thin layer DLC (Diamond-like Carbon) coatings based on WCC (Tungsten Carbon Carbide) have properties such as low coefficient of friction, high hardness and wear resistance. Because of these properties, DLC coatings are suitable for application to the surfaces of mechanical parts where high mechanical energy losses occur and the surface is worn out very quickly. This type of coating has very high hardness and requires substrate with similar hardness in order to reach desired properties. Ideal situation is when both coating and substrate reach the same hardness.

Tungsten-DLC (WCC) coating keeps high hardness and low coefficient of friction even for high temperature range. When applied to the surfaces of cutting tools, DLC coatings contribute to higher wear resistance. The occurrence of cold welds on contact surfaces is reduced to minimum for tribological applications working under conditions without sufficient lubrication. The coating has good cohesion properties and excellent adhesion to the surfaces which will be deposited. WCC is highly resistant to flaking because of excellent adhesion and therefore offers better protection of high speed cutting tools. This type of coating is also corrosion resistant, non-toxic and biocompatible what makes it especially suitable for medical applications [1].

Suitable heat treatment of substrate was chosen in order to reach its desired hardness. Thin DLC coating based on WC/C was deposited onto surface of substrate using PVD (Physical Vapor Deposition) method. We chose this method because of its low temperature deposition process which leads to almost no heat affection of substrate. Tribological properties of prepared samples were tested and "ball-on-flat" method was used.

1.1. Preparation of samples

The samples with dimensions of 25 x 80 mm and thickness of 5 mm were made from bearing steel 100Cr6. The samples were cut to desired dimensions in the first step. The second step consisted of grinding the upper surface on every sample on plane grinding machine BPH-20 and later the Struers grinder was used for final polishing of functional sample surfaces with diamond polishing paste with 3µm grit size. Prepared sample can be seen on Fig. 1.

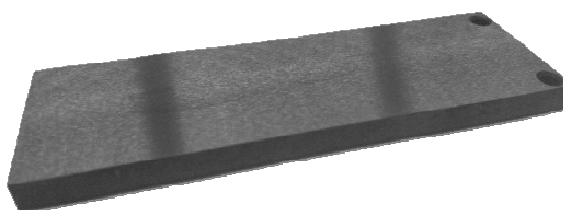


Fig. 1. Sample used in our experiments.

1.2. Heat treatment of 100Cr6 steel

There were three different heat treatment methods used which resulted in three different microstructures of a substrate: martensitic, bainitic and sorbitic. Microstructure of these materials is shown on Fig. 2.



Fig. 2. Microstructures after heat treatment: a) martensitic, b) bainitic, c) sorbitic.

The conditions of heat treatment, type of final structure and final hardness of used samples are listed in Tab. 1.

<i>Structure</i>	<i>Hardness [HRC]</i>	<i>Heat treatment</i>
Martensite	64	Hardening temperature: 830 °C Non tempered
Sorbite - hardening in oil and air tempering	63	Hardening temperature: 830 °C Tempered at 190 °C
Bainite - salt	58	Austenitization temperature: 830 °C Isothermal hold: 220 °C

Tab. 1. Microstructure types of substrate with corresponding hardness after heat treatment.

1.3. DLC coatings based on WCC

After all substrates were prepared according to our requirements, we could move to the next phase. Nano-metric WCC coatings were deposited to functional surfaces of all samples by company STATON Turany. Magnetron sputtering method was used. Chemically cleaned sample was placed to deposition chamber and the surface of the sample was ionic purified. Deposition process began right after purification and it was divided into two steps – thin layer of chromium was deposited for better adhesion properties and later thin WCC layer was deposited onto already deposited Cr layer. Schematic structure of both coatings deposited on the substrate and real structure can be seen on Fig. 3.

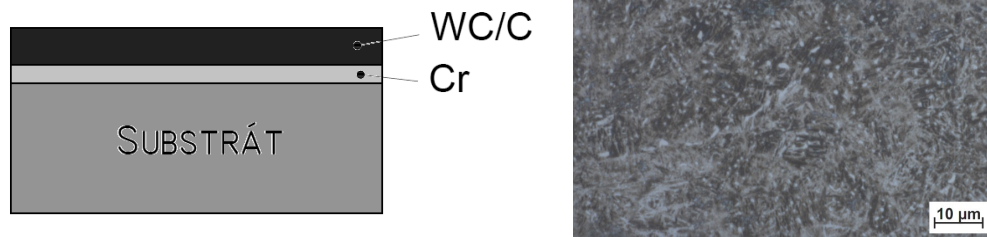


Fig. 3. Schematic structure of deposited coatings (left) and real structure of 100Cr6 steel with deposited coatings (right).

2. Experimental device

Tribological tests were performed in the laboratory of Department of Design and Mechanical Elements. This laboratory offers a wide range of devices dedicated to the measurement of the coefficient of friction. The most suitable device for the task was a linear tribometer.

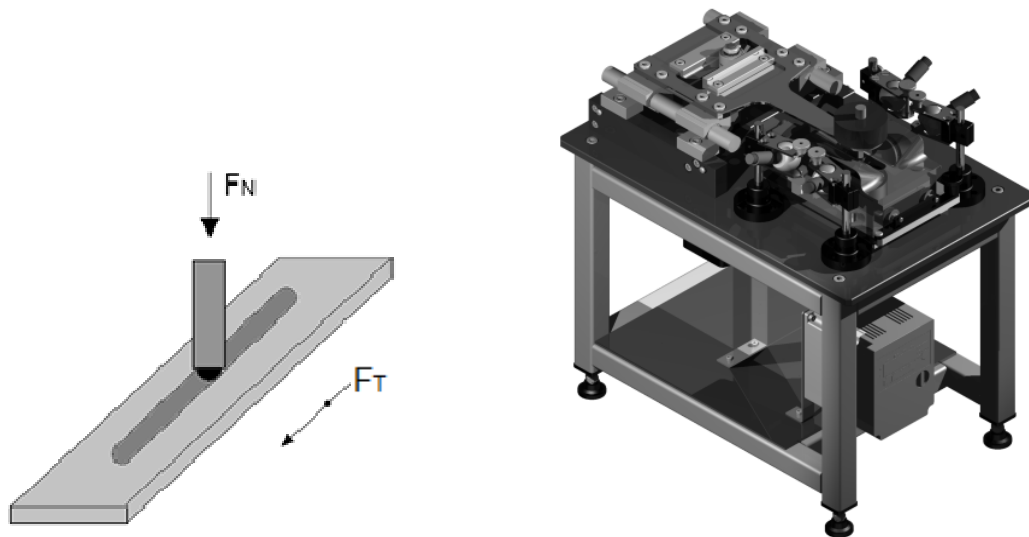


Fig. 4. Basic principle of tribometer (left), linear tribometer used for experiments.

This type of tribometer allows to measure the coefficient of friction by "ball-on-flat" method. Friction force F_T is measured with a tensometric sensor and data during the whole experiment are written to mass memory storage. Normal force F_N is generated by a set of weights with a desired mass.

2.1. Methodics of experiment

The tribological pair consists of measured samples with martensitic, bainitic and sorbitic structures with deposited WCC coating, another component was a standard 100Cr6 steel ball with 4 mm diameter.

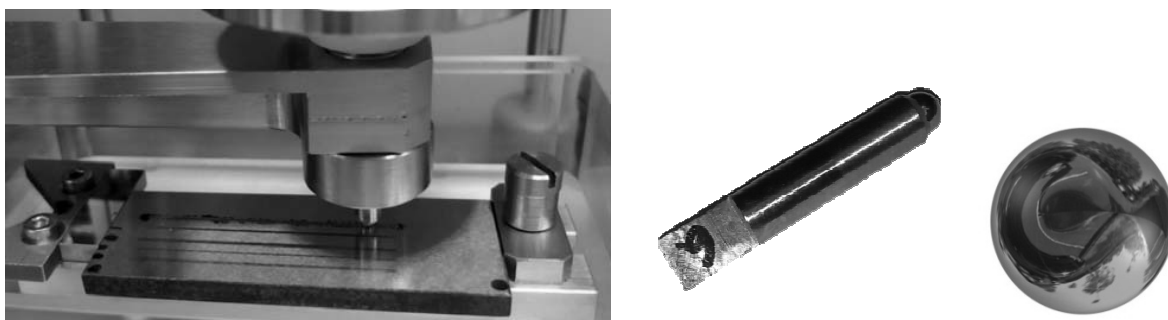


Fig. 5. Tribological pair during one of our tests on linear tribometer (left), ball holder and steel ball (right).

The conditions during the experiment were exactly the same for all tribological pairs. The experiments were conducted in atmospheric conditions and without lubrication. The velocity of steel ball was not constant, but it had sinusoidal behavior with velocity ranging from 0 to 20 mm². The load was constant with value of 10N. The duration of all experiments was 6000 seconds with 100 meter distance.

2.2. Results

The result of our experiment was the change of the coefficient of friction over time. Vertical axis shows the value of the coefficient of friction of all three samples with WCC coatings and horizontal axis represents time domain. All values of the coefficient of friction listed in the graph were obtained with constant 10 N load.

Initial value of the coefficient of friction for the sample with sorbitic structure was 0.33. Other samples (bainitic and martensitic) reached equal initial value of 0.43. The value of the coefficient of friction had decreasing tendency during our experiments and became almost constant after 5000 seconds. The lowest value of the coefficient of friction 0.15 was reached by the sample with bainitic structure at the end of our experiments. Martensitic and sorbitic structures reached only slightly higher value of the coefficient of friction. Detailed behavior of the coefficient of friction can be seen on Fig. 6.

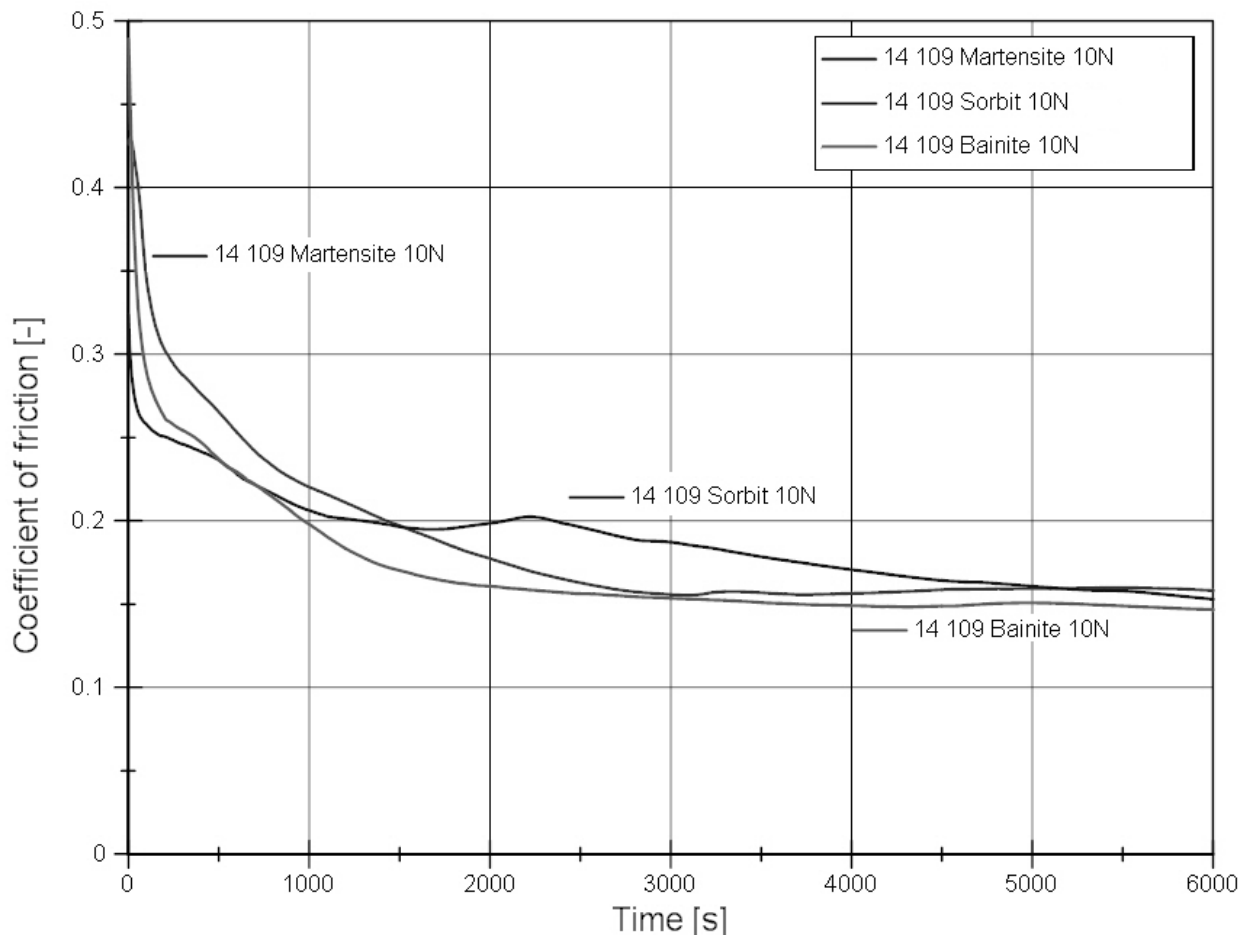


Fig. 6. Coefficient of friction for different heat treated 100Cr6 substrates with deposited WC/C layer.

The wear of steel balls was measured and evaluated after all experiments were finished. Initial coefficient of friction, Hertzian pressure and the area of worn surface of steel ball for samples with different structure of the substrate are listed in Tab 2.

Sample	Initial coefficient of friction [-]	Hertzian pressure P_{THEOR} [GPa]	Area of worn surface of steel ball [mm ²]	Load [N]	Number of tip
Martensite + WC/C	0.426	1.24	0.10	10	tip no.20
Sorbite + WC/C	0.341	1.24	0.07	10	tip no.17
Bainite + WC/C	0.442	1.24	0.06	10	tip no.12

Tab. 2. Chosen tribological properties.

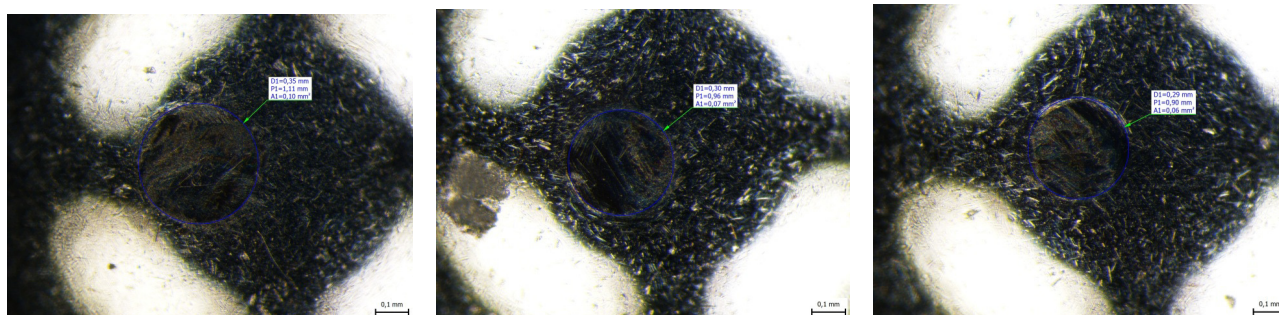


Fig. 7. Surface of steel balls after experiments on samples with different substrate: a) martensite, b) sorbite, c) bainite.

3. Conclusion

Tribological properties of WCC coatings were experimentally measured and evaluated. Based on our measured data we can conclude that the lowest value of coefficient of friction was reached with bainitic structure of the substrate. Low value of coefficient of friction for this material also led to the lowest value of wear rate when compared to martensitic and sorbitic structure of the substrate.

Acknowledgments

The research work reported here was made possible by project “Research Centre of University of Žilina”, ITMS 26220220183.

References

- [1] „NHBB”, 15 Marec 2015. [Online]. <http://nhbb.com/reference/mini-instrument-bearings/hard-coatings.aspx>
- [2] P. Blaškovič, J. Balla a M. Dzimko. *Tribology*. Bratislava: ALFA, 1990.
- [3] Stachowiak, Batchelor a Stachowiak, *Experimental methods in tribology*, ELSEVIER, 2004.
- [4] „Thin coatings,” 7 November 2013. [Online]. Available: https://mail-attachment.googleusercontent.com/attachment/?ui=2&ik=8491954ded&view=att&th=1420507fb6ca27c9&attid=0.1&disp=inline&safe=1&zw&saduie=AG9B_P9fP6BjnZHjVeRl2ssNdcD2&sadet=1383823739010&sads=lhpt1QS_z_9Iu0jzGXSP1DcrcEUo&sadssc=1. [Cit. 7 November 2013]. (In Slovak)



Multisensory measurements in modern production techniques

*Jakub Kulpa, *Grzegorz Witkowski

* Kielce University of Technology, Department of Mechatronics and Machine Building,
Tysiaclecia Państwa Polskiego 7, 25-314 Kielce, Poland, {jakub-kulpa, gwickowski }@wp.pl

Abstract. The technological development of production forces the need for continuous development of measurement systems. Modern production technologies such as Rapid Prototyping require specialized measurement systems. Additive technologies allow to manufacture parts with a complex geometry. Geometry measurement of such models by traditional methods is problematic or impossible to perform. The selection of an appropriate method of measurement is influenced by many factors: required accuracy, type of the object being measured (size, material, surface) and place of measurement. Multisensory Coordinate Measuring Machine (ang. CMM) use a combination of different types of measurement sensors such as: tactile sensors, tactile-optical sensors, laser sensors, cameras processing the image, and optical sensors. Complex measurement tasks often require the use of several types of sensors to measure the same object.

Keywords: Additive technologies, CCM, Sensor, Tactile, Coordinate.

1. Introduction

Coordinate metrology as a multipurpose and efficient technology is especially important for new needs of the market.

Coordinate Measuring Machines (CMM) collect data about the measured object using sensors. CMMs can be equipped with a many different sensor such us a tactile or optical trigger probes or measurement sensors. The main task of the trigger probes is to call the trigger signal when a probe tip get a contact with the measured surface. It makes it necessary to read the data with respect to all the axes of the machine to determine the coordinates of the interface in space. Movement against the axis is needed to determine the coordinates of the interface. The measurement sensors have an internal measuring range of up to a few millimeters. The interface is determined by overwriting the value read by the sensor over the coordinate values read by the measuring machine.

1.1. Multisensory of CMMs.

Typical CCMs are equipped with tactile measuring tip with the possibility of the selection of its diameter and length of the probe where the measuring tip is situated. This allows to measure the dimensions of various elements from several millimeters to several meters (Gantry CMMs) Although such measurements are the most accurate at the moment, they involve certain limitations. The first limitation are the dimensions of the measuring tips, the minimum diameter is about 0.3 mm. Another limitation is related to the physical contact of the measuring tip with the surface of the measured element; too much pressure on the element may damage its surface or cause the movement against the table.

During the last years, there is a strong emphasis on the development connected with multisensory coordinate measuring technology in order to meet the needs of the production market. There are a lot of elements that require to use different measuring sensors, i.e.: micro gears, implants, delicate elements made of glass or fabric, and more. Measurements of parts with size of a few millimeters to a few micrometers or the measurements of macroscopic elements of very low uncertainty require new measurement techniques based on current machines but with improved stiffness and thermal stability. Multisensory coordinate measuring machines use a combination of different types of measurement sensors such as: tactile measurement tips, tactile-optical tips, laser

sensors, cameras processing the image, optical sensor using autofocus, sensors scanning 3D tracks [1, 2, 3, 4].

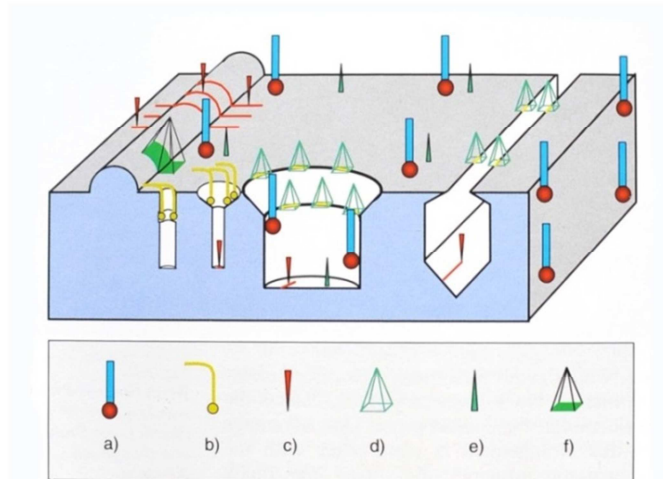


Fig. 1. Measurement sensors and their application [1]: a-tactile sensor; b- tactile-optical sensor; c- laser; d- sensor processing the image; e- autofocus; f- sensors scanning 3D tracks.

1.2. Additive technologies.

Additive technologies known as Rapid Prototyping (ang. RP) or „3D printing” allow to produce physical models based on a computer model developed in CAD software’s or generated by reverse engineering technologies. The general principle of production of these objects involves creating layered models. The concept of "Rapid Prototyping" combines the technologies that are automated physical modelling techniques through a layered sintering, bonding, splicing, melting and curing all kinds of material, by laser or other sources and energy. RP technology is mainly used for the production of prototypes but increasingly also for the production of small series. They allow you to significantly reduce the time and cost of the launch of a new product. Although these processes are the same at end, are very different in terms of the resulting final product. One of the most popular technologies with a lot of possibilities is the POLJET Matrix technology developed by Objet company. In Polyjet technology model is created by spraying photopolymer on tray by piezo-crystal working through electronically controlled (Fig. 2). Working material is fed to the nozzle with a very small pressure, then if a location is to be given the material to piezo-crystal voltage is applied to decrease a volume of the crystal. In resulting the photopolymer drop is squeezed through the nozzle. After the single layer, it is exposed to UV light that causes the immediate hardening of the material [5, 6, 7].



Fig. 2. Objet Connex 350 Printer and the manufactured thin wall cube model.

2. The use of multisensory CMM ZEISS O-INSPECT 442 for Rapid prototyping models.

Applying RP technology we can produce elements of geometry impossible to perform traditional techniques. Such models require the use of a variety of sensors in order to assess the accuracy of performance. There are many different RP technologies which differ in accuracy and the principle of the prototype production. Due to the development of RP technologies they are more and more popular and they are used not only for prototyping but also for the small series production. This necessitates a proper assessment of the accuracy of these technologies and determination of their capabilities. Multisensory coordinate measuring technique is very useful for the evaluation of the models produced with the use of RP technologies. One of the most popular of Multisensory CMMs is O-INSPECT 442 produced by Zeiss Company.

O-INSPECT 442 is equipped with a three different sensors:

- Tactile sensor - passive scanning head,
- Visual sensor – 2D optical CCD Camera with discovery zoom lens,
- Optical sensor – white light distance sensor.

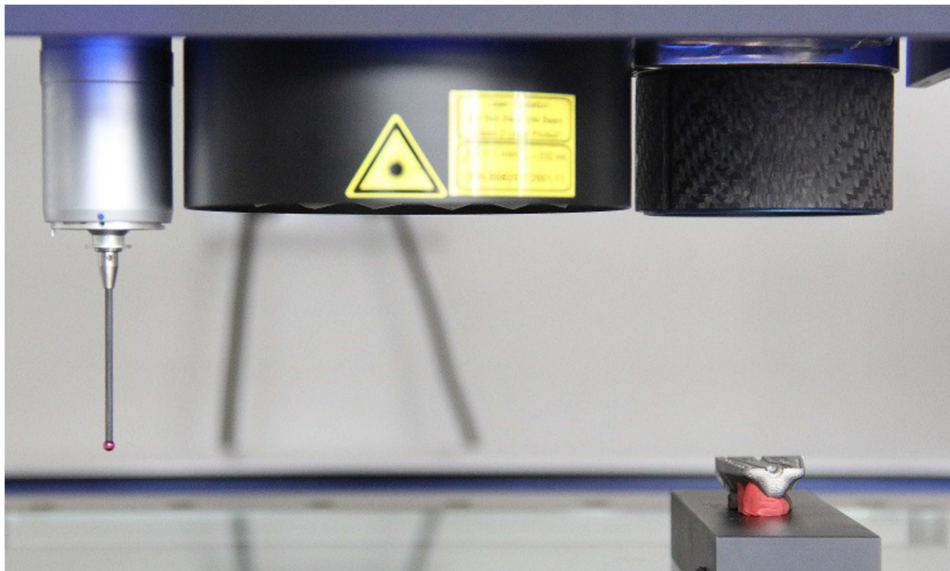


Fig. 3. O-INSPECT 442 sensors: from left side a) tactile sensor; b) 2D Camera; c) white light sensor.

Fig. 4 illustrates an exemplary application of multisensory CCMs for the evaluation of a prototype made of metal powders (SLM).

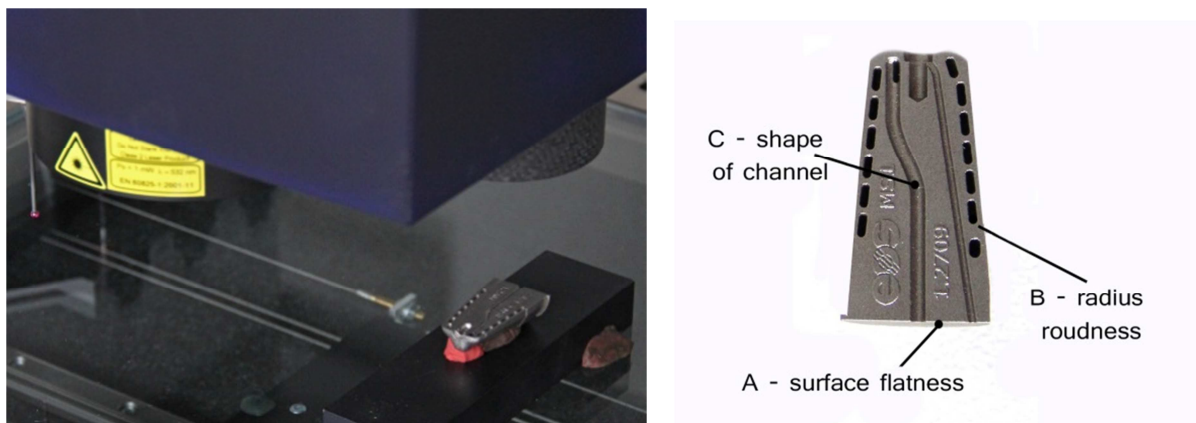


Fig. 4. Multisensory measurement of a prototype.

To measure three characteristics marked on the above prototype three different sensors were used. The evaluation of the flatness of the side wall was performed with the use of a tactile tip. The rounding radius of repeating slotted holes, due to the very small size, was determined by optical image processing method, and the shape of the channel cross-section was determined by the white light optical sensor as its dimensions did not allow the evaluation by the tactile method. The above example illustrates well the issues and complex measurement tasks posed to us by production technology by Rapid Prototyping. At this point, multisensory measurements are necessary for the correct evaluation of a prototype.

Visual and tactile sensors were compared to check their accuracy on O-Inspect CCM using Calypso5.2 software. The diametral stencil of the value equal 49.9865 mm specified by the Central Office of Measures was used as the object of the measurement. This object was measured with a ULM600 linear gage and its value was set to 49.9867 mm; it was accepted in further measurements as the nominal value. Both methods have been carried out in automatic mode with a fixed scan rate of 5m/s and 360 measurement points were collected. In both methods, software filtering and deleting of abnormal values were used. The measurement for each of the methods was carried out ten times. After calculations, the standard deviation obtained for the optical method was 0.0046 mm and 0.0024 mm for the tactile method. Deviation of the optical method is almost twice as large as the deviation of the tactile method, nevertheless, it is still satisfactory.

Tactile sensor was also compared to the white light sensor. The surface flatness of printed model was designated by both sensors. The result are shown on a Fig. 5 [8].

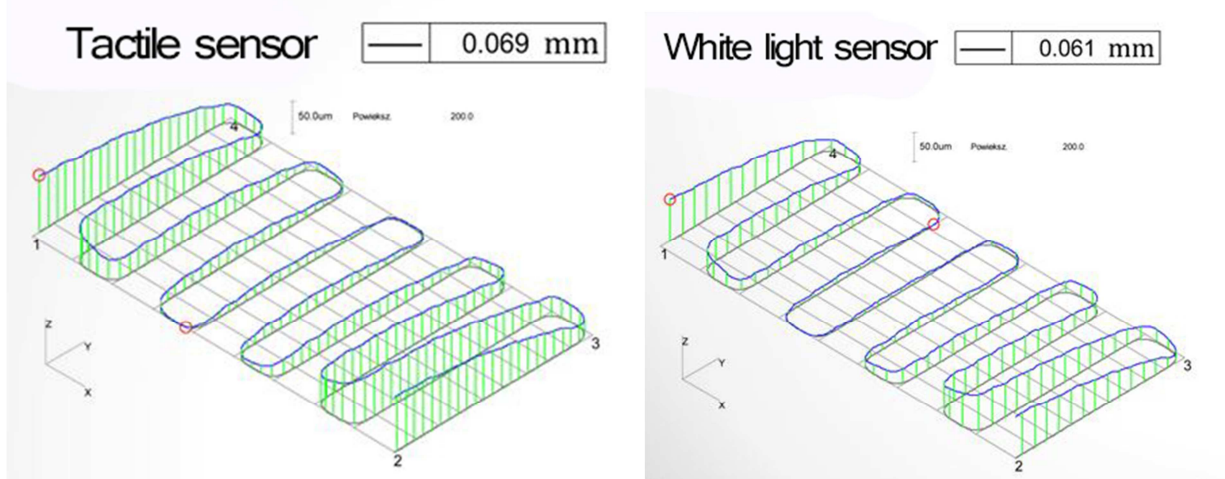


Fig. 5. Results of measure.

The obtained results of the measurements are very similar. There are currently hard to determine which of them will be more correct. Measurement by tactile sensor could be affected by the deformation of the material caused by the contact pressure of the measuring tip. The other hand, optical measurement could be affected by the model which was made of translucent material.

3. Conclusion

Multisensory measuring technique enables a comprehensive measurement of complex parts made of RP technologies. Optical sensors can be used with a small-sized elements and easily deformable materials. Highest accuracy of measurements we achieve by tactile sensor, however due to low accuracy of RP technologies we can use optical sensor with high precision. Optical sensor are much faster than the tactile sensor but not so precision. In many cases it is not possible to measure some details by contact methods, for example diameter of hole is smaller than the diameter of stylus tip. Optical method has a lot of limitations and may be used only where it is necessary.



References

- [1] CHRISTOPH R., NEUMANN H.J.: *Multisensory Coordinate Metrology*. Werth Messtechnik GmbH
- [2] SŁADEK J., KULPA J.: *Multisensory coordinate measuring technology*. XI Coordinate measuring Technique 2014
- [3] DE CHIFFRE L., HANSEN H. N.: *Metrological limitations of optical probing techniques for dimensional measurements*. Institute of Manufacturing Engineering, Technical University of Denmark
- [4] RATAJCZYK E., *Coordinate Measuring Technique (in Polish)*, Warsaw University of Technology Press, Warsaw, Poland, 2005.
- [5] KIETZMAN J.: *Rapid prototyping polymer parts via shape deposition manufacturing* . Doctors dissertation
- [6] GIBSON I., ROSEN D., STUCKER B.: *Additive Manufacturing Technologies*. Rapid Prototyping to Direct Digital Manufacturing. ISBN: 978-1-4419-1119-3
- [7] ADAMCZAK S., BOCHNIA J., KACZMARSKA B.: *Estimating the uncertainty of tensile strength measurement for a photocured material produced by additive manufacturing*. Metrology and Measurement Systems book 21
- [8] ADAMCZAK S., ŚWIDERSKI J.: *Przegląd wybranych współczesnych metod pomiarów zarysów nierówności powierzchni*. Sympozjum Klubu Polskie Forum ISO 9000 "Metrologia w Systemach Zarządzania -7"

Indirect Heat Water Heaters

*Richard Lenhard, *Martin Kasanický

*University of Žilina, Faculty of Mechanical Engineering, Department of Power engineering,
Univerzitna 1, 010 26 Žilina, Slovakia, {richard.lenhard, martin.kasanicky}@fstroj.uniza.sk

Abstract. To optimize water heating in indirectly heated hot water heater was created mathematical model. To verify the mathematical model, experimental measurements have been carried out. The results of experimental measurements is to determine the thermal performance of the heat exchanger. The results were then compared the results obtained from the mathematical model of hot water needs. The document also contains an analysis of the results.

Keywords: Experimental measurement, Experimental device, Water heater, Hot water.

1. Introduction

Indirectly heated water heaters used to heat and accumulation of heated drinking water. Offers high users comfort allowing hot water to supply a large number of deliveries points in residential buildings and even economic objects. In most cases, with one performance spiral heat exchanger Fig. 1 for hot water from an external source of heat.



Fig. 1. Indirectly heated water heater.

2. Experimental Measurement

For the experimental measurement was used indirectly heated water heater with the following geometrical parameters: height of the water tank 0.955 m, width of the water tank 0.520 m, volume of water tank 100 l, length of the spiral tube 9.880 m, inside diameter spiral tube 0.028 m, external pipe diameter 0.032 m spiral.

The experimental device was connected in Fig. 2. Water heater and the primary circuit was filled, while all the excess air squeezed out. V5 Control valve and valve V1 is closed and valve V2 is opened and the primary circuit was allowed to heat up to 80 °C. After achieving stable conditions in the primary circuit, the valve V1 open and valve V2 closed. When the temperature T2 at the top of the water heater temperature reached 15 °C, started the timer. During this heating period may be necessary to make fine adjustment of flow measured on FL1 by valve V3. When T₂ temperature reached 60 °C, the boiler is disconnected by opening valve V2 and closing valve V1. Read the elapsed time and recorded as heating time. The assembly is then allowed to stabilize about 1 min. After about 1 min. valve V1 is closed and valve V5 was opened and began to discharge, while in a fully open control valve V5 is set to flow outlet in STN EN with the valve V4. In our case, the flow of 0.25 l/s, because it is a 100 l water heater. While the flow was measured by the flow meter FL2. Subsequently, the timer started. When T₃ temperature has fallen below 40 °C, valve V5 is closed, and subtract the elapsed time and recorded as time of discharge. All measured values - initial and final temperature of the boiler, water heater temperature, inlet and outlet temperature of the water heater, the flow in the primary circuit and the flow discharged from the heater were recorded in the measurement units and were recorded using AMR - Win Control to your computer (PC) [1].

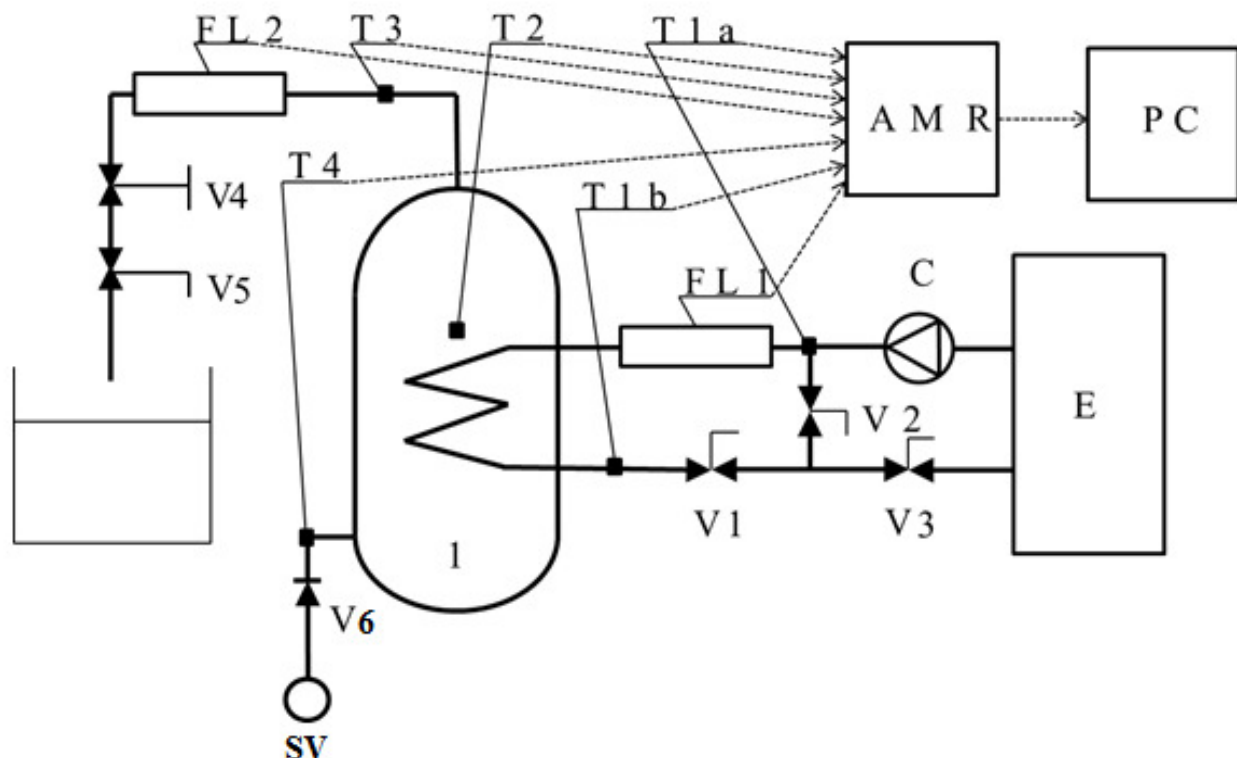


Fig. 2. Involvement of the experimental device. FL1, FL2 turbine flowmeters; V1, V2, V4, V6 stop-valves; V3, V5 adjusting valve; T1a, T2, T3, T4, T1b temperature gauge PT100; E boiler; C circulator; SV cold water, 1 experimental device.

2.1. Results of Experimental Measurements

Indirectly heated water heater was measured for a temperature drop 80/60 °C. During the measurements were recorded the following data - to the heating time was shown after 1 min and



temperature T11, T12 inlet and outlet temperature, T2 water temperature in the heater and Q heat output were averaged. Measured time to heat water from 15 °C to 60 °C was reached 19.72 min. Measurements the indirect discharges of heated water heater from 60 °C to 40 °C. Measured time is reached during discharge τ_v of water was fixed at 5.3 min.

The temperature of discharged water was observed in 5-liter increments. When at the end of 5 l increase in temperature has fallen below 40 °C was completed discharge. The values that have been achieved from measurements in the temperature gradient 80/60 °C were calculated performance of the heat exchanger, according to the following equation:

$$Q = \frac{(T_{av} - 15) \cdot V_{vyp}}{14,3 \cdot t} \quad [\text{kW}], \quad (1)$$

where: Q is the performance of the heat exchanger (kW), T_{av} is the average temperature of discharged water at 40 °C, V_{vyp} is the volume of water discharged at 40 °C or higher, t is the time needed to heat the water heater from 15 °C to 60 °C in min., the conversion ratio of 14.3 kW (860/60 min) [1].

3. Comparison of Results

Based on the results achieved from the measurement and mathematical model are compared, or set up a mathematical model of heating water indirectly heated hot water heater is working properly and it can be used to optimize heating. From the subsequent comparison of the measured and calculated power Fig. 3, was found to create a mathematical model of the hot water is working properly. Therefore, this model can be used to optimize water heating indirectly heated boiler water.

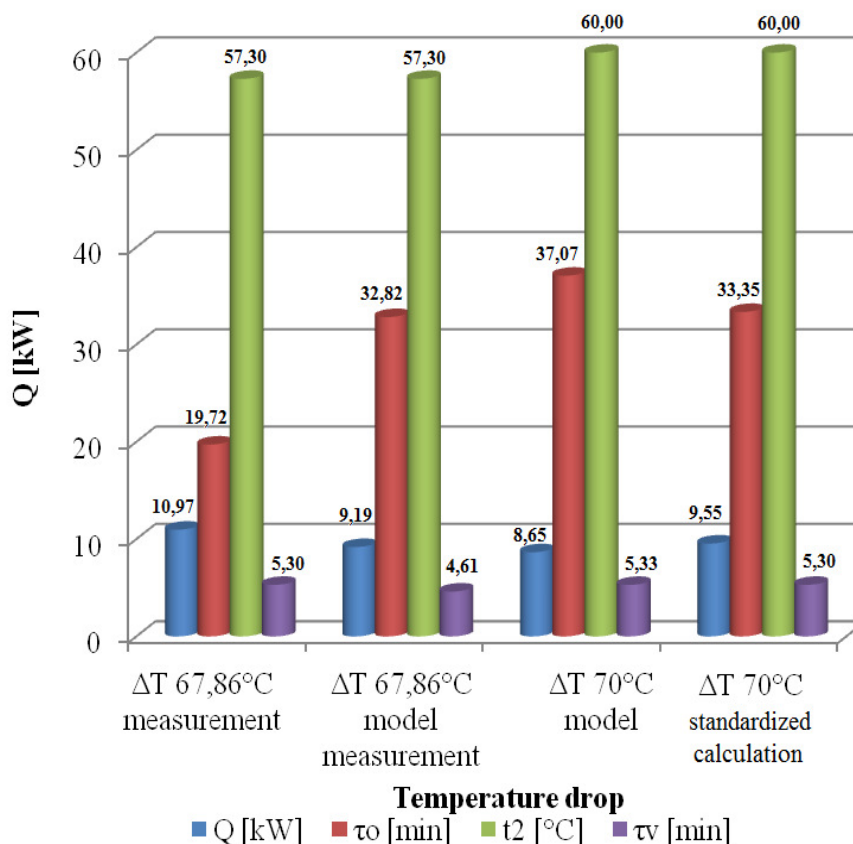


Fig. 3 Comparison of measured and calculated performance.



4. Conclusion

To verify the mathematical model of heating hot water was carried out experimental measurements, according to STN EN 12897:2007. The experimental measurement was carried out in the temperature gradient 80/60 °C. Heating rate reached 19.72 min and time of discharge was set at 5.3 min. Based on the measured values to calculate the performance of the heat exchanger, which went 10.97 kW. Performances achieved in the measurement and mathematical model were compared, and the following findings that the mathematical modeling of hot water heating is working properly, and can be used to optimize the heating of hot water. Optimization will focus on the change of geometric parameters indirectly heated hot water heater.

Acknowledgement

This article was created within the frame of project „Výskumné centrum Žilinskej univerzity“ ITMS 26220220183.

References

- [1] STN EN 12897:2007: *Vodárenstvo – Požiadavky na nepriamo vyhrievané neodvetrávané (uzatvorené) zásobníkové ohrievače vody*, 2007.
- [2] ĎURČANSKÝ, P., SMATANOVÁ, H., JANDAČKA, J. *Use of CFD methods at modelling of flow and transport of heat from shapely difficult pipe systems into the area of thermostatic chamber*. Energy transformation in industry, Technical university of Košice, Faculty of Metallurgy, 2013.
- [3] HRABOVSKÝ, P., PAPUČÍK, Š., JANDAČKA, J. *Ohrev vody pomocou tepelnej trubice*. Seminár z energetických procesov, 2014.
- [4] ČAJA, A., NEMEC, P., MALCHO, M. *Influence of the ambient temperature during heat pipe manufacturing on its function and heat transport ability*. EPJ Web of Conference, 2014.
- [5] JANDAČKA, J., PAPUČÍK, Š., KAPJOR, A., LENHARD, R. *Kombinované zdroje tepla na spaľovanie biomasy*. Vykurovanie, 2010.
- [6] ĎURČANSKÝ, P., LENHARD, R., JANDAČKA, J. *Výpočet parametrov výmenníka tepla pre nekonvenčnú mikrokogeneračnú jednotku*. 33th Conference of department of fluids mechanics and thermomechanics, 2014.
- [7] MIČIETA, J., LENHARD, R., JANDAČKA, J. *Návrh výmenníka tepla pre malý peletový kotol na spaľovanie fytomasy*. TechSoft Engineering ANSYS 2014 - Setkání uživatelů a conference, 2014.
- [8] KAPJOR, A., SMATANOVÁ, H., HUŽVÁR, J., GREŠŠÁK, T., JANDAČKA, J. *Optimization of heat transfer oriented surfaces by thermovision and using CFD method*. Structure and environment: architecture, civil engineering, environmental engineering and energy, 2013.
- [9] SULOVCOVÁ, K., JANDAČKA, J., NOSEK, R. *Influence of geometric parameters changes in flue gas path on particulate matter concentration*. Power control and optimization: proceeding of seventh global conference: Yangon, Myanmar, 2013.
- [10] NEMEC, P., HUŽVÁR, J. *Proposal of heat exchanger in micro cogeneration unit, configuration with biomass combustion*. Materials science and technology, 2011.
- [11] LENHARD, R., MALCHO, M. *Numerical simulation device for the transport of geothermal heat with forced circulation of media*. Mathematical and Computer Modelling, 2013.



Creation of a tilting bogie model for simulation purpose

*Mária Maňurová, *Andrej Suchánek

*University of Žilina, Faculty of Mechanical Engineering, Department of Transport and Handling Machines, Univerzitná 8215/1, 01026 Žilina, Slovak Republic, {maria.manurova, andrej.suchanek,}@fstroj.uniza.sk

Abstract. The article deals with usage of tilting bogie in public railway transport and determination of riding comfort value for a ride along a curve on the track. In the second chapter, the process of tilting bogie model creation in SIMPACK program with joints being defined is given. The bogie is modelled in the RAIL module of SIMPACK. The third chapter deals with method for calculation of individual bogie parameters, masses, static moments, center of gravity coordinates, moments of inertia and deviation moments. In the fourth chapter we characterize the track needed for the simulation of ride in a curve. In the last chapter, signals that are necessary for comfort value determination are given. The conclusion summarizes the simulations options that will be dealt with in the future.

Keywords: Model, Ride comfort, Tilting bogie, SIMPACK.

1. Introduction

A railway vehicle represents very complex mechanical system. In public transport the aim is to increase the driving velocity and the ride comfort of the vehicle.

The increase of driving velocity leads to introduction of a tilting body. Such attachment of a body on the bogie is much more complicated in the case of a standard railway vehicle. The role of the attachment is to increase felt while the vehicle rides in a curve and thus decrease the lateral unbalanced acceleration affecting the passengers and on the contrary, while keeping the lateral unbalanced acceleration measure, enable velocity increase for a ride in curve with the given radius [6].

The tilting bodies enable increase of a ride in curve only from the passenger comfort perspective, but they do not affect the rail strain from lateral forces [3]. The issue of tilting bodies was an impulse for creation of a tilting bogie model and the track, along which the bogie will ride [4]. The bogie and track models were created in a simulation program, which will also serve for the ride comfort analysis purposes.

2. Creation of tilting bogie model

The bogie model was created in the RAIL module of a SIMPACK program. Each model created in the program consists of certain bodies, which are connected to each other through joints with defined force elements. These parts of model are affected from the settings in of the Globals item in the model navigator tree.

The bodies are the main modeling elements, which depend on mass and inertial properties. They can be solid or flexible. SIMPACK provides three different types of bodies:

- Rigid bodies, which do not change their geometry or mass properties during the simulation.
- Flexible bodies defined in an FE code (mass matrix, stiffness matrix).
- Flexible bodies defined by SIMBEAM, which is an integrated finite element tool within SIMPACK that allows the user to model three-dimensional flexible beam structures including mass and inertia properties [1].

The input data for bodies can be set automatically or manually:

- Data Input – Manual: the total body mass, centre of gravity (coordinates of its position x , y and z with respect to the reference system), moments of inertia (with respect to the centre of gravity).
- Data Input – Auto. All these properties are being calculated on the bases of a density and geometry.

There are multiple options for the creation of a body geometry in the database of SIMPACK. The program enables also import of an external CAD model with geometry already define, which was also our case.

The bodies are connected with other objects or the reference system through Joint elements. Each connection of objects must be defined by Markers. Each body can have only one Joint. The type of Joint defines the amount of degrees of freedom of the body.

Springs, dampers and other passive or semi-active elements are modelled using the Force Elements. Force Elements serve to create relative force connections between individual bodies.

In the case of a bogie, it is also necessary to set the parameters for the Wheelsets, which provides logical connection between the left and right rail-wheel pair.

Most of the railway vehicle model parts are created from the standard modelling elements. Only the rail-wheel contact requires special modelling elements. The vehicle can move freely in the space or along the track, where the vehicle is also realistically restricted in the rail-wheel contact. The vehicle is forced to follow the track.

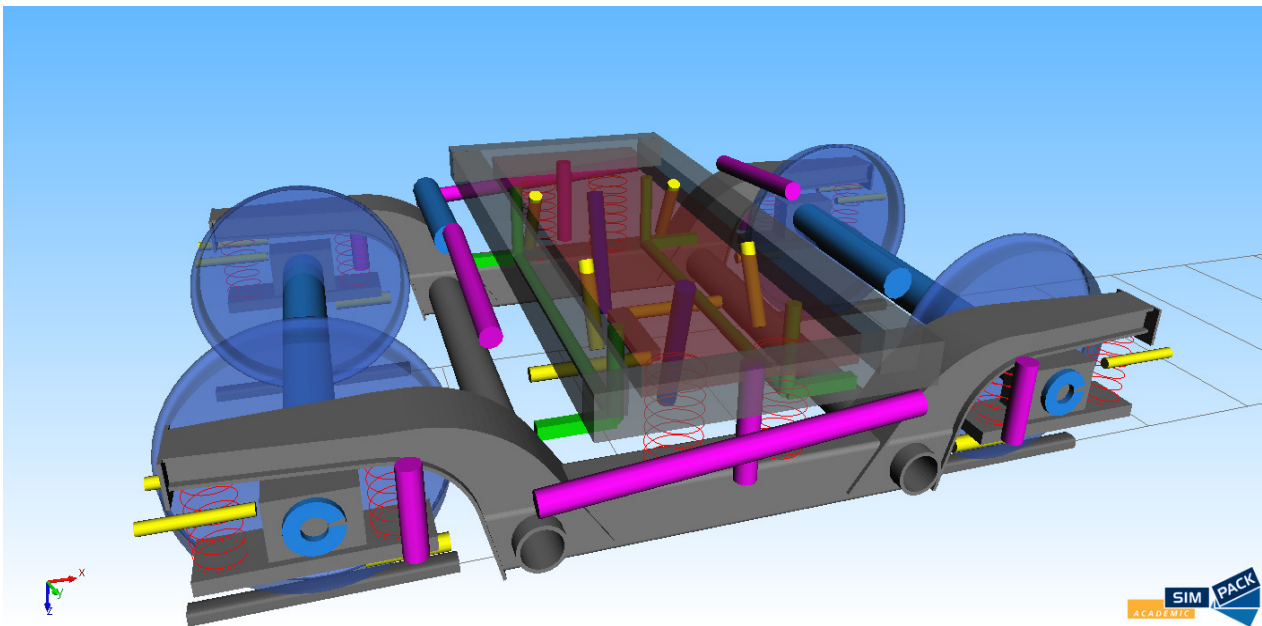


Fig. 1 Bogie model in SIMPACK.

3. Bogie parameters calculation

Geometrical parameters of bodies used for the automatically calculation of inertial properties are defined in parameters of each body composing the model. In our case, individual parts were modelled in CATIA programme and imported to SIMPACK afterwards. In the dialog menu of SIMPACK, multiple selections of individual bodies are possible for the calculation of inertial properties.

For the calculation of inertial properties, the so-called tessellation method instead of analytical expression is used. The tessellation method is a process, during which the former body is converted to irregular triangle mesh, that is individual geometrical elements are discretized using triangles and inertial parameters determined through integration on discretized volume of the bodies. The amount



of triangles used for discretization depends on the given geometrical parameters. The offered variants of tessellation are solid, shall, and wireframe [5].

The automatically calculation of inertial parameters in SIMPACK is a valuable tool for quick determination of these characteristic based on geometry. The calculated values are a rough estimation of properties and cannot guarantee exact results. Nevertheless, its universal concept makes it a suitable tool for standard geometrical shapes such as cylinder, cone etc. and also for arbitrary complex geometrical shapes of models imported from CAD software **Chyba! Nenašiel sa žiaden zdroj odkazov..**

Body mass m [kg] is defined as a density ρ [kg/m³] multiplied by integral of volumes:

$$m = \rho \int_{dV} dV . \quad (1)$$

Static moments of volumes to x , y , and z axis:

$$s_x = \rho \int_{dV} x dV, s_y = \rho \int_{dV} y dV, s_z = \rho \int_{dV} z dV. \quad (2)$$

Centre of gravity coordinates for x , y , and z axis: :

$$x_T = \frac{s_x}{m}, y_T = \frac{s_y}{m}, z_T = \frac{s_z}{m}. \quad (3)$$

When defining the moment of inertia of a continuously divided body it is necessary to use integral calculation. Moment of inertia of volume V to x , y and z axis are defined as addition of all volume element and squared distance of the centers of gravity from x , y and z :

$$I_x = \rho \int_{dV} x^2 dV, I_y = \rho \int_{dV} y^2 dV, I_z = \rho \int_{dV} z^2 dV. \quad (4)$$

Moment of deviation:

$$D_x = \rho \int_{dV} y^2 + z^2 dV, D_y = \rho \int_{dV} x^2 + z^2 dV, D_z = \rho \int_{dV} x^2 + y^2 dV. \quad (5)$$

In SIMPACK, there is a possibility to set the mass of the model manually and calculate the calculation of the center of gravity and the inertial parameters using the automatically function of the program [1].

4. Track characteristics

To determine the ride comfort, a simulation of a ride along a track has to be proceeded. Basic settings of the rail are done in the RAIL part of SIMPACK, where geometry of the rail and lateral position is defined. In the advanced settings, it is possible to modify its geometry. In the program, rail profiles from a library of existing profiles can be chosen. The program also allows to predict wear and loss of material on the rail or on the wheel.

In the track setting, the parameter Type plays an important role, which in our case is set to Rail option. By setting other parameters for length, radius of curve and cant are defined characteristics for line track [1]

In our case, the line is 3.5 km length. Track begins straights, followed by four (2 left, 2 right) curves which are connected straight line part and ends straights. Curve radius is 600 m.

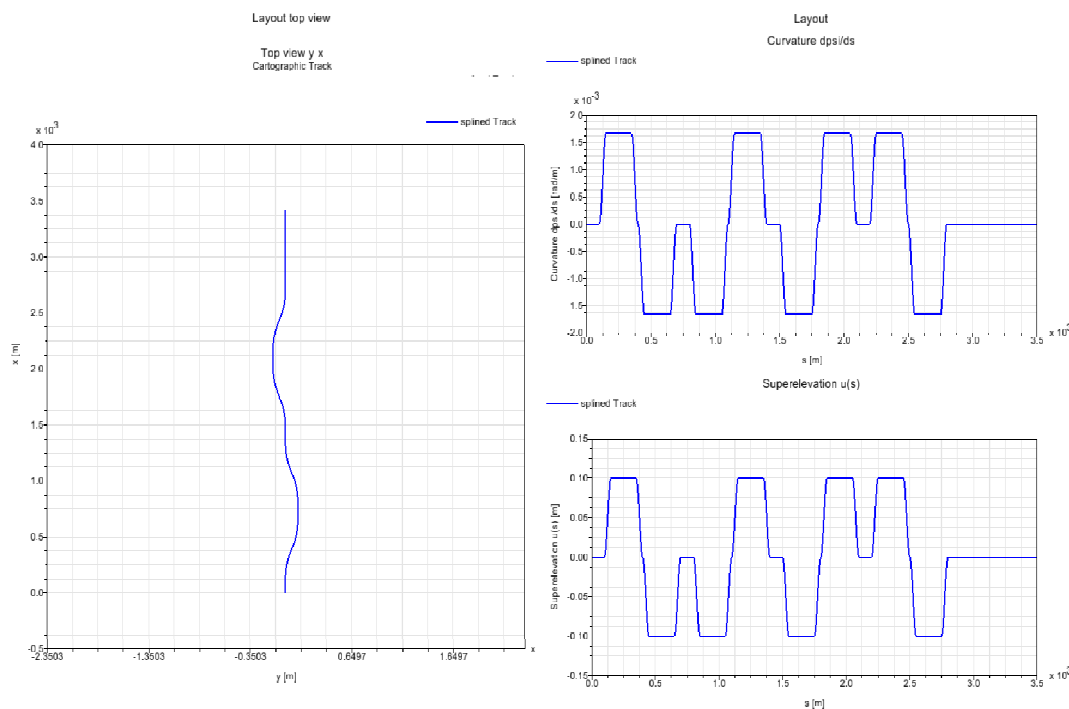


Fig. 2 Characteristic of a track.

5. Signals necessary for the calculation of ride comfort

Ride comfort is evaluated through comfort values, which are derived from test. In our simulation, the comfort during ride in curve P_{CT} will be evaluated. This value is described as discomfort perceived when entering the curve or perceived during ride through curves oriented in opposite direction. The comfort values will be specified according the STN EN 12299:2009 norm.

The following formula is used for calculating the value of comfort, where the member in brackets is taken to account only if it is ≥ 0 :

$$P_{CT} = 100 \cdot \left[(A\ddot{y} + B\ddot{\dot{y}} - C) + D\dot{v}^E \right], \text{ where:} \quad (6)$$

\ddot{y} is maximum value of lateral acceleration in the time period from beginning to end plus 1.6 s of the transition curve [$\text{m}\cdot\text{s}^{-2}$],

$\ddot{\dot{y}}$ is maximum value of lateral jerk in the time period from 1 s before the beginning to the end of the transition curve [$\text{m}\cdot\text{s}^{-3}$],

\dot{v} maximum value of body roll velocity in the time period from the beginning to the end of the transition curve [s^{-1}],

A, B, C, D, E are constants for P_{CT} comfort index in Tab. 1.

Condition	A [s^2/m]	B [s^3/m]	C [-]	D [s/rad]	E [-]
In rest - standing	0,2854	0,2069	0,1110	3,6400	2,283
In rest - seated	0,0897	0,0968	0,0590	0,9160	1,626

Tab. 1 Constants for A, B, C, D and E [2].

Formula (6) is used when entering the curve or opposite directed curve, which take at least 2 s. Following measurements are carried out [2]:

- lateral acceleration \ddot{y}^* in the middle of the vehicle body floor and the leading end of the passenger compartment,



- unbalanced lateral acceleration \ddot{y}_k ,
- roll velocity of the vehicle body $\dot{\phi}^*$, at a suitable position of the vehicle body,
- angle of tilting β (where is necessary),
- velocity v [29].

6. Conclusion

Passengers in public railway transport, place great importance on ride comfort in vehicle. They experience the biggest influence of ride during ride curve. The biggest acceleration affects the passengers there. The requirements for increase of ride comfort lead to construction of tilting vehicle body.

The article deals with procedure of creating a bogie for tilting bodies. Individual parts of bogie are created in CATIA program and imported into simulation program SIMPACK. It is necessary to specify basic model parameters of the vehicle and define joints between individual parts. With the use of the force elements it is also possible to model springs, dampers and other passive or semi-active elements.

The aim of further research will be evaluation of the values of ride comfort P_{CT} and force effects on the track with and without body tilting for empty and fully occupied vehicle. The load of vehicle has great influence on ride in curves and on body tilting. In the future simulation, the vehicle will drive through chosen track composed from curves and shorter straight sections. The outcome will be evaluation of the results and their graphical representation.

Acknowledgement

The work was supported by the Scientific Grant Agency of the Ministry of Education of the Slovak Republic and the Slovak Academy of Sciences in project No. 1/0347/12: "Railway wheel tread profile wear research under the rail vehicle in operation conditions simulation on the test bench", project No. 1/0383/12: "The rail vehicle running properties research with the help of a computer simulation." and the project No. APVV-0842-11: "Equivalent railway operation load simulator on the roller rig".

Research-Educational Center of Rail Vehicles (VVCKV)

References

- [1] SIMPACK Documentation. 2001. 4168 p.
- [2] STN EN 12299:2009. *Railway applications. Ride comfort for passengers. Measurement and evaluation.* 1. 10. 2009. 62 p. ICS 45.060.20.
- [3] KALINČÁK, D., GERLICI, J., LACK, T., KUKUČA, P., POLÁCH, O., SÁGA, M., LÁBAJ, J. *Transport vehicle – Calculation methods.* University of Žilina. 2005. 402 p. ISBN 80-8070-476-7. (In Slovak).
- [4] SÁGA, M., ŽMINDÁK, M., GERLICI, J., LACK, T., DEKÝŠ, V., SAPIETOVÁ, A. *Advanced Method in Computational and Experimental Mechanics.* 2013. 193 p. ISBN: 978-1-78434-069-8.
- [5] CHUDZIKIEWICZ, A., BOGACZ, R., OSTERMEYER, G-P.: *Selected Dynamical Problems in Mechanical Systems: Theory and Applications in Transport.* Oficyna Wydawnicza Politechniki Warszawskiej, 2014. 216 p. ISBN 978-83-7814-282-9.
- [6] GERLICI, J., LACK, T. *Rail geometry analysis (from the point of view of wearing in the operation).* In: Communications - scientific letters of the University of Žilina. ISSN 1335-4205. - Vol. 5, No. 1 (2003).
- [7] GERLICI, J., LACK, T. *Railway wheelset and track contact.* University of Žilina, 2004, ISBN 80-8070-317-5. (p. 200). (In Slovak).
- [8] GERLICI, J., LACK, T. *Wheelset/rail geometric characteristics assessment with regard to wheelset rolling.* In: Communications - scientific letters of the University of Žilina. ISSN 1335-4205. - Vol. 7, No. 1 (2005).



- [9] GERLICI, J., LACK, T. et al. *Transport means properties analysis: Volume 1* (2005) - 1st ed. - Žilina: University of Žilina, 2005. (p. 214), ISBN 80-8070-408-2.
- [10] LACK, T., GERLICI, J. *The usage of arcs radii profile variation for the synthesis of railway wheel and rail head profiles*. In: Communications - scientific letters of the University of Žilina. ISSN 1335-4205. Vol. 8, No. 2 (2006).
- [11] GERLICI, J., LACK, T. *Synthesis of railway wheel and rail head profiles via the usage of arcs radii profile variation*. In: Zeszyty naukowe Instytutu Pojazdów: mechanika, ekologia, bezpieczeństwo. - ISSN 1642-347X. 1 (60)/2006.
- [12] GERLICI, J., LACK, T. *Profiles synthesis through radii variation of arcs profile*. In: Archives of Transport. ISSN 0866-9546. Vol. 18, No. 3 (2006).
- [13] LACK, T., GERLICI, J. *Iterational method for railway wheel tread profile design*. In: XVIII konferencja naukowa - pojazdy szynowe: Katowice-Ustroń, 17-19 września 2008: Materiały konferencyjne.
- [14] LACK, T., GERLICI, J. *Iterative method for railway wheel profile design*. In: Communications: Scientific Letters of the University of Žilina. - ISSN 1335-4205. - Vol. 11, No. 2 (2009).
- [15] GERLICI, J., LACK, T. *Railway wheel profile development based on the geometric characteristics shapes*. In: Contact mechanics and wear of rail/wheel systems = CM2009: 8th international conference: 15th-18th September 2009, Firenze, Italy. - Firenze: AB EDITORE, 2009. ISBN 978-88-904370-0-7.
- [16] GERLICI, J., LACK, T. *Contact geometry influence on the rail / wheel surface stress distribution*. In: Procedia Engineering, ISSN 1877-7058. - Iss. 1 (2010).
- [17] GERLICI, J., LACK, T. *Railway wheel and rail head profiles development based on the geometric characteristics shapes*. In: Wear: an international journal on the science and technology of friction, lubrication and wear. ISSN 0043-1648. - Vol. 271, No. 1-2 Sp. iss. (2011).
- [18] YANG, Y. B. *Vehicle- bridge interaction Dynamics: with applications to high-speed railways*. 2004. ISBN-13: 978-9812388478.
- [19] LACK, T., GERLICI, J. *Vibrational analysis of mechanical system with concentrated masses*. In: Current problems in rail vehicles: 13. International conference. Univerzita Pardubice. ISBN 80-7194-105-0, (pp. 263-271). (In Slovak).
- [20] GERLICI, J., LACK, T. *Mechanical Systems analysis with Component Works TM*. In: Communications on the edge of the millenniums: 10th international scientific conference. 3rd section, Means of transport and electric traction equipment. Žilina: University of Žilina. ISBN 80-7100-518-5.
- [21] GERLICI, J., LACK, T. *Methods for vehicle vibration analysis in time domain*. In: Prace Naukowe. Transport. ISSN 1230-9265. Z. 63 (2007).
- [22] GERLICI, J., LACK, T. *Modified HHT method usage for vehicle vibration analysis in time domain*. In: Communications - scientific letters of the University of Žilina. ISSN 1335-4205, 2/2008.
- [23] GERLICI, J. – LACK, T. *Modified HHT method for vehicle vibration analysis in time domain utilisation*. In: Applied Mechanics and Materials. ISSN 1660-9336. Vol. 486 (2014), online ISSN 1662-7482, Trans Tech Publications, Switzerland.
- [24] LACK, T., GERLICI, J., MAŇUROVÁ, M. *Simulation analysis of railway wagon bogie model*. In: Dynamics of rigid and deformable bodies: conference proceedings of the XII. International scientific conference: Ústí nad Labem, 8.-10. 10. 2014. Ústí nad Labem: FVTM UJEP, 2014. ISBN 978-80-7414-749-4. - CD-ROM. (In Slovak).
- [25] LACK, T., GERLICI, J. *The Programme System DELTA Exploitation for Numerical Analysis Performances*. 18-th. International Conference “Current Problems in Rail Vehicles - PRORAIL 2007” Proceedings of lectures, Part II. pp. 11–22, EDIS, ISBN 978-80- 89276-07-3, Žilina. (In Slovak).
- [26] IWŃICKI, S., BEZIN, Y., ORLOVA, A., JOHNSON, P.-A., STICHEL, S., SCHELLE, H. The ‘SUSTRAIL’ high speed freight vehicle: *Simulation of novel running gear design*. Proceedings of the 23rd International Symposium on Dynamics of Vehicles on Roads and Tracks, p. 11. IAVSD. August 2013 Qingdao, China, 2013.
- [27] LACK, T., GERLICI, J. *Vehicles dynamical properties analysis from the point of view of comfort for passengers*. In: Archives of Transport. ISSN 0866-9546. Vol. 19, No. 1-2 (2007).
- [28] GERLICI, J., LACK, T., ONDROVÁ, Z. *Evaluation of comfort for passengers of railway vehicles*. In: Communications: Scientific Letters of the University of Žilina. ISSN 1335-4205. Vol. 9, No. 4 (2007).
- [29] LACK, T., GERLICI, J. *Analysis of vehicles dynamic properties from the point of view of passenger comfort*. In: Communications: Scientific Letters of the University of Žilina. ISSN 1335-4205. - Vol. 10, No. 3 (2008).
- [30] DIŽO, J. *Passenger ride comfort evaluation by means of computer simulation*. Dynamics of rigid and deformable bodies: conference proceedings of the XII. International scientific conference: Ústí nad Labem, 8.-10. 10. 2014. Ústí nad Labem: FVTM UJEP, 2014. ISBN 978-80-7414-749-4.
- [31] DIŽO, J. *Evaluation of Rode Comfort for Passenger by Means of Computer Simulation*. Manufacturing Technology. February 2015, Vol. 15, No. 1, Pp. 8-14. UJEP in Ústí nad Labem. ISSN 1213-2489.



Suspension of tilting bogie specification for calculations of dynamical behavior evaluation

*Mária Maňurová, * Andrej Suchánek

*University of Žilina, Faculty of Mechanical Engineering, Department of Transport and Handling Machines, Univerzitna 8215/1, 01026 Žilina, Slovak Republic, {maria.manurova, Andrej.suchanek}@fstroj.uniza.sk

Abstract. The article deals with use and calculation of coil springs for rail vehicles. There are three coil springs in the secondary suspension and two in the primary suspension of the bogie. In the primary suspension case, in addition to the vertical forces, there are also lateral forces acting, which affect the ride of the vehicle. The coil spring simulation was performed in SIMPACK program and the obtained values will be used in further simulations. The data obtained will be used as an input for a design of coil springs to be implemented in a tilting bogie model, on which the comfort values during ride in curve will eventually be determined.

Keywords: Coil spring, Stiffness, Lateral force, Vertical force.

1. Introduction

The basic task of tilting bodies of railway vehicle is larger slope in the ride in curve and reduce unbalanced lateral acceleration affected on passengers. The aim of the passenger transport is also increasing travel speed with the least impact on passenger comfort in the vehicle [1].

During the model construction, it is necessary to set the parameters of individual components. In the next chapters, we will deal with force elements in SIMPACK program, which allow the user to model springs, dampers, and other active or semi-active elements, forces in the contact between bodies, friction force, driving force, etc. During the setting of the parameters was made the analysis of stiffness in ANSYS program.

2. Suspension of rail vehicles

A spring is a flexible component of machines made of rods or beams, which allows deformation energy storage during its flexible deformation. Springs can be divided into steels or non-steel (rubbery, pneumatic or hydro-pneumatic). From the running quality perspective, the softest suspension possible is desired [27].

The deformation work of the spring represents the accumulated energy, which can be expressed in the form:

$$dA = Fdy = K_y dy, \text{ resp. } dA = Md\varphi = K_\varphi d\varphi; \quad (1)$$

where:

dA deformation work element [J],

F force [N],

dy deformation element [m],

M torque moment [N.m],

$d\varphi$ torsion angle element [rad],

K_y stiffness [N.m⁻¹],

K_φ torsion stiffness [N.m.rad⁻¹],



φ torsion angle [rad].

Deformation work is defined as [22]:

$$A = \int_0^y K y dy = \frac{1}{2} K y^2 = \frac{1}{2} F y, \text{ resp. } A = \int_0^\varphi K d\varphi = \frac{1}{2} K \varphi^2 = \frac{1}{2} M \varphi. \quad (2)$$

The force or moment that will cause the unit displacement or rotation of the spring rate:

$$k = \frac{dF}{dy}, \text{ ect. } k = \frac{dM}{d\varphi}. \quad (3)$$

Stiffness of the springs with linear characteristic is constant:

$$k = \frac{F}{y}, \text{ ect. } k = \frac{M}{\varphi}. \quad (4)$$

The first natural frequency serves as a sort of suspension quality indicator and can be approximately determined using the formula [20]:

$$f = \frac{1}{2\pi} \sqrt{\frac{k}{m}} \cong \frac{0.5}{\sqrt{z_{stat}}}; \quad (5)$$

where:

f is the natural frequency [Hz],

k is the total stiffness of the vertical suspension [kN/m],

m is the vehicle car body mass including the sprung parts of the bogie [t],

z_{stat} is the static press of the vertical suspension under the weight of the car body [m].

The natural frequency of the vehicle (reasonable running quality) should be between 1 and 1.5 Hz (better up to 1.25 Hz).

The results indicate, that the natural frequency value for the suspension is affected by the car body mass. This means, that an empty or low occupied car has a higher first natural frequency than a fully occupied car.

Default parameters of a coil spring are the mean diameter of the spring D [m], diameter of the wire d [m], amount of active threads n [-], amount of closing threads n' , free length of a spring H_0 [m] and gradient of the helix s [-]. The free length of a spring must be chosen in such manner, so maximal pressing z_{max} [m] (constrained by the buffers) would not come to contact with the threads, but a clearance will stay of at least 10 to 15 % diameter of the spring wire [2, 3, 6, 8, 11, 12, 26].

$$H_0 = (n + n')d + z_{max} + n(0.1 \text{ to } 0.15)d. \quad (6)$$

Deformation of the coil spring loaded by an axial force F is calculated from the formula:

$$z = \frac{64FR^3n}{Gd^4}; \quad (7)$$

where:

n is the amount of the active threads [-],

R is radius of spring [m]

G is the shear modulus [Pa].

Axial stiffness of the spring is [12]:

$$k = \frac{Gd^4}{64R^3n}. \quad (8)$$

3. Springs parameters in SIMPACK program

In program SIMPACK are the springs generated along the positive direction of the x-axis of the reference marker, which is located in the middle of the spring end (Fig. 1).

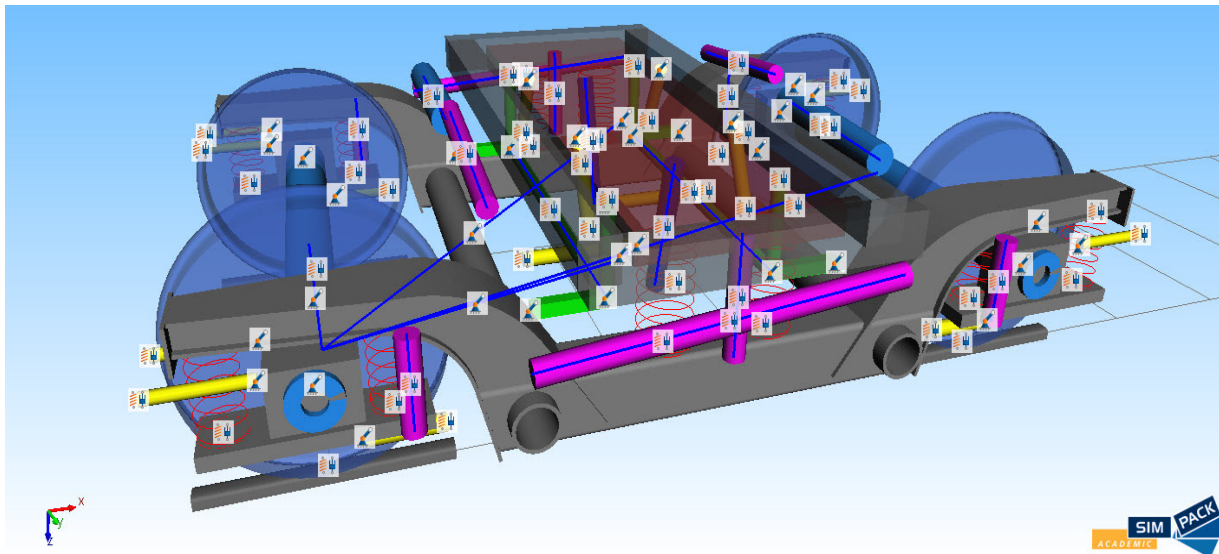


Fig. 1 Location of the primary and secondary suspension in the bogie.

By input of the spring characteristics, not all the parameters are always available:

- stiffness and damping parameters are lost, if the non-linear stiffness or damping characteristics are set through main input functions for individual directions,
- constants and input parameters, as well as nominal force parameters, are lost when the expression is assigned to the given direction.

Basic input parameters in SIMPACK program:

- nominal forces F_{nom_x} , F_{nom_y} , F_{nom_z} (Nominal force $f_{nom_x/y/z}$),
- stiffness k_x , k_y , k_z (Stiffness $k_{x/y/z}$),
- damping d_x , d_y , d_z (Damping $d_{x/y/z}$),
- input function F_{kx} , F_{ky} , F_{kz} , F_{dx} , F_{dy} , F_{dz} (Input Function $F_k(x/y/z)$, Input Function $F_d(xd/yd/zd)$),
- clearance in direction x , y , z , s_x , s_y , s_z ,
- root function - used for detection of the clearance constraints,
- reference marker for measurements and calculation - all the measurements of distance and speed between markers as well as all calculated forces use directions defined by the axis of the reference marker instead of *From Marker*,
- forces F_x , F_y , F_z , which describe the forces in three directions.

4. Calculation of the spring stiffness

The suspension used in our bogie is in vertical and lateral direction. The primary suspension is secured by two coil springs on each wheel supplemented by hydraulic dampers. The secondary vertical suspension is realised using coil springs with vertical and horizontal dampers. The secondary suspension is also in the lateral direction. Lateral suspension of the bogie is described as active, meaning that the centre of gravity of the car body is located in the longitudinal axis of the bogie.

The calculated axis forces in the secondary suspension springs in ANSYS program are shown in the Tab. 1. Longitudinal and lateral forces in springs are calculated for 4 degrees of turning of the spring. When the springs are turned, changes in the axial forces emerge, as can be seen in Fig. 2. There we can see an approximately linear force characteristic. If we turn the spring system around its vertical axis, the characteristic changes. An average force of -11 093.80 N applies in the vertical direction. The average value of stiffness in the axis direction is -221.88 N/mm (Fig. 3).

Depression [mm]	Rotation of spring 0 °		Rotation of spring 45 °		F_z [N]	Stiffness k [mm]
	F_y [N]	F_x [N]	F_x [N]	F_y [N]		
4	481.09	809.21	1066.50	559.77	-11071.00	-221.42
3	274.78	636.54	862.84	355.94	-11076.00	-221.52
2	69.04	434.30	659.07	155.44	-11081.00	-221.62
1	-136.86	232.00	454.90	-48.64	-11086.00	-221.72
0	-342.89	2.99	251.72	-253.00	-11091.00	-221.82
-1	-547.72	-174.96	47.52	-457.33	-11096.00	-221.92
-2	-753.84	-374.85	-155.58	-661.52	-11101.00	-222.02
-3	-975.62	-578.80	-359.50	-866.24	-11107.00	-222.14
-4	-1165.30	-780.43	-569.23	-1071.80	-11112.00	-222.24
-5	-1371.00	-982.56	-773.02	-1276.60	-11117.00	-222.34

Tab. 1 Calculated values of the secondary suspension.

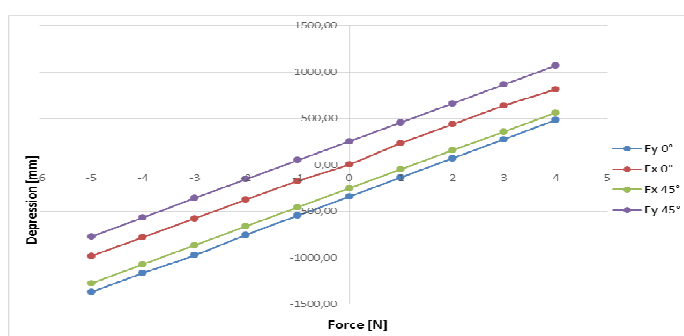


Fig. 2 Secondary suspension coil spring load by turning around the vertical axis.

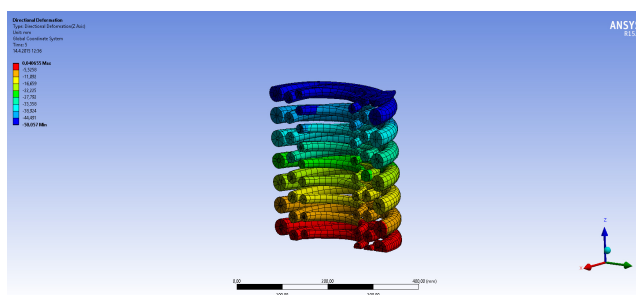


Fig. 3 Depression in the triple-springs.

In the primary suspension case, the situation is easier. No lateral forces affect the double-spring and therefore it is sufficient to calculate only vertical load from press and consequently determine the spring stiffness. From the calculated values in the Tab. 2 can be seen, that application of higher force leads to higher compression of the spring, but the stiffness remains unchanged with the average of 6599.20 N/mm (Fig. 4).

z [mm]	F_z [N]	k [N/mm]
1	6599.20	6599.20
2	13198.00	6599.00
3	19798.00	6599.33
4	26397.00	6599.25
5	32996.00	6599.20

Tab. 2 Calculated values of the primary suspension.

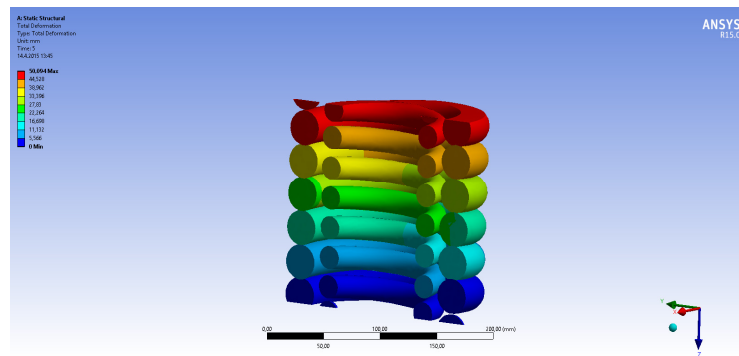


Fig. 4 Depression in the double-springs.

5. Conclusion

The increasing requirements on rail transport lead to permanent innovations of vehicle construction. In the case of passenger transport, great accent is focused on the passenger comfort. For that purpose, tilting car bodies were developed. Tilting bogies make an important part of the construction. Our aim is to create a model of such bogie and use it for a simulation of a ride on the track. In the case of primary suspension we have determined the stiffness in the vertical direction.

One of the important parts of a bogie is the suspension, in our case a double stage one - the primary suspension (composed of two springs) and the secondary suspension (composed of three springs). We created and analysed the model of the springs in the ANSYS program. As a result for both of the suspensions, the stiffness was constant -221.88 N/mm for the secondary suspension and 6599.20 N/mm for the primary suspension. The situation is more difficult by the secondary suspension. We found out, that the lateral stiffness of the spring is dependent on the turning of the spring and changes linearly with the compression. These results will be further used for simulations of the whole bogie and ride in curve of the track.

Acknowledgement

The work was supported by the Scientific Grant Agency of the Ministry of Education of the Slovak Republic and the Slovak Academy of Sciences in project No. 1/0347/12: “Railway wheel tread profile wear research under the rail vehicle in operation conditions simulation on the test bench”, project No. 1/0383/12: “The rail vehicle running properties research with the help of a computer simulation.” and the project No. APVV-0842-11: “Equivalent railway operation load simulator on the roller rig”.

Research-Educational Center of Rail Vehicles (VVCKV)

References

- [1] CHUDZIKIEWICZ, A., BOGACZ, R., OSTERMEYER, G-P. *Selected Dynamical Problems in Mechanical Systems: Theory and Applications in Transport*. Oficyna Wydawnicza Politechniki Warszawskiej, 2014. 216 str. ISBN 978-83-7814-282-9
- [2] KALINČÁK, D., GERLICI, J., LACK, T., KUKUČA, P., POLÁCH, O., SÁGA, M., LÁBAJ, J. *Transport vehicle – Calculation methods*. University of Žilina, 2005. - 402 p. ISBN 80-8070-476-7. (In Slovak)
- [3] SÁGA, M., ŽMINDÁK, M., GERLICI, J., LACK, T., DEKÝŠ, V., SAPIETOVÁ, A. *Advanced Method in Computational and Experimental Mechanics*. 2013. 193 p. ISBN: 978-1-78434-069-8.
- [4] LACK, T., GERLICI, J. *Vibrational analysis of mechanical system with concentrated masses*. (In Slovak). Current problems in rail vehicles: 13. International conference. Univerzita Pardubice. 1997. ISBN 80-7194-105-0.
- [5] GERLICI, J., LACK, T. *Mechanical Systems analysis with Component Works TM*. Communications on the edge of the millenniums: 10th international scientific conference. 3rd section, Means of transport and electric traction equipment. Žilina: University of Žilina. 1998. ISBN 80-7100-518-5.



- [6] GERLICI, J., LACK, T. *Methods for vehicle vibration analysis in time domain*. In: Prace Naukowe. Transport. ISSN 1230-9265. Z. 63 (2007).
- [7] GERLICI, J., LACK, T. *Modified HHT method usage for vehicle vibration analysis in time domain*. In: Communications - scientific letters of the University of Žilina. ISSN 1335-4205, 2/2008.
- [8] GERLICI, J. – LACK, T. *Modified HHT method for vehicle vibration analysis in time domain utilisation*. In: Applied Mechanics and Materials. ISSN 1660-9336. Vol. 486 (2014), online ISSN 1662-7482, Trans Tech Publications, Switzerland.
- [9] GERLICI, J., LACK, T. *Railway wheelset and track contact*. (In Slovak). University of Žilina, ISBN 80-8070-317-5. (p. 200).
- [10] GERLICI, J., LACK, T. *Wheelset/rail geometric characteristics assessment with regard to wheelset rolling*. Communications - scientific letters of the University of Žilina. ISSN 1335-4205. - Vol. 7, No. 1 (2005).
- [11] GERLICI, J., LACK, T. et al. *Transport means properties analysis: Volume 1 (2005) - 1st ed.* - Žilina: University of Žilina, 2005. (p. 214), ISBN 80-8070-408-2.
- [12] LACK, T., GERLICI, J. *Wheel/rail contact stress evaluation by means of the modified strip method utilization*. VSDIA 2012: proceedings of the 13th mini conference on Vehicle system dynamics, identification and anomalies: 5-7 November, 2012 Budapest, Hungary. - [S.l.: s.n.], 2012. - ISBN 978-963-313-102-2.
- [13] LACK, T., GERLICI, J. *Modified Strip method utilisation for wheel /rail contact stress evaluation*. 9th international conference on contact mechanics and wear of rail/ wheel systems (CM2012): 27.-30. August 2012, Chengdu, China: proceedings. Chengdu: Southwest Jiaotong University.
- [14] LACK, T., GERLICI, J. *A modified strip method to speed up the calculation of normal stress between wheel and rail*. In: Applied mechanics and materials. ISSN 1660-9336. Vol. 486 (2014), online ISSN 1662-7482.
- [15] LACK, T., GERLICI, J. *The FASTSIM method modification in speed up the calculation of tangential contact stresses between wheel and rail*. Manufacturing technology: journal for science, research and production. ISSN 1213-2489. - Vol. 13, no. 4 (2013).
- [16] LACK, T., GERLICI, J.: *Wheel/rail tangential contact stress evaluation by means of the modified strip method*. Communications: scientific letters of the University of Žilina. ISSN 1335-4205. - Vol. 16, no. 3A (2014).
- [17] GERLICI, J., LACK, T.: *Synthesis of railway wheel and rail head profiles via the usage of arcs radii profile variation*. In: Zeszyty naukowe Instytutu Pojazdów: mechanika, ekologia, bezpieczeństwo. - ISSN 1642-347X. 1 (60)/2006.
- [18] GERLICI, J., LACK, T. *Profiles synthesis through radii variation of arcs profile*. Archives of Transport. ISSN 0866-9546. Vol. 18, No. 3 (2006).
- [19] LACK, T., GERLICI, J. *Iterational method for railway wheel tread profile design*. XVIII konferencja naukowa - pojazdy szynowe: Katowice-Ustroń, 17-19 września 2008: Materiały konferencyjne.
- [20] LACK, T., GERLICI, J. *Iterative method for railway wheel profile design*. Communications: Scientific Letters of the University of Žilina. - ISSN 1335-4205. - Vol. 11, No. 2 (2009).
- [21] GERLICI, J., LACK, T. *Railway wheel profile development based on the geometric characteristics shapes*. Contact mechanics and wear of rail/wheel systems = CM2009: 8th international conference: 15th-18th September 2009, Firenze, Italy. - Firenze: AB EDITORE, 2009. - ISBN 978-88-904370-0-7.
- [22] GERLICI, J., LACK, T. *Contact geometry influence on the rail / wheel surface stress distribution*. Procedia Engineering. ISSN 1877-7058. - Iss. 1 (2010).
- [23] LACK, T., GERLICI, J., MAŇUROVÁ, M. *Simulation analysis of railway wagon bogie model*. (In Slovak). Dynamics of rigid and deformable bodies: conference proceedings of the XII. International scientific conference: Ústí nad Labem, 8.-10. 10. 2014. Ústí nad Labem: FVTM UJEP, 2014. ISBN 978-80-7414-749-4. - CD-ROM.
- [24] LACK, T., GERLICI, J. *The Programme System DELTA Exploitation for Numerical Analysis Performances*, (in Slovak). 18-th. International Conference “Current Problems in Rail Vehicles - PRORAIL 2007” Proceedings of lectures, Part II. EDIS, ISBN 978-80- 89276-07-3, Žilina.
- [25] GERLICI, J., LACK, T., ONDROVÁ, Z. *Evaluation of comfort for passengers of railway vehicles*. Communications: Scientific Letters of the University of Žilina. ISSN 1335-4205. Vol. 9, No. 4 (2007).
- [26] LACK, T., GERLICI, J. *Analysis of vehicles dynamic properties from the point of view of passenger comfort*. In: Communications: Scientific Letters of the University of Žilina. ISSN 1335-4205. - Vol. 10, No. 3 (2008)
- [27] GERLICI, J. *Comfort for passengers of rail vehicle assessment*. Advanced methods in computational and experimental mechanics. London: Pearson Education Limited, 2013. ISBN 978-1-78434-069-8.
- [28] BLATNICKÝ, M., DIŽO, J. *The design and functional calculation of the hydraulic arm of a track maintenance machines to lift of units loads* (In Slovak). In: Railway Transport and Logistic. Scientific and technical on-line journal about railway transport, traffic, logistics and management. 2014. ISSN 1336-7943.



Methodology of Assessment of Exhaust Gas Flow for a Small Jet Engine

* Jarosław Markowski, Jacek Pielecha, * Remigiusz Jasiński,
** Ślusarz Grzegorz, *** Wirkowski Paweł

* Poznan University of Technology, 10. Faculty of Machines and Transportation,
Institute of Combustion Engines and Transport, ul. Piotrowo 3, 60-965 Poznan, Poland,
{Jaroslaw.Markowski, Jacek.Pielecha}@put.poznan.pl, remigiusz.w.jasinski@doctorate.put.poznan.pl

** 2nd Tactical Wing, 61-716 Poznan, ul. Kosciuszki 92/98

*** Naval Academy, Faculty of Mechanical and Electrical, ul. Smidowicza 69, 81-103 Gdynia,
p.wirkowski@amw.gdynia.pl

Abstract. Exhaust emissions tests of engines for various applications are related to determination the concentration of harmful compounds and the mass of flowing exhaust. Modern measuring equipment enables fast measurement the concentration of compounds in the exhaust and also allows measurement the mass of flowing exhaust but with a relatively low speed. The common methods of flow measurements can not be used for turbine engines due to the high flow rates of the exhaust gas. The article proposes a methodology for evaluating flow exhaust from the turbine engine, which was verified by research. The study indicates the possibility of application the proposed method in the evaluation procedures of exhaust emissions from turbine engines.

Keywords: Jet engine, Exhaust emission, Exhaust mass flow.

1. Introduction

Methodology of measurement of the emission of exhaust compounds from turbine engines involves measuring the concentration of pollutants contained in the analysed exhaust gas sample collected from the stream of flowing gases with the use of a specially constructed measuring probe. In the provisions of ICAO – Annex 16 [2], the geometric parameters of probes are not specified, but the general guidelines are defined. The probe, which is in contact with the exhaust gas sample must be made of stainless steel or other non-reactive material. If a multi-hole probe is used, all orifices must be of the same diameter. The design of the probe must be such that at least 80% of the pressure acting on the probe assembly is drawn through the orifices. The number of gas sampling points cannot be less than 12. Sampling plane must be located as close to the plane of the exhaust nozzle exit as it is possible for given engine performance parameters, but in any case it must be within 0.5 of the diameter of the exit nozzle. The provisions state the necessity to prove to the certifying authorities that the proposed design of the probe and its localisation ensures obtaining a representative sample for each specific setting of the engine thrust [1, 2, 9].

The use of the multi-hole probe in the measurement of the emission of exhaust fumes results in obtaining an averaged sample of the exhaust gases. Averaging the exhaust gas sample is necessary as with increasing distance from the axis of the stream of outflowing exhaust gas, the concentration of the gas components diminishes. It depends on the type of engine design, including the way of its cooling and separating the engine assemblies from hot gases and turbulence occurring in the outflowing exhaust gas stream. Collected by several orifices of the probe gas samples, with different concentration of exhaust compounds [7], mix together, which in consequence leads to averaging the value of concentration of pollutants in the exhaust fumes [3, 5]. Thus, it is desirable to measure the concentrations of pollutants at the point where the exhaust gases are mixed with the air cooling the engine components, or air drawn in by the exhaust gases behind the engine exhaust

nozzle. By such a measure it is possible to estimate the actual composition of the gases, and using additional information – to determine the mass of outflowing exhaust gases and the hourly exhaust compounds emissions [4, 6, 8].

2. Methodology of Assessment of Exhaust Gas Flow for Turbine Engine

The idea of operation of the combustion engine is aimed at obtaining the performance parameters translating into the driving performance. For turbine jet engines vital is the outflow of the exhaust gases generating the thrust power. According to the basic equation defining thrust power, of great importance is also the mass and speed of outflowing gases. These indicators are related to such operational parameters as air consumption and fuel consumption, the total mass of which translates into a mass of the exhaust gases generated by the engine (Fig. 1). Knowing the instantaneous value of the fuel consumption and by measuring the chemical composition of exhaust gases enabling determination of the instantaneous value of the combustion air factor λ , it is possible to estimate the mass of air supplied at a particular moment to the engine.

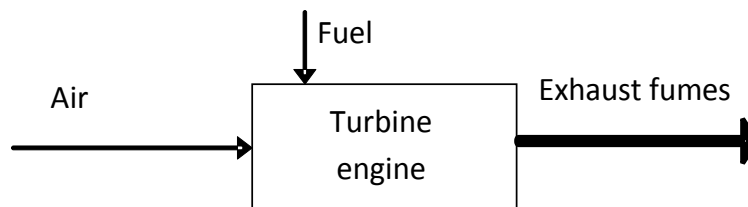


Fig. 1. Diagram of the input and output parameters of the turbine jet engine.

The sum of the values of fuel consumption and air consumption represents the value of a stream of generated exhaust gases:

$$\dot{m}_{air} + \dot{m}_{fuel} = \dot{m}_{exhaust} \quad (1)$$

where:

\dot{m}_{air} – stream of the air mass,

\dot{m}_{fuel} – stream of fuel mass,

$\dot{m}_{exhaust}$ – stream of the exhaust gas mass.

Assuming that it is possible to measure two out of three parameters, the value of the third parameter might be calculated. For this purpose were conducted tests the aim of which was to measure the fuel consumption and the value of the stream of emitted exhaust gases with simultaneous measurement of the concentration of the harmful compounds of exhaust gases and the combustion air factor λ . The research was conducted on the prepared test bench (Fig. 2), which included a small single flow turbine jet engine – GTM 120.

The engine was fueled from the integrated supplying module including the fuel flow meter ATMX 2040. The measurement of the exhaust gases flow was conducted with the use of the measuring system consisting of two exhaust gas flowmeters with a flow diameter of 125 mm. The use of two exhaust gas flowmeters was associated with the necessity to divide the exhaust gas stream and to reduce its flow rate, adjusting it to the measuring ranges of the flowmeters. Reduction of the flow rate of the exhaust gas stream is associated with the increase of the flow cross-section. Measurements of exhaust flow rate, concentration of harmful compounds contained in the gases and the values of the combustion air factor λ , were conducted with the use of the exhaust gas analyser Semtech of Sensors Inc.

The measurements were carried out for fixed values of engine thrust ranging from 10 N to 120 N in increments of 10 N. The research was carried out in such a way that first the setting of the engine thrust value was made while the system of separating exhaust gases with flowmeters was removed from the engine exhaust system. After obtaining the appropriate thrust value, the exhaust

nozzle of the system for exhaust gas separation along with measuring system were moved closer. Time of measurement of the exhaust gas flow and measurement of the concentration of pollutants for single setting of the thrust depended on achieving stability of the temperature of the measuring system and ranged from several to several tens of seconds. The obtained values of measured parameters were then analysed.

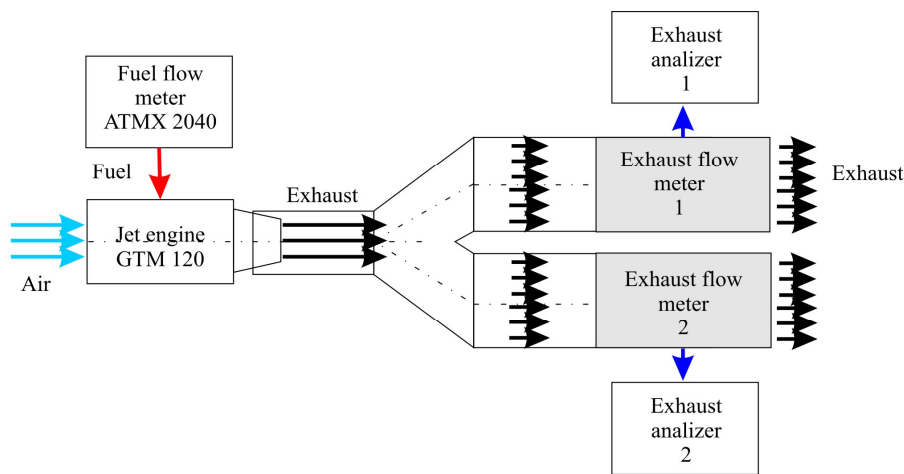
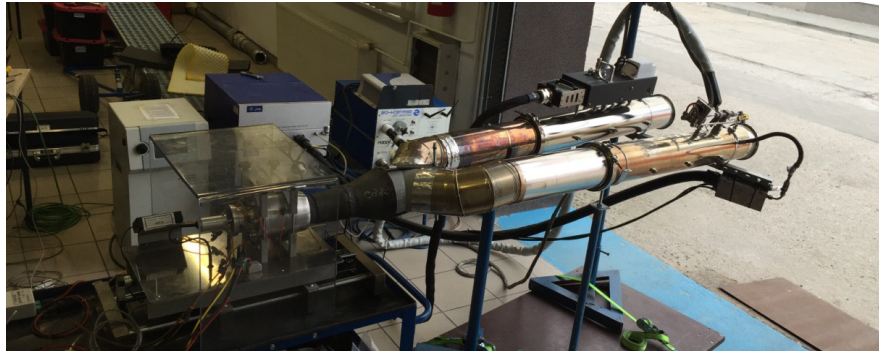


Fig. 2. View and diagram of the measuring test bench.

3. Test Results and their Analysis

During the conducted tests, for the assumed values of thrust power setting F were obtained values of the engine performance indexes (Tab. 1). An hourly measurement of fuel consumption G_e was conducted along with the measurement of combustion air factor resulting from the combustion process conditions λ , and the streams of the exhaust gas mass $\dot{m}_{exhaust}$ flowing through flowmeter 1 and flowmeter 2. There was also determined the total stream of exhaust gas mass as the sum of the streams of exhaust gas from two flowmeters.

In accordance with the assumed aim of the article, the attempt to estimate the value of the exhaust gas stream was made, based on the measured values of the hourly fuel consumption and the combustion air factor during combustion, which is determined on the basis of the composition of the exhaust gas. Bearing in mind that for complete combustion of one kilogram of fuel is needed approximately 14.5 kg of air, the following dependency might be proposed:

$$\dot{m}_{exhaust} = G_e \cdot \lambda \cdot 14,5 \left[\frac{\text{kg}}{\text{h}} \right] \quad (2)$$

With the use of the above dependency were conducted calculations resulting in obtaining the value of the exhaust gas mass stream (Tab. 2). The results obtained on the basis of calculations were compared with the values of the streams of exhaust gas mass obtained during measurements (Fig. 3). The comparison was made by calculating the percentage difference of the values in relation to the results of measurements of particular values of the thrust power.

F [N]	G_e [kg/h]	λ [-]	$\dot{m}_{exhaust\ 1}$ [kg/h]	$\dot{m}_{exhaust\ 2}$ [kg/h]	$\dot{m}_{exhaust}$ [kg/h]
10	7.2	3.80	195	274	470
20	9.0	3.94	388	183	571
30	10.8	4.16	375	320	695
40	12.6	4.27	373	441	814
50	14.0	4.39	497	452	949
60	15.5	4.39	497	452	949
70	17.3	5.11	808	417	1226
80	18.7	4.52	570	636	1206
90	19.8	4.50	609	712	1322
100	20.5	4.85	761	632	1394
110	21.6	4.31	636	756	1392
120	22.7	4.17	586	891	1477

Tab. 1. Values of the performance indexes obtained during measurements.

F [N]	$\dot{m}_{exhaust}$ [kg/h] (measurements)	$\dot{m}_{exhaust}$ [kg/h] (calculations)	The relative difference [%]
10	470	397	15.5
20	571	515	9.9
30	695	651	6.3
40	814	780	4.2
50	949	894	5.8
60	949	986	-3.9
70	1226	1281	-4.5
80	1206	1226	-1.6
90	1322	1291	2.3
100	1394	1443	-3.6
110	1392	1351	2.9
120	1477	1373	7.1

Tab. 2. Comparison of the values of the stream of the exhaust gas mass obtained from measurements and from conducted calculations.

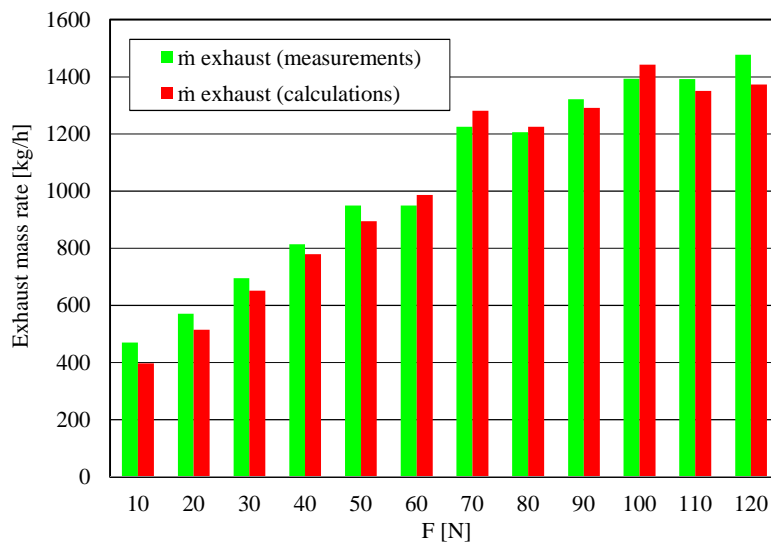


Fig. 3. Comparison of the values of the exhaust gas mass stream obtained during measurements and from calculations for particular settings of the thrust power of the GTD 120 engine.

Comparison of the values of the stream of the exhaust gas mass obtained during conducted tests with the values determined on the basis of calculations indicate that the calculated values of the exhaust gas stream are close to the values obtained during measurements. In order to make a qualitative assessment, the percentage differences between the values obtained from measurements were determined (Fig. 4).

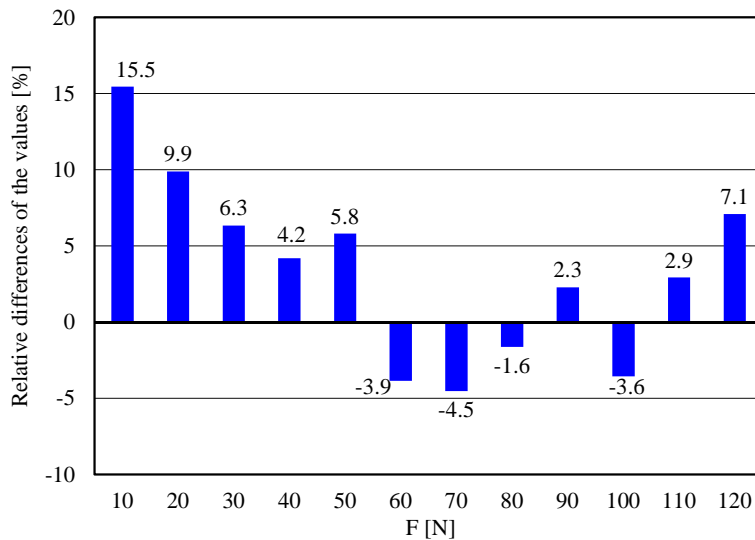


Fig. 4. Relative differences between the values of the exhaust gas mass stream obtained during measurements and from calculations.

4. Conclusion

The proposed analytical method of determining the stream of exhaust gas mass for jet engine enables obtaining results similar to the actual values. The nature of the distribution of measured values and values obtained from calculations is similar. The maximum difference between the values is approximately 15% and is related to the lowest setting of the thrust power. For other values, these differences do not exceed 10%. Therefore, it can be concluded that the proposed method for determining the stream of exhaust gas mass on the basis of the hourly fuel consumption and known value of the combustion air factor, determined on the basis of an analysis of the composition of the exhaust gases, can be used in relation to turbine engines.

References

- [1] Environmental Protection Agency, Control of Air Pollution from Aircraft and Aircraft Engines; *Proposed Emission Standards and Test Procedures*; Proposed Rule. Part II. Federal Register, Vol. 76, No. 144, 2012.
- [2] International Civil Aviation Organization, Annex 16: *Environmental Protection*, Vol. II, Aircraft Engine Emissions, 2008.
- [3] KOTLARZ, W., PIASECZNY, L., RYPULAK, A., ZADRĄG, R. *Tests of exhaust gas toxicity of jet turbine engine for take off and landing phases of flight*. Combustion Engines, No. 4, 2006.
- [4] MARKOWSKI, J., MERKISZ, J., PIELECHA, J., KARPINSKI, D., GALANT, M. *The investigation of the influence of the oxygen additive to fuel on the particle emissions from a small turbine engine*. 18 ETH-Conference on Combustion Generated Nanoparticles, Zurich, 2014.
- [5] MERKISZ, J., MARKOWSKI, J., PIELECHA, J. *Emission tests of the F100-PW-229 turbine jet engine during pre-flight verification of the aircraft*. In: J. W. S. Longhurst, C. A. Brebbia (Eds.), WIT Transactions on Ecology and the Environment, Vol. 174, WIT Press, Southampton, 2013.
- [6] MERKISZ, J., MARKOWSKI, J., PIELECHA, J. *Emission tests of the F100-PW-229 turbine jet engine during prestart trial of the F-16 aircraft*. The 26th International Conference on Efficiency, Cost, Optimization, Simulation and Environmental Impact of Energy Systems, Guilin, 2013.
- [7] MERKISZ, J., MARKOWSKI, J., PIELECHA, J. *Selected issues in exhaust emissions from aviation engines*. Nova Science Publishers, New York, 2014.
- [8] MERKISZ, J., MARKOWSKI, J., PIELECHA, J., ŚLUSARZ, G. *Analysis of engine operating parameters multi-role aircraft*. Logistyka, No. 6, 2014.
- [9] WYGONIK, P. *Selection criteria of turbine engine parameters for multi-purpose aircraft*. Combustion Engines, No. 4, 2006.



Validation of the Rail Vehicles' Suspension Damage Model

*Rafał Melnik, *Bogdan Sowiński

Warsaw University of Technology, Faculty of Transport, Department of Fundamentals of Transport
Equipment Construction, Koszykowa 75, 00-662 Warsaw, Poland, {rme, bso}@wt.pw.edu.pl

Abstract. The works within the framework of the MONIT project on the monitoring system of rail vehicle and track, included simulation and experimental study on the influence of chosen suspension damages on vehicle's dynamic behavior. Apart from development of suspension fault detection method for the monitoring system, it was an opportunity to validate numerical model of suspension damages, due to acquisition of data from real damaged vehicles. The validation process was carried out with use of proposed indicator of concordance, due to partial knowledge of vehicles' parameters.

Keywords: Rail vehicle, Suspension damage, Validation.

1. Introduction

The rail vehicle and track monitoring system has been developed under the framework of the project: MONIT – Monitoring of Technical State of Construction and Evaluation of its Lifespan Project. The system performs qualitative assessment of the vehicle's suspension condition (and thus of the running gear), as well as track condition monitoring. The piezoelectric sensors are used by the system in order to measure acceleration signals on bogie frame and body to assess primary and secondary suspension condition and on the wheelsets' bearing for track condition. The detailed description of the system is presented in [1, 2, 3].

During the development phase of the system its prototype was tested on experimental track in Żmigród, Poland. The system performed measurements on the rail vehicles (passenger and goods wagon) which were at first in nominal condition, and then suspension damages were introduced [1, 2]. The results of the experimental rides did not only prove a proper operation of the system but also provided information on the influence of suspension damages on recorded acceleration signals in actual operation conditions. However, the acquired data can be used in validation of the mathematical model of suspension damages.

The experiment on the test track was preceded by numerical investigation of vehicle's dynamic responses due to suspension characteristics variations. In order to check whether the built model of the rail vehicle for simulation is sufficiently accurate, it should be validated.

2. Experiment Conditions

The experimental rides of the wagons were conducted for two vehicles' conditions: undamaged and damaged. Introduced damages to suspension were as follows:

- Primary suspension stiffness reduction at one wheel of goods wagon – one packet of coaxial springs was removed from Y25 bogie.
- Secondary suspension damping reduction – removal of one secondary damper in passenger wagon.

Acceleration signals for suspension condition assessment were measured by piezoelectric accelerometers at sampling frequency $f_s = 500$ Hz, on track sections of 500 m long. The signals were processed by the following digital filters, according to [4, 5]:

- Low-pass 20 Hz – bogie frame, vertical motion,



- Low-pass 10 Hz – boogie frame, lateral motion,
- Bandwidth 0.4 – 10 Hz – body, vertical and lateral motion.

3. Validation Characteristic

For the suspension monitoring purpose, it was assumed that validation of the mathematical model, built in VI-Rail simulation software, covers comparison of the analyzes' results from numerical and experimental studies, and its character is qualitative. The built vehicle model represents typical Z-2 class wagon. Since we are interested in qualitative comparison, the passenger wagon model was also used for study of stiffness reduction which was introduced in goods wagon during the experiment. The exact parameters of passenger and goods wagon were unknown, since these vehicles, belonging to Railway Institute are modified, e.g. passenger wagon is a version of 111A coach converted into measurement wagon. It should be noted that during simulation phase, the current irregularities of the experimental track were also unknown. The irregularities used in simulation were generated basing on values from different track sections. This proceeding also influences qualitative character of the comparison.

The measures to compare for validation are diagnostic parameters of the obtained signals which provide information on suspension condition:

- Root mean square (RMS),
- Interquartile range (IQR),
- Zero-peak.

Direct comparison of the parameters' values from numerical investigation and experiment, due to simplifications of simulation models and stochastic character of vibrations of the real wagons, may lead to negative conclusion on the models usefulness. For the damage detection purpose, we focus on the trend of the diagnostic parameters' values. This approach indicates if the variation of suspension parameters is reflected in similar relative changes of diagnostic parameters' values. Concerning lack of required models' parameters (simulation) and stochastic nature of the vehicles' vibrations (experiment), we can cope with comparison by implementation of proposed indicator. The adopted indicator of concordance between results of experiment and simulation is (1):

$$C = \left\| \frac{S_{Dam} - S_{Nom}}{S_{Nom}} - \frac{E_{Dam} - E_{Nom}}{E_{Nom}} \right\| \cdot 100\% \quad (1)$$

The lower the value of C indicator, the better simulation model corresponds to real dynamic behavior due to suspension damages. However, the C indicator does not show direction of relative changes (increase or decrease).

4. Results of the Analysis

Tab. 1 depicts results comparison of stiffness reduction, for speed of 80 km/h. The difference between parameters' values referring to nominal and damaged condition is presented in [%].

Parameter	Condition	Lateral acceleration				Vertical acceleration			
		Simulation		Experiment		Simulation		Experiment	
RMS	Nom.	1.013			3.421	1.074			4.658
	Dam.	0.962	-5.0%	-3.7%	3.294	0.890	-17.1%	-11.9%	4.106
IQR	Nom.	1.186			4.303	1.277			6.053
	Dam.	1.143	-3.6%	-2.3%	4.203	1.103	-13.6%	-13.2%	5.251
Zero-peak	Nom.	4.998			13.299	5.268			17.595
	Dam.	4.557	-8.8%	-9.5%	12.031	3.512	-33.3%	-21.8%	13.754

Tab. 1. The results of the simulation and the experimental studies – primary suspension stiffness reduction, $v = 80$ km/h, parameters' values in $[m/s^2]$.

Fig. 1 presents calculated values of C indicator in case of stiffness reduction in goods wagon for acceleration signals in lateral (Y) and vertical (Z) direction.

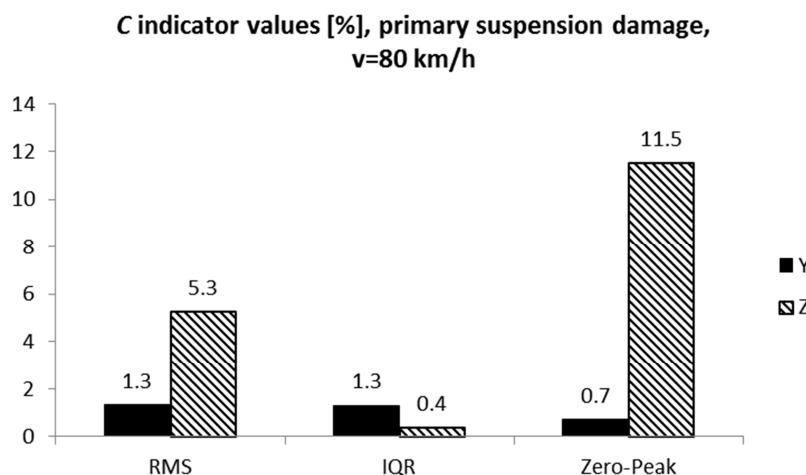


Fig. 1. C indicator values in case of primary suspension damage, $v=80$ km/h.

For $v = 80$ km/h, the damage caused reduction of the parameters' values (Tab. 1). The highest value of indicator C (Fig. 1) refers to Zero-peak of lateral acceleration signal and is equal to 11.5%, what shows only small difference between responses of simulation and experiment, taking into account sensibility of Zero-peak parameter. The highest concordance between simulation and experiment is achieved for IQR (below 1.5%).

The comparative analysis of the simulation and experimental results in case of damping reduction in passenger wagon for $v = 100$ km/h is presented in Fig. 2.

Parameter	Condition	Lateral acceleration			Vertical acceleration			
		Simulation	Experiment	Parameter	Simulation	Experiment		
RMS	Nom.	0.106	4.7%	0.108	0.120	11.7%	8.7%	0.138
	Dam.	0.111		0.115	0.134			0.15
IQR	Nom.	0.141	2.8%	0.129	0.153	11.1%	9.4%	0.18
	Dam.	0.145		0.155	0.170			0.197
Zero-peak	Nom.	0.388	7.0%	0.362	0.382	36.9%	-1.1%	0.45
	Dam..	0.415		0.439	0.523			0.445

Tab. 2. The results of the simulation and the experimental studies – secondary suspension damping reduction, $v = 100$ km/h, parameters' values in [m/s²].

The assessment of concordance, given by C indicator, in case of damping reduction in passenger wagon is depicted in Fig. 2

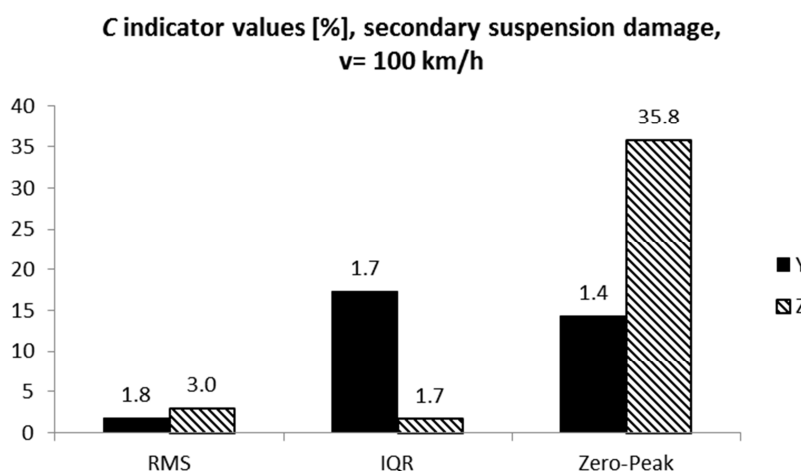


Fig. 2. C indicator values in case of secondary suspension damage, $v = 100$ km/h.



At $v = 100$ km/h, the increase of all parameter's values is noticed in case of both directions of signals acquisition (simulation and experiment, Tab. 2). The C indicator (Fig. 2) reached generally low values for both directions of signals acquisition, in case of RMS and IQR. However, there is a noticeable increase of C for Zero-peak of vertical signal due its sensitivity to shocks.

5. Conclusion

The adopted C indicator, used for comparison of simulation and experimental results, reached values in most cases several or over a dozen percent. It means that trend of parameters change is congruent for simulation and experiment. This measure can be used for qualitative comparison of phenomena – when the trend is in our focus, instead of exact values.

The simplified models of the track and the vehicles are sufficient for investigation of suspension damage influence on acceleration signals. However, the use of Zero-peak parameter may be arguable. It is assumed that in the monitoring process, data is collected from distance of a certain length (500 m). Zero-peak is a sensitive measure – its value may suddenly increase, what can be caused by random excitations. The measures of dispersion – RMS and IQR average signals and thus C indicator does not reach such the high values for these parameters.

The further development of suspension damage detection methods for the monitoring system may be based on studying dynamic behavior of a simple vehicle model without getting into constructional details of suspension elements.

Acknowledgement

The author expresses his gratitude for the financial support by the Polish Ministry of Science and Higher Education for the support of research within the framework of the project MONITORING OF TECHNICAL STATE OF CONSTRUCTION AND EVALUATION OF ITS LIFESPAN – MONIT. Action Operational Programme Innovative Economy.

References

- [1] MELNIK, R., KOSTRZEWSKI, M. *Rail vehicle's suspension monitoring system - analysis of results obtained from tests of the prototype*. Key Engineering Materials Vol. 518, 2012. ISBN-13: 978-3-03785-443-3. DOI 10.4028/www.scientific.net/KEM.518.281.
- [2] MELNIK, R., SOWINSKI, B. *Application of the Rail Vehicle's Monitoring System in the Process of Suspension Condition Assessment*. Communications- Scientific Letters of the University of Žilina, vol. 15, No. 4, 2013. ISSN 1335-4205.
- [3] MELNIK, R., SOWIŃSKI, B., CHUDZIKIEWICZ, A. *Experimental research of the rail vehicle and track monitoring system*. Slovak –Dynamical problems in rail vehicles 2013, Proceeding of the Workshop, University of Žilina, Department of Transport and Handling Machines, Žilina, Slovak Republic, 2013. ISBN 978-80-554-0841-5.
- [4] EN 14363: *Railway applications - Testing for the acceptance of running characteristics of railway vehicles - Testing of running behavior and stationary tests*. June 2005.
- [5] UIC 518: *Testing and approval of railway vehicles from the point of view of their dynamic behavior – Safety – Track fatigue – Ride quality*. 2nd edition, April 2003.



Simplified Model of Combustion Process in Fuel Bed

*Jozef Mičieta, **Jiří Hájek, *Jozef Jandačka

*University of Žilina, Faculty of Mechanical Engineering, Department of Power Engineering,
Univerzitná 8215/1, 010 26 Žilina, Slovakia, {jozef.micieta, jozef.jandacka}@fstroj.uniza.sk

**Brno University of Technology, Faculty of Mechanical Engineering, Department of Process and
Environmental Engineering, Technická 2896/2, 616 69 Brno, Czech Republic, hajek@fme.vutbr.cz

Abstract. Combustion of the solid fuel in the burner is an important issue when discussing the CFD simulation of combustion process in boiler. In the present work is employed a simplified method for modeling the bed, which is based on heat and mass balances in order to simplify the simulation of combustion in pellet boiler. The combustion model for solid fuel in a burner is created for the purpose of boiler simulations. Such approach does not require a detailed bed model of fired solid fuel. A simple model of the bed can be very useful for designers and engineers of automatic boilers. The described approach to modeling the combustion process in a burner helps to shorten the calculation time and simplify the model of pellet combustion in various types of automatic boilers for households.

Keywords: Simulation, CFD, Combustion, Biomass, Pellet, Boiler.

1. Introduction

CFD simulations may help to increase understanding and provide detailed prediction of combustion taking place in a boiler. However, modelling of combustion is more complex in biomass boilers than in gas or oil-fired boilers, due to the complexity of the heterogeneous reactions in the bed, the turbulent reactive flow in the freeboard and the very strong coupling between those two regions. However, it is usually not required to describe in depth and in every detail all phenomena that occur in a combustion system. Instead, CFD calculations should give an approximate view of system behavior, help in troubleshooting and provide insights necessary to fine-tune the system's operation, as well as give assistance when dealing with new designs [1].

From an engineer's point of view a detailed model of combustion process in a burner is too complicated to be useful, as it requires great amount of time and effort to set it up, run, and analyze its results. Therefore it can be useful to introduce some assumptions in order to simplify a boiler simulation. From an overall point of view on a boiler as a unit, only integral factors like heat and mass transfer in the bed and the boiler are relevant. A simplified method of bed modelling based on thermal and mass balances was employed in this work to describe pellet combustion process in the simulation of an experimental 20 kW boiler. The predictions from CFD simulation have been compared with the analytic results from thermal and mass analysis of the combustion process. The model employed in this work may be readily adapted for the modelling of other solid fuel burners and boiler designs. Several combustion parameters need to be defined if a practicable model is to be achieved.

1.1. Combustion process in a retort burner

The analyzed boiler (Fig. 1) is equipped with a retort burner, which works on underfeeding principle. Fuel (e.g. pellets) is fed from a fuel tank through a horizontal pipe by a feeding screw. The burner elbow changes the direction of movement and pellets are slowly pushed from the bottom into the mouth of the burner, where the combustion process starts. From long-time viewpoint, the pellet boiler operation is a steady process. In fact, the pellet supply to the burner is discontinuous, because the feeder is in operation for tens of seconds and then certain time in rest,



before the next pellet batch is fired. The primary air is usually blown into the feeder, but also directly to the fired pellets through slits in the burner mouth. The fuel is gradually fed to the bed, where it is heated and gradually releases volatile gases [10]. Depending on the specific fuel, volatile gases start to be released already from 150 – 200 °C. Gases then pass through the hot upper layer of bed, which leads to their ignition and subsequent burning in the combustion chamber [7]. The upper layer of bed consists mainly of fixed carbon and non-combustible inorganic material, with inter-particle space filled by gases.

Small part of the combustible gases burns in the bed, but the main combustion process takes place in the combustion chamber above the burner (freeboard). Burned pellets, or their parts are pushed away from the bed surface and then to burner edge, where they gradually burn out. The edge of the retort burner is usually made of cast iron, which resists well the hot environment and accumulates heat, so it creates favorable conditions for fuel gasification. Oxygen in the primary air, which is not used for the char combustion is preheated so that there is no problem with incomplete oxidation of combustible gases in the combustion chamber [9]. Residues (ash and unburnt fuel) are either (in the case of fine particles) blown away by the combustion air or (heavier particles) are gradually pushed out of the burner to the ashtray. Secondary air is introduced into the combustion chamber at a certain height above the burner through nozzles in the intermediate wall, which leads to the burnout of remaining combustible gases. Before secondary air blows into the combustion chamber, it is heated in the distribution channel, pipes and intermediate wall.

1.2. Biomass fuel

Ultimate and proximate analysis of the fuel that is used in the model is shown in Tab. 1. More physical and chemical properties of various biomass fuels could be found in databases, which are quoted in [8] or e.g. [5] and in similar work [3]. Parameters of fuel like moisture, ash content, ratio of char and volatile combustible compounds, and calorific value are obtained in proximate analysis, which is performed experimentally. From the point of view of energy content it is more practical and useful as the ultimate analysis of fuel and it defines fuel parameters necessary as input for CFD simulations.

Proximate analysis is in this work directly used to define composition of gases entering the combustion chamber. As noted above, primary air is supplied together with fuel to the bed. Gaseous products of fuel drying and devolatilization are thus mixed with primary air. This defines the composition of gas entering the combustion chamber.

Ultimate analysis		Proximate analysis		Bed and particle parameters	
Carbon	52.0 wt%	Moisture	8.5 wt%	Particle diameter	6 mm
Hydrogen	6.8 wt%	Ash	0.6 wt%	Average pellet length	12 mm
Oxygen	41.0 wt%	Fixed carbon	16.2 wt%	Void fraction	0.4
Nitrogen	0.2 wt%	Volatile	74.7 wt%	Net calorific value	18.3 MJ/kg

Tab. 1. Approximate composition and properties of the employed fuel.

2. CFD Model description

The present CFD model is set up within commercial code Ansys Fluent, but it would be the same in other software as well. The modeling of biomass boiler includes two main areas of interest: 1) combustion process of biomass in the bed and 2) homogeneous reactions and heat transfer in the combustion chamber (freeboard). These two processes are strongly coupled, as freeboard reactions depend on the gases leaving the bed, and as the radiative heat flux emitted by flames above the bed drives the processes inside the bed [1].

Combustible gases in reality begin to be released at the so-called devolatilization temperature, which according to the Ion`s work [4] is about 330 °C (about 600 K). With further increase of temperature, the composition of the released gases changes.



Thus, we see that devolatilization process is strongly coupled to the temperature in combustion chamber, which in turn depends on the amount and composition of the released volatile gases. Therefore, in the present simplified model it is necessary to select a reference temperature, which is key to determining the composition of released gases [3]. Here it has been decided to choose a temperature level of 600 K (about 330 °C) to estimate the composition of introduced volatile gases, adopting the individual mass fractions according to Ion [4] or Thunman [14]. We assume for simplicity that devolatilization is an instantaneous phenomenon of thermal transformation of fuel. Volatile gases are represented by CO, CO₂, H₂, H₂O, NH₃, plus CH₄ representing light hydrocarbons, and finally C₆H₆ representing heavy hydrocarbons (tar).

The amount of nitrogen in a majority of biomass fuels is below 1 %, (although some phytomass fuels may contain up to 4 %). It reacts by endothermic reaction (the energy gain is negative). The reaction can be neglected, because the relative energy gain is very small. Some authors have defined the biomass by a substitutive substance with the chemical formula C₆H_aO_b. It replaces biomass in dry, ash-free state, where *a* and *b* are coefficients [8, 13]. For this substance are defined physical parameters similar to the real for biomass. After gasification, only a solid substance remains in the bed. This charcoal can be considered for wood pellets as pure carbon, because the ash content is usually below 1 %. Sulphur content is at trace level, so it is neglected as well.

Char combustion is a complex process that is affected by the fuel composition, particle shape and boiler conditions. A simplified model is used by Porteiro [11], which considers a heterogeneous reaction of char to form CO and CO₂, where the ratio of the CO/CO₂ formation rate depends on the temperature. A representative char combustion temperature of 1373 K (about 1100 °C) is employed in this work to estimate the composition of the char combustion products [3].

The present work simulates combustion at nominal power of the boiler, as the most representative operating condition. In the long-term point of view, the combustion can be considered as continuous steady process. Adopting this assumption implies that the various zones in the boiler, where certain processes dominate (such as heating, drying, gasification, combustion of volatile gases and char combustion...) are fixed in space. Then the overall combustion process can be considered as steady. Main boundary conditions of the model then include mass flow inlet defined at the fuel inlet (burner) and flue gas outlet to the chimney (pressure outlet).

2.1. Model of fuel conversion - bed model

As noted above, it is evident that the most complicated processes occur in the burner. The top layer of burner volume that contains burning pellets is called the bed. Within the bed take place several phenomena, from the initial heating of fuel, through its drying, devolatilization, gas combustion and fixed carbon burnout. Reactants, which include the primary combustion air and the solid fuel, are fed to this bed layer. In the computational model devised in this work, the bed is a part of the computational domain and there is no separate bed model to define the boundary conditions, similarly as in [1].

When we consider boiler as a device for transformation of chemically stored energy into heat carried by hot utility water, then burner is a device for fuel transformation to combustible gases and consequently to flue gases, while the thermal energy is released. The subsequent combustion of devolatilized fuel takes place in the freeboard (combustion chamber). As detailed description of the processes occurring in the burner is not required in this work, the burner may be considered as the source (inlet) of flammable gases, thermal energy and primary combustion air, the oxygen in which is already partially consumed. Gas leaves the bed at a certain temperature, which is higher than the devolatilization temperature. If the gas species were inserted into the computational domain through mass sources, the FLUENT software provides no option to specify their inlet temperature. This problem can be eliminated by assuming that the volatile gases enter the domain through an inlet boundary. The inlet however may not be located at the interface of the bed and the freeboard, as in that case the bed would behave as a reflective surface (diffuse or specular). It is thus better to place the inlet below the porous fuel bed.



One role of the bed is to distribute fluid flow on the interface with freeboard evenly across the burner. Furthermore, the bed provides space and time to heat up the gas. Those two effects of the bed are closely coupled. The pellets fill up the bed volume and they have the shape of cylinders with known properties. With this assumption, it is possible to replace the bed volume by a porous zone. It is necessary to specify parameters of the porous zone to generate a correct pressure loss in the gas passing through the pellets.

Different flow regimes are expected in the boiler due to its complex geometry. The gases are practically still in some regions and, on the contrary, high gas velocities and fully turbulent flow are expected in areas such as the flame or secondary air injections. Beneath the bed is primary air inlet and in the bed take place various thermo-chemical processes, thus there is also expected turbulent flow. The realizable $k-\varepsilon$ model was employed to account for the effect of turbulence due to its proven effectiveness in industrial applications [6, 15].

In this work the modelling of a packed bed is performed without considering channeling effect. In turbulent flows, packed beds are modelled using both permeability α (a viscous resistance coefficient is $1/\alpha$) and an inertial loss coefficient C_2 . One technique for deriving the appropriate values of the porous properties involves the use of the Ergun equation [2]. It is a semi-empirical correlation applicable over a wide range of Reynolds numbers and for many types of packing.

The effect of the bed porosity on the gas flow is introduced by the addition of a source term S_i , calculated by the formula (1), into the momentum equation. Three parameters are needed in the CFD code to evaluate the source term: permeability α , inertial losses coefficient C_2 and porosity ε . The source term is composed of two parts: a viscous loss term (Darcy's, the first term in equation (1)), and an inertial loss term (the second term in the same equation (1) [12]. To cover the present case of simple homogeneous and isotropic porous media, it is sufficient to use the same porous properties in the whole bed volume.

$$\nabla p = S_i = - \left(\frac{\mu}{\alpha} v_i + C_2 \frac{1}{2} \rho_p |v| v_i \right) \quad (kg.m^{-2}.s^{-2}). \quad (1)$$

Here S_i is the source term for the i th ($x, y, \text{ or } z$) momentum equation, $|v|$ is the magnitude of the velocity, μ is the viscosity. In equations (2) and (3) that define permeability and inertial loss coefficient, d_{eq} is the equivalent particle diameter and ε is the void fraction, defined as the volume of voids divided by the volume of the packed bed region. Comparing Darcy's equation and equation for inertial loss in the porous media with Ergun equation, the permeability and inertial loss coefficient in each component direction may be identified as

$$\alpha = \left(\frac{\Psi^2 d_{eq}^2}{150} \frac{\varepsilon^3}{(1-\varepsilon)^2} \right) \quad (m^2), \quad (2)$$

$$C_2 = \frac{3,5}{\Psi d_{eq}} \frac{(1-\varepsilon)}{\varepsilon^3} \quad (m^{-1}). \quad (3)$$

Permeability (2) and inertial loss coefficients (3) is estimated by the Ergun equation using the mean diameter D_p of the fuel particles [12]. The sphericity Ψ and the spherical equivalent diameter d_{eq} are calculated from fuel parameters shown in Tab. 1. using formulae (4) and (5):

$$\Psi = \frac{\pi^{1/3} (6V_p)^{2/3}}{A_p} \quad (-), \quad (4)$$

$$d_{eq} = D_p \left(\frac{3L_p}{2D_p} \right)^{1/3} \quad (m). \quad (5)$$

The fuel in the burner is modeled by 4 layers with different porosity and total height 20mm, which are discretized by several layers of hexahedra. Mesh of bed should be sufficiently fine in order to cover fluid flow changes (Fig. 2.).

The computational model uses the symmetry of the boiler, and therefore it models only 1/4 of the boiler. The boundaries of the model in the radial direction are defined as symmetry planes, as there is no tangential flow. The wall of the burner, which is in contact with the bed, is considered adiabatic.

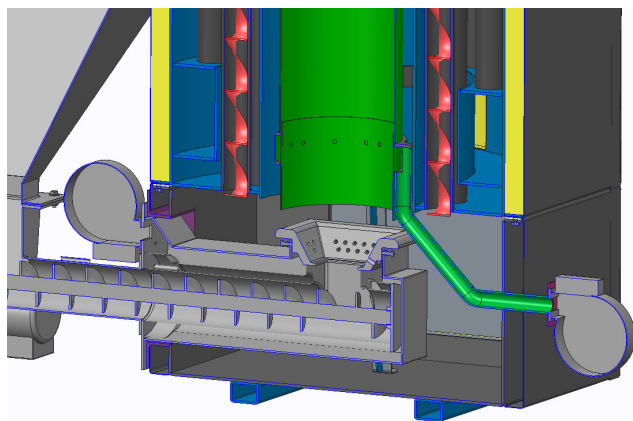


Fig. 1. 3D geometry of the burner and the freeboard.

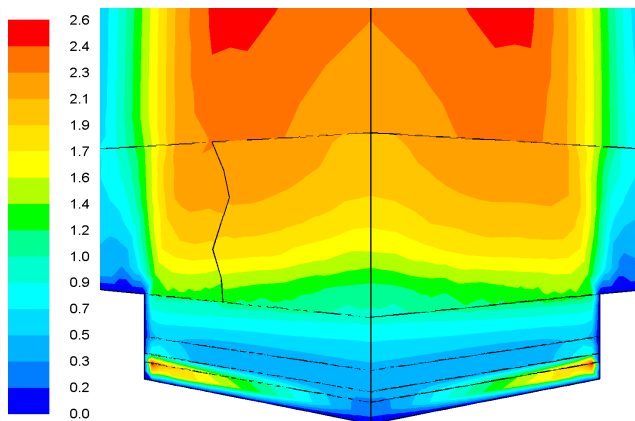


Fig. 2. Velocity [m/s] in the bed.

A significant effect on the temperature of combustion chamber has the radiative heat transfer in the fuel bed. Radiation increases the temperature inside the bed, as shown by the temperature fields on the symmetry planes in Fig. 3. and Fig. 4.

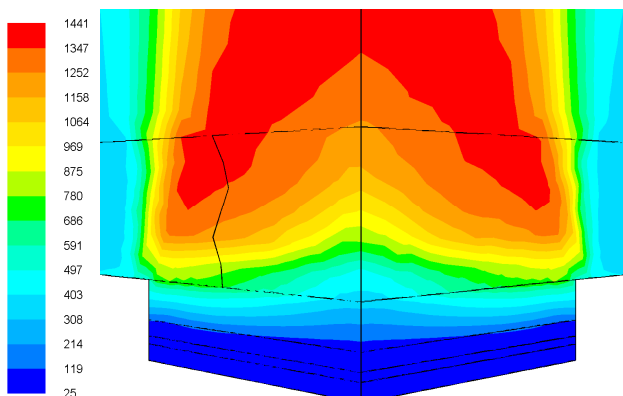


Fig. 3. Temperature [°C] in bed, without radiation.

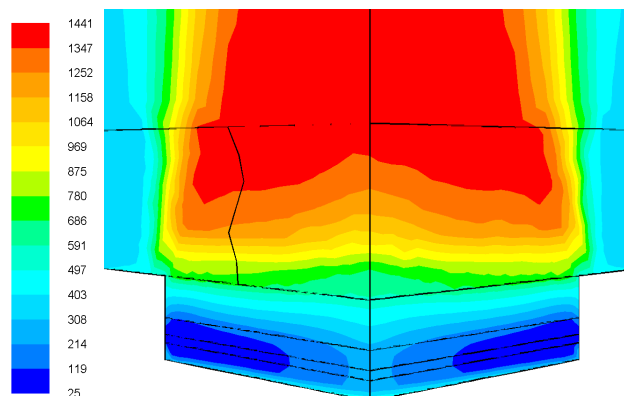


Fig. 4. Temperature [°C] in bed, with radiation.

In the model set-up, it is important to set the absorption coefficient of the burner walls equal to unity (black body). Otherwise, all radiative flux is reflected back. During the model development it was also found as very important to carefully design the porous fuel volume and the primary air inlet, because the area of the input boundary leads to radiation losses. The inlet area should therefore be small and shielded from the direct radiative flux of the combustion chamber. It also has to ensure uniform velocity and mass flux distribution on the bed-freeboard interface. In simulations, several design alternatives for the supply of reactants have been tested. The most appropriate method in this particular burner was from placing the inlets on the burner perimeter. The inlet has the shape of a narrow slit in under the porous bed. The space under the bed is open to horizontal flow, which helps to distribute the fluid flow. This solution ensures almost uniform flow in the layer above it.



3. Conclusion

The described model greatly simplifies the modeling approach for pellet combustion and also is simple and easy to apply for a user of CFD software. This simple model can be used for simulation in a relatively simple way and is able to predict the general behavior of solid fuel-fired boilers. In developing the model, it is necessary to consider the impact of the assumptions which may vary depending on the design of the burner and boiler.

The limitations of the bed model include the assumption that the reactants are well mixed with each other and that the heterogeneous combustion process is also uniform in space. Another important limitation of the model is that it considers constant temperatures of devolatilization and of char combustion. Perhaps the main simplifying assumption is that the production of volatiles in the bed is independent of the conditions in the combustion chamber. An advantage is that the model bed is set up directly in the CFD model and does not require programming of external libraries.

The present model does not substitute more advanced models and tools that can be used to design biomass combustion systems, such as three dimensional bed, transient modelling, solid to gas conversion or bed particles feeding. These all are however quite complex tasks, which require the implementation of external libraries. The work introduces a model that may provide help in the design of simple small boilers, where fuel consists of well-defined pellets, the fixed bed is small relative to the combustion chamber, and where high development costs preclude the application of more sophisticated tools.

Acknowledgement

This article has been prepared within the framework of the project R&D – APVV-0458-11 “Solving issues with low-melting ash during the biomass combustion“. The author JH gratefully acknowledges financial support of the Ministry of Education, Youth and Sports within the programme „National Sustainability Programme I“, project NETME CENTRE PLUS (LO1202).

References

- [1] COLLAZO, J. et al. *Numerical simulation of a small-scale biomass boiler*. Energy Conversion and Management. 2012. Vol. 64, pp. 87–96.
- [2] ERGUN, S., ORNING, A. A. *Fluid Flow through Randomly Packed Columns and Fluidized Beds*. Industrial & Engineering Chemistry. 1949. Vol. 41, no. 6, pp. 1179–1184.
- [3] GÓMEZ, M. A. et al. *Simulation of the Effect of Water Temperature on Domestic Biomass Boiler Performance*. Energies. 2012. Vol. 5, no. 12, pp. 1044–1061.
- [4] ION, I. V. et al. *A biomass pyrolysis model for CFD application*. Journal of Thermal Analysis and Calorimetry. 2013. Vol. 111, no. 3, pp. 1811–1815.
- [5] JANDAČKA, J. et al. *Biomasa ako zdroj energie : Potenciál, druhy, bilancia a vlastnosti palív*. 1. vyd. Žilina: Juraj Štefuň - GEORG, 2007. 241 p. ISBN 978-80-969161-3-9.
- [6] KLASON, T. et al. *Investigation of radiative heat transfer in fixed bed biomass furnaces*. In Fuel. 2008. Vol. 87, no. 10–11, pp. 2141–2153.
- [7] KOLONIČNÝ, J. et al. *Postupy správného topení*. Ostrava: Vysoká škola báňská – Technická univerzita Ostrava, Výzkumné energetické centrum, 2010. 131 p. ISBN 978-80-248-2255-6.
- [8] KOPPEJAN, J., LOO, S. VAN. *The handbook of biomass combustion and co-firing*. London: Earthscan Publications, 2010. 442 p. ISBN 978-1-84971-104-3.
- [9] LYČKA, Z. *Dřevní peleta II : spalování v malých zdrojích tepla*. 1. vyd. Krnov: LING Vydavatelství, 2011. 71 p.
- [10] NOSEK, R. et al. *Meranie emisií pri spaľovaní fytomasy v malých zdrojoch tepla*. 32. stretnutie katedrií mechaniky tekutín a termomechaniky. Vysoké Tatry - Tatranská Lomnica: Žilinská univerzita, 2013. pp. 205–208.
- [11] PORTEIRO, J. et al. *Numerical Modeling of a Biomass Pellet Domestic Boiler*. Energy & Fuels. 2009. no. 23. pp. 1067–1075.
- [12] SAS IP, INC. *ANSYS Fluent User's Guide*. U.S.A., 2013. 2692 p.



- [13]SHARMA, A. K. et al. *Modelling product composition in slow pyrolysis of wood*. SESI Journal. 2006. Vol. 1, no. 16, pp. 1–11.
- [14]THUNMAN, H. *Principles and models of solid fuel combustion*. Goteborg, Sweden: Chalmers University of Technology, 2001.
- [15]ZAHIROVIĆ, S. et al. *Advanced gas phase combustion models: validation for biogases by means of LES and experiments as well as application to biomass furnaces*. 7th European Conference on Industrial Furnaces and Boilers. Poto, Portugal: CENERTEC, 2006.



Hybridization way of better fuel utilization and decreasing emission

* Martin Mikolajčík, * Daniel Kalinčák

* Department of Transport and Handling Machines, Faculty of Mechanical Engineering, University of Žilina, Univerzitná 1, 010 26 Žilina, Slovakia. martin.mikolajcik@fstroj.uniza.sk, daniel.kalincak@fstroj.uniza.sk

Abstract. This article analyses the driving performance of shunting locomotives with conventional internal combustion engine (ICE) and suitable substitutes of conventional ICE for ICE with lower performance combined with hybrid propulsion. Installed performance of the ICE in shunting locomotive is high, the maximum power is used only for minimum working time of locomotive and it's leading to high fuel consumption and increasing operating costs and emission of carbon dioxide. Due to the introduction of stricter emission limits for rolling stocks are placed demands on more effective fuel efficiency and reducing greenhouse gases emissions. For this reason, there is an effort to introduce hybrid propulsion into rail vehicles operating in a wide range of performances, which replace the ICE with high performance. Hybrid drive consists of ICE, which is more powerful than average power of shunting (non hybrid) locomotive in shunting and hybrid system, which covers performance peaks.

Keywords: Hybrid traction drive of rail vehicles, Utilization power of ICE, Hybrid locomotives, Fuel utilization.

1. Introduction

Railway systems always have been described as competitive, sustainable and environmentally friendly modes of transportation. However, diesel engines appear more and more like the weak point in this good picture. Fortunately, fast-growing technologies offer everyday new opportunities for improving such a technical domain as railway [1].

Most diesel locomotives used on railways using outdated types of ICE that do not meet today's emission limits for this type of vehicle and using of their installed power is low. As suitable and cheaper solution to this problem, instead of buying a new rail vehicle seems to use a hybrid system in upgraded diesel locomotives and it brings the desired reduction in fuel consumption and reduce emissions. For suitable design of a hybrid propulsion of specific rail vehicle, it is necessary to know the operating parameters and make the analysis of operating parameters to determine the most appropriate design of the hybrid system and accumulators of energy. Improper design of a hybrid system would be extended return of investment in rebuilding and hybrid system could not be fully utilized. It is best use hybrid systems in rail vehicles, which often stop and then starting up again. In the following paper we will present the possibility of using a hybrid system in shunting locomotives.

2. Analysis of shunting and main line locomotive's operation parameters

It is known that the use of installed power capacity of ICE in motive power units (especially in shunting locomotives and locomotives for industrial transport) is very low. Average utilization of engine power is usually less than 20% of the installed power capacity and nominal engine performance is utilized only during minimal period of the total time of engine operation (at the level of approx. 1%). The result of this is that most of the operational time the internal combustion engine works in regimes that are far from optimum mode. It means that specific fuel consumption is high. At this type of locomotives operation the frequent and fast changes of engine regimes occur, which

results in increased fuel consumption and imperfect fuel combustion with increased quantity of harmful emissions [2].

2.1. Shunting service of locomotive Class 742

The measurements were carried out on the locomotive class 742 (ČKD in shunting service at railway station Trenčianska Tepla [3]. This class of locomotives has 883 kW nominal output of engine. The distribution of traction generator output is shown in the Fig. 1. The mean output of traction generator was only about 102 kW, which represents about 11.5 % of the nominal output of ICE [2].

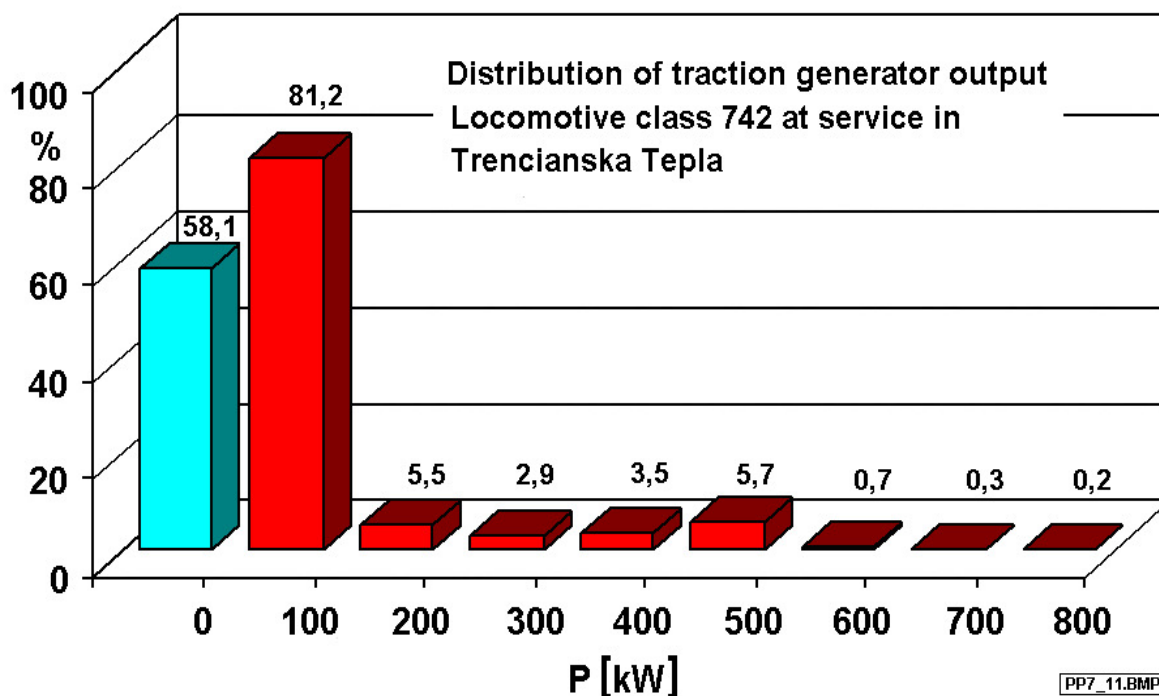


Fig. 1. The distribution of traction generator output of locomotive class 742 in the shunting service at Trenčianska Tepla [2].

As we can see at the Fig. 1, the maximum power of locomotive is using only short time period and main engine operation is idling and work with power output up to 100 kW. More efficient is using hybrid locomotives for these types of rail operations. In this case can be used ICE with power about 200 kW and it will cover 86.7% of power needs. The rest 13.3% have to be covered by energy from accumulator which will be charged during idling operation of ICE and recuperation braking. The accumulator should be able give short-time power about 680 kW, what is ambitious requirement. This high power of accumulators is needed for keeping up maximum traction effort of locomotive. The high power of accumulators is necessary for charging during regeneration of braking power as well.

By this way we can achieve that ICE will be working at optimal conditions and it will cause lower fuel consumption and emission. The next step in designing hybrid locomotive is to choose correct accumulator of energy, which can be fast charging and discharging with high power, which will not damage storage of energy during years of using. For shunting services is suitable use flywheel, ultracapacitors and superconducting magnetic energy storage system and Ni-MH or LiFePo4 batteries as storage of energy, because they can be charged and discharged by high power in short period.

2.2. Shunting service of locomotive Class 770

Another example of output distribution of locomotive class 770 (ČKD) during shunting operation on hump in railway station in Zilina is shown in the Fig. 2 [4]. The mean output of the locomotive with nominal rating of 993 kW was only 61 kW in this case, what represents only 6% of nominal output of ICE [2].

The Fig. 2 shows that ICE shunting locomotives working for a not insignificant duration in the idling mode (approx. 37%) in the area of high specific fuel consumption. This is from reason to power peripheral devices such as compressor. In the case of a hybrid propulsion would be peripherals driven by an electric motor and, if it is necessary, could be powered by energy from accumulator with turn off ICE. This would achieve the operation of the ICE in area of low specific fuel consumptions.

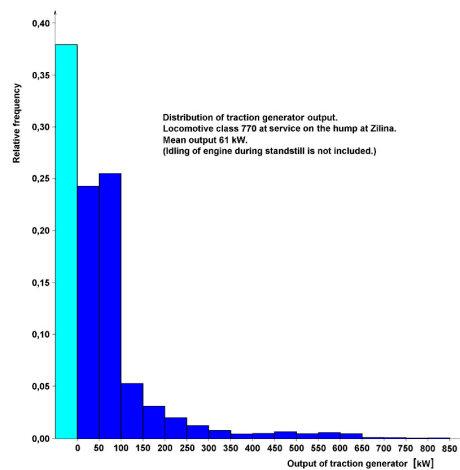


Fig. 2. The distribution of traction generator output of locomotive class 770 shunting at Zilina [4].

2.3. Passenger main line locomotive class 757

Modernized locomotive class 757 (Fig.3), intended for passenger transport, is equipped with diesel ICE with installed power of 1550 kW and EDB (electrodynamic brake). All auxiliaries are driven by electric motors. The measurements were carried out at railway line Zvolen- Banska Bystrica – Margecany – Banska Bystrica – Zvolen. Measurements were realized from 7:40 to 20:36. During this period engine was stopped 5 times with total duration of stopped ICE for 2 hours a 14 minutes.

The average distribution of the traction generator output was in this case approx. 317 kW, which represents about 20.5% of maximum output of ICE [6]. Distribution of traction generator output of locomotive class 757 is shown in Fig.4. From the figure follows, that the ICE is running most of the time with outputs up to 100 kW and also considerable part of the engine work is an idling ICE.



Fig. 3. Passenger main line locomotive class 757 after modernization [5].

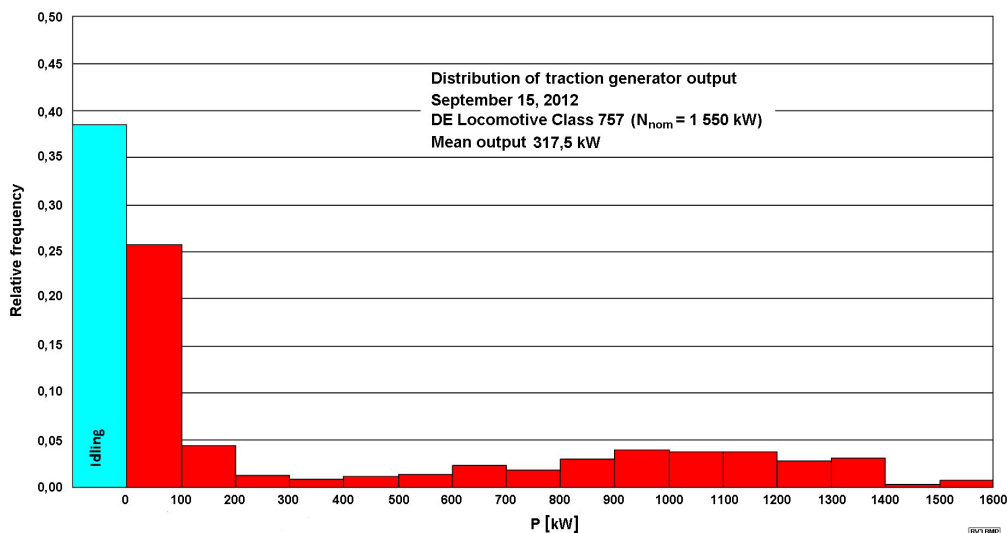


Fig. 4. The distribution of traction generator output of locomotive class 757 at main line operation [6].

The courses of some operational parameters of locomotive class 757 during all work shift is shown at the Fig. 5. and one part of shift is presented in more detailed form. Percentage of engine idling (approx. 38 %) is alike as in case of shunting and industrial locomotives. Distribution of electrodynamic brake (EDB) power and input of auxiliaries is shown in Fig.6. It is apparent that EDB was used quite frequently and its mean output was 59.9 kW which represents approximately 19 % of mean traction output (317 kW). The mean output of all auxiliaries was 33.3 kW. The auxiliaries include two fans of primary and secondary cooling circuit of engine, two fans of traction motors cooling, compressor of brake system and fan of traction and auxiliary generator and also ventilator of EDB brake resistors [6].

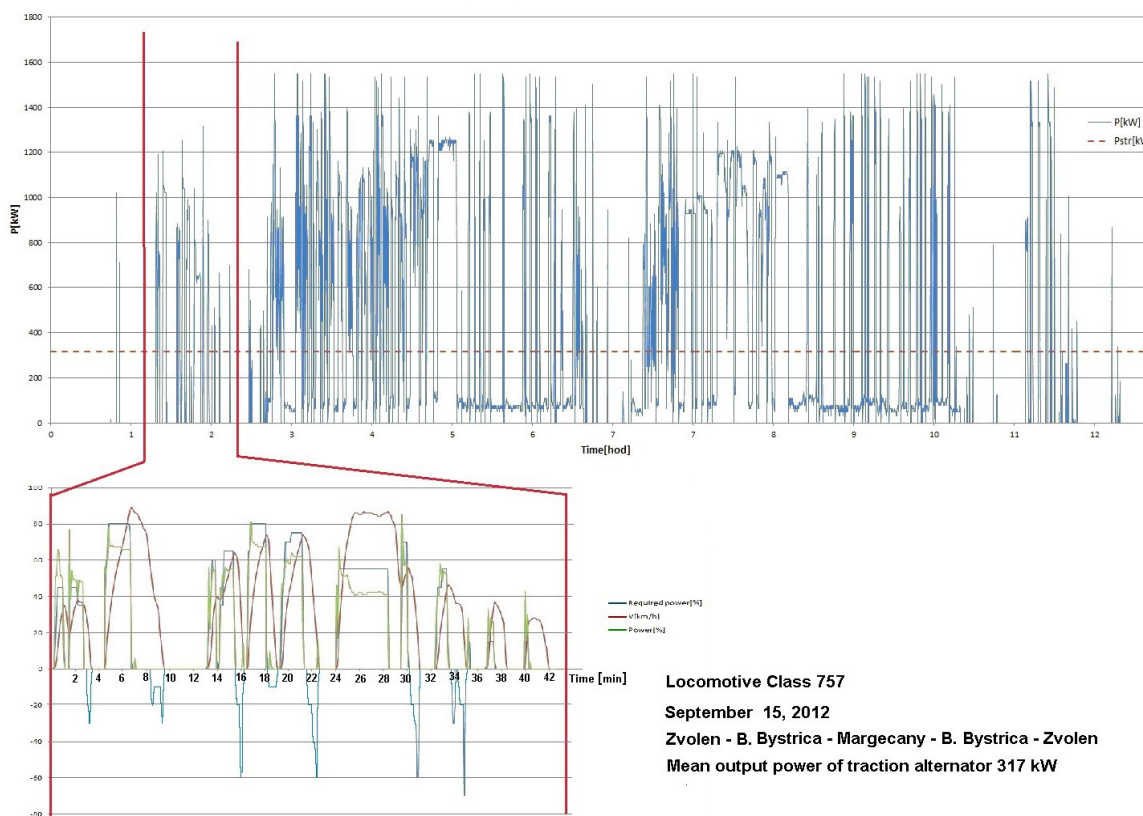


Fig. 5. The courses of some operational parameters of main line locomotive class 757 [6].

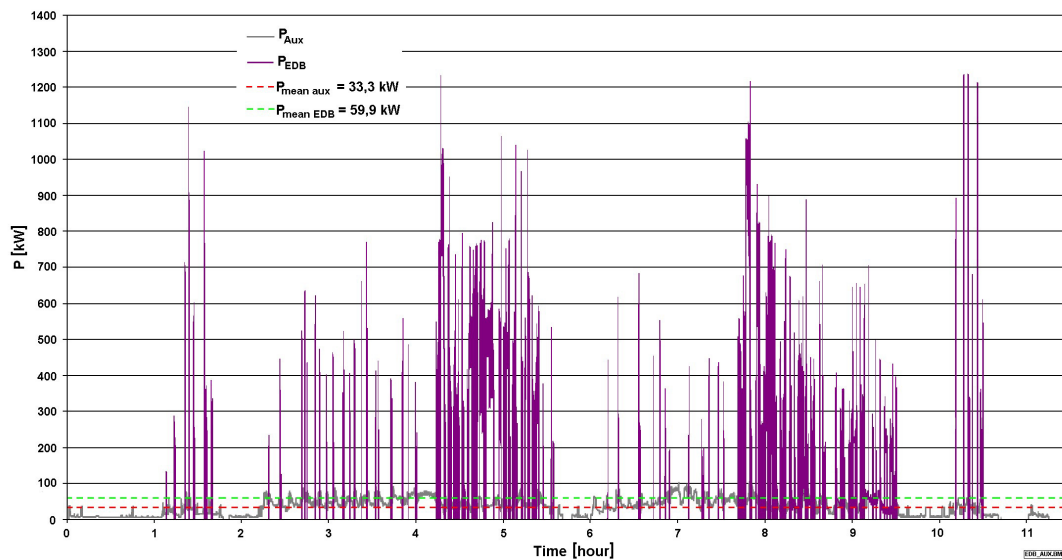


Fig. 6. The distribution of the electrodynamic brake and input of auxiliaries of locomotive class 757 [6].

Theoretically it would be possible to cover the energy consumption of auxiliaries with the energy produced during electrodynamic braking, but there is a problem with the storage, because EDB produces large amounts of energy for a short period of time. Therefore, they cannot be used for energy storage batteries, because they can't be charged with high power, which produces EDB, but must be used ultracapacitors, which are capable to accumulate large amount of energy over a relatively short period of time.

2.4. Comparison between shunting hybrid locomotive Class 718 and non-hybrid locomotive Class 730

In the former Czechoslovakia was in 1986 built the hybrid locomotive Class 718. There were carried out measurements for comparison this hybrid locomotive and non-hybrid locomotive Class 730. Design and operational properties of locomotive Class 718 was based on locomotive class 730. The results of measurements showed that hybrid locomotive is more effective in all type of shunting except of shunting to hump as it is shown in Tab. 1. It is possible to save up to 24% of fuel compare to non hybrid locomotive, but it's depend on type of shunting. Increasing fuel consumption of hybrid on shunting to hump is caused by using of hybrid traction drive on maximum. In this operational regime is regenerative braking rare. To reduction of fuel consumption significantly contributes using of regenerative braking, which save braking blocks or braking pads and achieves higher efficiency of hybrid drive. The measurements at this hybrid locomotive were executed with various loads up to 2500 t. Locomotive class 718 has ICE with power only 189 kW and replaced original ICE with power of 600 kW. It is only 31.5% power of original ICE which cause lower fuel consumption and emission compared to original ICE.

Type of shunting	Fuel consumption dm ³ /h		Ratio of fuel consumption
	Class 730	Class 718	
Shunting on hump	14,92	13,09	0,88
Pushing off and allocation of load	13,62	10,33	0,76
Shunting to hump	23,53	25,56	1,09
Pulling of load	12,87	10,86	0,84

Tab. 1. Comparison of fuel consumption in shunting service [7].



3. Conclusion

Rising prices of fossil fuels force designers and producers to improve efficiency of diesel locomotives. Better utilization of fuel and decreasing of greenhouse gases emission are required by strict emission limits for rolling stocks. One of the ways for better fuel utilization is introducing hybrid propulsion to rolling stocks. With hybrid propulsion it is possible to change kinetic energy of vehicle to electricity through regenerative braking. Kinetic energy is normally changed to heat in non-hybrid locomotives and it is lost during braking process. Another advantage of hybrids is possibility of replacing old ICE, which has high power and fuel consumption, for new ICE with lower power and fuel consumption, but with equal traction effort. The hybrid locomotives in shunting operations can reduce the fuel consumption up to approximately 22% and in some case even more.

The most reasonable is using hybrid propulsion in shunting services or at the regional railways where the needs of power are periodically changing and vehicles are still stopping and starting in short period during services. The power peaks are covered from energy stored in accumulators of energy and another power needs are covered by ICE.

Introduction of hybrid locomotives will probably rise in the future, but is necessary to solve problem with high prices of energy accumulators. We can hope that Tesla motors [8] will start massive production of batteries for electric vehicles and it will be possible to use those batteries for hybrid locomotives. Finally hybrid locomotives will cost less than now.

Acknowledgement

This article was supported by the Scientific Grant Agency of the Ministry of Education of the Slovak Republic and the Slovak Academy of Sciences in project no. VEGA 1/0927/15 "Research of the possibilities of using alternative fuels and hybrid propulsion in rail vehicles with the aim to reduce fuel consumption and production of air pollutants".

References

- [1] CHABAS, J. *Environmentally friendly technologies for railway application*, SNCF, Paris, 2001.
- [2] KALINČÁK, D., BARTÍK, E., GREŇČÍK, J. *Some ways of fuel consumption reduction of diesel railway vehicles*, Autobusy – Technika, Eksploatacja, Systemy Transportowe, Nr. 3/2013, Instytut Naukowo-Wydawniczy „SPATIUM“ sp. z o.o., Radom, ISSN 1509-5878. pp. 1957 – 1966, Radom, 2013.
- [3] PALKO, P. *Hybrid drive systems in rail vehicles* (in Slovak). Thesis. University of Žilina, 2008.
- [4] MÜLLER, J., KALINČÁK, D., POHL, R., RYBIČKOVÁ, D., TRUBAN, M., ŠEBO, L., DIVIŠOVÁ, H., HERZÁŇ, F., SMOLKOVÁ, A., BALALA, L. *Reliability of traction of rolling stock* (In Slovak). Report No SET – KKVMZ/2/85. VŠDS Žilina 1985.
- [5] ŽOS ZVOLEN. *Locomotive 757* (In Slovak), [online]. 2015 [cit. 2015-1-15]. Available on the internet: <<http://www.zoszv.sk/userfiles/image/produktove%20listy/757%20PL%20vsetky%20strany.pdf>>.
- [6] KALINČÁK, D., BARTÍK, E. *The possibilities of fuel economy – The hybrid traction propulsion*, In Prace Naukowe – Transport, z. 98, 2013, Oficyna wydawnicza Politechniki Warszawskiej. ISSN 1230-9265. Warszawa, 2013.
- [7] POHL, J. *Research result of hybrid – accumulators drive of locomotives* (In Czech), Railway technology 17/1987, pp. 206 - 211, Praha, 1987.
- [8] HORČÍK, J. *Tesla doesn't manage production, they want to build the largest plant for Li-ion batteries* (In Czech), online, Available on the internet: <http://www.hybrid.cz/tesla-nestiha-vyrabet-chce-postavit-nejvetsi-tovarnu-na-li-ion-baterie>, 2013.



The rotational speed differences of the vehicle wheels equipped and non-equipped with ABS system

*Diana Młodzińska, *Rafał S. Jurecki, *Emilia Szumska

*Kielce University of Technology, Faculty of Mechatronics and Machine Building, Department of Vehicles and Transport, Tysiąclecia Państwa Polskiego 7, 25-314 Kielce, Poland, {dmlodzinska, rjurecki, eszumska}@tu.kielce.pl

Abstract. There is a lot of vehicles equipped with ABS system currently. The system has been obligatory for all new models of the passenger cars since May 1st, 2004 in the EU countries. The device prevents wheel from lock during brake process and helps driver to acquire brake stability in emergency situations. The goal of paper is to present the results of the investigations of the rotational speed differences of the wheels ABS-equipped and non-ABS during braking process in winter conditions. Additionally the vehicle was fitted with summer and winter tires.

Keywords: ABS, Winter tires, Summer tires.

1. Introduction

Electronic active safety systems of modern passenger cars are intended to reduce or avoid the risk of a road accident. Nowadays, the majority of vehicles are equipped with ABS - an electronic device preventing the vehicle wheel from locking during brake process, ensuring the shortest possible brake distance and brake stability. As a result of the ABS action it is possible to avoid a collision with an obstacle. The driver has ability to control the vehicle in emergency situations. The ABS constantly monitors the rotational speed of each wheel. If it detects a wheel rotating significantly slower than the others, a condition indicating impending wheel lock, by reducing hydraulic pressure to the brake at the affected wheel it is possible to reduce the braking force on that wheel. The wheel then turns faster. Conversely, if the system detects a wheel turning significantly faster than the others, brake hydraulic pressure is increased, the braking force is applied, slowing down the wheel. In modern ABS systems pressure changes can occur up to 100 times per second [1, 2, 3, 4].

During braking is the wheel peripheral speed lower than the speed of the car motion. When the rotational speed of the wheels equals zero and the car is still in motion the maximum slip is observed. Braking efficiency is dependent on the type of road surface and weather conditions. The wheel slips most frequently on a slippery surface, such as a road which is wet, icy or covered with snow. Braking performances is also influenced by the tire condition. The vehicle tires must provide the best possible adhesion to the road surface [5].

Before the winter season some drivers are considering if it is reasonable to use snow tires in our climate zone or is it better to use the all-season tires. Winter tires are designed to provide enhanced traction on mud or slush road surfaces when the temperature drops below 0°C. Many European countries have obliged the car owners to use winter tires at a specified time of the year or on prevailing traffic conditions. Polish law has not establish such a requirement but a lot of Polish drivers change the tires before winter.

The aim of this contribution is to present some investigation results of the differences in rotational speed of the wheels for ABS-equipped and non-ABS equipped vehicles fitted with summer and winter tires during braking process on snow-covered asphalt.

2. Test procedure

Experiment was carried out on track section of the Kielce University of Technology located in Dąbrowa. Brake tests were conducted on asphalt covered by snow homogeneously. The ambient temperature was -4°C . The test procedure consisted of accelerating the car to specified speed and then rapid braking initiated by rapid pressing of the brake pedal. The initial velocity was sequentially 10, 15 and 20 km/h.

The experiment was conducted with use of two types of tires:

- summer tires Kleber Dynaxer HP3 185/65/R15 (read wear indicator = 0.1 mm),
- winter tires Fulda Kristall Montero 2 185/65/R15 (read wear indicator = 0.7 mm).

The vehicle tire pressures were set in accordance to the manufacturer's recommendations.



Fig. 1. The test track and test vehicle.

The test vehicle (Opel Astra G) was equipped with:

- ABS system,
- data acquisition station $\mu\text{EEP-12}$ - Corrsys - Datron (Kistler)[®] with ARMS[®] software and a control tablet, which enabled the collection, visualization and pre-processing of the results non-contact,
- optoelectronic sensor S-350 Corrsys - Datron[®] which can measure the longitudinal and transverse speed of the vehicle and a vehicle drift angle,
- directional linear acceleration sensor of measuring range $\pm 2g$ necessary to determine the longitudinal and lateral acceleration of a car body block,
- WPT (Wheel Pulse Transducer) for acquisition data delivered from vehicle wheel rotation.

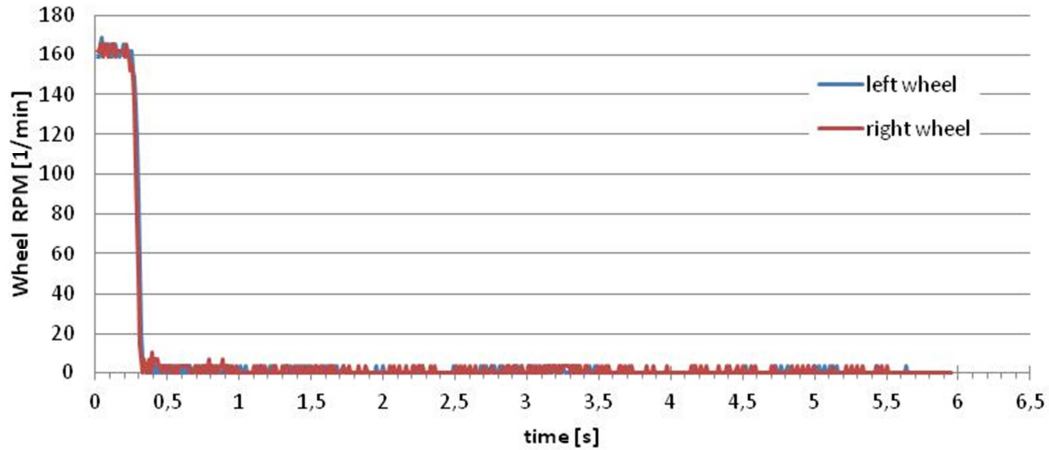
3. Results and verification

Wheel speed sensors were used to detect any sudden changes of the rotational speed of the wheel. It enabled collecting data of the wheels work and calculation of wheel speeds as well as the changes of the speed at the time, i.e. the acceleration and deceleration.

Fig. 2 presents a comparison of the rotational speed wheel changes of the ABS-equipped and ABS-unequipped vehicle during braking process. The initial speed was 20km/h. The summer tires were used for this experiment. The rotational speed of the wheels of the ABS unequipped vehicle decreased rapidly (within approx. 0.16 s) to zero, but the car was completely stopped after 5.5 seconds. In the same conditions with the ABS system working and with the wheels initially blocked, their rotation without slipping was restored after about 0.2 – 0.3 s.



a)



b)

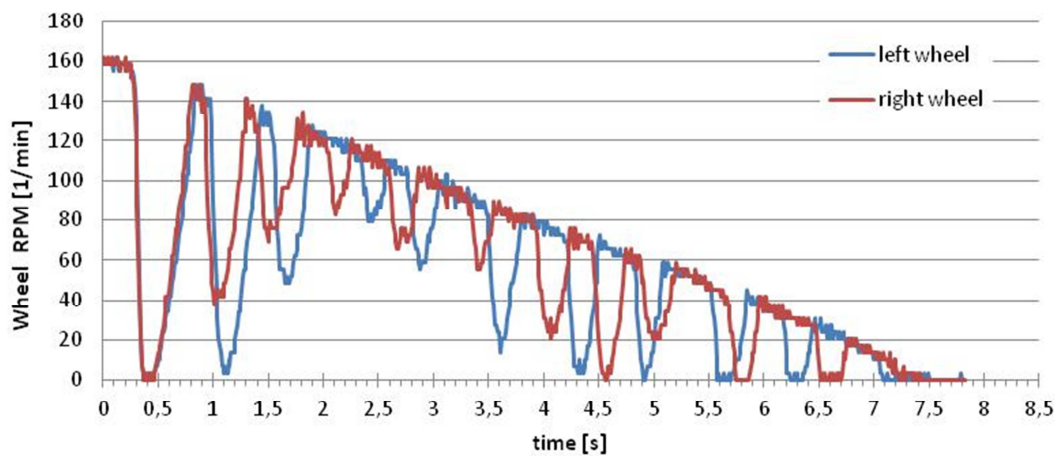
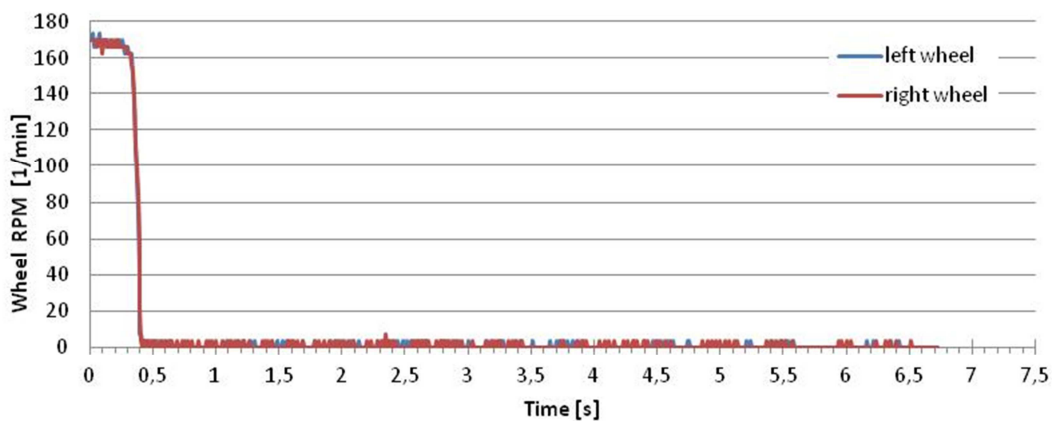


Fig. 2. The rotational speed of the wheels during braking with the summer tires: a) ABS unequipped, b) ABS-equipped vehicle.

Fig. 3 presents a comparison of the rotational speed of the wheels of the ABS-equipped and unequipped vehicle fitted with the winter tires during braking process. The initial speed was 20 km/h. The rotational speed of the wheels of the ABS unequipped car fallen to zero after approx. 0.2 s. The car stopped after 6.3 seconds. The ABS-equipped car wheels were blocked initially, but after about 0.2 - 0.3 s they restored to rotate. The wheels fitted with winter tires rolled longer without slipping than summer tires. The car stopped after 4 seconds.

a)



b)

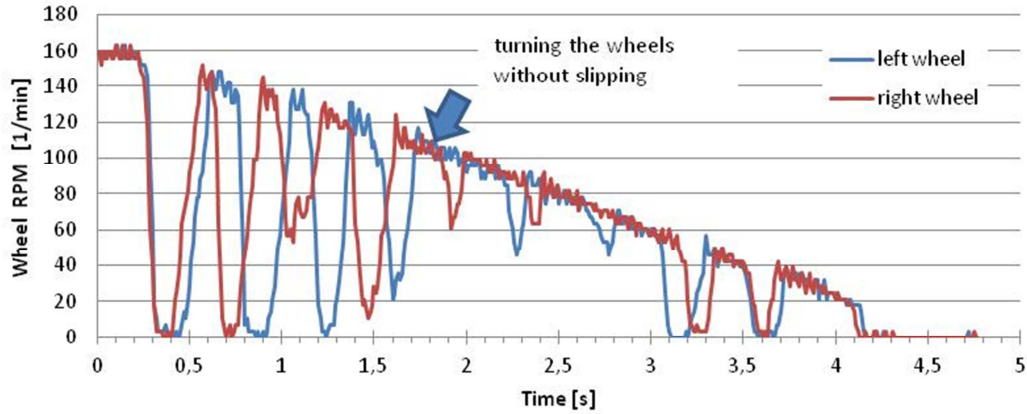


Fig. 3. The rotational speed of the wheels during braking with the winter tires: a) ABS unequipped, b) ABS-equipped.

Fig. 4 shows a comparison of the rotational speeds characteristics for the ABS-equipped vehicle fitted with winter and summer tires respectively during braking process. The intensity of the reduction of the rotational speed lines were traced. An average deceleration of a vehicle equipped with winter tires was 1.26 m/s^2 , whereas the average deceleration of a vehicle fitted with wheels with summer tires, was 0.75 m/s^2 .

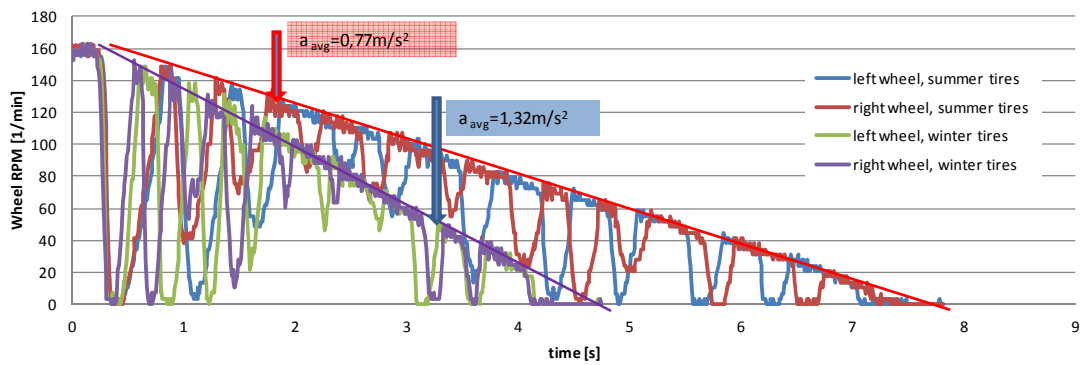
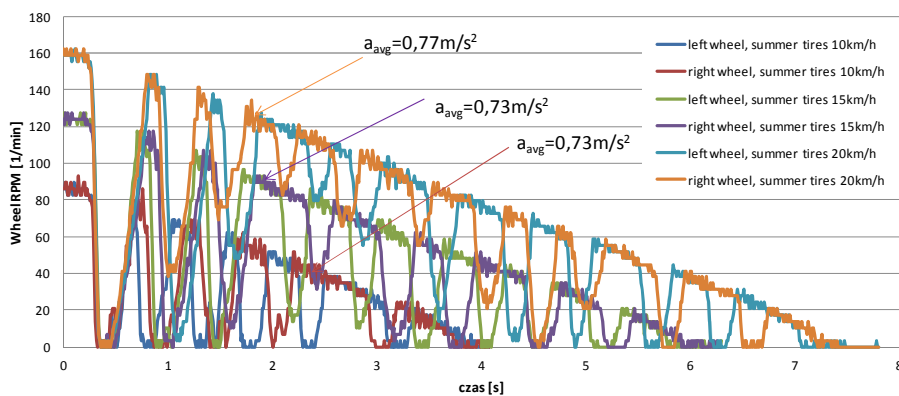


Fig. 4. The rotational speed of the wheels during braking ABS-equipped vehicle.

Fig. 5 presents the impact of an initial speed on average deceleration during braking process. The initials speed were small and amounted sequentially 10, 15 and 20 km/h. Differences in the average deceleration were not significant and the influence of the initial speed on average deceleration was negligible.

a)



b)

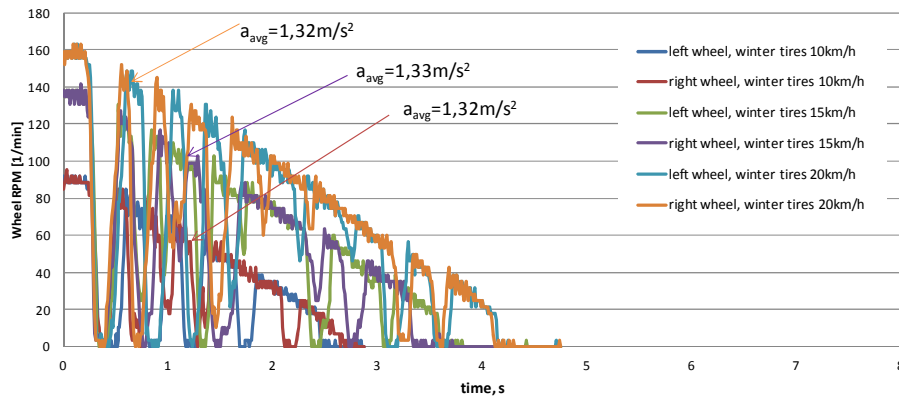


Fig. 5. The rotational speed of the wheels during braking ABS-equipped vehicle fitted with: a) summer tires, b) winter tires.

4. Conclusions

The test results indicated that during braking on snow-covered road:

1. Reduction of the intensity of the wheel rotation speed was dependent on the value of deceleration.
2. The initial braking speed value does not significantly affect on the value of the deceleration.
3. The braking process lasted longer for vehicle fitted with summer tires and ABS system.
4. The shortest braking time was observed for the car equipped with ABS system and winter tires.
5. The experiment showed that the usage of the winter tires on the snow-covered road is fully reasonable and recommended. The ABS system allows to keep control of the vehicle and enables the wheel to rotate without slipping in emergency situations.

Acknowledgement

This paper has been based on subsidy from LABIN – *Wsparcie Aparaturowe Innowacyjnych Laboratoriów Naukowo – Badawczych Politechniki Świętokrzyskiej w Kielcach* projekt nr POPW.01.03.00-26-016/09, „*Ruchome laboratorium badań bezpieczeństwa i komfortu w transporcie zbiorowym*” WND-RPSW.02.01.00-26-012/11, „*Ruchome laboratorium badań bezpieczeństwa i własności dynamicznych pojazdów samochodowych*” WND-RPSW.02.01.00-26-010/11 and *Modernizacja i rozwój infrastruktury dydaktyczno - badawczej dla innowacyjnego kształcenia na kierunku Transport* nr WND-RPSW.02.01.00-26-011/11.

References

- [1] GRZESIKIEWICZ W., POKORSKI J., SZWABIK B. *Modelowanie i badania eksperymentalne przyczepności hamowanego koła*, Przegląd Mechaniczny, Zeszyt 10/2003.
- [2] JURECKI R, JAŚKIEWICZ M. *Analiza stanu bezpieczeństwa na polskich drogach w latach 2000-2010*, VIII International Science-Technical Conference Automotive Safety, Kielce 6-8 February 2012.
- [3] POKORSKI J., SAR H., REŃSKI A. *Badania porównawcze przyczepności opon letnich i zimowych*, Zeszyty Naukowe Instytutu Pojazdów 4(90)/2012.
- [4] POKORSKI J., SAR H., REŃSKI A. *Badania przyczepności opon letnich i zimowych w różnych warunkach atmosferycznych*, IX International Science-Technical Conference „Automotive Safety 2014”, Rajecke Teplice Slovakia.
- [5] SZUMSKA E., MŁODZIŃSKA D., JURECKI R. *Wpływ stanu nawierzchni na skuteczność hamowania pojazdu*, Logistyka 6/2014:10430-10439.

Thermo-Mechanical Finite Element Analysis of Mold for Piston Casting

Martin Močilan *Milan Žmindák

*University of Žilina, Faculty of Mechanical Engineering, Department of Applied Mechanics, Univerzitna 1, 01026 Žilina, Slovakia, {martin.mocilan, milan.zmindak}@fstroj.uniza.sk

Abstract. The aim of this paper is the examination of the interaction of fluid and core molds for piston casting. Analysis of the core will be performed by finite element method. As a tool for FEM analysis will serve the commercial software ANSYS Workbench - Polyflow, which is often used in technical practice because of its fast and effective means of FEM model creation. The mold and core are both metal. The core cooling is ensured by drilled hole on the bottom side, into which is injected water. This paper is focused on analysis of stress inside the core molds for piston casting. As a result of uneven stress in the core, cracks begin to appear which have a negative influence on the longevity.

Keywords: Fluid flow, Interaction, Polyflow ANSYS, FEM analysis.

1. Introduction

Computer Aided Design / Engineering (CAD / CAE) tools allow engineers to design molds for piston casting. In the last decades, together with the development of computers rose also the popularity of the finite element method (FEM) for the simulation of miscellaneous technological processes, such as welding, quenching, casting, cutting, etc. [1, 2].

Softwares that are available today and are only used for simulation of casting, casting techniques, quality assurance, optimization etc. are, for example. CastCAE, MAGMA, NovaCast, Procast and SolidCAST. Simulation of casting replace or minimize the manufactory tests. Most of them use the finite element method (FEM). The main inputs to the geometry of the mold, thermo-physical properties (density, specific heat, thermal conductivity, material properties) [3] and boundary conditions [4, 5, 6].

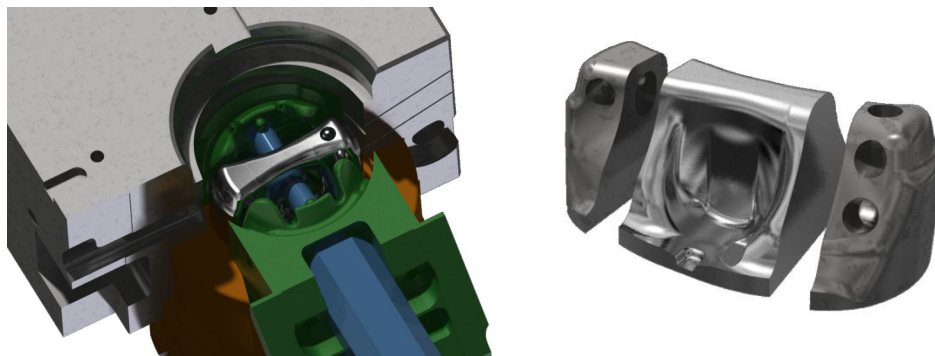


Fig.1. CAD model of the mold (left) with the core (right).

On the production line pistons for combustion engines made of aluminum alloy are cast into molds. In the mold is the core, which is heated by flame after insertion (Fig.1). The mold and the core are subjected to extreme temperature changes. These components are made of tool steel. Cast pistons are made of aluminum alloy. These materials are used to production the pistons because of low melting point, low weight of the piston, corrosion resistance, etc. Material properties core and alloy are in table (Tab.1).

The core is a massive forging, with nitrided surface. Core cooling is provided by a hole drilled in the bottom of the casting and water is injected into the hole. The melt is kept at a temperature of 775-785 ° C in the furnace. The mold filling time is 2-4 seconds. Opening of the bottom of the mold occurs after 60 seconds. The mold is preheated to a temperature of about 160 ° C.

		Alloy (Fluid) Al Si 17 Cu 3	Core Steel H13
Viscosity	μ [mPa. s ⁻¹]	2.7	-
Density	ρ [g. mm ⁻³]	2.5×10^{-3}	7×10^{-3}
Thermal conductivity	k [g. mm. s ⁻³ . K ⁻¹]	1×10^8	26.25×10^6
Heat capacity	C_p [mm ² . s ⁻² . K ⁻¹]	1163×10^6	490×10^6
Average temperature	T_p [K]	1024	433
Young's Module	E [Pa]	-	2.1×10^{11}
Poisson's ratio	ν	-	0,25
Coefficient of thermal expansion	α [K ⁻¹]	-	13×10^{-6}

Tab.1. Material properties.

We imported the geometry of the mold and core from the CAD software as *.stp into DesignModeler, which is integrated into the software ANSYS Workbench. We simplified the geometry of the mold to generate good mesh, reduce the number of elements and minimize errors in the simulation. We created a cut of the gating system common for the mold and the core. We eliminated the small fillets and chamfers, which were negligible in the calculation. The whole system is symmetrical, so we solved only one half. The picture shows the geometry of the core, which is the subject of our calculations. The core consists of three parts, the middle part is essential for us and we will focus on it in the simulations.

This paper is divided into two sections. The first part is a planar problem of non-isothermal Newtonian flow. It is a time-dependent simulation, where we examine the impact of fluid on the core. We want to evaluate the core temperature in contact with the liquid at different time steps.

In the second part of the paper are shown the numerical results of the core stress field. We will not investigate the whole core, but only the central part in which cracks occur, so in this part we are mostly interested in the stress at each time step.

2. Progress and discussion of results

Problem was solved as a 3D problem of non-isothermal Newtonian flow. This is a time-dependent simulation where we examine the impact of the liquid to the core. We want to find out what the core temperature in contact with the liquid at the end of the simulation time 2s (t=2s).

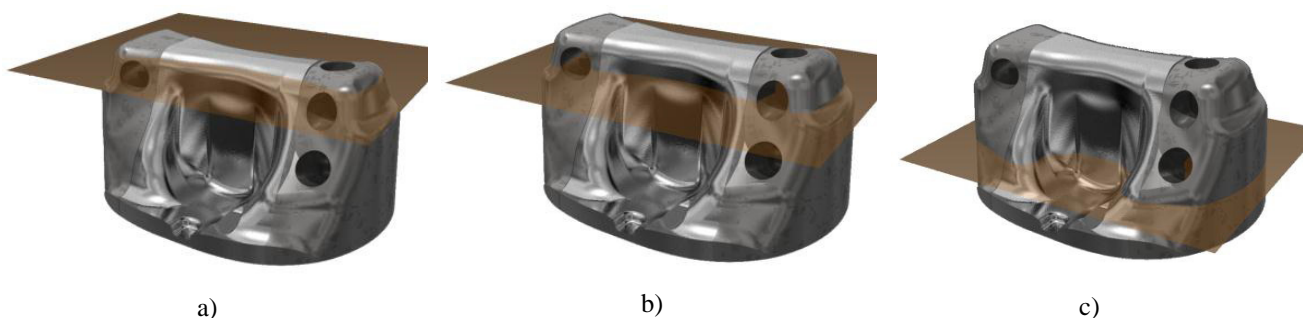


Fig.2. Section plane of the core a) section A b) section B c) section C.

The main goal of this paper was not to flow and distribution of fluids in the mold, but examination of the interaction of the fluid with the core, so we can simplify. It is a symmetrical

problem, we will solve only one half. Create a sections plane of the core (Fig. 2), where the change occurs geometry. In these areas we expect the greatest differences in core temperature changes.

In the simulation we used the adaptive mesh and remeshing. For mesh fluid was performed every 5 time steps. The size of elements was set to 1.5 mm, and the quality of the mesh 0.9 (Fig.3.). The areas of interaction have been set and zone sizes small elements to better fill the space around the core and accurate calculation.

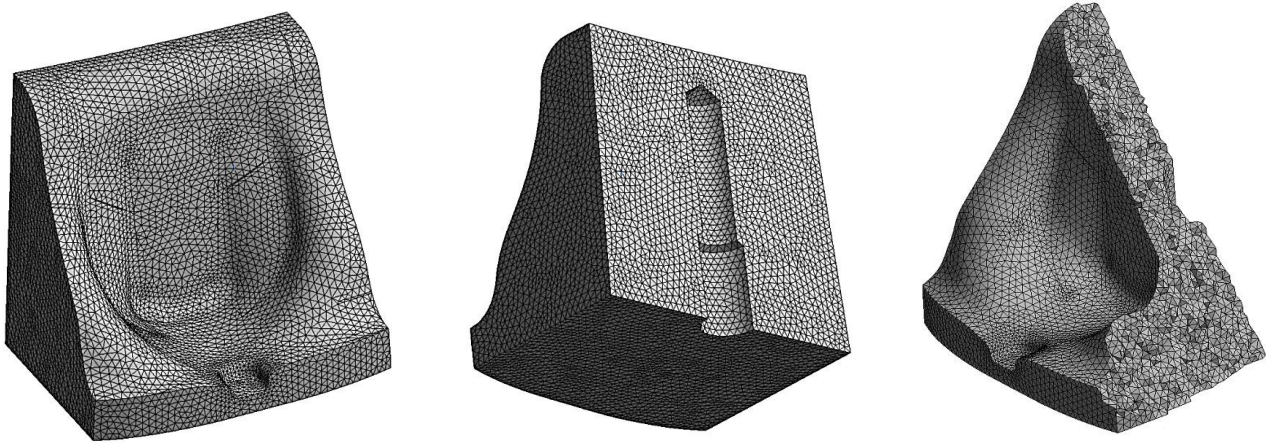


Fig.3. Discretization model of the core.

3. Result

The results for heat transfer at time step $t = 1s$ are visible in the following figures.

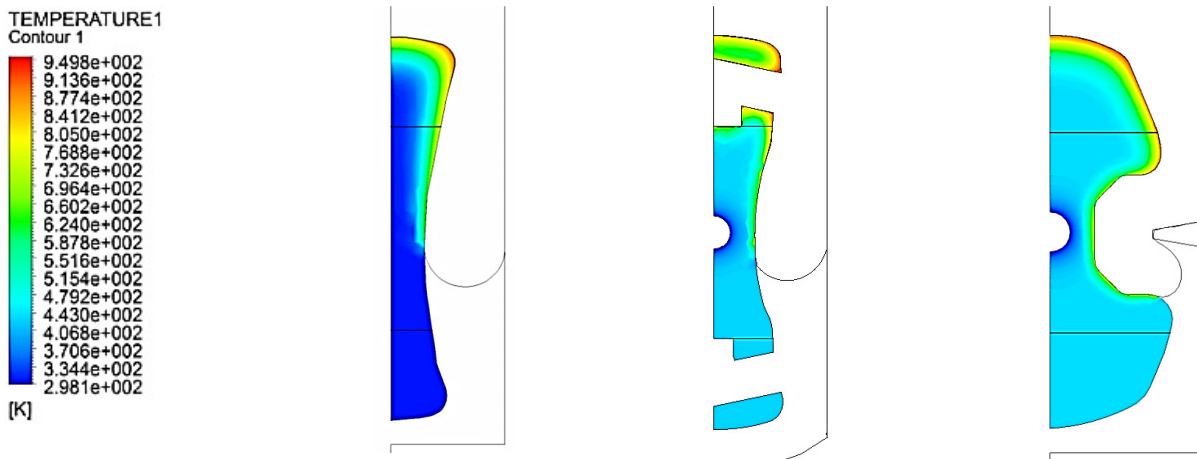


Fig.4. Heat distribution at $t = 1s$ a) section A b) section B c) section C

The results for heat transfer at time step $t = 2s$ are visible in the following Fig. 5.

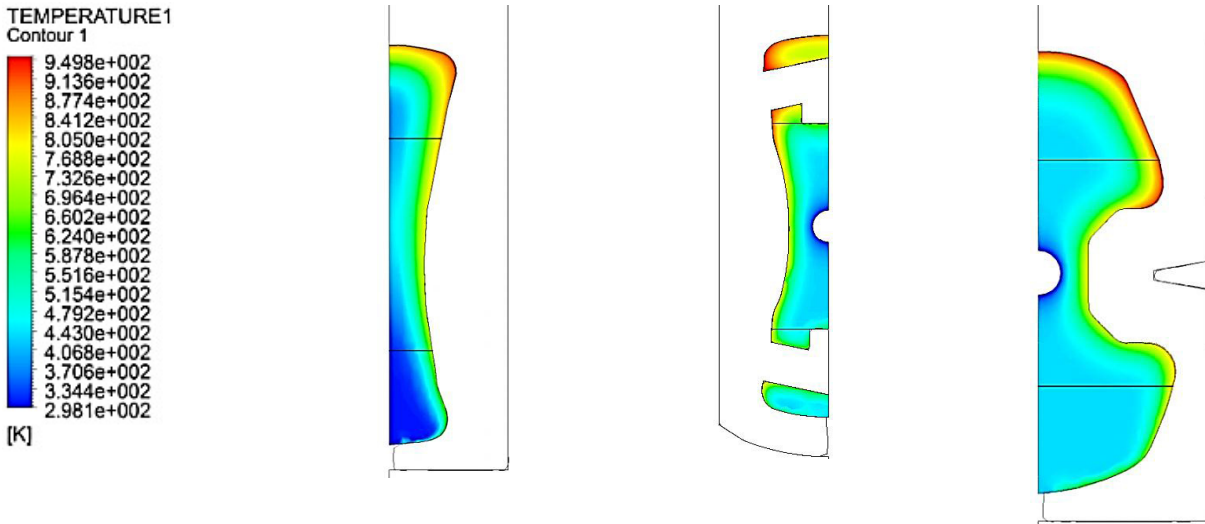


Fig.5. Heat distribution at $t = 2s$ a) section A b) section B c) section C

The results of surface elastic stress at $t = 1s$ can be seen in Fig. 6 to Fig.11.:

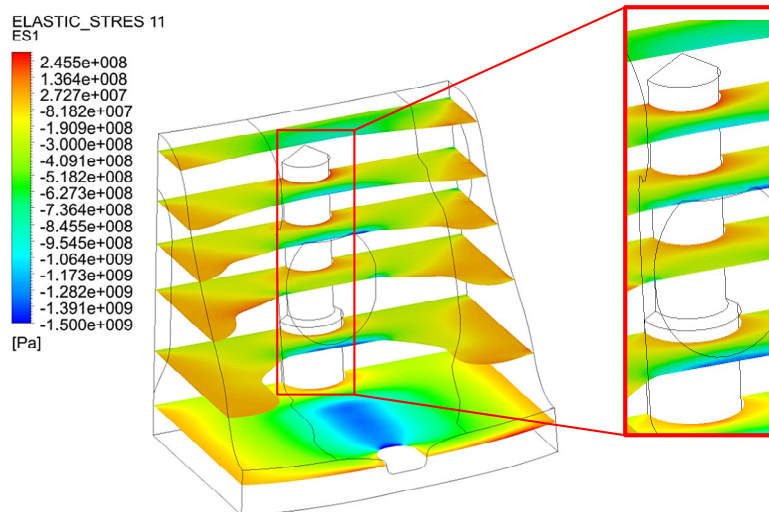


Fig.6. Surface elastic stress in the direction x.

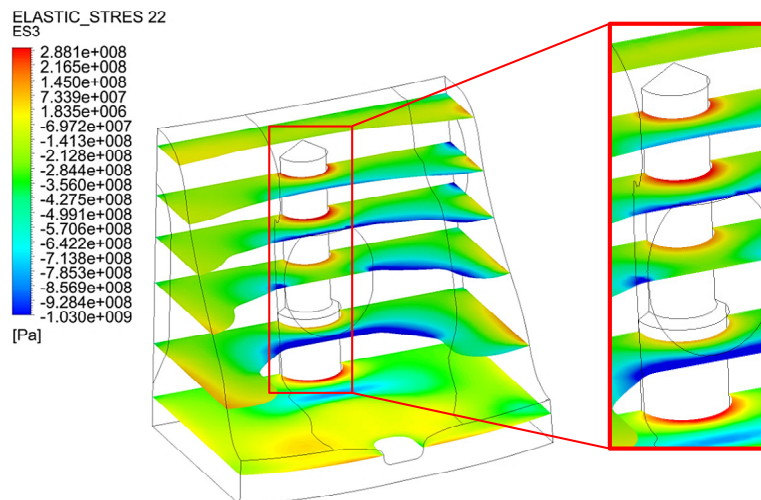


Fig.7. Surface elastic stress in the direction y.

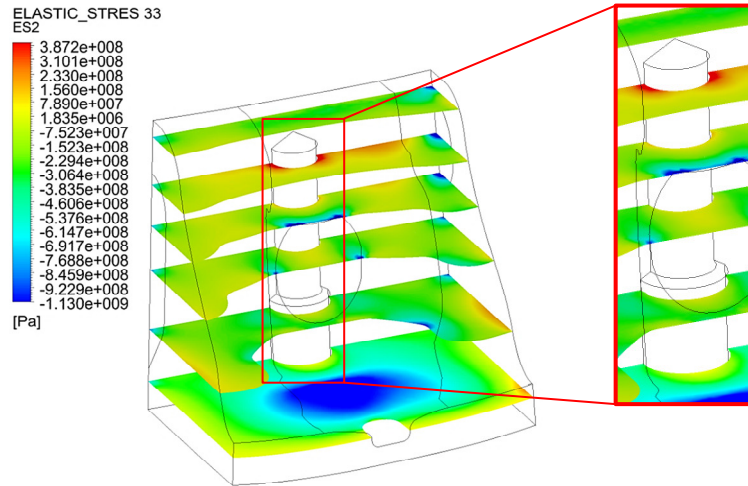


Fig.8. Surface elastic stress in the direction z.

The results of surface elastic stress at $t = 2s$ can be seen in the following figures:

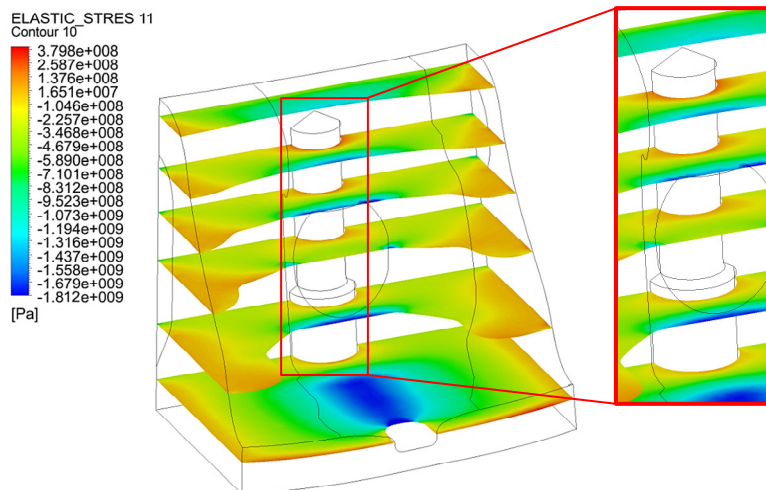


Fig.9. Surface elastic stress in the direction x.

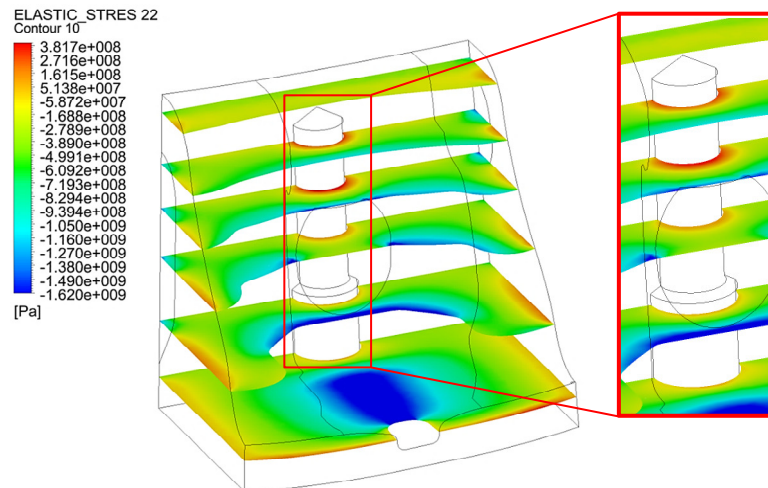


Fig.10. Surface elastic stress in the direction y.

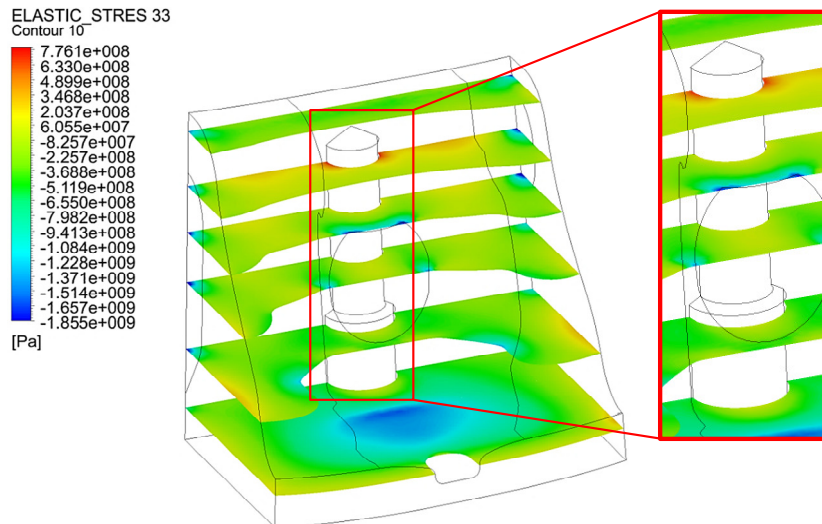


Fig.11. Surface elastic stress in the direction z.

4. Conclusion

Analysis of the core confirmed the assumption that the highest temperatures of the core are measured at the point of its longest contact with the liquid. The core surface temperatures are after 2.0 seconds considerably uneven and these differences are the cause of inner stress in the metal core. On the basis of heat stress, stress was determined including the speed of its changes. Given these changes, critical points were marked. In the next steps, core adjustments are going to be suggested with possible technologies of casting and cooling adjustments resulting in increased longevity. The current method of core heating before casting and after technological breaks with cooling solutions included will be assessed as well as this process may considerably influence longevity of the cores. In the next step, further core adjustments are going to be specified. These should lead to lowering of the number of core cracks. The newly designed shape is going to be analyzed with FEM and then tested in real operation.

Acknowledgement

The authors gratefully acknowledge for support the Slovak Grant Agency VEGA 1/0983/15.

References

- [1] MEŠKO, J., ZRAK, A., MULCZYK, K., TOFIL, S. *Microstructure Analysis of Welded Joints after laser Welding*, Manufacturing Technology, 14 (3).
- [2] ŽMINDÁK, M., NOVÁK, P., MEŠKO, J., *Metallurgy*, 49 (2), 2010.
- [3] SKOČILAS, J., SKOČILASOVA, B., SOUKUP, J.: *Determination of the rheological properties of thin plate under transient vibration*. Latin American Journal of Solids and Structures. Vol. 10(2013).
- [4] SCHOBIRI, M. *Fluid Mechanics for Engineers*. Springer, 2010.
- [5] FERZINGER, J. H., PERIČ, M. *Computational Methods for Fluid Dynamics*, London: Springer, 2002.
- [6] JANNA, W. S. *Introduction to Fluid Mechanics*, New York: CRS Press, 2009.



Increasing the Accuracy of Thermal Power of the Large Heat Source by Using Sensor Calibration

* Matej Palacka, * Michal Holubčík, * Peter Vician

*University of Zilina, Faculty of Mechanical Engineering, Department of Power Engineering, Univerzitna 1, 01026 Žilina, Slovakia, michal.holubcik@fstroj.uniza.sk

Abstract. Experiment is very important to obtain and verify the knowledge, experiences and hypotheses. The most important part of the experiment is to evaluate the measured values. Measurement accuracy depends on a number of factors. Deviations of instruments cannot eliminate or influence if it is neglect the possibility of using more precise measuring equipment. Another way for the most accurate results can be calibration. Calibration allows achieve measurement values with relatively high accuracy using less precision instruments. The paper deals about the problematic of thermal power measurement accuracy. Thermal power was measured on heat source with nominal thermal power 2 MW by using direct calorimetric method. There were used ultrasonic flow meter and type K thermocouples. Type K thermocouples are not very suitable for these applications because of their low precision. The paper presents the possibility of using calibrated thermocouples for the thermal power measurement with acceptable accuracy.

Keywords: Thermal power, Thermocouple, Resistance thermometer, Heat source, Calibration.

1. Introduction

Experiment is very important to obtain and verify the knowledge, experiences and hypotheses [1, 2, 3, 4]. The most important part of the experiment is to evaluate the measured values. It is necessary the measured values were the most accurate to achieve relevant results [5, 6, 7]. Measurement accuracy depends on a number of factors. The greatest factor is the accuracy of used measurement instruments. Deviations of instruments cannot eliminate or influence if it is neglect the possibility of using more precise measuring equipment. Another way for the most accurate results can be calibration [8, 9, 10].

Calibration is a comparison between measurements – one of known magnitude or correctness made or set with one device and another measurement made in as similar a way as possible with a second device. The device with the known or assigned correctness is called the standard [11, 12,]. Calibration allows achieve measurement values with relatively high accuracy using less precision instruments. As the result of the calibration is to increase confidence of the results and reduce requirements on measurement technology and costs of the experiment [13].

1.1. Thermocouples

Thermocouple is a sensor used to measure temperature. Thermocouples consist of two wire legs made from different metals. The wires legs are welded together at one end, creating a junction. This junction is where the temperature is measured. When the junction experiences a change in temperature, a voltage is created. The voltage can then be interpreted using thermocouple reference tables to calculate the temperature. This is due to Seebeck effect [14].

The Seebeck effect is the conversion of temperature differences directly into electricity. The Seebeck effect creates an electromotive force wherever there is a temperature gradient. This electromotive force can be used to perform work, however in the thermocouple it is used to develop an open-circuit voltage [15]. Under open-circuit conditions where there is no internal current flow, the gradient of voltage (∇V) is directly proportional to the gradient in temperature (∇T):

$$\nabla V = -S(T)\nabla T \quad (1)$$

where $S(T)$ is a temperature-dependent material property known as the Seebeck coefficient.

Type K thermocouples are the most common general purpose thermocouples with a sensitivity of approximately $41 \mu\text{V}/^\circ\text{C}$ (NiCr positive relative to Ni when the junction temperature is higher than the reference temperature). It is inexpensive, and a wide variety of probes are available in its -200°C to $+1350^\circ\text{C}$. [16]

Thermocouples including type K thermocouples are not appropriate for applications of thermal power of heat sources measurements [15]. The main problem is their low accuracy. There are the most frequently used paired resistance thermometers (for example PT100) for thermal power measurements.

1.2. The aim of the paper

The paper deals about the problematic of thermal power measurement accuracy on heat source with nominal thermal power 2 MW by using direct calorimetric method with thermocouples for measurement of heat-transfer fluid temperatures.

2. Thermal power of large heat source measurement

2.1. Heat source

The measurements were realized on heat source for straw burning with nominal thermal power 2 MW (Fig. 1). This device is located on southern part of Slovakia. It is used for heat production for dryer of agricultural crops for food industry. The energy chemically saved in straw is converted to the heat by burning square straw bales weighing 250 kg. Produced heat is transported from the heat source to the dryer by heat-transfer fluid (water) in twin tube system.



Fig. 1. The photo of tested heat source.

2.2. Thermal power measurement

Thermal power was measured on heat source by using direct calorimetric method. There were used ultrasonic flow meter and type K thermocouples for measurement of heat-transfer fluid (water) temperature in the inlet and in the outlet tube. There were used thermocouples NiCr – Ni OMEGA TFE with class 1 accuracy with deviations ± 1.5 K. The scheme of the measurement is on Fig. 2. The temperatures and volume flow of the heat-transfer fluid was recorded by logger in every 20 seconds and then measured values was exported to personal computer (PC).

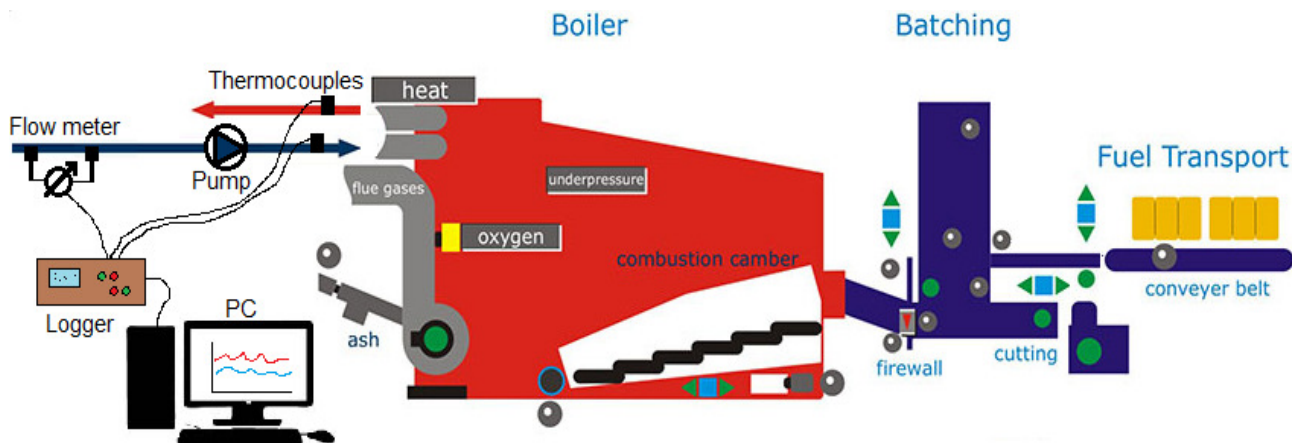


Fig. 2. The scheme of the thermal power of large heat source measurement.

On the Fig. 3 are time courses temperatures of inlet and outlet of heat-transfer fluid (water) and the thermal power of tested heat source.

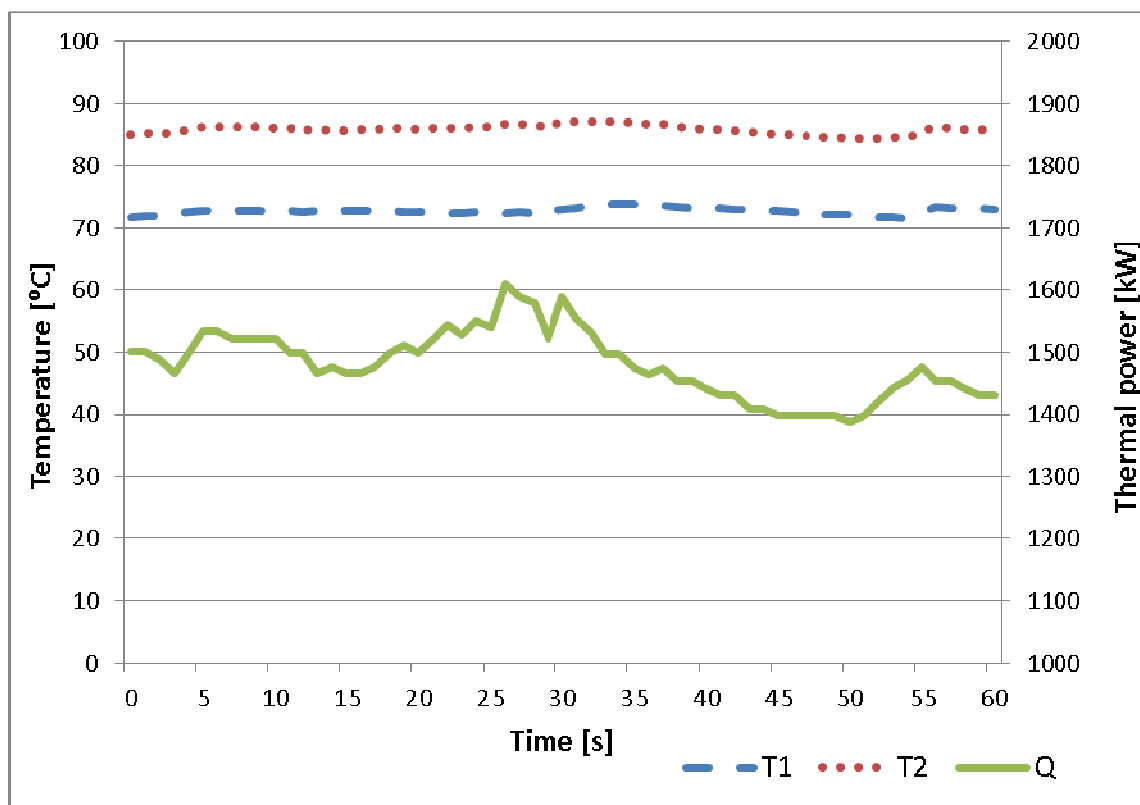


Fig. 3. Time courses of thermal power and temperatures

The thermal power of the heat source is depends on the temperature difference. In this measurement 1 °C temperature difference cause approximately 120 kW difference of the thermal power. Because of this it is necessary very accurate measurement of the temperature.



3. Calibration of the thermocouples

Calibration of the thermocouples was necessary because we wanted to reach the best possible accuracy of the thermal power measurement. Calibration of the thermocouples was realized by comparing the temperatures measured with thermocouples and resistance thermometer PT100 AHLBORN FPA32L0100 with 1/5 DIN class B accuracy. The maximum deviation of used PT100 thermometer is ± 0.06 K at 0 °C and ± 0.16 K at 100 °C. These values indicate that this used sensor is very accurate in comparison with thermocouples accuracy (± 1.5 K). The PT100 was connected to logger by connector ALMENO ZA9030FS5. Thermocouples and PT100 sensors were isolated in order to avoid mutual electrical influence of the sensors.

Requested constant temperature condition was secured through the heating/cooling circulator JULABO F34-HE with working temperature range $-30 \div 150$ °C and temperature stability 0.01 °C. The heating/cooling circulator was filled by distilled water and there were inserted the temperature sensors. After setting the desired constant temperature it was necessary wait to stabilize the temperatures and then the values can be recorded. The measurement was realized in temperature range $20 \div 95$ °C in steps 5 °C.

Measured values of the temperatures are in the tab. 1. The results show that the deviation between PT100 and thermocouples sensors was in range $-0.16 \div 0.35$ °C. During measurement on heat source temperature T_1 (Fig. 3) was between $70 \div 75$ °C (temperature difference was $-0.05 \div 0.02$ °C) and temperature T_2 was about 85 °C (temperature difference was 0.32 °C).

Temperatures [°C]				
PT100	T1	T2	$\Delta T1$	$\Delta T2$
20	20.06	20.24	0.06	0.24
25	25.04	25.20	0.04	0.20
30	30.10	30.14	0.10	0.14
35	34.84	35.09	-0.16	0.09
40	39.99	40.15	-0.01	0.15
45	44.95	45.25	-0.05	0.25
50	49.85	50.20	-0.15	0.20
55	54.90	55.30	-0.10	0.30
60	60.00	60.30	0.00	0.30
65	65.00	65.32	0.00	0.32
70	70.02	70.35	0.02	0.35
75	74.95	75.26	-0.05	0.26
80	79.96	80.23	-0.04	0.23
85	85.03	85.32	0.03	0.32
90	90.02	90.27	0.02	0.27
95	95.07	95.33	0.07	0.33

Tab. 1. Temperatures of and temperature differences of thermocouples.

4. Conclusion

The results of measurement show that the highest observed deviation of thermocouples in temperature range $20 - 95$ °C was 0.35 °C in comparison with more accurate PT100 thermometer. The deviations in temperature range of tested heat source with large nominal thermal power can cause relatively high differences in actually measured thermal power. Results of thermocouples calibration (-0.05 °C and 0.32 °C in the working temperature range $70 - 85$ °C) can cause thermal power differences about 42 kW of the tested large heat source with nominal thermal power 2 MW. This thermal power difference is pretty high value because this amount of heat would be enough for three average houses direct heating. Because of this it is necessary to use PT100 with higher accuracy or calibrated thermocouples for the thermal power determination of large heat sources.



Acknowledgement

This work was supported by the “Moderné zdroje tepla pre vykurovanie ”KEGA 070ŽU-4/2013” and “Výskumné centrum Žilinskej univerzity v Žiline ITMS 26220220183”.

References

- [1] MEŠKO, J., FABIAN, P., HOPKO, A., KONAR, R.: *Shape of heat source in simulation program SYSWELD using different types of gases and welding methods*. Strojárska technológia, vol. 16, n. 5, 2011, p. 6-11
- [2] KAPJOR, A., HUZVAR, J., FTOREK, B., VANTUCH, M.: *Criterion equations of heat transfer for “n“ horizontal pipes one above another at natural convection in linear method of approximation*, Communications: Scientific Letters of the University of Zilina. Vol. 16, no. 3A (2014), 54-61.
- [3] PILAT, P., PATSCH, M., MALCHO, M.: *Solar Heat Utilization for Adsorption Cooling Device*, EPJ Web of Conferences, vol. 25, 2012.
- [4] CERNECKY, J., NEUPAUEROVA, A., JANOSKO, I., SOLDAN, M.: *Environmental Technology (in Slovak)*, Technická univerzita: Zvolen, 274 p., 2010.
- [5] DELIISKI, N., DZURENDA L., BREZIN V.: *Calculation of the heat energy needed for melting of the ice in wood materials for veneer production*, Acta Facultatis Xylogiae Zvolen Vol. 55 No. 2/2013, pp. 21–32.
- [6] SOOS, L., KOLEJAK, M., URBAN, F.: *Biomass - Renewable Energy Source (in Slovak)*, Vert: Bratislava, 2012.
- [7] HUZVAR, J., KAPJOR, A.: *Micro-cogeneration incl. the Conversion of Chemical Energy of Biomass to Electric Energy and the Low Potential Heat*, Proc. of AIP Conference, vol. 1337, 2011, 40-42.
- [8] VITAZEK, I., VITAZKOVA, B., PLOTH, J.: *Production of Gas Emissions from Biomass Heat Source*. Engineering Mechanics, vol. 20, 2013, No. 3/4, 289-298. ISSN 1805-4633.
- [9] TAUS, P., TAUSOVA, M.: *Economic Analysis of FV Power Plants According to Installed Performance*, Acta Montanistica Slovaca, vol. 14, No. 1, 2009
- [10] ČAJA, A., NEMEC, P., MALCHO, M.: *Dependence of electric strength on the ambient temperature*, AIP Proceedings, Vol. 1608 (2014), p. 12-15., 2014
- [11] NEMEC, P., ČAJA, A., MALCHO, M.: *Mathematical Model for Heat Transfer Limitations of Heat Pipe*, Mathematical and Computer Modelling, vol. 57, No. 1-2, 2013, 126-136.
- [12] CHABADOVÁ, J., PAPUČÍK, Š., NOSEK, R.: *Particle emissions from biomass combustion*, AIP Proceedings, Vol. 1608 (2014), p. 67-70., 2014
- [13] PUŠKÁR, M., BRESTOVIČ, T., JASMINSKÁ, N. *Numerical simulation and experimental analysis of acoustic wave influences on brake mean effective pressure in thrust-ejector inlet pipe of combustion engine*. International Journal of Vehicle Design, vol. 67, iss. 1, s. 63-76, 2015
- [14] ČIERNY, J., PATSCH, M., JANDAČKA, J. *Mikrokogeneračné jednotky na zemný plyn pre zásobovanie domácností energiami*, Alternatívne zdroje energie ALER 2014. Liptovský Mikuláš : SES, p. 171-175, 2014.
- [15] KOLKOVÁ, Z., MALCHO, M. *Analysis of effect various types of working fluids on performance of pulsating heat pipe*, European International Journal of Science and Technology, , vol. 3, no. 4, p. 7-14, 2014
- [16] KOLKOVÁ, Z., MALCHO, M. *Effect of working fluids on thermal performance of closed loop pulsating heat pipe*. In: AIP Conference Proceedings, vol. 1608, p. 128-131, 2014



Comparison Study of Fully Stress Design Algorithms for Discrete Optimization of Truss Structures

*Peter Pecháč, *Milan Sága

*University of Žilina, Faculty of Mechanical Engineering, Department of Applied Mechanics, Univerzitná 1, 01026 Žilina, Slovakia, {peter.pechac, milan.saga}@fstroj.uniza.sk

Abstract. This paper deals with comparison of newly developed optimization algorithms based on the fully stress design (FSD) method for discrete optimization of truss structures subjected to stress constraint. The FSD method is based on the idea that every structural member of a structure should be loaded up to the stress limit, this means that the material is present only where it is needed and this way minimal weight can be achieved. The optimization algorithms were programmed in programming language Matlab and finite element models were created and calculated by software developed by the authors also in programming language Matlab. The first part of the paper is dedicated to the philosophy and capabilities of the FSD method, followed by theoretical basics of stress calculation in a truss finite element and description of four optimization algorithms based on principles of the FSD method. The second part contains testing example of a statically loaded truss structure. The conclusion deals with an assessment of performance of the proposed algorithms.

Keywords: Structural optimization, Fully Stress Design, Finite Element method, Regula – Falsi method, Newton's tangent method, Matlab.

1. Introduction

Structural optimization has always been a part of machine designing. Nowadays when the economic and ecologic situation calls for savings of material, lowering operational costs, fuel consumption and emissions, it has become more important than ever before. The complexity of problems being solved grows with the improvement of computer performance and as the products are improved through optimization, the optimization algorithms themselves also need to be improved, mainly in terms of their effectiveness.

Not all optimization algorithms are equally effective for every problem, some can excel in one problem but suffer great performance drop in other and some methods can be suitable for a wide range of problems but are significantly slower. The FSD method belongs to the group of algorithms which are extremely effective for one type of problem but cannot be used for other problems.

2. Fully stress design method

As the name fully stress design (FSD) suggests, this method is based on designing structural components to their stress limit. This method is popular for optimization of truss structures mainly due to its simplicity and effectiveness [4].

This method is indeed very effective however its use is limited and cannot be used for other criteria except stress constraint. Other optimization methods like gradient methods, simplex or genetic algorithms require evaluation of multiple points in the optimization landscape and the number of evaluations rises with the number of optimization variables. For example the Nelder - Mead simplex method and gradient based methods need $n+1$ evaluations per iteration (n is the number of optimization variables), global optimization methods like genetic algorithms generally require tens/hundreds/thousands of evaluations per iteration. On the other hand the FSD method requires only one evaluation per iteration, regardless of the number of optimization variables.

The importance of these properties rises when either the number of optimization variables or the time required for evaluation of objective function is high. The time required for evaluation using the finite element method can vary from mere seconds to hours or even days depending on the complexity of the model and so the evaluation of objective function can be considered as expensive.

Unlike the other mentioned optimization methods, the fully stress design method is not based on search for extremum (minimum or maximum), but on various root-finding algorithms. The proposed algorithms are based on the Regula Falsi method and Newton's method.

The Regula Falsi method (often called false position method) is based on similarity of triangles which have common vertex called "the false point" hence, the false position method. The Newton's method is based on an assumption that the examined function has continuous first derivative. All of the presented algorithms carry-out uni-dimensional optimization for every optimization variable independently and the derivative is approximated numerically from the results of previous iteration.

3. Calculation of stress and theoretical basics of finite element method for truss elements

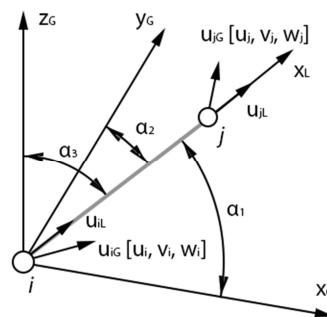


Fig. 1 truss element in 3D space

In three dimensional space we can write the relation between displacements in local and global coordinate system using direction cosines of angles α_1 , α_2 and α_3 as follows [1]:

$$\begin{bmatrix} u_{iL} \\ u_{jL} \end{bmatrix} = \begin{bmatrix} c_1 & c_2 & c_3 & 0 & 0 & 0 \\ 0 & 0 & 0 & c_1 & c_2 & c_3 \end{bmatrix} \cdot \begin{bmatrix} u_{iG} \\ v_{iG} \\ w_{iG} \\ u_{jG} \\ v_{jG} \\ w_{jG} \end{bmatrix} \Rightarrow \mathbf{u}_L = \mathbf{T} \cdot \mathbf{u}_G \quad (1)$$

where $c_1 = \cos(\alpha_1)$, $c_2 = \cos(\alpha_2)$, $c_3 = \cos(\alpha_3)$. Then the final relation for stiffness matrix of truss in 3D space will be:

$$\mathbf{K}_G = \mathbf{T}^T \cdot \mathbf{K} \cdot \mathbf{T} = \begin{bmatrix} c_1 & 0 \\ c_2 & 0 \\ c_3 & 0 \\ 0 & c_1 \\ 0 & c_2 \\ 0 & c_3 \end{bmatrix} \cdot \frac{E \cdot A}{l} \cdot \begin{bmatrix} 1 & -1 \\ -1 & 1 \end{bmatrix} \cdot \begin{bmatrix} c_1 & c_2 & c_3 & 0 & 0 & 0 \\ 0 & 0 & 0 & c_1 & c_2 & c_3 \end{bmatrix} \quad (2)$$

During the calculation of axial force in a truss we have to transform displacements from global coordinate system into local coordinate system. To simplify this complex and computationally expensive process we can use relations for direct calculation of axial forces from displacements in global coordinate system [2].

$$N = \frac{E \cdot A}{l} \cdot [c_1 \cdot (u_{jG} - u_{iG}) + c_2 \cdot (v_{jG} - v_{iG}) + c_3 \cdot (w_{jG} - w_{iG})] \quad (3)$$

Axial stress in the truss is then calculated as follows:

$$\sigma = \frac{N}{A} = \frac{E}{l} \cdot [c_1 \cdot (u_{jG} - u_{iG}) + c_2 \cdot (v_{jG} - v_{iG}) + c_3 \cdot (w_{jG} - w_{iG})] \quad (4)$$

4. Description of the proposed algorithms

4.1. Algorithm no. 1 – classical FSD

The algorithm no. 1 is the classical interpretation of the FSD method for optimization of cross-section areas of truss structures and will serve as a standard for performance assessment. This algorithm is based on the assumption of independence between axial forces and size of the cross-section areas of statically determined truss structures.

Geometrical interpretation of this method is depicted on Fig. 2. From the similarity of triangles 0AB and 0CD we obtain:

$$\frac{\sigma_{ieq}^{(k)}}{\left(\frac{1}{A_i}\right)^{(k)}} = \frac{\sigma_L}{\left(\frac{1}{A_i}\right)^{(k+1)}} \quad (5)$$

From the geometrical interpretation follows that the new estimation $A_i^{(k+1)}$ is approximated from points $[0, 0]$ and $\left[\left(\frac{1}{A_i}\right)^{(k)}, \sigma_L\right]$. In numerical mathematics this method is called Regula – Falsi. From the equation 5 we can derive familiar iterative formula for FSD:

$$\sigma \text{ pred}_n^{(k+1)} = \sigma^{(k)} \left(\frac{A^{(k)}}{A_n}\right) \quad (6)$$

Where i is the number of optimization variable, $\sigma \text{ pred}_n^{(k+1)}$ is predicted stress for cross-section area A_n in the $(k+1)^{\text{st}}$ step, $\sigma^{(k)}$ is stress in the k^{th} step for area $A^{(k)}$, $A^{(k)}$ is the area in the k^{th} step, A_n is the n^{th} area from the vector of design variables. After the prediction of stress for every design variable, the smallest cross-section area which satisfies the stress condition $\sigma^{(k)} \left(\frac{A^{(k)}}{A_n}\right) \leq \sigma_L$ is chosen.

4.2. Algorithm no. 2 – squared FSD

This method was used for optimization of shell structures, where it proved to be quite efficient. The linear prediction of stress from the algorithm no. 1 is changed to nonlinear by adding square to the ratio of cross-section areas see Fig. 3. This minor change reduces the change of optimization variable between iteration steps and stabilizes convergence [3]. Prediction of axial stress is done by following formula:

$$\sigma \text{ pred}_n^{(k+1)} = \sigma^k \left(\frac{A^{(k)}}{A_n}\right)^2 \quad (7)$$

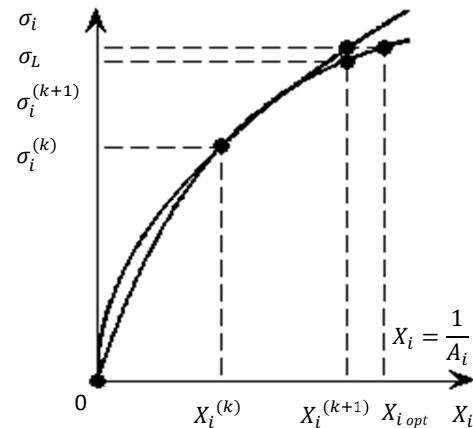
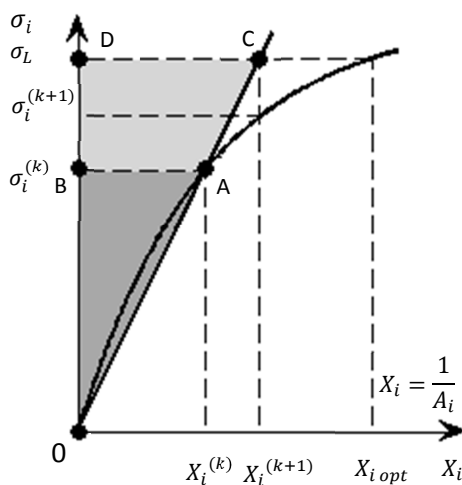


Fig. 2 Geometrical interpretation of the algorithm no. 1 Fig. 3 Geometrical interpretation of the algorithm no. 2

4.3. Algorithm no 3 – Newton’s method for prediction of axial stress

This method is based on Newton’s tangent method. The derivative of the unknown relation between cross-section area and axial stress is solved numerically using results from two previous iteration steps. Since results from two previous iteration steps are not available in the first iteration, another method has to be used. During the tests we used the algorithm no. 1 for the first iteration.

The geometrical interpretation of the stress prediction is depicted in the Fig. 4. From the similarity of triangles ABC and BDE we obtain relation:

$$\frac{\sigma_{ieq}^{(k)} - \sigma_{ieq}^{(k-1)}}{\left(\frac{1}{A_i}\right)^{(k)} - \left(\frac{1}{A_i}\right)^{(k-1)}} = \frac{\sigma_L - \sigma_{ieq}^{(k)}}{\left(\frac{1}{A_i}\right)^{(k+1)} - \left(\frac{1}{A_i}\right)^{(k)}} \quad (8)$$

Then we can derive the following iterative formula:

$$\left(\frac{1}{A_i}\right)^{(k+1)} = \left(\frac{1}{A_i}\right)^{(k)} + \frac{\sigma_L - \sigma_{ieq}^{(k)}}{\sigma_{ieq}^{(k)} - \sigma_{ieq}^{(k-1)}} \left[\left(\frac{1}{A_i}\right)^{(k)} - \left(\frac{1}{A_i}\right)^{(k-1)} \right] \quad (9)$$

However for consistency with the other algorithms we used modified formula for prediction of axial stress during tests. The predicted stress in (k+1) iteration step for area S_n is calculated as follows:

$$\sigma pred_n^{(k+1)} = \frac{-(A^{(k-1)}\sigma^{(k-1)}A^{(k)} - A^{(k-1)}\sigma^{(k-1)}A_n - A^{(k-1)}\sigma^k A^{(k)} + A^{(k)}\sigma^{(k)}A_n)}{(A^{(k-1)}A_n - A^{(k)}A_n)} \quad (10)$$

where $\sigma pred_n^{(k+1)}$ is the predicted axial stress for area A_n in (k+1)th iteration step, $\sigma^{(k)}$ is axial stress in kth iteration step for area $A^{(k)}$, $A^{(k)}$ is area in the kth iteration step, A_n is nth area from the vector of design variables, $A^{(k-1)}$ is the area in the (k-1st) step, $\sigma^{(k-1)}$ is axial stress in the (k-1st) step.

4.4. Algorithm no. 5 – Newton’s method for prediction of axial force

Similar approach as in the algorithm no. 3 is used for prediction of axial force. The geometrical interpretation of the prediction of axial force is depicted in the Fig. 5. Axial force is predicted based on similarity of triangles ABC and BDE. The predicted axial force is calculated as follows:

$$F pred_n^{(k+1)} = F^{(k)} + (F^{(k)} - F^{(k-1)}) \left(\frac{\left(\frac{1}{A_n} - \frac{1}{A^{(k)}}\right)}{\left(\frac{1}{A_n} - \frac{1}{A^{(k-1)}}\right)} \right) \quad (11)$$

The predicted axial stress can be calculated as follows:

$$\sigma pred_n^{(k+1)} = \frac{F_{approx}^{(k+1)}}{A_n} \quad (12)$$

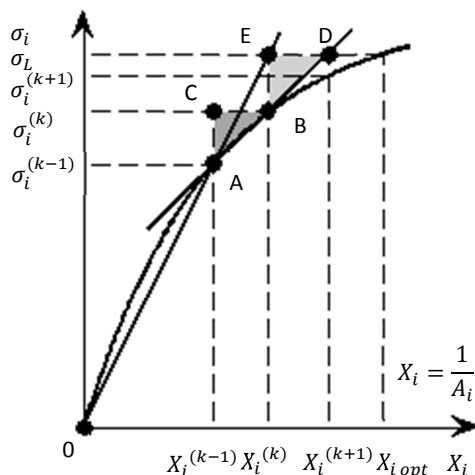


Fig. 4 Geometrical interpretation of algorithm no. 3

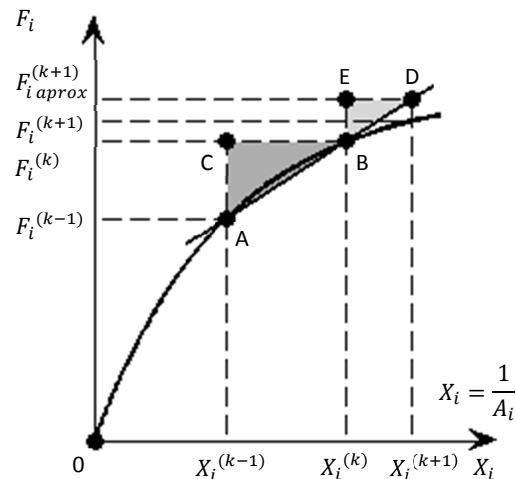


Fig. 5 Geometrical interpretation of algorithm no. 5

5. Testing example

5.1. Description of the problem

Truss structure is divided into 6 optimization groups (see Fig. 6). Design variables are discrete values of cross-section areas of normalized steel profiles.

Material model: linear elastic isotropic – steel $E = 210\,000\text{ MPa}$, $\sigma_L = 120\text{ MPa}$

Boundary conditions:

Load: lone forces (red arrows) and own mass, $g = 9,81\text{ ms}^{-2}$, $\rho = 7850 \cdot 10^{-9}\text{ kg mm}^{-3}$

$$F = \begin{bmatrix} 1000 \\ -1000 \\ -10000 \end{bmatrix}$$

Deformational:

The structure has fixeded degrees of freedom in 6 points marked by green color:

1. $[ux, uy, uz]$,
2. $[ux, uz]$,
3. $[ux]$,
4. $[uy, uz]$,
5. $[uz]$,
6. $[ux]$.

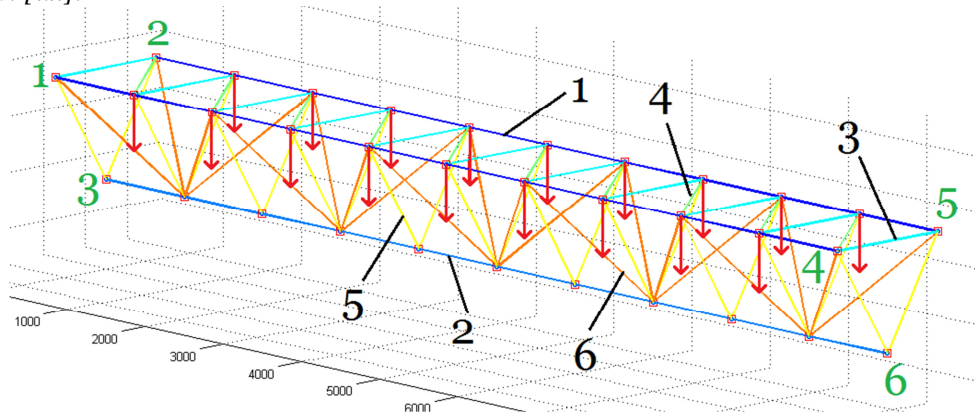


Fig. 6 Geometry, optimization groups and boundary conditions.

5.2. Results of the testing example

Algorithm	1	2	3	4
Final mass [Kg]	533.5	553.1	1123.4	548.4

Tab. 1. Final mass of the best solution found by algorithm 1 - 4.

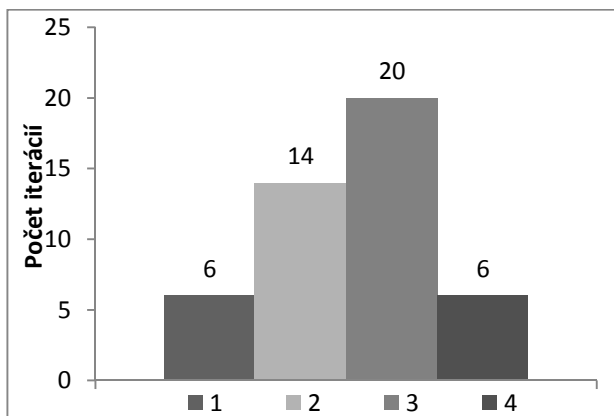


Fig. 7 Number of iteration steps for individual algorithms

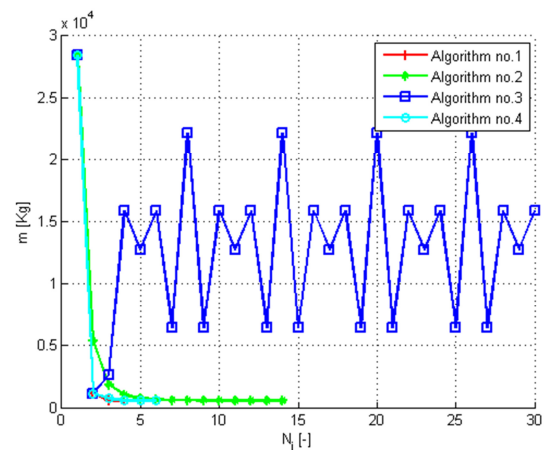


Fig. 8 history of mass convergence for each algorithm

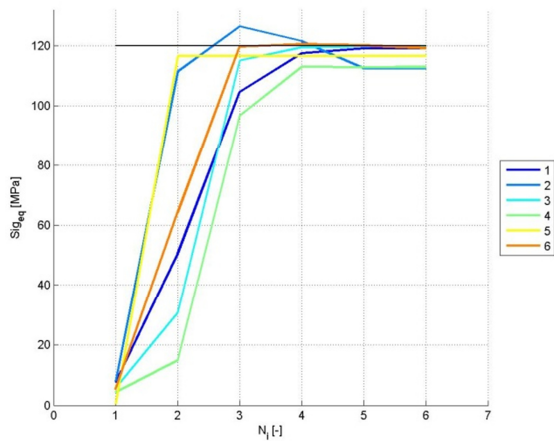


Fig. 9. History of stress convergence - Algorithm No. 1

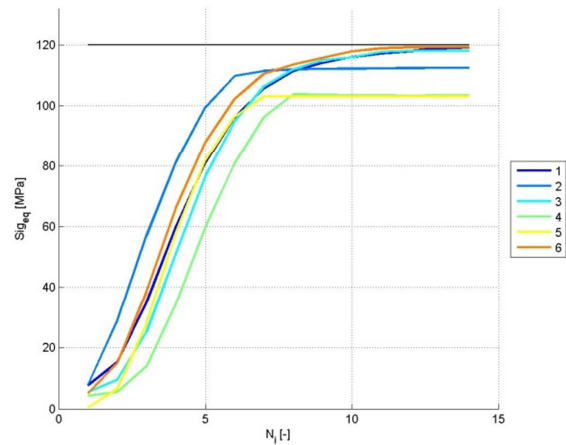


Fig. 10. History of stress convergence - Algorithm No. 2

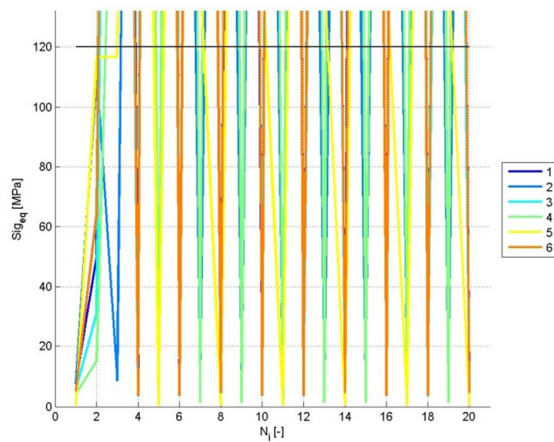


Fig. 11. History of stress convergence - Algorithm No. 3

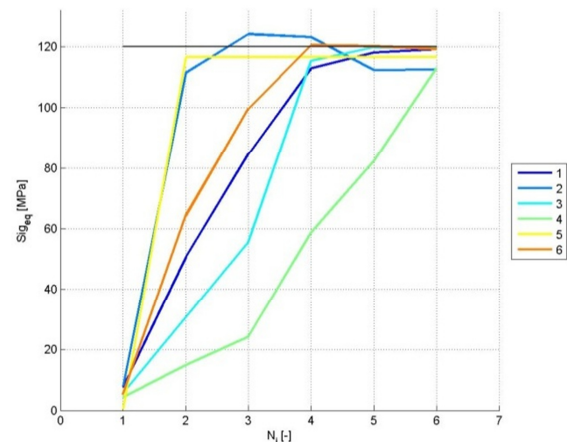


Fig. 12. History of stress convergence - Algorithm No. 4

6. Conclusion

The numerical testing proved that the classical approach to FSD method is indeed the most suitable method for optimization of truss structures. The algorithm no. 2 – squared FSD did not bring any improvement over the classical approach in contrary with our experience with thin shell structures. The algorithm no. 3 – Newton’s method for prediction of axial stress did not converge at all and showed similar behavior when tested on other models. On the other hand, algorithm no. 4 - Newton’s method for prediction of axial force performed well but when compared to the classical approach, despite its relative complexity it did not outperform the classical approach.

Acknowledgement

This work has been supported by grant project VEGA No. 1/0234/13.

References

- [1] BATHE, K. J., WILSON, E. 1976. *Numerical Methods in Finite Element Analysis*. New Jersey : Prentice-Hall, 1976. ISBN 9780136271901.
- [2] COOK, R. D. 1981. *Concepts and Applications of Finite Element Analysis*. New York : Wiley, 1981.
- [3] SÁGA, M., PECHÁČ, P., VAŠKO, M.. *FSD and its modifications for shell finite elements*. American Journal of Mechanical Engineering 1.7 (2013): 427-433.
- [4] SÁGA M., VAŠKO M., KOCÚR R., TOTĤ. E., KOHÁR R. 2006. *Aplikácia Optimalizačných Algoritmov v Mechanike Telies*. Žilina : Vedecko-Technická Spoločnosť pri Žilinskej Univerzite, 2006. ISBN 9788096916599.



Energy Accumulation and Storage of Natural Gas in the Form of Compressed Natural Gas, Liquefied Natural Gas and Methane Hydrates

*Štefan Rezníčák, *Milan Malcho

*University of Zilina, Faculty of Mechanical Engineering, Department of Power Engineering, Univerzitná 8215/1, 01026 Žilina, Slovakia, {stefan.reznicak, milan.malcho}@fstroj.uniza.sk

Abstract. This paper deals with accumulation of high potential energy through the process of methane hydrates generation. We will briefly describe three methods of energy storage of natural gas in the form of compressed natural gas, liquefied natural gas and methane hydrates. The paper takes into account the energy input necessary to achieve the temperature and pressure conditions necessary for the various forms of accumulation and storage. It also includes a comparison of pressure and temperature conditions between different forms. The last criterion is the specific energy, how much energy can be accumulated in 1 kilogram.

Keywords: Energy accumulation, Liquefied natural gas, Compressed natural gas, Methane Hydrates.

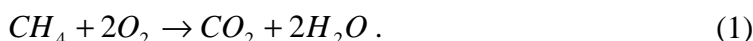
1. Introduction

Humanity currently uses different sources of energy: renewable forms of energy such as wind, hydro, solar and geothermal energy and non-renewable sources (coal, oil, and natural gas). Out of the non-renewable sources of energy natural gas is considered to be environmentally friendly fuel because it is a combination of the simplest saturated hydrocarbons, predominantly formed by methane. A high proportion of hydrogen in methane is the cause of the low proportion of CO₂ per unit of energy released.

Natural gas as a source of energy had been accumulated in the form of compressed natural gas and liquefied natural gas. After finding large deposits of methane hydrates, whether in permafrost or under the ocean floor, in addition to mining, people began to consider the possibility of accumulating the energy in this form. It was caused by the fact that methane hydrates are stable at relatively high temperatures up to 18 °C and low pressure, which is close to atmospheric pressure.

1.1. Methane

It is the simplest hydrocarbon and the main component of natural gas with the chemical formula CH₄. Under normal conditions (pressure of 101 325 Pa, the temperature of 0 °C) it is lighter than air, colourless, not poisonous, but suffocating and oppressive. Since it is odorless, it is odorized with tetrahydrothiophene [1]. Combustion of methane produces carbon dioxide and water "(1)."



Conditions	Temperature (K)	Pressure (MPa)
	273.15	atmospheric
Molar mass (kg/kmol)	16.04	
Density (kg/m ³)	0.71562	
Volume (m ³ /kg)	1.3974	
Heat value of methane (MJ/m ³)	36	
Heat value of natural gas (MJ/m ³)	34.776	

Tab. 1. Properties of methane under normal conditions.

2. Forms of Natural Gas Energy Accumulation

Up to the present, natural gas has been accumulated and stored as compressed natural gas and liquefied natural gas. Currently, methane hydrates are considered to be a new form of accumulation and storage.

2.1. Compressed natural gas (CNG)

It is natural gas compressed to the pressure of 20-22 MPa. It is used as fuel for buses of urban and suburban transport, cars and trucks as well as ships, trains, tractors and motorcycles. It is stored in containers of cylindrical or spherical shape, see Fig.1.

Conditions	Temperature (K)	Pressure (MPa)
	273.15	20
Density (kg/m ³)	141.253	
Volume (m ³ /kg)	0.0070795	
Energy volume (m ³ natural gas in 1 m ³)	198.81	
Energy density (GJ/m ³)	6.914	
Specific energy (MJ/kg)	48.946	
Energy inputs (kJ/kg)	856.885	

Tab. 2. Properties of compressed natural gas.



Fig. 1. Location CNG tank in the vehicle.

2.2. Liquefied natural gas (LNG)

It is natural gas in the liquid state. It does not occur naturally in the environment. After mining, LNG is liquefied under atmospheric pressure and at the temperature of -162 to -170 °C in order to be transported by means of tankers more easily. It is a bluish, clear, odourless, non-corrosive and non-toxic liquid with low viscosity. It is used as fuel for long-distance buses and freight transport and in refrigerated trucks, in which liquid gas is used as an evaporative cooling contractor. It is also used in LCNG filling stations where it is transported as a liquid under high pressure into the evaporator. From there it fills the gaseous CNG pressure container.

Conditions	Temperature (K)	Pressure (MPa)
	111.15	101.325
Density (kg/m ³)	410.5	
Volume (m ³ /kg)	0.002436	
Energy volume (m ³ natural gas in 1 m ³)	577.77	
Energy density (GJ/m ³)	20.093	
Specific energy (MJ/kg)	48.946	
Energy inputs (kJ/kg)	904.769	

Tab. 3. Properties of liquefied natural gas.



Fig. 2. Cryogenic tank of liquefied natural gas.

2.3. Methane hydrates

Methane hydrates are solid crystalline substances resulting from contact of liquid water with small hygroscopic molecules of methane. They form a cubic crystal structure I. It consists of two small spherical cavities with twelve pentagonal walls (5^{12}), followed by six large cavities with two hexagonal walls and twelve pentagonal walls ($5^{12}6^2$) [2].

Actually, it is frozen methane in ice. In this form it is stable at relatively high temperatures, up to 18 °C, and a low pressure, which is close to atmospheric pressure. 70-170 m³ of methane can be accumulated in one m³ of ice, which makes it a very interesting way energy accumulation for the future.

Conditions	Temperature (°C)	Pressure (MPa)
	0	1.77
Density (kg/m ³)	900	
Volume of methane in methane hydrates (kg/m ³)	120	
Volume (m ³ /kg)	0.00833	
Energy volume (m ³ natural gas in 1 m ³)	168.90	
Energy density (MJ/m ³)	5.873	
Specific energy (MJ/kg)	6.526	
Energy inputs (kJ/kg)	1 293.253	

Tab. 4. Properties of methane hydrates.



Fig. 3. Methane hydrate know also as “burning ice”.

Fig. 4 shows the comparison of energy inputs and pressure conditions. Fig. 5 shows the comparison of temperature conditions and specific energy.

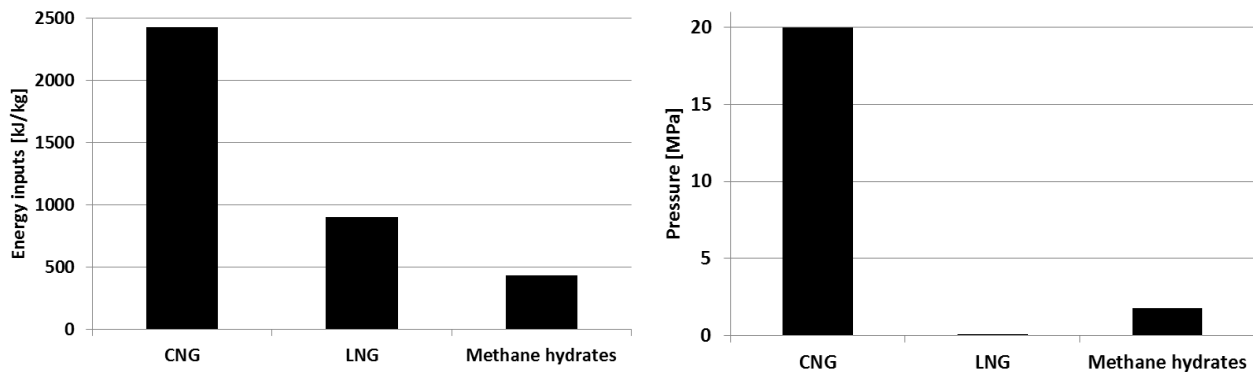


Fig. 4. Energy inputs and pressure conditions.

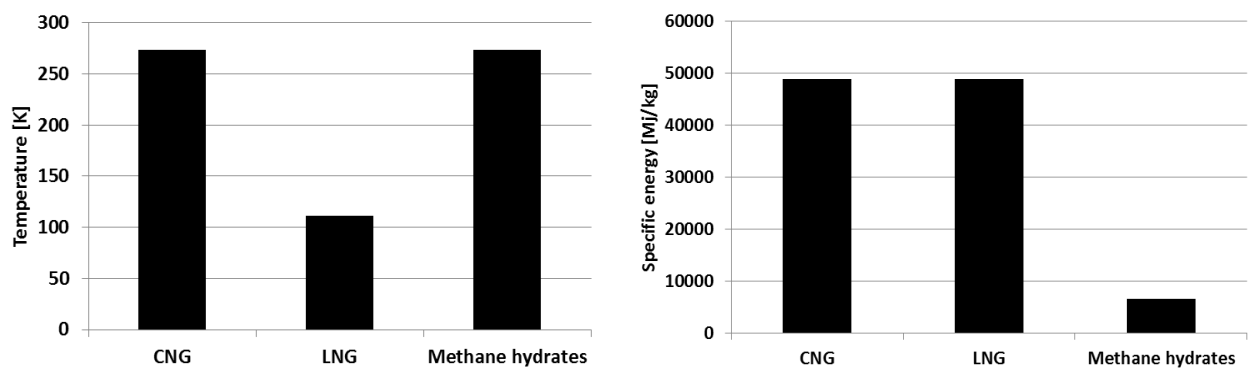


Fig. 5. Temperature conditions and specific energy.

3. Conclusion

The comparison shows that methane hydrates have the lowest energy input (432.21 kJ/kg). The largest energy input has CNG (2 429.58 kJ/kg) and the energy input of LNG is 905.71 kJ/kg. Compared to methane hydrates, the energy input of CNG and LNG is 5.6 times and 2.1 times higher. In terms of pressure conditions, the accumulation in the form of LNG and methane hydrates is more advantageous. When comparing temperature conditions, CNG and methane hydrates are preferable. When comparing the specific energy, methane hydrates have 7.5 times less energy than LNG and CNG at the same weight, because they consist of 86,6% water.

Acknowledgements

This paper was developed under the project “Chladienie výkonových elektronických systémov pomocou chladiacich obehov bez mechanických pohonov” APVV no. 0577 – 10.

References

- [1] PILÁT, P., PATSCH, M., JANDAČKA, J. *Analysis of problems with dry fermentation process for biogas production*. Experimental fluid mechanics 2011. Liberec, 2011.
- [2] CARROLL, J. J. *Natural gas hydrates: A guide for engineers*, Elsevier Science. Burlington, 2003.



The Heat Transfer from the Complex Shaped Piping System

*Štefan Rezničák, **Helena Smatanová, **Andrej Kapjor

*University of Zilina, Faculty of Mechanical Engineering, Department of Power Engineering, Univerzitná 8215/1, 01026 Žilina, Slovakia, {stefan.reznicak}@fstroj.uniza.sk

**University of Zilina, Faculty of Mechanical Engineering, Department of Power Engineering, Univerzitná 8215/1, 01026 Žilina, Slovakia, {helena.smatanova, andrej.kapjor}@fstroj.uniza.sk

Abstract. This paper describes the heat transport from the complex shaped piping system which is made of a tube of circular section wound up into a planar spiral. Its goal is to determine the thermal performance of the system and to verify the impact of the size of the geometric parameter on its thermal performance. The paper shows the results of experimental measurements of heat output and the verification of the influence of the geometric parameter on its thermal performance.

Keywords: heat transport, heat transfer, piping system, thermal performance of piping system.

1. Introduction

When discussing various piping systems with flow and heat transfer, the current issue is the efficiency of heat distribution in complex piping systems.

Complex shaped piping systems include piping systems of different cross-sections (circular, non-circular), various shapes (tubes, slats, ribbed tubes, ...), and various arrangement (vertical pipes, horizontal pipes, closed profiles, which have the appearance of a ladder, asymmetrically arranged tubes, tube coiled in a spiral, ...).[1]

Performance of complex piping systems depends on several factors:

- the arrangement of the heat exchange surfaces (tubes, slats),
- the size and material of the heat exchange surface,
- the speed of the fluid flow,
- regularization of the flow of heat transfer fluid in different parts (tubes) of the system.

Regularization of the flow in different parts of the system should result in a uniform distribution of surface temperatures in different parts (tubes) of the system and ultimately in the enhanced thermal performance.

2. Complex shaped piping system

The complex shaped piping system was made up of circular tubes with an external diameter of 20 mm, a wall thickness of 2 mm and length of 13 m, wound into a planar spiral. The pipes were made from multilayer polyethylene-aluminum (Ivar Alpex Turatec Multi PE-RT/AL/PE-RT 20 x 2), which is used for heating, underfloor heating and potable water installations.

Thermal conductivity (W/m.K)	0,45
Max. pressure (MPa)	1
Max. water temperature (°C)	95

Tab. 1. Properties of Ivar Alpex Turatec Multi PE-RT/AL/PE-RT 20 x 2.

Heat transfer from the surface of the pipe to the heated area of this system is carried out as a combination of natural convection and radiation. Here again, the determining parameters are the geometry arrangement of the pipes and the diameter of the pipes. An important parameter for the natural convection and radiation is the temperature of the pipe surface.[2]

3. Experimental measurement

The measurement of thermal performance of the system was performed by a method used for measuring the thermal performance of heaters according to STN EN 442-2 Radiators and convectors. Part 2: Test methods and rating.

Experiments have helped us to verify the accuracy of the calculation methods. Experimental results have also served to refine the calculation procedure. We experimentally determine the thermal performance of the system and verified the influence of the size of the gaps between the windings on thermal performance.

A total of 12 measurements were performed: three measurements for the two types of connection and for the two distances a), b), c), d), see Fig. 1. We performed measurements of the piping system at temperature differences: $\Delta T = (30 \pm 2.5)$ K, i.e. $t_s = 50$ °C, $\Delta T = (50 \pm 2.5)$ K, i.e. $t_s = 70$ °C, $\Delta T = (60 \pm 2.5)$ K, i.e. $t_s = 80$ °C. ΔT is the temperature difference of surroundings (20 °C) and the heat transfer fluid.[3] First to be realized was the measurement of temperature gradient 55/45 °C, then at nominal 75/65 °C and at the end of the temperature gradient 85/75 °C.

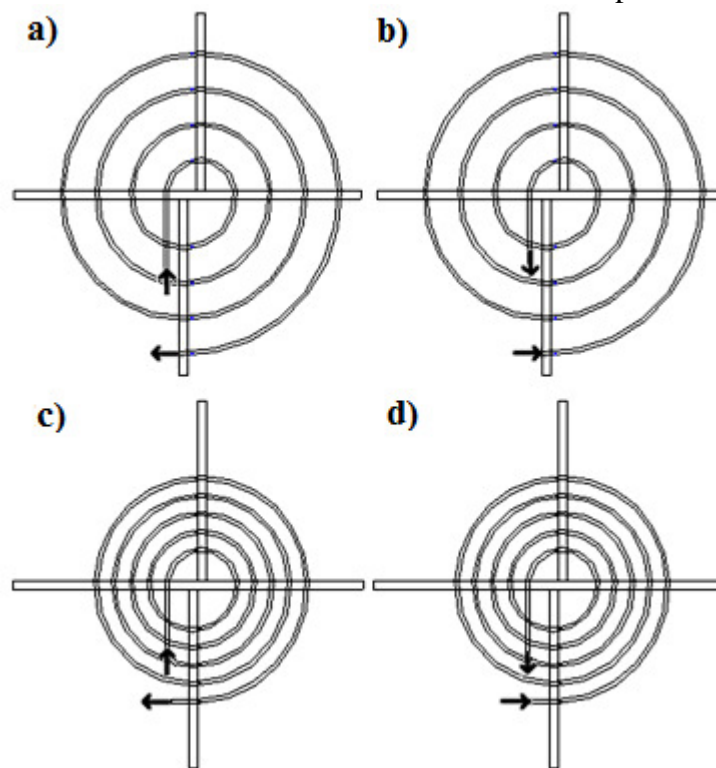


Fig. 1. Connection types: a) at a distance of 20 cm (10 d) between each winding and the inlet at the center of the system, b) at a distance of 20 cm (10 d) between each winding and the inlet on the edge of the system, c) at a distance of 10 cm (5 d) between each winding and the inlet at the center of the system, d) at a distance of 10 cm (5 d) between each winding and the inlet on the edge of the system.

The surface temperatures of windings were measured by thermocouple sensors NiCr-Ni. 8 sensors were used for the connections a) and b), and 10 sensors for the connections c) and d). The distribution of sensors is shown on Fig. 2.

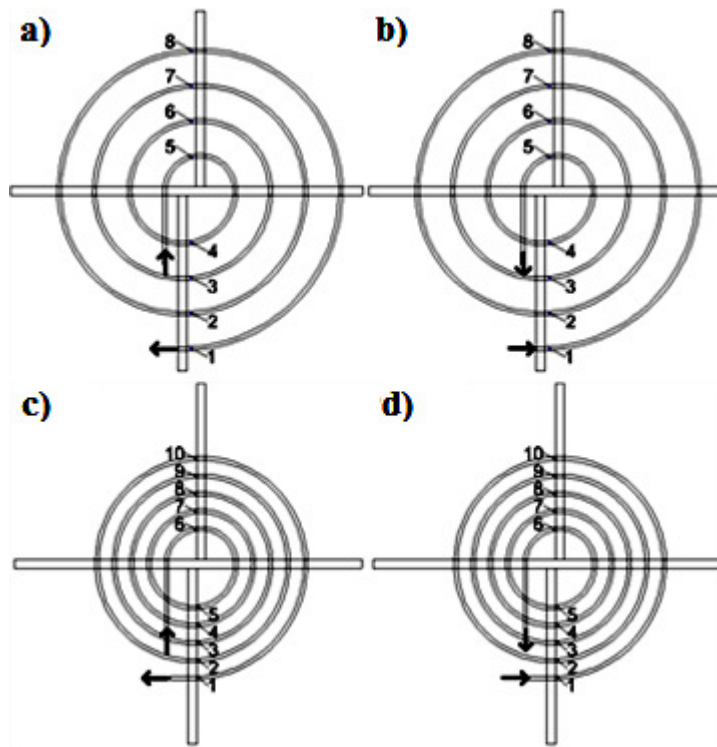


Fig. 2. The distribution of thermocouple NiCr-Ni.

Basic measured parameters were: reference temperature, the temperature at the inlet and outlet of the system, volume flow and the surface temperature of windings. The progress of measurement was recorded on infrared cameras.

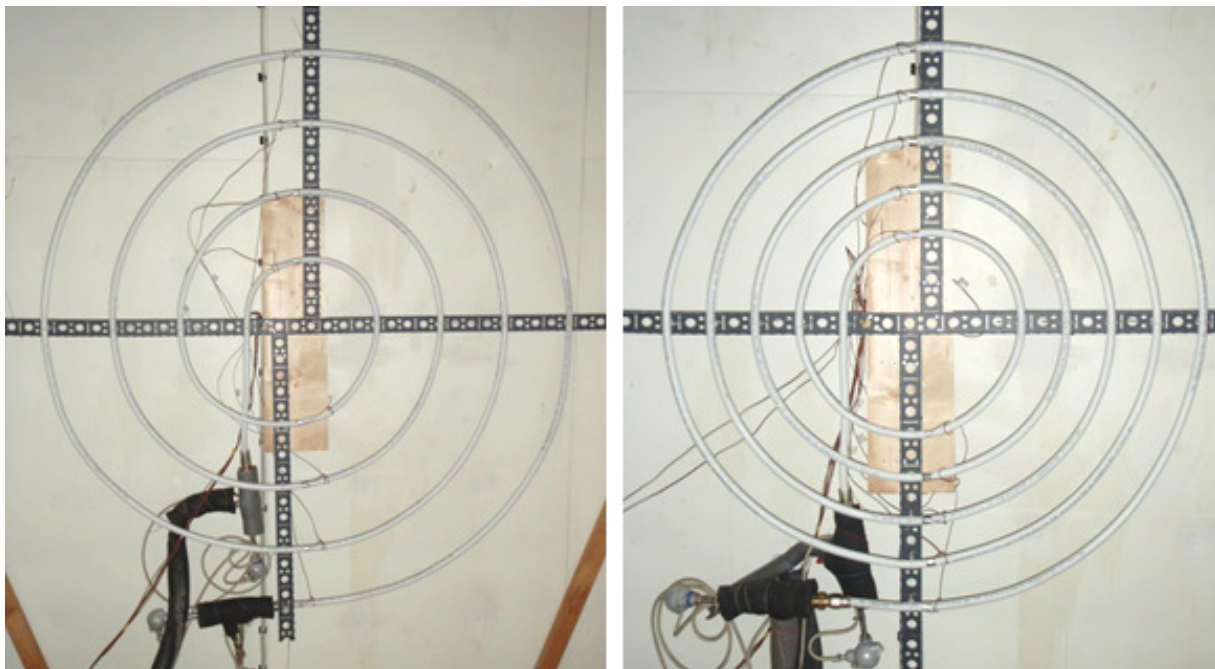


Fig. 3. Location of the system in the thermostatic chamber.

4. The measured values of thermal performance

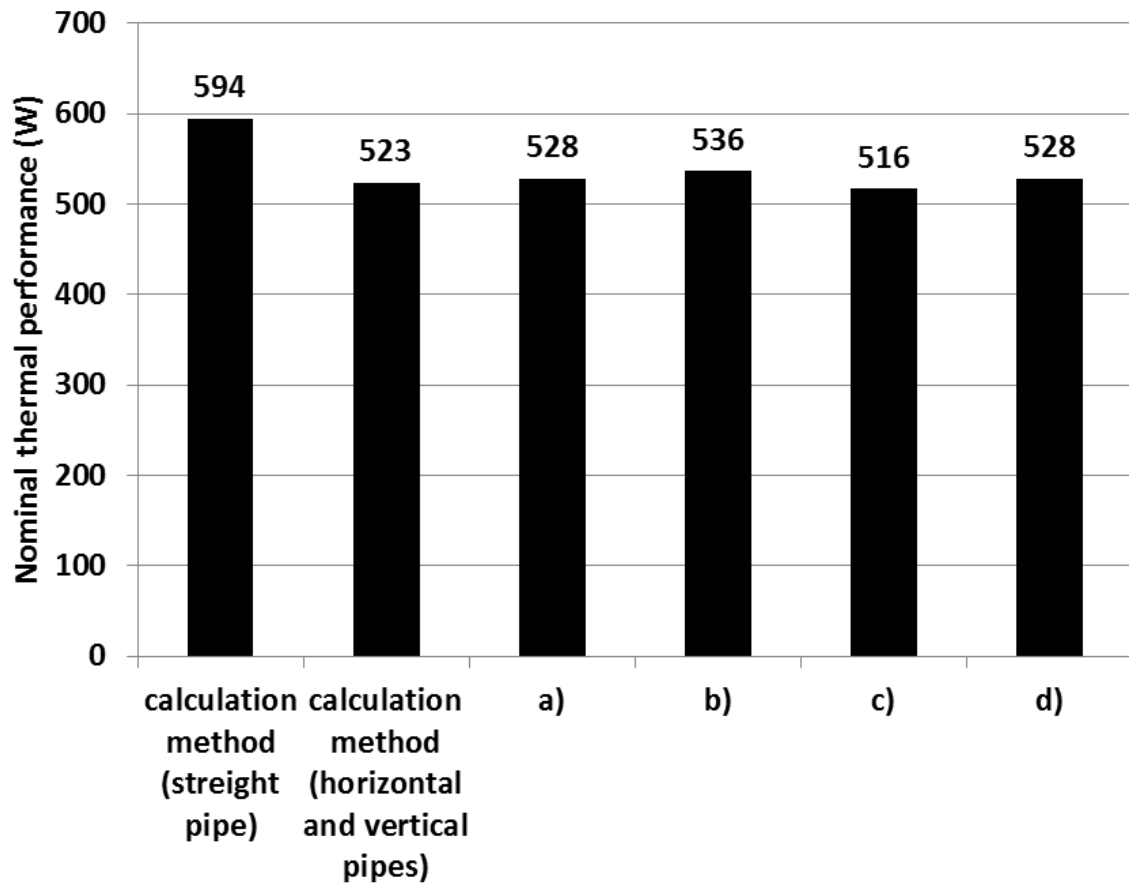


Fig. 4. Comparison of measured nominal thermal performance values and calculated nominal thermal performance values.

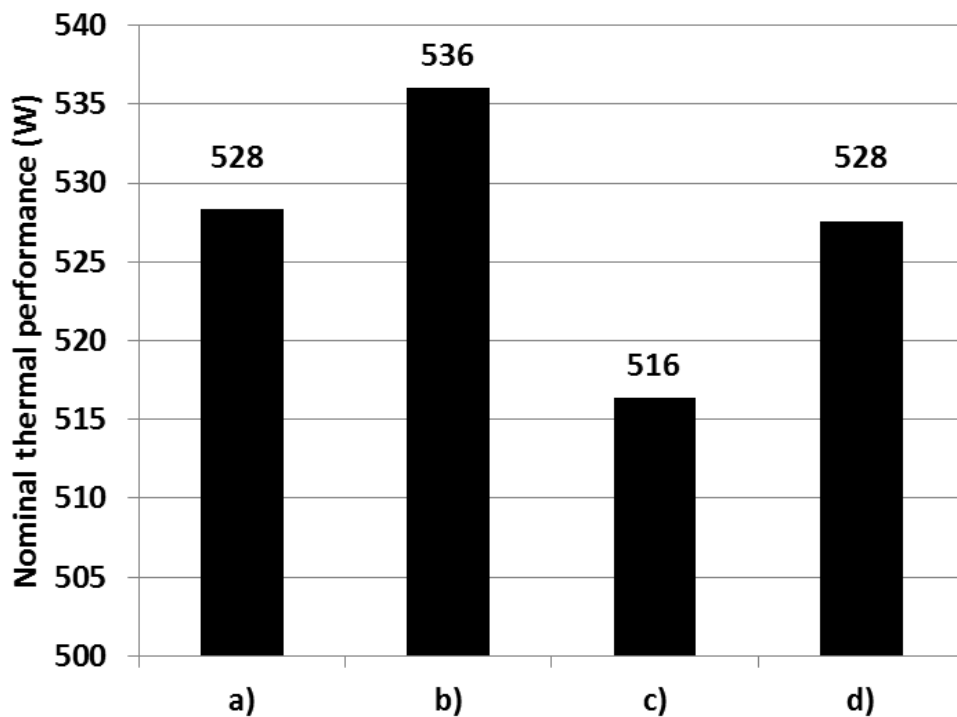


Fig. 5. Influence of the gaps size between the windings on heat output.



5. Conclusion

Fig. 4 shows that the measured values of nominal thermal performance are closest to the calculation in which the spiral was replaced by horizontal and vertical tubes. It is caused by the fact that the change of pipes position changes natural convection. Thus the characteristic dimension in the case of vertical pipe is the height. In the case of horizontal pipes (also when replaced with a straight pipe) the heat transfer coefficient is $\alpha_2 = 9.715 \text{ W/ m}^2 \text{ K}$. Vertical pipes have the transfer coefficient $\alpha_2 = 5.892 \text{ W/ m}^2 \text{ K}$.

Fig.5 shows that the difference between the nominal thermal performance of all types of connections is minimal. The difference between the connections a) and c) is 12 W and the difference between the connections b) and d) is 8 W. The comparison between the two sets of connections [a) to b) and c) to d)] has shown that when the inlet is on the edge of the system, the nominal thermal performance is higher. When we compared the connections a) and b), in which the distance between the coils was 20 cm, with the connections c) and d), in which the distance between the coils was 10 cm, the heat output of the latter was smaller. This means that with a smaller distance between each winding, the higher tubes are influenced by the free convection in such a way that the transfer from them is smaller.

Acknowledgements

This work was developed under the project “Transport tepla z orientovaných teplovýmenných plôch” KEGA no. 026ŽU-4/2014.

References

- [1] SMATANOVÁ, H. *Optimalizácia tokov teplotnosného kvapalného média cez rozvetvený systém rúrok pri uvažovaní neizotermického prúdenia*. ŽU v Žiline. Žilina., 2009.
- [2] KAPJOR, A., SMATANOVÁ, H., GREŠÁK, T., HUŽVÁR, J., JANDAČKA, J. *Optimization of heat transfer oriented surfaces by thermovision and using CFD method*. Structure and Environment. Kielce, 2013.
- [3] STN EN 442-2 Radiators and convectors. Part 2: Test methods and rating.



Methodology for calculating the LCC and LCP with the support of software

*František Ruman, *Juraj Grenčík

* Department of Transport and Handling Machines, University of Zilina, Univerzitná 1, 010 26 Žilina, Slovakia. {frantisek.ruman, juraj.grencik}@fstroj.uniza.sk

Abstract. It is a well-known fact that modern trams are designed and manufactured on much higher standard than older trams, many of them of obsolete concepts. On the other hand, nowadays tram designs are more complex and require much higher investment costs. Efforts to minimise costs and demonstrate the economic advantages of these new technologies and designs, throughout the life cycle (LC), launched a process of economic analysis called life-cycle cost analysis and life-cycle profit analysis (LCC and LCP).

The aim of the work was to create own methodology for the calculation of costs and profits for the life cycle of a rail vehicle in terms of manufacturer and the operator to comply with all the relevant principles of the EN 60300-3-3 standard. The created methodology was implemented into the MS Excel software. The data on costs and profits during the life cycle of a tram were input into the software data. The data are mutually interconnected and may be monitored for any individual change that will affect other costs or profits for life cycle of a tram.

Keywords: Tram, LCC, LCP, Software.

1. Introduction

The term LCC analysis, also referred to as the analysis of life-cycle costs, can be understood as a sequence of actions aimed at estimation of the total or part of the costs incurred for the purchase, use and disposal of fixed assets throughout their life cycle [8].



Fig. 1 Investigated tram [3].

The term analysis of the LCP, also referred to as the life-cycle profit analysis, can be understood as the total profit that physical asset, in our case railway vehicle, brings throughout its

life cycle. For the costs as well as for the profits it is important to know their distribution in time. Along with the time distribution, costs can be very easily identified when the owner will have insufficient funds for the operation [8].

The LCC methodology in detail is covered in the standard EN 60300-3-3 Dependability management, Part 3-3: Application guide, Life cycle costing [8].

In view of the above standard own methodology for calculating LCC and LCP was created, which was subsequently transferred to MS Excel software by the data needed to calculate the LCC and LCP of the selected transport company.

2. The proposed methodology for calculation of LCC and LCP

The costs and profits of the life cycle of tram can be observed from two points of view - from the point of view of producer of the tram and the point of view of the tram operator. The proposed methodology connects both views of calculating of LCC and LCP. Life Cycle Costs generally have to include all costs that the product incurs:

The period of manufacture.

- Period of use.
- Period of disposal.

Profits consist of the following components:

- Profits from the fares.
- Subsidies from the government and the regions.
- Profits from advertisements.

3. Calculation of life cycle costs

Costs consist of the following components:

$$C = \sum C = C_{ac} + C_m + C_c + C_a + C_s + C_e + C_{ps} + C_r + C_o; \quad (1)$$

where: C_{ac} - Acquisition costs, C_m - The costs of maintenance (preventive and corrective maintenance), C_c - The costs of cleaning, C_a - The costs of accidents, C_s - The costs of staff salaries, C_p - The costs of energy, C_{ps} - The costs of power supply, C_r - The costs of transport route, C_o - The costs of overhead.

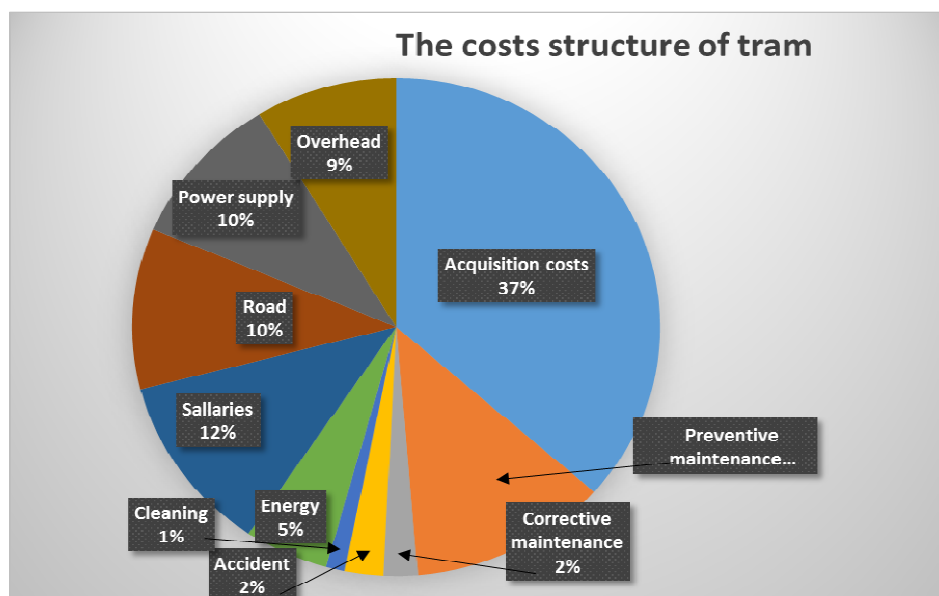


Fig. 2 The costs structure of tram [3].



Acquisition costs

In the price of the vehicle may or may not be included: financial costs, transportation, testing, approval, documentation, training, corrective maintenance during the guarantee, spare parts, tools and the like. In case of loan it is necessary to calculate the additional cost factor.

For the selected tram daily mileage of 172.8 km was assumed. Then annual throughput with regards to preventive and corrective maintenance which represents about 95% availability of the vehicle is 59 918.4 km. Thus the total mileage over the 30 years' service life is 1 797 552 km.

Acquisition cost of tram is about 2 450 000 €. When financed by a loan, the price of tram is 3 667 708 €. Acquisition costs calculated per km throughout the lifetime is the 1.363 €/ km.

Preventive maintenance

The costs of preventive maintenance for the life cycle of tram based on data on failures constitutes 816 371 €. Then the costs of preventive maintenance of life cycle of tram are 0.4542 €/km.

Corrective maintenance

Corrective maintenance is not planned – has random character (stochastic). Its occurrence and extent can be determined based on experience from the operation of similar vehicles and the detected data on failures. The approximate cost of corrective maintenance for the lifetime of the vehicle based on data on failures constitutes 123 649 €. These costs are approximately 15 % costs of preventive maintenance. Then the costs for corrective maintenance of life cycle tram are 0.0775 €/km.

Accidents

Traffic on city streets carries the risk of accident. Tram accidents are very common and occur about every 20 000 km. Usually, these are light damages, the costs are about 0.0885 €/km.

Energy

It is a simple calculation of performance-transport work. For tram, the specific energy consumption is about 100 kWh / 1000 tkm. The price of electricity for traction is 64.20367 €/MWh. Then the costs of energy of life cycle tram are 346 228.31 € and 0.1926 € / km.

Operating materials

It is a smallish item when calculated per kilometre run. These include sand, windscreen washer fluid, grease for flanges lubrication and the like.

Salary costs

The amount of the salary costs calculated on a passed kilometres decides in particular the number of board staff K_n , hourly wage M , employee productivity p , the ratio of labour costs to wages k_m , the ratio of the period of personnel service time to vehicles service k_s and turnaround in speed v_0 . Then salary costs represent around 0.4298 € / km.

Costs of the transport route

The costs of transport route are € 0.39 / km. These costs themselves contain all the items that are used to ensure smooth operation of trams and also imply the maintenance and repair of transport route.

Costs of cleaning

Maintaining internal and external cleanliness of tram is controlled at regular intervals like preventive maintenance. Are planned personnel costs and material costs (cleaning products) and technology (car wash, etc.). At present, the trend is to ensure cleaning and washing completes trams by using specialized cleaning companies. The cost of cleaning throughout the life cycle of trams is 76 230 €. After calculation the cleaning costs are 0.0424 €/ km.

Overhead costs

For large companies, it is necessary to ensure transparency - avoid meaningless billing cumulative administrative costs and overheads. Overhead costs throughout the life cycle trams are 581 867.58 €. After calculation the overhead costs are 0.3237 € / km.

Power supply costs

The cost of power supply throughout the life cycle of tram are 665 094.24 €. After calculation the power supply costs are 0.37 € / km.

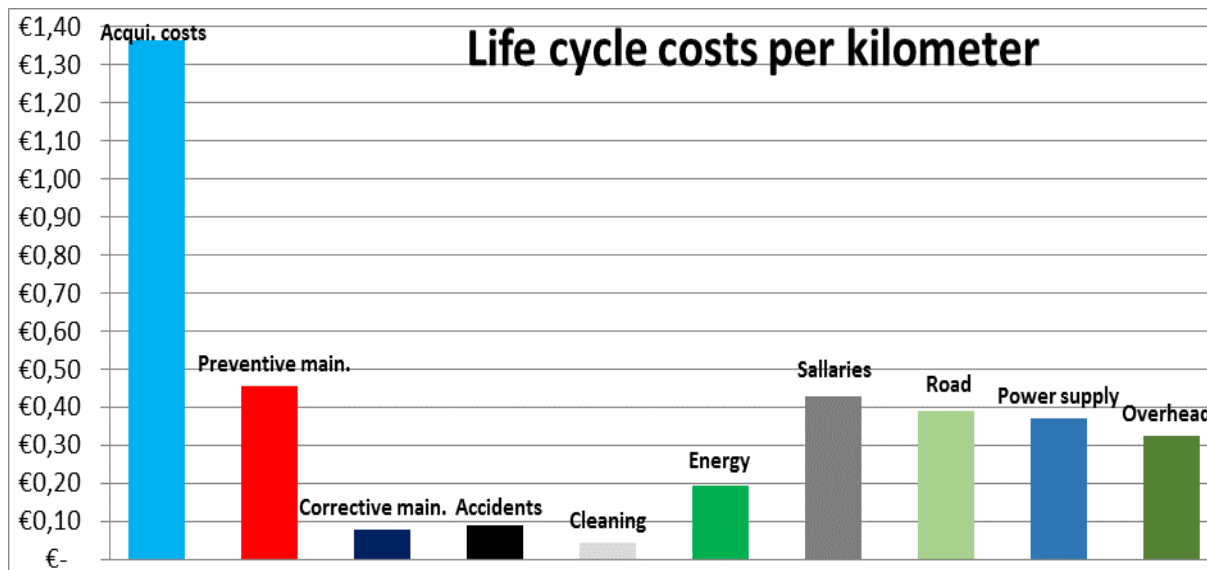


Fig.3 Life cycle costs per kilometre [3].

The calculations suggest that the total life cycle costs for the investigated tram and annual mileage of 59 918.4 km are 3.7919 € / km.

The calculations suggest that the total life cycle costs for the investigated tram with 52 seats and an annual mileage of 59 918.4 km are 0.0718 € /km / seat.

4. Calculation of life cycle profits

Public passenger transport by rail is the public service. And ensure their availability to the public is the main task of the state or region. Therefore, these services are funded from public regional budgets.

Profits consist of the following main components:

- Profits from the fares.
- Subsidies from the government and the regions.
- Profits from advertisements.

Profits from passengers

They range roughly between 1.1638 € per kilometre. The total approximate amount of sales for the full occupation of seats and the entire lifetime is the 2 091 942.75 €.

Subsidies from the customer traffic

Subsidies for region government are about 1.186 € /km. Overall subsidies for tram throughout its lifetime are therefore 2 131 896.67 €.

Profits from advertising

Advertising profits are ranging about 0.2 € / km. Profits from advertisements throughout the lifetime of tram are about 359 510.4 €.

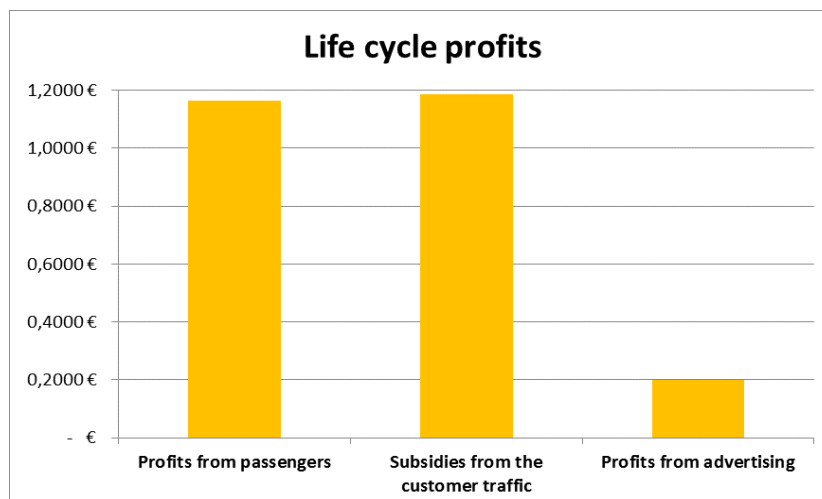


Fig. 4 The profit (revenues) structure of tram [3].

The calculations suggest that the total life cycle profits for 30 meter tram an annual mileage of 59 918.4 km are 2.5498 € / km.

The calculations suggest that the total lifecycle costs for 30 meter tram with 52 seats and an annual mileage of 59 918.4 km are 0.049 € / km / sæt.

5. Designed software to calculate LCC and LCP

The program is created in software MS Excel. The application consists of one file and several worksheets. There are connections among some worksheets, and all worksheets are connected to the input list. In the designed application costs and profits for the life cycle of selected tram are calculated.

The software consists of:

Global data, Acquisition costs, Preventive maintenance, Corrective maintenance, Accidents, Cleaning, Energy, Salaries, Transport route, Power supply, Overhead, Profits from passengers, Subsidies from the traffic customer, Advertising, Chart of LCC, Chart of LCP.

Life cycle of railway vehicle - tram			
Life cycle	Zaèiatok	2014	
	Koniec	2044	
	Poèet rokov	30	
Life cycle stages			
	Beginning	End	
Research and development		2011	2013
Manufacture		2013	2014
Operation and maintenance		2014	2043
Decommissioning and disposal		2043	2044
Life cycle costs per 1 km		3,7317 €	
Life cycle costs per 1 seat / km		0,0718 €	
Life cycle profits per 1 km		2,5498 €	
Life cycle profits per 1 seat / km		0,0490 €	
Number of seats		52	
Middle daily circulation		172,8 km	
Average annual circulation		59918,4 km	
Total circulation for life cycle		1797552 km	
Availability		95%	

Fig. 5 The software to calculate the LCC and LCP.



Purchase price	2 450 000 €
Price include loan 3M EURIBOR	3 667 708,19 €
The costs of preventive maintenance for the life cycle	816 370,84 €
The costs of corrective maintenance for the life cycle	139 306,27 €
The costs of accidents for the life cycle	159 090 €
The costs of cleaning for the life cycle	76 230 €
The costs of energy for the life cycle	346 228,31 €
The costs of salaries for the life cycle	772 632 €
The costs of transport route for the life cycle	701 045,28 €
The costs of power supply for the life cycle	665 094,24 €
The costs of overhead for the life cycle	581 867,58 €
The profits of passengers for the life cycle	2 091 942,75 €
The profits of subsidies for the life cycle	2 131 896,67 €
The profits of advertising for the life cycle	359 510,40 €

Fig. 6 The software to calculate the LCC and LCP.

6. Conclusion

The aim of the work was to create own methodology for the calculation of costs and profits for the life cycle of a rail vehicle in terms of manufacturer and the operator. The created methodology was implemented into the MS Excel software.

The calculations suggest that the total life cycle costs for the investigated 30 meter tram and annual mileage of 59 918.4 km are 3.7919 € / km. The calculations suggest that the total life cycle costs for the tram with 52 seats and an annual mileage of 59 918.4 km are 0.0718 € / km / seat.

The calculations suggest that the total life cycle profits for the investigated 30 meter tram and annual mileage of 59 918.4 km are 2.5498 € / km. The calculations suggest that the total lifecycle costs for the tram with 52 seats and the annual mileage of 59 918.4 km are 0.049 € / km / seat.

References

- [1] BRONČEK, M.: *Life cycle costs of railway vehicle* (In Slovak) Dissertation thesis, VŠB-TU Ostrava, 2005.
- [2] BRONČEK, M. *Problems with life cycle costs of railway vehicles*. (In Slovak) At present problems in railway vehicles. Level I. Žilina: VTS near Žilinskej univerzite v Žiline, 1999. s.29-35.
- [3] *Transport company of Bratislava*, internal materials. (In Slovak)
- [4] KJELLSSON, U.: Unife – Unilife and Unife – Unidata – the first European life cycle cost interface software model: research report, 2000. 8 pp.
- [5] LUKAČOVIČ, J., GREŇČÍK, J. *LCC and LCP analysis in operation and maintenance means of transports*. High Tatras : NFÚ , 2001. (In Slovak)
- [6] LUKAČOVIČ, J., GREŇČÍK, J. *LCC and LCP analysis utilisation*. Žilina : Transcom, 2001.
- [7] POHL, J.: *Principles and trends of trams transport*, *Transport magasin*, (In Slovak) 2/2008, pp. 24 – 29.
- [8] STN EN 60300-3-3: 2005 *Management of reliability. Part 3-3: Manual for using. Life cycle costs*. (In Slovak)
- [9] STN IEC 60050-191: 1993 *International electronical dictionary*. Chapter 191: Reliability and quality of service. (In Slovak)
- [10] STN EN 13306: 2011 *Maintenance. Terms of maintenance*. (In Slovak)



Simulation comparison of the operating characteristics of conventional and a new type of Stirling engine

*Wojciech Sadkowski, *Robert Pastuszko, **Mateusz Marciniowski, ***Krzysztof Ludwinek,
*Robert Kaniowski

*Kielce University of Technology, Faculty of Mechatronics and Mechanical Engineering, Department of Mechanics, Al. Tysiąclecia P. P. 7, 25–314 Kielce, Poland, {wsadkowski, tmprp, kaniowski}@tu.kielce.pl

**Kielce University of Technology, Faculty of Mechatronics and Mechanical Engineering, Department of Automotive Engineering and Transport, Al. Tysiąclecia P. P. 7, 25–314 Kielce, Poland, {mmarciniowski}@tu.kielce.pl

***Kielce University of Technology, Faculty of Electrical Engineering, Automatic Control and Computer Science, Department of Industrial Electrical Engineering and Automatics, Al. Tysiąclecia P. P. 7, 25–314 Kielce, Poland, {k.ludwinek}@tu.kielce.pl

Abstract: The paper presents a new type of Stirling engine. The structural differences between the traditional Stirling engine and the new type have been described. The advantages resulting from the proposed modifications have been presented. The program developed in the MATLAB / SIMULINK environment to simulate the Stirling engine operation has been described. The performance characteristics of the traditional Stirling engine and the new type with the same conditions are presented and compared. They were also compared with the theoretical and real Stirling cycle.

Keywords: Stirling Engine, Cam Mechanism, Thermodynamic Cycle, Rotary Displacer.

1. Introduction

The Stirling engine is a type of external combustion engine which operates over a closed, thermodynamic cycle with the ability to use a different energy sources.

The Stirling engines working principle is that when the gas pressure value is above the ambient pressure, the working piston is pushed. With the increase of the volume, the working gas pressure starts to decrease. Then, the gas is pushed into the cooled zone, the temperature decreases and hence the gas pressure decreases below ambient pressure. Now, the piston begins to move back. With the decrease of the volume, the pressure starts to rise. Then, the gas is pushed back into the heated zone and its pressure increases, the engine cycle of operation is closed [2].

There are many types of Stirling engines. Two solutions for moving the gas from the heated to the cooled zone and back are the most popular: the first one called alpha type consists of a system of two pistons in two cylinders, where one is heated and the other cooled (Fig. 1a) and the second one called beta type is a piston coupled to the displacer which pushes the gas from one zone to another (Fig. 1b).

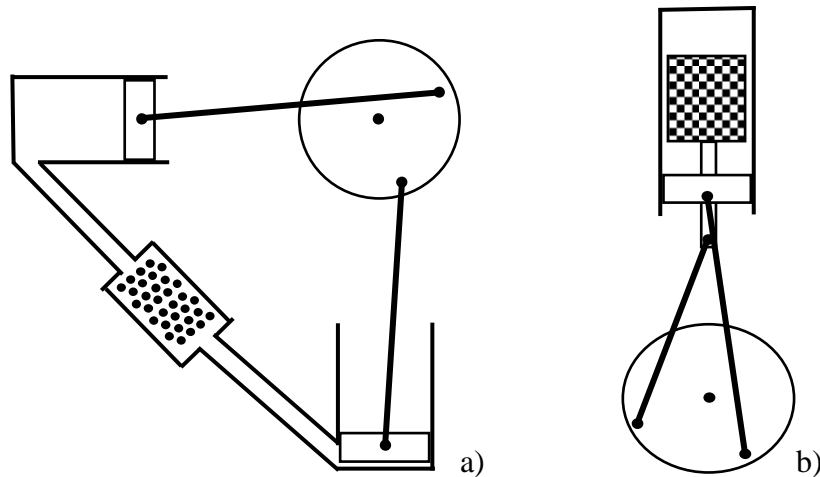
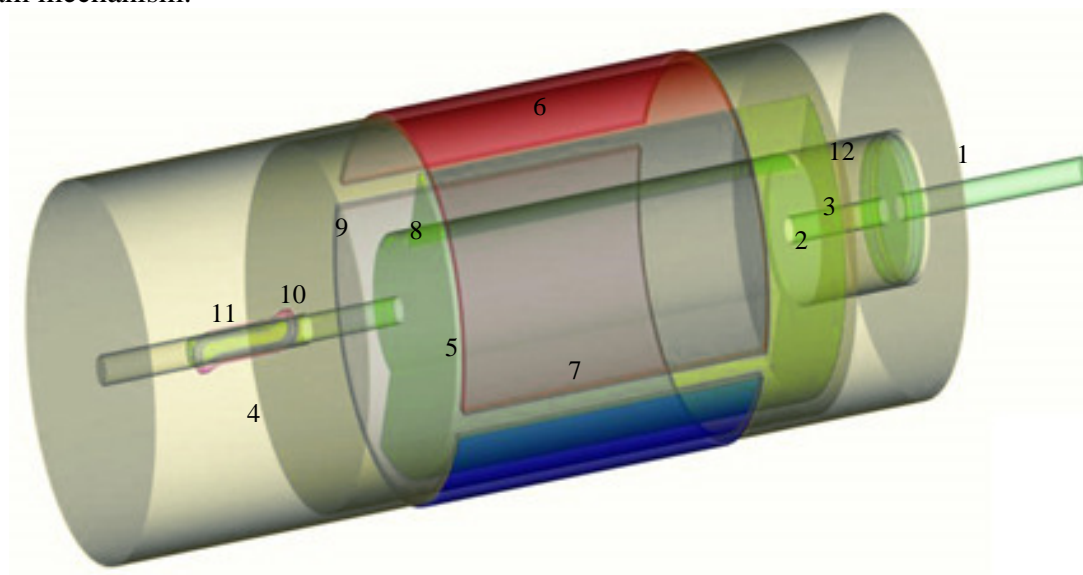


Fig. 1. The most popular types of Stirling engine a) alpha type, b) beta type.

There are many ways to couple the displacer with the piston movement. The crankshaft is the most popular solution used in conventional Stirling engines. However, it has a major drawback: a displacer is set in the position allowing to obtain the biggest heat transfer area for a very short time in relation to the time of one cycle of the engine. In the invented engine a cam mechanism has been applied, so that the displacer is set in this position for much longer time than in the case of the crankshaft. A good heat transfer is one of the most important parameter influencing the efficiency of the Stirling engine. Because of the cam mechanism the invented engine is characterized by a simple construction and only one movable sealing element.

There are several configurations of this engine type according to the positioning order of the piston, displacer and cam mechanism. It is also possible to improve the engine by stopping the rotation of the piston and the reciprocating movement of the displacer. Fig. 2a shows one of the simplest configurations of this engine with only one moving element. Fig. 2b shows an enlargement of the cam mechanism.



a)

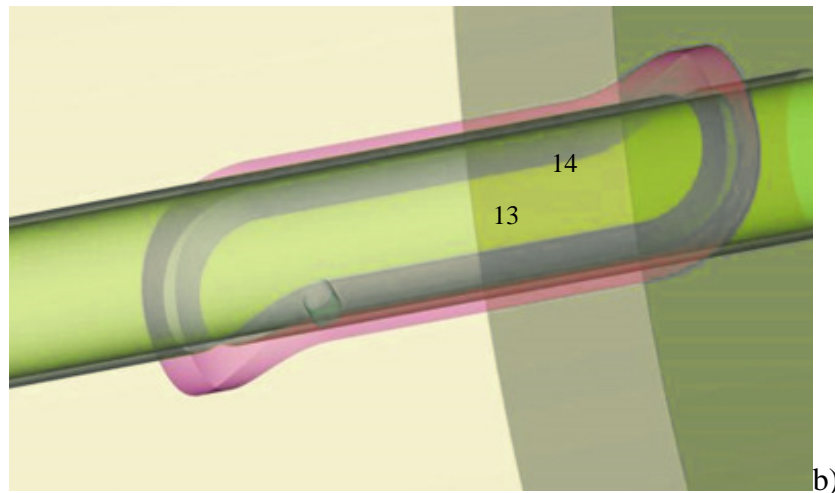


Fig. 2. Configuration of the investigated Stirling engine: a) view the entire engine, b) enlargement of the cam mechanism; 1 – shaft, 2 – cylinder, 3– piston, 4 – stator, 5 – displacer, 6 – heater, 7 – cooler 8 – balance element, 9 – heat exchange chamber, 10 – cam mechanism, 11 – sleeve, 12 – seal ring, 13 – cam channel, 14 – slider.

2. Simulation

The engine thermodynamic model was developed on the basis of the first law of thermodynamics (3) and the ideal gas law (5). The main relations and equations of the model are presented below.

Heat transfer rate from the heater (1), is achieved by using following formula:

$$\dot{Q}_G = A_G \cdot \frac{l_w \cdot 2 \cdot \pi \cdot \lambda_{wG} \cdot (T_G - T)}{\ln\left(\frac{r_z}{r_w}\right)} \quad (1)$$

where:

- l_w – exchanger length,
- λ_{wG} – the heater wall conduction,
- T_g – heater temperature,
- T – working gas temperature,
- r_z – exchanger external radius,
- r_w – exchanger internal radius.

Heat supplied in a single calculation step (2) is calculated as follows

$$\Delta Q = \dot{Q} \Delta t \quad (2)$$

where:

- \dot{Q} – heat transfer rate ,
- Δt – time of single calculation step.

Internal energy change of working gas in single calculation step (3) is calculated on the basis of the first law of thermodynamics [1]. The volume of working gas change results from the response of the mechanical system to the thermodynamic system operation.

$$\Delta U = \Delta Q - p \Delta V \quad (3)$$

where:

- p – working gas pressure,
- ΔV – working gas volume change ,
- ΔU – working gas internal energy change.

Temperature of working gas is given by a relation (4)

$$T = \frac{U}{m_g c_v} \quad (4)$$

where:

m_g – mass of working gas,

c_v – specific heat of working gas.

Pressure (5) is calculated on the basis of ideal gas law:

$$p = \frac{m_g \cdot R \cdot T}{V} \quad (5)$$

where:

R – specific gas constant for air.

The engine mechanical system equations of motion were also developed [3]. These relationships have been implemented in Matlab/Simulink environment. The resulting program allows to simulate the engine operation with different parameters of the thermodynamic and mechanical system and different shapes of the cam. The engine work simulation allows to display the most important characteristics of the engine.

3. Characteristics

In order to compare the work of classical Stirling engine with invented one, the simulations were carried out with two types of cams: the first one allowing the displacer movement in the way to increase the heat exchange and the second one providing the displacer movement as in the case of the classical Stirling engine. The engine indicator diagrams generated by the simulations are presented below: for the heater temperature 600°C on the Fig. 3 and for temperature 120°C on the Fig. 4. For comparison, Fig. 5 shows a theoretical shape of the Stirling cycle and Fig. 6 shows the real indicator diagram of an exemplary conventional Stirling engine.

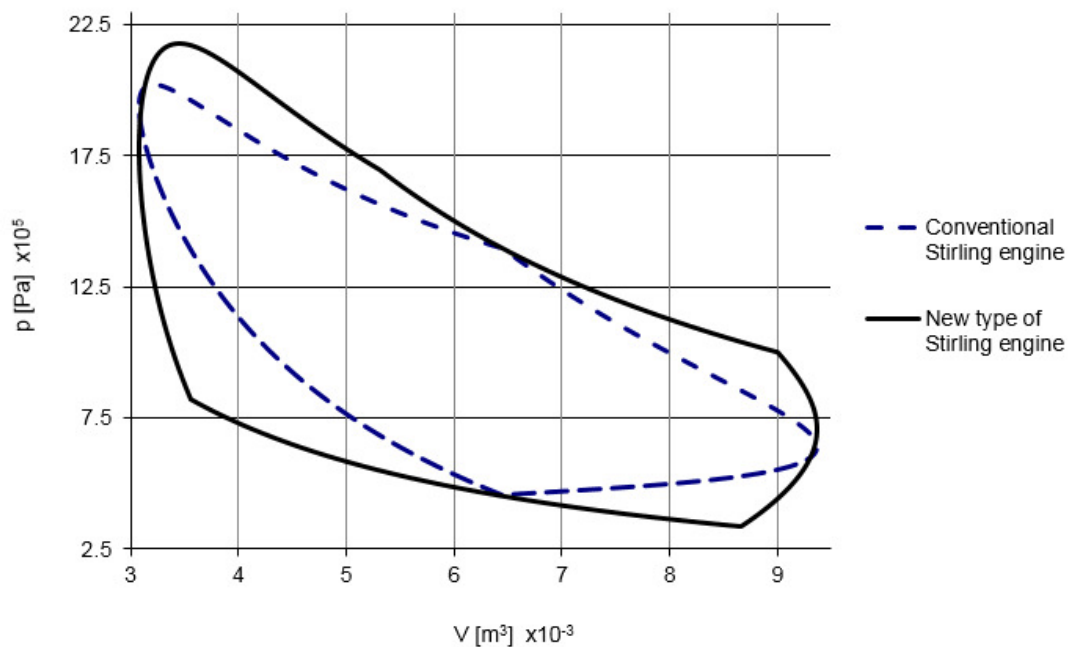


Fig. 3. Simulated indicator diagram of conventional Stirling engine and the diagram of investigated engine for heater temperature 600°C.

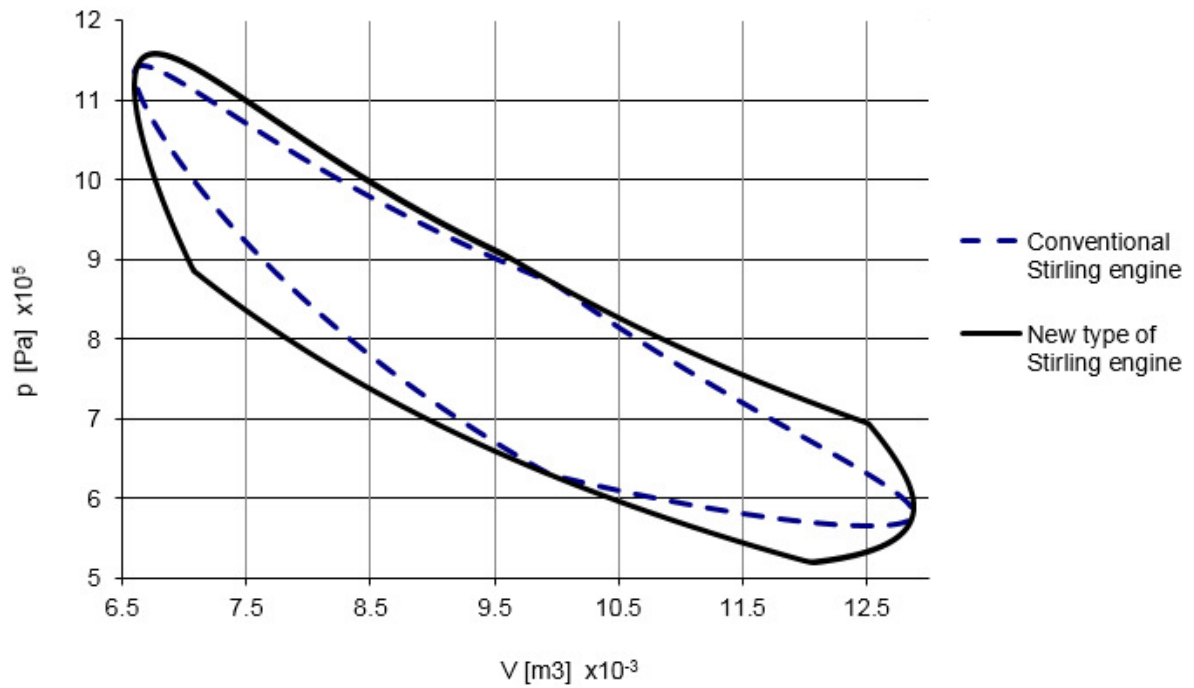


Fig. 4. Simulated indicator diagram of conventional Stirling engine and the diagram of investigated engine for heater temperature 120°C .

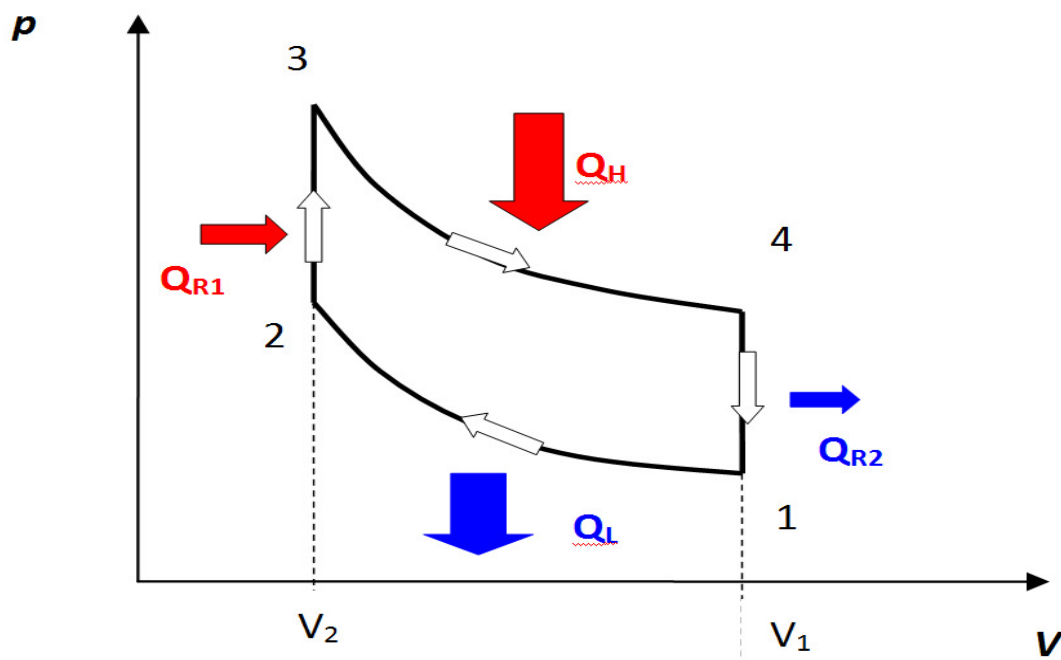


Fig. 5. Theoretical Stirling cycle.

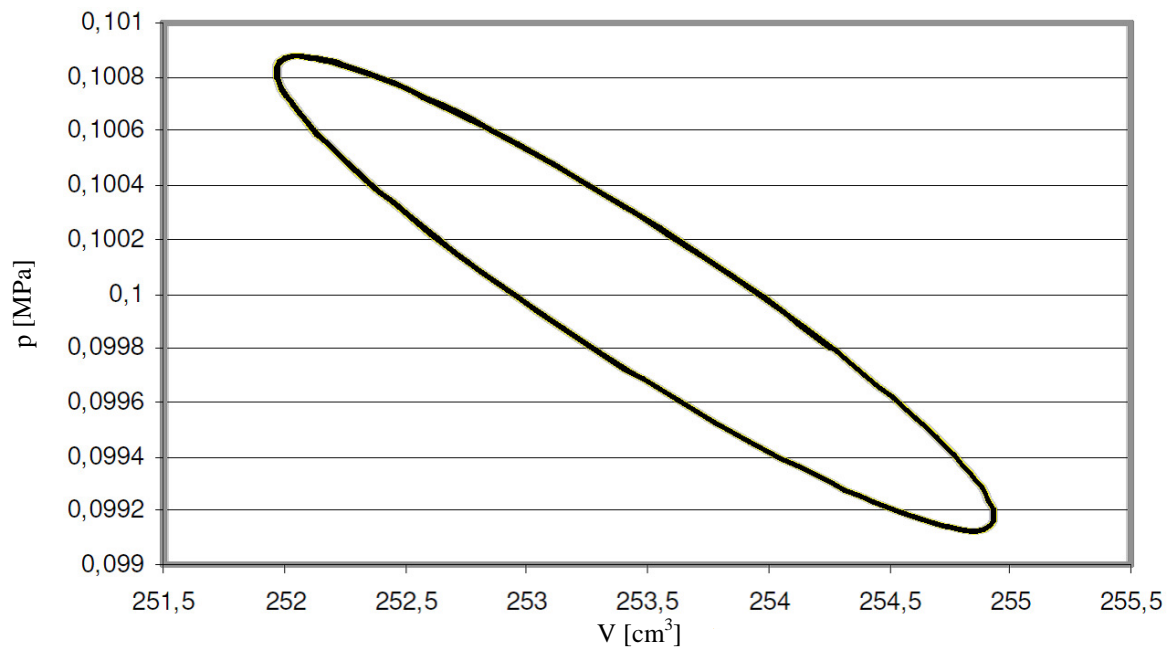


Fig. 6. The real indicator diagram of an exemplary conventional Stirling engine [5].

4. Conclusions

The indicator diagrams, simulated for the cam which increases heat transfer, are much more similar in shape to the ideal Stirling cycle. Moreover, they have larger surface area than the graphs generated for the cam providing the displacer movement as in the classical Stirling engine with crank system. The larger area of the resulting indicator diagram, obtained using the same simulation program with the same working conditions for the new engine type, shows its higher efficiency [4]. The indicator diagrams for the cam imitating the crank system work are similar in shape to the real exemplary Stirling cycles. This confirms the correctness of the simulation. The obtained results can be supported experimentally, when the construction of the new engine prototype will be completed.

Acknowledgement

This publication was created by the project "Innovative system for distributed processing of renewable energy" within the framework of action 1.4 IE OP - the task realized by the Kielce University of Technology.

References

- [1] STANISZEWSKI, B. *Termodynamika*. PWN, Warszawa 1982.
- [2] ŻMUDZKI, S. *Silniki Stirlinga*. WNT, Warszawa 1993.
- [3] SUNIL KUMAR SINGH. *Kinematics fundamentals*. Rice University, Houston, Texas 2008.
- [4] ZIABASHARHAGH, M., MAHMOODI, M. *Numerical solution of beta-type Stirling engine by optimizing heat regenerator for increasing output power and efficiency*. TextRoad Publication 2012.
- [5] SANZ MORENO, A. *Simulación del motor Stirling por el método LHA*. EINA /Área de Máquinas y Motores Térmicos 2012.

Process evaluation of the braking disc brake of a rail vehicle using vibration friction pad

*Wojciech Sawczuk, **Jakub Kowalczyk, **Dariusz Ulbrich

* University of Technology, Faculty of Machines and Transport, Division of Rail Vehicles,
M. Skłodowskiej-Curie sq. 5, 60-965 Poznan, Poland, wojciech.sawczuk@put.poznan.pl

** Poznan University of Technology, Faculty of Machines and Transport, Division of Motor Vehicles and
Road Transportation, M. Skłodowskiej-Curie sq. 5, 60-965 Poznan, Poland, {jakub.kowalczyk,
dariusz.ulbrich}@put.poznan.pl

Abstract. The reliability of the operation of the braking system of the vehicle depends to a large extent on the cooperation of the brake components forming a pair of friction e.g. brake disc-friction pad. Work instability arises between the occurrence of vibrations on friction element, which affects the lower efficiency of the braking process. In practice, this means that, during braking the vehicles currently alternative at a time of friction resistance may cause uneven braking process. The effects of these changes in accordance with the work [5] may be revealed in the form of a self-excited vibration. The vibrations generated by the assemblies are moved per vehicle, which also adversely affects ride comfort.

The purpose of the article is to assess the possibility of selected vibration parameters accompanying processes of friction in the disk brakes and use it for process evaluation braking of a rail vehicle.

Keywords: Brake disc, Friction pad, Coefficient of friction, Instantaneous value of vibration acceleration.

1. Introduction

Because of numerous advantages in comparison to a traditional air block brake, disc brakes, are more and more often utilized in passenger carriages and other railway vehicles.

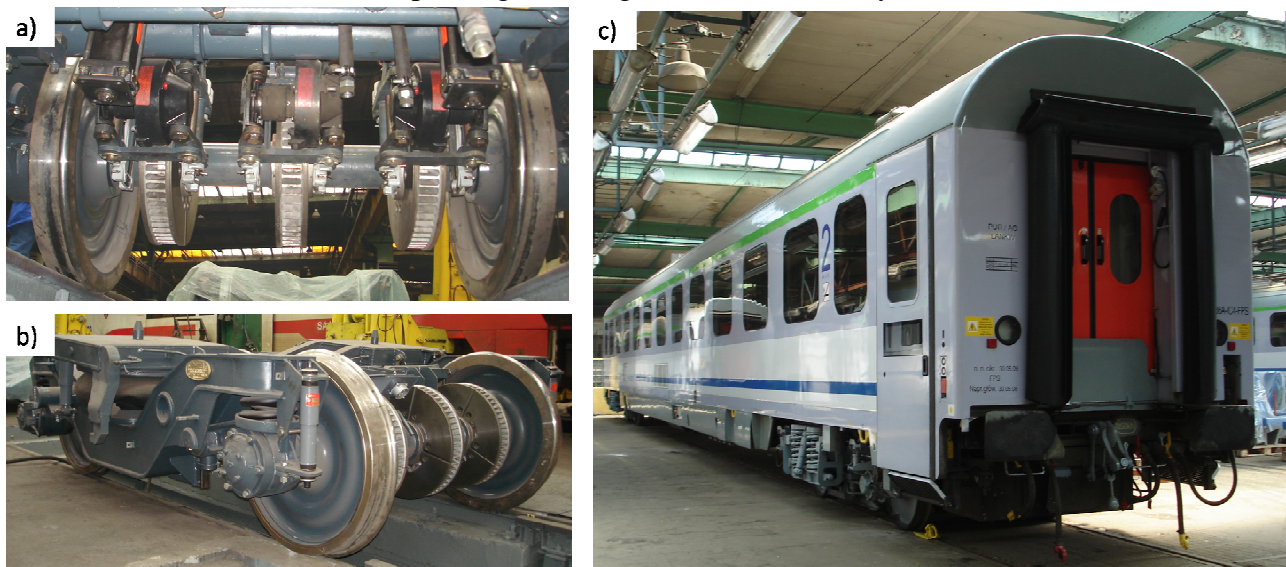


Fig. 1. View of passenger car with disc brake system: a) view of brake discs mounted on axle passenger car, b) view of bogie 25AN, c) passenger car.

In rail vehicle, because of constantly rising ride speed and to obtain required braking distance, disc brakes are used as primary brake. Additionally, according to UIC 546, speed of passenger trains of over 160km/h triggers application of disc brake. Stable and constant - in the whole speed

range- average coefficient of friction μ , with the value: $\mu = 0.35$ is a basic advantage of disc brake systems [6].

Few disadvantages of disc brake include a lack of possibility of controlling the condition of the friction set: brake and pad in the whole operation time. It is particularly observable in rail cars, where disc brakes are mounted on the axle of the axle set between the wheels (Fig. 1c) [3]. To check the wear of friction pads and brake discs it is necessary to apply specialistic station e.g. inspection channel to carry out inspections, and to carry out replacement of friction parts in case they reach their terminal wear [7].

Selection of friction materials of type disk and pad directly affects the braking process. Work instability arises between the occurrence of vibrations on friction element, which affects the lower efficiency of the braking process. In practice, this means that, during braking the vehicles currently alternative at a time of friction resistance may cause uneven braking process. The effects of these changes in accordance with the work [5] may be revealed in the form of a self-excited vibration. As a result, the growth of vibration friction pad causes changes in the activity of the temporary coefficient of friction during braking, as braking to. This will be presented in the next part of the article.

2. Methodology and research object

The research was carried out at internal station for tests of railway brakes. A brake disc type 610×110 with ventilation vanes and friction pads type 200 FR20H.2 made by Frenoplast constitute the research object (thickness of 15mm). A research program 2B1 (I) according to instructions of UIC 541-3 was applied.

The braking was carried out from speed of 120km/h. During the research pad's pressures to disc N of 28kN was realized as well as braking masses per one disc of $M=7.5t$ and during braking to stop [4]. This research was carried out in accordance with principles of active experiment [8]. After carrying out a series of brakings the friction pads were changed and values of instanteneous vibration accelerations were registered.

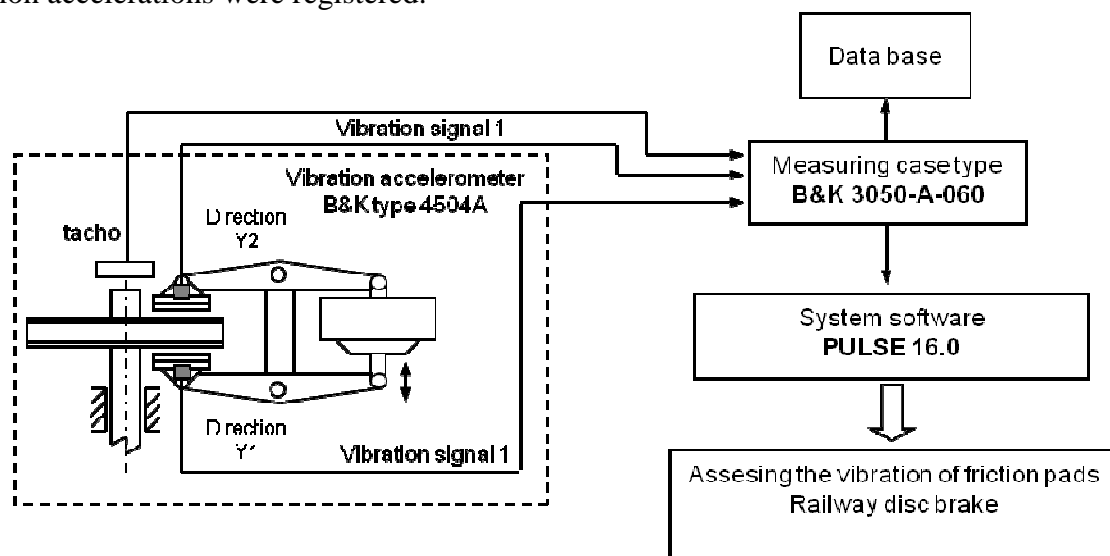


Fig. 2. Measurement set of vibration generated by caliper with pads.

Vibration converters were mounted on pad calipers with a mounting metal tile. During the research signals of vibration accelerations were registered in three reciprocally orthogonal directions [9]. To acquire vibration signal a measuring system consisting of piezoelectric vibration accelerations converter and measuring case type B&K 3050-A-060 with system software PULSE 16.0 was used. Fig. 2 presents the view of the measurement set [1, 2].

3. Research results

Fig. 3 shows an exemplary signal of instantaneous values of vibration accelerations of caliper and pad registered in direction Y_1 (orthogonal to the disc) during station research. The analysis of results of vibration tests showed that obtaining dependence of friction pads' thickness on the value of point parameters is possible by measuring vibration in directions Y_1 and Y_2 on an accelerometer mounted from the side of brake cylinder's case and brake cylinder's piston rod. Fig. 4 show the mileage instantaneous and average coefficient of friction for braking with speed $v=120$ km/h. The average coefficient of friction is calculated from (1) as the integral of the instantaneous coefficient of friction on the road braking s_2 [4].

$$\mu_m = \frac{1}{s_2} \int_0^{s_2} \mu \cdot ds, \quad (1)$$

where:

- s_2 – road braking from speed v to stop,
- μ – instantaneous coefficient of friction.

In fig. 4a) also shows the time braking for first and second braking.

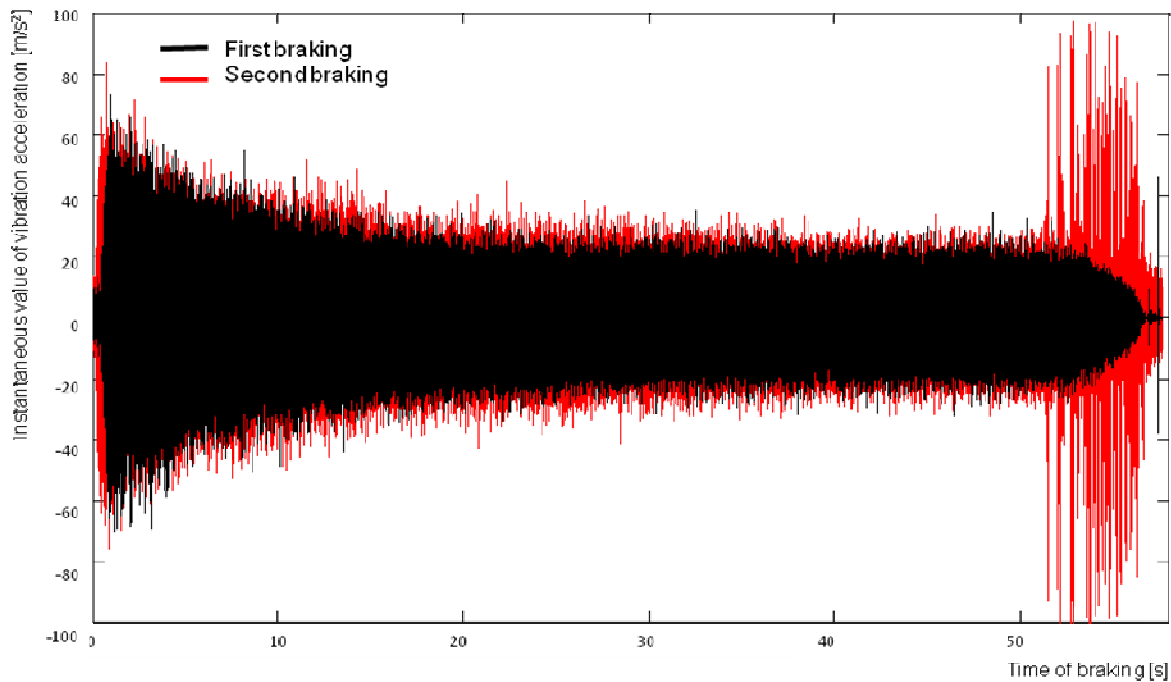


Fig. 3. Signal of vibration accelerations registered on pad caliper on direction Y_1 for different thickness of pads during braking to stop (Speed at beginning of braking $v=120$ km/h).

Both flaw detectors made it possible to obtain correct, while the data for the study of ultrasonic pulses systems. Examples of the pulses are shown in Fig. 4. It is clear that the pulse was obtained from the bottom of the connection, which means that full penetration was achieved. Current research aims to develop a technique that allows to location of melting boundary, which is important for car manufacturers and car equipment components producers.

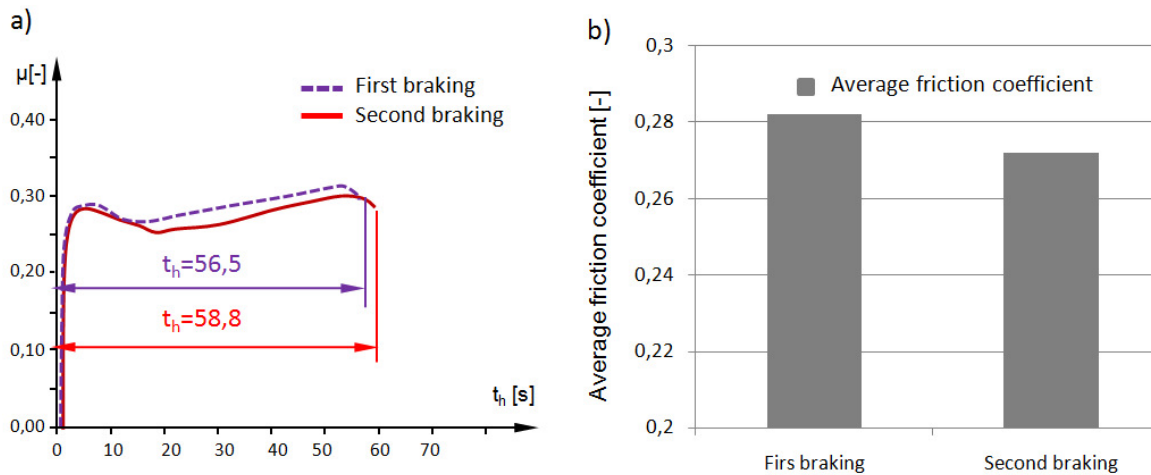


Fig. 4. The coefficient of friction obtained from the braking to stop reagent with velocity $v=120$ km/h for two braking: a) the instantaneous coefficient of friction, b) the average coefficient of friction.

4. Conclusion

Research conducted at the inertial station for tests of railway brakes, showed that there is a dependence of the growth acceleration of vibrations from instantaneous and average friction coefficient. Measurement of vibration accelerations in direction Y_2 orthogonal to friction surface of the disc and mounting vibration converter from the side of brake cylinder piston rod, is characterized as the most sensitive towards direction Y_1 , which is confirmed by values of coefficient of dynamics of changes. In addition, research conducted on the inertial station for tests of railway brakes, showed that the wear of the friction pads effect on the reduction of instantaneous and average friction coefficient of friction pads relative to the brake disc. In the result of worn brake friction pads increase the deceleration time. Studies have shown that the braking process is not repeated. At the same parameters of braking in some cases, there are vibration in the resonant character in the last phase of braking.

The project is funded by the National Centre for Research and Development, program LIDER V, contract No. LIDER/022/359/L-5/13/NCBR/2014

References

- [1] BRÜEL & KJÆR: *Piezoelectric Accelerometer Miniature Triaxial Delta Tron Accelerometer – Type 4504A*, oferta firmy Brüel & Kjør.
- [2] BRÜEL & KJÆR: *Measuring Vibration*, Revision September 1982.
- [3] GRUSZEWSKI M. *Wybrane zagadnienia eksploatacji hamulca tarczowego*. Technika Transportu Szynowego 1995, nr 6-7, s. 84-86.
- [4] KODEKS UIC 541-3: *Hamulec-Hamulec tarczowy i jego zastosowanie*. Warunki dopuszczenia okładzin hamulcowych. Wydanie 6, listopad 2006.
- [5] MARIO TRICHES JUNIOR, SAMIR N. Y. GERGES, ROBERTO JORDAN, *Analysys of brake squeal noise using finite element method: A parametric study*, Federal university of Santa Caterina, Brazylia 2007.
- [6] PIECHOWIAK T., *Hamulce pojazdów szynowych*, Wydawnictwo Politechniki Poznańskiej.
- [7] Rail Consult Gesellschaft für Verkehrsberatung mbH. *Wagon osobowy Z1 02, układ jezdny-tom 2*. Dokumentacja Techniczno-Ruchowa.
- [8] SAWCZUK W., TOMASZEWSKI F. *Assessing the wear of friction pads in disc braking system of rail vehicle by using selected amplitude characteristics of vibration signal*, *Vibration In Physical Systems*, Volume XXIV
- [9] SERRIDGE M., LICHT T. R.: *Piezoelectric accelerometers and vibration preamplifiers*, Brüel & Kjør 1987.



Thermal stress analysis of the plate with hole at fatigue testing machine

*Zuzana Stankovičová, *Vladimír Dekýš, *Pavol Novák, *Milan Uhříček, *Milan Sapieta,
**Leszek Radziszewski

*University of Žilina, Faculty of Mechanical Engineering, Department of Applied Mechanics,
Univerzitná 1, 010 01 Žilina, Slovakia,
{zuzana.stankovicova, vladimir.dekys, pavol.novak, milan.uhricik, milan.sapieta}@fstroj.uniza.sk
**Kielce University of Technology, Faculty of Mechatronics and Machine Design,
al. Tysiąclecia Państwa Polskiego 7, PL 25-314 Kielce, Poland, {lradzisz}@tu.kielce.pl

Abstract. This paper presents experimental measurement of the first stress invariant on the plate with hole at fatigue testing machine due to adiabatic elastic deformation. The theoretical part is concentrated on the theory of thermal stress analysis focusing on thermoelastic analysis. The experimental part is dedicated to the postprocessing of the measured data including analytical and numerical solutions for the plate with hole using finite element method (FEM).

Keywords: Thermoelastic stress analysis, Infrared camera, First stress invariant, Temperature change.

1. Introduction

The deformation of structural materials is followed by thermal effects. We recognize thermoelastic or thermoplastic stress analysis, depending on whether the load creates elastic or plastic strains. Thermoelastic stress analysis describes the relation between stress changes and temperature changes of a body in specimens. When the tensile deformation is in the elastic field specimen's temperature increases, on the other hand when there is a pressure load it decreases. The thermoplastic effect quantifies the heat generated by plastic deformation. In the elastic part it is possible under adiabatic conditions to determine the value of the first stress invariant on the material surface by measuring changes of the surface temperature. Adiabatic conditions are ensured by frequency higher than 2Hz for steel specimens and more than 20Hz for aluminum specimens. In plastic zone it is possible only to estimate the trace of stress tensor, because there is not a total conversion of mechanical energy into heat.

Surface temperature in thermal stress analysis was previously measured using thermocouples. The development of new technologies brought a new contactless method for measuring the temperature with greater sensitivity by using thermography. Infrared thermography is a unique technology which allows using an infrared detector to measure the surface temperature of an object. The measurement results is a thermographic image called thermogram. It is possible to determine the temperature changes on the surface of the measured object from the thermogram [1].

2. Thermal stress analysis

Thermoelastic and thermoplastic effect are summarized in a 3 – dimensional heat equation together with the effect of heat conduction [2]:

$$\rho C_{\varepsilon} \frac{\partial T}{\partial t} = k \left(\frac{\partial^2 T}{\partial x^2} + \frac{\partial^2 T}{\partial y^2} + \frac{\partial^2 T}{\partial z^2} \right) + T_0 \sum \frac{\partial \sigma_{ij}}{\partial T} \varepsilon_{ij}^e + \alpha_p \sigma_{ij} \varepsilon_{ij}^p, \quad (1)$$



where ρ is the material density, C_ε is specific heat capacity at constant deformation, T is absolute temperature, t is time, k thermal conductivity, x , y and z are spatial coordinates [3], T_0 is the initial temperature, σ_{ij} stress tensor, ε_{ij}^e is the rate of change of elastic deformation, α_p is the ratio of plastic deformation, which is converted to total heat of plastic deformation, ε_{ij}^p is the irreversible part of deformation tensor [2].

2.1. Thermoelastic effect

Thermoelastic effect is known as the conversion between mechanical forms of energy and heat. This transformation occurs when stress changes within a material element alter its volume. Density of energy generated in an object is transformed into local temperature changes. If specific heat of metal is high this phenomena is insignificant in terms of temperature change. Roughly 1 MPa change in stress state causes a temperature change of 1mK in steel [4].

The equation of thermoelasticity is derived from heat equation ignoring thermoplastic effect [5]:

$$\rho C_\varepsilon \frac{\partial T}{\partial t} = k \left(\frac{\partial^2 T}{\partial x^2} + \frac{\partial^2 T}{\partial y^2} + \frac{\partial^2 T}{\partial z^2} \right) + T_0 \sum \frac{\partial \sigma_{ij}}{\partial T} \varepsilon_{ij}^e. \quad (2)$$

To evoke the thermoelastic effect it is standard to load object cyclically so that no heat conduction takes place. Therefore the first term on the right side of (2) can be neglected. Time integration of (2) ignoring heat transfer leads to the following equation:

$$\rho C_\varepsilon \Delta T = T_0 \sum \frac{\partial \sigma_{ij}}{\partial T} \varepsilon_{ij}^e \text{ pre } i, j = 1, 2, 3. \quad (3)$$

Using Hooke's law and simple mathematical operations we obtain an expression that relates the trace of stress tensor (first stress invariant) σ_{ii} and temperature changes ΔT

$$\sum_{i=1,2} \sigma_{ii} = -\frac{\Delta T}{\alpha} \left[\frac{\rho C_\varepsilon}{T_0} - \frac{2\alpha^2 T_0}{(1-\nu)} \right]. \quad (4)$$

where ν - Poisson's ration (-)
 α - linear coefficient of thermal expansion (K^{-1}).

Equation (4) can be simplified by using the relationship between heat capacity at constant deformation C_ε and heat capacity at constant pressure C_p [5]:

$$C_\varepsilon = C_p - \frac{2E\alpha^2 T_0}{\rho(1-\nu)}, \quad (5)$$

where E - Young's modulus (Pa).

Substituting (5) to (4) we obtain

$$\Delta T = -\frac{\alpha}{\rho C_p} T_0 \sum_{i=1,2} \sigma_{ii}. \quad (6)$$

The term $\frac{\alpha}{\rho C_p}$ is a proportionality constant known as thermoelastic constant K . Therefore (6) can be rewritten as:

$$\Delta T = -KT_0(\sigma_1 + \sigma_2 + \sigma_3), \quad (7)$$

where σ_1 , σ_2 , σ_3 are changes in the principal stresses. The sum of principal stresses is known as the first invariant of stress or trace of stress tensor. Equation (7) says that the sum of the principal stresses is related to the dilatational component of deformation. Tensile load causes a decrease of temperature and vice versa.

3. Experimental part

The experimental part consists of measuring the temperature change by using an infrared camera in elastic field during cyclic tension – compression load. The measurement was carried out at the Department of material engineering, which has a frequency Zwick Roel pulsator. The sample was loaded by dynamic amplitude of 1kN with a frequency of 104 Hz. The measurement was performed on a plate with a hole. On the specimen a black emissivity spray (for LWIR) was applied to prevent the partial reflection of the surrounding surfaces. The emissivity spray for MWIR was not used, this problem is difficult and complex [6].

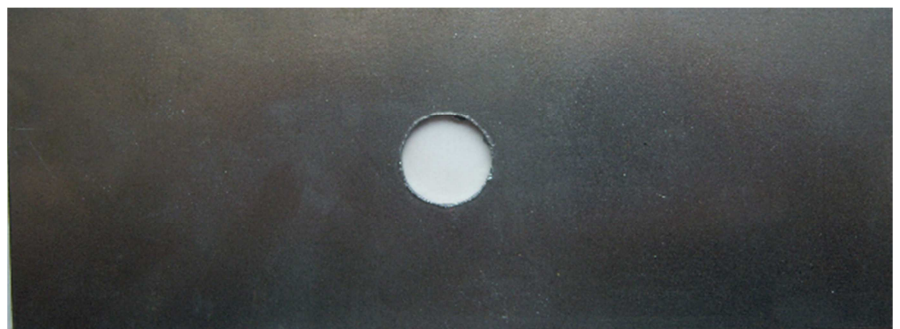
3.1. Measurement preparation

To measure the temperature change an infrared camera with a cooled detector FLIR SC7000 was used (Fig. 1a). Three softwares were used to evaluation the measured data: Research IR MAX, ALTAIR LI, ALTAIR. The software ALTAIR LI provides thermograms of stress fields using thermoelastic effect, which is based on a linear relationship between the temperature changes induced mechanical load and stress at the surface of the material. ALTAIR LI software is associated with the Lock In method that is used to extract the signal from noise and for synchronization signal load to signal measured data.

The sample used in the experiment was a steel plate with dimensions 50 x 111 mm with a thickness of 1 mm. In the middle of the plate a hole was drilled with a diameter of 12 mm (Fig. 1b). The specimen material is steel S355J.



a)



b)

Fig. 1 a) Infrared camera SC7000, b) Steel plate with hole.

3.2. Analytical solution

In plane stress problems during the applied loading of plate with hole results in stress concentration at the edge of the hole. For an infinite plate the stress is equal to three times the stress in full cross section. For finite plate (cantilevered on one side), the value is slightly higher. The maximum stress in place of stress concentrator is analytically calculated by the stress concentration factor K_t :

$$\sigma_{max} = K_t \cdot \sigma_{nom}. \quad (8)$$

The stress concentration factor is determined from the graph in Fig. 2. Nominal stress σ_{nom} is stress in cross section at half the length of the bar:

$$\sigma_{nom} = \frac{P}{(H - d).thickness} \quad (9)$$

where P is loading force in N and dimensions are given according to Fig. 2.

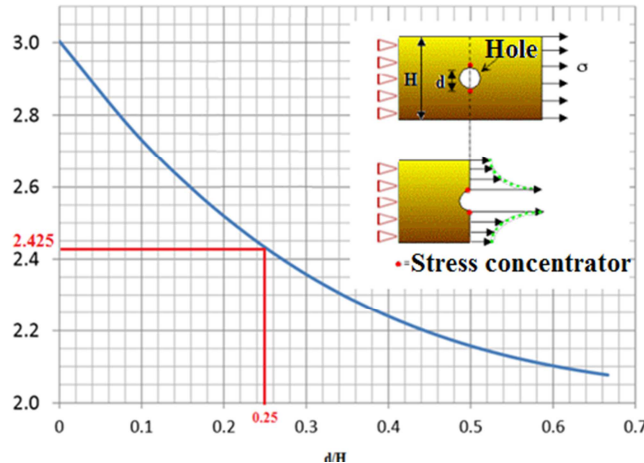


Fig. 2 Stress concentration factor (www.latech.com).

If the sample is loaded with force 1kN, the nominal stress is calculated:

$$\sigma_{nom} = \frac{P}{(H - d).thickness} = \frac{1000}{(50 - 12).1} = 26.3 \text{ MPa}, \quad (10)$$

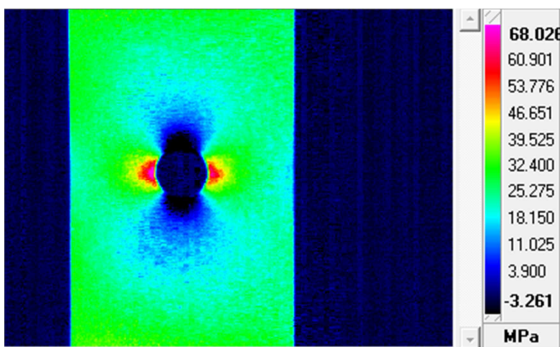
and the stress in the field of stress concentration:

$$\sigma_{max} = 2,425.26,3 = 63.8 \text{ MPa}. \quad (11)$$

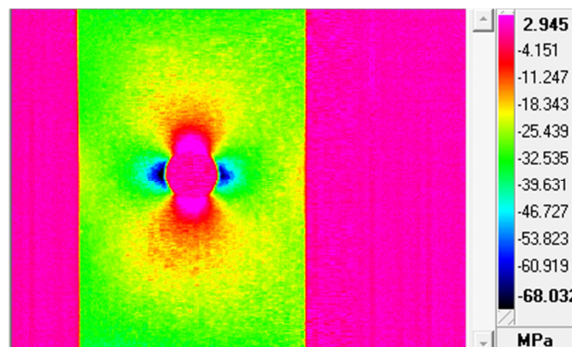
In full cross section stress evoked by loading force of 1kN is 20 MPa. In the place of stress concentration it is 64 MPa after rounding.

4. Measurement results

Figure 3 shows thermograms of stress fields under tension (Fig. 3a) and compression loading (Fig. 3b). Here we can see that the maximum stress is at the edge of the hole as we assumed in the analytical solution.



a)



b)

Fig. 3 Measured results for a) tension loading, b) compression loading.

Further processing of the results was carried out in ALTAIR software, which provides the user greater comfort with processing of measured data. For a sample in tension loading (Fig. 4) and compression loading (Fig. 5) was chosen transverse line and plotted curve of the first stress invariant in each pixel. In Fig. 4 you can see that maximum first invariant stress is on the edge of the hole and its value is 68.17 MPa. The maximum value during compression loading is -68.18 MPa.

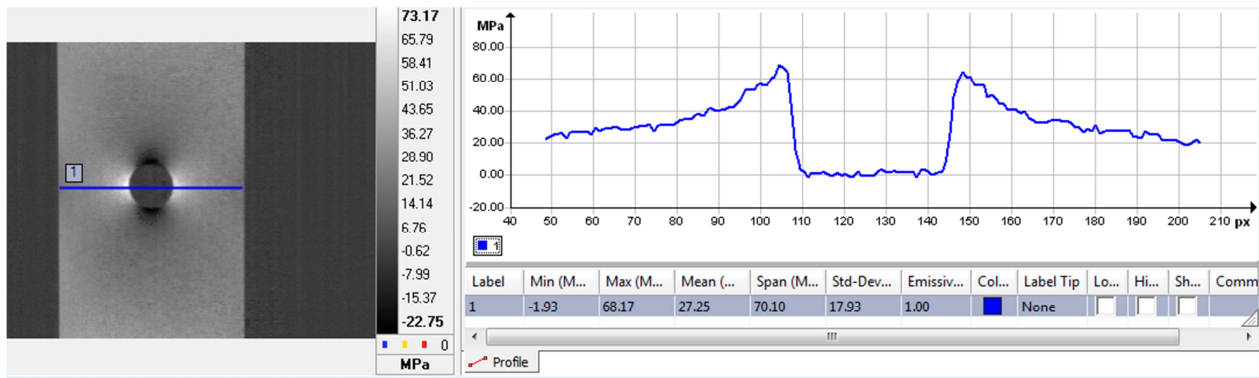


Fig. 4 Measured results for tension loading.

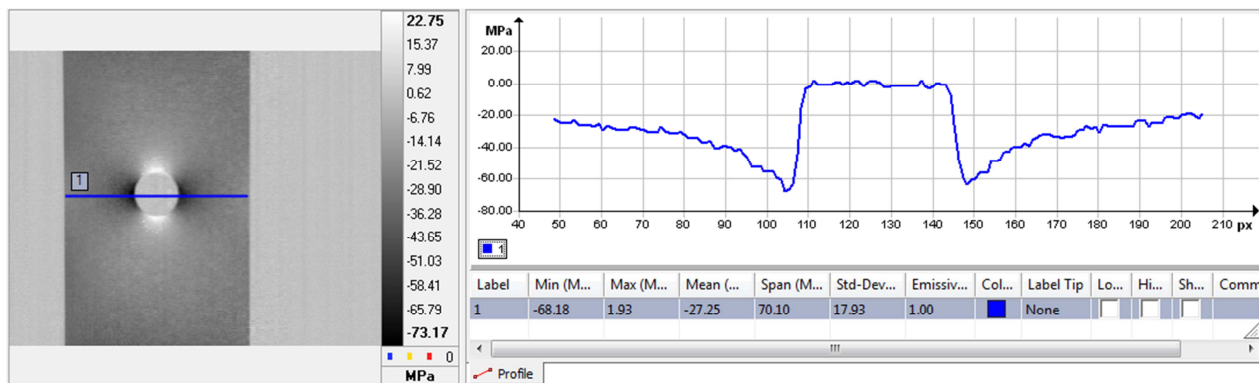


Fig. 5 Measured results for compression loading.

5. Numerical solutions

Numerical solution was performed in ANSYS FEM software. Structural analysis was created to find out stress field of the specimen during cyclic loading tension – compression. The mesh is generated by 4 node – Plane 42 elements. This is a 2D plane element which is used for modeling plane stress. The applied material is elastic, isotropic with properties of steel S355J:

- Young's modulus $E=200$ GPa,
- Poisson's ratio $\mu=0.3$,
- density $\rho=7800$ kg m⁻³.

The model is loaded by cyclic loading with amplitude of 1kN and frequency of 104 Hz. Boundary conditions were defined according to the experiment. The results of the structural analysis for tensile and compressive loading are presented in Fig. 6. Here we can see that maximum first invariant stress for tensile loading is 65.2 MPa after rounding and for compressive loading is -65.6 MPa.

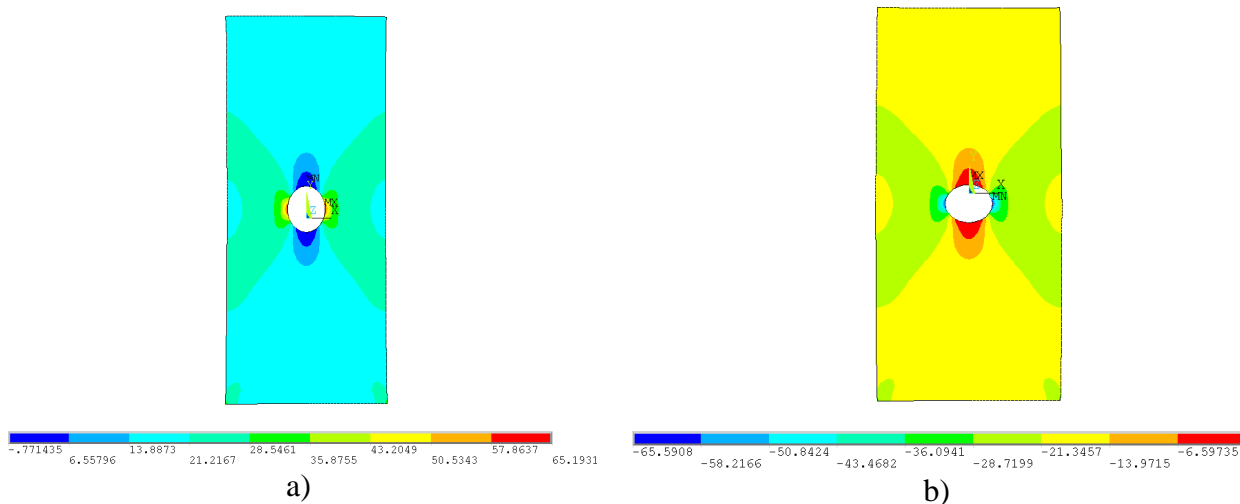


Fig. 6 Numerical solutions for a) tension loading, b) compression loading.

6. Conclusion

The paper deals with thermal stress analysis focusing on the thermoelastic analysis. The introduction provides an overview of the theory of thermal stress analysis. The experimental part is preceded by the preparation of the measurement including analytical solution for the plate with a hole. Measured data are compared with numerical solution using the finite element method.

In this paper we compare measured data with analytical and numerical solutions. The specimen used for measurement was selected due to better comparison of results. During solution of plane stress of plate with hole stress concentration at the edge of the hole occurs. For analytical solutions is the stress value 63.8 MPa. From thermograms we obtained the maximum first invariant of stress 68.17 MPa in tensile loading. The maximum value during compression loading is -68.18 MPa. Numerical solution was performed in ANSYS FEM software. The result of the structural analysis for tensile loading is 65.2 MPa and for compressive loading is -65.6 MPa. The error in measurements is less than 10 percent.

Acknowledgement

This work was supported by the Slovak Research and Development Agency under the contract No. APVV-0736-12.

References

- [1] EISENLOHR, A. 2012. *Adiabatic temperature increase associated with deformation winning and dislocation plasticity*. [online]. 2012. Available online at <www.sciencedirect.com>.
- [2] PLUM, R. a kol. 2010. *Extended thermoelastic stress analysis applied to carbon steel and CFRP*. [online]. 1999. Available online at: <<http://ebookbrowse.net/we5a3-pdf-d75918406>>.
- [3] WANG, G. a kol. 2012. *Thermographic studies of temperature evolutions in bulk metallic glasses: An overview*. In *Intermetallics*. [online]. 2012. Available online at: <www.sciencedirect.com>. ISSN: 0966-9795.
- [4] BRÉMOND, P. 2007. *New developments in ThermoElastic Stress Analysis by Infrared Thermography*. [online]. 2007. Available online at: <<http://www.ndt.net/article/panndt2007/papers/138.pdf>>.
- [5] BARTON, J. 1999. *Introduction to thermoelastic stress analysis*. In *Strain* [online]. 1999. Available online at: <<http://onlinelibrary.wiley.com/doi/10.1111/j.1475-1305.1999.tb01123.x/abstract>>. ISSN: 0039-2103
- [6] HONNER M. – HONNEROVA, P. 2015. *Survey of emissivity measurement by radiometric methods*. In: *Applied Optics*, Vol. 54, 2015, pp. 669-683. <<http://dx.doi.org/10.1364/AO.54.000669>>.



Evaluation of structural properties of braked railway wheel

* Andrej Suchánek, * Jozef Harušinec

University of Žilina, Faculty of Mechanical Engineering, Department of Transport and Handling Machines,
Univerzitná 1, 01026 Žilina, Slovakia, {andrej.suchanek, jozef.harusinec}@fstroj.uniza.sk

Abstract. Article deals with the detection of reduced stress in a braked railway wheel based on thermal transient analysis on virtual models, because they influence the characteristics of the railway wheels. Structural analysis was performed by means of the ANSYS Multiphysics program system package. Thermal transient analysis deals with the detection of temperature fields which are result of braking by brake block. The applied heat flux represents the heat generated by friction of brake block. It is applied to the quarter model because of the acceleration calculation. This analysis simulates two braking with subsequent by cooling. Distribution of the equivalent stress was detected in the cross section railway wheel, at selected points. The input parameters were used from the thermal transient analysis. These equivalent stresses result due to thermal load.

Keywords: Railway wheel, Brake block, Residual stress, Transient thermal analysis.

1. Introduction

The brake system of railway vehicles is an important subsystem in terms of driving safety. Investigated property is process of non-stationary temperature fields, generated by the braking railway vehicles. Thermal load of railway wheels arises when braking by the brake blocks [2, 3, 4]. It has significant share of the impacts that lead to wear - modifications of the driving wheel profile and damage to the wheel tread [7, 8]. We have to consider two factors in the process of braking. Railway wheel is overheated by the brake block at the point of contact. It is loaded by the normal and tangential stress, which is the source of the braking process. Brake blocks are structurally designed as adhesive brakes. The braking effect of the vehicle with respect to the track is carried out in the wheel-rail contact via the contact surface.

Professional public must pay attention to studying the effects of thermal and mechanical loading wheels of railway vehicles of reasons: the operation of vehicles, protection of life and health of the traveling public, reliable transport material and minimizing the negative effects of rail traffic on the environment [5].

Article deals with the detection of reduced stress in a braked railway wheel based on thermal transient analysis. Railway wheel is loaded by heat flux, which is applied on the contact surface. This topic is discussed in more detail in [6, 11, 12, 13].

2. ANSYS program package

The program ANSYS (Fig. 1) uses the finite element method. Modeling of the finite element method belongs to the group of numerical methods. This method develops due to the continuous increase in computing power. Its core is the discretization of bodies on the files of finite elements [1, 10]. These elements form analogue after parts field that can be mathematically written [9].

The ANSYS program is generally nonlinear, multiphysics program including structural and thermodynamic analysis, analysis of flow continuum, analysis electrostatic and electromagnetic fields, and acoustic analysis. All these analyses can be performed individually, but thanks ANSYS multiphysics conceived program can also be included in one common analysis. The ANSYS

program allows you to not only check calculations, but also enables optimization and sensitivity analysis due to parameterized computational models, as well as the calculations of reliability.

ANSYS Mechanical product is intended to simulate the structural and thermodynamic tasks. The program includes the complete set of linear and nonlinear simulation with using linear and non-linear elements, material models, and contact non-linear algorithms.

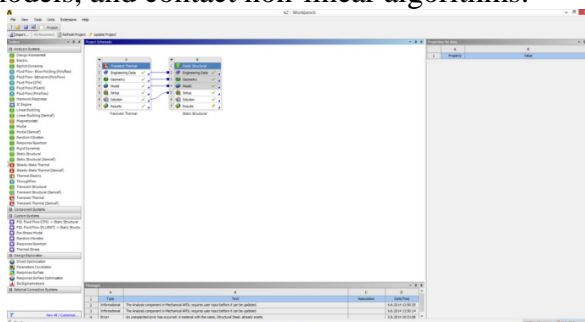


Fig. 1 ANSYS Workbench program system environment.

3. Transient thermal analysis in ANSYS program

The problem simulates heating of the railway wheel tread. The railway wheel is braked by the brake block. The heat generated by friction of brake block, represents the heat flux of 40 kW. It is around the circumference of the wheel. The Analysis simulated two braking for time 100 seconds. The heat flux is applied to the tread. Railway wheel cools for 200 seconds after each braking. The value of heat flux is then zero. A quarter model of railway wheel was created using CATIA program and imported into ANSYS program.

3.1. The definition of material properties

Railway wheel is made of steel DIN 40Mn4. The thermal properties used in the simulation are shown in Tab. 1.

Property	Railway wheel	Air
Density ρ [kg.m ⁻³]	7850	1.170
Heat capacity C_p [J.kg ⁻¹ .K ⁻¹]	486	1100
Thermal conductivity k [W.m ⁻¹ .K ⁻¹]	52	0.026
Emissivity [-]	0.28	-
Dynamic viscosity [Pa.s]	-	$1.8 \cdot 10^{-5}$

Tab. 1 Thermal properties of materials.

3.2. Definition of boundary conditions

A quarter model was used because of the acceleration calculation. The symmetry has been applied to the model. The values of the heat flux (power) (Fig. 3) are shown in Tab. 2. Dependence heat flux to time is shown in Fig. 2.

Step	Time [s]	Heat flux [W]
1	0	0
1	10	10000
2	100	10000
3	101	0
4	300	0
5	310	10000
6	400	10000
7	401	0
8	600	0

Tab. 2 Dependence heat flux to time.

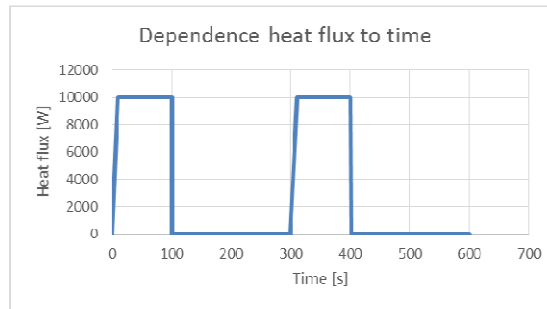


Fig. 2 Dependence of a heat flux to time.

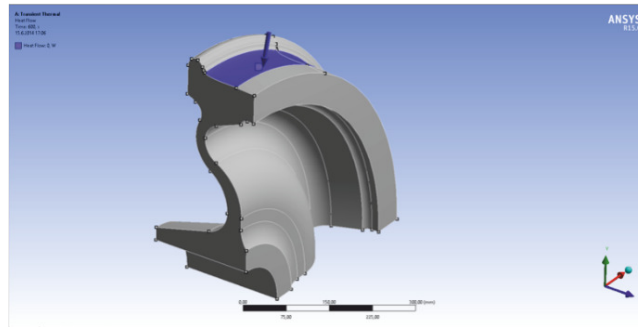


Fig. 3 Heat flux applied to the tread of the rail wheel.

Reference ambient temperature was set to 20°C.
Thermal radiation was set to all areas of railway wheel.
Six degrees of freedom were taken to the railway wheel (Fig. 4).

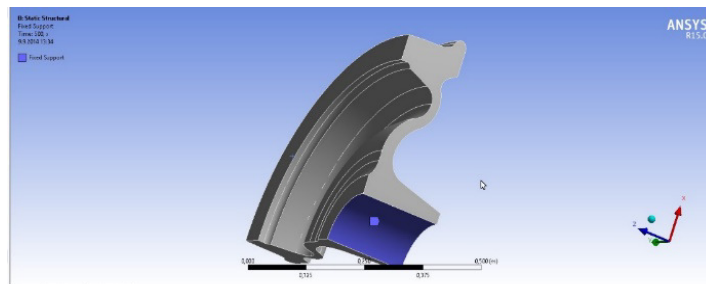


Fig. 4 Applied boundary conditions.

Finite element mesh (Fig. 5) was created according to the dimensional parameters with the following parameters:

- element size: 10 mm,
- element type: SOLID 90,
- number of elements: 5075,
- number of nodal elements: 26156.

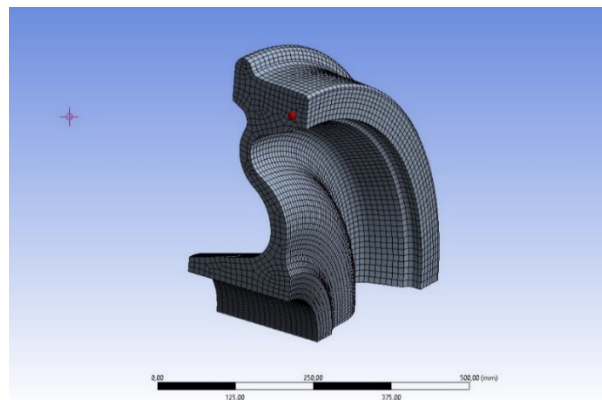


Fig. 5 Finite element model.

Setting solver:

- direct solver with fixed setting step and automatic control of convergence.

Computation parameters:

- processor: Intel Core i7 3.3 GHz (6 core),
- memory (RAM): 64 GB,
- computation time about 25 minutes.

3.3. Results

The maximum temperature value was 172°C at the time of 400 seconds (Fig. 6), which is at the end of the second braking. The maximum value of the temperature was 138.8°C at the end of the first braking. The maximum values were detected in the surface layer of the rail wheel.

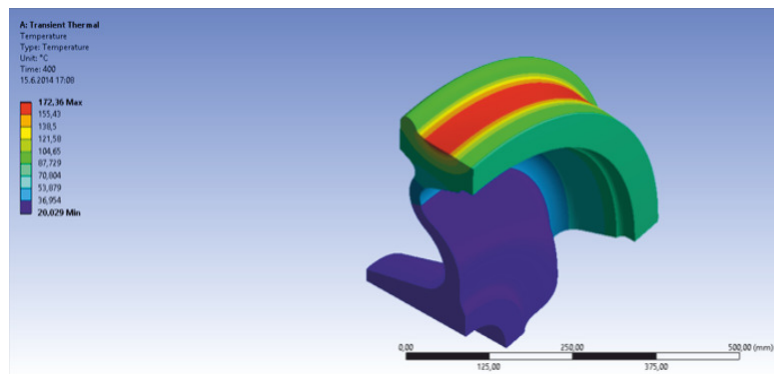


Fig. 6 Temperatures in railway wheel at the end of braking (time 400 s).

The temperatures in the cross section of the rail wheel, at selected points (Fig. 7), are shown in Fig. 8.

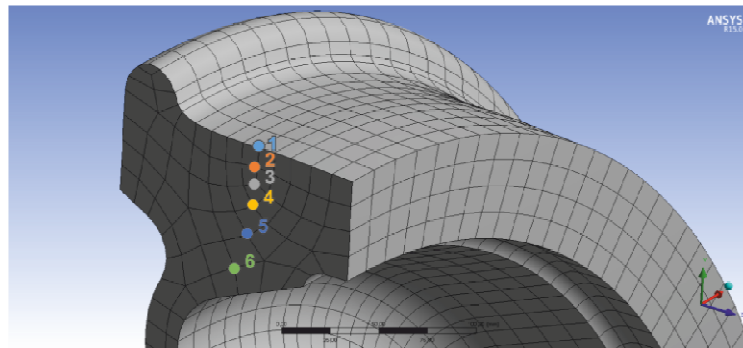


Fig. 7 The selected points, where were evaluated the temperatures and stresses.

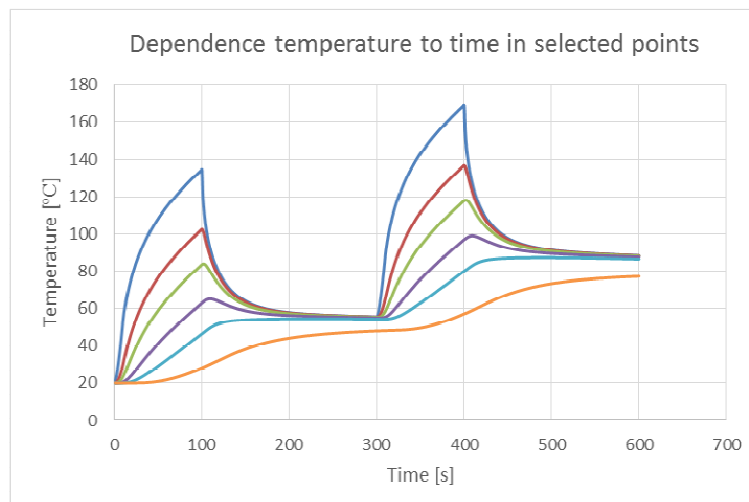


Fig. 8 Dependence temperature to time in selected points.

4. Calculation of equivalent stress

Distribution of equivalent stress can be detected based on thermal transient analysis of braked railway wheel. These stresses result due to thermal load. We could use the parameters from the previous thermal transient analysis thanks the ANSYS program.

The maximum equivalent stress (von - Mises) value was 212.55 MPa at the time of 400 seconds (Fig. 9).

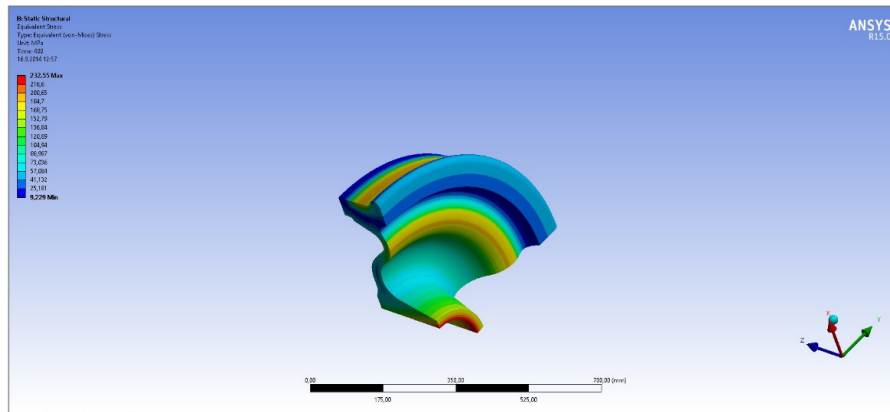


Fig. 9 Equivalent stress in railway wheel at the end of braking (time 400 s)

The equivalent stresses in the cross section of the rail wheel, at selected points (Fig. 7), are shown in Fig. 10.

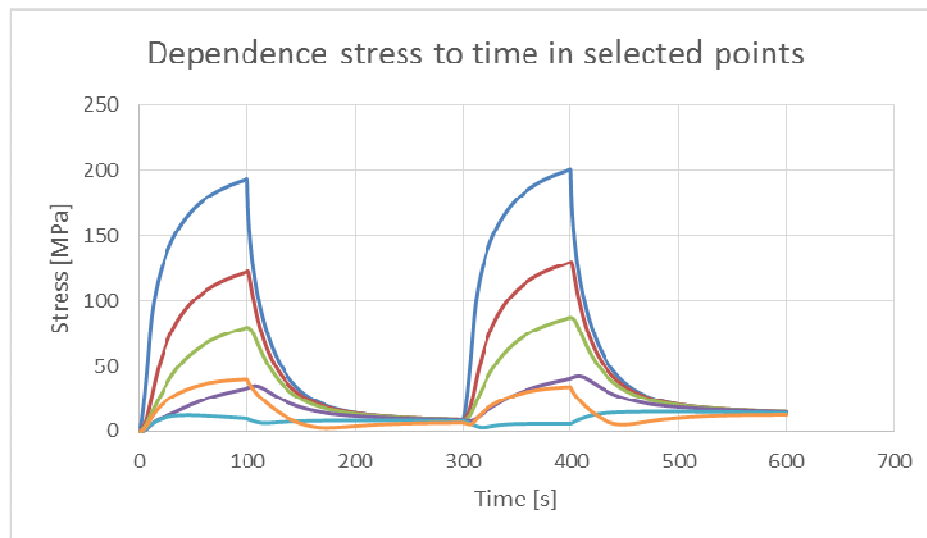


Fig. 10 Dependence stress to time in selected points.

5. Conclusion

One possibility for identifying the impact of thermal and mechanical loading on braked railway wheel is the use of appropriate software and implementation of computer analyzes.

The article deals with the detection of structural properties braked railway wheel using a program that uses the finite element method.

Structural analysis was done on the basis of thermal transient analysis, where it was possible to determine the distribution of temperature fields during braking with constant heat flux. Thermal loads are used as input parameters from the previous thermal transient analysis. Distribution of equivalent stresses is the result of the analysis. These stresses result due to thermal load. This problem was solved in ANSYS program, which was suitable for this assignments.



Acknowledgement

The work was supported by the Scientific Grant Agency of the Ministry of Education of the Slovak Republic and the Slovak Academy of Sciences in project No. 1/0347/12: “Railway wheel tread profile wear research under the rail vehicle in operation conditions simulation on the test bench”, project No. 1/0383/12: “The rail vehicle running properties research with the help of a computer simulation.” and the project No. APVV-0842-11: “Equivalent railway operation load simulator on the roller rig”.

Research-Educational Center of Rail Vehicles (VVCKV)

References

- [1] GERLICI, J., LACK, T. *Test benches computer control software tools development*. Scientific bulletin of North University of Baia Mare: Fascicle: Mechanics, Tribology. Technology of Machine Manufacturing. - ISSN 1224-3264. - Series C, Vol. XVII. Baia Mare 2003.
- [2] GERLICI, J., ŘEZNÍČEK, R.. *Temperature fields in the brake blocks when braking on an incline*; XI. International conference "Current problems in rail vehicles". (In Slovak). Česká Třebová. 1994.
- [3] GERLICI, J., HLAVŇA, V., ŘEZNÍČEK R. *Simulation of down-hill braking with a shoe brake*, 4.th mini conference on vehicle system dynamic, identification and anomalies. Technical university of Budapest, 1994.
- [4] GERLICI, J., LACK, T., KALINČÁK, D. *Laboratory simulation of braking with a shoe brake*.
- [5] SITARZ, M.: *Railway wheelsets*. Monograph. ISBN 83-7335-151-5. Chapter 5. Silesian university of technology, Gliwice Poland, 2003.
- [6] GERLICI, J., LACK, T., HARUŠINEC, J. *The test stand load modulus implementation for the realistic railway operation in the laboratory conditions*. Manufacturing technology: journal for science, research and production. - ISSN 1213-2489. - Vol. 13, no. 4 (2013).
- [7] HARUŠINEC, J., SUCHÁNEK, A., GERLICI, J., LACK, T. *Locomotive brake unit modification for laboratory experimental tests*. (In Slovak). DTDT 2012. J. E. Purkyně University. ISBN 978-80-7414-510-0.
- [8] LACK, T., GERLICI J. *Contact area and normal stress determination on railway wheel / rail contact*. Communications, the scientific letters of the University of Zilina, 1/2005. ISSN 1335-4205, EDIS – Publishing Institution of the University of Zilina 2005.
- [9] LACK, T., GERLICI J. *The FASTSIM method modification in speed up the calculation of tangential contact stresses between wheel and rail*. Manufacturing technology: journal for science, research and production. - ISSN 1213-2489. - Vol. 13, no. 4.
- [10] MAN, K. W. *Contact mechanics using boundary elements*. Topics in engineering. Volume 22. Computational mechanics publication. ISBN: 1 85312 334 X. p. 185. Southampton 1994.
- [11] ŘEZNÍČEK R., GERLICI J., LACK T. *Stress analysis monoblock wheels braked by FEM* (In Slovak). ŽELSEM '93, Savings in railway", University of Zilina 1993. Loučeň, 1993.
- [12] SUCHÁNEK, A., HARUŠINEC, J., GERLICI, J., LACK, T. *Analysis of models for simulation computations and experimental detection of stress in braked railway wheel*. TRANSCOM 2013, section 6. EDIS – Publishing Institution of the University of Zilina, 2013. ISBN 978-80-554-0695-4.
- [13] SUCHÁNEK, A., GERLICI, J., HARUŠINEC, J., LACK, T. *Analysis of temperature distribution in a braked railway wheel during braking by the brake block*. TRANSCOM 2013, section 6. EDIS – Publishing Institution of the University of Zilina, 2013. ISBN 978-80-554-0695-4.
- [14] SUCHÁNEK, A. *Analysis of stress distribution in a braked railway wheel* (In Slovak), PhD thesis, University of Zilina, Faculty of Mechanical Engineering.



Visualization and measurement of flow in flue gas path by particle image velocimetry method

*Katarína Sulovcová, *Jozef Jandačka, *Štefan Papučík

*University of Žilina, Faculty of Mechanical Engineering, Department of Power Engineering, Univerzitna 1, 01026 Žilina, Slovak Republic, {katarina.sulovcova, stefan.papucik, jozef.jandacka}@fstroj.uniza.sk.

Abstract. Higher particulate matter concentration in ambient air has harmful influence, therefore it is important to decrease their amount from every source. In small combustion installation with biomass combustion we can influence amount of particulate matter in flue gas path. Particle image velocimetry can be used for visualization and measurement of fluid medium and also particles flow. This method is able to measure velocity and direction of vectors without affecting of flow and help to change the flow in flue gas path with regard to decreasing particulate matter concentration. Particle image velocimetry is also good tool for verification of simulation from computational fluid dynamic program.

Keywords: Particulate matter, Small combustion installation, PIV method,

1. Introduction

Approximately 14 % of the world's energy use is derived from biomass and in developing countries the corresponding figure is 35 %. Many countries also encourage the adoption of biomass combustion in order to reduce emissions of greenhouse gases, improve energy security and rural development. However, combustion of biomass, along with many other industrial, commercial and transport activities, leads to emissions of air pollutant that are potentially harmful to human health [1].

Residential wood combustion (small heat sources) for heat production has been assessed to be a major source of fine particle mass emissions, particulate polyaromatic hydrocarbons (PAHs) and certain gaseous pollutants such as volatile organic compounds (VOCs) throughout Europe [2]. Those small sources are not controlled and not monitored and especially during heating season produce large amounts of pollutants.

Many European countries observed increased particulate matter concentration in ambient air, what has negative influence on air quality and on human health. Particulate matter pollution can cause or aggravate cardiovascular and lung diseases, heart attacks and arrhythmias, affect the central nervous system, the reproductive system and cause cancer [3][2].

Therefore is also important to decrease particulate matter production from those sources.

1.1. Particulate Matter

Bigger attention is paid to particulate matter with smaller diameter. Particles PM10 with diameter under 10 micrometer and particles PM2,5 with diameter less than 2.5 micrometer belong into the group of smallest particles Those particles are able to infiltrate deep into the lungs and cause serious damage. They contribute to rising of cardiovascular and respiratory problems too. Moreover they are able to keep longer time in the atmosphere and could be drifted hundreds of kilometers from the source of pollution. In contrast to fine particles are course particles (bigger than 10 microns) filtered during breathing by natural process in a top part of respiratory system and don't charge the organism. Bigger particles with diameter above 100 microns are relatively quickly settled down near the source of pollution [1], [3],[2][4].

2. Modelling of Particulate Matter Flow

Modelling of physical changes by simulation program (computational fluid dynamics - CFD) is advantage for science and technology. It is safer, more economical and more environmentally friendly and it may significantly reduce the “trial and error” development time needed if experiments only are used for design optimization. For example it can be used as an option to observe influence of construction changes on the flue gas flow with particulate matter [5].

Results of modelling are velocity, temperature and particle layout, which can be used for particulate matter behaviour observation inside the flue gas path (Fig.1). Form and velocity of flow influence particulate matter capture in the flue gas path. Optimized geometry of flow can decrease particulate matter emission from small heat sources. Therefore is useful for optimizing to know vector maps of flow.

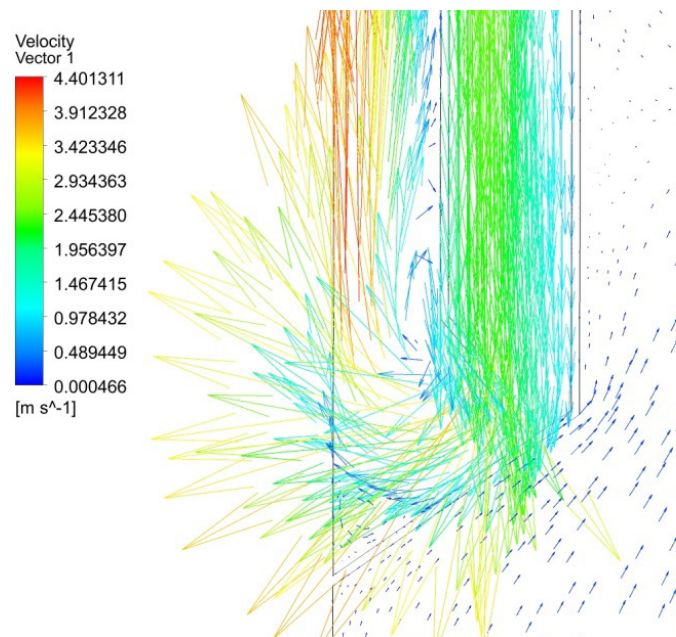


Fig. 1 Vector map of flow.

3. Particulate Image Velocimetry Method

Particle Image Velocimetry (PIV) is a whole-flow-field technique which provides instantaneous velocity vector measurements in a cross-section of a flow. Two velocity components are measured, resulting in 2D velocity vectors, but use of a stereoscopic approach permits all three velocity components to be recorded, resulting in instantaneous 3D velocity vectors for the whole measured area. The use of modern digital cameras and dedicated computing hardware, results in real-time velocity maps [6].

Principle of velocity measurement is based on recording of particles movement in flow and subsequent evaluation of this motion (Fig.2). The seeding particles in the target area of fluid flow are illuminated by laser pulses with defined time difference and the velocity vectors are derived from sub-sections of the target area of the particle-seeded flow by measuring the movement of particles between two light pulses. Positions of seeding particles are recorded on digital camera. The camera is able to capture each light pulse in separate image frames [6], [7].

Elementary equation, which evaluate those recordings is equation (1):

$$v = \frac{x}{t} \quad (1)$$

where distance x is movement of particle in fluid flow per time interval t .

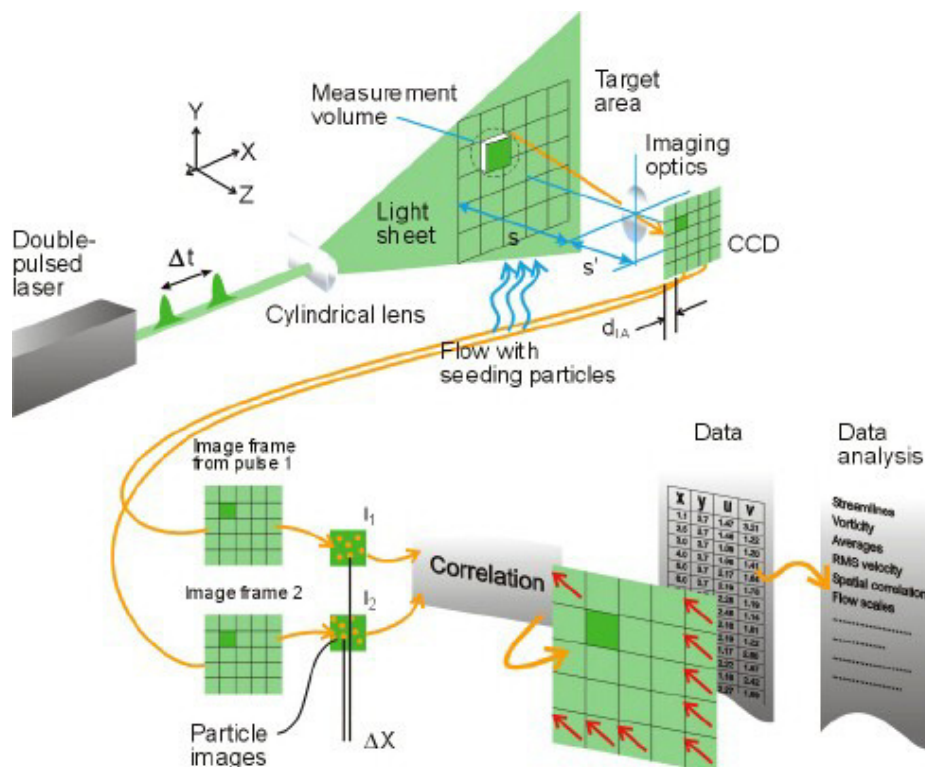


Fig. 2 Scheme of PIV principle [6].

Once a sequence of two light pulses is recorded, the images are divided into small subsections called interrogation areas. The interrogation areas from each image frame, I_1 and I_2 , are cross-correlated with each other, pixel by pixel (Fig. 3) [6].

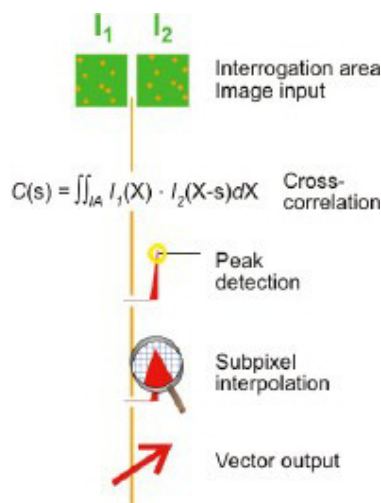


Fig. 3 The correlation of the two interrogation areas, I_1 and I_2 , results in the particle displacement represented by a signal peak in the correlation [6].

The correlation produces a signal peak, identifying the common particle displacement. An accurate measure of the displacement - and thus also the velocity - is achieved with sub-pixel interpolation. A velocity vector map over the whole target area is obtained by repeating the cross-correlation for each interrogation area over the two image frames captured by the camera [6], [7].

According simulation model which was used for modelling of flow is prepared real model from plexiglass for measurement by PIV method. For experiment is necessary to prepare the same condition as was set up in the simulation, it means to use approximately same temperature of air (as in simulation) and set up the same chimney draft. Position of devices for PIV measurement is done according scheme of the experiment in Fig. 4, where camera is able to record fluid flow.

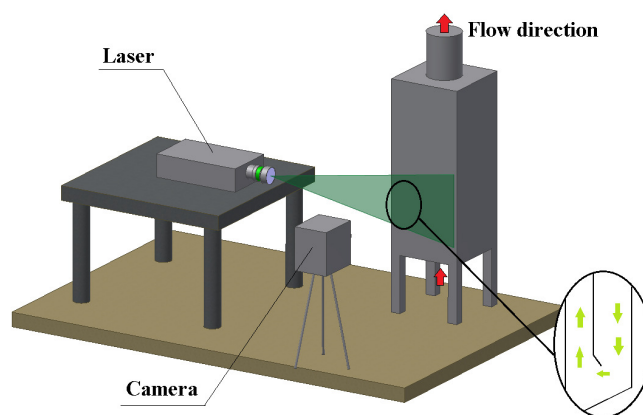


Fig. 4: Experiment scheme.

4. Verification

Verification of changed, optimized results can be done by gravimetric method in real small heat source. Gravimetric method is the manual single method with sampling of the flow gas by probe. It is based on determination of the median concentrations by sampling from multiple points of measurements cross-section and their subsequent gravimetric assessment. Solid contaminants are usually separated by an external filter [8].

According final particulate matter concentration is possible to observe if geometrical changes also change the amount of particulate matter in flue gas path.

5. Conclusion

There are efforts to reduce particulate matter emission from small heat sources. Construction changes of combustion appliances can satisfy the following requirement. Use of CFD simulation is good tool for observation of particulate matter behaviour. For verification is suitable measurement by PIV method. CFD simulation together with PIV measurement method can be appropriate solution how to find out how is flow of particulate matter in combustion devices influenced and see how particulate matter concentration can be depending on construction changes. That can also help to do construction changes with regard to decrease particulate matter pollution.

Acknowledgement

This work is supported by the financial assistance of the project VEGA 1/0548/15

References

- [1] ABBOT, J., STEWART, R., FLEMING, S., STEVENSON, K., GREEN, J., COLEMAN, P. *Measurement and Modelling of fine particulate emission (PM10 & PM2.5) from wood – burning biomass boilers*, Edinburg 2008,
- [2] TISSARI, J., *Fine particle emissions from residential wood combustion*, online: Doctoral dissertation, Kuopio University Publications, C. Natural and Environmental Sciences 237, 2008. p. 63. (PDF), Finland, Kuopio 2008
- [3] GUERREIRO, C. , DE LEEUW, F., FOLTESCU, V., SCHILLING, J., VAN AARDENNE, J., LÜKEWILLE, A., ADAMS, M., *Air quality in Europe – 2012 report* ,European Environment Agency,
- [4] JANDACKA.; M. MALCHO.: *Biomass as energy source*. Zilina, Editorship Juraj Stefun GEORG, 2007, Slovakia;.
- [5] VAN LOO, S., KOPPEJAN, J., *The Handbook of Biomass Combustion and Co-firing*, London : Washington, 2008.
- [6] Dantec Dynamics. *Particle Image Velocimetry measurement principles*. Online: <http://www.dantecdynamics.com/measurement-principles-of-piv>
- [7] KOPECKÝ, V. : *Laserová enometrie v mechanice tekutin*, Liberec 2008
- [8] NOSEK R., HOLUBČÍK, M., *Measurement of particulate matter during the combustion of phytomass in small heat sources* Power control and optimization : proceeding of seventh global conference : Yangon, Myanmar, 2013. -



Design of Non-Standard Long Railway Wagon with Variable Use of Loading Platform

*Pavol Šťastniak

University of Žilina, Faculty of Mechanical Engineering, Department of Transport and Handling Machines,
Univerzitná 8215/1, 010 26 Žilina, Slovakia, pavol.statniak@fstroj.uniza.sk

Abstract. The article present the design of non-standard long railway freight wagon with variable use of loading platform with regard to the safe operation and assessment of the properties by the calculation methods of simulation analysis. 3D model of wagon was created in a computer program PTC/Creo. Wagon chassis frame was subjected to the static and dynamic analysis in programs ANSYS and ADAMS/Rail. On the basis of computer aided simulation analysis was optimized the frame of the wagon. This wagon chassis frame will be able to offer even more capacity and utilize less resources and energy than current wagons for intermodal transport.

Keywords: Wagon design, Chassis frame, Computer simulation analyzes.

1. Introduction

Indeed nowadays about 1.5 billion t/km are transported in Europe by lorry at distances farther than 150 km, conversely only 0.4 billion t/km (20%) are transported by train [1], this entails important costs for fossil fuels. In the nearby future when transportation has to be more sustainable it seems quite clear that freight railways will win the mode choice more often.

For this to happen though, it is necessary that freight railways, apart from lowering their prices, significantly improve highly increase the quality of transportation. In that sense, quality standards such as reliability, flexibility, availability, cargo security and safety, punctuality, customisation, marketability, traceability, complementary servicing and time for transport among others have to be improved by railways as well.

Hence, rail freight has the challenge to become excellent and to gain in reputation. There are many actions to increase quality in rail freight transport; one of them is the optimisation of the current wagon fleet to improve availability, flexibility, marketability, commercial speed, cargo security and cost [2]. This optimisation has to respond to the actual trends of transport demand and has to be in consonance with the required and feasible infrastructure upgrades.

The basic idea of new wagon is that in the future, longer loading surfaces without interruptions, as well as more capable platforms with higher axle loads and with lower loading heights will be necessary to increase the capacity of the freight railway transportation.

The time schedule is divided to several subtasks as shown in Fig. 1.

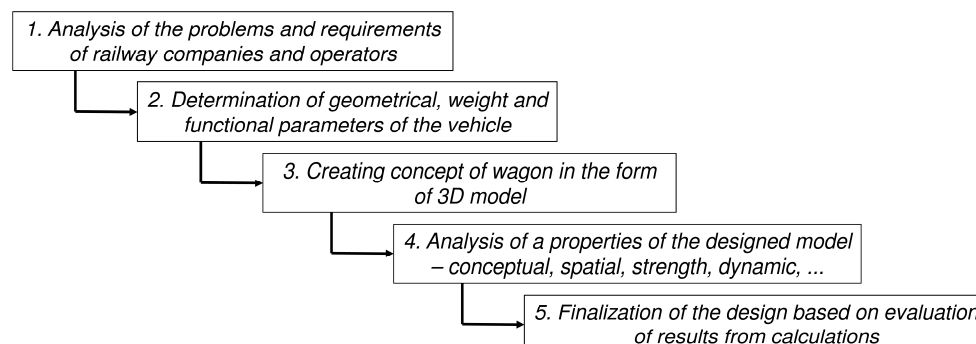


Fig. 1. The time schedule segmented into several subtasks.

2. Analysis of the problems and requirements of railway operators

Intermodal continental transports utilize a large amount of unit types (much more than hinterland (sea) transportation) and that increases the amount of possible loading cases for the trains. In that sense, there would be an optimal wagon for each case but this wagon could be sub-optimally utilized for other cases. This variety of cases makes difficult to know which wagon is the optimal for an averaged situation.

Wagons represent an important investment for companies (c.a. 100 000 € per wagon) and they should be extensively utilized during their whole life cycle (25-30 years) to achieve profitability. For this reason, wagons specialized in one kind of units are usually employed for other unit types even if they are not 100% efficient at it [3].

From individual wagons were created four trains, whose maximum length were 500 m and have been investigated the parameters listed in Fig. 2.

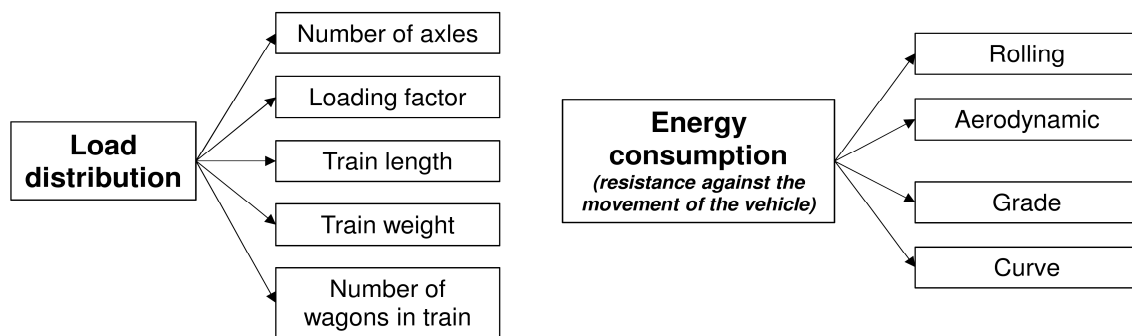


Fig. 2. Load distribution and energy consumption - Investigated parameters.

Concluding that:

- 106 ft wagon suits optimally the FTL (full truck load, semitrailers) segment and performs quite reasonably in other segments except the pure bulk ones,
- 60 ft wagon is the optimal wagon for the pure bulk segment,
- 80 ft wagon would offer better performance than 106 ft in averaged situations (mainstream shuttles), but it is not recommended for specialized FTL transports, however it performs better than 106 ft wagon in bulk segments,
- 90 ft wagon would offer better performance than 80 ft if in the future the 45 ft unit is widely introduced.

The results of the capacity simulations have showed that an 80 ft long wagon could lead to an important advantages in efficiency. These advantages would be amplified by averaged cases with mixture of units, for example in the case of a shuttle between the two important continental terminals with an unknown and varying proportion of units [4].

It could be concluded that the 80 ft wagon would bring about an important gain for continental transports since it would enable better utilization of space (loading length) on trains than existing wagon technologies. The 80 ft wagons would be able to transport same or even more amount of units with the fewer axles and the less deadweight. Furthermore the aerodynamics would improve (fewer gaps between containers, fewer bogies per meter) and the noise emissions would be reduced due fewer axles per train.

Longer loading lengths 85 ft and 90 ft could have an advantage too, but only if the 45 ft unit is widely introduced and if it dominates in intermodal traffics, which is not the actual case. A revision of this issue has to take place in the approximately 5 years.

The strategic procedure would be to design a 80 ft without pocket and try to make it as cheap as possible. By this it could be very competitive in its market segment [5, 6].

3. Concept of wagon in the form of 3D model

The model presents a complete structure of the 4 – axle freight wagon (Fig. 3) for transportation of ISO containers and swap bodies which should meet prescriptions TSI-WAG, valid regulations UIC, agreement on the reciprocal use of freight wagons in international traffic AVV (RIV), recommendations ERRI and norms EN.

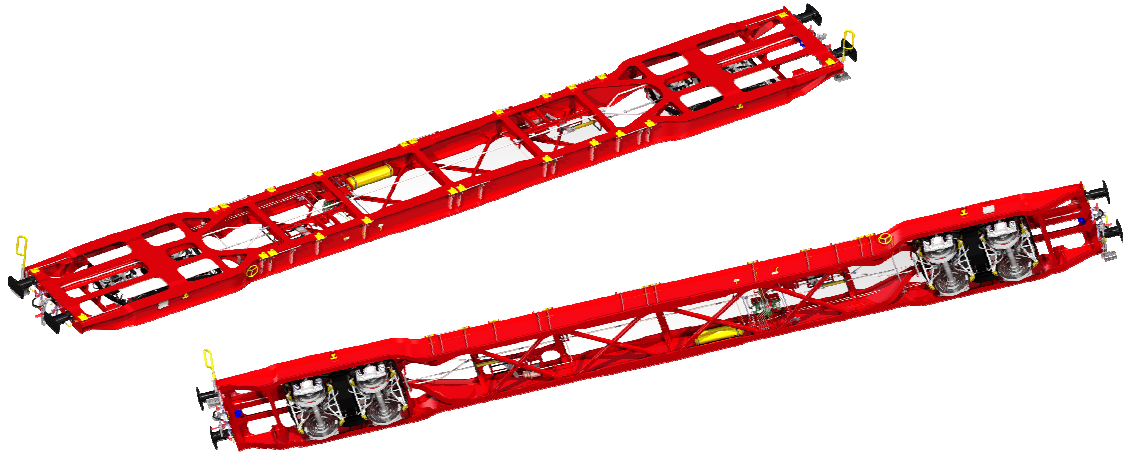


Fig. 3. The 3D wagon model designed in program PTC/Creo.

Chassis frame (Fig. 4) is welded the steel construction consisting of two side longitudinal beams (in the most of “I” profiles various sections) which through the cross beams create a support frame. On lower flange plate of main cross-beam there is rotating lead for upper of rotating pivot standard type and arms for sprung side bearers. The passage from the front to the center part of the wagon is branched because of better layout longitudinal forces. The center section of chassis frame contains the cross brace by reason optimizing the torsional stiffness of the wagon. The material thickness of individual structural parts has been optimized based on strength analysis simulations [7].

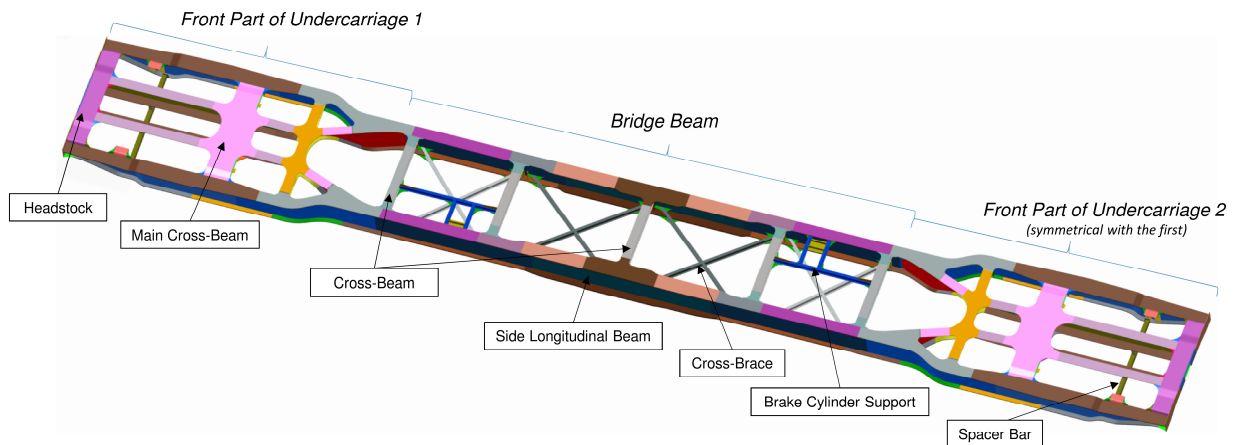


Fig. 4. Main parts of the chassis frame.

4. Computer aided simulation analyzes

Integral part of the development of rail vehicles are ride tests performed on test tracks and static tests on test stands. These tests are expensive and nowadays are using the modern computer technologies that can simulate riding a vehicle/train on the track and detect selected parameters [8, 9, 14, 15].

For the proposed wagon were performed several simulation analyzes which there are shown in Fig. 5.

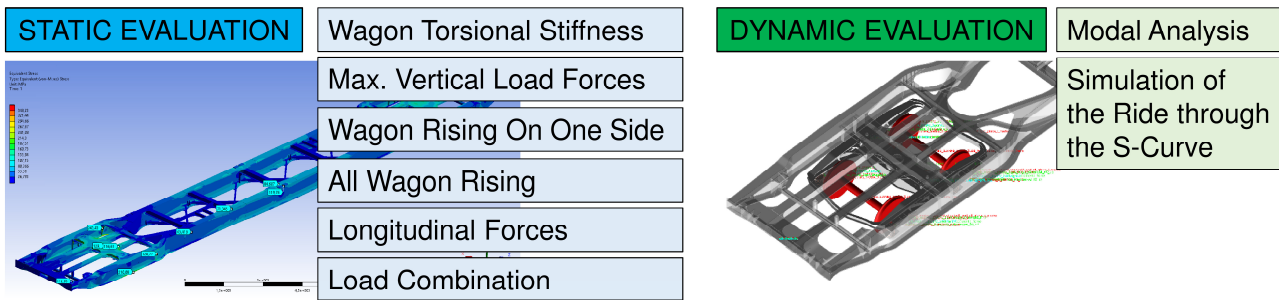


Fig. 5. The layout of static and dynamic evaluations.

Investigated construction was subjected to static structural analysis (program ANSYS) based on the standards EN 12663-2 and ERRI B12/RP17. On the basis of the 3D model of chassis frame was created calculation model which characteristics are shown in Fig. 6.

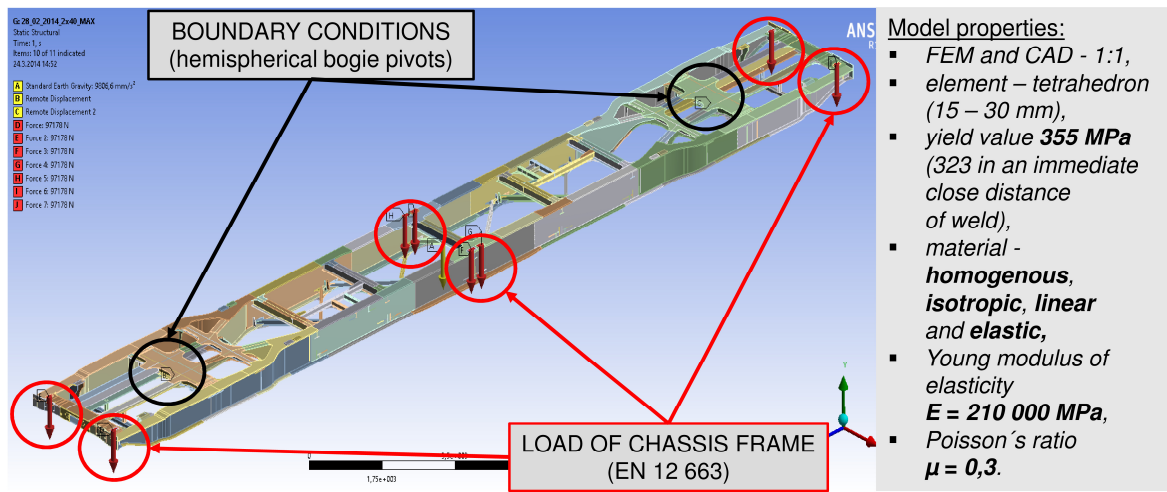


Fig. 6. Computational model – boundary conditions, loads and properties.

The task of structural analysis was to simulate behaviours of stresses and deformations in the proposed construction loaded maximum vertical forces.

The simulation analysis shows that the greatest deflection investigated structures (middle of the wagon) will be 29.928 mm. The report ERRI B12/RP17 states that the maximum deflection of the chassis frame must not exceed 3% of the distance between bogie pivots respectively axis of wheelsets. The results of the simulations show that the chassis frame satisfies strength conditions. For further development respectively production of this type of construction it is necessary to verify the results on the real construction on the test stand [11, 12].

Behaviour of displacements and stresses is shown in Fig. 7.

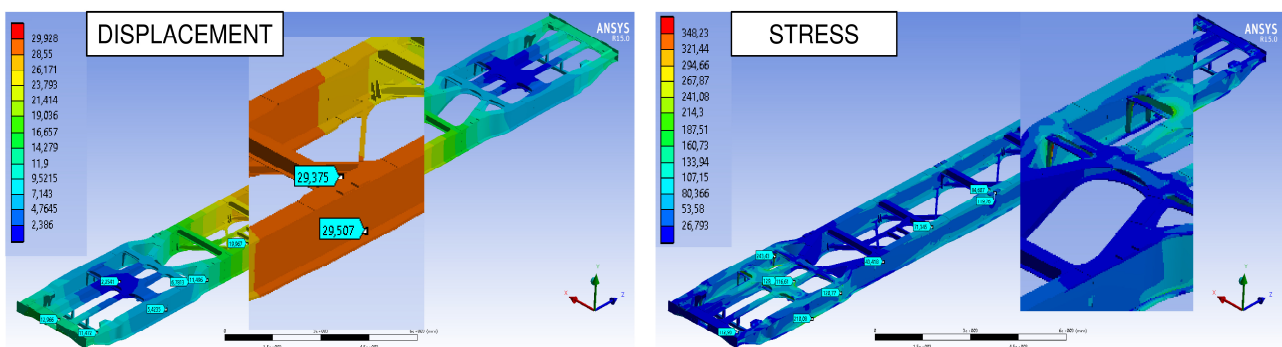


Fig. 7. Results of static simulation analysis – max. displacement and stress.

Dynamic simulation (verify enough overlap of buffers, when the vehicle ride through S-curve) was performed in the program Adams/Rail.

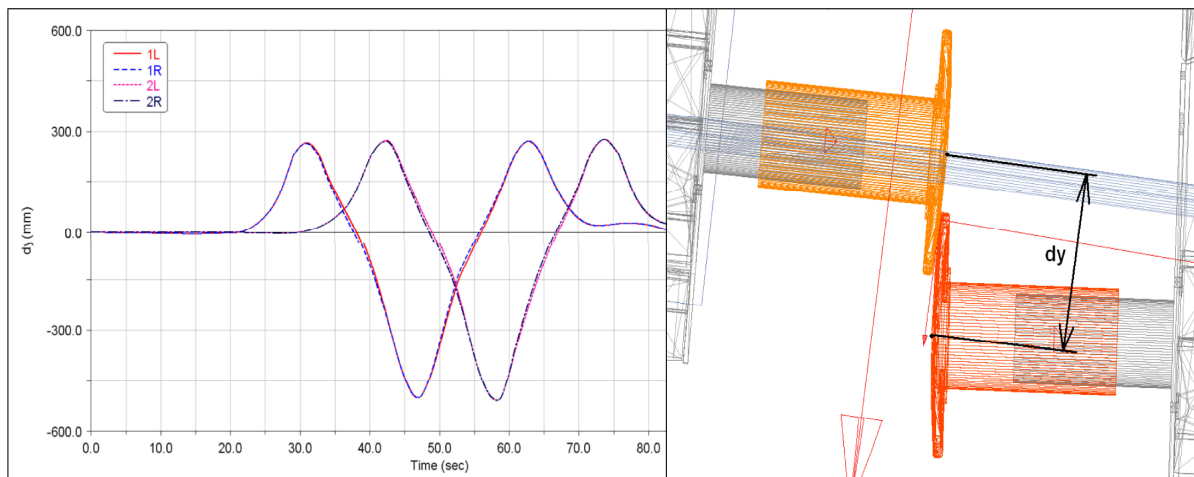


Fig. 8. Lateral displacement of buffer axis.

The buffers (according TSI) should have such size that it is not possible to lock two vehicles in horizontal curves or opposite curves [13, 16, 17].

The simulation calculation shows that the maximum lateral deviation from the center line of the buffers d_y (Fig. 8) reached the value 510 mm, which corresponds to 70 mm overlap. The minimum acceptable overlap according TSI is 50 mm. It can be concluded that the used buffers (width of plate 650 mm) satisfy the conditions of safe operation.

5. Conclusion

It is estimated that this wagon will be a sustainable wagon that will be able to offer the same or even more capacity and utilize less resources and energy than current wagons for intermodal transport.

The analysis of the intermodal traffic has enabled to carry a simulation in which wagon capacity performance has been assessed. The primary results speak for an increase of capacity due to wagon use of about 10% in comparison to a realistic reference case. This capacity increase is mainly produced by a better arrangement of containers and by reduction of deadweight of the wagon. When it comes to energy consumption wagon could save up to 18% of the energy necessary to transport a units. This is mostly due to an improvement of the loading factor that enables a better compression of the containers, fewer gaps, a reduced number of axles and a lighter tare per units.

Main advantages over existing design are:

- lower loading plane = transport of containers and swap bodies all dimensions in kinematic gauge G1 (including HiCube containers and swap bodies with a wide of up to 2600 mm),
- distance between pivots to 18 000 mm = no special permissions.

Due to the reduced amount of axles, for same or even more units capacity, wagon will bring about important savings in maintenance and very importantly, it will reduce the noise emissions per train.

Acknowledgement

The work was supported by the Scientific Grant Agency of the Ministry of Education of the Slovak Republic and the Slovak Academy of Sciences in project No. 1/0347/12: “Railway wheel tread profile wear research under the rail vehicle in operation conditions simulation on the test bench”, project No. 1/0383/12: “The rail vehicle running properties research with the help of a



computer simulation.” and the project No. APVV-0842-11: “Equivalent railway operation load simulator on the roller rig”.

Research-Educational Centre of Rail Vehicles (VVCKV)

References

- [1] VEL-WAGON Consortium (2011) Deliverable Report 1.1: State of the art and concept drafting.
- [2] FABIÁN, P., GERLICI, J., MAŠEK, J., MÁRTON, P. (2013) *Versatile, efficient and long wagon for intermodal transport in Europe*. In: Communications: scientific letters of the University of Žilina. ISSN 1335-4205. Vol. 15, no. 2, p. 118-123.
- [3] VEL-WAGON Consortium (2012) Deliverable Report 2.1: Intermodal application of Wel-Wagon.
- [4] FABIÁN, P., GERLICI, J., MAŠEK, J., MÁRTON, P. (2013) *Development of a new wagon for intermodal freight transport*. In: EURO - ŽEL 2013: 21st international symposium "Recent challenges for European railways": symposium proceedings: 4th-5th June 2013, Žilina, Slovak Republic. Brno: Tribun EU, 2013. ISBN 978-80-263-0380-0. CD-ROM, p. 298-306.
- [5] ŠŤASTNIAK, P., HARUŠINEC, J., GERLICI, J., LACK, T. (2012) *Containers Transport Wagons Design* (In Slovak). In: Dynamics of rigid and deformable bodies, Ústi nad Labem, Czech Republic: University J. E. Purkyně. ISBN 978-80-7414-510-0. CD-ROM, [7] p.
- [6] ŠŤASTNIAK, P., HARUŠINEC, J., GERLICI, J., LACK, T. (2013) *Railway vehicles design solutions for intermodal transport* (In Slovak). In: Computational and experimental methods in applied mechanics I. Ústi nad Labem, Czech Republic: University J. E. Purkyně. ISBN 978-80-7414-609-1. p. 167-172.
- [7] ŠŤASTNIAK, P., HARUŠINEC, J., GERLICI, J., LACK, T. (2014) *Structural design of long freight railway wagon with variable use of loading space*. In: Dynamics of rigid and deformable bodies, Ústi nad Labem, Czech Republic: University J. E. Purkyně. ISBN 978-80-7414-749-4. CD-ROM, [8] p.
- [8] DIŽO, J. (2014) *The freight wagon analysis using computer simulation*. In: EURO - ŽEL 2014: 22nd international symposium "Recent challenges for European railways": symposium proceedings: 3rd-4th June 2014, Žilina, Slovak Republic. Brno: Tribun EU, 2014. ISBN 978-80-263-0700-6. CD-ROM, p. 44-51.
- [9] DIŽO, J. (2015) *Evaluation of Ride Comfort for Passengers by Means of Computer Simulation*. In: Manufacturing Technology: Journal for science, research and production. ISSN 1213-2489. Vol. 15, No. 1, p. 8-14.
- [10] ŠŤASTNIAK, P., HARUŠINEC, J. (2013) *Computer Aided Simulation Analysis for Computation of Modal Analysis of the Freight Wagon*. In: Communications: scientific letters of the University of Žilina. ISSN 1335-4205. Vol. 15, no. 4, p. 73 - 79.
- [11] HARUŠINEC, J., ŠŤASTNIAK, P., DIŽO, J. (2013) *Calculations and Simulations in the Rail Vehicle Constructions Development* (In Slovak). In: Technológ, University of Žilina, EDIS – Žilina University Publisher. ISBN 1337-8996, p. 239 – 244.
- [12] ŠŤASTNIAK, P., HARUŠINEC, J. (2014) *Simulation analysis of selected parameters by the development of non-standard freight wagon*. In: Experimental and Computational Methods, I. international conference for young scientists, Ústi nad Labem, Czech Republic: University J. E. Purkyně. ISBN 978-80-7414-725-8. CD-ROM, [8] p.
- [13] ONDROVÁ, Z., GERLICI, J., LACK, T. (2008) *Dinamic simulation analysis of a railway vehicle running on a real track*. In: Dynamics of rigid and deformable bodies, Ústi nad Labem, Czech Republic: University J. E. Purkyně. ISBN 978-80-7414-030-3. p. 133-138.
- [14] GERLICI, J., LACK, T. (2007) *Methods for vehicle vibration analysis in time domain*. In: Prace Naukowe. Transport. ISSN 1230-9265. Vol. 63.
- [15] GERLICI, J., LACK, T. (1997) *Systems with concentrated masses dynamics analysis* (in Slovak). In: Current problems in rail vehicles: 13. International Conference. Pardubice: University of Pardubice. ISBN 80-7194-105-0. p. 263-271.
- [16] SVOBODA, M., SKOČILAS, J., SOUKUP, J. (2011) *Analysis of vertical vibration of mechanical system*. In: Dynamical systems. Analytical /Numerical Methods, Stability, Bifurcation and Chaos. pp. 261 - 268. Department of Automation and Biomechanics. Polytechnika Lodž.
- [17] NANGOLO, F. N., SOUKUP, J., SVOBODA, M. (2012) *Modeling of vertical dynamic response of railway vehicle system with experimental validation*. In: Machine Modeling and Simulation. Polytechnika Poznańska, Rokosovo, Poland. ISBN 978-83-923315-2-0.



Modification of spring element in the system for the angle of attack setting

*Veronika Štefaňaková

*University of Žilina, Faculty of Mechanical Engineering, Department of Transport and Handling Machines, Univerzitná 1, 01026 Žilina, Slovakia, veronika.stefanakova@fstroj.uniza.sk

Abstract. The aim of the article is to present necessary changes at the conception of the angle of attack setting mechanism and the modification of the spring element at the load module SIMRAIL, part of roller rig RAILBCOT. During the measurements were recorded imperfections, which could influence continuous testing, and would lead not to reliable and fully trustworthy results. The article describes three steps to improve the situation. The first step describes the stabilization of the members to prevent the occurrence of clearance. In the second step were started measurements at the roller rig at different operating speeds. In the third step the angle of attack setting mechanism is modified where mechanical spring element was changed by the hydraulic spring element. Mentioned, increasing the stiffness of the spring element is also needed, which the lack of stiffness caused loss of stability before the requesting speed. The gear lever was modified, where the transmission ratio and dimensioning of spring element was changed.

Keywords: RAILBCOT, SIMRAIL, Modification of mechanisms.

1. Introduction

Researchers at the University of Žilina have been intensively interested in railway research mainly in fields of friction tests performance with the brake test stands and rail/wheel contact analysis from various points of views. By means of the flywheel test stand UIC was possible to perform the investigation of the phenomena that appears in accordance to braking of railway vehicles. Contact geometry is closely connected with wheel/rail surface contact stress analysis. The contact analysis was performed by means of more sort methods. These analyses led to the investigation of wheel/rail profiles mutual attitude and their influence on ride behavior of vehicles and the values of contact stresses. New profiles were established on the requested geometrical or the contact stress options. RAILBCOT test stand was developed as a research project in years 2009 - 2012. Because of the stand creates the test stand and research core, there was need to complete it with the load modulus of the test stand for the realistic simulation of railway operation in laboratory conditions – SIMRAIL.

2. Load module SIMRAIL

Load module SIMRAIL (acronym for SIMulation module for the realistic simulation of RAILway operation under laboratory conditions), was created at the request to generate force and position inputs at the roller rig RAILBCOT that faithfully simulates the behavior of the vehicle on a real track (change the angle of attack, acting lateral forces to the wheelset simulated passing arc and also change the size of the vertical wheel forces when passing arc, or asymmetrically loaded vehicle).

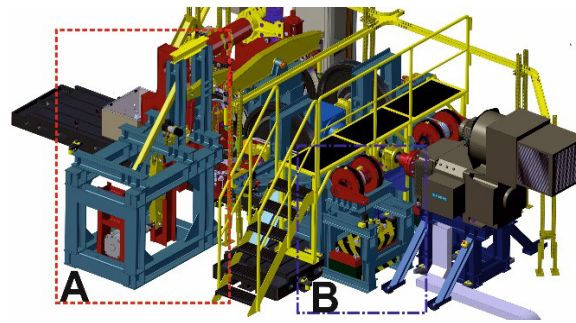


Fig. 1. 3D model of the test bench RAILBCOT (B) equipped by the load device SIMRAIL (A).

The RAILBCOT test stand represents the operational conditions of the four-axle railway wagon. Based on dynamic simulations and measurements performed on a roller rig RAILBCOT during operation, it was necessary to modify the parameters of the load module SIMRAIL and modify or replace some elements of mechanisms which acting on the wheelset during the test drive. SIMRAIL device consists of two separate modules shown in Fig.1.

Module A provides the changes for the angle of attack during the test, creates a lateral forces acting on the wheelset and also allows the wheel oscillation along the x axis in the test around the fixed angle of attack.

Module B compensates the changing wheel forces, whether in passing the arc, or as a substitute to asymmetrically loaded vehicle. Also leads weights in the lateral and longitudinal directions and prevents their swinging out.

3. Mechanism for the setting the angle of attack

The system for setting the angle of attack is in the module A and the elements are described in Fig. 2. The roller rig RAILBCOT is connected with the pivot lever (1) by a connector (0). The lever is pivotally clamped to the frame of module SIMRAIL (10) with bearing (2). This pair transmits the moment caused by the difference of tensile forces T_{x1} and T_{x2} on flexible bond (4), which leads to capture this moment of force caused by means of a pivot joint (3). Flexible bond is due to this force pressed by the value of displacement adequate to the force in positive or negative direction. Flexible bond (4) is not connected to the frame (10) directly, but through the gear lever (7), fixed to it by a dowel joint (5). The gear lever is running fitted in the frame through of a friction bearing (6). On the frame is actuating device for adjusting the angle of attack (9). It is connected to the gear lever (7) with pivot pin (8). Gripping the actuating device is rotatable by means of pins supplied with the gearbox of the actuating device.

Description of the Fig. 2: 0 – connector of system with the device RAILBCOT, 1 - lever for the transmission of oscillating moment, 2 - the bearing of the lever for the transmission of oscillating moment, 3 - a connecting pin for the transmission lever and the oscillating motion of the actuating device, 4 - actuating device, 5 - connecting pin of actuating device and gear lever, 6 - location of the gear lever, 7 - gear lever, 8 - connecting pin of the gear lever and the actuating device, 9 – actuating device, 10 – frame.

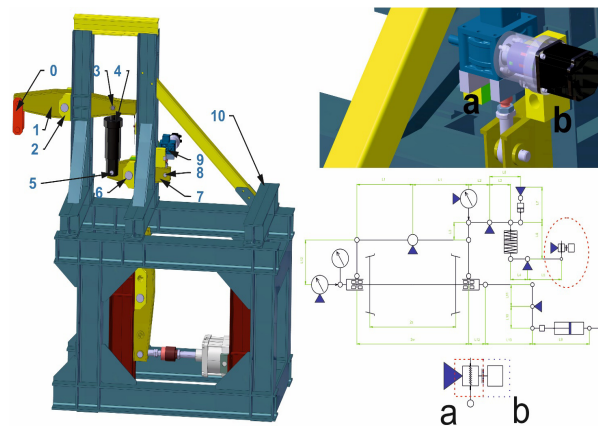


Fig. 2. Parts of the system for the angle of attack setting.

In Fig. 2 the detail of the actuating device is shown, which consists of two parts. For tapping a moment and rotational movement of the shaft is used a servomotor (b) with a nominal output of 0.75kW, which is manageable by the number pulses. It is equipped with a brake that enables detent the final position. The control electronics monitors through the feedback the device position, in consequence the propulsion dispose with information about the actual location. Engine (b) is connected with a lifting gear (a), whereby there is a change of the transmission ratio, as well as the screw on output changes rotation movement of the motor shaft to linear motion of the screw.

Gear ratio is 1:36, this is achieved through worm gear and except sensitive separation is also self-locking, which ensures when the brake failure in the engine there is no change the angle of attack by acting a forces in roller rig RAILBCOT. Modifying the rotational motion of the worm wheel provides screw with trapezoidal thread Tr 30x6, where per one rotation of the worm wheel is change of vertical position of the resilient member 3 mm, as the shifting lever has an aspect ratio of 2:1. In all, for the displacement of 1 mm is necessary 12 rotation of the shaft of the servomotor. Lifting gear is designed for total load of 25 kN and that load is transferred by actuating device is 50 kN. Elastic member consist of two spring units of 13 against the embedded pre-stressed springs for half of the maximum compression. Whereas within the operating range works only with compression between 0.25 to 0.75 of maximum and preload is always guaranteed. Thus compiled spring, when pressing 7 mm, deduces the strength 30 311.5 N, therefore $k = 4\,330.2$ N/mm, which represents a deviation of 1 per cent.

4. Operation

During the operation of device for changing the angle of attack was registered some specific imperfections in the construction. At startup the roller rig has occurred in the device excitation of oscillations due to clearances, which are reflected in the imposition of the working screw in the lifting gear. Impact of the clearance, which was 0.2 mm at the beginning and during the test operation was extended to 0.5 mm. There have been damaged polyamide bearing, where is mounted a lifting gear. After the replacing with Teflon bearing the device worked for a short time in accordance with the requirements. As a consequence of bruising the material of Teflon bearings after a short time the affect of clearance has reflected the lever bearings. The measurements were performed with the software developed at the University of Žilina.

As a result of this roller rig RAILBCOT had semi-unstable behavior even at engine speeds 300 rpm. and there was an expectation of damage of other elements of the roller rig. Then was carried out the modifications in construction and the problem was solved for short time. Plain Teflon bearing has been replaced by bronze housing. Bronze housing better tolerate shock loads and in places of heavy drive fit was used a putty to prevent beat out the bond caused by beats. On working screw was installed female screw with thread TR 30x6 that eliminated the clearances in the lift gear.

But this has inhibited the possibility to change the angle of attack during measurement. After the changes is evident, that the clearances were eliminated in the mechanism.

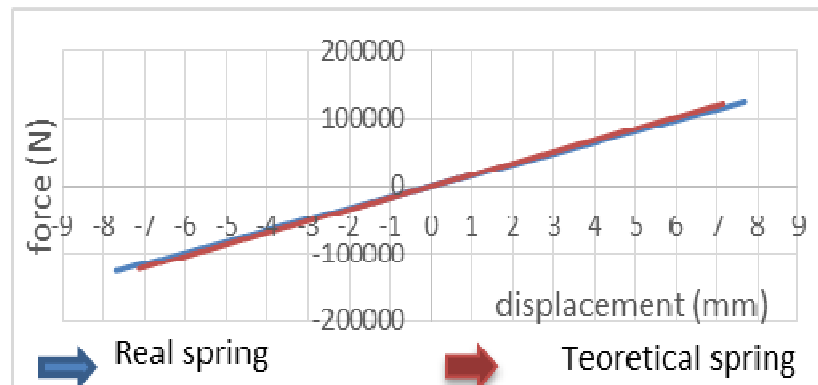


Fig. 3. Characteristics of required and achieved spring stiffness of rebuilt actuating device.

After a stabilization of the mechanism for changing the angle of attack has followed the detection of stability of roller rig across whole spectrum of operating speeds of simulated drive at the wheelset on the rail. During the tests were increasing rotational speed of the rail and the displacement was with the position sensor, which monitors the oscillation of the wheelset about the x axis. To the speed of 400 rpm. was the displacement in the stable area but at speeds above 450 rpm. has increased the deflection. This confirmed the results of the simulation program SIMPACK.

5. Spring element stabilization

For modification of activating device there was two possible ways. In the first case the creation a new body of activating device was considered. The second case was the originating body, as the activating device was designed for higher loads than the initial proposal. As required stiffness, was determined four times value of the stiffness 17 142.85 N/mm. Because the device was already in the proposal designed for possible adjustments in the stiffness of the activating device, therefore were used disc springs. It was also necessary to take into account the fact that the production of activating device body was expensive and this element is only for one special purpose, its further use would be questionable. So the chosen path was to rearrangement the flexible elements. As a good option, has been found suitable arrangement in Fig.4.

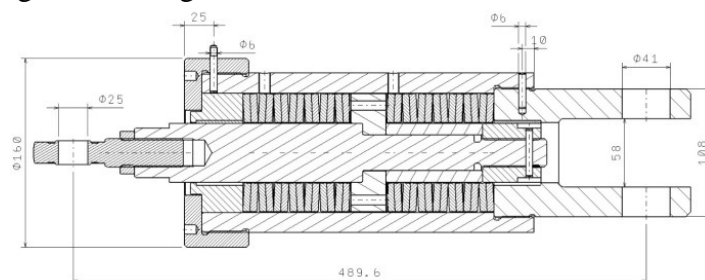


Fig. 4. New arrangement of flexible element.

There are 14 springs arranged in pairs opposite each other. So for the compression of the spring the has to be double force and total active spring deflection is reduced, at double force will be the spring half-pressed and thus we reached almost four – time higher stiffness.

In Fig. 3 the comparison of the achieved and required stiffness is shown, where the stiffness has reached a value of 16 288.6 N/mm. For the verification of the mechanical properties or modifying particular components were done strength calculations for doubled maximum load, where the condition for applicable condition was not to exceed the yield strength. It is for heat – treated material 423CrMo4 min 550 MPa for proportions of material from 100 to 160 mm and for sizes 16 to 40 mm it is 750 MPa. The actuating device is at the specified load able to pass this burden.

6. Optimizing the mechanism for the angle of attack setting

After adjusting the characteristics of the activating device was necessary to adjust and overdesign the mechanism for adjusting the angle of attack. The original design is shown in Fig. 2. The new solution had to maintain a gear lever, but change its gear ratio to increase the sensitivity of the steering but activating device will be modified or changed.

Double-acting hydraulic cylinder was complemented by spring hydraulic brake, which fixes the device during the stable phase. This occurs at a time when there is no need to change the angle of attack and also in case of a sudden power failure or hose rupture or failure of hydraulic pump.

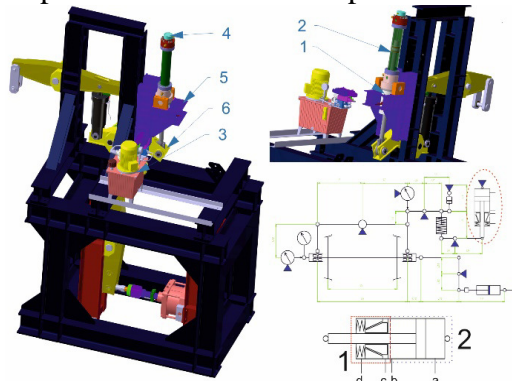


Fig. 5. New adjustment of mechanism for the angle of attack setting.

The final set up and scheme is in Fig. 5: 1 - hydraulic brake, 2 - hydraulic cylinder, 3 - hydraulic power unit, 4 - position sensor, 5 - frame for fixing the actuator, 6 - selector lever. The changes are mainly at the gear lever (6), which has in the new version the ratio of arms 1:3 compared to the original gear ratio 1:2. Rebuilt were also fastenings of pivots in lever, where are used clamping sleeves to eliminate the clearances and they are also made of bronze. To the original frame is mounted actuating device (5) consisting of hydraulic cylinder (2) with a work force of 50 kN at working pressure 20 MPa and hydraulic brake (1) with braking force of 50 kN at an operating pressure of 16 MPa. In body of the hydraulic cylinder (2) is an integrated position sensor Baluff BTL-A510-M0350-C-SR32 with range of 0 - 350 mm. Whole device is powered by using the compact hydraulic power unit mounted with a hydraulic generator with working pressure 20 MPa with a flow of 1.6 l/min.

The hydroelectric generator is powered by three-phase asynchronous electric engine with an output of 0.75 kW.

7. Conclusion

The article describes the changes in concept of mechanism for changing the angle of attack and modification of the actuating device. The introduction describes the structure, principles of operation and basic parameters of the module SIMRAIL In this configuration the test measurements aimed to verify the functionality of individual elements of construction equipment have been carried out. When the long – term tests were performed, were found, that some deficiencies has to be eliminated. Eliminating of this condition consisted of three steps. In the first step the parts of device was stabilized. In the second step, the verification of stability of the roller rig at different operating speeds. The third step the mechanism for the change the angle of attack was to adjust. At the verification of the stability of the roller rig was found, that the used actuating device has a low stiffness, which caused a loss of stability in the speeds of 61-70 km/h. Therefore, it was necessary to increase the stiffness of the actuating device. This was achieved by rearranging the segments of disk springs. After this change required flexibility of rigid member at a minimum cost for rebuilding has been achieved. The next chapter describes the modification of the mechanism for changing the angle of attack. Here was the original mechanical actuator replaced by a hydraulic actuator. The



selector lever has been also adjusted, where the gear ratio has increased from the original value of 1:2 to 1:3. Also the actuating device was dimensioned for double load. Connections were also modified to prevent the parasitic clearances.

Acknowledgement

The work was supported by the Scientific Grant Agency of the Ministry of Education of the Slovak Republic and the Slovak Academy of Sciences in project No. 1/0347/12: “Railway wheel tread profile wear research under the rail vehicle in operation conditions simulation on the test bench”, project No. 1/0383/12: “The rail vehicle running properties research with the help of a computer simulation.” and the project No. APVV-0842-11: “Equivalent railway operation load simulator on the roller rig”.

Research-Educational Center of Rail Vehicles (VVCKV)

References

- [1] GERLICI, J., LACK, T., HARUŠINEC, J., MÜLLER, R., DOLEŽEL, P. *Rail vehicles brake components test stand*. (In Slovak). In: PRORAIL 2011: Žilina, 21.-23.9.2011, conference proceedings. - Žilina: Scientific and Technical Society at the University of Žilina, 2011. ISBN 978-80-89276-30-1.
- [2] GERLICI, T., LACK, T., HARUŠINEC, J. *Test stand properties analysis for wheel-tread wear in accordance with the laboratory simulated railway operation*. In: VSDIA 2012 : proceedings of the 13th mini conference on Vehicle system dynamics, identification and anomalies: 5-7 November, 2012 Budapest, Hungary. - [S.l.: s.n.], 2012. - ISBN 978-963-313-102-2.
- [3] GERLICI, J., LACK, T., HARUŠINEC, J. *RAILBCOT - Rail vehicles brake components test stand* (In Slovak). *Computational and experimental methods in applied mechanics*. - Ústí nad Labem: Faculty of production technologies and management University J. E. Purkyně, 2012). ISBN 978-80-7414-377-9.
- [4] GERLICI, J., LACK, T., HARUŠINEC, J. *RAILBCOT - The rail vehicles brake components test stand* (In Slovak). *Computational and experimental methods in applied mechanics*. - Ústí nad Labem: UJEP, 2012. - ISBN 978-80-7414-377-9.
- [5] VALČÁKOVÁ, L., LACK, T., GERLICI, J., HARUŠINEC, J. *Rail vehicles brake components test stand dynamic properties evaluation*. TRANSCOM 2013: 10-th European conference of young researchers and scientists: Žilina, June 24-26, 2013, Slovak Republic. - Žilina: University of Žilina. ISBN 978-80-554-0695-4.
- [6] GERLICI, J., LACK, T., HARUŠINEC, J. *Wheels tread wear stand analysis in accordance to the laboratory simulated railway operation*. *Dynamical problems in rail vehicles 2013: Slovak - Polish scientific workshop: Žilina June 24th and 25th, 2013 Slovak Republic*. Žilina: University of Žilina, Department of Transport and Handling Machines. ISBN 978-80-554-0841-5.
- [7] GERLICI, J., LACK, T., HARUŠINEC, J. *Development of test stand prototype for rail vehicles brake components testing*. In: *Communications*. ISSN 1335-4205. - Vol. 16, no. 3A (2014).
- [8] GERLICI, J., LACK, T., HARUŠINEC, J. *Realistic simulation of railway operation on the RAILBCOT test stand*. *Applied mechanics and materials*. ISSN 1660-9336. - Vol. 486 (2014), online ISSN 1662-7482.
- [9] GERLICI, J., LACK, T., DOLEŽEL, P., HARUŠINEC, J. *Test stand mechanical system dynamics analysis*. *Prace Naukowe. Transport: Analiza i ocena elementów systemów transportowych*. ISSN 1230-9265. - Z. 101 (2014).
- [10] GERLICI, J., LACK, T. *Rail vehicles brake components test bench utilisation*. *Applied mechanics and materials*. ISSN 1660-9336. - Vol. 486 (2014), online ISSN 1662-7482.
- [11] GERLICI J., LACK T., HARUŠINEC J. *Rail vehicles wheels and brake blocks wear laboratory test stand utilization*. *Prace Naukowe. Transport: Analiza i ocena elementów systemów transportowych*. ISSN 1230-9265. - Z. 101 (2014).
- [12] SUCHÁNEK, A., HARUŠINEC, J., GERLICI, J., LACK, T. (*Test stand for railway wheels wear investigation function parts modification*). (In Slovak). *Computational and experimental methods in applied mechanics I*. - Ústí nad Labem: Faculty of production technologies and management UJEP, 2013. ISBN 978-80-7414-609-1.
- [13] GERLICI J., LACK T., HARUŠINEC J. *SIMRAIL - the load modulus of the test stand for the realistic simulation of railway operation in laboratory conditions*. *Dynamics of flexible and rigid bodies 2013: proceedings of the XI. International scientific conference, Ústí nad Labem, 9.-11.10 2013*. FVTM UJEP, 2013. ISBN 978-80-7414-607-7.
- [14] GERLICI J., LACK T., HARUŠINEC J. *The test stand load modulus implementation for the realistic railway operation in the laboratory conditions*. Paper number: M2013183. *Manufacturing technology*. Vol. 13, Nr.4.,



ISSN 1213-2489. Journal for science, research and production. December 2013. Issued by J.E. Purkyně University in Ústí nad Labem, Faculty of Production Technology and Management.

- [15] ŠTEFAŇAKOVÁ, V., GERLICI J., LACK T., HARUŠINEC, J. *Test stand load modulus construction proposal for the realistic simulation of railway operation*. TRANSCOM 2013: 10th European conference of young researchers and scientists : Žilina, June 24-26, 2013, Slovak Republic. - Žilina: University of Žilina, 2013. ISBN 978-80-554-0695-4.
- [16] ŠTEFAŇAKOVÁ, V. *Test stand loading modul for realistic simulation of rail vehicle operation*. (In Slovak). Experimental and computational method in engineering: Conference proceedings. 11. - 13. 6. 2014, Ústí nad Labem, Czech Republic. 2014. ISBN 978-80-7414-725-8.
- [17] HARUŠINEC, J., GERLICI, J., LACK, T., ŠTEFAŇAKOVÁ, V. *Angle of attack setting on the test stand system concept modification* (In Slovak). Dynamics of flexible and rigid bodies 2014: Proceedings of the XII international scientific conference. 8.-10.10. 2014. FVTM UJEP, 2014. ISBN 978-80-7414-749-4.
- [18] GERLICI, J., LACK T. *Test benches computer control software tools development*. Scientific bulletin of North University of Baia Mare: Fascicle: Mechanics, Tribology. Technology of Machine Manufacturing. ISSN 1224-3264. - Series C, Vol. XVII (2003).



Vehicle suspension and damping

*Maria Tomasikova, ** Leszek Krzywonos, *Frantisek Brumercik

* University of Zilina, Faculty of mechanical engineering, Department of design and machine elements,
Univerzitna 1, 01026 Žilina, Slovakia, tomasikovam@fstroj.uniza.sk

** Lublin University of Technology, Faculty of Mechanical Engineering, Department of Machine Design and
Mechatronics, Nadbystrzycka 36, 20 618, Lublin, Poland, l.krzywonos@pollub.pl

Abstract. The article is about damping. It is resume of basic information about springs and dampers, shock absorbers. Article includes information about the function and importance of the spring and damping mathematical relations for calculation of forces in the spring and a brief overview of the different types of vibration dampers.

Keywords: Suspension, Damper, Spring.

1. Introduction

In a vehicle, shock absorbers reduce the effect of traveling over rough ground, leading to improved ride quality and vehicle handling. While shock absorbers serve the purpose of limiting excessive suspension movement, their intended sole purpose is to damp spring oscillations. Shock absorbers use valving of oil and gasses to absorb excess energy from the springs. Spring rates are chosen by the manufacturer based on the weight of the vehicle, loaded and unloaded. Some people use shocks to modify spring rates but this is not the correct use. Along with hysteresis in the tire itself, they damp the energy stored in the motion of the unsprung weight up and down. Effective wheel bounce damping may require tuning shocks to an optimal resistance.

Spring-based shock absorbers commonly use coil springs or leaf springs, though torsion bars are used in torsional shocks as well. Ideal springs alone, however, are not shock absorbers, as springs only store and do not dissipate or absorb energy. Vehicles typically employ both hydraulic shock absorbers and springs or torsion bars. In this combination, "shock absorber" refers specifically to the hydraulic piston that absorbs and dissipates vibration.

Because surface unevenness the wheels have to do movement- up and down. Under fast ride this movements are undertaken in very short time interval and then acceleration and deceleration are formed in vertical direction by the direction of runway, which ones are multiple of Earth's gravitational acceleration. Impact forces influence on vehicle, which increase with the mass in movement. Suspension with damping is tasked absorbs impacts from traffic and convert them to vibration.

Damping is the control of motion or oscillation, as seen with the use of hydraulic gates and valves in a vehicle's shock absorber. This may also vary, intentionally or unintentionally. Like spring rate, the optimal damping for comfort may be less than for control.

Damping controls the travel speed and resistance of the vehicle's suspension. An undamped car will oscillate up and down. With proper damping levels, the car will settle back to a normal state in a minimal amount of time. Most damping in modern vehicles can be controlled by increasing or decreasing the resistance to fluid flow in the shock absorber.

2. Springs

Springs support the weight of the vehicle. In vehicle suspensions coil springs, air springs, torsion bars, and leaf springs are used (Fig. 1).

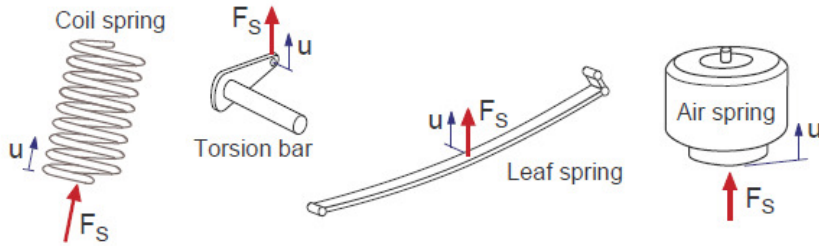


Fig. 1. Vehicle suspension springs.

Coil springs, torsion bars, and leaf springs absorb additional load by compressing. Thus, the ride height depends on the loading condition. Air springs are rubber cylinders filled with compressed air. They are becoming more popular on passenger cars, light trucks, and heavy trucks because here the correct vehicle ride height can be maintained regardless of the loading condition by adjusting the air pressure.

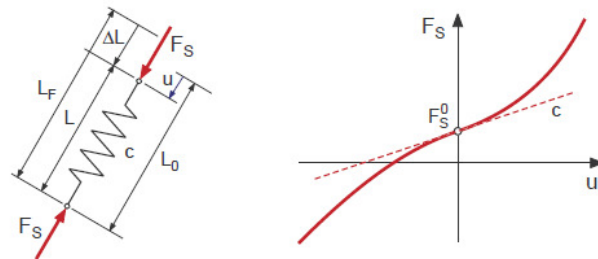


Fig. 1. Linear coil spring and general spring characteristics.

A linear coil spring may be characterized by its free length L_F and the spring stiffness c , fig. 2. The force acting on the spring is then given by

$$F_s = c(L_F - L). \quad (1)$$

where L denotes the actual length of the spring. Mounted in a vehicle suspension the spring has to support the corresponding chassis weight. Hence, the spring will be compressed to the configuration length $0 < L < L_F$. Now, (1) can be written as

$$F_s = c(L_F - (L_0 - u)) = c(L_F - L_0) + cu = F_s^0 + cu, \quad (2)$$

where F_s^0 is the spring preload and u describes the spring displacement measured from the spring's configuration length.

In general the spring force F_s can be defined by a nonlinear function of the spring displacement u

$$F_s = F_s(u). \quad (3)$$

Now, arbitrary spring characteristics can be approximated by elementary functions, like polynomials, or by tables which are then inter- and extrapolated by linear functions or cubic splines. The complex behavior of leaf springs and air springs can only be approximated by simple nonlinear spring characteristics, $F_s = F_s(u)$.

3. Damper

Dampers are basically oil pumps, Fig. 3. As the suspension travels up and down, the hydraulic fluid is forced by a piston through tiny holes, called orifices. This slows down the suspension motion.

Today twin-tube and mono-tube dampers are used in vehicle suspension systems. Dynamic damper model, compute the damper force via the fluid pressure applied to each side of the piston. The change in fluid pressures in the compression and rebound chambers are calculated by applying the conservation of mass.

In standard vehicle dynamics applications simple characteristics

$$F_D = F_D(v). \quad (4)$$

are used to describe the damper force F_D as a function of the damper velocity v .

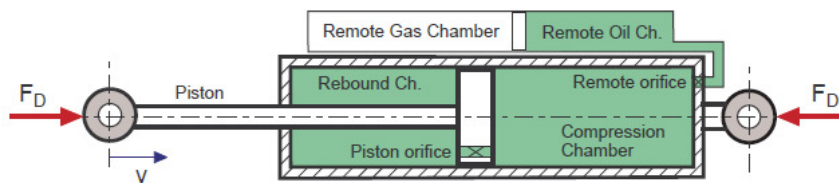


Fig. 2. Principle of a mono- tube damper.

Types of shock absorbers

Twin Tube Gas

This type of shock absorber has two tubes. An outer reservoir tube and inner pressure tube. The piston moves up and down inside the pressure tube and oil is forced through the compression valve or the rebound valve.

As the oil displaces, an inert gas such as nitrogen at relatively low pressure (around 5 atmospheres) is maintained on the oil in the reservoir tube.

The reason why an inert gas at pressure is used is to reduce the chances of aeration.

This type of shock absorber eventually will fade if used hard and simply requires time to cool for full damping to return.

Foam cell

Again a twin tube but an interesting design where instead of allowing any gas to come in contact with the hydraulic oil, nitrogen impregnated foam cells are used.

These shock absorbers virtually eliminate aeration and will generally hang on a bit longer than the twin tube gas shock absorbers before fading. Unfortunately if this type of shock absorber is overheated, it will not regain its damping qualities when cooled.

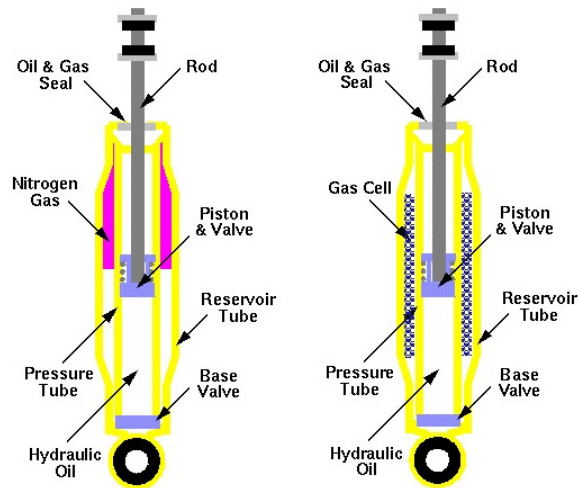


Fig. 3. Twin Tube Gas and Foam cell.

Mono tube

As the name implies, this type of shock absorber uses only one tube and the piston valving controls both rebound and compression damping. A floating piston separates the nitrogen gas from the oil and the gas is at a high pressure generally above 20 atmospheres.

This type of shock absorber is more prone to stone damage than the twin tube types. Once the tube is hit, the rod piston and/or floating piston will no longer seal properly against the cylinder wall. With the gas at the bottom of the shock absorber, it's difficult to design one with as much travel as the twin tube designs above. As such it's a popular shock absorber on road cars and as it heats up, the gas pressure increases and exerts more force on the oil. The end result is that the damping rates increase with heat

Twin tube hydraulic

This type of shock absorber is similar to the twin tube gas type except instead of using an inert gas at pressure, it simply uses air at atmospheric pressure. Generally, it's prone to aeration and will fade quickly. Allowing the shock absorber to cool will see a return of its damping qualities.

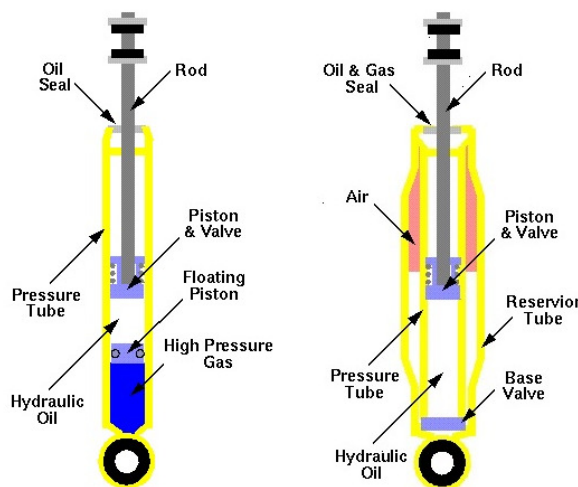


Fig. 4. Mono Tube and Twin tube hydraulic.



4. Conclusion

The suspension system affects both the driver's control of the car and the comfort of the occupants. The springs allow the wheels to move up to absorb bumps in the road and reduce jolting, while the dampers prevent bouncing up and down. Various mechanical links keep the wheels in line.

Acknowledgement

This work was supported by the Scientific Grant Agency of the Ministry of Education, Science, Research and Sport of the Slovak Republic under the contract no. V-1/0844/13 - Research on guidance elements of rolling bearing and their design.

References

- [1] DROZDZIEL, P. – KOMSTA, H. – KRZYWONOS, L. *An analysis of unit repair costs as a function of mileage of vehicles in a selected transport company*. Transport Problems, Vol. 9, Issue 4, 2014, pp. 73-81.
- [2] DROZDZIEL, P., KRZYWONOS, L. *The estimation of the reliability of the first daily diesel engine start-up during its operation in the vehicle*. Maintenance and Reliability 1(41), 2009, pp. 4-10, ISSN 1507-2711.
- [3] DROZDZIEL, P. – KOMSTA, H. – KRZYWONOS, L. *Repair costs and the intensity of vehicle use*. Transport Problems, Vol. 8, Issue 3, 2013, pp. 131-138.
- [4] DROZDZIEL, P. – KRZYWONOS, L. – MADLENAK, R. – RYBICKA, I. *Selected aspects of analyses of failure rates of active safety systems in buses*. Communications, Vol. 16, Issue 3, 2014, pp. 114-119.
- [5] KAMPF, R., LIZBETIN, J., LIZBETINOVA, L. *Requirements of a Transport System User*. Communication, Vol. 14, Issue 4, 2012, pp. 106-108.
- [6] BUKOVA, B., BRUMERCIKOVA, E., MADLENAK, R. *Doprava a elektronické podnikanie*. Bratislava : Wolters Kluwer, 2014. - 172 s. : obr., tab. - ISBN 978-80-8168-130-1
- [7] BUKOVA, B., BRUMERCIKOVA, E., KOLAROVŠZKI, P.: *Zasielateľstvo a logistika*. Bratislava : Wolters Kluwer, 2014. - 318 s. : obr., tab. - ISBN 978-80-554-0925-2



Vehicle steering geometry

*Maria Tomasikova, ** Anna Machrowska, *Frantisek Brumercik

* University of Zilina, Faculty of mechanical engineering, Department of design and machine elements,
Univerzitna 1, 01026 Žilina, Slovakia, tomasikovam@fstroj.uniza.sk

** Lublin University of Technology, Faculty of Mechanical Engineering, Department of Machine Design and
Mechatronics, Nadbystrzycka 36, 20 618, Lublin, Poland, a.machrowska@pollub.pl

Abstract. This article is about steering and wheel alignments. In clear and concise way describes principle of steering system, its function, properties and basic parts. The important chapter of article is about Ackermann geometry- explanation of the principle of geometry and formulas. And at least it mentioned wheel alignments.

Keywords: Steering, Ackermann geometry, Caster, toe, Camber.

1. Introduction

The steering system is a very important interface between driver and vehicle. The most conventional steering arrangement is to turn the front wheels using a hand-operated steering wheel which is positioned in front of the driver, via the steering column, which may contain universal joints (which may also be part of the collapsible steering column design), to allow it to deviate somewhat from a straight line. Other arrangements are sometimes found on different types of vehicles, for example, a tiller or rear-wheel steering.

Via the steering wheel the driver controls the vehicle and gets a feedback by the steering torque. The traditional steering system of high speed vehicles is a mechanical system consisting of the steering wheel, the steering shaft, the steering box and the steering linkage. Usually the steering torque produced by the driver is amplified by a hydraulic system. Nowadays, hydraulic power steering are widely use in every vehicle. It contains a power steering pump that use to pump hydraulic in the steering rack which will make the turning of vehicle easier. Today, new technology was invented which is electric power steering that fully controlled by the electronic device.

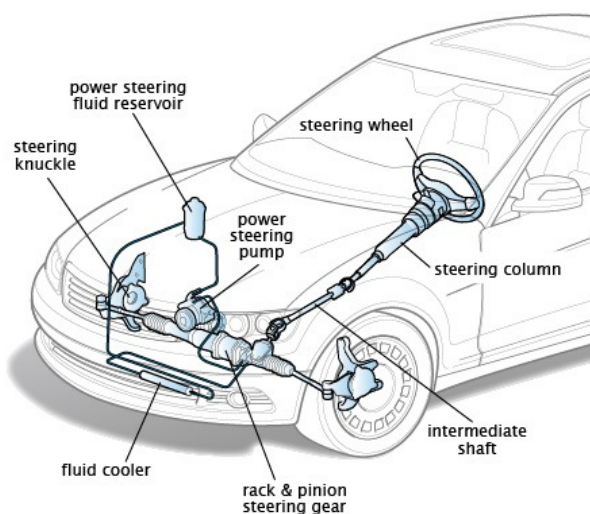


Fig. 1. Car steering system.



Modern steering systems use an overriding gear to amplify or change the steering wheel angle. Recently some companies have started investigations on 'steer by wire' techniques. In the future steer-by-wire systems will be used probably. Here an electronically controlled actuator is used to convert the rotation of the steering wheel into steer movements of the wheels. Steer-by-wire systems are based on mechanics, micro-controllers, electro-motors, power electronics and digital sensors. At present fail-safe systems with a mechanical backup system are under investigation. The steering system must guarantee easy and safe steering of the vehicle. The entirety of the mechanical transmission devices must be able to cope with all loads and stresses occurring in operation.

The basic aim of steering is to ensure that the wheels are pointing in the desired directions. This is typically achieved by a series of linkages, rods, pivots and gears. One of the fundamental concepts is that of caster angle – each wheel is steered with a pivot point ahead of the wheel; this makes the steering tend to be self-centering towards the direction of travel.

The steering linkages connecting the steering box and the wheels usually conforms to a variation of Ackermann steering geometry, to account for the fact that in a turn, the inner wheel is actually travelling a path of smaller radius than the outer wheel.

2. Ackermann steering geometry

Within the validity limits of the kinematic tire model the necessary steering angle of the front wheels can be constructed via the given momentary pivot pole M , Fig. 2. At slowly moving vehicles the lay out of the steering linkage is usually done according to the Ackermann geometry.

Then, the following relations apply

$$\tan \delta_1 = \frac{a}{R} \text{ and } \tan \delta_2 = \frac{a}{R + s}, \quad (1)$$

where s labels the track width and a denotes the wheel base. Eliminating the curve radius R , we get

$$\tan \delta_1 = \frac{a}{\frac{a}{\tan \delta_1} + s} \text{ or } \tan \delta_2 = \frac{a \tan \delta_1}{a + s \tan \delta_1}. \quad (2)$$

The deviations $\Delta \delta_2 = \delta_2^a - \delta_2^A$ of the actual steering angle δ_2^a from the Ackermann steering angle δ_2^A , which follows from (2), are used, especially on commercial vehicles, to judge the quality of a steering system.

At a rotation around the momentary pole M , the direction of the velocity is fixed for every point of the vehicle. The angle β between the velocity vector v and the longitudinal axis of the vehicle is called side slip angle. The side slip angle at point P is given by

$$\tan \beta_P = \frac{x}{R} \text{ or } \tan \beta_P = \frac{x}{a} \tan \delta_1, \quad (3)$$

where x defines the distance of P to the inner rear wheel.

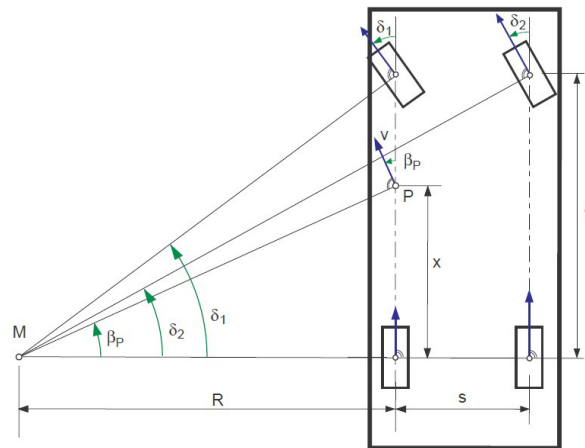


Fig. 1. Ackermann geometry.

3. Wheel alignments

Wheel alignments ensure that all four wheels are consistent with each other and are optimized for maximum contact with the surface of the road. The way a wheel is oriented on your car is broken down to three major components; camber, caster, and toe.

3.1. Camber

Camber angle is the measure in degrees of the difference between the wheels vertical alignment perpendicular to the surface. If a wheel is perfectly perpendicular to the surface, its camber would be 0 degrees. Camber is described as negative when the top of the tires begin to tilt inward towards the fender wells. Consequently, when the top of the tires begin to tilt away from the vehicle it is considered positive.

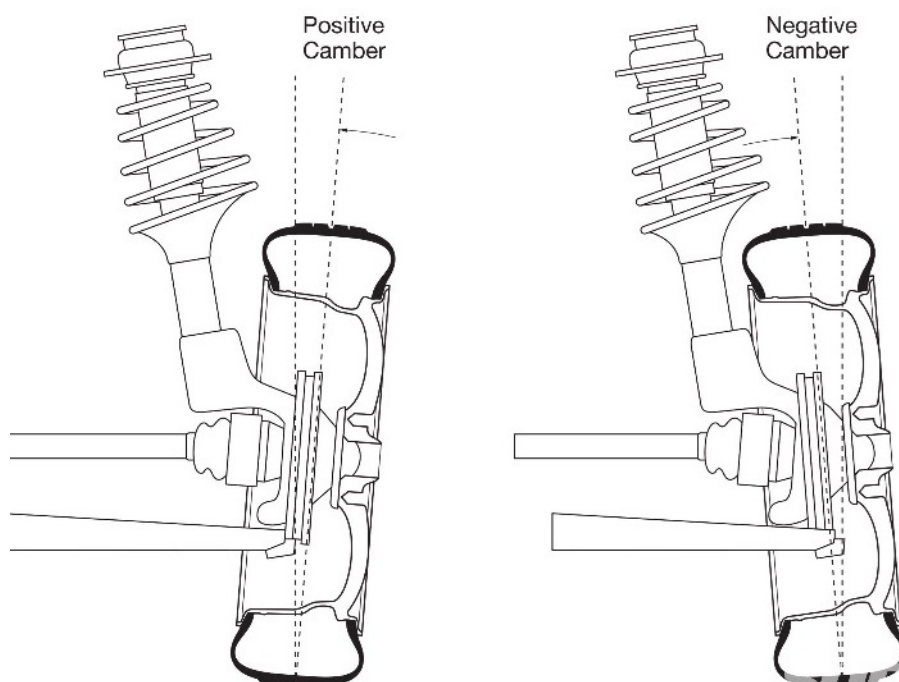


Fig. 2. Camber.

Negative camber is becoming increasingly more popular because of its visual appeal. The real advantages to negative camber are seen in the handling characteristics. An aggressive driver will enjoy the benefits of increased grip during heavy cornering with negative camber. During straight acceleration however, negative camber will reduce the contact surface between the tires and road surface.

3.2. Toe

Toe represents the angle derived from pointing the tires inward or outward from a top-down view – much like looking down at your toes and angling them inward or outward. Correct toe is paramount to even tread wear and extended tire life. If the tires are pointed inward or outward, they will scrub against the surface of the road and cause wear along the edges. Sometimes however, tread life can be sacrificed for performance or stability.

Positive toe occurs when the front of both tires begins to face each other. Positive toe permits both wheels to constantly generate force against one another, which reduces turning ability. However, positive tow creates straighter driving characteristics. Typically, rear wheel drive vehicles have slightly positive tow in the rear due to rolling resistance – causing outward drag in the suspension arms. The slight positive toe straightens out the wheels at speed, effectively evening them out and preventing excessive tire wear.

Negative toe is often used in front wheel drive vehicles for the opposite reason. Their suspension arms pull slightly inward, so a slight negative toe will compensate for the drag and level out the wheels at speed. Negative toe increases a cars cornering ability. When the vehicle begins to turn inward towards a corner, the inner wheel will be angled more aggressively. Since its turning radius is smaller than the outer wheel due to the angle, it will pull the car in that direction. Negative toe decreases straight line stability as a result. Any slight change in direction will cause the car to hint towards one direction or the other.

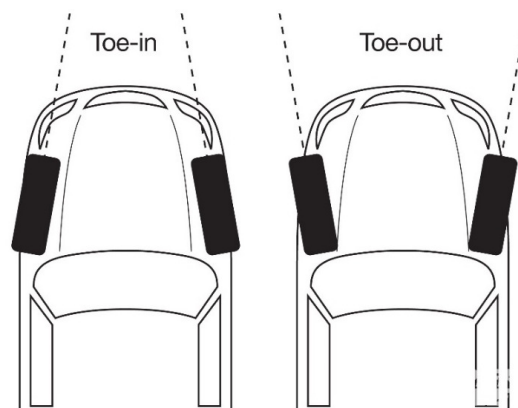


Fig. 3. Toe.

3.3. Caster

Caster is a bit harder to conceptualize, but it's defined as the angle created by the steering pivot point from the front to back of the vehicle. Caster is positive if the line is angled forward, and negative if backward.

Typically, positive caster will make the vehicle more stable at high speeds, and will increase tire lean when cornering. This can also increase steering effort as well.

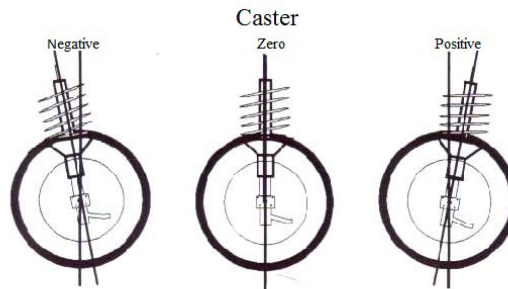


Fig. 4. Caster.

4. Conclusion

Countless hours of research and development go into designing suspension components and steering systems. The steering system converts the rotation of the steering wheel into a swivelling movement of the road wheels in such a way that the steering-wheel rim turns a long way to move the road wheels a short way.

Acknowledgement

This work was supported by the Scientific Grant Agency of the Ministry of Education, Science, Research and Sport of the Slovak Republic under the contract no. V-1/0844/13 - Research on guidance elements of rolling bearing and their design.

References

- [1] DROZDZIEL, P. – KOMSTA, H. – KRZYWONOS, L. *An analysis of unit repair costs as a function of mileage of vehicles in a selected transport company*. Transport Problems, Vol. 9, Issue 4, 2014, pp. 73-81.
- [2] DROZDZIEL, P., KRZYWONOS, L. *The estimation of the reliability of the first daily diesel engine start-up during its operation in the vehicle*. Maintenance and Reliability 1(41), 2009, pp. 4-10, ISSN 1507-2711.
- [3] DROZDZIEL, P. – KOMSTA, H. – KRZYWONOS, L. *Repair costs and the intensity of vehicle use*. Transport Problems, Vol. 8, Issue 3, 2013, pp. 131-138.
- [4] DROZDZIEL, P. – KRZYWONOS, L. – MADLENAC, R. – RYBICKA, I. *Selected aspects of analyses of failure rates of active safety systems in buses*. Communications, Vol. 16, Issue 3, 2014, pp. 114-119.
- [5] KAMPF, R. – LIZBETIN, J. – LIZBETINOVA, L. *Requirements of a Transport System User*. Communication, Vol. 14, Issue 4, 2012, pp. 106-108.
- [6] BUKOVA, B. – BRUMERCIKOVA, E. – MADLENAC, R. *Doprava a elektronické podnikanie*. Bratislava : Wolters Kluwer, 2014. - 172 s. : obr., tab. - ISBN 978-80-8168-130-1
- [7] BUKOVA, B. – BRUMERCIKOVA, E. – KOLAROVSKZI, P. *Zasielateľstvo a logistika*. Bratislava : Wolters Kluwer, 2014. - 318 s. : obr., tab. - ISBN 978-80-554-0925-2



Vehicle drivetrain modelling

*Maria Tomasikova, ** Aleksander Nieoczym, *Frantisek Brumercik

* University of Zilina, Faculty of mechanical engineering, Department of design and machine elements,
Univerzitna 1, 01026 Žilina, Slovakia, tomasikovam@fstroj.uniza.sk

** Lublin University of Technology, Faculty of Mechanical Engineering, Department of Machine Design and
Mechatronics, Nadbystrzycka 36, 20 618, Lublin, Poland, a.nieoczym@pollub.pl

Abstract. This article is about modeling in Matlab SimDriveline. In the example model of vehicle powertrain is showed some basic block like engine, planetary gear and tires. Every using block is explained by description its function and how put the block in to the vehicle model. Step by step you make your own vehicle model.

Keywords: Vehicle model, SimDriveline, Simulation.

1. Introduction

SimDriveline™ provides component libraries for modeling and simulating one-dimensional mechanical systems. It includes models of rotational and translational components, such as worm gears, planetary gears, lead screws, and clutches. You can use these components to model the transmission of mechanical power in helicopter drivetrains, industrial machinery, vehicle powertrains, and other applications. Automotive components, such as engines, tires, transmissions, and torque converters, are also included.

2. Vehicle drivetrain model

SimDriveline has many possibilities, good way to show you is make one simple example model, that can be reused for controls development. Basic concept for a vehicle model is shown in fig. 1. The blocks of the drivetrain parts are described below.

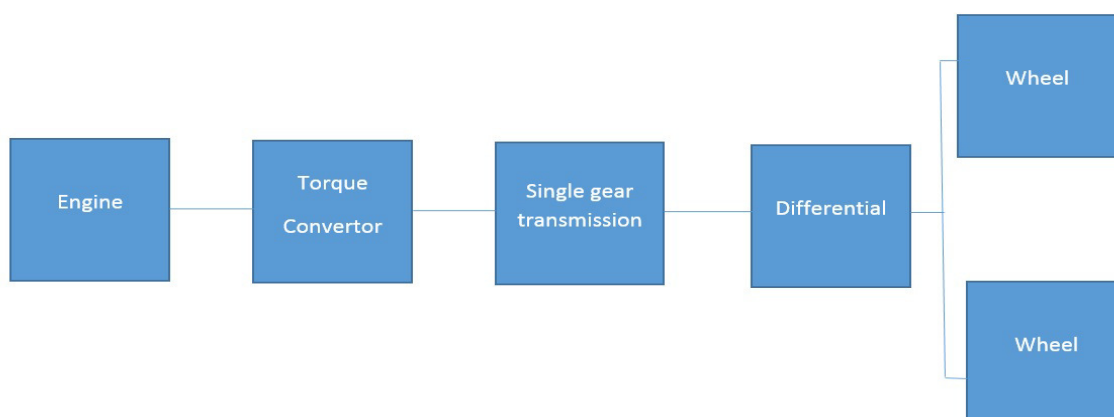


Fig. 1. Block schema of vehicle model.



Generic engine

The block represents a general internal combustion engine. Engine types include spark-ignition and diesel. Speed-power and speed-torque parameterizations are provided. A throttle physical signal input specifies the normalized engine torque. Optional dynamic parameters include crankshaft inertia and response time lag. A physical signal port outputs engine fuel consumption rate based on choice of fuel consumption model. An optional speed controller prevents engine stall and enables cruise control.

Torque convertor

A torque converter couples two driveline axes, transferring torque and angular motion by the hydrodynamic action of a viscous fluid. Unlike a friction clutch, a torque converter cannot lock the axes together. The Torque Converter block acts between the two ports I and T. The block acts as a lookup function of the relative angular velocity of the two connected driveline axes. This function is defined at discrete angular velocities.

In our model we need to specify the inertia on the other side to the torque converter—simply copy and paste exist inertia block. Set the inertia of the shaft is different.

Simple gear

The Simple Gear block represents a gearbox that constrains the two connected driveline axes, base (B) and follower (F), to corotate with a fixed ratio that you specify. You can choose whether the follower axis rotates in the same or opposite direction as the base axis. If they rotate in the same direction, ω_F and ω_B have the same sign. If they rotate in opposite directions, ω_F and ω_B have opposite signs.

The next part in our model is the transmission. Put a simple gear and connect that to model. In simple gear we can specify parameters like: main, meshing losses, viscous losses. We change just the output shaft rotates in the same direction as input shaft.

Differential gear

The Differential block represents a differential gear that couples rotational motion about the longitudinal driveshaft axis to rotational motion about two lateral or side axes. The differential is composed of a simple gear and two symmetric sun-planet bevel gears. The simple gear comprises a differential crown gear attached to the carrier of one of the sun-planet bevel gears, plus a bevel gear attached to the driveshaft.

The next component in our model is differential gear. Differential gear split the torque between the 2 wheels on the rear axle.

Tire

The Tire (Magic Formula) block models the longitudinal dynamics of a vehicle axle-wheel-tire combination, with road contact represented by the Magic Formula and optional deformation compliance. The convention for the vertical load is positive downward. If the vertical load is zero or negative, the horizontal tire force vanishes. In that case, the tire is just touching the ground or has left the ground. The longitudinal direction lies along the forward-backward axis of the tire. We put 2 tire block in to our example model. By the differential is torque split between this tires. Tires are connected with differential by mechanical connections.

Vehicle body

The Vehicle Body block models a two-axle vehicle, with an equal number of equally sized wheels on each axle, moving forward or backward along its longitudinal axis.

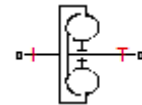


The model includes the following vehicle properties: mass, number of wheels on each axle, position of the vehicle's center of gravity (CG) relative to the front and rear axles and to the ground, effective frontal cross-sectional area, aerodynamic drag coefficient, initial longitudinal velocity
 Our vehicle model needs a model of longitudinal vehicle dynamic. Drag this into the model and connect mechanical connections to tires blocks. Tires blocks need to know the normal force, so that it can calculate the slip. We use the normal force calculation from a longitudinal vehicle dynamics model.

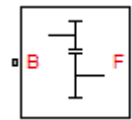
Generic engine



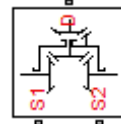
Torque convertor



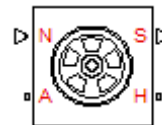
Simple gear



Differential gear



Tire (Magic formula)



Vehicle body

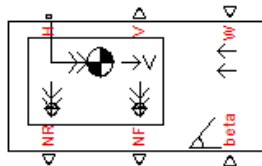


Fig. 2. Symbols of blocks.

Scope

We use the scope to plot the vehicle speed (Fig. 3). The vehicle speed is calculated by our vehicle dynamics model. To set the units of the speed of the vehicle to be plotted will use the converter block.

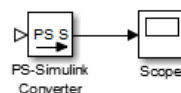


Fig. 1. The converter block + Scope.

We need also to set up the solvers for our simulation because we model a physical systems and use special solver technology need access to some additional solver settings and we get those through this offer configuration block. Then, the model is complete and ready to the simulation (Fig. 4).

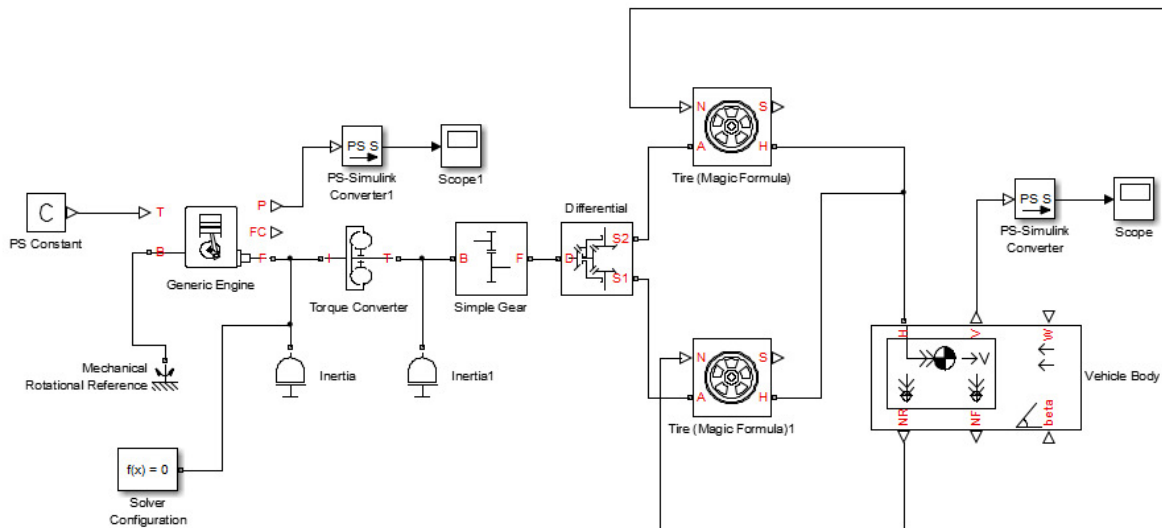


Fig. 2. Complete model ready for the simulation.

The last step is choose the solver for simulation - ode15s, which is a full implicit solver.

3. Conclusion

SimDriveline™ provides component libraries for modeling and simulating one-dimensional mechanical systems. It includes models of rotational and translational components, such as worm gears, planetary gears, lead screws, and clutches. This setting help you create your own models easier. This is one example from many others.

Acknowledgement

This work was supported by the Scientific Grant Agency of the Ministry of Education, Science, Research and Sport of the Slovak Republic under the contract no. V-1/0844/13 - Research on guidance elements of rolling bearing and their design.

References

- [1] DROZDZIEL, P. – KOMSTA, H. – KRZYWONOS, L. *An analysis of unit repair costs as a function of mileage of vehicles in a selected transport company*. Transport Problems, Vol. 9, Issue 4, 2014, pp. 73-81.
- [2] DROZDZIEL, P., KRZYWONOS, L. *The estimation of the reliability of the first daily diesel engine start-up during its operation in the vehicle*. Maintenance and Reliability 1(41), 2009, pp. 4-10, ISSN 1507-2711.
- [3] DROZDZIEL, P. – KOMSTA, H. – KRZYWONOS, L. *Repair costs and the intensity of vehicle use*. Transport Problems, Vol. 8, Issue 3, 2013, pp. 131-138.
- [4] DROZDZIEL, P. – KRZYWONOS, L. – MADLENAC, R. – RYBICKA, I. *Selected aspects of analyses of failure rates of active safety systems in buses*. Communications, Vol. 16, Issue 3, 2014, pp. 114-119.
- [5] KAMPF, R. – LIZBETIN, J. – LIZBETINOVA, L. *Requirements of a Transport System User*. Communication, Vol. 14, Issue 4, 2012, pp. 106-108.
- [6] BUKOVA, B. – BRUMERCIKOVA, E. – MADLENAC, R. *Doprava a elektronické podnikanie*. Bratislava : Wolters Kluwer, 2014. - 172 s. : obr., tab. - ISBN 978-80-8168-130-1
- [7] BUKOVA, B. – BRUMERCIKOVA, E. – KOLAROVŠZKI, P. *Zasielateľstvo a logistika*. Bratislava : Wolters Kluwer, 2014. - 318 s. : obr., tab. - ISBN 978-80-554-0925-2



Determine the Fatigue Lifetime for Aluminium Alloy EN AW 2007.T3 During Cyclic Bending – Torsion Loading Under In-and-out of Phase Shift $\varphi = 0^\circ$ and $\varphi = 90^\circ$

*Milan Uhrčík, *Peter Kopas

* University of Žilina, Faculty of Mechanical Engineering, Department of Material Engineering, Univerzitná 1, 010 26 Žilina, Slovak Republic, {milan.uhricik, peter.kopas}@fstroj.uniza.sk

Abstract. The article is focused on determine of fatigue lifetime of aluminium alloy EN AW 2007.T3 during by multiaxial cyclic loading. The theoretical part deals with the fatigue and with the criteria for evaluation of multiaxial fatigue lifetime. The experimental part deals with modeling of combined bending - torsion loading and determining the number of cycles to fracture in region low-cycle and high-cycle fatigue and also during of loading with the sinusoidal wave form under in phase $\varphi = 0^\circ$ and out phase $\varphi = 90^\circ$.

Keywords: Multiaxial fatigue, Criteria, Stress, Aluminium alloy, Fatigue lifetime.

1. Introduction

Aluminium is the world's most abundant metal and is the third most common element, comprising 8% of the earth's crust. The versatility of aluminium makes it the most widely used metal after steel. Pure aluminium is soft, ductile, corrosion resistant and has a high electrical conductivity. It is widely used for foil and conductor cables, but alloying with other elements is necessary to provide the higher strengths needed for other applications. Aluminium is one of the lightest engineering metals, having a strength to weight ratio superior to steel. By utilising various combinations of its advantageous properties such as strength, lightness, corrosion resistance, recyclability and formability, aluminium is being employed in an ever-increasing number of applications. This array of products ranges from structural materials through to thin packaging foils [1, 2].

Fatigue failures in metallic structures are a well-known technical problem. In a specimen subjected to a cyclic load, a fatigue crack nucleus can be initiated on a microscopically small scale, followed by crack grows to a macroscopic size, and finally to specimen failure in the last cycle of the fatigue life. Understanding of the fatigue mechanism is essential for considering various technical conditions which affect fatigue life and fatigue crack growth, such as the material surface quality, residual stress, and environmental influence. This knowledge is essential for the analysis of fatigue properties of an engineering structure [3, 4].

Fatigue under combined loading is a complex problem. A rational approach might be considered again for fatigue crack nucleation at the material surface. The state of stress at the surface is two-dimensional because the third principal stress perpendicular to the material surface is zero [5]. Another relatively simple combination of different loads is offered by an axle loaded under combined bending and torsion. This loading combination was tested in our and also in many others experiments [6,7]. In spite of this fact, fatigue mechanisms are still not fully understood. This is partly due to the complex geometrical shapes and also complex loadings of engineering components and structures which result in multiaxial cyclic stress-strain states rather than uniaxial.



2. Criteria

Criteria valid for the fatigue lifetime calculation can be classified in three different categories: strain based methods, strain-stress based methods and energy based approaches [8].

Goodman used main stresses for evaluating the fatigue under multiaxial loading. Normal stresses are calculated for each plane and their ranges are used for calculation of fatigue lifetime. If the point of the combined stress is below the relevant Goodman line then the component will not fail. This is a less conservative criteria based on the material ultimate strength yield point S_{ut} . To establish the factor of safety relative to the Goodman's criteria can be written as:

$$\frac{K_f \times \sigma_{amp}}{S_e} + \frac{\sigma_{mean}}{S_{ut}} = \frac{1}{f_f} \quad (1)$$

Findley criterion is the first critical plane criterion. He suggested that the normal stress σ_n , acting on a shear plane might have a different linear influence on the allowable alternating shear stress, $\Delta\tau/2$. Criterion has the following form:

$$\frac{\Delta\tau}{2} + k \times \sigma_n = \tau'_f \times (N_f)^b \quad (2)$$

Sines published his works throughout the fifties of the last century. His criteria are very much alike, utilizing the amplitude of second invariant of stress tensor deviator (which corresponds to the von Mises stress) as the basis. Another term is added to the equation in order to cope with the mean stress effect – while Sines prefers the mean value of first invariant of stress tensor (i.e. hydrostatic stress σ_h). His resulting failure criterion can be expressed as:

$$\frac{\Delta\tau_{oct}}{2} + \alpha \times (3 \times \sigma_h^{mean}) = \tau'_f \times (N_f)^b \quad (3)$$

Minimum circumscribed ellipse (MCE) – The origin of this method goes out from minimum circumscribed circle method (MCCM). This method was first presented by Papadopoulos. Its major feature is its explicitness in determination of mean shear stress. Papadopoulos later shows that such minimum circumscribed circle can be obtained by a search through all pairs and triads of points in the shear stress path, but such an approach can be very lengthy. The contrast in comparison with MCCM is clear – it should offer a better solution of phase shift effect problems. Nevertheless, as regards the definition of mean shear stress, it does not offer any new approach. For proportional loading this will always be a straight line and for non-proportional loading histories will have some complex shape.

$$\tau_a = \sqrt{R_A^2 + R_B^2} \quad (4)$$

Fatemi and Socie [9] observed that the Brown and Miller's idea could be successfully employed even by using the maximum stress normal to the critical plane, because the growth rate mainly depends on the stress component normal to the fatigue crack. Starting from this assumption, he proposed two different formulations according to the crack growth mechanism: when the crack propagation is mainly MODE I dominated, then the critical plane is the one that experiences the maximum normal stress amplitude and the fatigue lifetime can be calculated by means of the uniaxial Manson-Coffin curve; on the other hand, when the growth is mainly MODE II governed, the critical plane is that of maximum shear stress amplitude and the fatigue life can be estimated by using the torsion Manson-Coffin curve [9]. Criterion has the following form:

$$\frac{\Delta\gamma}{2} \times \left(1 + k \times \frac{\sigma_{n,max}}{\sigma_y} \right) = \frac{\tau_f'}{G} \times (2 \times N_f)^{b_\gamma} + \gamma_f' \times (2 \times N_f)^{c_\gamma} \quad (5)$$

Smith, Watson and Topper (SWT) created a parameter for multiaxial load, which is based on the main deformation range $\Delta\varepsilon_I$ and maximum stress $\sigma_{n,max}$ to the main plane. Criterion has the following form:

$$\sigma_{n,max} \times \frac{\Delta\varepsilon_I}{2} = \frac{\sigma_f'^2}{E} \times (2 \times N_f)^{2b} + \sigma_f' \times \varepsilon_f' \times (2 \times N_f)^{b+c} \quad (6)$$

Brown and Miller [10] observed that the fatigue life prediction could be performed by considering the strain components normal and tangential to the crack initiation plane. Moreover, the multiaxial fatigue damage depends on the crack growth direction. Different criteria are required if the crack grows on the component surface or inside the material. In the first case they proposed a relationship based on a combined use of a critical plane approach and a modified Manson-Coffin equation, where the critical plane is the one of maximum shear strain amplitude. Criterion, which was created, has the following form:

$$\frac{\Delta\gamma_{max}}{2} + S \times \Delta\varepsilon_n = A \times \frac{\sigma_f' - 2 \times \sigma_{n,mean}}{E} \times (2 \times N_f)^b + B \times \varepsilon_f' \times (2 \times N_f)^c \quad (7)$$

Liu created a virtual model of the deformation energy, which is a generalization of the axial energy on the basis of prediction of fatigue life. Criterion has the following form:

$$\Delta W = 4 \times \sigma_f' \times \varepsilon_f' \times (2 \times N_f)^{b+c} + \frac{4 \times \sigma_f'^2}{E} \times (2 \times N_f)^{2b} \quad (8)$$

Where: γ_f' is the fatigue ductility coefficient in torsion; ε_f' is the fatigue ductility coefficient; σ_f' is the fatigue strength coefficient; σ_h^{mean} is the mean hydrostatic stress; σ_n is the normal stress; $\sigma_{n,max}$ is the maximum stress; $\sigma_{n,mean}$ is the mean stress; σ_y is the stress in the direction of the axis y; τ_a is the equivalent shear stress; τ_f' is the fatigue strength coefficient in torsion; $\Delta\gamma_{max}$ is the maximum shear strain range; $\Delta\varepsilon_I$ is the principal strain range; $\Delta\varepsilon_n$ is the normal strain range; $\Delta\tau/2$ is the alternating shear stress; $\Delta\tau_{oct}$ is the octahedral shear stress; ΔW is the virtual strain energy; b is the fatigue strength exponent; b_γ is the fatigue strength exponent in torsion; c is the fatigue ductility exponent; c_γ is the fatigue ductility exponent in torsion; N_f is the number of cycles to fracture; S_e is the modified fatigue strength; S_{ut} is the ultimate tensile strength; f_f is the factor of safety applicable the fatigue; A , B , S , k , α are material parameters; E is the elasticity modulus in tension; G is the elasticity modulus in torsion; R_A is the major axis of the ellipse; R_B is the maximum distance of stress point.

3. Numerical calculations and results

In ANSYS software was created the model of the test bar. The real geometry of this component is shown in Fig.1. The rod bar had a circular shape with a defined section, in which was expected an increased concentration of stress and creation a fatigue fracture.

The ends of this model were loaded by reversed bending moment on the one side and by reversed torsion moment on the opposite site. The values of presented stresses and strains in the middle of the rod radius were taken from computational analysis using finite element method. We used the following parameters in finite element model: used material was aluminum alloy EN AW 2007.T3 (AlCu4PbMg) with Young's modulus $E = 0.817 \times 10^{11}$ Pa, Poisson number $\mu = 0.3$ and with the strength limit $R_m = 491$ MPa. From computational analysis can be seen that the area with greatest

concentration of stresses or eventually the place with the higher deformation was localized in the middle of the rod radius (see Fig.2).

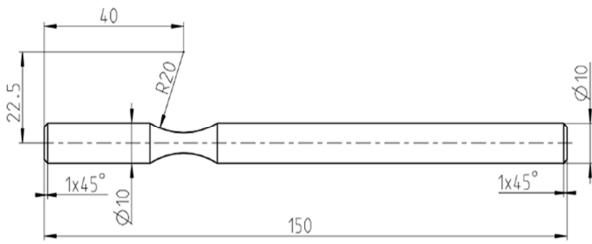


Fig.1 Shape and dimension fatigue test specimen (dimension in mm)



Fig.2 Result of FEM analysis

Obtained values of the stresses from finite element analysis were next computational analyzed using Fatigue Calculator software. This is a program which can quickly calculate fatigue lifetime of selected material. After starting the calculation, Fatigue Calculator displayed the number of cycles to failure for different models of damage. In our calculation we considered with all multiaxial criteria described above which can be applied to low-cycle and also to high-cycle fatigue region. All the tests were performed under controlled bending and torsion moments. Frequency of each analysis was equal to 30 Hz. It was first detected the number of cycles to fracture for multiaxial high-cycle fatigue with amplitudes in the phase shift 0° and then out of the phase shift 90° for stress. The same was done for multiaxial low-cycle fatigue.

The obtained number of cycles are processed into Wöhler curves $\sigma_{xx} - \log N_f$ for multiaxial cyclic combined bending - torsion loading. For multiaxial high-cycle fatigue with phase shift 0° , Wöhler curves are shown in Fig.3. For multiaxial high-cycle fatigue with phase shift 90° , Wöhler curves are shown in Fig.4.

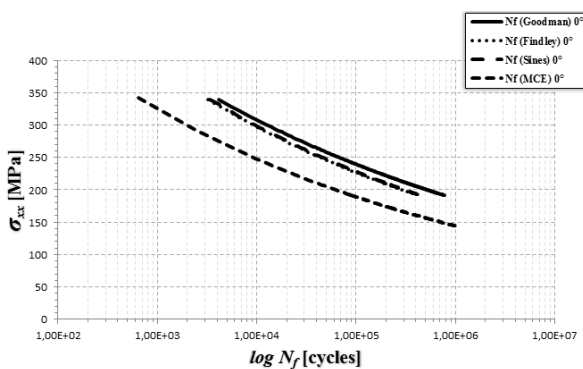


Fig.3 Wöhler curves for multiaxial high-cycle fatigue with phase shift 0° .

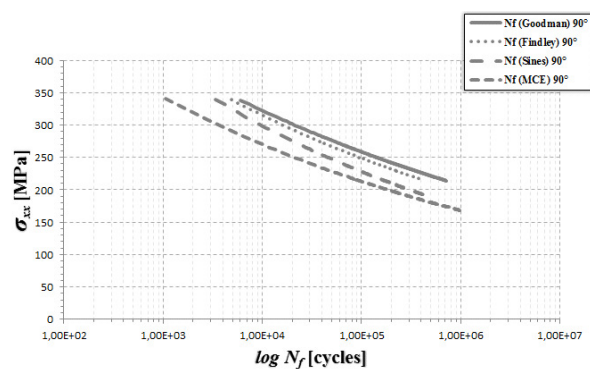


Fig.4 Wöhler curves for multiaxial high-cycle fatigue with phase shift 90° .

For multiaxial low-cycle fatigue with phase shift 0° and with phase shift 90° , Wöhler curves are shown in Fig.5 and in Fig.6.

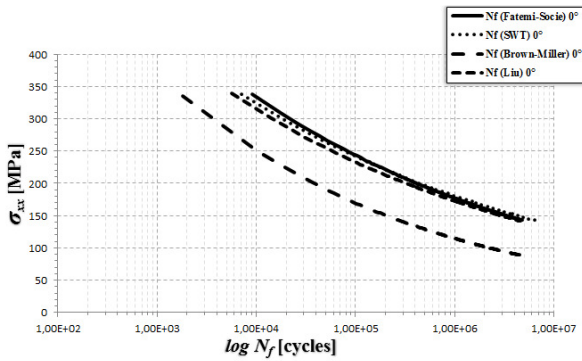


Fig.5 Wöhler curves for multiaxial low-cycle fatigue with phase shift 0°.

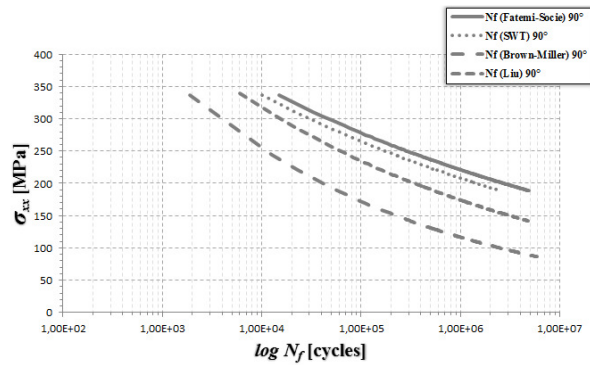


Fig.6 Wöhler curves for multiaxial low-cycle fatigue with phase shift 90°.

4. Conclusion

All multiaxial models applied to fatigue lifetime calculation of aluminum alloy EN AW 2007.T3 increases with decreasing stress amplitude continuously in the cycles of number region.

Comparing Wöhler curves for low-cycle fatigue (Fig.7), for amplitudes of the load with phase shift 0° (black lines) and for amplitudes of the load with phase shift of 90° (gray lines), it can be seen that some models (such as Fatemi-Socie and SWT) give higher resistance to fatigue damage in the phase shift than the synchronized load amplitudes. This may be caused by, that the bending loading and neither torsion loading not active with the maximum value on the sample at the same time during the phase shift, but alternately. In this way, as if the sample was loaded by lower value of stress or deformation in a given time (phase shift of 90°). For other models, this shift of amplitudes did not cause any significant changes and the differences are minimal.

Comparing Wöhler curves for high-cycle fatigue (Fig.8), for amplitudes of the load with phase shift 0° (black lines) and for amplitudes of the load with phase shift of 90° (gray lines), it can be seen that all models (except for Sines) gives a higher resistance against fatigue damage in the phase shift than in the synchronized amplitudes of loading. Probably the reason will be same as for low-cycle fatigue.

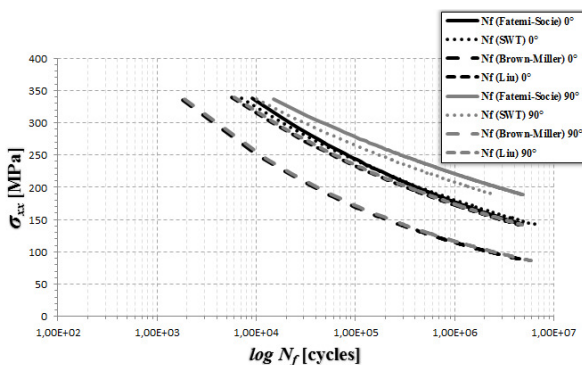


Fig.7 Comparison of Wöhler curves for multiaxial low-cycle fatigue

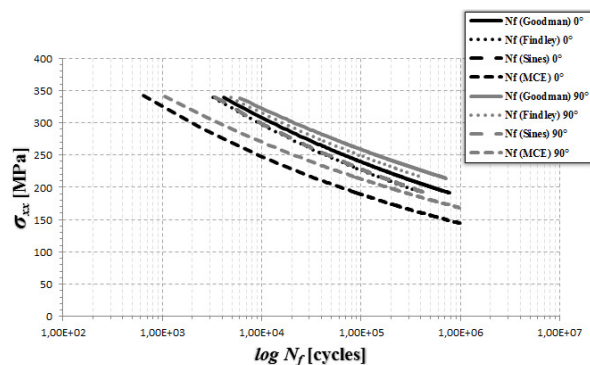


Fig.8 Comparison of Wöhler curves for multiaxial high-cycle fatigue

It was observed that a phase shift 90° is the cause of "rotating" curves of fatigue life, which may have an impact on partial increase of fatigue life for the area of low-cycle and high-cycle fatigue.



Acknowledgement

This work has been supported by Scientific Grant Agency of Ministry of Education of Slovak Republic and Slovak Academy of Sciences, No.1/0797/12, No.1/0533/15.

References

- [1] www.aalco.co.sk
- [2] HURTALOVÁ, L., TILLOVÁ, E. *Elimination of the negative effect of FE-rich intermetallic phases in secondary (recycled) aluminium cast alloy*. Manufacturing Technology, 2013, Vol.13, No.1, pp.44-50.
- [3] BOKŮVKA, O., NICOLETTO, G., KUNZ, L., PALČEK, P., CHALUPOVÁ, M. *Low & high frequency fatigue testing*. CETRA and Univerzity of Žilina, Žilina, 2002.
- [4] BATHIAS, C. *Fatigue in the very high cycle regime*. Vienna, Austria, 2001.
- [5] BANNANTINE, J. A., SOCIE, D. F. *A multiaxial fatigue life estimation technique*. In: Advances in Fatigue Lifetime Predictive Techniques, ASTM STP 1122. Eds: M. R. Mitchell a R. W. Landgraf. Philadelphia, American Society for Testing and Materials, 1992, pp. 249-275.
- [6] GOUGH, H.J. AND POLLARD, H.V., *Some experiments of the resistance of metals to fatigue under combined stresses*. Min. of Supply, Aero Res. Council, RSM 2522, Part I, 1951.
- [7] LEGER, J. *Fatigue life testing of crane drive shafts under crane-typical torsional and rotary bending loads*. Schenck Hydropuls Mag., Issue 1/89, 1989, pp.8–11.
- [8] www.efatigue.sk
- [9] FATEMI, A. , SOCIE, D. F. *A critical plane approach to multiaxial fatigue damage including out-of-phase loading*. Fatigue Fract. Engng. Mater. Struct , 1988, pp.149-166.
- [10] BROWN, M. W., MILLER, K. J. *A theory for fatigue under multiaxial stress-strain conditions*. In: Proc. Inst. Mech. Engrs, Vol. 187, 1973, pp.745-755.



RAILBCOT – SIMRAIL System Dynamics analysis

*Lenka Valčáková

*University of Žilina, Faculty of Mechanical Engineering, Department of Transport and Handling Machines,
Univerzitná 1, 01026 Žilina, Slovakia, lenka.valcakova@fstroj.uniza.sk

Abstract. The paper is devoted to the mechanical system dynamic properties investigation of the test stand RAILBCOT (RAIL vehicles Brake Components Test stand). Using sensors attached to some parts values of positions, the longitudinal, vertical and transversal forces, revolutions and accelerations have been measured. There was created computational model of the mechanical system in SIMPACK software system environment. There were performed model establishment, starting and boundary condition setting and simulation computations to determine the dynamic properties parameters. The measured values were compared with calculated values. Subsequent verification has been confirmed the necessity of modification of the flexible member of the bench. The paper consists of issue definition and the comprehensive references specification from the field of investigation of working team at the University of Žilina relevant to this field of study.

Keywords: Test bench, Multibody system dynamics, RAILBCOT, SIMPACK, Simulation computations.

1. Introduction

Experimental investigation of interaction rotating rails and a wheelset is a complex interaction of test stand construct design and test sample, which is represented by a wheelset and a collection of computer controlled loading conditions for the realization of tests. Test stand is a part the laboratory, affecting with results of its running and also current state of the environment affects the running of test stand and test results [1, 2, 3, 4, 5, 6, 7]. The functional core of the test stand is equipped by the system SIMRAIL (SIMulation modul for the realistic simulation of RAILway operation under laboratory conditions) [8, 9, 10, 11, 12].



Fig. 1 Overview of the test stand RAILBCOT.

To assess the behavior of the test bench in operation at the specified boundary conditions, it is often necessary, sometimes indispensable to do simulating calculations taking into account all important parameters future experimental work. The test bench is equipped with measurement technology with characteristic sensor ranges. For ensuring the best use of the range and accuracy of the sensors, as well as the entire measurement chain the specification of the anticipated values of the measured magnitudes is significant contribution. Computer simulation of the movement of the wheelset, pressed against the rotating rails is another important contribution in analysis of its interaction, when loading forces affect.

2. The purpose of test bench

The purpose of test bench RAILBCOT is the analysis of changes in the geometry of rail thread driving profiles railway wheelset induced by change in the simulated operating load in laboratory conditions to imitate the real operation as closely as possible.

Activity of test bench lies in active loading the tested wheelset by various forces that will be simulated simultaneously in combination with the change of engine torque, engine speed, wheel load change, changing the size of the free channel gauge, changing the angle of attack of a wheelset and fluctuating braking mode, which is based on independent activities of two and two brake units with the option to change their arrangement, shape and material composition of brake blocks, while also considering the possibility of simulation under different weather conditions.

The specific focus of this test bench has to be the analysis the driving characteristics of wheelsets for freight wagons with a wheel diameter of 920 mm for axle boxes V84, with emphasis on placement in bogie Y25, at traffic load 22.5 tons per axle, the maximum test speed of 160 km h⁻¹ and when using an electric motor with a maximum output of 434 kW and torque of 3900 Nm.

3. Operating principle of test bench

Driving motor (1) transmits the torque through conical gear (2) and rotates rotating rails (3). Rotating rail is connected with gearbox shaft by gear clutch (11). This stationary part of the bench is firmly secured to the base grid (9). Against the discs of the rotating rails (3) the wheelset (8), placed in the support frame (7) is pressed.

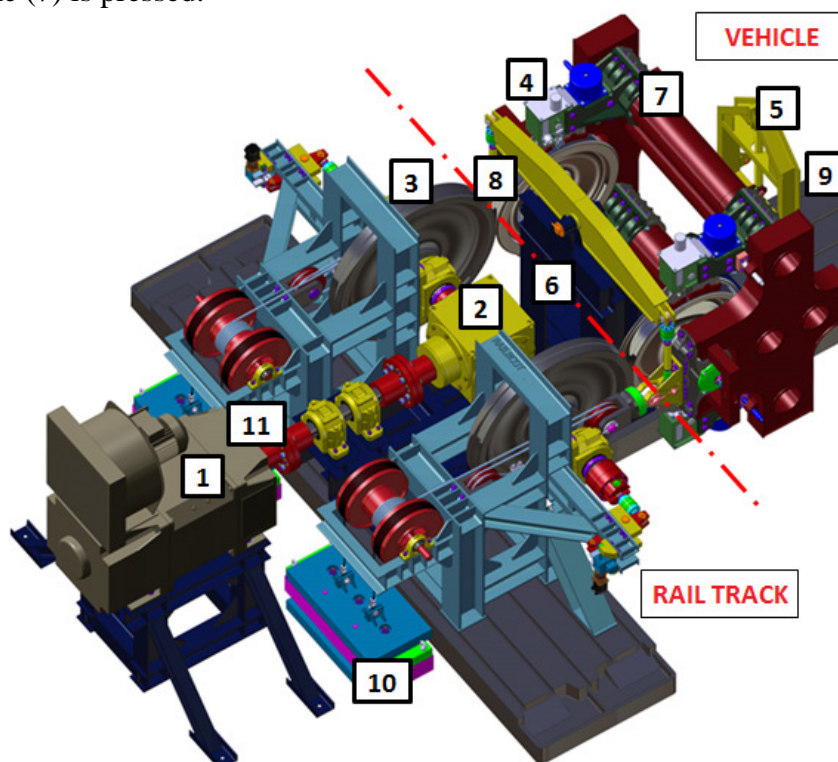


Fig. 2 Operating principle of the test stand core.

Discs can zoom in and out with each other, simulating the change of gauge. Frame (7) is hanged on two front hinges (6) and one back hinge (5). The wheelset (8) in frame (7) is pressed against the discs (3) by the cable transmission that is connected to the weights (10). The frame with the wheelset creates the moveable part, which represents the rail vehicle. The frame has the opportunity to move in a limited extend in the transverse direction (in axle of the wheelset). It can be tilted. Each wheel is braked by a pair of modified brake units.

4. Monitored values and location of sensors

Development of methodology for analyzing the wear is based on scientific knowledge of phenomena in rail-wheel contact. Therefore, it is important to analyze and evaluate the phenomena arising during braking between rail wheel and brake block, as well as phenomena in contact of rail wheel and (simulated rotating) rail track. An integral part of the work of this stage is to finalize the installation of sensors and integrated sensory technology to the bench, verifying their activity, testing of measuring instruments and data acquisition and evaluation.

Based on these information it is possible to test and apply methods of evaluating the measured data, the results of which may give a relevant view of an operation state of the contact components and provide verified materials to predict the development of the wear of brake components by the expected operation.

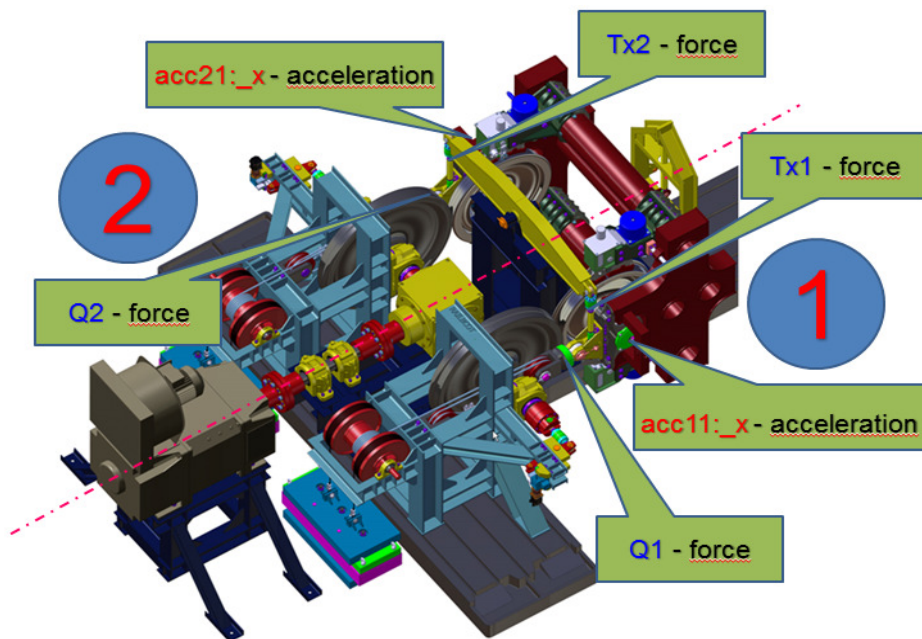


Fig. 3 Measured parameters on the bench according to placement of sensors.

Realization of each test lies not only in obtaining the measured data, but also in the manner of its management. This management is normally done via PC and control software, which guide trained staff in the so-control center.

For the purposes of carrying out measurements on the test stand are used mainly sensors for:

- force measurement: wheel forces, longitudinal forces between wheel/rail, guiding forces and force in the rear rod of the middle frame,
- revolutions measurement: engine, wheelset,
- acceleration measurement: wheelset / frame.

Currently on the bench are situated these sensors of:

- *longitudinal force* – HBM, type U3, are located on the hinge of the wheelset,
- *lateral force* – HBM, type U3, are fixed to the rotating frame of the rail,
- *vertical force* – HBM, type U10M, are situated between connection of the wheelset and the weights attached via rollers to the frame of rotating rail,
- *contact force* – EMSYST, type EMS70, located in the brake units on the brake hinge,
- *friction force* – EMSYST, type EMS100, placed in the brake units body in the setup of remoteness of brake pads,
- *motor velocity* - LARM, type IRC315/360, integrated directly on the motor,
- *wheelset velocity* – LARM, type IRC315/360, connected to the axle,
- *acceleration* – TML, type ARF-100A and ARF-100A-T, located on the bearing housing and weights.

The Fig. 3 marked the location of the sensors, by which are measured certain key parameters on the test bench RAILBCOT. It is clear that for the implementation of the various sensors it was necessary produce the relevant adapter that sensors are attached to the construction of the bench to form the desired chain.

In Fig. 4 - Fig. 8 the comparison of two different physical quantities measured by two different devices can be observed. The basic measurement is Acc_x acceleration, measured data acquisition systems HBM QuantumX.

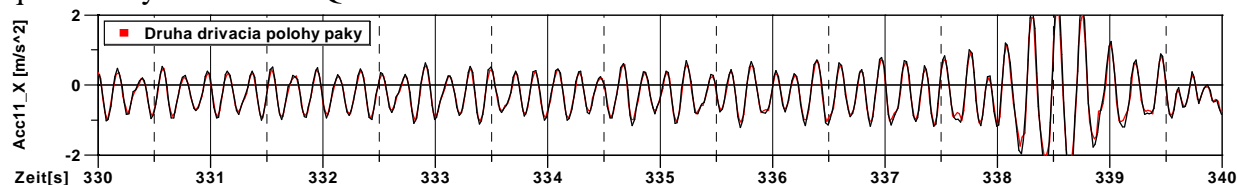


Fig. 4 Second derivation of the lever position – right side.

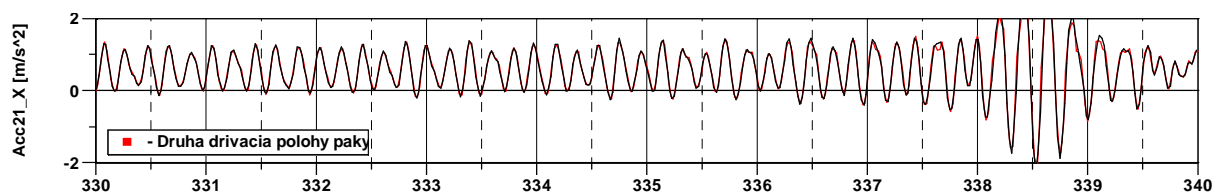


Fig. 5 Second derivation of the lever position – left side.

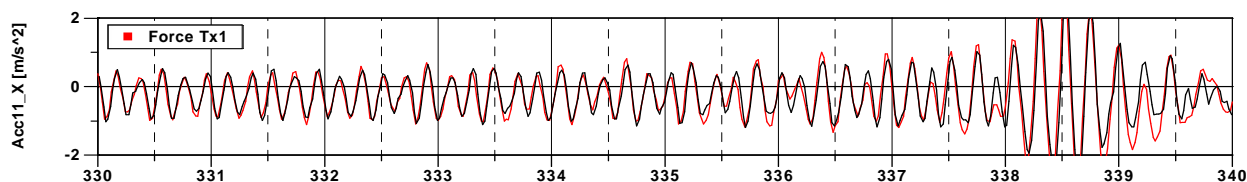


Fig. 6 Longitudinal forces and wheelset right side measured by means of sensors (n*Tx1).

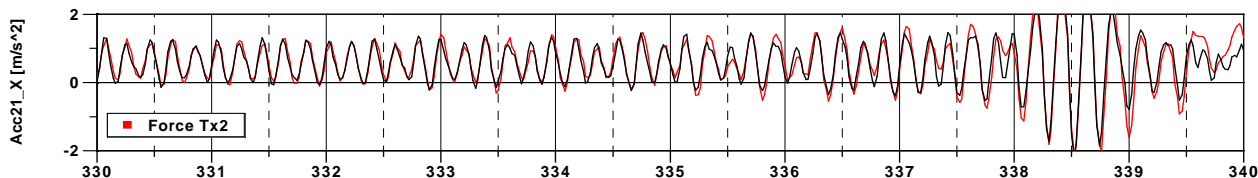


Fig. 7 Longitudinal forces and wheelset left side measured by means of sensors.

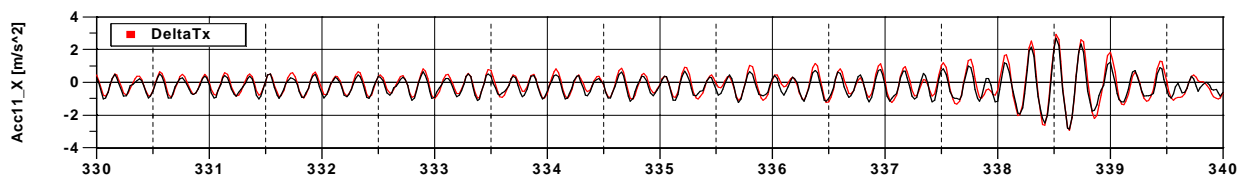


Fig. 8 Longitudinal forces difference and acceleration in x- direction.

Fig. 9 shows the course of the difference of forces T_{x1} and T_{x2} and the torque that has been calculated as x - lever position * stiffness of spring element (4285715N/m)+ lever position derivation * bumper contact (3000N*s/m).

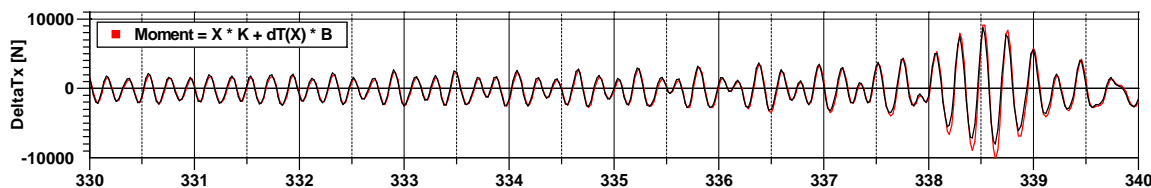


Fig. 9 Comparison of the course of DeltaTx and the torque.

In Fig. 10 and Fig. 11 the dominant frequency of the signal DeltaTx (Fig. 11 x-lever position) corresponds with the frequency of the rotating speed rail. Dominant excitation of inequality rails

cause getting into resonance with its own frequency and then starts to act dominant excitation of the wheelset and un-roundness.

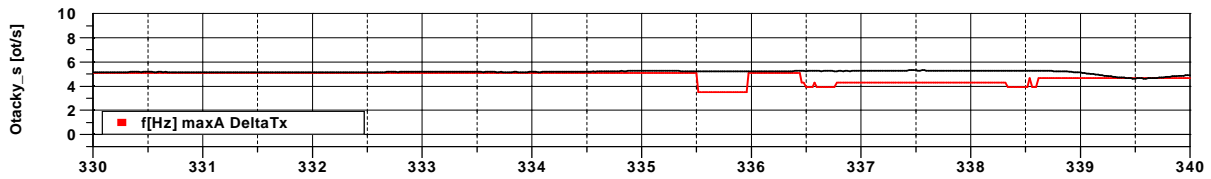


Fig. 10 Rail disc revolutions [rev*s-1] and Delta Tx frequencies (frequency of harmonic part with maximum amplitude).

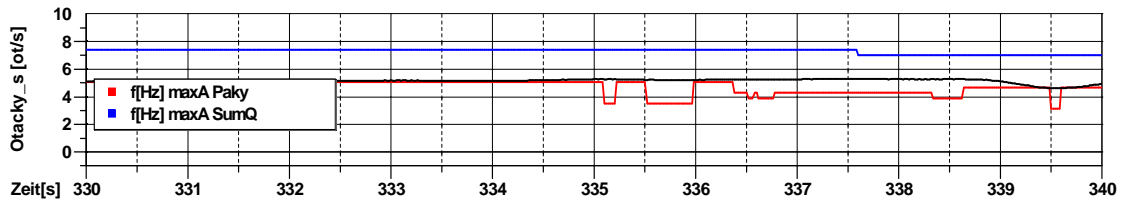


Fig. 11 Rail disc revolutions [rev*s-1] and max Amplitudes of lever and max Amplitudes of Sum of wheel forces frequencies (harmonic part frequency with maximum amplitude rot the lever position and the sum of Q).

Fig. 12 shows a frequency analysis of the acceleration signal and the difference T_{x1} and T_{x2} forces in the time domain 330-340s.

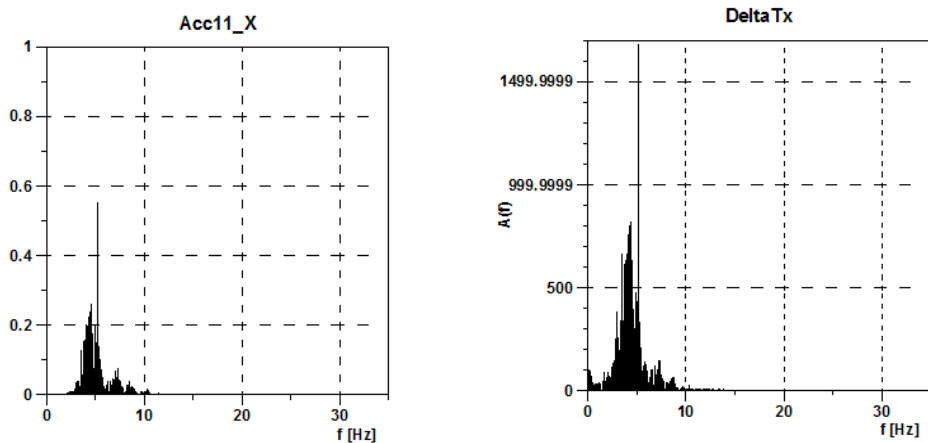


Fig. 12 FFT analysis of acceleration Acc1_x signal and DeltaTx forces signal.

Correlation of acceleration in Fig. 13a with a correlation coefficient of 0.965 confirms the value of the quadratic moment of inertia about 3121m^4 .

Correlation of the calculated torque in Fig.13b with a correlation coefficient of 0.978 confirms that moment \approx DeltaTx.

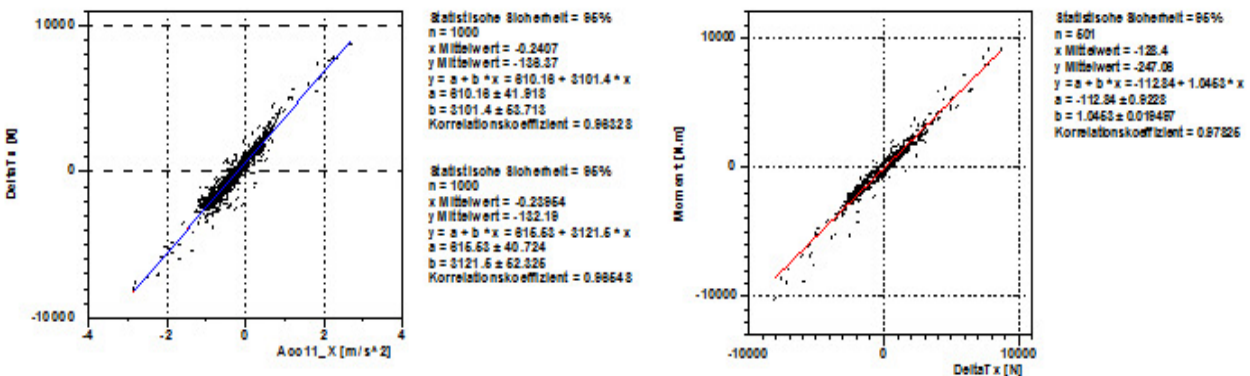


Fig. 13 a) Correlation of acceleration in the time range 330-340s (left) b) Correlation of (calculated) torque in the time range 330 – 340s (right).

From the transfer functions of Fig. 14 it is clear that the value of the natural frequency, at which the resonance imaging, corresponds to the moment of inertia about 3100 m^4 (left) and DeltaTx value of about 1.00 (right).

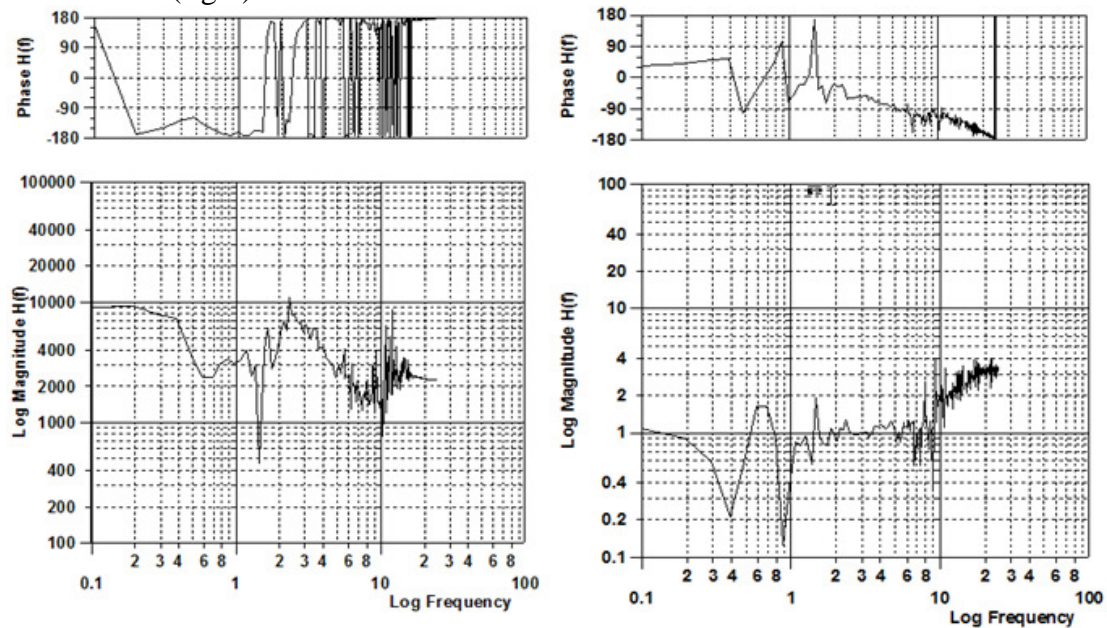


Fig. 14 Transfer function of signals Acc11_x and DeltaTx (left) and Moment and DeltaTx (right).

5. The results of dynamic analysis

After starting the dynamic analysis starts increasing angular velocity of the rotating rail, which rotates the wheelset as well as its roundness excited driven oscillations. Fig. 15a shows the model in system SIMPACK and Fig. 15b shows two time-dependent courses. On the graph below is seeing an increase in the angular velocity of the wheelset (red) and the rotating rail (black), which are bound constant gear ratio between wheel and rail, caused by different diameter of wheels. On the graph above is displayed angular deflection of the lever at the time, which corresponds to an increase of angular speed of rail. Extreme deflections occur at lower speeds than 20 rad/s, which does not fall within the scope of our work.

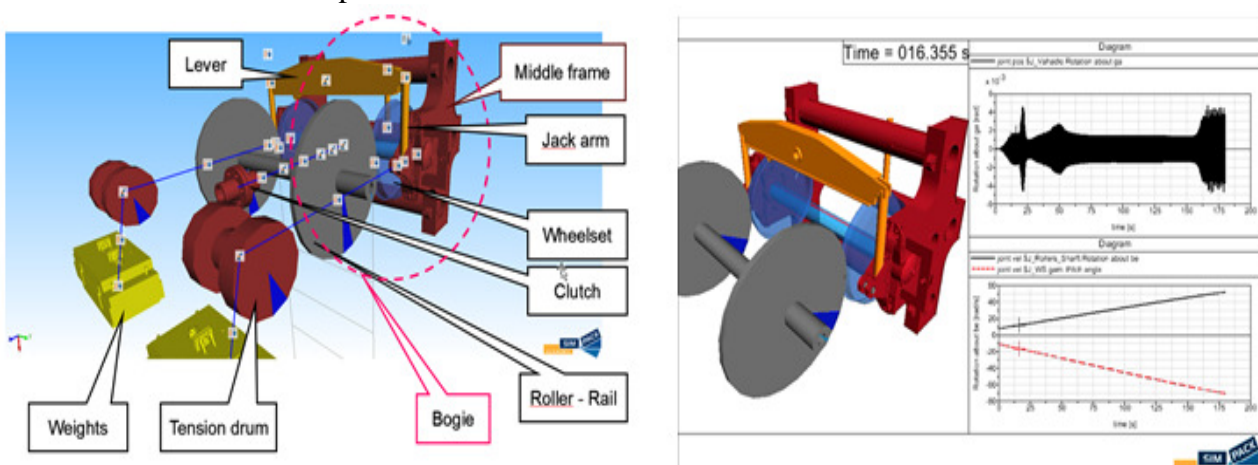


Fig. 15 a) Simplified mechanical system dynamic schema (left) b) Dynamic analysis in SIMPACK (right).

The natural frequency of the rotary movement of middle frame (boogie) reached at resonance by dynamic analysis in SIMPACK value 5.42 Hz at a speed of about 70 km/h.



6. Conclusion

Verification of comparison of measured and calculated values confirmed the need to change the structural parameters of the structure of the bench.

After determining the natural frequency of the moving frame 5.42Hz at velocity approximately at 70 km/h, when the resonance occurs, it is necessary to increase the stiffness of the elastic member at least twice. Then the natural frequency increases and the resonance will occur at higher working speed about 98 km/h, which is sufficient for further measurements.

Acknowledgement

The work was supported by the Scientific Grant Agency of the Ministry of Education of the Slovak Republic and the Slovak Academy of Sciences in project No. 1/0347/12: “Railway wheel tread profile wear research under the rail vehicle in operation conditions simulation on the test bench”, project No. 1/0383/12: “The rail vehicle running properties research with the help of a computer simulation.” and the project No. APVV-0842-11: “Equivalent railway operation load simulator on the roller rig”.

Research-Educational Center of Rail Vehicles (VVCKV)

References

- [1] GERLICI, J., LACK, T., HARUŠINEC, J., MÜLLER, R., DOLEŽEL, P. *Rail vehicles brake components test stand*. (In Slovak). PRORAIL 2011: Žilina, 21.-23.9.2011, conference proceedings. - Žilina: Scientific and Technical Society at the University of Žilina, 2011. ISBN 978-80-89276-30-1.
- [2] GERLICI, J., LACK, T., HARUŠINEC, J. *RAILBCOT - Rail vehicles brake components test stand (In Slovak). Computational and experimental methods in applied mechanics*. Ústí nad Labem: Faculty of production technologies and management University J. E. Purkyně, 2012). ISBN 978-80-7414-377-9.
- [3] GERLICI, J., LACK, T., HARUŠINEC, J. *RAILBCOT - the rail vehicles brake components test stand (In Slovak). Computational and experimental methods in applied mechanics*. - Ústí nad Labem: UJEP, 2012. - ISBN 978-80-7414-377-9.
- [4] GERLICI, J., LACK, T., HARUŠINEC, J. *Development of test stand prototype for rail vehicles brake components testing*. Communications: scientific letters of the University of Žilina. - ISSN 1335-4205. - Vol. 16. (2014).
- [5] GERLICI, J., LACK, T. *Rail vehicles brake components test bench utilisation*. Applied mechanics and materials. ISSN 1660-9336. Vol. 486 (2014), online ISSN 1662-7482. Trans Tech Publications, Switzerland.
- [6] GERLICI J., LACK T., HARUŠINEC J. *Rail vehicles wheels and brake blocks wear laboratory test stand utilization*. Prace Naukowe. Transport: Analiza i ocena elementów systemów transportowych. ISSN 1230-9265. (2014).
- [7] SUCHÁNEK, A., HARUŠINEC, J., GERLICI, J., LACK, T. *Test stand for railway wheels wear investigation function parts modification*. (In Slovak). Computational and experimental methods in applied mechanics I. - Ústí nad Labem: Faculty of production technologies and management UJEP, 2013. ISBN 978-80-7414-609-1.
- [8] GERLICI J., LACK T., HARUŠINEC J. *SIMRAIL - the load modulus of the test stand for the realistic simulation of railway operation in laboratory conditions*. Dynamics of flexible and rigid bodies 2013: proceedings of the XI. International scientific conference, Ústí nad Labem, 9.-11.10 2013. FVTM UJEP, 2013. ISBN 978-80-7414-607-7.
- [9] GERLICI J., LACK T., HARUŠINEC J., *The test stand load modulus implementation for the realistic railway operation in the laboratory conditions*. Paper number: M2013183. Manufacturing technology. Vol. 13, Nr.4. ISSN 1213-2489. Journal for science, research and production. December 2013. Issued by J.E. Purkyně University in Ústí nad Labem, Faculty of Production Technology and Management.
- [10] ŠTEFAŇÁKOVÁ V., GERLICI J., LACK T., HARUŠINEC J. *Test stand load modulus construction proposal for the realistic simulation of railway operation*. TRANSCOM 2013: 10th European conference of young researchers and scientists: Žilina, June 24.-26. 2013, Slovak Republic. - Žilina: University of Žilina, 2013. ISBN 978-80-554-0695-4.



- [11] HARUŠINEC, J., GERLICI, J., LACK, T., ŠTEFAŇAKOVÁ, V. *Angle of attack setting on the test stand system concept modification* (In Slovak). Dynamics of flexible and rigid bodies 2014: Proceedings of the XII international scientific conference: Ústí nad Labem, 8.-10.10.2014. FVTM UJEP, 2014. ISBN 978-80-7414-749-4.
- [12] LACK, T., GERLICI, J. *The Programme System DELTA Exploitation for Numerical Analysis Performances*. (In Slovak). 18-th. International Conference "Current Problems in Rail Vehicles - PRORAIL 2007" Proceedings of lectures, Part II. EDIS, ISBN 978-80- 89276-07-3, Žilina 2007.
- [13] LACK, T., GERLICI, J. *Modified Strip Method utilisation for wheel /rail contact stress evaluation*. 9th international conference on contact mechanics and wear of rail/ wheel systems (CM2012): 27.-30. August 2012, Chengdu, China: proceedings. Chengdu: Southwest Jiaotong University.
- [14] LACK, T., GERLICI, J. *Wheel/rail contact stress evaluation by means of the modified Strip method*. Communications: scientific letters of the University of Žilina. ISSN 1335-4205. - Vol. 15, no. 3 (2013).
- [15] LACK, T., GERLICI, J. *The FASTSIM method modification in speed up the calculation of tangential contact stresses between wheel and rail*. Manufacturing technology: journal for science, research and production. ISSN 1213-2489. - Vol. 13, no. 4 (2013).
- [16] LACK, T., GERLICI, J. *A modified strip method to speed up the calculation of normal stress between wheel and rail*. Applied mechanics and materials. ISSN 1660-9336. Vol. 486 (2014), online ISSN 1662-7482.
- [17] LACK, T., GERLICI, J. *A modified strip method to speed up the tangential stress between wheel and rail calculation*. Applied mechanics and materials. ISSN 1660-9336. Vol. 486 (2014), online ISSN 1662-7482. Trans Tech Publications, Switzerland
- [18] LACK, T., GERLICI, J. *Wheel/rail tangential contact stress evaluation by means of the modified strip method*. Communications: scientific letters of the University of Žilina. ISSN 1335-4205. - Vol. 16, no. 3A (2014).
- [19] GERLICI J., LACK T. *Test benches computer control software tools development*. Scientific bulletin of North University of Baia Mare: Fascicle: Mechanics, Tribology. Technology of Machine Manufacturing. ISSN 1224-3264. - Series C, Vol. XVII (2003).
- [20] GERLICI, T., LACK, T., HARUŠINEC, J. *Test stand properties analysis for wheel-tread wear in accordance with the laboratory simulated railway operation*. VSDIA 2012: proceedings of the 13th mini conference on Vehicle system dynamics, identification and anomalies: 5-7 November, 2012 Budapest, Hungary. - [S.l.: s.n.], 2012. - ISBN 978-963-313-102-2.
- [21] VALČÁKOVÁ, L., LACK, T., GERLICI, J., HARUŠINEC, J. *Rail vehicles brake components test stand dynamic properties evaluation*. TRANSCOM 2013: 10-th European conference of young researchers and scientists: Žilina, June 24-26, 2013, Slovak Republic. - Žilina: University of Žilina, 2013. - ISBN 978-80-554-0695-4.
- [22] GERLICI, J., LACK, T., DOLEŽEL, P., HARUŠINEC, J. *Test stand mechanical system dynamics analysis*. Prace Naukowe. Transport: Analiza i ocena elementów systemów transportowych. ISSN 1230-9265. - Z. 101 (2014).
- [23] VALČÁKOVÁ, L. *Dynamics analysis methods of mechanical system of the test stand*. (In Slovak). Experimental and computational methods in engineering: conference proceedings [Ústí nad Labem : Univerzita J. E. Purkyně], 2014. ISBN 978-80-7414-725-8.
- [24] GERLICI, J., LACK, T., HARUŠINEC, J. *Realistic simulation of railway operation on the RAILBCOT test stand*. Applied mechanics and materials. ISSN 1660-9336. Vol. 486 (2014), online ISSN 1662-7482. Trans Tech Publications, Switzerland.
- [25] LACK, T., GERLICI, J., VALČÁKOVÁ, L. *Test stand dynamics properties research by means of simulation computations*. (In Slovak) Dynamics in rigid and deformable bodies. Proceedings from the XII. International scientific conference: Ústí nad Labem, 8.-10.10.2014. - Ústí nad Labem: FVTM UJEP, 2014. - ISBN 978-80-7414-749-4.



Examination of Modal Characteristics of currying frame and gearbox for extruder

*Peter Weis

University of Žilina, Faculty of Mechanical Engineering, Department of Design and Mechanical Elements,
Univerzitna 2, 01026 Žilina, Slovakia, peter.weis@fstroj.uniza.sk

Abstract. The paper presents examination of the Modal characteristic of currying frame and gearbox for extruder. Finite element analysis (FEA) is divided into analysis of currying frame, which is under load from mass and inertial effects of motor and gearbox and into analysis of separate gearbox, which is under load from torque moment. We performed FEA in software ANSYS Workbench.

Keywords: Gearbox, Extruder, Modal analysis, Contact of bodies, Finite element mesh.

1. Introduction

Gearbox has been designed in Transmisie engineering a.s. Martin. On gearbox together with the currying frame were detected increased vibration at 17 rpm on the output shaft. Based on the vibration analysis was developed new design of currying frame. The aim of the design changes was to move natural frequencies of the system outside the scope of excitation effects. We performed finite element analyzes after these design changes.

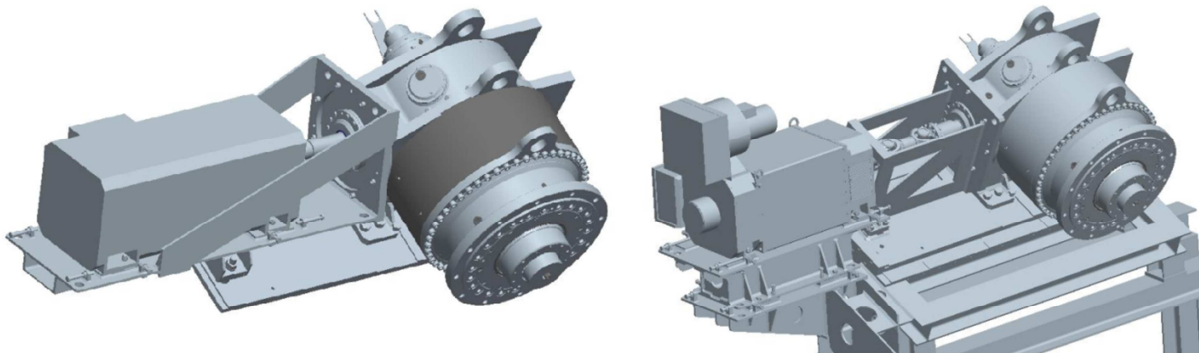


Fig. 1 Gearbox together with currying frame (before and after design changes).

2. Basics of Modal analysis

Modal analysis, or the mode-superposition method, is a linear dynamic-response procedure which evaluates and superimposes free-vibration mode shapes to characterize displacement patterns. Mode shapes describe the configurations into which a structure will naturally displace. Typically, lateral displacement patterns are of primary concern. Mode shapes of low-order mathematical expression tend to provide the greatest contribution to structural response. As orders increase, mode shapes contribute less, and are predicted less reliably. It is reasonable to truncate analysis when the number of mode shapes is sufficient.

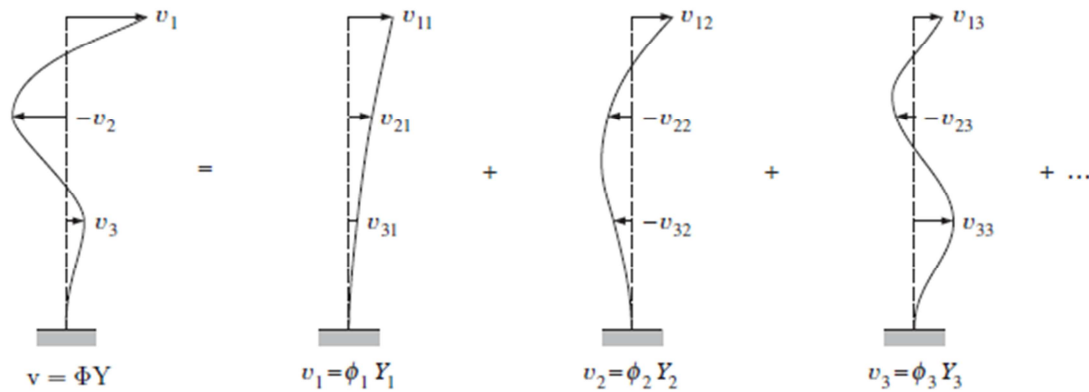


Fig. 2 Resultant displacement and modal components.

For the most basic problem involving a linear elastic material which obeys Hooke's Law, the matrix equations take the form of a dynamic three-dimensional spring mass system. The generalized equation of motion is given as:

$$M\ddot{q}(t) + C\dot{q}(t) + Kq(t) = f(t), \quad (1)$$

where M is the mass matrix, C is a damping matrix, K is the stiffness matrix, \ddot{q} acceleration, \dot{q} is the velocity, q is the displacement and f is the force vector.

The general problem, with nonzero damping problem, is a quadratic eigenvalue problem. However for vibrational modal analysis, the damping is generally ignored, leaving only the mass matrix M and the stiffness matrix K .

$$M\ddot{q}(t) + Kq(t) = 0. \quad (2)$$

3. Modal analysis of gearbox and currying frame

Due to the high computational demands is even nowadays perform a complex analysis of large 3D model, consisting primarily of volume solids big challenge. Therefore, we performed two independent analyzes. At first we performed finite element analysis of currying frame in consideration of mass and inertial effects of the motor and gearbox. Second was finite element analysis of gearbox under load of torque moment on input shaft. 3D model was supplied by Transmie engineering a.s. in the native format Creo Parametric 2.0.. It was necessary to modify geometry of the whole 3D model regarding to finite element analysis demands.

3.1. Finite element analysis of currying frame

We have removed all welds from 3D model of currying frame due to avoid possible complications when calculating finite element mesh. Also, since their removal would not change significantly the weight and stiffness of the currying frame. We created one part from all parts, which included assembly.

We used material model with the following properties:

- Young's modulus $E=205$ MPa,
- Poisson's ratio $\mu=0.3$,
- density $\rho=7850$ kg m⁻³.

On the currying frame we applied mass and inertial effects of the motor and gearbox using "Point mass".

	Hmotnosť m [kg]	Moment zotrvačnosti I_x [kg.m ²]	Moment zotrvačnosti I_y [kg.m ²]	Moment zotrvačnosti I_z [kg.m ²]
Prevodovka	4600	1263,8027	1103,7918	1580,9491
Motor	1650	-	6,3	-

Tab. 1. Mass and inertial effects.

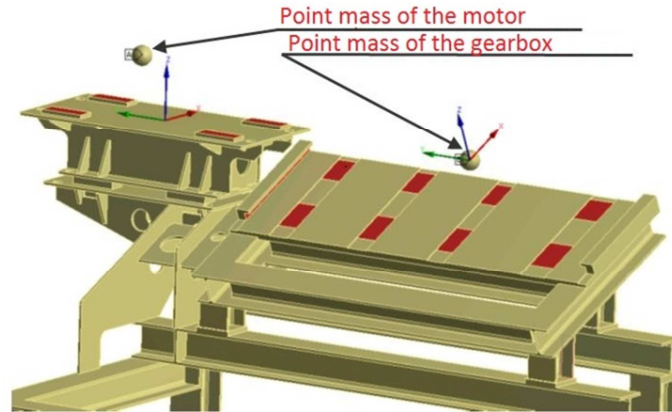


Fig. 3 Point mass.

We removed all Degree of Freedom (DOF) from four lower surfaces.

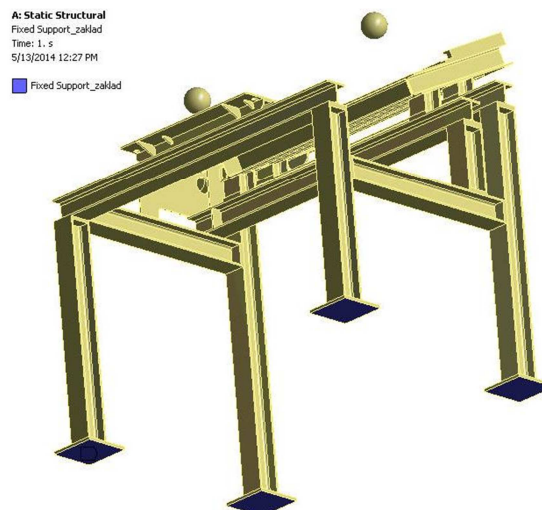


Fig. 4 Fixed support.

When creating finite element mesh we were trying achieve compromise between the number of generated elements and the accuracy of the results. We performed four analyzes with different finite element mesh in order to increase the accuracy of results. Software ANSYS Workbench automatically uses element type SOLID185. Is defined by eight node points with three degrees of freedom movable in X, Y, Z. It can be modified to element type SOLID 186 with twenty node with three degrees of freedom movable in X, Y, Z.

To solve static analysis was chosen direct solver SPARSE. From this solution we obtained state of stress in currying frame. Therefore, stiffness also changed. After static analysis we performed in ANSYS Workbench modal analysis with the new stiffness matrix. We calculated the first twenty natural frequencies and mode shapes.

Exciting frequency was detected at 17 rpm on the output shaft, which is 0.283 Hz. From solution we obtained the lowest frequency $f = 4.48$ Hz, which is below exciting frequency. Therefore, there is no resonance.

3.2. Finite element analysis of gearbox

Before finite element analysis we had to manage complex modification of the 3D model. At first we have removed all components from gearbox, which were not needed for analysis (seals, bearing elements, plugs etc.). Secondly we had to simplify geometry of various parts, which could cause problems when generating the finite element mesh.

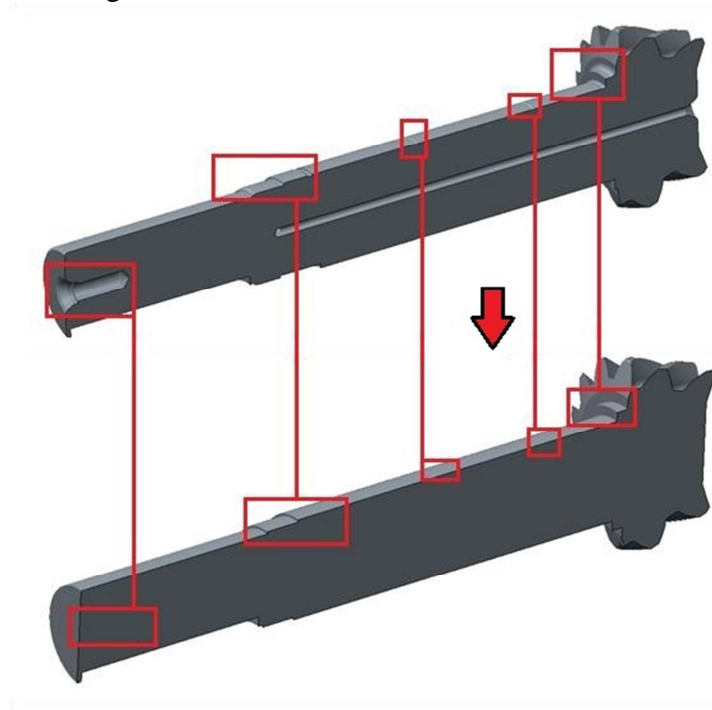


Fig. 5 Simplifying geometry of the input shaft.

In *Design modeler* module, which is included with the software ANSYS Workbench, we add individual parts into smaller components.

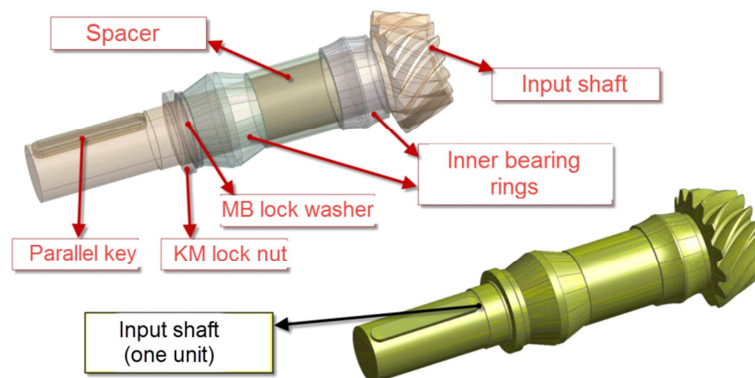


Fig. 6 Adding of individual parts.

After geometry modification we have defined contact pairs between all components. We replaced all bearings in gearbox for *Spherical Joint*. These *Spherical Joints* represent constraint equations. We applied torque moment on the input shaft. We also removed all DOF on the output shaft and on eight lower surfaces.

The biggest challenge was to generate the finite element mesh. On contact surfaces we used CONTA174 and TARGE170 elements. We were trying to use the fewest number of finite elements but with sufficient accuracy of results. The final finite element mesh consists of 12353489 elements and 2504988 nodes.

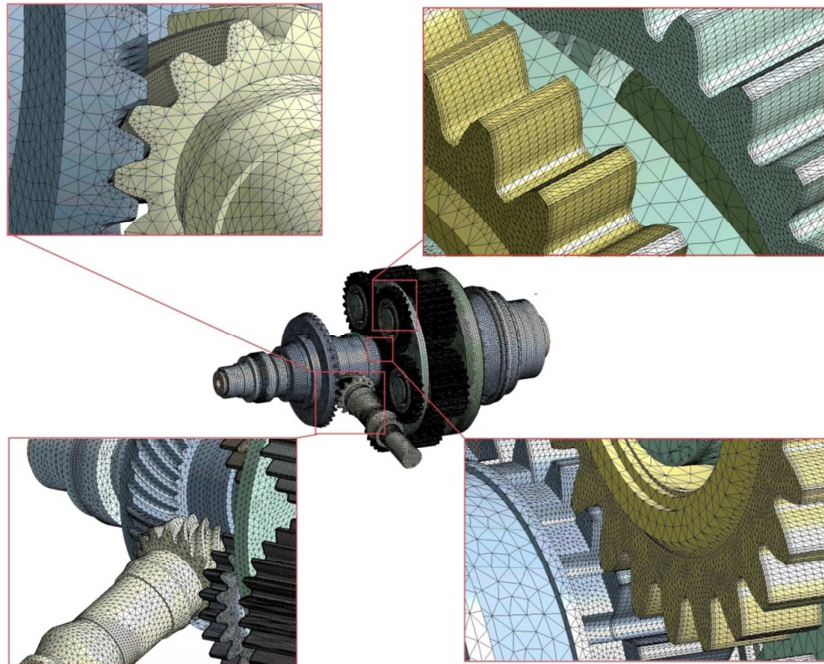


Fig. 7 Finite element mesh.

To solve static analysis was also chosen direct solver SPARSE. From this solution we obtained state of stress in the gearbox with the new stiffness matrix. After static analysis we performed in ANSYS Workbench modal analysis. We calculated the first twenty natural frequencies and mode shapes.

The lowest calculated frequency is 31.568 Hz, which is below exciting frequency. Therefore, there is no resonance.

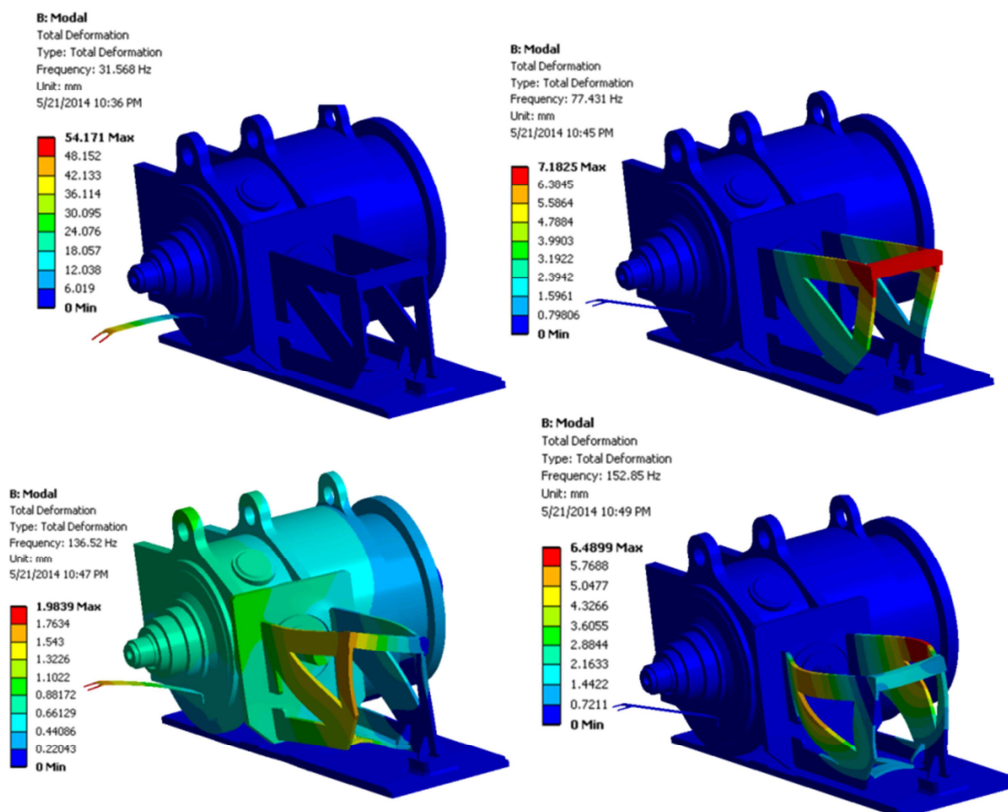


Fig. 8 The first mode shapes.

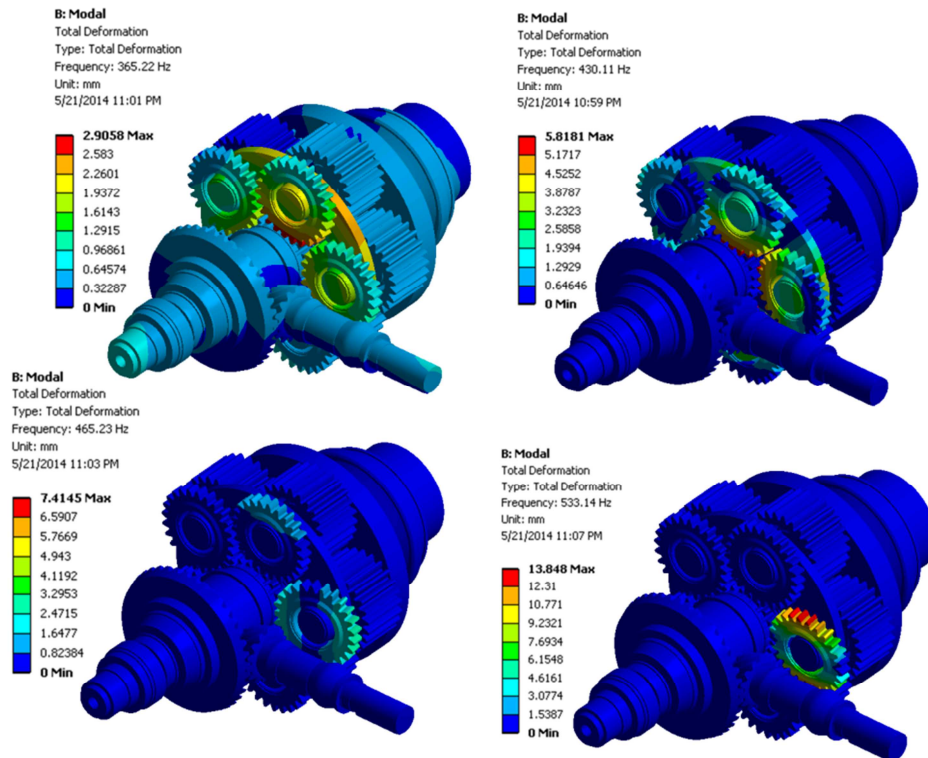


Fig. 9 Some mode shapes inside the gearbox.

4. Conclusion

The paper presents examination of the Modal characteristic of currying frame and gearbox for extruder. The introduction provides an overview of the examined gearbox and currying frame. We performed two independent analyzes. At first we performed finite element analysis of currying frame in consideration of mass and inertial effects of the motor and gearbox. We calculated the first twenty natural frequencies and mode shapes. Exciting frequency was detected at 17 rpm on the output shaft, which is 0.283 Hz. From solution we obtained the lowest frequency $f = 4.48$ Hz, which is below exciting frequency. Therefore, there is no resonance. Second was finite element analysis of gearbox under load of torque moment on the input shaft. The lowest calculated frequency is 31.568 Hz, which is also below exciting frequency. Therefore, there is no resonance.

Acknowledgement

This work was supported by the Scientific Grant Agency of the Ministry of Education, Science, Research and Sport of the Slovak Republic under the contract no. V-1/0844/13 - Research on guidance elements of rolling bearing and their design.

References

- [1] BENČA, Š. 2004. *Výpočtové postupy MKP pri riešení lineárnych úloh mechaniky*. Bratislava: STU Bratislava, 2004. 150 s. ISBN 80-227-2032-1.
- [2] FRANKOVSKÝ, P. 2011. *Využitie modálnej analýzy pri diagnostike vibrácií strojných zariadení*. [online]. 2011. Available online at: < <http://www.sjf.tuke.sk/transferinovacii/pages/archiv/transfer/19-2011/pdf/178-184.pdf> >.
- [3] CHAVAN, D. 2013. *Modal Analysis of Power Take Off Gearbox*. [online]. Available online at: < http://www.ijetae.com/files/Volume3Issue1/IJETAE_0113_12.pdf >.

TRANSCOM 2015

Proceedings, Section 6

Published by University of Žilina

First Editions

Printed by EDIS - Žilina University publisher

Printed in 500 copies

ISBN 978-80-554-1048-7

ISSN of Transcom Proceedings CD-Rom version: 1339-9799

ISSN of Transcom Proceedings online version: 1339-9829

(<http://www.transcom-conference.com/transcom-archive>)

